

## THE CHEMISTRY OF SULFUR IN COAL—A HISTORICAL PERSPECTIVE

William H. Calkins  
Department of Chemical Engineering  
University of Delaware  
Newark, Delaware 19716

### Introduction

Coal represents 85–90% of the fossil energy resources in the United States, and a quarter of the world's coal resources (1). Yet the full utilization of these resources has been limited by the presence of high levels of sulfur in many of the major deposits. (Fig. 1) This has been a recognized problem for many years. In the early part of the century, high sulfur content made use of some coals unsuitable for making of coke for metallurgical purposes. In recent years, the high sulfur content of coal has been recognized as the source of air pollution problems (acid rain), particularly from electricity generation and in industrial boilers. The Clean Air Act Amendments of 1990 were enacted to mitigate these problems. Earlier legislation restricted allowable SO<sub>2</sub> emissions in new power plants. The 1990 act however requires phased in limitation of SO<sub>2</sub> emissions in all power plants of over 25 MW capacity beginning in 1995, and is projected to reduce annual SO<sub>2</sub> emissions by about 10 million tons by the year 2000. A wide variety of methods of limiting SO<sub>2</sub> in flue gas have been devised from wet and dry limestone scrubbers, hot scrubbers, fluidized bed combustors, limestone injection into burners or ducts and others. Many of these are being developed and tested on a commercial scale under the Clean Coal Initiative. Under the 1990 Clean Air Act utilization of high sulfur coal without scrubbers or other remedial measures will not be permitted, although credits for lower than permitted levels may be used to compensate for emissions over permitted levels. This legislation will be expensive in new investment and operating costs and consumers are going to feel it.

### The Origin of Sulfur in Coal

Much of the sulfur in low sulfur coal derives from the sulfur content of the plant material making up the original peat. Sulfur contents greater than a few tenths of a percent have long been known to derive from the depositional environment. Sea water or brackish water in the coal beds contain sulfates. The sulfates undergo bacterial reduction to H<sub>2</sub>S which reacts with iron in the water to form pyrite and with the organic material or the sulfate reducing bacteria to form the organic sulfur structures. The reactions involved are not understood, but isotopic sulfur ratios support this conclusion (2,3).

### Sulfur in the Mineral Matter in Coal

It is well known that high sulfur coal usually contains both mineral sulfur which is largely pyrite, but can also include other metal sulfides and sulfates, and in some cases small amounts of elemental sulfur. It also contains sulfur in organic structures of a variety of types. (Table 1) There are well established methods for removal of much of the mineral sulfur compounds, based on density or wettability or other characteristics of the mineral.

Stock (4) and Buchanan (5,6,7) have shown that elemental sulfur is not present in pristine coal, but derives by oxidation of pyrite primarily. In any event, it is generally present in relatively small amounts even in oxidized coals.

### The Organic Sulfur Structures in Coal

Removal of the organic sulfur is much more difficult than the pyritic sulfur, as it is part of the organic coal structure itself. Processes have been developed for removal of both organic and inorganic sulfur involving molten caustic at high temperatures (e.g., the TRW Gravimelt Process) or oxidizing agents such as air, or chlorine in the presence of strong alkali (e.g., the Ames, PETC and Ledgemont oxydesulfurization Processes). (8) None of these appear to be economically practical at the present time. All of them have been developed without any real knowledge of the chemistry of the organic sulfur they

are supposed to remove. In the Second Supplementary Volume of the "Chemistry of Coal Utilization" which came out in 1981 it says:

"Since there are few methods for determining the functionality of sulfur, especially in mixtures, and the few that are available either are ambiguous or give questionable results with coal, the nature and bonding of the organic sulfur in coal is still unknown."

Since that was written, much progress has been made by many researchers including our Storch Awardee and his coworkers. I am therefore going to devote the limited time I have to outline some of the scientific advances that have been made toward understanding the chemistry of the organic sulfur components, and the status of our knowledge of the organic sulfur structures in coal, as I perceive it today. This progress has been the result of development of a number of new analytical techniques that have become available and considerable research ingenuity by a number of coal scientists.

The organic sulfur in coal can vary from a few tenths of a percent to several percent. Usually, the pyritic sulfur content is similar to the organic sulfur content. In some rare coals however, the pyritic sulfur is very low and the organic sulfur very high. That is the case for two coals from Spain and Yugoslavia (see table 2) which have been the subject of considerable study by coal scientists because they allow the study of the organic sulfur with little interference from the pyrite (46,47,48). Similar coals exist from India and New Zealand.

It has been known for many years, that coal produces thiophenic compounds as tars upon coking, pyrolysis or in coal hydrogenation. That these heterocycles are actually part of the coal structure and not formed in the processing was demonstrated by Hayatsu (9,10) with sodium dichromate oxidation of a range of coal ranks from lignite to anthracite and converting the resulting acids to the methyl esters. Of some 141 aromatic structures obtained in this work were thiophene, benzothiophene, dibenzothiophene and a number of methyl substituted compounds of those same heterocycles. Since that time, Nishioka et al. (11, 12), Curt White (13,14), Sinnighe Damste and de Leeuw (15, 16) and a number of other workers have identified other heterocyclic structures either produced by solvent extraction, pyrolysis or coal hydrogenation. The development of Flame Photometric Detectors (FPDS) was important in some of this work. Winans and Neill (17) also found a number of multiple- heteroatom-containing sulfur compounds where there was oxygen or nitrogen or both in addition to the sulfur by flash pyrolysis of coal into a high resolution mass spectrometer (fig. 2). There can be little doubt that there are sulfur heteroatoms in the aromatic clusters of most high sulfur coals. But is that the only form of sulfur in the organic portion of coal?

When Pittsburgh 8 coal which contained about 1.5% organic sulfur was pyrolyzed by a pyroprobe into a high resolution mass spectrometer many sulfur containing products including low molecular weight compounds such as  $H_2S$ ,  $CO$ ,  $CH_3SH$ ,  $SO_2$ , and  $CS_2$  as well as a whole range of heterocyclic structures from thiophene, benzothiophene, dibenzothiophene and many alkyl substituents of these heterocycles were detected. (18) When the same coal had over 90% of the mineral matter removed by a non-chemical process so as not to affect the organic structures present, a very similar set of pyrolysis products were produced with only the  $SO_2$  and  $CS_2$  largely eliminated. (Table 3) With the mineral sulfur compounds removed from the system, this suggests that the low molecular weight sulfur compounds are produced by breakdown of some relatively unstable organic sulfur structures in the coal, while the more stable heterocyclic sulfur structures pyrolyze into the mass spectrometer unchanged. What are these unstable sulfur structures?

Coal of course is a very heterogeneous material, consisting not only of mineral matter as I have already mentioned, but also quite distinct macerals, deriving from different components of the plant material which went into forming the coal. Raymond of Los Alamos (19,20) studied the organic sulfur content of the various macerals, without separation, from 8 different coals by electron probe microanalysis and showed that the sulfur content is not the same in the various macerals of a given coal. Wert et al. at the University of Illinois (21) made similar measurements on Illinois #5 coal by Transmission Electron Microscopy and showed that the sporinite contained twice as much sulfur as the vitrinite (Fig. 3). Purified

macerals prepared by Dyrkacz' (22) method for separating the various macerals from coal by Density Gradient Centrifugation have been shown by Dyrkacz and Wert (23) and Hippo and Crelling (24) to also have different organic sulfur contents in the various macerals of the same coal.

"Pure" macerals, we must remember still consist of mixtures of macromolecules having a rather random distribution of component molecules. In most cases these are cross-linked and insoluble and therefore intractable. Most researchers in the field therefore resort to trying to identify the various sulfur functional groups or substituents in coal without regard to the rest of the coal structure, since they are the components whose chemistry we want to identify and presumably remove.

In the late 1970s Attar and his coworkers (25,26,27) developed an interesting approach to determining the sulfur functional groups in coal by catalytic programmed temperature reduction to H<sub>2</sub>S. He obtained "kinetograms" (fig. 4) which showed peaks of H<sub>2</sub>S production at various temperatures which from model compound experiments he identified with the various sulfur functional groups which were present. This approach had the problem of requiring adequate contact of a solid catalyst with a solid coal, and recoveries of the sulfur were often low. However he did obtain discrete peaks which he associated with such functional groups as thiolic (mercaptan), thiophenolic, aliphatic sulfide, aryl sulfide, thiophenic and pyrite.

LaCount and coworkers (28,29) came up with a similar approach based on the programmed temperature oxidation of coal in which the sulfur components were oxidized to SO<sub>2</sub> which was detected by FTIR. SO<sub>2</sub> evolution peaks were obtained at various temperatures which were again related to specific sulfur functional groups by comparison with model polymeric sulfur compounds. Peaks were identified with pyrite, non-aromatic sulfur and aromatic sulfur, which presumably includes thiophenic sulfur. In a recent paper, LaCount showed the presence of significant amounts of non-aromatic sulfur groups which he found to be a larger proportion of the total organic sulfur in the low rank coals than in the higher rank coals.

Similar results were obtained in isothermal flash pyrolysis experiments (18). If model sulfur compounds are pyrolyzed at various temperatures at fast heat up rates and very short contact times, to avoid secondary reactions, a set of curves such as those shown in figure 5 are obtained. The aliphatic mercaptans, sulfides and disulfides break down to form H<sub>2</sub>S at a much lower temperature than the aromatic sulfides and thiophenic compounds. When similar isothermal pyrolysis experiments are applied to coals, significant amounts of H<sub>2</sub>S are produced at temperatures in the range where the aliphatic sulfur groups are unstable. The proportion of organic sulfur groups of the thermally unstable types are found to be higher in the low rank coals, and decrease as the rank increases. This suggests that coalification either converts the unstable sulfur structures of the coal to thiophenic structures, or destroys them leaving the thiophenic sulfur structures intact.

It would of course be desirable to have an analytical method for the various sulfur functional groups without the danger of thermally converting the sulfur compounds to other sulfur structures. In the process, as could be the case with the three methods I have described. At least two laboratories undertook to do this with X-ray methods. Gorbaty and coworkers at EXXON used Sulfur K edge X-ray absorption near edge structure spectroscopy (XANES) and X-ray Photoelectron spectroscopy (XPS) (30,31), and Huffman and coworkers at the University of Kentucky also used XANES (32,33). The EXXON group found it necessary to use a third derivative analysis of the XANES spectra to get a resolution of the aliphatic, aromatic and pyritic sulfur forms, while with the XPS they were able to deconvolute the original spectra into identifiable sulfur components. Table 4 shows the breakdown of sulfur types they obtained on the 8 Argonne premium coal samples. The Kentucky group after initially being unable to see the aliphatic structures were able to deconvolute the XANES spectra into component sulfur types at which time the presence of the aliphatic sulfur components became apparent (fig. 6). Suffice it to say that both aliphatic and aromatic or heterocyclic sulfur structures are resolvable in the various coals, and the previously observed trend of higher aliphatic sulfur in the low rank coals decreasing in the higher rank coals is also apparent.

Comparison of analysis of sulfur type on the same low pyrite-high organic sulfur coals by flash pyrolysis and X-ray methods shows quite a reasonable agreement concerning the content of the more reactive aliphatic sulfur components. (34) (Table 5) The higher aliphatic value for the Rasa coal by pyrolysis than by X-ray apparently is due to the presence of some aromatic disulfide which was shown to be less stable than other aromatic sulfides. Combined pyrolysis and X-ray studies also provided evidence that aliphatic sulfidic sulfur is thermally converted to aromatic or heterocyclic sulfur forms, supporting the view that coalification results at least in part in conversion of aliphatic to aromatic and heterocyclic sulfur. (35)

Recently, Brown of CANMET and coworkers (36,37) have introduced another X-ray method based on the sulfur L edge X-ray absorption near-edge spectra. This method offers the potential of greater resolution than the K edge analysis. It has the disadvantage of requiring high vacuum, (the K edge method can be run at atmospheric pressure) thereby limiting the range of samples that can be run. However the greater resolution makes further investigation of this technique worthwhile.

While unoxidized (pristine) coals clearly contain sulfur in the reduced state, the X-ray techniques can also distinguish among the oxidized forms of sulfur such as sulfoxides, sulfones, sulfonic acids and sulfate. This was utilized by both the EXXON (38) and U. of Kentucky groups (39) to show that the aliphatic sulfides are selectively oxidized to sulfoxides and sulfones, and in some cases sulfonic acids, if disulfides are present.

Hippo and the group at Southern Illinois University (40) have done oxidation studies on coals and coal macerals derived from them, using peroxyacetic acid which solubilized most of the coals. The oxidation products were methylated with diazomethane and analyzed in a gas chromatograph using a flame photometric detector. Ten or twelve sulfur compounds were detected, with methyl sulfonic acid being a major product, presumably derived from aliphatic disulfides or thiophene.

The existence of organic sulfur in coal as both aliphatic and aromatic or heterocyclic sulfur forms was dramatically demonstrated by Stock and coworkers together with the EXXON group. They showed that single electron transfer reagents such as potassium naphthalenide in tetrahydrofuran will attack and destroy heterocyclic sulfur compounds and not the aliphatic or sulfidic sulfur. (41) They also showed that strong organic bases such as n-butyl lithium and potassium t-butoxide in heptane remove the sulfidic sulfur from model compounds without affecting the thiophenic compounds. (42) They performed these treatments individually on Illinois #6 coal from which the pyrite had been removed, and showed that the organic sulfur type corresponding to the particular method of treatment was removed as shown by the XANES method. Also, stepwise treatment of the same coal with each reagent eliminated both sulfidic and heterocyclic sulfur types from the coal. (43)

As I have discussed, we now have considerable evidence that the sulfur in coal exists as both aliphatic and aromatic or heterocyclic forms, and several methods exist for the approximation of the amounts of each. Low rank coals contain more of the organic sulfur in aliphatic or labile forms, whereas higher rank coals contain predominantly heterocyclic sulfur. Reaction of coals with methyl iodide (18) suggests that at least some of the aliphatic sulfur is present as thioether, and some possibly as disulfides. Very little appears to be present as mercaptan.

### Sulfur Removal from Coal

What are the implications of this information for the development of an effective high yield low cost process for sulfur removal from coal? Since there are at least two distinct organic sulfur forms, any process devised for such removal must take this into account. Palmer and Hippo et al. (44) found that a combination of peroxyacetic acid treatment and either thermal or base treatment removed much of the organic sulfur. Stock's two processes appear to be unlikely to be practical on a commercial scale, but may lead to similar lower cost methods. With the lower rank coals containing a larger percentage of the less stable aliphatic sulfur, removal of that portion of the organic sulfur together with the pyritic sulfur with strong alkali may be sufficient for most purposes. There is also a number of research programs

underway investigating bacteriological methods for sulfur removal (45). These might be expected to be slow but low in cost if the proper organisms are found.

### Summary and Conclusions

- 1) At least two classes of organic sulfur structures appear to be present in coals, with the low rank coals generally containing a larger percentage of the total sulfur as more reactive aliphatic sulfur components. As rank increases, the more stable heterocyclic sulfur structures increase and become predominant.
- 2) Analytical methods exist for approximating the amount of the two component classes, although more precise methods are needed.
- 3) We now have the fundamental basis and analytical methods for further development of processes for removal of organic sulfur from coal. Such processes must recognize the presence of the two types of sulfur structures.
- 4) We still do not understand the reactions occurring between  $H_2S$  and the biomass that formed the organic sulfur structures in the first place.
- 5) We also do not understand the reactions of  $H_2S$  and/or elemental sulfur with coal or char at elevated temperatures as has often been observed.

### References

- 1) Energy Security A Report to the President, U. S. DOE March 1987
- 2) Chou, C. L. ACS Symposium Series 429 Chapter 2, p 30-52
- 3) Smith, J. W. and Batts, B. D. *Geochimica et Cosmochimica Acta*, 1974, Vol 38, p 121
- 4) Duran, J. E., Mahasay, S. R. and Stock, L. M. *Fuel* 65 (8)1167 (1986)
- 5) Buchanan, D. H., Coombs, K. J., Chaven, C., Kruse, C. W., and Hackley, K. C. *Processing and Utilization of High-Sulfur Coals III* 1990 p 79
- 6) Hackley, K. C., Buchanan, D. H., Coombs, K., Chaven, C., and Kruse, C. W. *Fuel Processing Technology* 24 (1990) 431-436
- 7) Buchanan, D. H., Coombs, K., Murphy, P. M., Chaven, C., Hackley, K. C., Kruse, C. W. *Proceedings: Fourteenth Annual EPRI Conference on Fuel Science GS-6827, May 1990*
- 8) Morrison, G. F. *Chemical Desulfurization of Coal*, Report number JCTJS/TR115, June 1981
- 9) Hayatsu, R., Scott, R. G., Moore, L. P., Studier, M. H. *Nature* 257, p 380
- 10) Hayatsu, R., Winans, R. E., Scott, R. G., Moore, L. P. and Studier, M. H. *Fuel* 1978, Vol 57, p 541
- 11) Nishioka, M., Lee, M. L. and Castle, R. N. *Fuel* 1986, Vol 65, p 390
- 12) Nishioka, M. *Energy and Fuels* 1988, 2, p 214-219
- 13) White, C. and Lee, M. L. *Geochimica et Cosmochimica Acta*, Vol 44, p 1825
- 14) Lee, M. L., Willey, C., Castle, R. N. and White, C. M. *Fourth International Symposium on Analysis, Chemistry and Biology* Battelle Press, Columbus Ohio 1980
- 15) Sinninghe Damste, J. S. and de Leeuw, J. W. *Fuel Processing Technology* 30 (1992) p 109-178.
- 16) Lee, M. L. and Castle, R. N. *Technical Progress Report DOE/EV/10237-2*, May 1, 1981
- 17) Winans, R. E. and Neill, P. H. ACS symposium Series 429, p 249 (1989)
- 18) Calkins, W. H. *Energy and Fuels* 1987, 1, p 59
- 19) Raymond, R. and Gooley, R. *Scanning Electron Microscopy* 1978, vol 1, p 93
- 20) Raymond, R. ACS Symposium Series 205 1982 p 191
- 21) Wert, C., Ge, Yungpei, Tseng, B. H. and Hsieh, K. C. *Journal of Coal Quality* 1988, vol 7, p 118-121
- 22) Dyrkacz, G. R., and Horwitz, E. P. *Fuel* 1984, 63, 1125
- 23) Tseng, B. H., Buckentin, M., Hsieh, K. C., Wert, C. A. and Dyrkacz, G. R., *Fuel* 1986, vol 65, p 385
- 24) Palmer, S. R., Hippo, E. J., Krue, M. A., and Crelling, J. C. ACS Symposium Series 429, p 296
- 25) Attar, A. and Dupuis, F. ACS Fuel Div Preprints 24 (1), 166 (1979)
- 26) Attar, A. *Analytical Methods for Coal and Coal Products Vol III*, p 585
- 27) Attar, A. *Hydrocarbon Processing*, January 1979, p 175

- 28) LaCount, R. B. , Gapen, D. K. , King, W. K. , Dell, D. A. , Simpson, F. W. and Helms, C. A. ACS Symposium Series 169, p 415
- 29) LaCount, R. B. , Kern, D. B. , King, W. P. , Trull, T. K. , Walker, D. K. ACS Fuel Div. Preprints, 37 (3) 1083
- 30) George, B. N. , Gorbaty, M. L. , Kelemen, S. R. and Sansone, M. Energy and Fuels 1991, 5, p 93-97
- 31) Kelemen, S. R. , George, G.N. and Gorbaty, M. L. Fuel 1990, 69, p 939
- 32) Huffman, G. P. , Huggins, F. E. , Mitra, S. , Shah, N. , Pugmire, R. J. , Davis, B. , Lytle, F. W. , and Gregor, R. B. Energy and Fuels, 1989, p 200-205
- 33) Huffman, G. P. , Mitra, S. , Huggins, F. E. , Shah, N. , Vaidya, S. and Lu, F. Energy and Fuels 191, 5, p 574-581
- 34) Calkins, W. H. , Torres-Ordonez, R. J. , Jung, B. , Gorbaty, M. L. , George, G. N. and Kelemen, S. R. Energy and Fuels 1992, 6, p 411-413
- 35) Kelemen, S. R. , Gorbaty, M. L. , George, G. N. , Kwiatek, P. J. and Sansone, M. Fuel 1991, 70, p 396-402
- 36) Kasrai, M. , Brown, J. R. , Bancroft, G. M. , Tan, K. H. and Chen, J. M. Fuel 1990, 69, p 411-414
- 37) Brown, J. R. , Kasrai, M. , Bancroft, G. M. , Tan, K. H. and Chen, J. M. Fuel 1992, 71, p 649-653
- 38) Gorbaty, M. L. , George, G. N. and Kelemen, S. R. Fuel 1990, 69, p 1065-1067
- 39) Taghiei, M. M. , Huggins, F. E. , Shah, N. and Huffman, G. P. Energy and Fuels, 1992, 6, p 293-300
- 40) Palmer, S. R. , Hippo, E. J. , Kruge, M. A. and Crelling, J. C. ACS Symposium Series 429, p 296-315 (1989)
- 41) Chatterjee, K. Wolny, R. and Stock, L. M. Energy and Fuels 1990, 4, p 402-406
- 42) Chatterjee, K and Stock, L. M. Energy and Fuels 1991, 5, p 704-707
- 43) Chatterjee, K, Stock, L. M. Gorbaty, M. L. George, G. N. and Kelemen, S. R. Energy and Fuels 1991, 5, 772
- 44) Palmer, S. R. , Hippo, E. J. , Kruge, M. A. and Crelling, J. C. Coal Preparation 1992, 10, p 93-106
- 45) C & E. News August 29, 1988, p 36-37
- 46) White, C. M. , Douglas, L. J. , Anderson, R. R. , Schmidt, C. E. and Gray, R. J. ACS Symposium Series 429, p 261
- 47) Torres-Ordonez, R. J. , Calkins, W. H. and Klein, M. T. ibid, p 287
- 48) Ignasiak, B. S. , Fryer, J. F. and Jademak, P. Fuel 1978, 57, p 578-584.

Table 1. Sulfur Content Of Some United States Coals (Wt. %)

Type of Sulfur	Texas Lignite Martin Lake	Wyodak Subbit.	Hi Vol Bit.	
			Ill #6	Ohio #6
Pyritic	0. 14	0. 11	1. 06	1. 15
Sulfate	0. 03	0. 12	0. 12	0. 03
Organic	1. 05	0. 70	2. 17	2. 01
Total	1. 22	0. 93	3. 35	3. 19

Table 2. Total and Organic Sulfur Contents of Two High-Sulfur Low-Pyrite Coals

Coal	Country of Origin	% Carbon (maf basis)	% Total Sulfur	% Organic Sulfur
Mequinenza	Spain	68. 6	12. 6	11. 8
Rasa	Yugoslavia	80. 2	11. 8	11. 4

Table 3. Pyroprobe GC/MS Analysis of Pittsburgh 8 R & F High Sulfur Coal

Product	% Tot. Area	
	raw	90% of Pyrite Removed
H <sub>2</sub> S	3. 03	4. 83
COS	0. 48	0. 31
CH <sub>3</sub> SH	0. 32	0. 34
SO <sub>2</sub>	2. 13	0. 02
CS <sub>2</sub>	0. 27	0. 06
thiophene	0. 25	0. 22
methylthiophene-1	0. 34	0. 23
methylthiophene-2	0. 23	0. 10
dimethylthiophene-1	0. 49	0. 46
dimethylthiophene-2	0. 47	0. 38
dimethylthiophene-3	0. 38	0. 24
dimethylthiophene-4	0. 07	0. 05
trimethylthiophene-1	0. 19	0. 10
trimethylthiophene-2	0. 22	0. 16
tetramethylthiophene	low	0. 04
benzothiophene	0. 29	0. 24
methylbenzothiophene-1	0. 06	0. 04
methylbenzothiophene-2	0. 13	0. 15
methylbenzothiophene-3	0. 20	0. 19
methylbenzothiophene-4	0. 15	0. 14
methylbenzothiophene-5	0. 17	0. 12
methylbenzothiophene-6	—	0. 02
Dimethylbenzothiophene-1	0. 11	0. 11
dimethylbenzothiophens-2	0. 06	0. 05
dimethylbenzothiophene-3	0. 12	0. 14
dimethylbenzothiophene-4	0. 07	0. 10
dimethylbenzothiophene-5	0. 05	0. 04
dimethylbenzothiophene-6	0. 07	0. 08
dimethylbenzothiophene-7	0. 05	0. 04
dimethylbenzothiophene-8	0. 05	0. 03
dimethylbenzothiophene-9	0. 03	0. 02
dibenzothiophene	0. 08	+

Calkins, W. H. (18)

Table 4. Approximate Quantification of Organically Bound Sulfur Forms in Argonne Premium Coal Samples

Coal	%C dmmf	Mole percent (+10) by XANES		
		aliphatic	aromatic	thiophenic
Beulah-Zap	74. 05	35	25	38
Wyodak-Anderson	76. 04	33	22	45
Illinois #6	80. 73	33	26	41
Blind Canyon	81. 32	24	28	47
Pittsburgh 8	84. 95	22	34	44
Lewiston-Stockton	85. 08	19	20	60
Upper Freeport	88. 08	13	30	57
Pocohontas #3	91. 81	13	23	64

G. N. George, M. L. Gorbaty, S.R. Kelemen and M. Sansone (30)

Table 5. Percent of Organic Sulfur as Aliphatic Sulfur by Pyrolysis and X-ray Methods

coal	country of origin	% carbon (maf basis)	% total S	% organic S	by pyrolysis	% aliphatic sulfur		mol % H <sub>2</sub> S by TPD
						by X-ray		
						XANES	XPS	
Mequinena	Spain	68.6	12.6	11.8	67	48	66	75
Beulah-Zap	USA	72.9	0.88	0.70	39	37	37	45
Wyodak-Anderson	USA	75.0	0.63	0.47	36	33	37	
Charming Creek	NZ	78.7	5.85	5.76	26	28	38	29
Rasa	Yugoslavia	80.2	11.8	11.4	47	30	26	40

Calkins, W. H. , Torres-Ordonez, R. J. , Jung, B. , Gorbaty, M. L. , George, G. N. and Kelemen, S. R. (34)

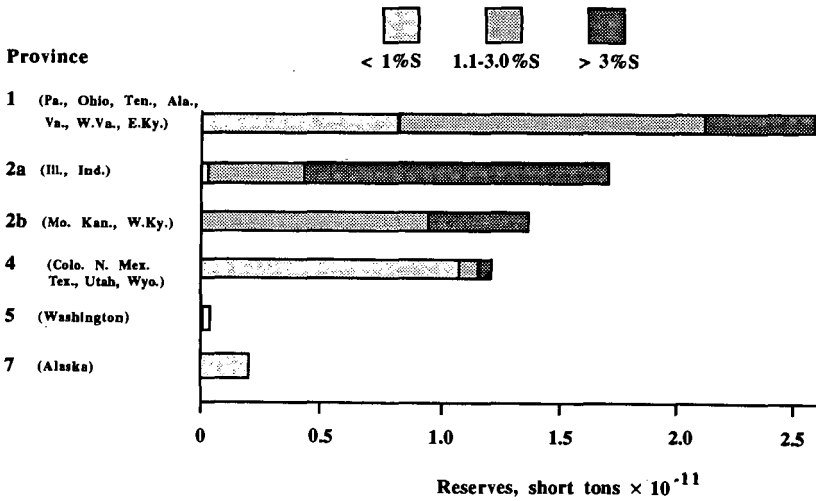


Figure 1. Distribution of U.S. bituminous coals by geological province and sulfur content.

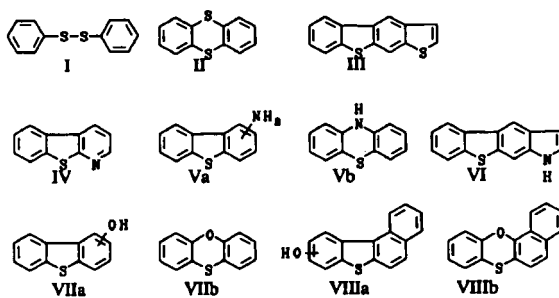


Figure 2. Possible Multiple-heteroatom-containing pyrolysis products. [R. E. Winans and P. H. Neill (17)]

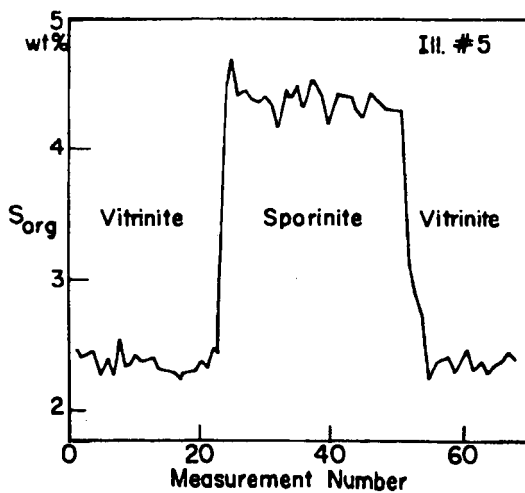


Figure 3. Change in organic sulfur concentration for a maceral of sporinite embedded in a maceral of vitrinite, Illinois #5 Coal. [C. Wert, Y. Ge, B. H. Tseng, and K. C. Hsieh (21).]

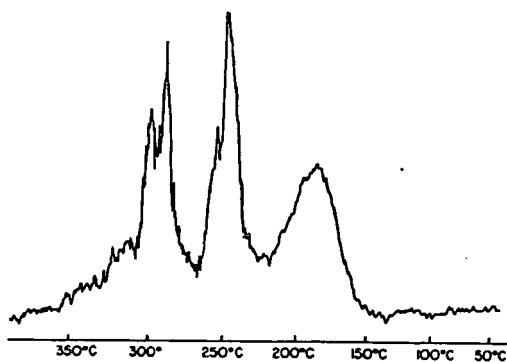


Figure 4. Reductive Kinetogram of Illinois #6 Coal. [A. Attar and F. Dupuis (25).]

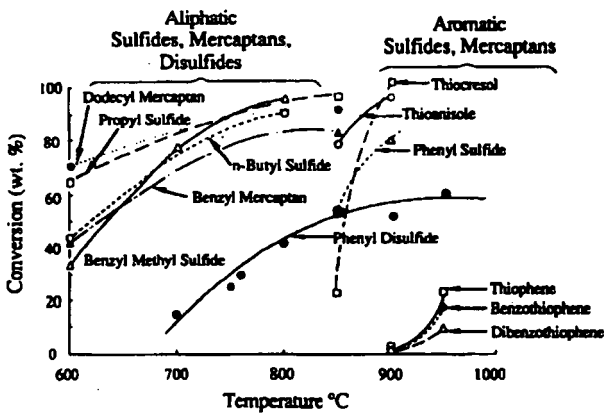


Figure 5. Pyrolysis of Model Sulfur Compounds (% Conversion vs. Temperature) 0.5 sec. Contact time. W. H. Calkins (18)

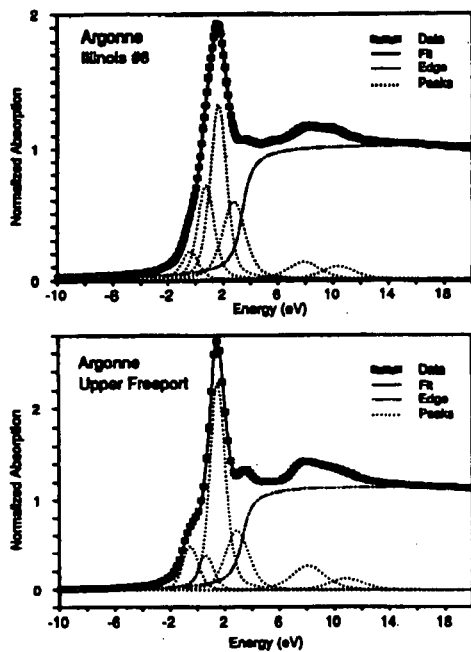


Figure 6. Least Squares Fits of the XANES of Illinois #6 and Upper Freeport Coals. [G. P. Huffman, S. Mitra, F. E. Huggins, N. Shah, S. Vaidya, and F. Lu (33).]

## **SULFUR SPECIATION STUDIES IN COAL AND OTHER FOSSIL ENERGY MATERIALS BY S K-EDGE XANES SPECTROSCOPY**

G.P. Huffman, F.E. Huggins, N. Shah, F. Lu, and J. Zhao, CFFLS 233 Mining & Minerals Res. Bldg., University of Kentucky, Lexington, KY 40506-0107

**Keywords:** sulfur speciation, XANES, XAFS, rubber, resids, coal.

### **ABSTRACT**

Sulfur K-edge XANES spectroscopy has been shown to be an excellent technique for quantitative speciation of sulfur in fossil fuels. Earlier studies focused on establishing the method and applying it to sulfur speciation in coal. More recently, it has been applied to a variety of additional problems, including investigation of coal desulfurization processes, and speciation of sulfur in such materials as asphalts, kerogens/asphaltenes, coal liquefaction resids, and rubber. Some of the more interesting results from this research will be presented. Additionally, a comparison will be made of sulfur K-edge and L-edge XANES results for the same coal.

### **INTRODUCTION**

Sulfur K-edge x-ray absorption fine structure (XAFS) spectroscopy has been shown to be an excellent method of speciating the sulfur in coal and related materials. Two methods have developed for sulfur speciation which involve analysis of the x-ray absorption near-edge structure (XANES) region of the XAFS spectrum. The method developed by Gorbaty and coworkers[1-3] analyzes the XANES by a third derivative method, which yields peaks whose heights are proportional to the percentages of sulfidic and thiophenic sulfur. In the method developed by our group[4-6], a direct least squares analysis of the XANES is carried out by fitting it to a series of mixed Lorentzian-Gaussian peaks. The peak areas are then used to determine the percentages of different sulfur forms present, using empirically determined calibration constants.

In the current article, we will briefly review some recent applications of this technique. These include speciation of sulfur in desulfurized coals, asphalts, coal liquefaction resids, and rubber. A comparison will also be made of sulfur speciation by sulfur K-edge and L-edge XANES spectroscopy for one coal.

### **RESULTS AND DISCUSSION**

The experimental procedures used in these experiments have been discussed in detail elsewhere[3-6]. We will merely note that all experiments were carried out on beamline X-19A at the National Synchrotron Light Source (NSLS) in the fluorescent XAFS mode, using a Si(111) double crystal monochromator and a Lytle detector.

**Desulfurization studies:** XANES results for coals desulfurized by a number of methods have been summarized in recent papers[7,8]. Here we will briefly the principal results for different desulfurization methods.

**Perchloroethylene(PCE) treated samples:** Results have been obtained for a fairly large number of samples before and after extraction with boiling PCE. For the samples investigated to date, it is concluded that the primary effect of the treatment is to remove elemental sulfur. The samples which show elemental sulfur before treatment normally also exhibit a significant amount of sulfate, indicative of oxidation. Fresh coals are unaffected by PCE treatment, suggesting that an oxidative step is required to produce the elemental sulfur that is removed by PCE. These results are discussed in detail in reference 8.

**Treatment with single electron transfer(SET) and basic reagents:** Chatterjee and Stock have discussed the removal of organic sulfur by treatment with SET[9] and basic reagents[10]. A suite of these desulfurized coals have been investigated by XANES spectroscopy using both the third derivative method of Gorbaty et al.[11] and the least squares analysis method[7]. The results for the raw coal, an Illinois #6 from the Argonne Premium Coal Sample Bank, are similar to those reported earlier[4]. After treatment with lithium aluminum hydride(LAH), all of the pyrite is removed, and the percentage of organic sulfide appears to have decreased somewhat relative to thiophenic sulfur. Following SET treatment, the thiophenic sulfur percentage is significantly decreased, while the BASE treatment produces a substantial decrease in sulfidic sulfur, exactly as proposed by Stock and Chatterjee[9,10]. The results are obscured somewhat, however, by the appearance of an unidentified sulfide peak in the spectra of the treated coals, which is believed to be due to potassium sulfide.

**Biological desulfurization:** XANES has been used to investigate two samples of Illinois #6 coal before and after biodesulfurization using the microbe *Rhodococcus rhodochrous* by Kilbane[12]. Pyrite was removed from the coal before biotreatment, leaving a sulfur distribution that consisted of approximately 48% thiophenic sulfur, 31% sulfidic sulfur, 10% sulfate and minor amounts of other components. Following biotreatment, the organic sulfur content was reduced by approximately 2 wt.% and 1 wt.% for two separate samples. The relative percentages of the various sulfur functional forms, however, was unchanged within the error of the measurement( $\pm$  5%), indicating that the biotreatment does not discriminate between different sulfur forms.

**Molten caustic leaching:** A molten caustic leaching process has been developed by TRW Corporation for the removal of sulfur and ash from coal[13]. The results obtained by least squares analysis of the XANES for a Kentucky #9 and a Pittsburgh #8 coal subjected to this process establish that the forms of sulfur are drastically changed and reduced[7]. Specifically, no pyrite or organic sulfide remain, and thiophenic sulfur, which is the dominant organic sulfur form in the original coals is reduced to only about 0.1% in the treated coals. Elemental sulfur, sulfone, and sulfate are the dominant sulfur species remaining at levels of approximately 0.2%, indicating rather severe oxidation.

**Sulfur speciation in asphalts:** The sulfur functional groups present in a

number of asphalt samples were determined by least-squares analysis of their sulfur K-edge XANES spectra[14]. In unoxidized asphalts, oxidized sulfur forms are generally absent, and the principal sulfur form observed is thiophenic. Thiophenic sulfur varied from 54% to 78% of the total sulfur, with the balance being primarily sulfidic. Oxidation tests aimed at mimicing asphalt ageing were carried out at the Western Research Institute. Comparison of the sulfur forms before and after oxidation shows that only the aliphatic sulfur oxidizes to sulfoxide.

**Sulfur speciation in rubber:** Recently, we completed an XANES analysis of the sulfur forms in rubber tread material provided by Michelin. This is the same rubber used by Farcasiu and Smith in experiments on the coliquefaction of rubber and coal[15]. The XANES spectrum of this rubber is shown in Figure 1. As seen, the major feature of the spectrum can be deconvoluted into the  $s \rightarrow p$  transition peaks of polysulfide(0.0 eV), monosulfide(0.8 eV), and thiophenic sulfur(1.5eV). The conversion of peak area percentages into sulfur percentages gives the following results: polysulfides - 38%; sulfides - 29%; thiophenes - 27%; and sulfoxides - 5%. The polysulfides, and possibly the sulfides, are believed to be the sulfur chains formed between polymer chains during vulcanization. A more detailed summary of this work will be prepared for publication elsewhere.

**Sulfur speciation in coal liquefaction resids:** Sulfur speciation has been carried out on THF soluble extracts from a series of coal liquefaction resids from Wilsonville and on the resids themselves. In the resids, pyrrhotite derived from added iron catalyst is the dominant sulfur form. In the extracts, thiophenic sulfur is dominant, sulfidic sulfur is low relative to the original coals, and most samples exhibit some oxidized sulfur, principally sulfoxide and sulfone.

**Comparison of sulfur K-edge and L-edge results:** Recently, Brown et al.[15] have examined the sulfur in coal by sulfur L-edge XANES spectroscopy. Analysis of the sulfur forms in Mequinenza lignite[16] by L-edge XANES gave the following results: 40% thiophenic(4.0 wt%), 20% aryl sulfide, 20% aliphatic sulfide, and 20% disulfide(2.0 wt.% for each sulfide form). The K-edge spectrum of this sample is shown in Figure 2. The major white line component was fitted to three peaks that correspond, with increasing energy, to di/polysulfide, organic sulfide, and thiophenic sulfur. Minor amounts of sulfoxide and sulfate are also observed. The results for the percentages of total sulfur and the wt.% of sulfur in each sulfur form identified are summarized in Table 1. Generally speaking, the results for sulfur speciation by K-edge and L-edge spectroscopy agree within the error of the measurements if the aryl and aliphatic sulfide categories of the L-edge measurement are combined for comparison to the K-edge organic sulfide category.

## REFERENCES

1. George, G.N.; Gorbaty, M.L. *J.Am.Chem.Soc.* **1989**, *111*, 3182.
2. Gorbaty, M.L.; George, G.N.; Kelemen, S.R. *Fuel*, **1990**, *69*, 1065.

3. George, G.N.; Gorbaty, M.L.; Kelemen, S.R.; Sansone, M. *Energy & Fuels*, **1991**, *5*, 93.
4. Huffman, G.P.; Mitra, S.; Huggins, F.E.; Shah, N.; Vaidya, S.; Lu, F. *Energy & Fuels*, **1991**, *5*, 574-581.
5. Huggins, F.E.; Mitra, S.; Vaidya, S.; Taghiei, M.; Lu, F.; Shah, N.; Huffman, G.P. *Processing and Utilization of High Sulfur Coals IV*, **1991**, Elsevier Sci. Pub., 13-42.
6. Taghiei, M.M.; Huggins, F.E.; Shah, N.; Huffman, G.P.; *Energy & Fuels*, **1992**, *6*, 293-300.
7. Huffman, G.P.; Huggins, F.E.; Vaidya, S.; Shah, N. *Amer. Chem. Soc. Div. of Fuel Chem. Preprints*, **1992**, *37(3)*, 1094-1102.
8. Huggins, F.E.; Vaidya, S.V.; Shah, N.; Huffman, G.P.; submitted to *Fuel Processing Technology*.
9. Chatterjee, K.; Wolny, R.; Stock, L.M. *Energy & Fuels*, **1990**, *4*, 402.
10. Chatterjee, K.; Stock, L.M. *Energy & Fuels*, **1991**, *5*, 704-707.
11. Chatterjee, K.; Stock, L.M.; Gorbaty, M.L.; George, G.N.; Kelemen, S.R. *Energy & Fuels*, **1991**, *5*, 771-773.
12. Kilbane, J.J.; *Proceedings: 1991 Second International Symposium on the Biological Processing of Coal*, Ed., S. Yunker; EPRI GS-7482, 1991, pp. 5-1-5-18.
13. Anastasi, J.L.; Barrish, E.M.; Coleman, W.N.; Hart, W.D.; Jonis, J.F.; Ledgerwood, L.; McClanathan, L.C.; Meyers, R.A.; Shih, C.C.; Turner, W.B. *Processing and Utilization of High Sulfur Coals III*; Eds., Markuszewski, R.; Wheelock, T.D.; Elsevier Sci. Pub., **1990**, 371-377.
14. Huggins, F.E.; Vaidya, S.V.; Huffman, G.P.; Mill, T.; Youtcheff, J.; *Amer. Chem. Soc. Div. of Fuel Chem. Preprints*, **1992**, *37(3)*, 1376-1382.
15. Farcasiu, M.; Smith, C.M. *Amer. Chem. Soc. Div. of Fuel Chem. Preprints*, **1992**, *37(1)*, 472.
16. C.M. White et al., paper in preparation.

**Table 1**  
**Results of Least-Squares Fitting of**  
**Sulfur K-edge Spectrum of Mequinenza Lignite**

<u>Sulfur Form</u>	<u>% of Total Sulfur</u>	<u>Wt% S in Lignite<sup>1</sup></u>
Pyritic Sulfur	nd	(<0.5)
Di-sulfide	10	1.0
Sulfide	33	3.3
Thiophenic	42	4.2
Sulfoxide	9	0.9
Sulfone	0	0.0
Sulfate	5	0.5

---

<sup>1</sup>Based on 10.0 wt% (dry) non-pyritic sulfur in lignite. nd - Not determined

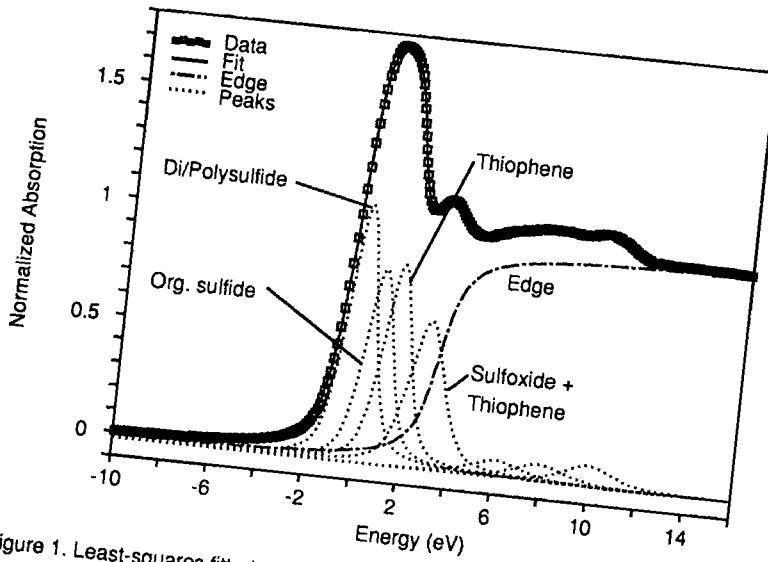


Figure 1. Least-squares fitted sulfur K-edge XANES spectrum of rubber tread material.

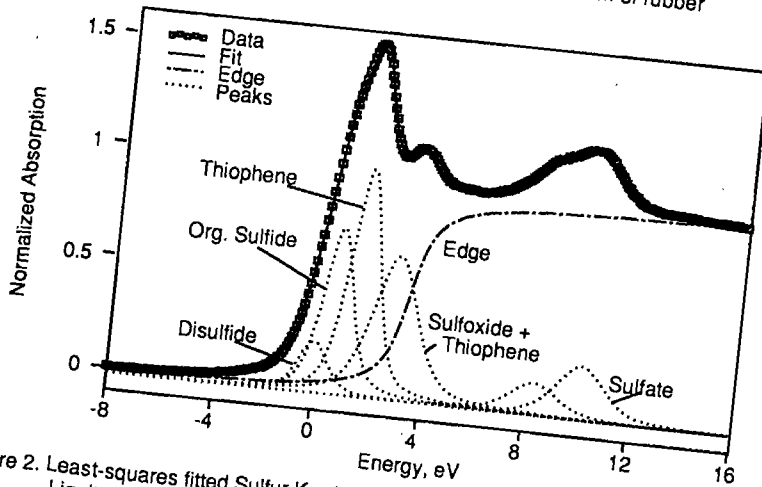


Figure 2. Least-squares fitted Sulfur K-edge XANES spectrum of Mequinenza Lignite

DETERMINATION OF SULFUR COMPOUNDS IN COAL BY  
MASS SPECTROMETRY, CORRELATED WITH XANES AND XPS\*

R. E. Winans, P. E. Melnikov, G. R. Dyrkacz, and C. A. A. Bloomquist  
Chemistry Division, Argonne National Laboratory  
Argonne, IL 60439

M. L. Gorbaty, S. R. Keleman, and G. N. George  
Exxon Research and Engineering Company  
Annandale, NJ 08801

Keywords: Macerals, Sulfur, High Resolution Mass Spectrometry, XANES, XPS

INTRODUCTION

The objective of this study is to identify important organic sulfur-containing compounds in the Argonne Premium Coals and in selected, separated coal macerals. In-source, desorption/pyrolysis high resolution mass spectrometry is being used to characterize the volatile species of whole coals, macerals, and their extracts. To examine the possibility of secondary reactions and undesirable selectivity, the MS data is compared to data from direct techniques, XANES and XPS. The MS results correlate very well which supports the suggestion that the species seen are indigenous to the original sample. Therefore, specific structural assignments to the sulfur species can be made.

Quantitative speciation of organic sulfur in coals has been accomplished by both XANES<sup>1,2</sup> and XPS<sup>2</sup> with what appears to be good reliability. Mass spectrometry approaches provide more detailed molecular information, but suffer from problems with sampling.<sup>3</sup> In the past we have found it difficult to isolate aliphatic sulfur compounds by thermal desorption or pyrolysis due to their thermal transformation to aromatic species. However, recently we have found that with in-source pyrolysis the occurrence of secondary reactions is reduced significantly. Results from both a selected set of the Argonne Premium Coal Samples and a set of three macerals from the Lewiston-Stockton coal (APCS 7) will be discussed.

Table 1. Analysis of the APCS 7 Macerals.

	%C(maf)	H	Per 100 Carbons			
			N	S	O	fa
Whole Coal	85.5	76	1.6	.3	8.9	.76
Liptinite	81.7	110	1.0	.5	8.3	.56
Vitrinite	80.2	78	1.7	.3	11.5	.75
Inertinite	85.4	46	1.3	.7	7.5	.89

## EXPERIMENTAL

The preparation of the macerals by a continuous flow density gradient technique has been discussed and analysis of these samples is presented in Table 1.<sup>1</sup> The XANES and XPS methods have also been published.<sup>2</sup>

The desorption chemical ionization (DCI) and desorption electron impact (DEI) mass spectra were obtained on a three-sector high resolution, Kratos MSS0 spectrometer operating at 10,000 resolving power. This lower resolution was used to enable a more rapid scanning rate (10 sec/decade). In the CI experiments iso-butane was the reagent gas. Samples are deposited on a small platinum coil that is inserted directly into the source body adjacent to the electron beam and heated electrically at 100°C/minute from 200° to 700°C.

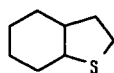
Table 2. Sulfur Distribution in a Selected Set of Argonne Premium Coal Samples.

Coal	%C	S/100C	XANES		XPS		HRMS	
			Al	Ar	Al	Ar	Al	Ar
Lignite	74.1	0.4	37	63	45	55	31-41	69-59
Upper Freeport	88.1	0.3	13	87	19	81	5-7	93-95
Pocahontas	91.8	0.2	13	87	0	100	3-4	96-97

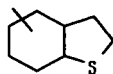
## RESULTS AND DISCUSSION

Initially, a set of pyridine extracts was examined by DEIHMS. Extracts have been found to be quite representative of the whole coal and they typically give higher yields of volatiles compared to the whole, unextracted coals. The results for a lignite and two high rank coals are shown in Table 2 along with the published XANES and XPS results.<sup>2</sup> Although the MS results are only semi-quantitative, they agree very well with the directly obtained data. The trend of decreasing aliphatic sulfur with increasing rank is evident. It can be concluded that the sulfur containing species seen in the mass spectrometer are likely to represent most of the coal.

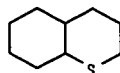
There are some interesting trends in the aliphatic sulfur species seen in the lignite coal. Molecules containing eight and nine carbons tend to dominate. This is especially true at a hydrogen deficiency (rings + double bonds = HD) of two. Possible structures could be:



I

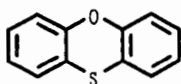


II

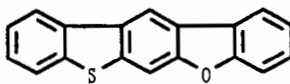


III

Thiolanes (I and II) have been observed in sediments.<sup>3</sup> In addition, partially reduced thiophenes such as dihydrobenzothiophenes are also quite abundant.



I V



V

In the higher rank coals polycyclic thiophenes and sulfur-oxygen species (for example IV or V) dominate. There is evidence that phenoxathiim (IV) occurs in high sulfur bituminous coals.<sup>6</sup> The distribution for the Pocahontas Iv bituminous coal is shown in Figure 1.

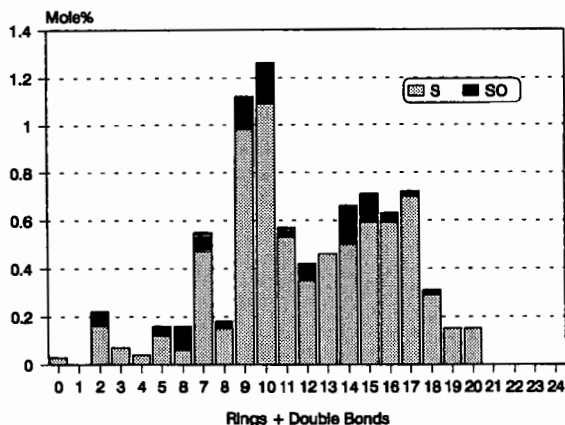


Figure 1. Distribution of organic sulfur containing species as a function of hydrogen deficiency.

XANES and the first XPS results for a set of separated macerals are shown in Table 3. Huffman and co-workers have examined a different set of macerals by XANES.<sup>4</sup> They found, as is shown in this study, that sporinites typically contain much more aliphatic sulfur compared to either vitrinite or inertinite. The amounts are very similar to those found in lignite coals (Table 2). Since these sporinite macerals have been subjected to more rigorous coalification conditions than the lignite, the sulfur compounds such as those seen in lignite (i.e., thiolanes) would be aromatized. Initial examination of the MS data shows a lack of these compounds. The sulfur compounds are possibly incorporated into extended straight<sup>2</sup>chair aliphatic networks, which has been observed with alginites.<sup>3</sup> As expected the inertinites contain more aromatic thiophenes similar to those seen in the high rank coals. Analysis of this data is continuing.

Table 3. Sulfur Distribution in Lewiston-Stockton Coal and Separated Macerals.

	XPS		XANES		HRMS	
	Al	Ar	Al	Ar	Al	Ar
Whole Coal	14	86	20	80		
Liptinite	35	65	50	50		
Vitrinite	8	92	0	100		Pending
Inertinite	9	91	0	100		

#### CONCLUSIONS

Results on the distribution of sulfur compounds determined by in-source pyrolysis HRMS correlates very well with organic sulfur data from XANES and XPS.

#### ACKNOWLEDGMENT

This work was performed under the auspices of the Office of Basic Energy Sciences, Division of Chemical Sciences, U.S. Department of Energy, under contract number W-31-109-ENG-38.

#### REFERENCES

- Huffman, G.P.; Mitra, S.; Huggins, F.E.; Shah, N.; Vaidya, S.; Lu, F. *Energy Fuels*, 1991, 5, 574-581.
- George, G.N.; Gorbaty, M.L.; Kelemen, S.R.; Sansone, M. *Energy Fuels*, 1991, 5, 93-97.
- Winans, R.E. "Mass Spectrometric Studies of Coals and Coal Macerals," In *Advances in Coal Spectroscopy*, Meuzelaar, H.L.C., Ed.; Plenum Press, New York, 1992, 255-274.
- Joseph, J.T.; Fisher, R.B.; Masin, C.B.; Dyrkacz, G.R.; Bloomquist, C.A.A.; Winans, R.E. *Energy Fuels*, 1991, 5, 724-729.
- ten Haven, H.L.; Rullkötter, J.; Sinnighe Damste, J.S.; de Leeuw, J.W. "Distribution of Organic Sulfur Compounds in Mesozoic and Cenozoic Sediments from Atlanta and Pacific Oceans and the Gulf of California." In *Geochemistry of Sulfur in Fossil Fuels*, Orr, W.L. and White, C.M., Eds.; ACS Symposium Series 429, 1990, 613-632.
- Winans, R.E.; Neill, P.H. "Multiple-Heteroatom-Containing Sulfur Compounds in a High Sulfur Coal," In *Geochemistry of Sulfur in Fossil Fuels*, Orr, W.L. and White, C.M., Eds.; ACS Symposium Series 429, 1990, 249-260.

## TOWARD ORGANIC DESULFURIZATION

Leon M. Stock and Kuntal Chatterjee

Chemistry Division  
Argonne National Laboratory  
Argonne, IL 60439

Keyword: Desulfurization

### INTRODUCTION

Advances in the organic desulfurization of coals and resids depend upon the discovery of methods for the secure definition of the sulfur forms in fossil fuel materials as well as upon the discovery of innovative chemical desulfurization strategies. This report deals with the coupling of selective chemical methods with XANES in an investigation of the desulfurization of Illinois No. 6 bituminous coal and Rasa subbituminous coal.

### EXPERIMENTAL PART

The Argonne National Laboratory Premium sample of Illinois No. 6 bituminous coal and a sample of Rasa subbituminous coal that was provided by Ljiljana Ruscic were used in these experiments. The Illinois No. 6 coal contains 81% C (maf) with 2.0%S in organic compounds and 2.8%S in pyrite. The Rasa coal contains 73%C (maf) with 11.7%S in organic compounds.

The procedures that we used for selective desulfurization with lithium aluminum hydride (1-3), potassium naphthalene (-1), (3), and n-butyllithium-potassium t-butoxide (4) have been described previously. Conventional isolation procedures were used in most experiments, however, the facility with which some of the residual sulfur-containing compounds underwent air oxidation prompted us to protect the reaction products from oxygen in certain experiments.

All of the sulfur analyses were performed by Commercial Testing and Engineering of South Holland, IL.

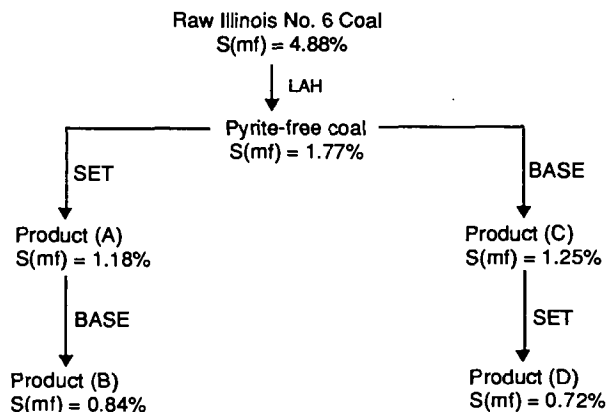
The XANES measurements were carried out by Gorbaty and his associates (5).

## RESULTS AND DISCUSSION

The Illinois No. 6 coal was treated with lithium aluminum hydride to remove pyrite (1-3). As already reported, this method reduces the iron content of this coal to less than 0.1% by weight without altering the organic sulfur content. Several lines of evidence secure this point. First, pyrite reflections are absent in X-ray spectrum. Second, the XANES spectra of the product and the starting material indicate that the distribution of the sulfur forms is unchanged.

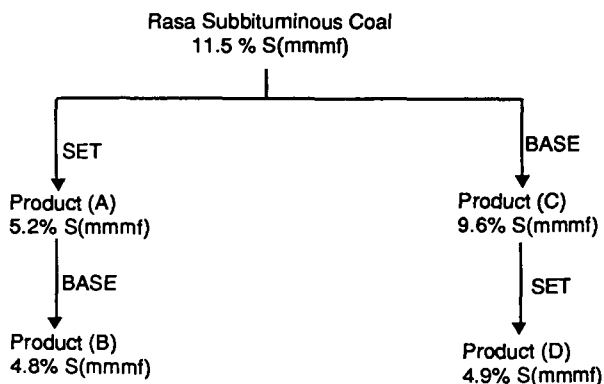
The pyrite-free coal was then treated with a single electron transfer reagent (SET) to react selectively with aromatic sulfur compounds including the sulfur heterocycles (3). We used potassium naphthalene(-1) in tetrahydrofuran at 67°C for 24 hours in most experiments. In an attempt to remove sulfidic sulfur, we used Lochmann's base (BASE), a very reactive mixture of *n*-butyllithium and potassium *t*-butoxide, in heptane at 98°C for six hours (4).

The results of the desulfurization experiments, which have been reported elsewhere (6), are summarized in the equation.



The XANES spectra of each product were recorded by Gorbaty and his colleagues at the Exxon beamline at National Synchrotron Light Source at Brookhaven National Laboratory (6). In brief, Gorbaty has shown that the sulfur XANES spectra of pyrite-free, unoxidized coals exhibit key features near 2469.6 and 2470.5 eV. The feature at 2469.6 eV arises from sulfidic sulfur compounds such as aromatic and aliphatic thiols, aliphatic sulfides, and aryl alkyl sulfides. The feature near 2470.5 eV is dominated by sulfur bound to sp<sup>2</sup> hybridized carbon atoms. The sulfur heterocycles and diaryl sulfides exhibit their absorptions in this region of the spectrum. The pyrite-free Illinois No. 6 coal contains 65 mole % aromatic sulfur and 35% sulfidic sulfur (7). As already reported, SET selectively reduces the aromatic sulfur content and the signal at 2470.5 eV is selectively decreased. On the other hand, BASE removes certain sulfidic forms that contribute to the intensity at 2469.6 eV.

With these results in hand, we turned our attention to the Rasa coal. The work with this subbituminous coal provided the results shown in the equation.



The Rasa coal undergoes extensive desulfurization with the SET reagent. It removes 55% of the sulfur when it is used as the first reagent and 41% of the sulfur when it is used as the second reagent. BASE is much less effective. It removes only 17% of the sulfur when it is employed as the first reagent, and even less, 3%, of the sulfur when it is used after the SET reagent. We also found that when the Rasa coal was treated with BASE and SET and

then treated with SET again, the sulfur content was reduced to 2.2%. When the BASE treatment was omitted entirely, dual SET reactions again reduced the sulfur content to 2.2%.

The XANES spectra for selected products were recorded. It was found that the sulfur bonded to  $sp^2$  carbon in diaryl sulfides and heterocycles is virtually eliminated in the dual SET reactions, but that the feature at 2469.6eV remains.

In the course of our studies with the Illinois coal, we also found that the sulfur compounds that remained after SET and BASE reactions were thermally labile, and were also decomposed by vigorous acid hydrolysis.

## CONCLUSIONS

Although space limitations do not permit a full discussion of all the results, the chemical and spectroscopic observations when coupled with information about the known chemistry of SET and BASE suggest the following conclusions.

First, the SET reagent selectively removes sulfur from heterocyclic sulfur compounds and aromatic sulfides. BASE does not remove the sulfur from the heterocycles but does react with sulfur compounds such as alkyl aromatic sulfides that are susceptible to base catalyzed elimination reactions. Neither of these reagents is effective for the removal of sulfur from aliphatic thiols under the mild conditions that were used in these experiments.

Second, the sulfur compounds that remain after the treatment with SET and BASE are probably aliphatic substances including alkyl and allylic thiols.

Third, BASE can be effective for partial organic desulfurization in some coals, but, generally speaking, the SET reactions, while slow, are more effective and purge sulfur selectively from the organic compounds in these coals without appreciable loss in the heat content.

## ACKNOWLEDGEMENT

This work was supported by the Office of Basic Energy Sciences, Division of Chemical Sciences, U.S. Department of Energy, under contract number W-31-109-ENG-38.

## REFERENCES

1. Kuhn, J. K.; Kohlenberger, L. B.; Shimp N. F. *Environ. Geol. Notes* **1973**, *66*.
2. Westgate, L. M.; Anderson, T. F. *Anal. Chem.* **1982**, *54*, 2136.
3. Chatterjee, K.; Wolny R.; Stock, L. M. *Energy & Fuels* **1990**, *4*, 402-406.
4. Chatterjee, K.; Stock, L. M. *Energy & Fuels* **1991**, *5*, 704-707.
5. George, G. N.; Gorbaty, M. L. *J. Am. Chem. Soc.* **1989**, *111*, 3182-3186 and subsequent publications in this series.
6. Chatterjee, K.; Gorbaty M. L.; George, G. N.; Keleman, S. R. *Energy & Fuels* **1991**, *5*, 771-773.
7. George, G. N.; Gorbaty, M. L.; Kelemen, S. R.; M. Sansone *Energy & Fuels* **1991**, *5*, 93-97.

## Quantification of Nitrogen Forms in Argonne Premium Coals

S. R. Kelemen, M. L. Gorbary, S. N. Vaughn and P. J. Kwiatek  
Exxon Research and Eng. Co., Annandale, N.J. 08801

### Abstract

X-ray Photoelectron Spectroscopy (XPS) was used to investigate the organic nitrogen forms present in fresh Argonne premium coals. In addition to the anticipated presence of pyrrolic and pyridinic nitrogen forms, a detailed analysis of the nitrogen (1s) line shape indicates the presence of quaternary type nitrogen species. A trend of decreasing level of quaternary nitrogen type with increasing coal rank is observed.

### 1. Introduction

The ability to quantify heteroatom functionalities in complex carbonaceous systems such as coal and petroleum residua can provide valuable insight into the organic macromolecular structure. Direct spectroscopic probes such as X-ray Photoelectron Spectroscopy (XPS) [1, 2] and X-ray Absorption Near Edge Structure (XANES) spectroscopy [3-7] have proven to be viable nondestructive techniques for organic sulfur speciation in non-volatile and solid carbonaceous materials. Results from these direct probes for organic sulfur have been compared to results based on pyrolysis methods [8]. XANES and XPS has been used to study the thermal chemistry of sulfur in coal [2] and these results provide insight into the transformations of organic sulfur that occur during pyrolysis based analytical probes. These results also provided insight into some of the processes at work during coal metamorphism [9].

A similar understanding of the chemistry of nitrogen in coal has not yet emerged. Progress has been made with XPS [10-14] and XANES [15] in the quantification of organic nitrogen forms. Development of both of these techniques is essential for a more complete understanding of chemical reactivity of coal. Mass transport of reactants and products is always a concern when dealing with coal. XPS has the advantage of being a probe the near surface (e.g. first 50 Angstroms) while XANES can derive its signal from the entire sample.

XPS methods have been widely used in the study of nitrogen forms in coal. Initial studies established that the energy position of the nitrogen (1s) signal was close to that expected for pyrrolic nitrogen [10,11]. It was possible to further curve resolve the XPS nitrogen (1s) spectra of coal into two peaks corresponding to pyrrolic and pyridinic types [10-13]. In a more recent study of a series of eight UK coals covering the range of 80-95 Wt% carbon it was found that the XPS nitrogen (1s) spectra could be curve resolved into two major components, pyrrolic and pyridinic [14]. The XPS sensitivity for nitrogen in this study was estimated at 0.1 atom % nitrogen and the total nitrogen content of the coals ranged from about 0.8 to 2.0 atom % [14]. In another recent XPS study of nitrogen, pyrrolic and pyridinic were the major forms identified in coal and its derived products with only minor unidentified components present in some samples at higher binding energy [13]. The first XANES studies of coal and petroleum asphaltenes supports the position that pyrrolic and pyridinic groups are the most abundant nitrogen forms in these materials [15]. An error estimate based on the unnormalized XANES nitrogen fraction, is considered to be about 10% [15].

A detailed analysis of the XPS nitrogen (1s) line shape has been used to quantify both the major and minor forms of nitrogen present in fresh Argonne premium coals. Changes in the distribution of nitrogen functionalities

due to pyrolysis and hydrolysis have been examined for Illinois #6 bituminous and Wyodak subbituminous coal. The relevance of these results toward understanding coal metamorphism will be discussed.

## II. Experimental

XPS spectra were obtained with a Vacuum Generators (VG) ESCA Lab system using MgK alpha non-monochromatic radiation and a either a single or a five channel detection arrangement. The five channel signal system provided a five times greater XPS signal for the same X-ray exposure time. The coal and model compound samples were made into fine powders and mounted to a metallic sample block by means of Scotch double sided non-conducting tape. An energy correction was made to account for sample charging based on the carbon (1s) peak at 284.8 eV. All spectra were obtained at an analyzer pass energy of 20 eV and a constant analyzer transmission mode. Under these conditions the full width at half maximum (FWHM) of 1.7 eV was obtained for the carbon (1s) spectrum of Argonne premium Pocahontas coal. The carbon (1s) line shape of Pocahontas coal is dominated by signal from hydrocarbons because of the very low total heteroatom content.

The nitrogen (1s) signal was curve resolved using a mixed Gaussian-Lorentzian line shape and a FWHM of 1.7 (eV). With these parameters it was possible to fit the nitrogen (1s) signal from pure model compounds, where nitrogen exists in a single chemical environment, with a single peak having these characteristics. The nitrogen (1s) spectra from coal were more complex. These spectra were curve resolved using the same theoretical line shape using peaks at 398.7, 400.2 and 401.3 ( $\pm 0.05$ )(eV). These peaks correspond to the energy positions found for pyridinic, pyrrolic and quaternary type nitrogen functionalities respectively [13]. The peak shape and peak energy positions were fixed and only the amplitudes of these peaks varied to obtain the best fit to the experimental XPS data.

Elemental data for the coal samples were obtained from the Users Handbook for the Argonne Premium Sample Program [16]. Other elemental analytical data were obtained from Galbraith Analytical Laboratories, Knoxville, TN. Elemental data was also derived from XPS measurements from the areas of the XPS peaks after correction for atomic sensitivity. The sensitivity factors were obtained from VG sensitivity tables and experimentally measured standards. The elemental concentrations are presented relative to carbon.

Pyrolysis experiments were done in a quartz lined reactor in helium at 1 atm. The reactor temperature was raised to 400°C at approximately 0.5°C/sec. and held for 5 min. Under these conditions, little of the ultimate amount of hydrocarbons expected from the volatile matter determination are released while much of the oxygen as CO<sub>2</sub>, H<sub>2</sub>O and CO evolves [2]. Hydrolysis was accomplished in a closed reactor pressurized at room temperature to 70 atm. with a 95% hydrogen 5% helium mixture. The reactor temperature was raised to 427°C at a heating rate of 0.05°C/sec. and held for 30 min. These conditions favored the retention of coal hydrocarbon components and hydrocarbon products in the hydrolysis chars.

## III. Results

The amount of nitrogen measured by XPS for the fresh coal samples was compared to bulk elemental data. The results are shown in Table I and there is excellent agreement for all coals except Illinois #6 and Lewiston coals. The generally good agreement indicates that there is no systematic enhancement or depletion of nitrogen at the coal surface. Illinois #6 and Lewiston coals gave lower nitrogen values with XPS. The origin for the difference with bulk

value for these two coals is not yet resolved. The precise nature of the XPS results was demonstrated by numerous measurements on fresh coals of different particle sizes. The XPS nitrogen values for Illinois #6 coal were consistent throughout thermal and reductive treatment. Previous XPS investigations of other coal samples gave reasonable agreement between XPS and bulk values for nitrogen [10-14, 17, 18]. A tendency toward lower XPS values was noted [11, 13, 14] and a possible uncertainty in the XPS sensitivity factor for nitrogen was suggested as one possible cause for the discrepancy. This is an inadequate explanation in the present case of Argonne premium coals. Nevertheless, XPS has good precision for nitrogen quantification and the results are significant for identification of chemical changes in coal functionality.

The XPS nitrogen (1s) signals for the fresh Argonne premium coal samples is shown in Figure 1. Included in Figure 1 are the results of the curve resolution analysis for nitrogen forms. In each case the individual peaks and the total simulated spectrum are shown with the actual spectrum. The anticipated pyrrolic (402.2 eV) and pyridinic (398.7 eV) nitrogen forms were the most abundant species identified. The two forms could almost completely describe the nitrogen (1s) spectrum from a high rank coal such as Pocahontas, however, in all other cases it was necessary to include a peak for quaternary nitrogen ion (401.3 eV). Notice the relatively good signal to noise (S/N) characteristics of each spectrum and how well the sum of theoretical peaks fit the actual data. There are limited degrees of freedom in the curve resolution methodology, described in the experimental section. Data with good (S/N) provide a good test for the curve resolution methodology. Additional samples of fresh Argonne Premium coal were prepared, the XPS nitrogen (1s) signal recorded and curve resolved using the same methodology the gave essentially the same result, namely, that it was necessary to include in all cases a peak representative of quaternary nitrogen in addition to the ones representative of pyrrolic and pyridinic species. The estimated experimental precision for nitrogen forms is ( $\pm$ ) 3.0 mole %.

The average numerical results of the curve resolution analysis are shown in Table 2. In all cases pyrrolic and pyridinic species are the dominant nitrogen forms in agreement with previous findings for coal [10-14]. There is a significant contribution of quaternary nitrogen signal, especially in the lower rank Argonne premium coals. The data from each individual curve resolution analysis for nitrogen forms was plotted as a function of the weight % carbon in coal. Figure 2 shows these results. The solid and open points were obtained using a five and a single channel detection system respectively. These results show a distinct trend of decreasing relative amount of quaternary nitrogen with increasing coal rank for Argonne premium coals. A distinct trend for the relative level of pyrrolic nitrogen is not evident but there appears to be a tendency for the relative level of pyridinic nitrogen to increase with increasing coal rank.

The changes in the total level of organic nitrogen and oxygen following pyrolysis and hydrolypyrolysis of Illinois #6 and Wyodak coal were examined. The results of total nitrogen in the residual pyrolysis and hydrolypyrolysis chars are shown in Table III along with the results for total organic oxygen based on XPS analysis. For Illinois the level of organic oxygen drops nearly in half during hydrolypyrolysis. Less organic oxygen is lost during pyrolysis. There is only a slight increase in the relative level of total nitrogen after pyrolysis and hydrolypyrolysis. For Wyodak coal the organic oxygen level drops in half after pyrolysis and to one third of its initial value after hydrolypyrolysis. In contrast the relative level of nitrogen remain close to the initial value. The loss of organic oxygen after mild pyrolysis and hydrolypyrolysis conditions employed here is likely a result of loss of organic oxygen functionalities as CO<sub>2</sub>, H<sub>2</sub>O and CO [19, 20]. The loss of nitrogen as small gaseous molecules (i.e. NH<sub>3</sub>, HCN, etc.) does not occur at low temperature (T < 450°C) [21] prior to the devolatilization of hydrocarbons. Since some carbon is lost with CO<sub>2</sub> and CO as well as through formation of small quantities of methane or other small hydrocarbon gases a slight increase in the level of nitrogen relative to carbon would be expected if nearly all of the initial nitrogen is retained in the pyrolysis and

hydropyrolysis chars.

The changes in the XPS nitrogen (1s) line shape following mild pyrolysis and hydropyrolysis of Illinois #6 and Wyodak coal have been studied. Figure 3 shows the The XPS nitrogen (1s) signals following hydropyrolysis. Included in Figure 3 are the results of the curve resolution analysis for nitrogen forms. In each case the individual peaks and the total simulated spectrum is shown with the actual spectrum. The anticipated pyrrolic (402.2 eV) and pyridinic (398.7 eV) nitrogen forms were the dominant species present. The two forms could describe the nitrogen (1s) spectrum following hydropyrolysis of Illinois #6 coal, however it was still necessary to include a small peak at the position expected for the quaternary nitrogen species.

The numerical results of the curve resolution analysis for nitrogen forms after pyrolysis and hydropyrolysis are shown in Table IV. There is a decline in the relative level of quaternary nitrogen for both coals after reaction. The decline is greater following hydropyrolysis. There is a significant increase in the relative level of pyridinic nitrogen for both coals after hydropyrolysis.

#### IV. Discussion

Detailed analysis of the XPS nitrogen (1s) signal has been used to determine the relative level of nitrogen forms in fresh Argonne premium coal samples. In agreement with previous investigations of other coals [10-14] pyrrolic and pyridinic species were the dominant nitrogen forms. In all cases it was necessary to include a peak found at the position expected for quaternary nitrogen ion. The relative level quaternary nitrogen decreases with increasing coal rank. It seems plausible that the quaternary nitrogen ion is associated with oxygen and the observed functional trend is caused by the loss of organic oxygen functionalities during coal metamorphism.

Quaternary nitrogen species have been identified in the XPS nitrogen spectrum of derived products of coal quaternarized with methyl iodide and examples shown where quaternary nitrogen is the most abundant species [12, 13]. The presence of quaternary nitrogen forms in fresh coal samples has not been reported before. The estimated experimental precision in the present study Argonne premium coal samples is estimated at ( $\pm$ ) 3 mole %. It is possible that quaternary nitrogen species in lower rank coals was not measured in previous studies because the confidence level in the curve resolution process was substantially poorer on the order of ( $\pm$ ) 10 mole %.

The XPS analysis for nitrogen forms in pyrolysis and hydropyrolysis chars showed that the relative level of quaternary nitrogen declines following reaction and is accompanied by a decline in the relative level of organic oxygen. There is ample reason to believe that nearly all of the nitrogen initially present is retained in the coal chars after reaction. The preferential retention of nitrogen [22] compared to sulfur and oxygen [2, 19, 20, 22] has been noted before. In the case of hydropyrolysis chars the relative level of pyridinic nitrogen increases substantially. It is concluded that the quaternary nitrogen species present in Illinois #6 and Wyodak coal are associated with oxygen and that the associations are broken during reaction. Furthermore, it appears likely that the quaternary nitrogen species is transformed during reaction and is largely retained in the coal char as a pyridinic nitrogen form. The appearance of quaternary nitrogen in fresh lower rank coal and the partial retention of these forms after mild pyrolysis indicates that these represent a significant class of strong non-covalent interactions present in the macromolecular structure of coal.

A detailed analysis of the XPS nitrogen (1s) line shape indicates the presence of quaternary type nitrogen species in addition to the anticipated pyrrolic and pyridinic forms. A trend of decreasing level of quaternary type

nitrogen with increasing coal rank is observed. The quaternary nitrogen species is lost with the loss of oxygen functionalities during pyrolysis. The ratio of pyridinic to pyrrolic nitrogen increases after pyrolysis. These observations suggest that the quaternary nitrogen species is associated with oxygen and that the association is broken as a result of thermal reactions. Furthermore, it appears that the quaternary nitrogen is transformed and remains in the coal char as a pyridinic nitrogen form.

#### V. Summary

Curve resolution analysis of the XPS nitrogen (1s) spectra of Argonne Premium coal showed that pyrrolic and pyridinic nitrogen are the most abundant forms. Quaternary nitrogen species are a significant fraction in lower rank coals and the trend is toward decreasing level of this species with increasing coal rank. Most nitrogen is retained in the remaining coal after mild hydrolysis. The relative amount of pyridinic nitrogen increases and while the level of quaternary nitrogen decreases after hydrolysis of Wyodak and Illinois #6 coal.

#### References

- 1) Kelemen, S. R.; George, G. N.; Gorbaty, M. L., *Fuel* 1990, 69, 939.
- 2) Kelemen, S. R.; Gorbaty, M. L.; George, G. N.; Kwiatek, P. J.; Sansone, M., *Fuel*, 1991, 70, 396.
- 3) Gorbaty, M. L.; George, G. N.; Kelemen, S. R., *Fuel* 1990, 69, 945.
- 4) George, G. N.; Gorbaty, M. L.; Kelemen, S. R.; Sansone, M., *Energy and Fuels*, 1991, 5, 93.
- 5) Huffman, G. P.; Mitra, S.; Huggins, F. E.; Shah, N.; Vaidya, S.; Lu, F., *Energy and Fuels*, 1991, 5, 574.
- 6) Taghiei, M. M.; Huggins, F. E.; Shah, N.; Huffman, G. P., *Energy and Fuels*, 1992, 6, 293.
- 7) Brown, J. R.; Kasrai, M.; Bancroft, M. G.; Tan, K. H.; Chen, J. H., *Fuel*, 1992 71, 649.
- 8) Calkins, W. H.; Torres-Ordóñez, R. J.; Jung, B.; Gorbaty, M. L.; George, G. N.; Kelemen, S. R., *Energy and Fuels*, 1992, 6, 411.
- 9) Kelemen, S. R.; Gorbaty, M. L.; Vaughn, S. N.; George, G., Preprint, Am. Chem. Soc., Div. of Fuel Chem., 1991, 36, 1225.
- 10) Jones, R. B.; McCourt, C. B.; Swift, P., Proc. Int. Conf. Coal Sci., Dusseldorf, 1981, p. 657.
- 11) Perry, D. L.; Grint, A., *Fuel* 1983, 62, 1029.
- 12) Bartle, K. D.; Perry, D. L.; Wallace, S., *Fuel Proc. Technol.* 1987, 15, 351.
- 13) Wallace, S.; Bartle, K. D.; Perry, D. L., *Fuel* 1989, 68, 1450.
- 14) Burchill, P.; Welch, L. S., *Fuel* 1989, 68, 100.
- 15) Kirtley, S. M.; Mullins, O. C.; van Elp, J.; Cramer, S. P., Preprint, Am. Chem. Soc., Div. of Fuel Chem., 1992, 37, 1103.

- 16) Vorres, K. S., Ed. The Users Handbook for the Argonne Premium Coal Sample Program; Argonne National Laboratory: Argonne, IL, 1989; ANL-PCSP-89-1.
- 17) Clark, D. T.; Wilson, R., Fuel 1983, 62, 1034.
- 18) Weitzsacker, C. L.; Gardella, J. A. Jr., Anal. Chem. 1992, 64, 1068.
- 19) Solomon, P. R.; Serio, M. A.; Carangelo, R. M.; Bassilakis, R.; Gravel, D.; Baillargeon, M.; Baudais, F.; Vail, G., Energy and Fuels 1990, 4, 320.
- 20) Burnham, A. K.; Oh, M. S.; Crawford, R. W., Energy and Fuels, 1989, 3, 42.
- 21) Bassilakis, R.; Serio, M. A.; Solomon, P. R.; Preprint, Am. Chem. Soc., Div. of Fuel Chem., 1992, 37, 1712.
- 22) Fiedler, R.; Bendler, D., Fuel, 1992, 71, 381.

Table I

Coal	Nitrogen/Carbon Atom Ratio (x100)	
	Total XPS	Total Bulk
Beulah Zap	1.5	1.5
Wyodak	1.3	1.4
Illinois #6	1.2	1.7
Blind Canyon	1.6	1.7
Pittsburgh #8	1.2	1.3
Lewiston	1.0	1.7
Upper Freeport	1.5	1.6
Pocahontas	1.2	1.3

Table II

Coal	XPS Pyridinic	Mole Percent Pyrrolic	(± 3.0) Quaternary
Beulah Zap	26	58	16
Wyodak	25	60	15
Illinois #6	26	62	12
Blind Canyon	31	55	14
Pittsburgh #8	32	61	7
Lewiston	31	60	9
Upper Freeport	28	65	7
Pocahontas	33	64	3

Table III

Coal	XPS Atom Ratio (x100)	
	Organic Oxygen/C	Organic Nitrogen/C
Illinois #6 (Initial)	9.0	1.2
Illinois #6 (Pyrolysis)	6.7	1.3
Illinois #6 (Hydropyrolysis)	4.8	1.5
Wyodak (initial)	16.9	1.3
Wyodak (Pyrolysis)	8.8	1.3
Wyodak (Hydropyrolysis)	5.6	1.4

Table IV

Coal	XPS	Mole Percent	(± 3.0)
	Pyridinic	Pyrolic	Quaternary
Illinois #6 (Initial)	26	62	12
Illinois #6 (Pyrolysis)	30	64	6
Illinois #6 (Hydropyrolysis)	35	65	0
Wyodak (initial)	25	60	15
Wyodak (Pyrolysis)	29	62	9
Wyodak (Hydropyrolysis)	35	65	3

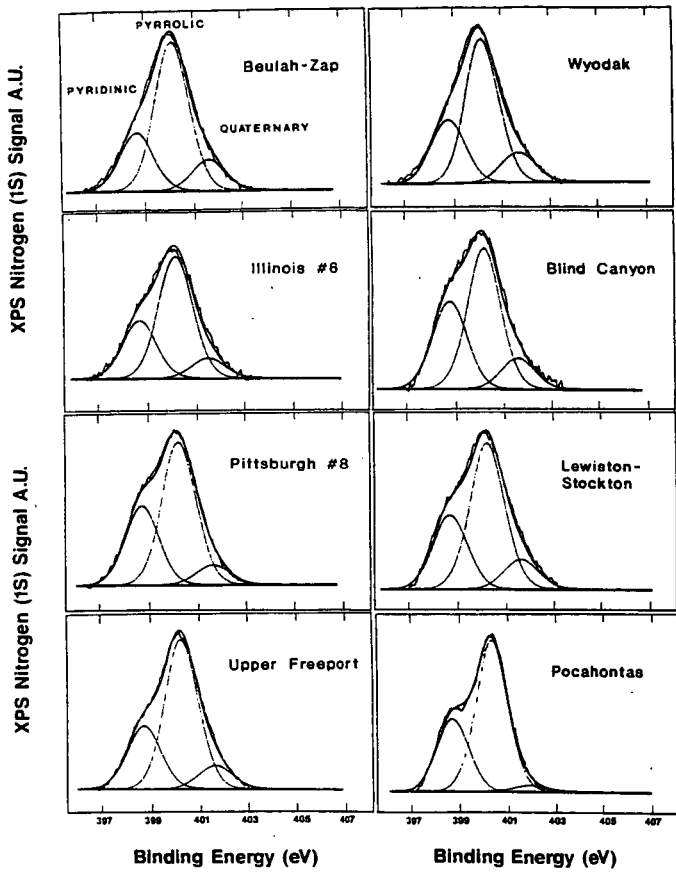


Figure 1. XPS Nitrogen (1s) Curve Resolution of Argonne Premium Coals

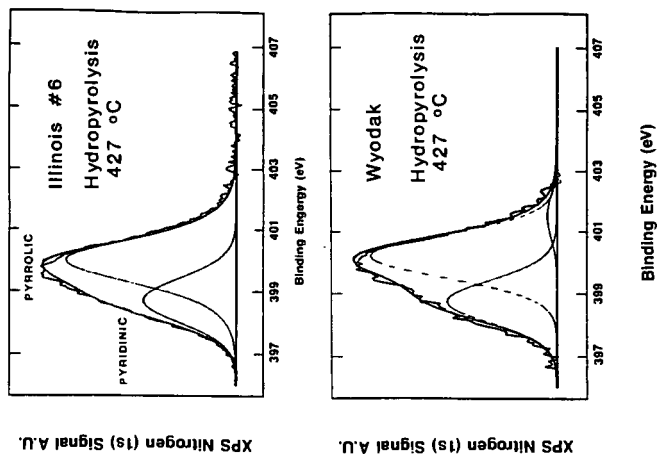


Figure 3. XPS Nitrogen (1s) Curve Resolution of Hydrolyzed Coals

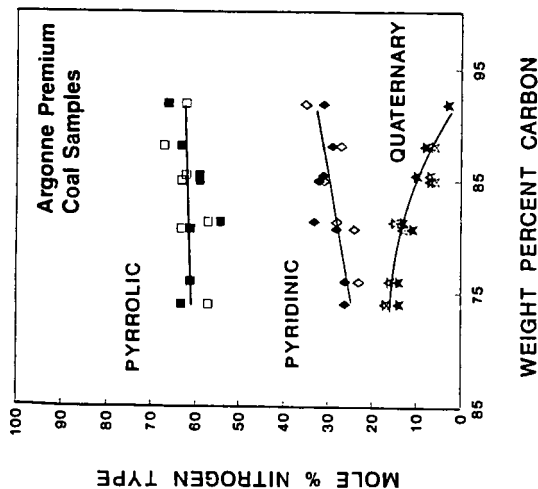


Figure 2. Nitrogen Functional Groups By XPS Curve Resolution Analysis

## A PERSONAL VIEW OF COAL SCIENCE: PAST, PRESENT AND FUTURE

Martin L. Gorbaty  
Exxon Research and Engineering Company  
Annandale, NJ 08801-0998

### INTRODUCTION

Coal is our most abundant fossil fuel resource. Its major commercial use today is for electric power generation through combustion, and to a lesser extent as a feed for the manufacture of metallurgical coke. The potential uses for coal are broader, such as feeds for producing liquid fuels and chemicals; technologies are available, but are not economically competitive. New, more efficient and environmentally sound technologies for coal utilization will be required in the future, and these will arise from more detailed fundamental knowledge of coal structure and reactivity. What follows is a personal assessment of the state of the art in several areas of coal science, some critical opportunities for new chemistry in these areas, and some guesses about the impact such new information might have. Taken together, these suggested research areas could provide the scientific bases from which the required technologies of the future could emerge.

It should be noted that significant progress in basic understanding of coal structure and reactivity has been made in the last decade. In order to assess the extent of this progress, it is instructive to review what were considered to be key research needs at that time. In 1979 the writer and his colleagues detailed such needs (1), and in this paper they will be referred to as starting points for assessing current state of the art.

### COAL CHARACTERIZATION

Today, as in the past (2,3), coal is thought of as a complex heterogeneous "organic rock", made up of fossilized remnants of primordial plant matter and incorporated inorganics. Coal is also a porous rock. Thus coals have organic, inorganic and physical structures. Because of the inherent heterogeneity of coals, and limitations in analytical instrumentation, systematic studies of these structures were limited in 1979. With the advancement of many modern characterization approaches, not available in 1979, clearer, more precise and in-depth knowledge of each of these structures has been attained, and understanding the ways in which they affect coal reactivity becomes possible.

### ORGANIC STRUCTURE

Many average molecular models representative of the organic material in coals have been and continue to be proposed (4-8), and as expected, become more refined as new information is obtained. An excellent review of this area, published in 1981, is still relevant (9). These models are useful to guide thinking, but must be used with care, since they are average structures meant to represent functional group distributions and may not be completely accurate. All recent model structures may be viewed as "islands" of aromatic ring clusters, many of which contain substituents, held together by largely aliphatic, or aliphatic-heteroatomic "bridges". The relative sizes of the islands, bridges and substituents vary depending on rank.

About a decade ago, major unknowns of coal structure included the types and amounts of oxygen, nitrogen and sulfur functionalities, carbon aromaticities, the ring size distributions, and bridging structures for coals of different rank. Since then characterization techniques have been developed which allow much of this information to be obtained:

Organically bound oxygen functionalities (hydroxyl, carboxyl, and ethers by difference) may now be accurately determined by the O-alkylation method (10). This knowledge makes possible the understanding of the role of oxygen functionalities during coal reactivity. For example, the effect of hydroxyl group hydrogen bonding on the caking properties of bituminous coals has been demonstrated (11).

An X-Ray Photoelectron Spectroscopy (XPS) method has been developed to accurately speciate and quantify forms of organically bound nitrogen (12), including the basic pyridines and quinolines and the weakly acidic or neutral indoles and carbazoles. It is necessary to know how nitrogen is incorporated in the organic matrix, since it has been apparent for some time that nitrogen species play a role in coal asphaltene behavior (13) and in coal conversion chemistry (14).

Since 1979 major advances have been made in speciating and approximately quantifying forms of organically bound sulfur, involving reactive and direct measurements. The reactive method uses flash pyrolysis (15), while the direct measurements involve XPS (16) and X-ray Absorption Near Edge Structure Spectroscopy (XANES) (17, 18). The latter methods were applied to the suite Argonne Premium coals (19), and it was shown that aromatic sulfur forms increased directly with increasing rank of the coals studied (17). In addition these methods are now being used to follow the chemistry of organically bound sulfur under mild oxidation (20) and pyrolysis conditions (21).

Knowledge of ring size distributions has grown significantly in the last several years. In 1979, solid state <sup>13</sup>C nuclear magnetic resonance (nmr) held real potential for this purpose, which has since been fulfilled. Aromatic ring cluster sizes have been estimated for the Argonne Premium coal samples based on some very elegant nmr experiments (22). For this sample suite varying from lignite to low volatile bituminous, the striking result is that the average ring cluster ranged between 9 (lignite) and 20 carbons (lvb), with most subbituminous and bituminous coals of this suite containing 14. This indicates an average size of 2-3 rings per cluster.

Another indicator of ring size distribution comes from coal depolymerization experiments (23). High levels of naphtha and distillate yields from a number of coals treated by this method indicate that average ring size distributions in the coals studied range from 1-3.

While methods are available today to get detailed information of the important coal structural features, they have not been uniformly applied to a standard suite of coals, and this represents an important research opportunity. Only the sulfur, nitrogen and nmr work described above have been done on the exact same suite of coals. This is necessary in order to get an idea of the parametric variations as a function of coal rank. Also, major opportunities now exist for using these methods to characterize starting and reacted coals and their products in order to be able to provide a basis for elucidating and understanding the detailed the chemistry taking place during conversion procedures.

## INORGANIC STRUCTURE

Although the amounts of mineral matter in coals vary considerably, most contain about 10% (24). Mineral matter is inorganic material deposited before, during or after coalification of partially decayed biomass, and is largely in a reduced chemical state. Mineral matter is not necessarily inert during coal conversion processes, and has been reported to act beneficially in some cases as a catalyst for

gasification (25) and liquefaction (26) or detrimentally (27, 28). Therefore, a knowledge of the structures of the minerals present and their reactivities is important. Unfortunately, not much progress has been made in this type of characterization. Furthermore, the ways in which the inorganic matter is bound to the organic matter is not well understood. When coal is burned, the remaining inorganic mixture of oxides is called ash. Techniques to characterize the chemical compounds in ash, many of which are non-stoichiometric, are required. Sensitive probes to determine the compounds in which trace elements exist in native coals and in ash are being developed (29).

This information can impact on all forms of coal utilization including beneficiation, combustion, gasification, and liquefaction. For example, if mineral matter has catalytic effects during liquefaction, identification of the chemical species involved could lead to ways of enhancing its catalytic behavior. Better understanding of organic-inorganic interactions is needed to improve current coal cleaning procedures, and the determination of the compounds that make up slags found in furnaces might lead to ways of controlling the slagging phenomenon.

## PHYSICAL STRUCTURE

The physical structure of coal has been described as a porous macromolecular gel (30). From the "porous rock" point of view, methods for determining surface areas and pore volumes on coals are needed. Depending on the coal, the adsorbing gas, the procedures used to acquire adsorption data and the equation used for the calculation, values of from 2-200 m<sup>2</sup>-g have been reported for the same sample (31). The difficulty in making these measurements is compounded because pore structures of subbituminous and lower rank coals collapse upon drying (32). Knowledge of surface areas and pore volumes are needed in order to help establish correlations between surface areas and chemical reactivity, particularly regarding access of gases and liquids to the interior of a coal particle.

From the "macromolecular network" point of view, much progress has been made in recent years in characterizing coals, and some reviews are available (33). It is well known that coals imbibe solvents, swell appreciably, and in some ways swollen coal networks take on elastomeric properties (35). Much work in recent years has focussed on adapting solvent swelling as applied to polymers to defining coal macromolecular structure in terms of  $M_c$ , the molecular weight between cross-links. There are many difficulties with translating polymer science techniques to coal (34), and the opportunities remain for finding reliable methods to determine  $M_c$ . This vital parameter could be used to follow the extent of coal network "depolymerization" during processing and for determining how many bonds need to be cleaved to reduce the "molecular weight" of coal from a solid macromolecular network to desired liquid products.

In recent years, another view of coal physical structure has been proposed (36), based on observed rapid and slow proton relaxation rates in nmr experiments. In this view, the macromolecular network is an "immobile phase" and is "host" to a number of many presumably smaller, mobile molecules, the "mobile phase", called by some "guests". As yet it has not been possible to distinguish between a long chain mobile molecule which exists independent of the network, and a similar molecule bound at a point to the network. Evidence to date suggests this model of unbound materials embedded in a rigid network may be valid for lignites and brown coals (37), but may not be for bituminous coals (38, 45). Regardless, this model has spawned some very important new work which addresses the true nature of

the bonding in coals.

If one assumes the host-guest, or two-phase model to be correct, then one would assume that a solvent or set of solvents could be found which would be able to dissolve large portions of the coal structure under mild solvent extraction conditions. Indeed recent reports suggest that N-methyl pyrrolidone (NMP) alone (39), or in combination with carbon disulfide (40) is capable of extracting up to 70% of some bituminous coals. The phenomenon is rank dependent, and appears to be most effective for low and medium volatile bituminous coals (40). Further understanding of this could help provide a basis for a low temperature procedure for obtaining liquid products from coals.

These observations, along with many others have called into question the nature of the bonding interactions in coals. It is fair to state that in 1979, most researchers believed that coal networks were held together almost entirely by covalent bonds, with minor contributions of ionic bonding in low rank coals (1). Perhaps the most important development in the last ten years and also the greatest opportunity for more research has been the realization that other bonding forms exist and exert major influences. The effect of aromatic-aromatic ( $\pi$ - $\pi$ ) interactions have been proposed and discussed (41, 42), as has charge transfer interactions (43). These interactions appear to contribute more and more to binding of coal structures as coals increase in rank and develop more aromaticity. Proton nmr relaxation experiments have differentiated between mobilities caused by heat and solvent swelling (44, 45) and confirm that non-covalent polar linkages become increasingly important with increasing rank. Computer modeling studies of proposed coal structures are consistent with this idea (46), and a qualitative representation of the types of bonding in coals as a function of rank has been proposed (47).

One important implication of this new understanding of how coals are held together is that it may be possible to convert solid coal into liquids using milder approaches than thermolysis, since these other interacting bonds are of much lower energy than covalent links. Use of milder conditions also has the potential of increasing the selectivity of the conversion of solid coal to lower molecular weight products, by avoiding the retrogressive reactions common to high temperature treatments. This area needs to be investigated further.

## COAL LIQUEFACTION

Ten years ago, a number of coal hydroliquefaction processes were being developed, all based on a thermal conversion step, but differed in how hydrogen was provided: either from organic donors or molecular hydrogen, with or without catalysts (48), and these development programs were accompanied by relatively short-term laboratory research programs. During this same period, there were no process developments for pyrolysis and laboratory research was limited. Many of the hydroliquefaction process developments were completed by the mid 1980's, and provided the basis for substantial technological progress. For example, equipment performance was demonstrated on a large scale, and scale up issues were addressed. It was also demonstrated that coal liquids could be upgraded to transportation fuels using standard petroleum refining operations. Finally, successful methods of dealing with potentially harmful plant emissions were developed.

Major advances have since been made in the technology of coal hydroliquefaction in terms of

significantly increased yields of lighter, cleaner liquids, along with higher conversion selectivities and process efficiencies and costs. These improvements have come about largely by use of process staging and by having catalysts present in each stage. The scope of this progress has been reviewed in a recent U. S. Department of Energy needs assessment study (49). The current estimated cost of liquid transportation fuels produced from coal hydroliquefaction is in the range of US\$ 35 per barrel (50).

It must also be mentioned that fundamental research also progressed during this period. Notable among the recent discoveries are the proposal of new mechanisms for hydrogen donation, involving solvent assisted processes (51), and new bond breaking chemistry, such as the use of water to cleave refractory diaryl ether covalent bonds (52). There is also new interest in pyrolysis as a result of the discovery that the catalyzed hydrolysis of bituminous coals can lead to liquid yields approaching 60% (53).

The study mentioned above lists many research opportunities in priority order, and the interested reader is referred to it for greater detail (49). In the writer's opinion, numerous research opportunities exist to gain understanding of the catalysis mechanisms involved in coal hydroliquefaction (54). For example, it is generally recognized that it may be relatively easy to affect the course of reactions after the primary products are out of the coal particle; by this time, however, the product distribution may already be determined (49). If a catalyst could be found which could influence the product distribution of the primary products as they are formed, entirely different types and quantities of products might be formed. Better understanding of catalysis mechanisms could lead to catalysts which use hydrogen more efficiently, and even to modification of naturally occurring mineral matter to improve its catalytic properties (26).

A more in depth understanding of the chemistry occurring as coal is heated to reaction temperature is a fertile area for new research (49). This would include the building of kinetic models containing intrinsic rate expressions for conversion of individual components, and include bond breaking, cross-linking, hydrogen donation, mass transport, and effects of solvents. This understanding can lead to methods to mitigate the retrogressive, i.e., molecular weight growth, reactions which are believed to take place at and even below presently used coal conversion temperatures. This might lead to pretreatment methods which would allow much lower temperatures to be used for the conversion process, presumably resulting in higher thermal efficiencies and greater selectivities to lighter products than now achievable. Finally, a coal structure-reactivity model needs to be developed, based on the coupling of the knowledge base of coal structure and kinetic models of its reactivity.

## FUTURE OUTLOOK

By its nature, coal is a highly complex organic material, and many different approaches are required to gain the necessary scientific understanding. It is not at all certain that all of those have been mentioned in the above. In this context, the writer cannot help but remark that ten years ago the accomplishments of today's bio-science and technology, and specifically their application in coal science were not even thought of. Also, many environmental issues have not only surfaced, but been placed in the scientific and political forefront in the past ten years. To be applied, new science must have associated with it answers to any environmental concerns connected with it. Thus it is apparent that new research in coal science must be multi-disciplinary, including not only the familiar organic,

inorganic, physical and analytical chemistry, and chemical and mechanical engineering, but also solid state-condensed matter physics, geology, biology, and environmental science. No doubt, ten years from now, there will be others. As with recent advances in other fields involving complex materials, the greatest chance of success will come as a result of interactions among people specializing in these disciplines. The writer believes that the time for coal science to make major advances has arrived, and awaits the contributions of the scientific community.

#### REFERENCES

- 1) Gorbaty, M. L.; Wright, F. J.; Lyon, R. K.; Long, R. B.; Schlosberg, R. H.; Baset, Z.; Liotta, R.; Silbernagel, B. G.; Neskora, D. R. *Science*, **206**, 1029.
- 2) van Krevelen, D. W. "Coal", Elsevier, Amsterdam, 1961.
- 3) Francis, W. "Coal: Its Formation and Composition", Edward Arnold, Ltd., London, 1961.
- 4) Given, P. H. *Fuel*, **1960**, *39*, 147.
- 5) Wisner, W. H. Proceedings of the EPRI Conference on Coal Catalysis, Palo Alto, CA, **1973**, p3.
- 6) Solomon, P. R. in *New Approaches in Coal Chemistry*, Am. Chem. Soc. Sym. Ser. **1981**, *169*, 61.
- 7) Shinn, J. H. *Fuel*, **1984**, *63*, 1187.
- 8) Huttinger, K. J.; Michenfelder, A. W.; *Fuel*, **1987**, *66*, 1164.
- 9) Davidson, R. M. in "Coal Science", Vol 1, Gorbaty, M. L., Larsen, J. W., Wender, I., eds., Academic Press, New York, **1982**, pp.83-160.
- 10) Liotta, R. *J. Am. Chem. Soc.*, **1981**, *103*, 1735.
- 11) Liotta, R. *Fuel*, **1981**, *60*, 453.
- 12) Burchill, P.; Welch, L. S. *Fuel*, **1989**, *68*, 100; Wallace, S.; Bartle, K. D.; Perry, D. L. *Fuel*, **1989**, *68*, 1450; Kelemen, S.R.; Gorbaty, M. L.; Kwiatek, P. Preprints ACS Fuel Chem Div., **1993**.
- 13) Sternberg, H. W.; Raymond, R.; Schweighardt, F. K. *Science*, **1975**, *188*, 49.
- 14) McMillen, D. F.; Malhotra, R.; Chang, S.-J. Proceedings, 1987 International Conference on Coal Science, pp. 197-199 and references cited therein. Atherton, L. F.; Kulik, C. J. EPRI Journal, **1982**, pp. 31-34.
- 15) Calkins, W. H. *Energy Fuels*, **1987**, *1*, 59.
- 16) Kelemen, S. R.; Gorbaty, M. L.; George, G. N. *Fuel*, **1990**, *69*, 939.
- 17) George, G. N.; Gorbaty, M. L.; Kelemen, S. R.; Sansone, M. *Energy Fuels*, **1991**, *5*, 93.
- 18) Taghiei, M. M.; Huggins, F. E.; Shah, N.; Huffman, G. Preprints ACS Fuel Chem Div., **1991**, *36*, 757.
- 19) For more information on the Argonne Premium Coal Sample program see Vorres, K. *Energy Fuels*, **1990**, *4*, 420.
- 20) Kelemen, S. R.; Gorbaty, M. L.; George, G. N. *Fuel*, **1990**, *69*, 1065.
- 21) Kelemen, S. R.; Gorbaty, M. L.; George, G. N.; Kwiatek, P. J.; Sansone, M. *Fuel*, **1991**, *70*, 396.
- 22) Solum, M. S.; Pugmire, R. J.; Grant, D. M. *Energy Fuels*, **1989**, *3*, 187.
- 23) Shabtai, J.; Zhang, Y. Proceedings, 1989 International Conference on Coal Science, pp. 807-810 and references cited therein.
- 24) O'Gorman, J. V.; Walker, P. L. *Fuel*, **1971**, *50*, 135.
- 25) Johnson, J. L., Preprints ACS Fuel Chem Div., **1975**, *20*, 85.
- 26) Montano, P. A.; Bommanavar, A. S. *Fuel*, **1982**, *61*, 523.
- 27) Gorbaty, M. L. Proceedings, 1989 International Conference on Coal Science, pp. 691-694 and references cited therein.

- 28) Joseph, J. T. *Fuel*, 1991, 70, 459; Cronauer, D.; Swanson, A. J. Preprints ACS Fuel Chem. Div. 1991, 36, 67.
- 29) Doughton, M. W.; Gillison, J. R. *Energy Fuels*, 1990, 4, 426.; Skeen, C. J.; Libby, B. J.; Crandell, W. B. *Energy Fuels*, 1990, 4, 431.; Palmer, C. A. *Energy Fuels*, 1990, 4, 436.; Evans, J. R.; Sellers, G. A.; Johnson R. G.; Vivit, D. V.; Kent, J. *Energy Fuels*, 1990, 4, 440.; Wertz, D. L. *Energy Fuels*, 1990, 4, 442.
- 30) Gorbaty, M. L.; Mraw, S. C.; Gethner, J. S.; Brenner, D. *Fuel Process. Technol.*, 1986, 12, 31.
- 31) Gan, H.; Nandi, S. P.; Walker, P. L. *Fuel*, 1972, 51, 272.
- 32) Gorbaty, M. L., *Fuel*, 1978, 57, 796.
- 33) Green, T; Kovac, J.; Brenner, D.; Larsen, J. W.; Coal Structure, Meyers, R., ed., Academic Press, 1982, Chapter 6.
- 34) Suuberg, E. M.; Yun, Y. *Energy Fuels*, 1992, 6, 328; Painter, P. *Energy Fuels*, 1992, 6, 863.
- 35) Brenner, D. *Fuel*, 1985, 64, 167.; Preprints ACS Fuel Chem Div., 1982, 27, 244.
- 36) Given, P. H.; Marzec, A.; Barton, W. A.; Lynch, L. J.; Gerstein B. C. *Fuel*, 1986, 65, 155 seq.
- 37) Redlich, P. J.; Jackson, W. R.; Larkins, F. P. *Fuel*, 1985, 64, 1983.
- 38) Nishioka, M.; Gorbaty, M. L. *Energy Fuels*, 1990, 4, 70.
- 39) Renganathan, K.; Zondlo, J. W.; Stiller, A. H.; Phillips, G.; Mintz, E. A. Proceedings, 1987 International Conference on Coal Science, pp. 367-370.
- 40) Iino, M.; Takanoashi T. *Energy Fuels*, 1990, 4, 452. Iino, M.; Takanoashi, T.; Ohsuga, H; Toda, K. *Fuel*, 1988, 67, 1639.
- 41) Nishioka, M.; Larsen, J. W. *Energy Fuels*, 1990, 4, 100.
- 42) Larsen, J. W.; Wei, Y.-C. *Energy Fuels*, 1988, 2, 344.
- 43) Nishioka, M.; Gebhard, L. A.; Silbernagel, B. G. *Fuel*, 1991, 70, 341.
- 44) Barton, W. A.; Lynch, L. J. Proceedings, 1989 International Conference on Coal Science, pp. 13-16.
- 45) Barton, W. A.; Lynch, L. J. *Energy Fuels*, 1989, 3, 402.
- 46) Carlson, G. A. Preprints ACS Fuel Chem Div., 1991, 36, 398.
- 47) Aida, T. Proceedings 45th Conference of Hokkaido Coal Research Group, 1989, 34, 780.
- 48) Summaries of many of these processes may be found in "Coal Handbook", Meyers, R. A., ed., Marcel Dekker, New York, 1981.
- 49) "Coal Liquefaction: A Research Needs Assessment", Vol II, DOE-ER-400, 1989, (a)pp. 4-76 seq.; (b) pp. 5-6 seq.
- 50) Lumpkin, R. E. *Science*, 1988, 239, 873.
- 51) McMillen, D. F.; Malhotra, R.; Hum, G. P.; Chang, S.-J.; *Energy Fuel*, 1987, 1, 193; McMillen, D. F.; Malhotra, R.; Tse, D. S. *Energy Fuel*, 1991, 5, 179.
- 52) Siskin, M.; Katrizky, A. R.; Balasubramanian, M. *Energy Fuels*, 1991, 5, 770.
- 53) Snape, C. E.; Lafferty, C. J.; Stephens, H. P.; Dosch, R. G.; Klavetter, E. *Fuel*, 1991, 70, 393.; Snape, C. E.; Bolton, C.; Dosch, R. G.; Stephens, H. P. *Energy Fuels*, 1989, 3, 421.
- 54) Derbyshire, F. J. "Catalysis in Coal Liquefaction: New Directions for Research", IEA Coal Research, London, 1988; *Energy Fuel*, 1989, 3, 273.

## Activated carbons from bituminous coals; a comparison of H<sub>3</sub>PO<sub>4</sub> and KOH activants

Marit Jagtoyen, Chris Toles and Frank Derbyshire

University of Kentucky Center for Applied Energy Research  
3572 Iron Works Pike, Lexington, KY 40511-8433

### INTRODUCTION

An earlier study was made of the generation of activated carbons from bituminous coals, using phosphoric acid as a chemical reagent [1-4]. Other work has shown that potassium hydroxide is an effective reagent for the production of high surface area carbons from starting materials such as brown coal [5,6], and other coals, petroleum coke, or mixtures of these [7]. High surface area carbon fibres can also be prepared from charcoal cloth (carbonized viscose rayon cloth) by chemical activation with alkali hydroxides such as KOH at 500°C [8].

For these reasons, the research has been extended to examine the relative effectiveness of H<sub>3</sub>PO<sub>4</sub> and KOH as activants for the synthesis of activated carbons from bituminous coal, and the influence of these reagents on reaction mechanisms, porosity development, and adsorptive properties.

### EXPERIMENTAL

An Illinois Basin bituminous coal (IBC 106) was supplied by the Illinois Basin Coal Sample Program. Before being used for carbon synthesis, the coal was first ground and cleaned to lower the ash content, using a laboratory scale flotation unit [2]. Properties of the parent and cleaned coals are given in Table 1.

The carbon synthesis procedure has been described in detail elsewhere [2,4]. Briefly, a 20 g sample of dry coal is thoroughly mixed with a given volume of reagent solution at room temperature. The mixture is then reacted first at a low heat treatment temperature (HTT), and subsequently at a higher HTT, in both cases in flowing nitrogen. The solid products are leached with distilled water to pH=6 and vacuum dried at 110°C before further analysis. The tar and oil products are collected in cold traps, and gaseous products are collected in a calibrated graduated gas cylinder.

The conditions normally used with H<sub>3</sub>PO<sub>4</sub> were: wt. ratio of acid to dry coal= 0.96, added as 30 cm<sup>3</sup> of 50% acid solution; low HTT 170°C for 0.5 to 3h; upper HTT 350 - 650°C for 1h. The corresponding conditions for KOH were: weight ratio=1.42 of KOH to dry coal, added as 28.4 g KOH to 20 g coal in 100 cm<sup>3</sup> H<sub>2</sub>O; low HTT 75°C for 2h; upper HTT 400 - 900°C for 1h. In some experiments, the reagent to coal ratio was varied. Thermal blank experiments were performed under the same conditions for comparison.

The leached and dried heat treated solids were routinely analyzed for H, C, O, N, S, ash and moisture contents. Fourier transform infrared (FTIR) spectra were obtained from 0.4% loaded KBr discs using a Nicolet 20SX spectrophotometer.

Surface area measurements were obtained from nitrogen adsorption isotherms at 77 K using a Quantachrome Autosorb 6 apparatus. Specific surface areas, S<sub>BET</sub>, were obtained from the adsorption isotherms using the BET equation. Mesopore surface areas were obtained using the α<sub>s</sub> method [9]; standard isotherm data were taken from Rodriguez-Reinoso et al. [10].

## RESULTS AND DISCUSSION

### *Chemical Change*

Both reagents promote chemical change at lower temperatures and more extensively than is achieved by thermal reaction. The H/C atomic ratio of carbons produced by different treatments is shown as a function of HTT in Figure 1. In the presence of either activant, dehydrogenation is considerably enhanced [2,4]. Gas analyses have shown that significant quantities of hydrogen may be evolved during chemical activation: for KOH activation up to 70-90% of the parent coal hydrogen is released as H<sub>2</sub>, around 7% with H<sub>3</sub>PO<sub>4</sub> treatment, and a negligible amount on thermal treatment. In parallel with these observations, Fourier transform infrared spectroscopy of the carbons shows that chemical activation results in the earlier disappearance of aliphatic absorption bands.

The oxygen content of the carbon products was determined by difference, and hence there is a reasonable margin of error in the data. With this caveat, it seems that the oxygen content of H<sub>3</sub>PO<sub>4</sub> carbons falls quickly with HTT, from 12% in the starting coal to about 5% by 350°C, and remains in the range 3-5% between 350 and 650°C. The pattern is different for KOH, where there appears to be an initial reduction in oxygen content, followed by an increase at 400-500°C to values higher than that in the parent coal. Subsequently, the oxygen content is reduced, falling to negligible values at 800 and 900°C. With both reagents, FTIR spectroscopy shows the appearance of carbonyl absorption bands at temperatures from about 75 to 500°C. This band is not evident in the thermal products, and the formation of C=O groups appears to be an intrinsic part of the chemical activation mechanism. Presumably, at high HTT, the carbonyl groups are eliminated by thermal reaction: CO and CO<sub>2</sub> begin to be evolved at HTT over same temperature range where the C=O adsorption bands are reduced in intensity.

Reaction with H<sub>3</sub>PO<sub>4</sub> or KOH effects the removal of both inorganic and organic sulfur. Pyritic sulfur is eliminated with relative ease, while some residual organic sulfur remains to high HTT, Figure 2. The mode of sulfur removal is found to depend upon the reagent used: with phosphoric acid, a large proportion of sulfur is liberated as H<sub>2</sub>S [1,2,4], whereas with KOH it is released as a water-soluble sulfide during leaching of the heat treated solid, Figure 3. Some sulfatic sulfur is also produced upon KOH activation. Research with model compounds has shown that dibenzothiophene, benzothiophene and thiophenol are desulfurized by reaction with bases, such as KOH, at 375 - 400°C. Ring opening is followed by sulfur removal, probably as a soluble potassium sulfide. Oxygen-containing analogs, indole and benzofuran, also experience ring-opening but no subsequent loss of the heteroatom [11]. Analogous behavior can be anticipated for H<sub>3</sub>PO<sub>4</sub>, with the sulfur released as H<sub>2</sub>S instead of K<sub>2</sub>S.

### *Porosity*

The ratio of reagent to precursor is important to the development of carbon pore structure. As shown in Figure 4, a minimum weight ratio is required to maximize the BET surface area: approximately 0.75 to 1.0 for H<sub>3</sub>PO<sub>4</sub> and 1.0 to 1.3 for KOH. At higher ratios, the specific BET surface area decreases. In both series of carbons, there were significant increases in ash content at the highest ratios (9.1% for H<sub>3</sub>PO<sub>4</sub> and 11.2% for KOH). It can be concluded that there is no gain to be made from using excess reagent, since it is consumed by reaction with coal mineral matter to form insoluble products [3], and it lowers the surface area per unit mass. If it is assumed that the ash has negligible porosity, then expressing the surface area on an ash-free basis should compensate for this reduction. As shown in the figure, this appears to be the case.

Operating above the minimum ratios, the development of BET surface area is shown as a function of HTT in Figure 5. The two series of chemically activated carbons develop similar surface areas up to HTT of about 500°C. At higher temperatures, the microporosity of the phosphoric acid carbons decreases slightly from a maximum surface area around 840 m<sup>2</sup>/g, while that of the KOH-activated carbons continues to increase: at HTT 900°C, the BET surface area approaches 1700 m<sup>2</sup>/g. Evidently, the two reagents have quite different temperature dependencies. The thermal products

have negligible accessible surface area, and would have to be subjected to partial gasification in steam or  $\text{CO}_2$  to open up the pore structure.

The ash content of the  $\text{H}_3\text{PO}_4$  carbons increases with temperature from 3.0% at 350°C to 12.0% at 650°C. In contrast to the behavior found with increasing the ratio KOH: coal, the ash content of the KOH carbons decreases with HTT from 6.9% at 400°C to 3.7% at 900°C: a similar observation has been made in related studies [12]. Expressing the data on an ash-free basis, shows that the maximum in the surface area of the  $\text{H}_3\text{PO}_4$  carbons is flattened, Figure 5. However, the correction does not eliminate the possibility of its existence. Other studies with subbituminous coal, coconut shell and wood precursors [13, 14, 15] have also shown the existence of maxima in surface area at similar HTT. The low ash content of the biomass precursors, and the sharpness of the reported maxima render it unlikely that increases in ash content of the carbons can account for the loss of surface area at high HTT. The more likely causes are considered to be due to the acid becoming inactive for the promotion of further porosity development, and the influence of dimensional contraction of the carbon at high HTT [15].

The mesopore capacities of the chemically activated carbons are low and in the range 20 - 75  $\text{m}^2/\text{g}$ . For the KOH carbons, there is no clear trend with increasing HTT, whereas that of the  $\text{H}_3\text{PO}_4$  carbons passes through a shallow maximum at 500-550°C.

It is supposed that, at lower HTT, the chemical reagents promote the formation of crosslinks within the coal structure by ionic mechanisms, leading to the establishment of a rigid, three-dimensional matrix, that is less prone to volatile loss and volume contraction upon heating to higher temperatures. The formation of a crosslinked structure can help to preserve the elements of porosity in the starting material. These suppositions, and the implicit assumption of increased carbon yield have been demonstrated by other work on the phosphoric acid activation of white oak [15]. This more recent work on the activation of white oak has shown that acid treatment actually causes an expansion of the structure that corresponds directly to porosity development. In comparison, extensive shrinkage of the thermal products leads to a collapse of the pore system, making it more difficult to access until carbon is removed by partial gasification.

At high HTT, there is a continuing development of surface area upon KOH activation, and an increase in amount of CO released to the gas phase. On the other hand, with  $\text{H}_3\text{PO}_4$  treatment, there is clearly no further increase in surface area above about 500°C. It is known that, with increasing temperature, orthophosphoric acid undergoes progressive dehydrogenation [16]. Above about 400°C, extensive polymerization and the elimination of water leads to the formation of metaphosphoric acid  $(\text{HPO}_3)_n$ . The formation of polyphosphates is also indicated by measurements by  $^{31}\text{P}$  NMR and FTIR. This species may be inactive with respect to porosity development, and further increase in HTT above 500°C results in volume contraction accompanied by a reduction in surface area. The same phenomenon could be explained by a structural rearrangement and associated contraction, if the crosslinks formed at low HTT have reached their limit of thermal stability.

### *Adsorptive properties*

The synthesized carbons were subjected to standard test methods to assess their utility [17, 18]. The iodine number provides an indication of the adsorption capacity for small molecules and is usually found to be directly proportional to the BET surface area. The determination was made for a suite of KOH activated carbons, and not surprisingly the highly microporous KOH carbons gave high values for the iodine number.

The methylene blue molecule is much larger than iodine, and its adsorption is restricted mainly to the mesopores. It is a useful indicator of the ability of the carbons to adsorb larger molecules, such as colour bodies from solution. A positive relationship was found between mesopore volume and the methylene blue value for a number of phosphoric acid activated carbons. However, the methylene blue values were low, consistent with the low mesopore surface areas; the values for KOH activated carbons were still lower. It may be concluded that these carbons are not ideally suited for the adsorption of large molecules.

Phenol adsorption capacity can be used to assess a carbon's performance for adsorbing polar compounds. Many of the KOH activated carbons proved to be able to adsorb phenol to a similar extent as a commercial water treatment carbon. The capacity of the acid activated carbons was much less, and disproportionately lower than could be explained by the differences in surface area. Phenol, being a polar molecule, will be attracted to polar sites in the carbon, and it is possible that KOH activation produces carbons with more favorable surface chemistry.

## SUMMARY

In the synthesis of activated carbons from bituminous coal using  $H_3PO_4$  and KOH, it is found that both reagents promote chemical change: the removal of hydrogen, oxygen, and organic and inorganic sulfur. Upon KOH activation, up to 70-90% of the parent coal hydrogen can be released as  $H_2$ , and much less upon reaction with  $H_3PO_4$ . Both inorganic and organic sulfur are eliminated; pyritic sulfur removal is relatively facile but some residual organic sulfur remains to high HTT. The mechanism for sulfur removal depends upon the reagent: with phosphoric acid, a large proportion of sulfur is liberated as  $H_2S$  and with KOH much is released as a water-soluble sulfide.

The extent of porosity development is found to be influenced by the ratio of reagent to precursor: a minimum ratio is required to maximize the BET surface area. With increasing HTT, the chemically activated carbons develop similar surface areas up to about 500°C. At higher temperatures, the microporosity of the phosphoric acid carbons decreases slightly, while that of the KOH-activated carbons continues to increase. The mesopore capacities of both series of chemically activated carbons are low and in the range 20 - 75  $m^2/g$ . The thermal products have negligible accessible surface area.

The mechanism of chemical activation is considered to involve the formation of crosslinks at low HTT, leading to the establishment of a rigid, three-dimensional matrix, that is less prone to volatile loss and volume contraction upon heating to higher temperatures. The resulting structure can help to preserve the elements of porosity in the starting material. With KOH, there is continuing development of surface area with HTT. With  $H_3PO_4$  treatment, there is no further increase in surface area above about 500°C. This may be due to the formation of inactive species (polyphosphates), or by structural rearrangement and associated contraction, if the crosslinks formed at low HTT have reached their limit of thermal stability.

As they are dominantly microporous, both series of carbons have high adsorptive capacities for small molecules (iodine number), but low capacities for larger molecules (methylene blue value). The KOH carbons have a higher capacity for phenol adsorption than the  $H_3PO_4$  carbons which cannot be explained on the basis of surface area alone. It is suggested that KOH activation produces carbons with more favorable surface chemistry.

## ACKNOWLEDGEMENTS

The authors wish to acknowledge the assistance of Danny Turner, Hengfei Ni and Bob Rathbone of the CAER. This work has been sponsored by the State of Kentucky and by the Illinois Department of Energy and Natural Resources through its Coal Development Board and Illinois Clean Coal Institute.

## REFERENCES

1. Derbyshire, F.J., Jagtoyen, M., McEnaney, B., Rimmer, S. M., Stencel, J. M., Thwaites, M. W., Proceedings 1991 ICCS Conference, 480-483, Newcastle, England, 16-20 September, 1991, Butterworth-Heinemann Ltd, 1991.
2. Derbyshire, F.J., Jagtoyen, M., McEnaney, B., Sethuraman, A. R., Stencel, J. M., Taulbee, D. and Thwaites, M.W., American Chemical Society, Fuel Division Preprints, 36 (3), 1072-1080, 1991.
3. Jagtoyen, M., McEnaney, B., Stencel, J. M., Thwaites, M.W. and Derbyshire, F. J., American Chemical Society, Fuel Division Preprints, 37 (2): 505-511, 1992.
4. Jagtoyen, M., Thwaites, M.W., Stencel, J. M., McEnaney, B. and Derbyshire, F.J., *Carbon*, 30 (7), 1089-1096, 1992.
5. Durie, R.A., Schafer, G.N.S. *FUEL*, 58, 472-476, 1978.
6. Guy, P.J., Verheyen, T.V., Felber, M.D., Heng, S., Perry, G., Australian Coal Science Conference, Brisbane, 380-386, 1990.
7. Wennerberg, A.N., Grady, T.M., United States Patent 4.082,694, 1978.
8. Audley, G. J., European Patent 0 312 395 A2, The British petroleum company p.l.c, 1989.
9. Gregg, S.J., Sing, K.S.W. in Adsorption, Surface Area and Porosity, 2nd ed., 94-100, Academic, London, 1982.
10. Rodriguez-Reinoso, F., Martin-Martinez, J. M., Prado-Burquette, C.P. and McEnaney, B., *J. Phys. Chem.*, 91, 515-516, 1987.
11. Friedman, S., Utz, B. R., Nowak, M. A., Fauth, D. J., Schmidt, C. E. "Base catalysed desulfurization and heteroatom elimination from coal-model heteroatomic compounds", 1987 International Conference on Coal Science, edited by J. A. Mouljin et al., Elsevier Science Publishers B. V., Amsterdam, 1987.
12. Verheyen, T. V., Derbyshire, F. J. and Jagtoyen, M., paper in preparation for Carbon.
13. Derbyshire, F.J., Jagtoyen, M., McEnaney, B., Rimmer, S.M., Stencel, J.M. and Thwaites, M.W., *Extended Abstracts, 20th Biennial American Conference*, 52-53, Sta. Barbara, Ca., 23-28 June, 1991.
14. Laine, J., Calafat, A. and Labady, M., *Carbon*, 27, 191-195, 1989.
15. Jagtoyen, M., Derbyshire, F. J., submitted for publication, 1993.
16. A. Cotton, G.Wilkinson, P. Gaus, *Basic Inorganic Chemistry*, 2. ed., John Wiley & Sons, New York, 1987.
17. Activated Carbon Evaluation and Selection, Autochem-Cecarbon, Tulsa, Oklahoma, 15-17.
18. CEFIC, Test Methods for Activated Carbons, European Council of Chemical Manufacturers Federations, 21-27, 1986.

Table 1: Composition of coals.

Coal	Av.P.Diam ( $\mu\text{m}$ )	Ash (%)	C	H	N	S	O
			(% daf basis)				
106	80	9.6	83.2	5.5	2.0	3.9	5.4
106clean	5	3.3	84.8	5.5	2.0	2.6	5.1

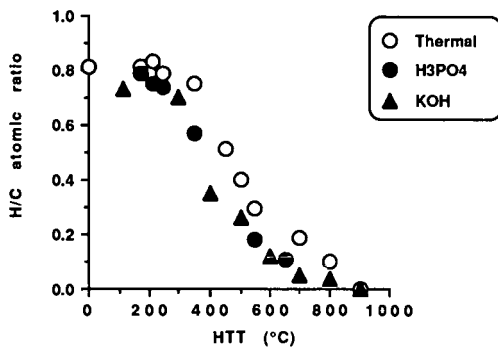


Figure 1: Change in H/C ratio for carbons synthesized from bituminous coals.

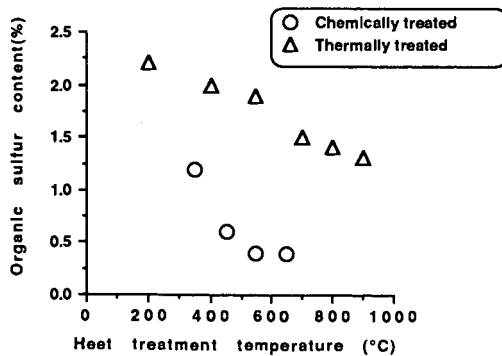


Figure 2: Organic sulfur removal is promoted by chemical treatment.

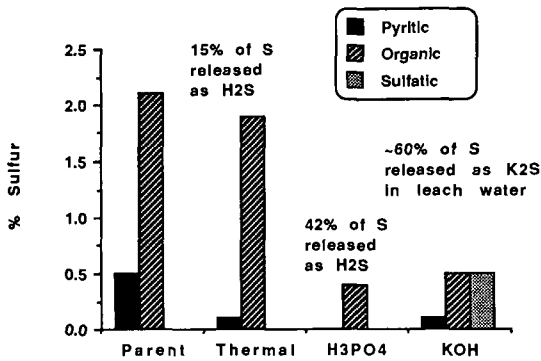


Figure 3: Mode of sulfur removal depends on type of treatment.

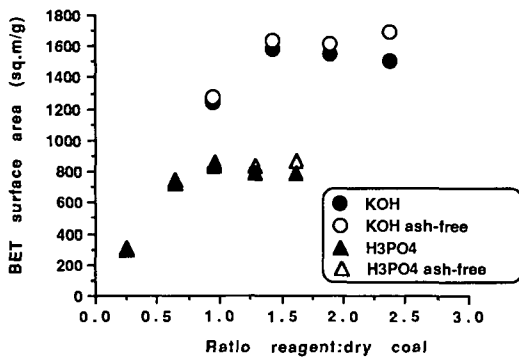


Figure 4: Ratio of reagent to precursor influences surface area (HTT: H3PO4, 500C; KOH, 800C)

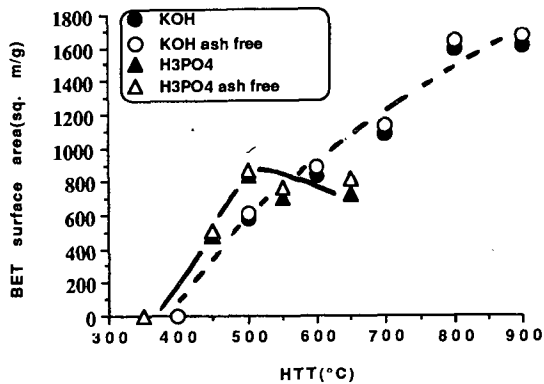


Figure 5: Surface area dependence upon HTT.

## TREATMENT OF ACTIVATED CARBONS FOR DENSIFICATION

Mark L. Stewart and John M. Stencel  
Center for Applied Energy Research  
University of Kentucky, Lexington, KY 40511

**Keywords:** Surfactant, densification, activated carbon

### ABSTRACT

Although activated carbons can have very high surface areas and micropore volumes, their adsorption capacity is generally achieved at the expense of density. Decreased density limits the applicability of carbons for adsorption storage of compressed natural gas and vehicular fuels, even though their potential use has been shown to offer advantages where storage volume is limited.

In this study, activated carbons were treated with surface active agents to increase their bulk and pressed densities. This treatment, along with a hydraulic pressing procedure, are described in which the carbon densities are enhanced without significant adverse effects on their adsorbent properties. It is also shown that surface active agent treatment decreases the work needed to densify the carbons and that specificity in densification is influenced by the ionic character of the agent. As a result, even higher volumes of adsorption storage is expected relative to untreated adsorbents, especially for carbons having very high surface areas ( $\sim 2000 \text{ m}^2/\text{g}$ ) and low densities ( $\sim 0.2 \text{ g/cc}$ ).

### INTRODUCTION

In general, the  $\text{N}_2$  adsorption surface areas of activated carbons are very high, and in the range  $600 - 2800 \text{ m}^2/\text{g}$ . As a consequence, they have inherently low densities ( $\sim$  or  $< 0.4 \text{ g/cc}$ ), and the amount or mass of carbon that can be accommodated in a limited volume is restricted. Ideally, a combination of high surface area, microporosity, and high density would be desirable for particular applications; for example, in the storage or adsorption of hydrogen, methane, or natural gas, it is imperative to maximize density while maintaining surface area and microporosity(1-4).

The purpose of this communication is to address the concept of densifying activated carbons produced from fossil resources with a surface active agent while maintaining reasonable levels of microporosity and adsorption capacity. The process uses low concentrations of inexpensive additives called surface active agents (surfactants) to enhance densification. These commercially available surfactants are anionic, cationic or amphoteric in nature and are interacted with activated carbons before or during densification processes that could be used in the carbons industry. This process was devised to enhance the density of activated carbon at a lower and more economical work input while maintaining inherent surface area and porosity in comparison to that obtained when using standard compaction, extrusion or pelletization without the addition of surface active agents.

## EXPERIMENTAL

Three commercial activated carbons were used in the study; they were supplied by Amoco Research and Development, Norit N. V. Activated Carbon, and Sutcliffe Speakman Carbons Ltd. The BET surface areas and densities for each carbon respectively are as follows: 2600 m<sup>2</sup>/g, 2000 m<sup>2</sup>/g, 850 m<sup>2</sup>/g and 0.18 g/cc, 0.21 g/cc, and 0.38 g/cc.

Two surfactants were used in the experiments and are classified as anionic and cationic in charge. These surfactants were dissolved into distilled de-ionized water with stirring at a temperature at which dissolution was rapid, ~ 50° C. Surfactant concentrations in the range 0 - 1.0% by weight were used, since at levels in excess of approximately 1.0% surfactant solubilities typically reach a critical point of saturation, thereby causing unwanted agglomeration and formation of micelles. The activated carbons were treated and then heated to approximately 50° C with stirring. This temperature is not a factor controlling the effects of the surfactant on carbon density, but rather enable it to uniformly deposit and interact with the carbon without causing excess water boil-off or surfactant decomposition. The solution-carbon mixture was then filtered and dried at temperatures of 100-200° C to remove excess water. As a control to verify the attributes of surfactant addition, each of the samples was also treated with only distilled, de-ionized water (i.e. 0% surfactant) using a procedure identical to that used for preparing surfactant treated samples.

Apparent density measurements of the carbons were obtained in accordance to ASTM procedure D-2854 (5). This procedure is commonly practiced in industry. Carbon samples are fed through a feed funnel into a 100 ml graduated cylinder. The apparent density is then calculated as grams of carbon per unit volume. Any mechanical or vibrational packing effects were minimized in an effort to measure true inherent apparent densities.

Secondly, the pressed density of the carbons were obtained through the use of a pressing/pelleting technique. In determining pressed density, a cylindrical stainless steel die was used with a hydraulic press to supply the pressure on a graduated plunger. A premeasured mass of activated carbon was compressed under a steadily increasing hydraulic force of 0 - 89,000 N. By using the cylindrical volume (V) relationship ( $V=4\pi r^2h$ , where r is the radius of the plunger and h is the height of compacted carbon in the die) the change in volume vs. pressure was obtained. The volume of the pressed carbons was calculated using predetermined hydraulic forces - 11,125, 22,250, 44,500, 66,750, and 89,000 N; and, at these forces, the density was calculated using the mass per volume relationship  $\rho=m/v$ , where m was the premeasured mass of the sample before pressing. In addition to the density measurements, work and force relationships were calculated using standard equations to look at potential ramifications of the procedure.

Surface area measurements were performed on the control and the surfactant treated samples to evaluate effects of the treatment on adsorption capacities. Standard nitrogen adsorption (6) using a static volumetric flow process was used, employing a Coulter Omnisorp 100CX sorption system. All surface areas were calculated using the standard BET equation between relative pressures of 0.05 - 0.25. All samples were pretreated under similar conditions to ensure uniformity in data interpretation.

## RESULTS AND DISCUSSION

Figure 1 displays the percent increase in apparent density relative to the standard data given in Table 1 for the carbons when treated with a 0.4 and 0.8% anionic surfactant. The maximum increase in apparent density is near 11% for the Norit activated carbon when using 0.8% by weight surfactant. The increased density of the 0.8% treated carbons suggests a cumulative effect which entails the ability to sufficiently cover the activated carbon surface with a minimum surface layer of surfactant. It has also been determined that treatments at concentrations of 1.0% or greater can cause decreased density in comparison to a 0.8% treatment. Hence, there is a maximum in density as a function of surfactant concentration rather than an increasing density with increasing surfactant concentration.

Using a cationic surfactant, the apparent density changes relative to the standard are displayed in Figure 2. The maximum increase in apparent density is 9% for the Amoco activated carbon when using a 0.8% surfactant treatment. The effects of cationic surfactant treatment are significantly different than the effect of the anionic surfactant treatment. This specificity is probably related to fundamental physical and chemical differences between the surfactants and their interaction with the carbons. This suggests possible inherent charge differences between the particles have been neutralized in the surfactant densification procedure. In addition, the data displayed in Figures 1 and 2 imply that a variable control of carbon density might be possible with either step-wise anionic/cationic treatments or amphoteric surfactants.

Figure 3 illustrates the work input needed to compact the Amoco activated carbon powder through a range of densities. The work-density plots for the Norit and A207 samples show similar behavior. Commercially it is imperative to increase carbon densities to maximize either the mass incorporated into a limited volume and/or to produce compacted pellets or extrudates which are resistant to decrepitation (1-4). Analysis of the data in Figure 3 show that the work required to achieve a particular density is significantly less for a sample that has been treated with surfactant. In the case of the Amoco activated carbon, the work input needed to compact the carbon to densities between 0.7-1.4 g/cc decreases by approximately 35% after treatment. This work input data implies that there is a potential and significant economic benefit to using surfactants during compaction, extrusion, or pelletization. It is also, however, imperative to retain specific or reactive surface area of the carbons if surfactant treatment is to be used during carbons processing.

Nitrogen BET surface areas of the pressed carbons are displayed in Figure 4. In general, the precision of the surface area measurement is (+/-) 5%. Within this precision limit, anionic and cationic surfactant treatments did not cause significant changes in the surface areas of the carbons. Surface area analysis on the carbon in their powdered, unpressed form showed similar results except for a marked decrease in surface area for the cationic treatments. Hence, the benefit of surfactants for powdered carbons, in which both density and surface area are considered, is dependent on the ionic character of the surfactant.

## CONCLUSIONS

Surfactant treatment has shown to be beneficial in the densification of high surface area activated carbons for potential natural gas storage applications. This simple and inexpensive procedure has been shown to increase the densities of activated carbons without significantly inhibiting their adsorption storage potential. For applications in which storage volume is limited at certain pressures, a combination of high density and porosity can be achieved through a combination of surfactant treatment and hydraulic pressing of activated carbons. It is known that activated carbons can contain either positively or negatively charged surfaces and that the magnitude of the charge can be influenced by chemical treatment of the carbon (7-10). In the examination of anionic and cationic surfactant treatments, it appears that selective neutralization and alteration of surface charge is surfactant dependent. The action of the surfactants in enhancing carbon density and in decreasing the work necessary to produce a densified carbon is therefore tentatively related to the elimination or minimization of surface charge.

## ACKNOWLEDGEMENTS

Appreciation is extended to Amoco Research and Development, Norit N. V. Activated Carbon and Sutcliffe Speakman Carbons Ltd. for supplying the activated carbon samples.

## REFERENCES

1. B. Buczek and L. Czepirski, *Adsorp. Science & Technol.*, **4**, 217(1987).
2. S.S. Barton, J. R. Dacey and D. F. Quinn, *Fundam. Adsorpt., Proc. Eng. Found. Conf.*, (Ed. A. L. Myers, G. Belvort Eng. Found), 65(1983).
3. K. Otto, *Adsorption of Methane on Active Carbons and Zeolites*, (Hemisphere Publ. Corp.), **4**, 241(1982).
4. "Natural Gas Storage", D. F. Quinn and J. A. MacDonald, *Proc., Workshop on Adsorbent Carbon*, 6/20-21/91, Lexington KY.
5. Standard Test Method for Apparent Density of Activated Carbon, ASTM Committee D-28 - D2854-89, p. 329, (3/31/89).
6. S. Brunauer, P. H. Emmett, and E. Teller, *J.A.C.S.* **60**, 309(1938).
7. M. K. Abotsi Godfried and A. W. Scaroni, *Fuel Proc. Tech.* **22**, 107(1989).
8. V. A. Gareten and D. A. Weiss, *J. Chem.*, **10**, 309(1957).
9. B. R. Puri, *Chemistry and Physics of Carbon*, Vol. **6**, (Marcell Dekker, NY), Ed. P. L. Walker, 1970.
10. J. B. Donnet, *Carbon* **6**, 161(1968).

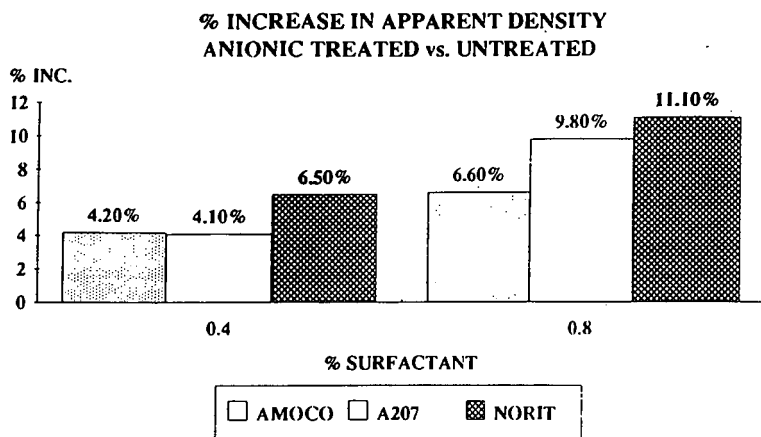


Figure 1.

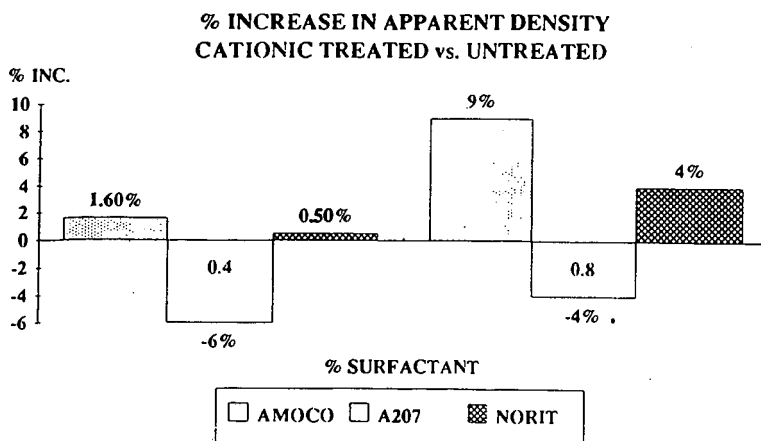


Figure 2.

**AMOCO ACTIVATED CARBON**  
**Work vs. Density**

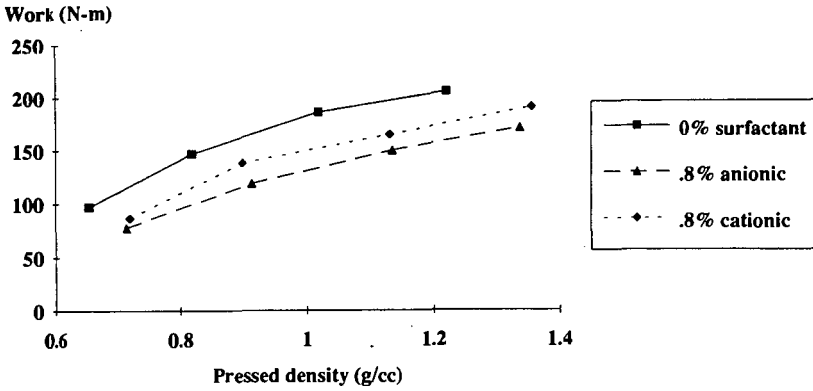


Figure 3.

**SURFACTANT TREATED PRESSED CARBONS**  
**BET SURFACE AREA**

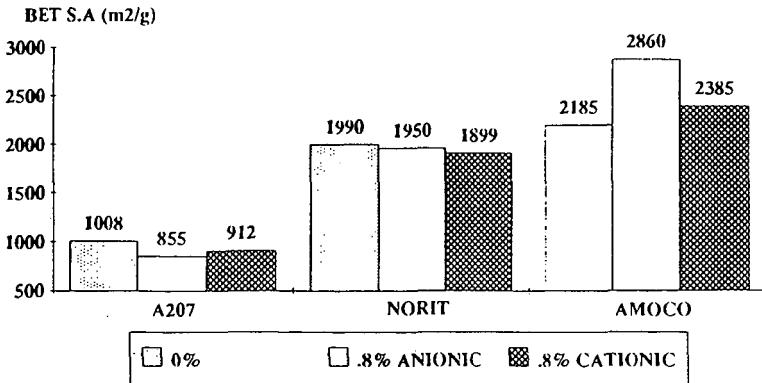


Figure 4.

## Formed Activated Carbons from Bituminous Coals by KOH Activation

Vincent Verheyen, Marit Jagtoyen\* and Frank Derbyshire\*

Coal Corporation of Victoria, PMB No.1 Morwell,  
3840 Australia

University of Kentucky, Center for Applied Energy Research,  
3572 Iron Works Pike, Lexington, KY 40511-8433

**Keywords:** activated carbon, potassium hydroxide, bituminous coal, nitric acid

### INTRODUCTION

Coals of various ranks are important precursors for the synthesis of activated carbons in powder, granular or extrudate forms. The commercial manufacture of carbons from bituminous coals generally involves carbonization followed by steam activation of the char to generate the required pore structure and surface area. Pitch binders can be used to produce hard pelletized products. Large size carbons have higher market value than powders, as they can be used in fixed bed adsorbers, allowing cyclic operation, and regeneration.

Low rank brown coals can be processed into pelletized highly microporous carbons using a different approach to that described above (1, 2). This involves alkaline digestion of the humic acid rich coal with potassium hydroxide to form an extrudable paste which can be carbonized and activated in a single heat treatment step, although a subsequent leaching step is required to recover the reagent. The KOH promotes both binding and chemical activation, and no further activation with steam or CO<sub>2</sub> is required. Even though KOH has been shown to be an effective chemical activant for producing powdered activated carbons from petroleum cokes and bituminous coals (3, 4), these precursors do not contain humic acids or sufficient acidic functional groups to enable their colloidal dissolution in aqueous KOH. Therefore the successful pelletization of bituminous coal/KOH mixtures is not normally possible without added binder.

To attempt to circumvent this difficulty, an approach has been taken in which bituminous coals are subjected to an oxidative pretreatment in order to modify the coal structure, remove mineral matter, enhance digestion in KOH, and induce strong binding properties. This paper describes an investigation of the effects of pre-oxidation with HNO<sub>3</sub> on the production and properties of pelletized activated carbons from bituminous coals using KOH. Nitric acid was chosen because of its known ability to oxidize coals (5, 6), and because it has the advantage over other strong oxidants such as Cr<sub>2</sub>O<sub>7</sub> in being able to generate humic acids in high yield (7,8). The research is germane to the diversification of use of coal resources, many of which face increasing environmental constraints on their direct utilization as fuels.

### EXPERIMENTAL

Western Kentucky No.9 seam (high vol.C) coal was dried, ground to minus 100 mesh, and oxidized by reaction with an aqueous solution of HNO<sub>3</sub> at concentrations from 0.25 to 2N. The reaction was conducted with vigorous stirring at 373K for 8 hours, or until visible signs of reaction had ceased. The oxidation product was filtered and washed with distilled water prior to drying.

Extrudable pastes were prepared by slowly blending the appropriate dry feedstock in a paddle mixer with a concentrated KOH solution. A KOH/fixed carbon ratio of 1:1 was maintained for all feedstocks. Sufficient water was added to prepare a paste of suitable consistency for extrusion. A low-pressure screw extruder, equipped with a multi-hole die, was used to prepare the spaghetti-like product. The extrudate was dried overnight at 353K to form hard brittle strands which were then roller crushed and sealed in moisture proof bags.

Both HNO<sub>3</sub> and HNO<sub>3</sub>/KOH treated feedstocks were carbonized in a N<sub>2</sub> purged tube furnace which was temperature programmed from ambient to 1173K at 15K/min., with a 60 min. dwell at the maximum temperature. After cooling, the product was water washed, boiled with a 5% HCl soln. to remove excess potassium, and dried. Proximate analyses were obtained using a LECO-MAC 400.

Information on the carbon pore structure was derived from nitrogen adsorption isotherms obtained at 77K on a Coulter Omnisorb 100CX apparatus; the micropore volume W<sub>0</sub> was determined using the Dubinin-Raduskevich equation (9). The average width of slit shaped pores was determined using the expression suggested by Stoekli et al. (10), which is valid for pores of diameter 0.45-2.5 nm;

$$L(\text{nm})=30/E_0+5705/E_0^3+0.028E_0-1.49$$

Specific surface areas, S<sub>BET</sub>, were obtained from the adsorption isotherms using the BET equation.

Non-microporous surface areas, S'<sub>BET</sub>, and micropore volumes were obtained using the α<sub>s</sub> method (11); standard isotherm data were taken from Rodriguez-Reinoso et al. (12).

Relative carbon hardness was estimated using the Takeda microstrength hardness test method (13). Fourier transform infrared (FTIR) spectra of the HNO<sub>3</sub> treated coals were obtained from 0.4% loaded KBr discs using a Nicolet 20SX spectrophotometer.

## RESULTS AND DISCUSSION

Nitric acid oxidation of the coal produced an expected decrease in ash content, due to leaching the acid-soluble minerals, Table 1(a). However, treatment with 0.25N and 0.5N HNO<sub>3</sub> did not remove all of the pyrite present in the coal, as the remaining pyrite separated from the lower density oxidation products during water washing. At low HNO<sub>3</sub>/coal ratios the fixed carbon content of the oxidation products increased above that reported for the coal. This may indicate that, under conditions of moderate oxidation, products are generated that participate in thermally induced condensation reactions, resulting in a net increase in fixed carbon content. The test to determine the fixed carbon content provides conditions under which such reactions can take place. With more severe oxidation, there was a reduction in fixed carbon as, presumably, the increased oxygen content of the coal contributed to the loss of carbon as volatile products.

The FTIR spectra presented in Figure 1 reveal a progressive increase in the intensity of acidic hydroxyl (broad 3700-2400 cm<sup>-1</sup>), carbonyl/carboxyl (~1700 cm<sup>-1</sup>) and NO<sub>2</sub> (1547cm<sup>-1</sup>) absorption bands with increasing severity of HNO<sub>3</sub> treatment. Interestingly, the spectra of the 1N and 2N HNO<sub>3</sub> oxidation products are comparable to those of untreated lignites or brown coals, such as Beulah (North Dakota, USA) and Loy Yang (Victoria, Australia), indicating that the acid treatment may have the desired result of effectively lowering the coal rank. The absorption bands associated with clays/silicates are unaffected by the HNO<sub>3</sub> treatment, while the intensities of the bands associated with aliphatic absorbance (~2900cm<sup>-1</sup> and 1450cm<sup>-1</sup>) decrease with increasing oxidation severity. However, the loss of aliphatic structure may be exaggerated by changes in the infrared extinction coefficients.

Thermal treatment of the  $\text{HNO}_3$  oxidized coals produced yields of char, Table 1(b), that were somewhat higher than the fixed carbon contents of the starting materials. Due to the loss of volatile matter on heat treatment, there was a general increase in ash content with oxidation severity.

The presence of KOH during heat treatment produced carbons with consistently lower yields than the corresponding thermal products, and these decreased with increasing oxidation severity, Table 1(c). Despite the lower carbon yields, the ash contents are reduced, rather than being further concentrated by the loss of carbonaceous material. Obviously, reaction with KOH converts some of the coal mineral constituents to soluble products that are removed upon product washing. Similar effects have been found in studies of the KOH activation of powdered bituminous coal (4).

Calculations based on the fixed carbon content, Table 1(b) and (c), show that fixed carbon is lost during KOH activation of the coals subjected to mild oxidation. In contrast, KOH activation of the more severely oxidized feedstocks results in negligible loss of fixed carbon during thermal treatment. Unpublished research has shown that no significant fixed carbon burnoff occurs on the activation of brown coal/KOH pellets (14). These observations suggest that the loss of fixed carbon during chemical activation by KOH exhibits an inverse rank dependence, with the more severely oxidized bituminous coals behaving similarly to low rank coals.

The nitrogen adsorption isotherm data presented in Table 2 reveal that  $\text{HNO}_3$  oxidation decreases the already low surface area and pore volume of the bituminous coal feedstock. Thermal treatment also produces solid products with negligible porosity. These results contrast with the well established ability of  $\text{HNO}_3$  to regenerate spent activated carbons (15).

On the other hand, the activated carbons produced with KOH reveal that even low levels of  $\text{HNO}_3$  oxidative pretreatment have a marked effect on the generation of microporosity, Table 2. At the lowest level of oxidation, the BET surface area increases by over 30% and the micropore volume by about 75%. Increasing the severity of oxidation further enhances the development of surface area and micropore volume, which are increased by over 50% and 100% respectively, after treatment with 2.0N  $\text{HNO}_3$ . The increase in surface area and pore volume of these carbons may help to explain their lower ash yields, since the high porosity will allow greater access during acid washing, leading to the more effective removal of soluble ash constituents.

The relative microstrength hardness of the active carbons is presented in Figure 2 along with some commercial carbons for comparison. The feedstocks and chars produced from the parent coal and after 0.25N  $\text{HNO}_3$  oxidation did not form extrudable mixtures with KOH. At higher oxidation levels, the extent of reaction and dissolution in the KOH solution was found to increase with severity of treatment. The reaction between the 1N and 2N  $\text{HNO}_3$  oxidation products and KOH was strongly exothermic with some  $\text{NH}_3$  evolution. These mixtures behaved like colloidal gels and were readily extruded. A dramatic increase in product carbon hardness was found on going from 0.5N to 1N  $\text{HNO}_3$  oxidation. Oxidation with 2N  $\text{HNO}_3$  improved the carbon hardness above that determined for commercial bituminous coal-derived activated carbons.

## SUMMARY

The pretreatment of bituminous coals by nitric acid oxidation produces a feedstock that, in the presence of KOH, is suitable for extrusion and for the synthesis of hard, high surface area activated carbons. Nitric acid serves several roles in the formation of pelletized carbons from bituminous coal:

- (1) it reduces the ash content,
- (2) it introduces sufficient acidic functionalities, including regenerated humic acids, to the

coal to enable dissolution in KOH solution, conferring binding properties for the formation of hard, shaped carbon precursors: the strength is retained during heat treatment, and

(3) it increases the ability of the KOH to generate microporosity.

#### REFERENCES

1. Guy, P.J.; Perry, G.J. *Fuel* 1992, **71**, 1083.
2. Guy, P.J., Verheyen, T. V., Heng, S., Felber, M. D. and Perry, G. J., *Proc. Int. Conf. Coal.Sci.* 1989, 23.
3. Marsh, H., Crawford, D., O'Grady, T. M. & Wennerberg, A., *Carbon* 1984, **22**,603.
4. Derbyshire, F.; Jagtoyen, M., "Synthesis of Adsorbent Carbons from Illinois Coals", Final Technical report to ICCI, August 31st., 1992.
5. Lowry, H.H. *J.Inst.Fuel* 1937, **10**, 294
6. Lilly, V.G.; Garland, C.E. *Fuel* 1932, **11**, 392.
7. Yohe, F.R.; Harman, C.A. *Trans.Illinois State Ac.Sci.* 1939, **32**, 134.
8. Lowry, H.H.(ed)*Chemistry of coal utilization.*Vol 1.1945, 358.
9. Dubinin, M. M. Zaverina, E. D. and Raduskevich, L. V. *Zh. Fiz. Khimii* , 1947, 1351.
10. Stoekli, H.F, Ballerini, L. De Bernadirmi, S., *Carbon*, 1989, **27**, 501.
11. Gregg, S.J.; Sing, K.S.W. *Adsorption, Surface Area and Porosity.* 2nd ed. 1982, 98.
12. Rodriguez-Reinoso, F., Martin-Martinez, J. M., Prado-Burquette, C.P. and McEnaney, B., *J. Phys. Chem.*, 1987, **91**, 515.
13. Takeda Chemical Industries Ltd (Japan). *Bulletin: Test procedures for activated carbon*, 1973.
14. Coal corporation of Victoria, internal reports.
15. Mueller, G., Ramsteiner, R., Graf, F. and Hupfer, L., *Fed. Rep. Ger. Patent DE 3536263 A1*, April, 1987.

#### ACKNOWLEDGEMENTS

T. V. Verheyen acknowledges the exchange visitors program between the Coal Corporation of Victoria and University of Kentucky, Center for Applied Energy Research that made this research possible.

Table 1: Analysis of HNO<sub>3</sub> treated coals and heat treated products.

(a) oxidized coal

HNO <sub>3</sub> Normality (W/W)	HNO <sub>3</sub> /Coal Ratio	Ash	Volatiles	Fixed Carbon
		dry basis		
0	-	14.48	36.00	49.52
0.25	0.22	7.60	36.05	56.35
0.5	0.44	6.87	37.07	56.06
1.0	0.88	5.66	44.89	49.46
2.0	1.76	5.93	56.06	38.01

(b) Thermally treated coals(1173K)

HNO <sub>3</sub> Normality	Yield (%w/w)	Fixed C Yield (%w/w)	Ash	Volatiles	Fixed Carbon
			dry basis		
0.0	66	110	11.17	2.33	86.50
0.25	69	107	8.73	2.29	88.97
0.5	59	95	8.77	<.1	91.18
1.0	55	98	7.98	2.41	89.61
2.0	52	117	9.94	3.29	86.77

(c) KOH activated coals (1173K; 1:1 KOH:Fixed Carbon)

HNO <sub>3</sub> Normality	Yield (%w/w)	Fixed C Yield (%w/w)	Ash	Volatiles	Fixed Carbon
			dry basis		
0.0	54	83	5.02	7.91	87.07
0.25	53	84	3.73	8.60	87.67
0.5	52	81	5.83	7.18	86.98
1.0	49	95	4.65	5.84	89.51
2.0	45	108	4.01	3.26	92.73

**Table 2: Nitrogen Adsorption Isotherm Data**

(a): BET surface area of feedstocks and thermally treated coals (1173K)

HNO <sub>3</sub> Normality	BET Surface Area (m <sup>2</sup> /g <sup>-1</sup> )	
	Feedstocks	Thermally treated
0	21	2
0.25	6	1
0.5	2	1
1.0	6	4
2.0	1	11

(b): Activated Carbons

HNO <sub>3</sub> Normality	Micropore Volume (cm <sup>3</sup> g <sup>-1</sup> )	BET Surface Area (m <sup>2</sup> g <sup>-1</sup> )	Mean Pore Width Angstrom	Mesopore Surface Area (m <sup>2</sup> g <sup>-1</sup> )
0	0.37	1035	-	36.6
0.25	0.65	1374	7.08	69.6
0.5	0.72	1473	7.63	38.1
1.0	0.71	1517	6.08	34.8
2.0	0.74	1602	7.13	52.2

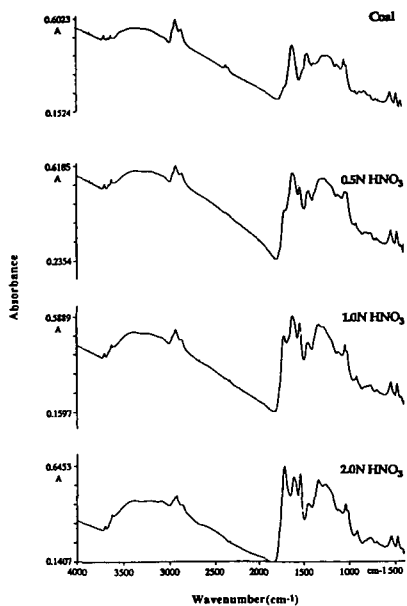


Figure 1: FTIR spectra of Western Kentucky No.9 bituminous coal and its solid HNO<sub>3</sub> oxidation products

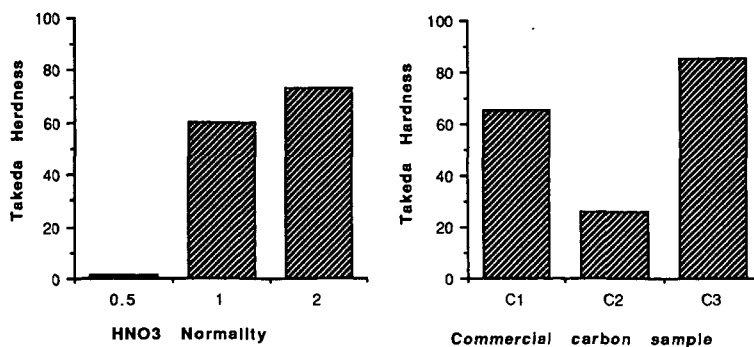


Figure 2: Takeda hardness of activated carbons and commercial samples. (C1 and C2: bituminous coal derived, C3: coconut shell derived)

## SO<sub>2</sub> AND NO<sub>x</sub> REMOVAL AT AMBIENT TEMPERATURES USING ACTIVATED CARBON FIBERS

S. Kisamori, S. Kawano, I. Mochida,  
Institute of Advanced Material Study, Kyushu University  
Kasuga, Fukuoka, 816 Japan.

Key words: SO<sub>2</sub> removal, NO<sub>x</sub> reduction, Activated Carbon Fiber(ACF)

### Abstract

The activity of polyacrylonitrile (PAN) and pitch based activated carbon fibers (ACF) has been studied for the removal of SO<sub>2</sub> and the reduction of NO<sub>x</sub> from air at ambient temperatures. The PAN-ACF was found to be active for oxidizing SO<sub>2</sub> and hydrating the product of H<sub>2</sub>SO<sub>4</sub>. The acid flows down from the ACF bed, maintaining the activity for SO<sub>2</sub> removal, and allowing the acid to be recovered. The influences of temperature, humidity, and contact time on the rate of SO<sub>2</sub> removal will be presented.

The pitch-ACF, when further activated with H<sub>2</sub>SO<sub>4</sub> at 400°C, was found to remove NO<sub>x</sub> at low concentrations (around 10ppm) by reaction with NH<sub>3</sub> at temperatures around 10°C and at 100% humidity. Heating the air to reduce the relative humidity was found to effectively enhance activity. Further, heat treatment of the fibers in inert atmosphere before activation enhanced the activity under high humidity. The cause of catalytic activity in the ACFs will be discussed.

### Introduction

In spite of extensive efforts to keep the atmosphere clean, acid rain problem is still growing globally. Extensive and efficient removal of SO<sub>x</sub> and NO<sub>x</sub> from the atmosphere as well as flue gas is strongly wanted to be developed.

The present authors have been involved in the dry removal of SO<sub>x</sub> and reduction of NO<sub>x</sub> with NH<sub>3</sub> using activated carbon fibers (ACF). SO<sub>x</sub> in the flue gas was oxidatively adsorbed as H<sub>2</sub>SO<sub>4</sub> on ACF at 100–150°C until its saturation, and was reductively recovered in concentrated SO<sub>2</sub>, consuming C of ACF as CO<sub>2</sub> to regenerate the adsorption ability of ACF. Such a deSO<sub>x</sub> has been commercialized with cheaper active coke, and polyacrylonitrile based ACF (PAN-ACF) exhibited very high capacity to reduce the volume of the reactor. However, the adsorption-recovery/regeneration sequence consumption of not cheap C, and large volume of reactor may prohibit current application.

NO<sub>x</sub> in flue gas has been found to be reduced with NH<sub>3</sub> on active coke at 120°C. Hence the deSO<sub>x</sub> and deNO<sub>x</sub> has been performed on the same coke in the three moving bed sequence of deSO<sub>x</sub>, recovery/regeneration and deNO<sub>x</sub>. However, the catalytic activity is not satisfactory especially at ambient temperatures. ACFs were found very active for this reaction.

In the present study, removal of SO<sub>2</sub> to be recovered in H<sub>2</sub>SO<sub>4</sub> and reduction of NO<sub>x</sub> in low concentration (≈10ppm) were both examined at ambient temperatures (0–80°C) using PAN-ACF and pitch based ACF (pitch-ACF), respectively. Very simple cleaning of atmosphere can be performed by very handy ways.

### Experimental

#### SO<sub>2</sub> removal

The SO<sub>2</sub> removal was carried out in the fixed bed flow reactor at 100, 80, 50, and 30°C using PAN-ACF as the catalyst. Its analysis is summarized in Table 1. The reactant gas contained 1000ppm SO<sub>2</sub>, 5% O<sub>2</sub>, 10, 20, and 30% H<sub>2</sub>O and the balance N<sub>2</sub>. The weight of ACF and total flow rate were 0.5 g and 100 ml, respectively. The SO<sub>2</sub> concentration in inlet and outlet gases were analyzed by a flame photometric detector.

#### NO<sub>x</sub> reduction

A pitch based active carbon fiber (OG-5A) was supplied from Osaka Gas in a yarn form. OG-5A was further activated with 12N-H<sub>2</sub>SO<sub>4</sub> (300 wt%) through impregnation, drying, and heat-

treatment up to 400°C for 4 h (abbreviated as OG-5A 3/400/4). The ACF was further activated with H<sub>2</sub>SO<sub>4</sub> under the same conditions. The analysis and surface areas of the as-received and further activated ACF are also summarized in Table 1.

Reduction of NO with NH<sub>3</sub> was performed in a fixed bed U-shaped flow type reactor. The weight and length of fiber bed, flow rate, the concentrations of NO and NH<sub>3</sub> in air, and reaction temperatures were 0.5 g, 70 mm, 50 ml·min<sup>-1</sup>, 10–400 ppm, 10–400 ppm, and 0–30°C, respectively. Air was humidified at the reaction temperature or some temperatures lower by 5 to 25°C than the reaction temperature. Reactant and product gases were analyzed by NOx meter (ECL-77A, YANAGIMOTO Co.,Ltd.).

## Results

### Capture of SO<sub>2</sub> in recoverable H<sub>2</sub>SO<sub>4</sub>

Figure 1 illustrates the capture profile of SO<sub>2</sub> in an atmosphere of 5% O<sub>2</sub>, 10% H<sub>2</sub>O on PAN-ACF at a temperature range of 30–100°C. W/F of this series of runs in the figure was 5x10<sup>-3</sup>g·min·ml<sup>-1</sup> (SV≈3000h). At 100°C, SO<sub>2</sub> was completely removed for 5h on the ACF and then broke through completely after 11h. Under the conditions, the desulfurization process is obligated to consist of capture, and recovery/regeneration steps. A lower temperature of 80°C prolonged the period of complete removal of SO<sub>2</sub> until 9h when SO<sub>2</sub> in the outlet gas started to increase gradually to reach 65% of the inlet concentration at 27h and stayed at this concentration until at least 45h.

Aq. H<sub>2</sub>SO<sub>4</sub> was found to fall down from the vertical reactor to be stored in the reservoir placed below the reactor. A further lower temperature of 50°C further prolonged the period of complete removal to 11h, delayed the increase of SO<sub>2</sub> concentration and reduced the stationary concentration after 45h to 35%. An ambient temperature of 30°C allowed complete removal up to at least 60h. The SO<sub>2</sub> concentration while its complete removal was as low as 10 ppm at highest.

Figure 2 illustrates the influences of humidity on the removal of SO<sub>2</sub> at 100°C and 80°C. Higher humidity favored the deSO<sub>x</sub> by prolonging the period of complete removal and enhanced the stationary removal. Humidity of 20% allowed 20% stationary removal at 100°C. Lower temperatures emphasized the influences. Humidity of 20 and 30% provided 40 and 90 % stationary removal of SO<sub>2</sub> at 80°C respectively. At 50°C, complete removal could continue by humidity of 20% until at least 60h.

Figure 3 illustrates SO<sub>2</sub> removal at various W/F at 30°C. W/F of 5.0x10<sup>-3</sup>g·min·ml<sup>-1</sup> allowed complete removal of SO<sub>2</sub> when humidity was fixed at 10%. A half value of W/F reduced the removal to 90%, indicating catalytic process of SO<sub>2</sub> oxidation and hydration on the ACF.

### Reduction of NO<sub>x</sub> on a pitch ACF and its activated ones

Figure 4 illustrates NO conversion at 22°C over a pitch (OG-5A) and its activated ones with H<sub>2</sub>SO<sub>4</sub>. The as-received ACF (Figure 4-1) provided a NO conversion of 50% at the start of the reaction, however the conversion decreased very rapidly to zero before 5h after the reaction started. Adsorption of NO is suspected. Activation of the ACF with H<sub>2</sub>SO<sub>4</sub> increased the conversion very significantly (OG-5A-S(3/400/4) Figure 4-2) the stationary conversion after the rapid decrease with in 5h was as high as 60%.

Humidity in the feed gas retarded the reaction very significantly, as shown in Figure 4-3. The stationary conversion on OG-5A-S(3/400/4) in 100% humidity decreased 15%, which was, however, nontrivial.

Figure 5 illustrates influences of humidity on NO reduction at 22°C. Pitch ACFs all activated with sulfuric acid lost severally the activity by increasing humidity. It is noted that an ACF of higher surface area appeared to provide lower catalytic activity.

### Heattreatment of ACFs

Influences of heattreatment to control the surface oxygen functional groups on ACF were examined on the NO<sub>x</sub> reduction. As shown in Figure 4, the heattreatment at 800°C (H-800) is very significant to provide an excellent conversion of 40% in dry air and 25% in wet air. Activation with H<sub>2</sub>SO<sub>4</sub> (S(3/400/4)) of the heattreated ACF was also significant to provide conversions of 70% in dry air and 40% in wet air. The heattreatment at this temperature to the H<sub>2</sub>SO<sub>4</sub> activated

ACF was interesting. The conversion in dry air decreased to 50% from 60%, but the conversion in wet air increased to 35% from 12%. Small retardation by humidity on the heat-treated ACF is also shown in Figure 5.

#### Discussion

##### SO<sub>2</sub> removal

The present study succeeded to capture SO<sub>2</sub> and recover it in H<sub>2</sub>SO<sub>4</sub>. The PAN-ACF showed excellent activity to oxidize and hydrate SO<sub>2</sub> and to push H<sub>2</sub>SO<sub>4</sub> flow down through its bed. PAN-ACF is very unique to show such a high oxidation activity very probably through its oxygen and nitrogen surface functional groups. Their cooperation may increase the oxidation activity. Humidity appeared very essential for the present process. Hydration of SO<sub>2</sub> and some dilution of H<sub>2</sub>SO<sub>4</sub> may be keys to allow H<sub>2</sub>SO<sub>4</sub> to flow down. Surface functional groups on ACF should interact with H<sub>2</sub>O vapor. Hence their control may allow the smaller humidity for the recovery of H<sub>2</sub>SO<sub>4</sub>.

##### NO<sub>x</sub>

The ACF surface can activate NO<sub>x</sub> and NH<sub>3</sub> at the same time to reduce the former into N<sub>2</sub>, as discussed in previous papers. The major concept in the present study is related to the retardation of water vapor which certainly inhibits adsorption of NO. At temperature above 100°C, such a retardation is rather negligible but becomes distinct at room temperature probably because of the high coverage by condensation. Hence hydrophobic pitch ACF is effective. Its heat treatment may delicately control the surface functional groups to enhance the catalytic activity. In previous papers, the authors emphasized the importance of NH<sub>3</sub> adsorption in the NO-NH<sub>3</sub> reaction since adsorption of NH<sub>3</sub> is slightly disturbed with water vapor. However, the heat treatment enhances the activity in spite of a significant decrease of NH<sub>3</sub> adsorption. Activation of NO should be emphasized, although active sites for NO is not clarified yet. In conclusion, PAN-ACF and pitch ACF are found very useful to capture SO<sub>2</sub> and reduce NO at ambient temperatures. Their practical application appears feasible.

Table 1 Profiles of ACFs

	Elemental Analysis(%)						Surface area
	C	H	N	O	S	Ash	(m <sup>2</sup> /g)
FE-300	78.1	1.4	4.5	16.0	-	0.3	1141
OG-5A	92.3	1.0	0.8	5.6	tr.	0.3	680
OG-5A(3/400/4)	80.0	1.5	0.7	16.1	0.7	1.0	770

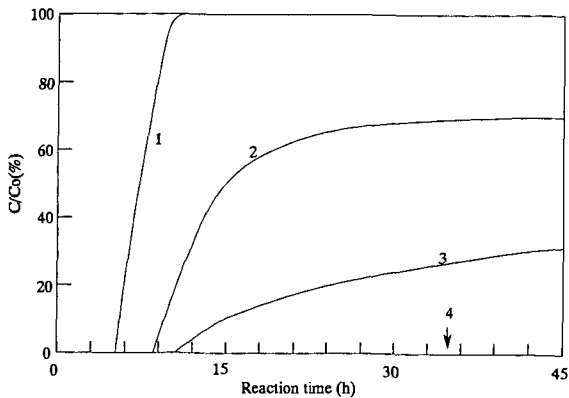


Fig.1 Breakthrough Profiles at Several Temperatures  
 $\text{SO}_2$  1000ppm,  $\text{O}_2$  5%,  $W/F=5.0 \times 10^{-3} \text{ g} \cdot \text{min} \cdot \text{ml}^{-1}$

- 1 : 100°C
- 2 : 80°C
- 3 : 50°C
- 4 : 30°C

No.4 adsorbed  $\text{SO}_2$  completely at least 60 hours

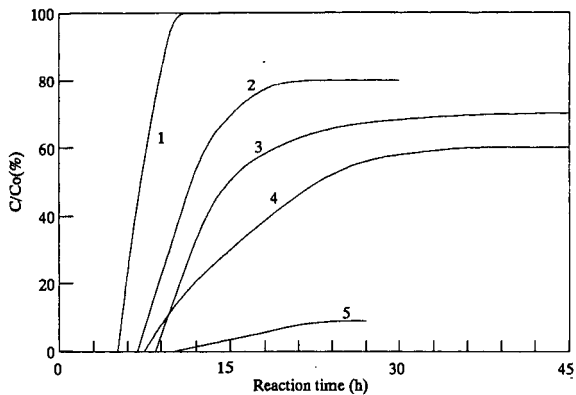


Figure.2 Influence of H<sub>2</sub>O Concentration for SO<sub>2</sub> Removal  
 SO<sub>2</sub> 1000ppm, O<sub>2</sub> 5%, W/F=5.0 × 10<sup>-3</sup> g · min · ml<sup>-1</sup>

- 1 : 100°C, H<sub>2</sub>O 10%
- 2 : 100°C, H<sub>2</sub>O 20%
- 3 : 80°C, H<sub>2</sub>O 10%
- 4 : 80°C, H<sub>2</sub>O 20%
- 5 : 80°C, H<sub>2</sub>O 30%

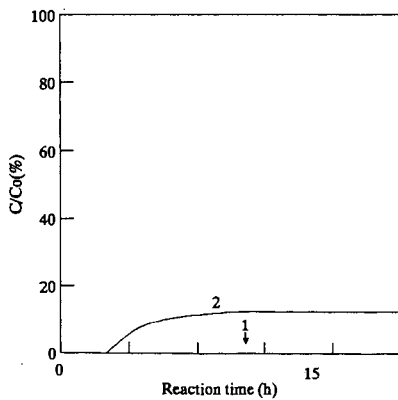


Fig.3 Effect of W/F for SO<sub>2</sub> Removal at 30°C  
 SO<sub>2</sub> 1000ppm, O<sub>2</sub> 5%, H<sub>2</sub>O 10%

- 1 W/F=5.0 × 10<sup>-3</sup> g · min · ml<sup>-1</sup>
- 2 W/F=2.5 × 10<sup>-3</sup> g · min · ml<sup>-1</sup>

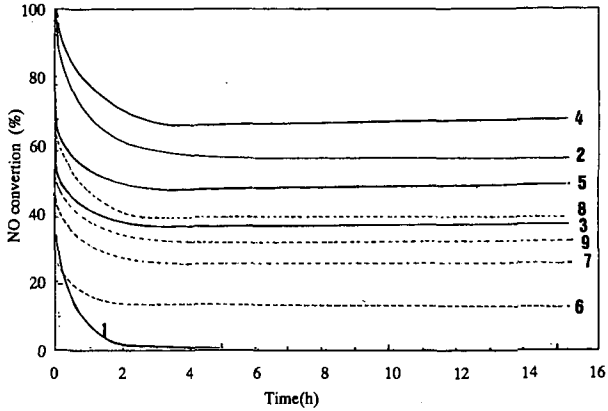


Figure 4 Conversion of NO in dry and wet air at room temperature over ACFs further activated with H<sub>2</sub>SO<sub>4</sub>

NO 10ppm, NH<sub>3</sub> 20ppm, W/F =  $5 \times 10^{-3} \text{g} \cdot \text{min}^{-1} \cdot \text{ml}^{-1}$   
Temp. : 22°C

Dry air (r.h.:0%)	Wet air (r.h.:100%)
1 : OG-5A	6 : OG-5A-(300/400/4)
2 : OG-5A-(300/400/4)	7 : OG-5A-H800
3 : OG-5A-H800	8 : OG-5A-H800-S(300/400/4)
4 : OG-5A-H800-S(300/400/4)	9 : OG-5A-S(300/400/4)-H800
5 : OG-5A-S(300/400/4)-H800	

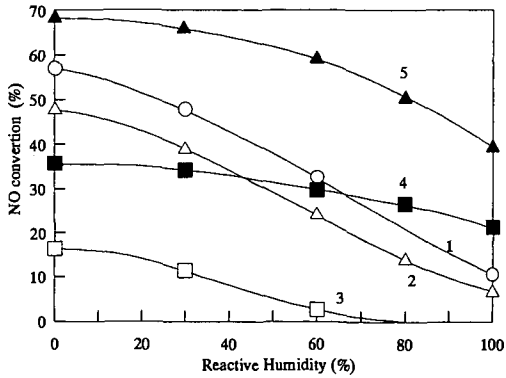


Figure 5 Stationary NO conversion vs. relative humidity(r.h)

Stationary conversion was observed at 15h after the reaction  
NO 10ppm, NH<sub>3</sub> 20ppm, W/F =  $5 \times 10^{-3} \text{g} \cdot \text{min}^{-1} \cdot \text{ml}^{-1}$   
Temp. : 22°C

1 : OG-5A(3/400/4)	4 : OG-5A-H800
2 : OG-10A(3/400/4)	5 : OG-5A-H800-S(3/400/4)
3 : OG-20A(3/400/4)	

## **CARBON FIBERS AND ACTIVATED CARBON FIBERS FROM RESIDUAL SHALE OIL**

**You Qing Fei, Frank Derbyshire and Thomas Robl**

**University of Kentucky, Center for Applied Energy Research,  
3572 Iron Works Pike, Lexington, KY 40511-8433**

**Keywords:** Carbon fibers, Activated carbon fibers, Shale oil

### **Introduction**

Oil shale is one of the largest fossil fuel reserves, and an important potential source of liquid fuels and chemicals. One of the disadvantages of oil shale liquids is their high nitrogen content, which causes difficulties in their upgrading to premium quality products[1]. To accentuate the problem, the nitrogen-containing species tend to be more concentrated in the higher boiling fractions of the retorted product [2]. An alternative solution may lie in investigating the use of the residual liquids as precursors for the synthesis of high added-value advanced carbon materials. The ability to generate valuable by-products could enhance the economics of oil shale retorting.

Carbon fibers (CF) and activated carbon fibers (ACF) are commercially produced from polyacrylonitrile (PAN) and petroleum and coal-tar pitches. The PAN-based fibers have very high strength for which reason they command a higher price than pitch-based ones. Other factors that contribute to the price are the high raw material cost, and low yield [3]. Pitch-based fibers can be formed by directly processing the precursor, to produce moderate strength isotropic carbon fibers, or after heat treatment to induce mesophase formation, when the fibers can have high modulus, and high thermal and electrical conductivity [4].

Activated carbon fibers produced from PAN have several unique properties[5], including the ability to adsorb NO<sub>x</sub>, SO<sub>x</sub> and vitamin B12[6,7], and where there may be novel metal-support interactions[8]. This may be related to their nitrogen content, which can lead to the presence of basic functional groups on the adsorptive surface. For similar reasons, it is considered that carbon fibers and activated carbon fibers produced from oil shale residues might exhibit unusual properties that are not possessed by fibers from petroleum or coal tar pitches. Accordingly, a program of work has been initiated to study the synthesis of carbon fibers from residual oil shale liquids.

In the study presented here, an asphaltene fraction was isolated from a shale oil residuum produced by the Kentort II process[9]. The fraction was processed by melt spinning, oxidative stabilization, carbonization and activation to produce carbon fibers and activated carbon fibers. The products were characterized by SEM, elemental and surface area analyses.

### **Experimental**

A shale oil residue (SOR), produced in the Kentort II process from eastern oil shale[9], was used as the starting material. The asphaltene fraction, SOR-AS, (hexane insoluble, benzene soluble) was separated as follows. The hexane soluble fraction of the shale oil residue was removed by extraction

with boiling hexane[10]. The hexane insoluble fraction was then Soxhlet extracted with benzene, following which the benzene was removed from the extract by rotary evaporation. A petroleum-derived isotropic precursor pitch (PP) was selected for comparison.

Continuous single filament carbon fibers were produced from the shale oil asphaltenes and the petroleum pitch by melt spinning, using a spinneret (capacity about 8g, nozzle diameter 0.3 mm) that is operated under nitrogen pressure. The shale oil and petroleum precursors were spun under 150–300 kPa pressure at about 240 and 300°C, respectively. The resulting fibers were then chopped into 15–20 mm lengths and stabilized by oxidation in air for 90 minutes at 180 and 230°C for the shale oil and petroleum pitch fibers, respectively. The stabilized fibers were carbonized in nitrogen at 850°C for 30 minutes. Carbon fibers were activated by reaction at 850°C for 60 minutes in 50 vol% steam or carbon dioxide, in nitrogen. The sequence of process steps for the preparation of carbon fibers (CF) and activated carbon fibers (ACF) is shown in Figure 1.

The morphology of the carbon fibers and activated carbon fibers was studied at magnifications up to  $\times 10^4$  by SEM (Hitachi S-2700). The BET surface area of activated fibers was measured by nitrogen adsorption at 77K, using a Quantachrome Autosorb 6.

## Results and Discussion

### Carbon Precursors

Analyses of the shale oil residue, its asphaltene fraction, and the petroleum pitch are shown in Table 1. The asphaltenes represent about 20 wt% of the original residue. It can be seen that the slightly higher nitrogen content of the residue (compared to the petroleum pitch) is considerably concentrated in the asphaltene fraction. The sulfur contents of the three materials are similar, but the petroleum pitch has a somewhat lower ash content. The shale oil asphaltene fraction has a softening point of 183°C, which is lower than that of the petroleum pitch, consistent with its higher hydrogen content.

### Carbon Fibers

Carbon fibers were successfully produced from the shale oil asphaltene fraction. SEM micrographs of the carbonized fibers are shown in Figure 2. Small particles (100–500 nm) were observed on the fiber surfaces: their origin is tentatively ascribed to the ash components in the precursor.

The form of the fibers was clearly retained after carbonization, indicating that the conditions chosen for stabilization were sufficient. The stabilization temperature of 180°C used here is much lower than those for conventional isotropic or mesophase pitches[11]. This suggests that the precursor have a very high oxidation reactivity.

While the freshly spun fibers had similar diameters for both precursors, the diameter of the shale oil carbonized fibers was smaller (in the range of 5–12  $\mu\text{m}$ ) than that of petroleum-derived ones (6–15  $\mu\text{m}$ ), as shown in Table 2. The greater degree of contraction of the shale oil fibers reflects their lower carbonization yield (50% versus 71%), or higher volatile matter content.

### ***Activated Carbon Fibers***

The morphology of activated carbon fibers derived from petroleum pitch and shale oil asphaltenes, and produced by activation of the respective carbonized fibers is shown in Figures 3 and 4. Ridges are apparent on the surfaces of the petroleum fibers, and they tend to follow the fiber circumference. Despite this, the surface appears relatively smooth and there are no evident cracks or pores. With the shale oil fibers, an irregular distribution of small pits or pores have developed over the fiber surfaces. In addition, particles can be observed on the surfaces of some of the pore walls. It may be that some of the ash components can have a catalytic influence on the activation or gasification of the fibers, and are instrumental in the generation of these features. The SEM micrographs also suggest that there are some differences in the internal morphology of the two types of fiber.

As shown in Table 3, under similar conditions, the shale oil carbon fibers experienced much greater burn-off during steam activation than the petroleum pitch fibers. This finding also indicates that the former are more reactive to reactions with oxidizing gases, either due to certain inherent aspects of their composition and structure, or to the catalytic effect of ash constituents. Predictably, activation in carbon dioxide, which is known to be a slower reaction, caused lower burn-off than steam under the same conditions. Despite the different degrees of burn-off, the steam activated fibers from pitch and shale oil had very similar BET surface areas. There may be significant differences in their pore size distributions, although this has yet to be determined, as does the dependence of pore structure on burn off.

### ***Nitrogen Content***

The changes in nitrogen content (N/C atomic ratio) during carbonization and activation for both kinds of precursor are shown in Figure 5. For the petroleum pitch, the nitrogen content increased upon carbonization and then kept unchanged through steam activation. As already noted, the N/C atomic ratio was much higher in the shale oil asphaltenes. It was slightly reduced upon carbonization, and then remained at a similar level upon activation: the N/C ratio for activated carbon fibers was about 0.025.

### ***Synopsis***

Preliminary studies have been made of the feasibility of producing carbon fibers from high boiling shale oil liquids. Single filament carbon fibers and activated carbon fibers have been produced successfully from an asphaltene fraction of shale oil residuum, by spinning, oxidative stabilization, carbonization, and activation. Comparisons were made with fibers derived from a petroleum pitch.

The yield of the shale oil carbonized fibers was around 50% while that for the petroleum pitch was about 70%. Differences in yield are attributed to the different volatile contents of the precursors.

Activated carbon fibers were obtained by steam activation of the carbonized fibers at 850°C. A BET surface area of around 960 m<sup>2</sup>/g was obtained at 63% burn off for the shale oil fibers. A similar surface area was obtained for the petroleum pitch based fiber after reaction under the same conditions but with only 38% burn off. The greater reactivity of the shale oil fibers may be due to

their inherent structure and/or to the catalytic effect of ash constituents: some evidence for catalysis is provided by microscopic observations. High reactivity of green fibers is also indicated by the low reaction temperature required for oxidative stabilization. The high nitrogen content of the activated shale oil fibers may provide unusual adsorptive or catalytic properties.

### Acknowledgments

The authors wish to thank Mark Stewart and Darrell Taulbee of the University of Kentucky Center for Applied Energy Research for surface area measurements, and for providing shale oil liquids, respectively.

### References

1. S.A. Homes and L.F. Thompson, Proc. 14th Oil Shale Symposium, Colorado, 1981, p.235.
2. J.W. Bunker, P.A.V. Devineni and D.E. Cogswell, American Chemical Society, Fuel Division Reprint, 37(2), 581(1992).
3. G.P. Daumit, Carbon, 27(5), 759(1989).
4. L.S. Singer, in Concise Encyclopedia of Composite Materials, Edited by Anthony Kelly, The MIT Press, 1989, p.47.
5. I.N.Ermolenko, I.P.Lyubliner and N.V.Gulko, in Chemically Modified Carbon Fibers, (Translated by E.P.Titovets), VCH Publisher, New York, 1990, p.198.
6. H. Fujitsu and I. Mochida, in Kaseitan (Activated Carbon), Edited by Y. Sanada, M. Suzuki and K. Fujimoto, Kotansha Scientific, Tokyo, 1992, p.195.
7. K. Sato, M. Hirai and K. Shimazaki, TEXTILE TEKHNOLGY'84, Industrial Fabrics Association International 72nd Annual Convention, 1984.
8. I. Mochida, Y.N. Sun, H. Fujitsu, S. Kisamori and S. Kawano, Nippon Kagakugakaishi (J.Chemical Society of Japan) No.6, 885 (1991).
9. S.D. Carter, T. Robl, A.M. Rubel and D.N. Taulbee, Fuel, 69(9), 1124 (1990).
10. Y.Q. Fei, K. Sakanishi, Y.N. Sun, R. Yamashita and I. Mochida, Fuel, 69(2), 261 (1990).
11. J.B. Donnet and R.C. Bansal, in Carbon Fiber, Marcel Dekker, New York, 1990, p.55.

Table 1 Analyses of precursor materials

Sample *	Elemental Analysis (wt%)				Atomic Ratio (%)		Content of Ash (wt%)	Softening Point (°C)
	C	H	N	S	H/C	N/C		
PP	92.88	4.63	0.31	1.99	0.60	0.29	0.21	258
SOR	83.22	9.60	0.51	1.82	1.38	0.53	0.82	< 25
SOR-AS	80.98	6.64	2.54	1.96	0.98	2.69	0.97	183

\* PP, petroleum-derived isotropic pitch; SOR, shale oil residue; SOR-AS, asphaltenes: hexane insoluble, benzene soluble.

**Table 2 Carbonization of two kinds of green fibers**

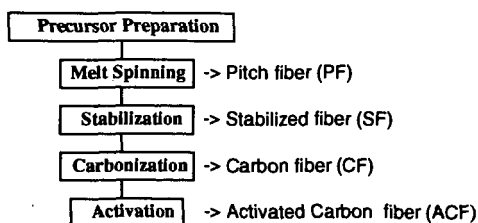
Sample Code	Precursor Type	Yield (wt%)*	Diameter of CF (mm)
CF-P1	PP	71	6 ~ 15
CF-S1	SOR-AS	50	5 ~ 12

\* carbonized at 850°C for 30 min; yield as % of green fibers.

**Table 3 Activation of petroleum and shale oil-derived carbon fibers**

Sample Code	Precursor Type	Activating Agents	Burn-off (wt%)*	Diameter of ACF (mm)	Surface Area (m <sup>2</sup> /g)
AF-P1	PP	H <sub>2</sub> O/N <sub>2</sub> (50:50)	38	4 ~ 12	978
AF-S1	SOR-AS	H <sub>2</sub> O/N <sub>2</sub> (50:50)	63	3 ~ 10	960
AF-S2	SOR-AS	CO <sub>2</sub> /N <sub>2</sub> (50:50)	49	3 ~ 10	566

\* activation at 850°C for 60 min; yield as % of carbonized fibers.

**Figure 1 Flowsheet of the preparation of carbon fibers and activated carbon fibers.**

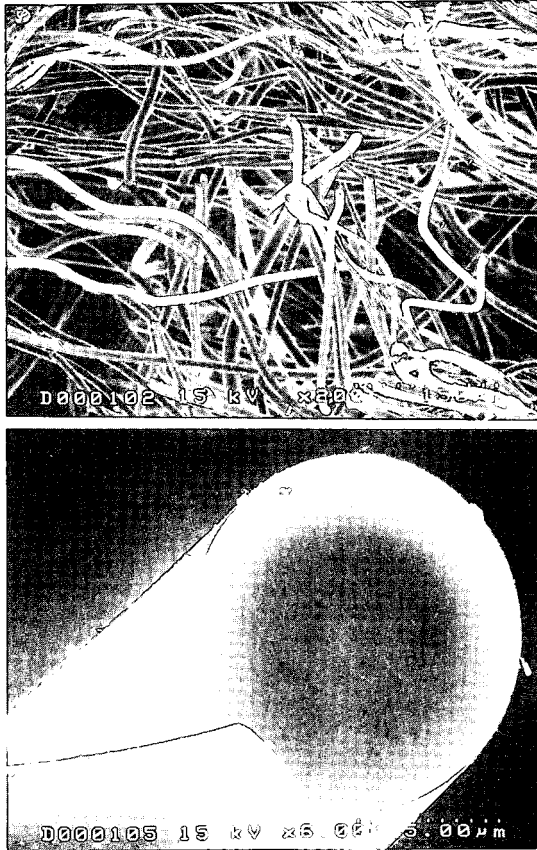


Figure 2 SEM micrographs of carbon fibers produced from shale oil.

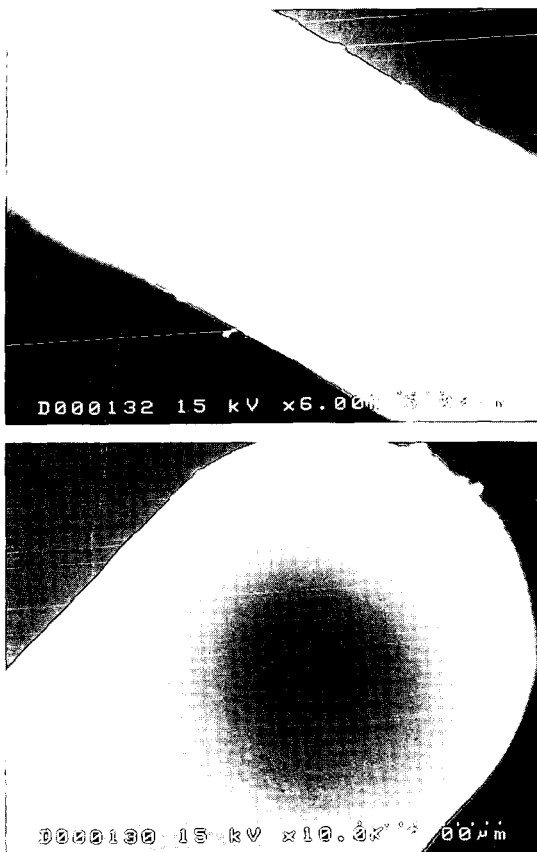


Figure 3 SEM micrographs of activated carbon fibers from petroleum pitch by steam activation.

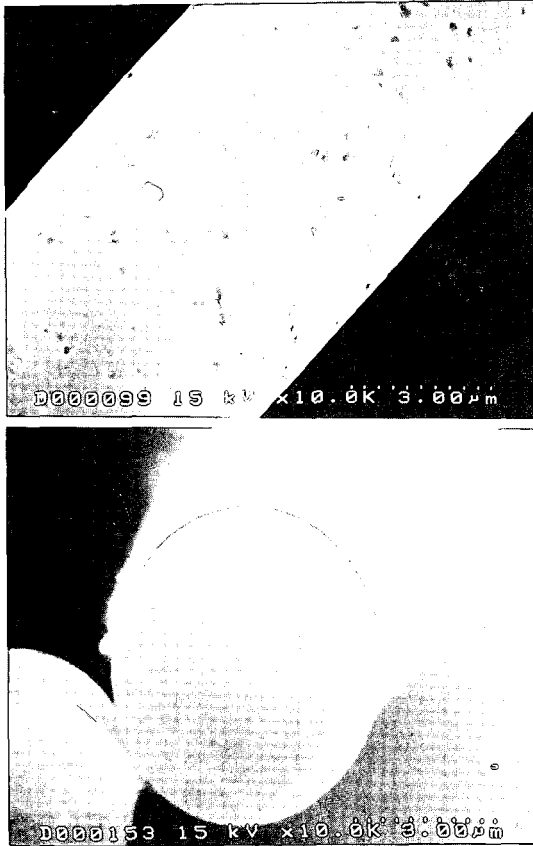


Figure 4 SEM micrographs of activated carbon fibers from shale oil by steam activation.

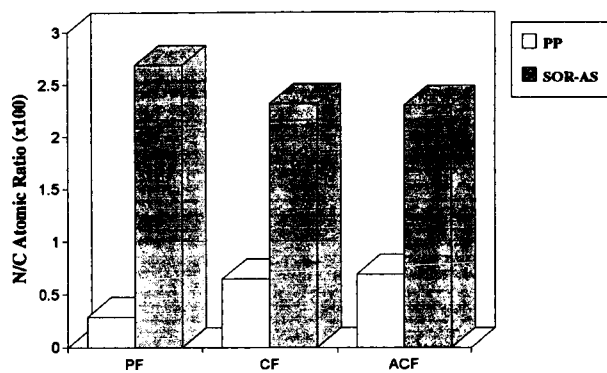


Figure 5 Changes in nitrogen content during the preparation of carbon fibers and activated carbon fibers from shale oil (SOR-AS) and petroleum (PP) precursors.

## HIGH PERFORMANCE, MODERATE COST MESOPHASE PITCH BASED CARBON FIBERS

I. Mochida, Y. Korai, S. H. Yoon, F. Fortin, L. C. Ling, K. Kanno\*

Institute of Advanced Material Study, Kyushu University,  
Kasuga, Fukuoka 816, Japan

\*Mitsubishi Gas Chemical Company, Inc.  
Chiyoda-ku Tokyo 100, Japan

### ABSTRACT

Mesophase pitch has been successfully prepared at very highly yield from aromatic hydrocarbons with low contaminant levels using HF/BF<sub>3</sub> as the catalyst. The derived carbon fiber is expected to be of high performance and to be produced at reasonable cost. The synthesis, structure, and properties of the mesophase pitches, which are strongly dependent upon the starting aromatic hydrocarbons and preparation conditions, will be described. The spinning process can control the shape and texture of the fiber, both of which are intimately related to performance. Fibers with a flat cross section, as thin as 1.5 μm, and round fibers with random texture can be produced when the spinning nozzle and the mesophase pitch are properly selected. Acceptable compression strength has been obtained with the random texture in the round fiber. Very high tensile strength as well as Young's modulus are realized by slow heating during stabilization. Some other applications of mesophase pitch will be addressed.

Key words: Mesophase pitch, Carbon fiber, HF/BF<sub>3</sub>

### INTRODUCTION

Mesophase pitch has been recognized as the most promising precursor for the carbon fiber of excellent properties and reasonable cost. Because of their low price, the residues from coal tar as well as petroleum have been selected as the starting substances. However, high cost of their refining, the lower yield, difficulty in spinning or the control of their molecular structure, and low reactivity lead to unacceptable price and insufficient quality. Carbon fibers produced from latter ones are of high price and their properties are unsatisfactory except for better Young's modulus which is better than that of PAN-based one<sup>1)-3)</sup>, limiting the broad application. Hence, lower price and better performances of the mesophase pitch are most relevant for the pitch based high performance carbon fiber.

Mitsubishi Gas Chemical company and Kyushu University proposed an application of HF/BF<sub>3</sub> as the catalyst for the condensation of aromatic hydrocarbon into mesophase pitch<sup>4)-11)</sup>. In the present paper, preparation conditions, structure, and physical and chemical properties of the mesophase pitch produced using HF/BF<sub>3</sub> were examined.

## EXPERIMENTAL

HF and  $\text{BF}_3$  are low boiling points of 19.9 and  $-101.1^\circ\text{C}$ , respectively. Such a liquid and a gas catalysts can promote the homogeneous reaction of monomer, being recovered and recycled completely by the distillation. HF has high dissolving power for organic compounds and can accelerate ionic reaction through the carbenium ion because of its high polarity. The ionic polymerization at lower temperatures is able to design the structure of mesophase pitch by virtue of the selective reaction under mild preparative conditions. Thus, mesophase pitches from naphthalene, anthracene and methylnaphthalene were prepared directly using HF/ $\text{BF}_3$  at a temperature range of 180 -  $300^\circ\text{C}$ .

These mesophase pitches were spun into fiber using mono hole spinneret of round, Y and slit shape under various conditions. After stabilization in air, fibers are carbonized in argon at 1300 to  $2500^\circ\text{C}$ .

## RESULTS AND DISCUSSION

### 1. Preparation of mesophase pitch

Catalytic polymerization reactions of naphthalene are illustrated in Fig. 1. The protonated complex exists in excess HF as a suitable proton donor. It reacts with other monomer at the position of the highest electron density to produce dimeric structure without dehydrogenation. Such a non-dehydrogenative reaction will be repeated to produce aromatic oligomers such as trimers and tetramers, carrying hydrogens as many as a number of polymerization reaction. These hydrogens are finally stabilized in the produced pitch as naphthenic hydrogens.

Preparation conditions of pitches at a temperature range of 180 to  $300^\circ\text{C}$  are shown in Table 1. Mesophase pitch of 100 vol% anisotropy could be prepared catalytically from naphthalene at  $210 - 300^\circ\text{C}$ . Amount of HF and  $\text{BF}_3$  is important to develop the anisotropy, no anisotropy being observed when ratios of HF/naphthalene and  $\text{BF}_3$ /naphthalene were 0.30 and 0.15 in molar ratio at  $260^\circ\text{C}$ , respectively. However, a higher temperature ( $300^\circ\text{C}$ ) induced 100 vol% anisotropy even with a small amount of HF/ $\text{BF}_3$ . Mesophase pitch of 100 vol% anisotropy could be prepared directly from anthracene at  $220^\circ\text{C}$ . Anthracene is more reactive than naphthalene, providing the pitch of higher softening point with a small amount of the catalyst. The larger planar of anthracene may be favorable for its oligomer to develop anisotropy. Mesophase pitch of 100 vol% anisotropy could be prepared also from methylnaphthalene at  $265^\circ\text{C}$  for 5 h under autogenous pressure in an autoclave. Its softening point of  $205^\circ\text{C}$  should be noted very low, suggesting that methyl group of the monomer influences on properties of the resultant mesophase pitch. A pitch prepared from methylnaphthalene at  $260^\circ\text{C}$  by the same period carried 80 vol% of anisotropy. The methyl group may hinder cationic polymerization.

### 2. Some properties of mesophase pitches

General properties of mesophase pitches prepared from naphthalene, anthracene, methylnaphthalene are summarized in Table 2. Their softening point, solubility, H/C

ratio varied according to preparation temperature and starting materials. Anthracene mesophase pitch tends to exhibit higher softening point and a low solubility. Methyl naphthalene pitch has a softening point of as low as 205°C and 57 % solubility in benzene.

**Table 3** summarizes the hydrogen distribution in the BS and BI-PS fractions of the mesophase pitches. The higher preparation temperature tends to provide a more aromatic mesophase pitch. Aromaticity of anthracene mesophase pitch (AP-220) and naphthalene mesophase pitch (NP-260) are similar. The methyl naphthalene mesophase pitch is most aliphatic, carrying many methyl groups in spite of the severest preparation conditions. The representative molecular species of BS fraction of each mesophase pitches are illustrated in **Fig. 2**.

### **3. Molecular assembly of the mesophase pitches**

Molecular assembly of the mesophase pitches at their fused states is examined using a high temperature horizontal X-ray diffractometer<sup>12</sup>. Changes in Lc values of some pitches calculated from the half width of C(002) are shown in **Fig. 3**. MNP-265 shows the largest Lc value of 5.8 nm at room temperature which stays almost constant up to 210°C of its softening point. Then, Lc decreases sharply at higher temperatures than its softening point. At 350°C, Lc of MNP-265 decreases to less than a half of that at room temperature. These results reveal that the mesogen molecules in the mesophase pitch are certainly stacked as observed with conventional liquid crystals, the thickness or number and d-space of the layers being temperature-dependent and different from one pitch to another. Among the mesophase pitch, MNP-265, exhibits the largest Lc (average thickness).

The values of Lc change according to the temperature especially above the softening point. The thermal motion of molecules above the softening point may compete the intermolecular interaction to liberate the stacking and to enlarge the d-space. Lc in MNP-265 decreases most sharply and those of NP-265-5 and AP-220 do gradually. The molecular motion should influence the stacking thickness and d-space in the similar manners, however, the former should be also influenced by the solubility of the stacking fraction in the isotropic matrix which is more strongly molecular structure - dependent.

### **4. Viscoelastic properties of mesophase pitches**

The mesophase pitch exhibited viscoelastic properties, reflecting its molecular structure and assembly. Typical viscoelastic properties of MNP-265 and NP-265-5 are shown in **Fig. 4**. Very different profiles may be due to the different assembling structure described above. The viscoelastic properties define the alignment in the spinning nozzle, dieswelling at the outlet of nozzle, and alignment at the extension. Hence such properties influence strength, shape, and texture of the resultant carbon fiber.

### **5. Carbon fiber from the mesophase pitch**

A variety of mesophase pitches provide various pitch based carbon fibers, which can achieve high tensile strength, Young's modulus<sup>1,2</sup> and compressive strength. Shapes of molecules and their stacking influence alignment of aromatic planes in

the pitch fiber under the spinning conditions which are fixed by stabilization. The alignment, thickness, and length of the graphite units along the fiber axis are recognized as the common origin of these strengths, the thicker the stacking the higher the modulus or stiffness of the carbon fiber. This occurs at a sacrifice of compressive strength. Hence, the complete controls of molecular shape and its alignment during the preparation of mesophase pitch and spinning are major targets to be achieved for the development of higher performance pitch-based carbon fiber. Table 4 summarizes the mechanical properties of carbonized fibers from naphthalene(NP-260-3) and anthracene(AP-220) mesophase pitches. Tensile strength of their carbonized fiber from NP-260-3 was 2.60 GPa at 1500°C and gradually increased with graphitization, reaching higher than 3.0 GPa by 2550°C. In contrast, tensile strength of carbonized fiber from AP-220 was limited to around 2.0 GPa, even after graphitization at 2550°C, indicating defects at its spinning. Tensile modulus of both fibers are very high, achieving 800 GPa by 2550°C. AP-220 tends to give higher values of Young's modulus than NP-260-3 when the graphitization temperature is lower. It may be due to the constituent molecules of the former mesophase pitch which consist of anthracene units tend to have wider planar structure for developing better graphitization and orientation. Because the spinning properties of AP-220 is inferior to that of NP-260-3, tensile strength of the former fibers may be limited due to micro-defects introduced at spinning. Careful preparation of AP-220 for its better spinning is expected to increase the tensile strength of its resultant carbon fiber.

#### **6. Improvement of mechanical properties of pitch based carbon fiber**

Because the physical properties and mechanical properties of carbon fibers strongly depend on their transversal shape and texture<sup>(3)-15)</sup>, it is believed that controls of transversal shape and texture of carbon fiber during the spinning is most relevant<sup>14)</sup>. The present authors examined some methods to change the flow pattern of molten pitches during spinning in order to control the transversal texture. Fig. 5 shows transversal sections of carbon fibers from methylnaphthalene derived mesophase pitch (MNP-265), using circular or non-circular shaped spinning nozzles at 285°C. It is noted that circular shaped fiber is obtainable at this temperature regardless of the nozzle shapes. Transversal texture of carbon fibers from Y and slit shaped spinning nozzles exhibited random or random-onion textures, respectively. In contrast, circular shaped spinning nozzle gives a radial one with open wedge, even though melt viscosities of molten pitches are much the same at the spinning temperature. This indicates that the flow pattern of molten mesophase pitch is changed and distorted against fiber axis during extrusion before solidification.

Table 5 shows mechanical properties of carbon fibers. Tensile strengths of graphitized carbon fibers spun with Y and slit shaped spinning nozzles are improved by 0.25 and 0.55 GPa, respectively. Young's modulus and compressive strengths of graphitized fibers spun with Y and slit shaped spinning nozzles are also improved by 160 and 0.13 GPa, and 120 and 0.04 GPa, respectively. Importance to control the texture is suggested to improve the mechanical properties of the resultant fiber. Slow heating rate of 0.5°C at the stabilization was found to improve very significantly the tensile strength up to 5 GPa.

Fig. 6 shows the transversal shape and texture of graphitized tape, which is spun through the slit nozzle. The thickness of the tape is as thin as  $1.6\ \mu\text{m}^{15}$ . Its excellent mechanical properties are noted. Tensile strength, Young's modulus and compressive strength of the graphitized tape are as high as 3.65 GPa, 810 GPa, and 0.71 GPa, respectively.

### 7. Further application of the mesophase pitch

The present mesophase pitches with moderate softening points and naphthenic hydrogens can be used as precursor pitches for a variety of carbon materials. The following are some examples: Carbon fiber-mesophase pitch prepreg<sup>17</sup>, high density carbon materials, binder of MgO brick<sup>18</sup>, porous carbonaceous materials, precursor for the solid lubricant, and oxidation prohibitors.

### REFERENCES

- 1) S. Ohtani, A. Watanabe and H. Ogino, Bull. Chem. Soc. Japan **45**, 3715 (1972)
- 2) L. S. Singer, Fuel **60**, 839 (1981)
- 3) E. Fitzer, Carbon **27**, 62(1989)
- 4) I. Mochida, K. Shimizu, Y. Korai, H. Otsuka and S. Fujiyama, Carbon **26**, 843 (1988)
- 5) I. Mochida, K. Shimizu, Y. Korai, Y. Sakai and S. Fujiyama, Chem. Lett. 1893 (1989)
- 6) I. Mochida, K. Shimizu, Y. Korai, H. Otsuka, Y. Sakai and S. Fujiyama, Carbon **28**, 311 (1990)
- 7) I. Mochida, K. Shimizu, Y. Korai, Y. Sakai and S. Fujiyama, Bull. Chem. Soc. Japan **63**, 2945 (1990)
- 8) I. Mochida, K. Shimizu, Y. Korai, Y. Sakai, S. Fujiyama, H. Toshima and T. Hino, Carbon **30**, 55 (1992)
- 9) I. Mochida, K. Shimizu, Y. Korai, Y. Sakai and S. Fujiyama, High Temperature-High Pressure, in press.
- 10) I. Mochida and S. Fujiyama, Japanese Open Patent Shouwa 63-146920 (1988)
- 11) I. Mochida, Y. Sakai and H. Ohtsuka, Japanese Open Patent Heisei 1-139621(1989)
- 12) Y. Korai and I. Mochida, Carbon **30**, 1019 (1992)
- 13) I. Mochida, S. H. Yoon, and Y. Korai, J. Mater. Sci. to be published
- 14) I. Mochida, S. H. Yoon, and Y. Korai, J. Mater. Sci. in press
- 15) I. Mochida, S. H. Yoon, and Y. Korai, Chem. Letter. 1111 (1992)
- 16) H. M. Hawthorne and E. Teghtsoonian, J. Mater. Sci. **22**, 41 (1975)
- 17) I. Mochida, R. Fujiura and Y. Korai, TANSO, No.155, p.398 (1992)
- 18) I. Mochida, Y. Korai, N. Akashi, R. Fujiura and K. Ito, TANSO No.149, p.256 (1991)

Table 1 Preparation conditions of pitches and their some properties.

Sample	HF (mol%)	BF <sub>3</sub> (mol%)	Temp. (°C)	Yield (wt%)	A. C. (vol%)	S. P. (°C)
NP-180	0.67	0.25	180	52	0	202
NP-200	0.81	0.30	200	52	15	199
NP-210	0.83	0.30	210	74	98	216
NP-260-1	0.59	0.15	260	71	95	219
NP-260-2	0.30	0.25	260	37	0	95
NP-260-3	0.47	0.20	260	68	100	212
NP-300	0.64	0.10	300	58	100	285
AP-220	1.00	0.20	220	90	100	238
AP-260	1.00	0.10	260	82	100	275
MNP-260	0.52	0.15	260	>80	80	205
MNP-265	0.52	0.15	265	76	100	205

NP: naphthalene derived pitch., AP: anthracene derived pitch.

MNP: methylnaphthalene derived pitch.

The amount of aromatic hydrocarbon: 1 mol.

Preparation time is 4 hr except for MNP-265(5 hr)

Table 2 Some properties of mesophase pitches.

Sample	S.P. (°C)	A. C. (vol%)	Solubility(wt%)				H/C
			BS	BI-PS	PI-QS	QI	
NP-260-4	215	100	52	19	6	23	0.67
NP-260-5	212	100	57	15	12	16	-
NP-300	285	100	12	29	6	53	0.58
AP-220	238	100	44	12	19	25	0.62
AP-260	275	100	19	32	16	33	0.65
MNP-260	205	80	72	10	10	8	0.68
MNP-265	205	100	57	13	4	26	0.69

Table 3 Hydrogen distribution of BS and BI-PS fractions in the mesophase pitches.

		Hydrogen distribution(%)				
		Haro	H <sub>α</sub>	H <sub>β</sub>	H <sub>γ</sub>	fa
NP-260-4	BS	50	36	13	1	0.82
	BI-PS	66	25	8	1	0.90
NP-300	BS	65	23	10	2	0.89
	BI-PS	71	15	9	5	0.92
AP-220	BS	56	26	15	3	0.85
	BI-PS	57	20	19	4	0.87
MNP-265	BS	44	40	13	3	0.81
	BI-PS	47	35	15	3	-

Haro: aromatic hydrogen(6-10 ppm), H<sub>α</sub>: α-position hydrogen(2.1-5.0 ppm)

H<sub>β</sub>: β-position hydrogen(1.1-2.1 ppm), H<sub>γ</sub>: γ-position hydrogen(0.3-1.1 ppm)

fa: aromaticity

Table 4 Mechanical properties of carbon fiber produced from NP and AP.

	HTT (°C)	$\Delta l$ (%)	T.S. <sup>1)</sup> (GPa)	Y.M. <sup>1)</sup> (GPa)
NP-260-3	1500	1.0	2.60	250
	2000	0.6	2.50	500
	2550	0.4	3.50	800
AP-220	1500	0.6	1.70	270
	2000	0.3	2.00	570
	2550	0.3	2.00	810

1) JIS R7601 monofilament method

HTT: heat-treatment temperature,

T.S.: tensile strength,

$\Delta l$ : strain to break,

Y.M.: Young's modulus

Table 5 Mechanical properties of graphitized fibers.

nozzle	fiber. shape	texture	diameter ( $\mu\text{m}$ )	$\Delta l$ (%)	DO (%)	Lc (nm)	T.S. (GPa)	Y.M. (GPa)	CS (GPa)
	circular	radial-crack	7.0	0.35	95.4	21	2.85	740	0.58
Y	triangle	random	9.0	0.40	94.2	39	3.10	900	0.71
slit	circular	random-onion	9.0	0.45	95.4	23	3.40	860	0.62

DO: degree of orientation

CS: compressive strength tested by composit method( $V_f=60\%$ )  
proposed by H. M. Hawthorne et. al. (ref. 15)

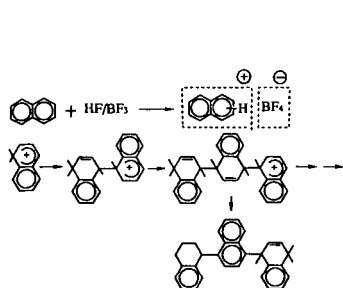


Fig. 1 Catalytic polymerization of naphthalene with  $\text{HF}/\text{BF}_3$ .

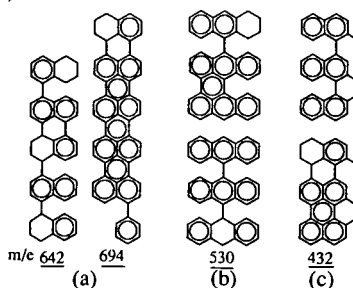


Fig. 2 Model structure of BS in the mesophase pitches.  
(a)NP-260, (b)AP-220, (c)MNP-265

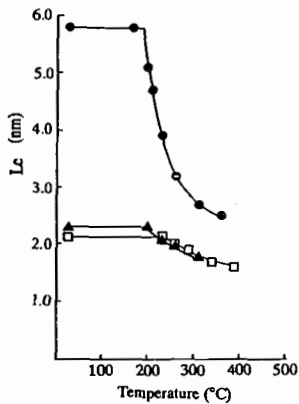


Fig. 3 Change in  $L_c$  at higher temperatures.  
 ○:MNP-265, ▲:NP-265-5,  
 □:AP-220

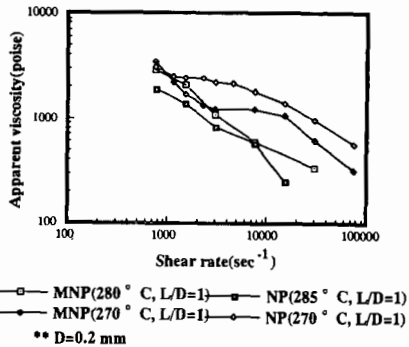


Fig. 4 Typical viscoelastic properties of MNP-265 and NP-265-5

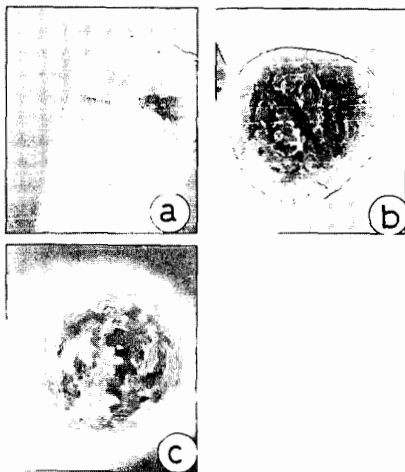


Fig. 5 SEM photographs of carbon fibers spun with circular or non-circular shaped spinning nozzles.  
 (a) circular-shaped nozzle  
 (b) Y-shaped nozzle  
 (c) slit-shaped nozzle

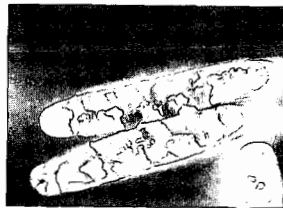


Fig. 6 SEM photograph of carbon tape graphitized at 2500°C

## LASER PYROLYSIS PRODUCTION OF NANOSCALE CARBON BLACK

Xiang-Xin Bi<sup>1</sup>, Wen-tse Lee<sup>1</sup> and Peter C. Eklund<sup>1,2</sup>

<sup>1</sup>Center for Applied Energy Research

<sup>2</sup>Department of Physics and Astronomy

University of Kentucky

Lexington, KY40506, USA

M. Endo<sup>3</sup>, K. Takeuchi<sup>3</sup>, S. Igarashi<sup>3</sup>, and M. Shiraishi<sup>4</sup>

<sup>3</sup>Shinshu University

Department of Electrical Engineering

<sup>4</sup>National Research Institute for Resources and Environment

Nagano-city 380, JAPAN

Key words: laser pyrolysis, carbon black, catalysis, fullerenes

### INTRODUCTION

Laser pyrolysis [1] is a versatile non-equilibrium thermodynamic process for the production of nanoscale particles involving fast growth, and rapid heating/cooling rates (~100,000 °C/s) in the reaction zone defined by the intersection of a reactant gas stream and high power infrared (CO<sub>2</sub>) laser. Using this technique, we have recently produced nearly pure phase nanocrystalline particles of  $\alpha$ -Fe, Fe<sub>3</sub>C, and Fe<sub>7</sub>C<sub>3</sub> [2]. This research, and our interest in fullerenes (e.g., C<sub>60</sub>), motivated us to consider whether or not we could extend the laser pyrolysis technique to produce the other endpoint material, e.g., pure, or nearly pure nanocrystalline carbon, and perhaps fullerenes. CO<sub>2</sub> laser pyrolysis production of carbon soot from acetylene (C<sub>2</sub>H<sub>2</sub>) decomposition was reported by Maleissye et al. [3] and Yampolskii et al. [4]. They found reaction products are close to those obtained in a classic pyrolysis. In this paper, we report the results of a study involving catalytic decomposition of benzene (C<sub>6</sub>H<sub>6</sub>) to produce carbon black. Using small quantities of Fe as a catalyst, we obtained nearly pure carbon soot comprised of amorphous, spherical carbon particles with an average dia.~ 20 nm. These carbon nanoparticles appear to best resemble acetylene black, which identifies a nanoscale carbon soot prepared by the oxidation or thermal decomposition of acetylene [5]. We have furthermore subjected our nanoscale soot to a 2800 °C high temperature treatment (HTT) under Ar gas which promotes the transformation of the disordered spherical soot particles to particles of approximately the same size, but with polygonal facets and, in many cases, a hollow core. Pyrolytic carbon planes are observed aligned parallel to the facets on the heat treated particles, as seen in TEM lattice fringe images. We have no evidence, as yet, that fullerenes were produced along with the nanoscale soot.

To produce nanocrystalline  $\alpha$ -Fe and Fe-carbides, we have investigated recently the laser driven reaction of Fe(CO)<sub>5</sub> and ethylene (C<sub>2</sub>H<sub>4</sub>) following the process described in patents submitted by Exxon researchers [6, 7] who reported the production of Fe<sub>3</sub>C (cementite). To produce carbon black as an extension of this reaction, we first tried the obvious step, namely that of reducing the relative concentration of Fe(CO)<sub>5</sub> in the reactant gas stream. These experiments failed to produce significant amounts of carbon black, yielding instead nanoscale Fe<sub>7</sub>C<sub>3</sub> with a thick coating of pyrolytic carbon. We next tried the addition of benzene (C<sub>6</sub>H<sub>6</sub>) to the reactant gas stream, and large amounts of fairly uniform size nanoscale carbon soot was thereby produced. Subsequent experiments revealed that this reaction requires the presence of only small amounts of

Fe(as a catalyst) to promote the formation of the carbon black. Carbon soot prepared in this way is the subject of this paper.

## SYNTHESIS

Our laser pyrolysis system is shown schematically in Fig. 1, and is similar to that described by Haggerty [1]. The reactants ( $\text{Fe}(\text{CO})_5$ ,  $\text{C}_2\text{H}_4$  (99.99%) and  $\text{C}_6\text{H}_6$  (HPLC grade)) are introduced into the reactant gas stream by bubbling  $\text{C}_2\text{H}_4$  through a solution of  $\text{C}_6\text{H}_6:\text{Fe}(\text{CO})_5 = 50:1$  (by volume) contained in a trap, as shown. The reactant gases then flow vertically out of a stainless steel nozzle inside the 6-way stainless steel cross (chamber) and intersect a horizontal beam from a  $\text{CO}_2$  laser (Laser Photonics Model 150). The  $\text{C}_2\text{H}_4$  flow rate was regulated to be  $\sim 100$  sccm. Using  $\sim 15,000\text{W}/\text{mm}^2$  incident power density in the reaction zone, a bright white flame was observed. The energy coupling of the laser to the reactant gas is realized by tuning the laser frequency to the P20 line ( $945\text{ cm}^{-1}$ ), which is shifted  $5\text{ cm}^{-1}$  relative to the strongest nearby rotational-vibrational absorption line of  $\text{C}_2\text{H}_4$  at  $950\text{ cm}^{-1}$ . A ZnSe lens was used to adjust the position of the  $\text{CO}_2$  laser beam waist relative to the nozzle tip. If no  $\text{Fe}(\text{CO})_5$  is present in the stream, almost no soot is produced. From our previous work [2], if no benzene is present (only  $\text{C}_2\text{H}_4$  and  $\text{Fe}(\text{CO})_5$ ), then Fe-carbides are formed. We therefore speculate that  $\text{Fe}(\text{CO})_5$  in the presence of both  $\text{C}_2\text{H}_4$  and  $\text{C}_6\text{H}_6$  acts as a catalyst, dehydrogenating the benzene and forcing the benzene molecule to fragment in the pyrolysis flame, leading to carbon soot formation. The chemical role of the  $\text{C}_2\text{H}_4$  may not be important, other than to allow heat energy from the laser to be pumped into the reaction.

After leaving the pyrolysis zone, the particles, protected by a lamellar, co-axial flow of Ar gas, are collected in a Pyrex trap (Fig. 1). A teflon membrane filter (pore size 200 nm) was used to protect the mechanical pump. In the steady state, using a reactant gas nozzle with circular 5 mm dia. opening, a 4 - 6 mm diameter, well-collimated stream of particles can be seen to drift up the center of the 1 cm (I.D.) glass tube connecting the 6-way cross and Pyrex particle trap. A 0.5g/hour production rate of carbon black was obtained under the conditions described above. Mass flow controllers were used to control the supply of Ar (99.999%) to the coaxial sheath and to the cell windows; a separate controller was used to control the flow of the reactant gas mixture. Further details of our laser pyrolysis apparatus are available elsewhere [2].

## RESULTS AND DISCUSSION

Subsequent to the synthesis, standard elemental analyses were applied to our carbon black samples for Fe, C, N, and H. The results of this analysis yield a composition  $\text{C}_{10}\text{Fe}_{0.01}\text{H}_{1.2}\text{N}_{0.1}$ . It should be noted that the C:H ratio is  $\sim 8$ , close to the ideal value  $\sim 10$  predicted for acetylene black using a polycondensation model, and this value is lower than that obtained for a typical acetylene black, which has C:H  $\sim 40$  [5]. The C:Fe ratio was also measured using electron microprobe analysis (EDX), resulting in C:Fe  $\sim 700$ , consistent with the value  $\sim 1000$  obtained from the elemental analysis.

Shown in Fig. 2 are the high resolution TEM data taken using a JOEL 4000 electron microscope on "as synthesized" (2a, 2b) and heat treated ( $2800^\circ\text{C}$  in Ar) (2c, 2d) carbon blacks produced by laser pyrolysis. As shown in Fig. 2a, untreated carbon black particles present, on average, a well developed spherical shape, with an average particle diameter on the order

of 20 nm. Typical of acetylene black, significant agglomeration was observed [5]. It is difficult to determine to what extent the particles might be fused, however. Fig. 2b is a magnified image within particle. Although the formation of very primitive carbon planes is observable in some regions of selected particles, most carbon black particles appear to exhibit an image of a highly disordered graphitic carbon (see the discussion of the x-ray results below).

Using the standard N<sub>2</sub> BET technique, we determined a value 50 m<sup>2</sup>/g surface area for the "as-synthesized" carbon black. This value is slightly lower than 70 m<sup>2</sup>/g reported for a typical acetylene black, and is lower than the theoretical surface total surface area for a 20 nm spherical particles (150 m<sup>2</sup>/g). Consistent with this observation of a lower surface area, is that no significant cracking of the particle surface or accessible internal pores are apparent in the TEM photos (Fig. 2b) and that agglomeration (with possible fusion) of the particles is also observed.

Furthermore, the carbon black samples subjected to 2800 °C HTT in Ar show clear evidence for graphitization, consistent with lattice fringes from parallel carbon planes and the associated lattice plane spacing (Fig. 2d). As shown in Fig. 2c and 2d, heat treated particles, in many cases, exhibit parallel carbon layers in polygonal shapes about a hollow center. This suggests that crystallization is initiated at the particle surface. Finally, we did not observe any evidence for the presence of Fe or Fe carbides as small particles within the carbon black particle, or, in particular, at the particle core, or as a separate nanoparticle. This is consistent with the small amount of Fe observed in the carbon black (0.5wt %), suggesting that the Fe may be atomically dispersed throughout the soot.

Shown in Fig. 3 are XRD results obtained with a Rigaku powder diffraction unit using Cu K<sub>α</sub> radiation. Results for "as synthesized" (Fig. 3a) and low temperature HTT (900 °C in N<sub>2</sub>) (Fig. 3b) carbon black samples are presented. The low HTT sample was produced with a higher than normal amount of Fe(CO)<sub>5</sub>. As a result, this sample exhibited x-ray diffraction peaks associated with the existence of nanocrystalline α-Fe and γ-Fe, as indicated. The diffraction peaks for the "as synthesized" sample are similar in width to that of a typical acetylene black [5]. Broad peaks are observed and indexed according to a convention for acetylene blacks based on graphite: in decreasing intensity, they are the 002, 10, and 11 diffraction lines, respectively. The average lattice constant along the c-axis, as determined from the 002 peak position, is found to be 3.65 Å, somewhat larger than normally observed (<3.5 Å) for acetylene black. A significant shift of 002 peak is observed after a 900 °C HTT in N<sub>2</sub> for 24 hrs (Fig. 3b), where again from the 002 peak, the lattice constant has decreased to 3.48 Å, closer to that of a typical acetylene black (3.43 Å).

Further work will be necessary to determine the role of Fe as a catalyst in the production of carbon black by the laser pyrolysis process.

#### ACKNOWLEDGEMENTS

This work was supported, in part, by the University of Kentucky Center for Applied Energy Research and the United States Department of Energy. We wish to thank Gerald Thomas and Mark Stewart for assistance in the characterization of the carbon black, and acknowledge helpful discussions with Frank Derbyshire.

## REFERENCES

1. J. S. Haggerty, "Sinterable Powders from Laser-Driven Reactions", in *Laser-induced Chemical Processes*, Editor, J.I. Steinfeld, 1981, Plenum Press: New York.
2. Xiang-Xin Bi, B. Ganguly, G. Huffman, E. Huggines, M. Endo, and P. C. Eklund, *J. of Material Research*, Submitted, 1992.
3. J. T. d. Maleissye, F. Lempereur, and C. Marsal, *C. R. Acad. Sci., Paris, Ser.*, **275**: p. 1153, 1972.
4. Y. P. Yampolskii, Y. V. Maximov, N. P. Novikov, and K. P. Lavrovskii, *Khim. Vys. Energ.*, **4**: p. 283, 1970.
5. Y. Schwob, "Acetylene Black: Manufacture, Properties, and Applications", in *Chemistry and Physics of Carbon*, Editor, J. Philip L. Walker and P.A. Thrower, 1979, Marcel Dekker, Inc.: New York and Basel. p. 109.
6. R. A. Fiato, G. W. Rice, S. Miso, and S. L. Soled, United States Patent, **4,637,753**1987.
7. G. W. Rice, R. A. Fiato, and S. L. Soled, United States Patent, **4,659,681**1987.

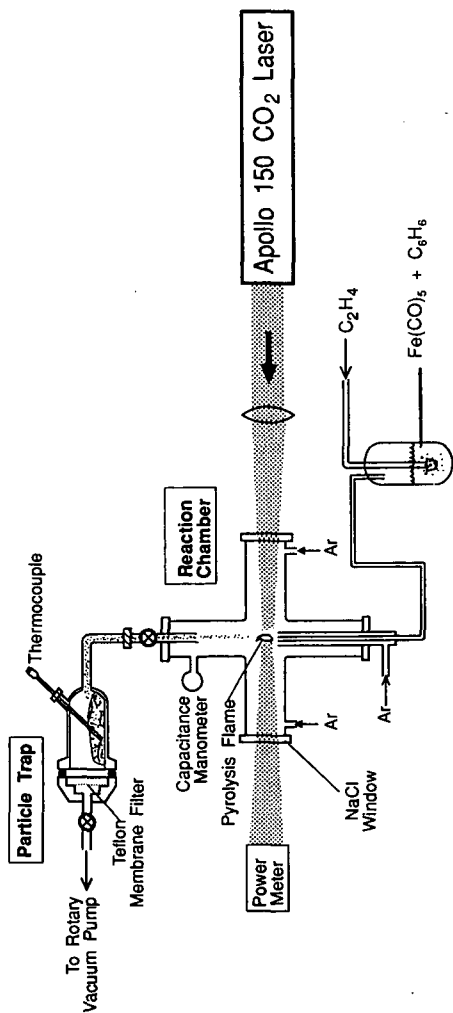


**Fig. 1 Laser pyrolysis system for the production of carbon blacks.**

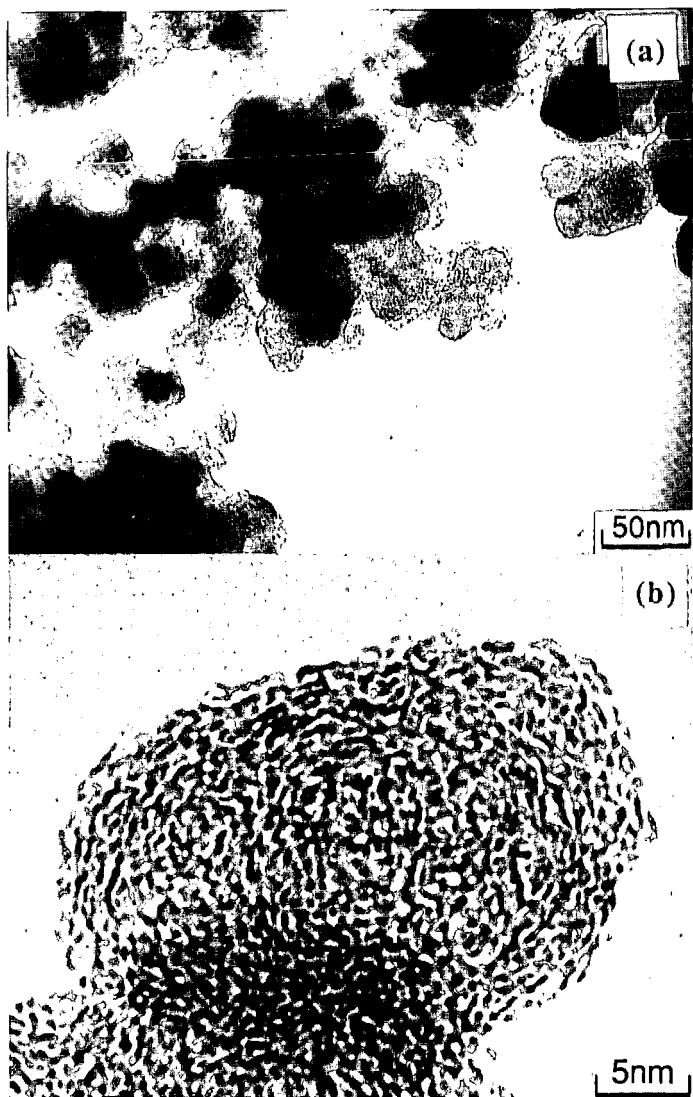


**Fig. 2a,b** TEM data for “as synthesized” carbon blacks produced by laser pyrolysis.

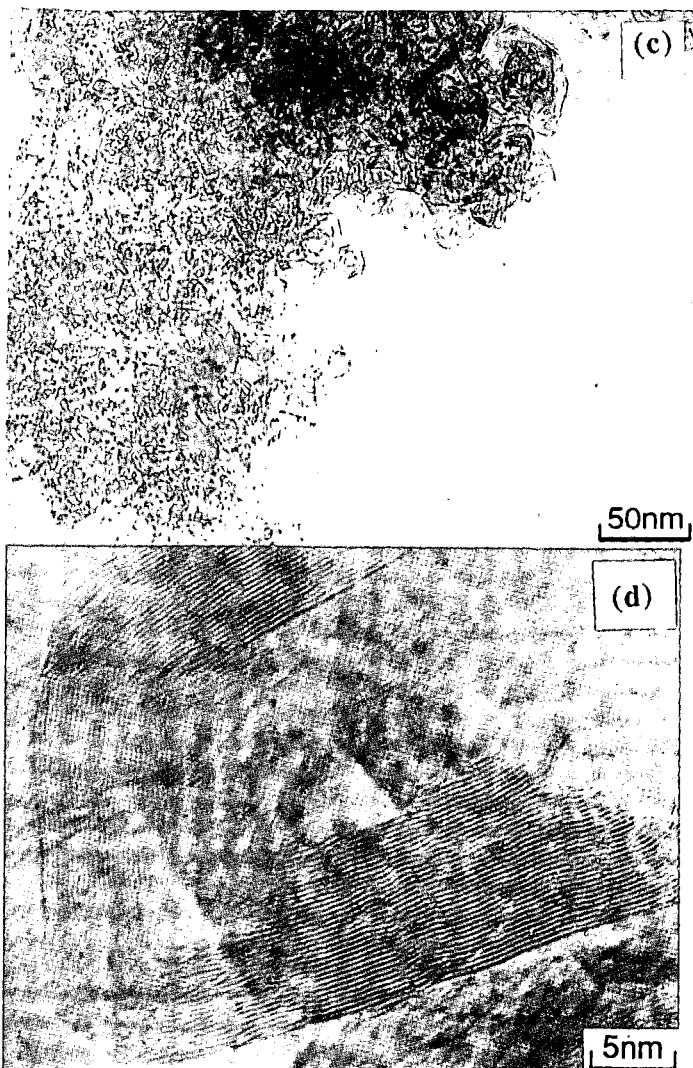


**Fig. 2c,d** TEM data for heat treated (2800 °C in Ar) carbon blacks produced by laser pyrolysis.

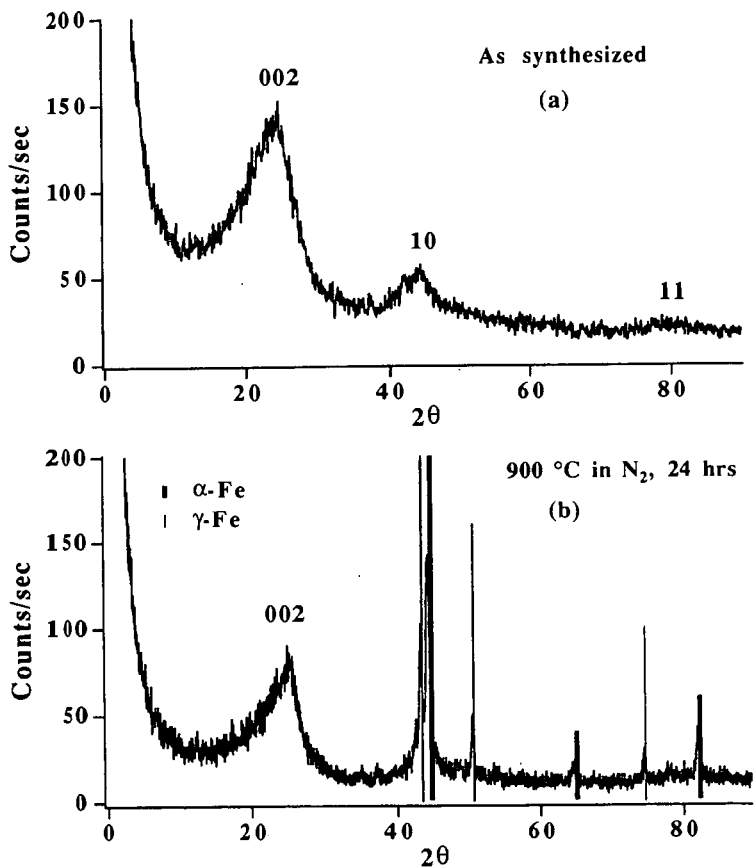


Fig. 3 XRD(Cu  $K\alpha$ ,  $\lambda=1.5418 \text{ \AA}$ ) data for "as synthesized" (3a) and heat treated (900 °C in N<sub>2</sub>) (3b) carbon black samples produced by laser pyrolysis. Vertical lines are obtained from standard powder diffraction data file.

## A GC/MS ANALYSIS AND CARBONIZATION OF DECANT OILS

S. Eser and Y. Liu

Fuel Science Program, The Pennsylvania State University  
209 Academic Projects Building, University Park, PA 16802

### ABSTRACT

Six fluid catalytic cracker decant oils (FCC-DO) samples were characterized by gas chromatography/mass spectroscopy (GC/MS) and carbonized to study the relationships between the chemical constitution and the optical texture of derived needle cokes. Ion chromatograms for each sample were studied, and more than 50 molecular and fragment ions were selected for a semi-quantitative analysis. Although the GC/MS technique and the selected ion integration method used have certain limitations, some correlation was observed between the chemical constitution of the decant oils and the quality of the resulting needle cokes.

### INTRODUCTION

Fluid catalytic cracker decant oil is used as feedstock to produce premium needle cokes. However, FCC decant oils may have significantly different chemical composition and carbonization behavior(1). Gas chromatography(GC) and size exclusion chromatography(SEC) were used to characterize carbonization feedstocks(2, 3). Recently, two-dimensional high performance liquid chromatography(HPLC) and heated probe MS analysis were developed and applied to FCC decant oil characterization(4). The reported results indicate that compounds up to seven or eight ring aromatics are found in decant oils, but in general, three and four ring aromatics and long chain normal alkanes were found to be the dominant components in decant oils(4). These results suggest that the distribution of major components in decant oil can be studied by GC/MS methods. In this study, six samples from four decant oil sources were analyzed by GC/MS using the selected ion integration method. The Carbonizations of decant oils were also carried out to study the relationships between chemical constitution of decant oils and resulting semi-cokes.

### EXPERIMENTAL

GC/MS analysis was carried out on FCC decant oil samples designated FDO #1 to FDO #6. FDO #1 and FDO #2 were received from the same source but at different time, as were samples FDO #5 and #6. An HP 5890 Gas

Chromatography interfaced to an HP 5971A Mass Selective Detector was employed. The samples were dissolved in chloroform and injected, using the splitless mode, into a J&W DB-17 GC column. The GC column temperature was controlled from 40 °C to 280 °C at heating rate of 4 °C/min.

Decant oils were carbonized in tubing reactors at 500 °C for 3 hours under a nitrogen atmosphere. Semi-cokes obtained after carbonization were embedded in epoxy resin and polished using conventional techniques. A polarized-light microscope (nikon-microphot-FXA II) was used to examine the optical textures of resultant semi-cokes.

## RESULTS AND DISCUSSION

A GC/MS total ion chromatogram (TIC) for samples FDO #1 to FDO #6 are shown in Figure 1. Most abundant ion peaks in FDO #1 and #2 are normal alkanes. Aromatic compounds become gradually important in going from FDO #1 to FDO #6. The dominant compounds in samples FDO #5 and #6 are pyrene and its methyl substituted analogs. For all the samples, constituent compounds consist of two to four ring aromatics with different degrees of ring substitution. The GC/MS TIC shows a hump of unresolved peaks around 45 to 65 minutes of retention time for each sample. A method of using selected ion chromatograms was employed to resolve the overlapping peaks.

Selected Ion Chromatograms(SIC) of mass 57, a stable aliphatic fragment, for samples FDO #1 to FDO # 6 are shown in Figure 2. All the samples show a long chain alkane distribution from C16 to C32 except sample FDO #4, which shows a significant shift towards the lower molecular weight alkanes (C12-C26). Sample FDO #3 shows a bimodal distribution of normal alkanes.

All the major aromatic peaks have been identified by mass spectroscopy. They are categorized into four series of compounds: naphthalenes, three ring aromatics (phenanthrene and anthracene), peri- and cata- four condensed ring aromatic compounds. Chromatograms of selected ions for these compounds, including alkyl substituted analogs and alkanes for FDO #3, are plotted in Figure 3. The labels "A, B, C, D" following ion mass numbers represent different isomers of the same compound. Table 1 gives the compound identification of the mass numbers used in Figure 3. Integrated intensities for ions of mass 55, 57, 69, 71, 83, 85, 97, 99 and 113 were obtained from one peak, the maximum alkane peak in each MS chromatogram.

The areas for isomers from each ion were added and the sum was divided by the area of the pyrene peak for normalization. The distribution of these summed ratios is presented in Figure 4. Columns marked alkane

present the sum of peak area ratios for 55, 57, 69, 71, 83, 85, 97, 99 and 113. Samples FDO #1 and FDO #2 show similar component distributions. The alkane contents in these two samples are higher than the other samples. Furthermore, the three ring aromatics are the most abundant components in samples FDO #1 and #2. Samples FDO #1 and #2 produced inferior optical textures upon carbonization. In contrast, samples FDO #5 and #6 produced premium needle cokes. These two samples contain less alkanes than the other samples. The dominant components in FDO #5 and #6 are pyrene and alkyl pyrenes. Sample FDO #3 contains more alkanes than FDO #4, but the former sample produced significantly better semi-coke than the latter. This implies that alkane composition may not be the only factor to affect needle coke quality. Both aliphatic and aromatic component distributions for sample FDO #4 are shifted toward lower molecular weight compound direction. This reveals why FDO #4 produced poor semi-coke.

#### REFERENCE

1. Mochida, I. ; Korai, Y.; Nesumi, Y. and Todo, Y. *Carbon* **1989**, 3, 357
2. Lewis, L. C. *Carbon* **1982**, 20(6), 519
3. Greinke, R. A. and Singer, L. S. *Carbon* **1988**, 26(5), 665
4. Liu, Y.; Eser, S. and Hatcher, P. G. *Am. Chem. Soc., Div. Fuel Chem., Preprints* **1992**,37(3), 1227

Table 1. List of selected ions

Mass	compound's name
128	Naphthalene
142	Naphthalene -methyl
156	Naphthalene -ethyl or dimethyl
170	Naphthalene -C3
178	Phenanthrene
192	Phenanthrene methyl
206	Phenanthrene ethyl or dimethyl
220	Phenanthrene - C3
202	Pyrene
216	Pyrene -methyl
230	Pyrene -ethyl or dimethyl
244	Pyrene -C3
228	chrysene
242	chrysene -methyl
256	chrysene -ethyl or dimethyl
270	chrysene -C3
55	n-C4 alkene
57	n-C4 alkane
69	n-C5 alkene
71	n-C5 alkane
83	n-C6 alkene
85	n-C6 alkane
97	n-C7 alkene
99	n-C7 alkane
113	n-C8 alkane

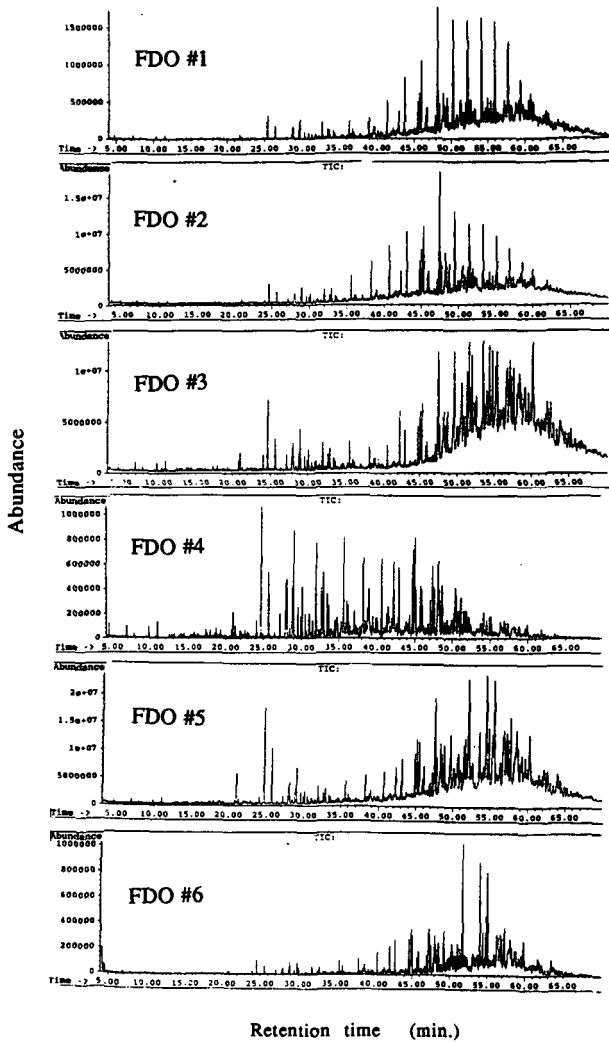


Figure 1. Total ion chromatograms for samples FDO #1 - #6

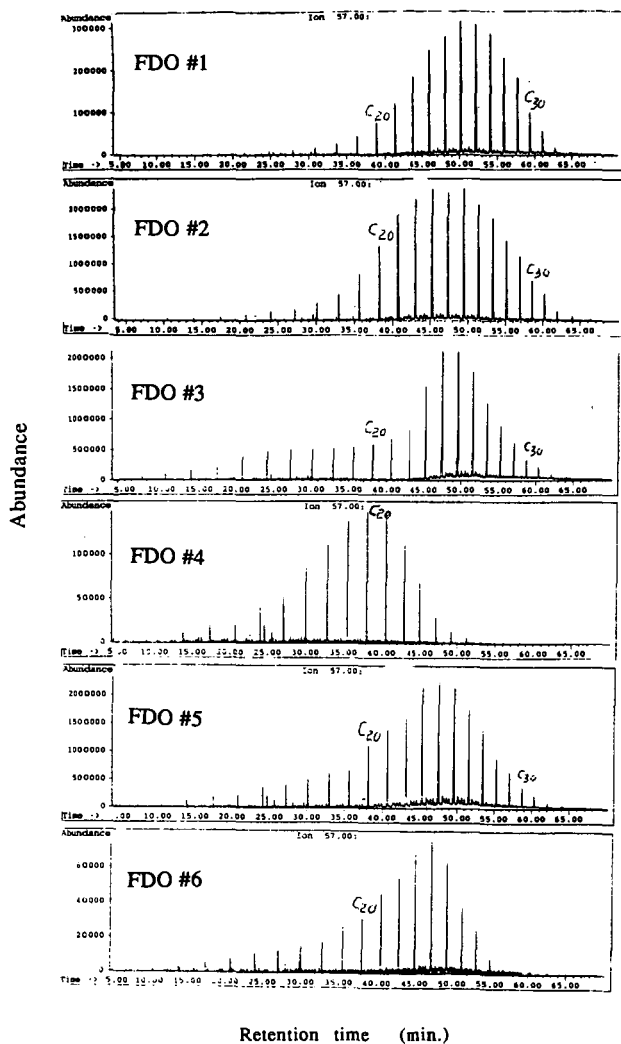
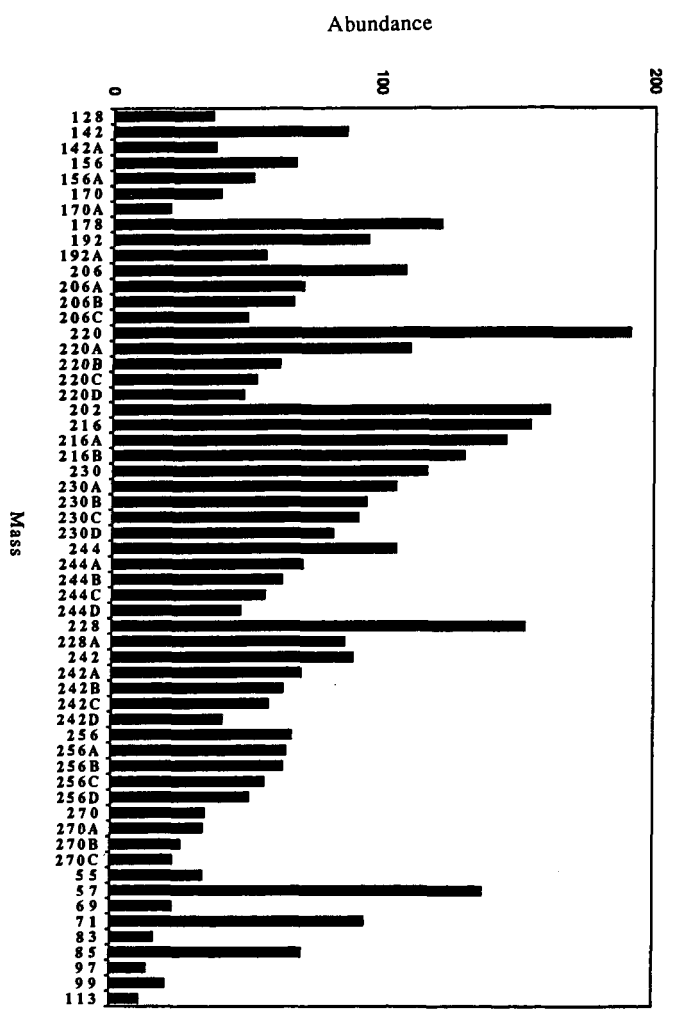


Figure 2. Selected ion (mass 57) chromatograms for FDO #1 - #6

Figure 3. A distribution of selected ions for decant oil FDO #3



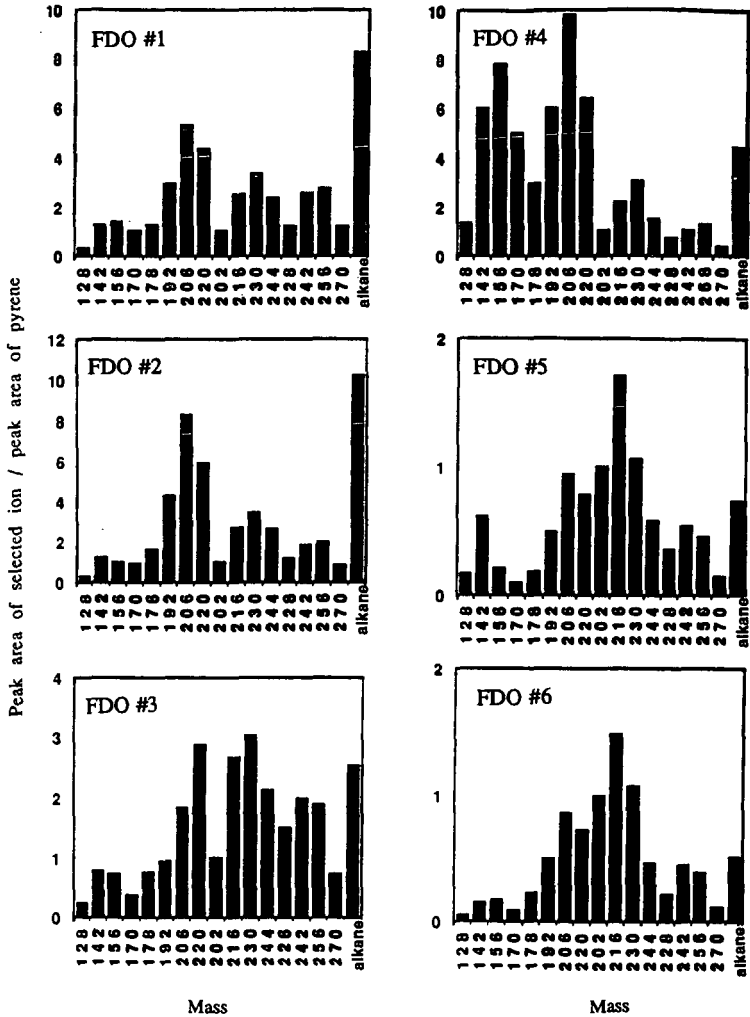


Figure 4. A distribution of selected ions for decant oil FDO #1 -#6

**CHARACTERIZATION OF THE PRODUCTS OF MILD GASIFICATION  
AT THE UNIVERSITY OF NORTH DAKOTA ENERGY AND ENVIRONMENTAL  
RESEARCH CENTER**

Brian D. Runge, Robert O. Ness, Laura Sharp  
Energy and Environmental Research Center  
University of North Dakota  
Box 8213, University Station  
Grand Forks, ND 58202

**Keywords:** Mild Gasification, Value-Added Products, Coal Utilization

**ABSTRACT**

The primary objective of the Energy and Environmental Research Center (EERC) Mild Gasification project has been to demonstrate a process that will produce several value-added products from a high-sulfur midwestern bituminous or a low-sulfur western subbituminous coal. Indiana No. 3 and Wyodak were the coals used for the majority of testing. The products of the process are a low-Btu gas, a hydrocarbon condensate, and a low-volatile char.

The testing was carried out on 4- and 100-lb/hr units. Initial yield data were generated using the 4-lb/hr continuous fluid-bed reactor (CFBR). The preliminary data were then used to plan production runs on the 100-lb/hr process research unit (PRU). An extensive survey was conducted to determine possible markets for the products. The survey indicated that the best slate of products would consist of a metallurgical form coke product from the solids, a feedstock for specialty chemicals from the liquids, and the gas being burned in the plant for utility heat or in a small electric cogeneration unit. The program was then tailored in an attempt to optimize the raw products to meet the industry standards for the desired end products. In the area of form coke, the EERC investigated organic and inorganic binders in both pelletizing and briquetting schemes. The heavy pitch fraction of the liquid products can be utilized as an organic binder in the briquetting process. The lighter liquids have been analyzed to determine their potential as a source of cresylic acid as well as for use as a liquid motor fuel.

**INTRODUCTION**

Coal is the largest indigenous energy resource in the United States. As the price of oil, both foreign and domestic, increases, it will become necessary to tap America's vast coal reserves to augment and in some cases to replace the use of petroleum. The replacement of oil with coal in production of electric power is relatively simple, and the EERC also proposes the use of coal in the chemical market.

The mild gasification process is similar in concept to an oil refinery in which a varied slate of products can be produced from a raw feedstock. The capability to alter product distributions, either by changing feedstocks or process conditions, would permit timely response to the ever-changing market. The current mild gas process consists of a rapid devolatilization of raw coal under mild conditions of temperature and pressure, resulting in a low-Btu gas, a hydrocarbon condensate, and a reactive, low-volatile char.

**RESULTS**

The major findings of the work at the EERC in mild gasification are summarized based on data from the tests on Indiana No. 3, Wyodak, and Cannelton coals in the thermogravimetric analyzer (TGA), the CFBR, and the PRU. All yields reported are as percentages of moisture- and ash-free coal.

## The Effect of Process Conditions on Char Yield and Char Quality for Indiana No. 3, Wyodak, and Cannelton Coals

### PRU Test Results

Operability of the PRU carbonizer was satisfactory for both the Indiana No. 3 and Wyodak coals. Table 1 shows the char yields and char quality from tests on the PRU and CFBR. The Indiana char values are for cleaned and uncleaned char. The lower yields for the cleaned char are due to the amount of char that is rejected in each gravity/magnetic separation that occurs between processing steps. No internal oxidation was assumed, which raised the carbonizer yield by 16%. Internal oxidation was only used to maintain reactor temperature due to heat loss.

The Wyodak char was the only char that met metallurgical coke specifications. The volatile content was higher than typical coke; however, testing indicated that briquettes produced from this char had acceptable strength properties. The Cannelton char data are reported without physical cleaning. If the relative reduction of ash in the Indiana No. 3 char can be used as a comparison, the Cannelton char could be reduced to 12%-13% ash, which would be slightly higher than the specifications. The volatile content is quite low, which should produce a high-strength coke substitute. The Indiana char did not meet the ash or sulfur content desired.

Char yields in the PRU with internal oxidation for the Indiana tests varied from 44.9% to 59.3% over a temperature range of 1020° to 1200°F (550° to 650°C) with limited agglomeration that presented no operational difficulties. The major variation was due to oxidation in the reactor for some test points in order to meet the desired run temperature. Only one mass balance was completed for the Wyodak coal, which had a yield of 49% at 1100°F (600°C).

### CFBR Test Results

Operability of the CFBR was satisfactory on noncaking Wyodak subbituminous coal. Satisfactory operation on mildly caking Indiana No. 3 and Cannelton bituminous coal was accomplished only by temperature staging, using char produced at lower-temperature runs as feed for a subsequent run at a higher temperature. Temperature stages used were 660°, 750°, 840°, 930°, and 1470°F (350°, 400°, 450°, 500°, and 800°C). Other methods that were tried for controlling agglomeration were of very limited success, including preoxidation of the coal feed, internal oxidation, and use of a limestone bed.

Char yields were determined in the CFBR between 930° and 1110°F (500° and 600°C) for Wyodak coal, at staged temperatures between 660° and 1470°F (350° and 800°C) for Indiana No. 3 coal, and at staged temperatures between 660° and 1290°F (350° and 700°C) for the Cannelton coal. The char yields decreased with increasing temperature and were significantly higher for the Indiana No. 3 coal, which yielded about 74 wt% char at 930°F (500°C) and 61 wt% at 1470°F (800°C). Corresponding yields for Wyodak were about 60 wt% at 930°F (500°C) and 50 wt% at 1110°F (600°C). Yields for the Cannelton coal were 82 and 74 wt% at 930° and 1290°F (500° and 700°C), respectively.

A calcining temperature of 1470°F (800°C) was needed to reduce the volatile content of the Indiana No. 3 char below 10%, as required for use in form coke. At this temperature, a typical analysis for Indiana No. 3 char was 8.5% volatile matter, 74% fixed carbon, 19% ash, and 3.4% sulfur without upgrading.

## **The Effect of Process Conditions on Condensable and Gas Yields**

### **PRU Test Results**

A wide variety of yields and boiling point distributions were observed for the three coals, as shown in Table 2. This table has data from the PRU and the CFBR. The Wyodak condensables approximated a liquid that was lighter than a decant oil (#6 diesel). The Indiana No. 3 liquids were the lightest and produced a 17.8% yield. Gas yields are shown in Table 3. The Indiana No. 3 yields are adjusted for no internal oxidation, which resulted in a reduction of CO<sub>2</sub>.

Initially, operation difficulties were encountered with the tar scrubber. The problems were eliminated by lowering the outlet temperature of the tar scrubber and redesigning the scrubber cyclones to eliminate mist entrainment. This increased the amount of liquid condensed in the scrubber, decreasing the coal fines/liquid ratio. The lower outlet temperature increased the light oil content of the recycle loop. This light oil then acted as a solvent for the heavy tars.

The sieve tower and water scrubber performed very well over a wide range of gas velocities and heat loads. During the course of operation, the outlet temperature of the sieve tower was reduced to below the dew point of water, in response to the reduction in outlet temperature of the tar scrubber. This reduced the heat duty on the water scrubber that served as a backup unit to remove entrained organics from the sieve tower.

### **CFBR Test Results**

Total gas yield for the Wyodak coal ranged from 31% to 51% between 930° and 1110°F (500° and 600°C), generally increasing with temperature. The total yield of gas from Indiana No. 3 coal ranged from a low of 2% to 5% at 660°F (350°C) to about 20% at 1470°F (800°C). Yields of all major gas components generally increased along with temperature. The measured gas compositions varied widely, but typical ranges were 50% to 70% for CO<sub>2</sub>, 8% to 14% for CH<sub>4</sub>, 3% to 12% for CO, and up to 3% for H<sub>2</sub>.

Yields of condensable organic liquids were higher for Indiana No. 3 bituminous coal than for Wyodak subbituminous. The cumulative yields obtained by staged heating of Indiana No. 3 coal increased along with temperature from less than 1% at 660°F (350°C) to about 18% at 930°F (500°C) and remained at 18% at the calcining temperature of 1470°F (800°C), owing to essentially zero liquid yield upon further heating of product char prepared at 930° to 1470°F (500° to 800°C). The maximum yield was less than that predicted by the Fischer Assay correlation, possibly due to the short residence time of the fine coal/char feed fraction in the fast fluidized-bed reactor.

The liquid yield for Wyodak coal was highest (10.7%) at the lowest test temperature of 930°F (500°C), and decreased by varying amounts to levels between 0.2% and 9.7%, depending on the gas atmosphere in the carbonizer.

The gas yield for the Cannelton coal was considerably lower than for the other two coals. Yields varied from 5% to 8% at temperatures from 930° to 1290°F (500° to 700°C). Condensable yields ranged from 14% to 19% over the same temperature range, with a large quantity in the 430° to 700°F (220° to 370°C) boiling point range. The most important feature of the Cannelton liquids was the quality. It resembled a #3 diesel fuel.

### **The Effect of Gas Atmosphere Including Steam on Liquid Yield and Quality (CFBR Test Results)**

The use of steam increased the liquid yield from Wyodak coal in three different gas atmospheres, including 1) CO<sub>2</sub>; 2) N<sub>2</sub>/CO<sub>2</sub>, representing flue gas; and 3) N<sub>2</sub>/CO<sub>2</sub>/2% O<sub>2</sub>, representing flue gas with

excess air. The effect of steam was noted primarily at the highest test temperature of 1110°F (600°C), where in all cases an increase in steam partial pressure caused an increase in liquid yield, which, in the case of the  $N_2/CO_2$  gas atmosphere, amounted to an increase from 0.2% liquid at 21% steam to 9.7% at 88% steam. The presence of 2%  $O_2$ , surprisingly, did not reduce the liquid yield, which was higher with 2%  $O_2$  than for  $N_2/CO_2$  alone at a low-steam partial pressure and which was about the same at higher levels of steam. At the lower temperatures of 1020° and 930°F (550° and 500°C), the Wyodak liquid yield varied with steam partial pressure in a manner that did not define a systematic trend.

For Indiana No. 3 coal, liquid yield increased consistently, but only slightly, along with an increase in steam at lower staging temperatures between 660° and 750°F (350° and 400°C). At higher temperatures, no consistent trend was observed.

The boiling point profiles and compound distributions for the two test coals differed, as shown in Table 4. The 3% to 4% low boiling aromatic fraction (BTX) is believed to be lower than the amount actually produced because of losses in the condensation train. Wyodak coal when carbonized without steam produced the highest yield of phenolics, boiling between 330° and 430°F (170° and 220°C). The 430° to 700°F (220° to 370°C) fraction was higher for Indiana No. 3 coal, but the even higher boiling pitch fraction was nearly missing for this coal as tested.

The most prominent effect of steam was to promote higher liquid yields from Wyodak coal at the higher carbonization temperature of 1110°F (600°C). At this condition, the steam is believed to have prevented the retrograde condensation and polymerization of organic compounds on the highly reactive surface of the Wyodak char. Another possible scenario is that the steam provides a better mechanism for removing the tar from the char pore structures. At any given temperature, the condensable yield with steam produced an amount of liquids equivalent to that produced under a higher operating temperature without steam.

#### **The Effect of Process Conditions on Sulfur Removal**

Sulfur reduction played a major role in the development of the process, as the main feed coal had a sulfur content over 4.2%. Since the program was to provide engineering data for commercialization, only proven, low-cost sulfur-reduction techniques were reviewed and incorporated into the process.

A series of tests were conducted to establish the database using a TGA and the CFBR in conjunction with analytical techniques that include scattered electron microscopy (SEM) with elemental mapping. A summary of the findings on in-process sulfur removal includes the following points:

- Pyritic sulfur was effectively reduced to low levels, but organic sulfur, as defined by ASTM analytical methods, was not appreciably reduced.
- Residence time had an important influence on the amount of pyritic and total sulfur removed. The effect extended beyond the 20- to 30-minute residence time at staging temperatures in the TGA and CFBR, since the greatest reduction in total sulfur content (from 3.9% to 1.2%) was observed after 6 hours of residence time in the 30-lb/hr fluidized-bed reactor.
- Gas atmosphere had a minor effect on sulfur removal. Larger reductions in total sulfur content in TGA tests were noted in either reducing ( $CO$  or  $H_2/CO$ ) or oxidizing atmospheres than in  $N_2$ . The use of steam in the 4-lb/hr CFBR did not increase the extent of sulfur removal.

- The chemical forms of sulfur in char were found to be more complex than the pyritic, sulfitic, and organic forms defined by the ASTM procedure. Analysis of char surfaces using scanning electron microscopy/energy dispersive spectroscopy (SEM/EDS) and electron spectroscopy for chemical analysis (ESCA) indicated that important changes in the physical and chemical form of sulfur occurred at 720° to 840°F (380° to 450°C) coincident with the onset of coal agglomeration and with the loss of sulfur from pyrite (FeS<sub>2</sub> to FeS). The principal change observed was that discrete crystals containing sulfur (possibly pyrite) present at 660°F (350°C) had disappeared at 840°F (450°C) and were replaced by a low concentration of sulfur that was detected over the entire char surface. SEM mappings of elements indicated some coincidence in the location of sulfur with Fe and Ca.
- After heating to calcining temperatures, most of the sulfur remaining in the coal is in the ASTM organic form. No combination of time, temperature, and gas atmosphere investigated in this study was successful in systematically removing this stable form of "organic sulfur."

#### **Results of Char Upgrading for the Production of Metallurgical Coke Substitutes Using Inorganic Binders (PTC Process)**

Table 5 includes a compilation of the compressive strengths, impact numbers, and tumble tests for the green pellets, dried pellets, and hardened pellets for the char with/without limestone. The individual tests for inorganic and organic binders use slightly different methods, so only general comparisons can be made between the two binders.

The initial Wyodak char submitted to Pellet Technology Corporation (PTC) for testing contained an uncharacteristically high ash content of 27%, owing to contamination from the limestone bed in the 30-lb/hr fluidized-bed reactor used to produce this bulk sample.

- CaO-SiO<sub>2</sub>-bonded carbon pellets and carbon-iron ore pellets of 1-inch diameter were successfully produced by induration in saturated steam at 420°F (215°C) and 300 psig.
- The finished pellets exhibited satisfactory strength, density, and abrasion resistance with 10% CaO-SiO<sub>2</sub> binder, but not with 5% binder. Since the addition of inorganic binder increases the amount of slag in the iron smelting process, a smaller amount of binder would be a significant benefit.
- The char-iron ore pellets were reduced to iron metal at very high rates upon heating to 2700°F (1480°C). The 5 minutes required for reduction was estimated to be fivefold less than it would have been using coke-iron ore pellets, owing to the high reactivity of the Wyodak char.

The inorganic tests yielded marginally acceptable compressive strength pellets for the Indiana No. 3 and Wyodak chars. The char-iron ore agglomerates were superior in all categories. The sulfur and volatile contents of the agglomerates are considerably lower since they are made of 25% char and 75% iron ore.

#### **Results of Char Upgrading for the Production of Metallurgical Coke Substitutes Using Organic Binders**

The Wyodak and Indiana chars were briquetted using a variety of organic binder types and binder levels that ranged from molasses and starch acrylic copolymer emulsions to coal-derived liquids. The briquettes were then subjected to compressive strength, tumble, and impact tests for the purpose of comparison with PTC pellets. The following is a summary of the organic binder briquette tests:

- Indiana and Wyodak chars when mixed with the asphalt emulsions, FMC formcoke® pitch, P028 scrubber tar, and P027 scrubber tar distillation resid as binders yielded durable oven-cured tablets with high compressive strengths.
- When the briquettes of Indiana char together with 15 wt% P027 scrubber tar distillation resid and the briquettes of Wyodak char with 20 wt% P028 scrubber tar were coked, their strength approached that of FMC formcoke®.
- Wyodak or Indiana char briquettes containing 15 wt% or less P028 scrubber tar or 15 wt% asphalt emulsion did not meet the strength criteria.
- Coked Indiana and Wyodak char briquettes were resistant to moisture absorption under simulated conditions of water soaking and rain showers.
- Wyodak char briquettes, with strength and durability similar or superior to that of a commercial barbecue briquette, can be prepared using starch binders at concentrations of ~4 wt%. Exceedingly strong briquettes with almost complete shatter and abrasion resistance can be prepared with 7 wt% starch.

Table 5 includes a compilation of the compressive strengths, impact numbers, and tumble tests for the dried pellets and hardened pellets for the two chars. The two examples shown in the table are those with the coal-derived liquid. The Wyodak pellet had a high sulfur content due to the use of Indiana tar as the binder, and the char produced was a combination of Wyodak and Indiana No. 3 char.

#### **Results of Char Upgrading for the Production of Activated Carbon**

The production of activated carbon for use in the adsorption of  $\text{SO}_2$  was investigated by producing calcined char with a small amount of steam present in the reactor. The resulting char was pelletized using the PTC process to provide a uniform particle of sufficient size and strength to be used in a filter device.

Sulfur capture was determined by using a TGA with an argon/sulfur dioxide sweep gas. The activated carbon produced at 1380°F (750°C) with 26% of the fluidization gas being steam had the highest  $\text{SO}_2$  adsorption. The char increased in weight by 8.1%. Pelletizing the char had no effect on the adsorption capabilities of the char and produced a product that had much better material-handling capabilities. Higher steam partial pressures should be investigated as the experimental matrix did not find the upper limit of steam partial pressure in relation to increased  $\text{SO}_2$  adsorption.

#### **Results of Condensable Upgrading for the Production of Cresylic Acid**

The Indiana No. 3 liquids yielded cresylic acids in quantities less than 5% of the original sample. It would not be economical to recover such a small quantity of cresylic acid from the liquid stream. However, the Wyodak condensables that were provided to Merichem from the Western Research Institute (WRI) mild gasification project contained 40% usable cresylic acids. This amount merits further consideration into the economic merits.

#### **Results of Condensable Upgrading for the Production of Diesel Fuel Additives**

The results from the diesel fuel testing being conducted by Oak Ridge National Laboratories under a separate DOE contract were not available by the publication deadline.

TABLE 1. Char Yields and Quality

Coal Specifications	Coal			
	Wyodak <sup>a</sup>	Indiana <sup>b</sup>	Indiana <sup>c</sup>	Cannelton
930°F	60.0	74.0		81.7
1110°F	49.0	68.0	54.4	
1290°F		55.1	30.1	74.3
Proximate Analysis, wt%				
Temperature, °F	1110	1290	1290	1290
Fixed Carbon	74.6	65.3	59.6	73.1
Volatiles	< 10	15.0	10.3	6.7
Moisture		1.5	2.0	0.5
Ash	< 10	8.9	22.5	16.1
Sulfur	< 1	0.5	3.5	2.9

<sup>a</sup> Uncleaned.

<sup>b</sup> No internal oxidation.

<sup>c</sup> Cleaned (low yields due to coal reject in cleaning steps).

TABLE 2. Condensable Yields and Quality

	#2 Diesel Decant Oil		Wyodak		Indiana		Cannelton		
	%	%	Yield	%	Yield	%	Yield	%	
ibp - 330°F	10		0.3	3	0.7	4	0.1	1	Gasoline Octane Enhancers, Benzene Cresylic Acids, Phenols Diesel Fuel Blends Briquetting Binders, Anode Carbon
330° - 430°F	86		3.2	34	6.2	35	2.7	14	
430° - 700°F	4	44	3.9	41	10.7	60	14.1	74	
700° - 1020°F		56	2.1	22	0.2	1	2.1	11	
	100	100	9.5	100	17.8	100	19.0	100	

TABLE 3. Gas Yields

	Wyodak	Indiana <sup>a</sup>	Cannelton
930°F	31.0	10.0	5.0
1110°F	42.0	19.0	
1290°F		22.0	8.0

<sup>a</sup> No internal oxidation.

TABLE 4. Comparison of Wyodak and Indiana No. 3 Condensable Boiling Point Fractions

Boiling Point Range and Major Compound Type	Percent of Liquid Produced		
	Wyodak 1110°F 0% Steam	Wyodak 1110°F 99% Steam	Indiana Staged to 1470°F 30% Steam
ibp to 330°F, BTX	4.0	3.4	3.6
330° to 430°F, phenolics	44.0	34.1	35.4
430° to 700°F, multiring aromatics and alkylated phenolics	34.7	40.6	59.6
above 770°F, crude pitch	17.4	21.9	1.4

TABLE 5. Summary of Inorganic and Organic Pelletizing Tests<sup>a</sup>

	Indiana No. 3		Indiana No. 3 <sup>b</sup>		Wyodak		Wyodak <sup>b</sup>		Indiana No. 3		Wyodak	
	PTC Process Inorganic Binder											
Inorganic Content	24.4	76.2	28.0	77.9	47.8	27.0	21.0					
Sulfur Content	3.3	0.6	0.8	0.2	0.6	2.8	3.0					
Volatile Content	10.6	2.1	10.2	2.1	7.7	<6.0	6.4					
Green Pellets												
Compressive Strength, lb	13.6	7.7	16.7	9.9	80.6							
Impact Number	>26.0	6.4	>25.0	12.3	46.6							
Dried Pellets												
Compressive Strength, lb	6.4	6.4	7.7	7.0	1.5	108.0	89.0					
Impact Number	2.0	1.0	2.0	1.6	1.6							
Hardened Pellets												
Compressive Strength, lb	20.3	146.4	46.2	104.0	340.0	163.0	64.0					
Impact Number	6.2	>25.0	16.8	>25.0	>100							
Density, g/cm <sup>3</sup>	1.3	2.5	1.0	2.4	2.1	1.1	1.0					
Tumble Test, %												
+3 mesh	68.0	98.0	92.5	97.2	98.2	89.0	87.0					
+14 mesh	2.8	0.2	0.2	0.1	0							
-14 mesh	29.2	1.8	7.4	2.7	1.8							

<sup>a</sup> Numbers reported are those for the coke produced that provided the best specifications. The PTC pellets reported here are only char.

<sup>b</sup> Iron/char agglomerate.

<sup>c</sup> Wyodak char contained 16% limestone.

<sup>d</sup> Crushed Indiana char with 16% coal-derived tar and 16% limestone.

<sup>e</sup> Crushed Wyodak char with 4.1% Sta-Lok and 4.6% Indiana coal-derived tar.

## **Ion Exchange Properties of Selected North American Low Rank Coals.**

C.J. Lafferty<sup>(1)</sup>, J.D. Robertson<sup>(1,2)</sup>, J.C. Hower<sup>(1)</sup> and T.V. Verheyen<sup>(3)</sup>.

1) Center for Applied Energy Research  
University of Kentucky  
3572 Iron Works Pike  
Lexington KY 40511.

2) Department of Chemistry  
University of Kentucky  
Lexington KY 40506.

3) Coal Corporation of Victoria.  
PMB No.1  
Morwell  
Victoria 3840  
Australia.

**Keywords:** Lignite, Ion Exchange, Metal Adsorption.

### **Introduction**

One of the main problems with the use of low rank coal for combustion purposes lies in its inherently high oxygen content. The high oxygen content results in increased coal reactivity and degradation during mining and storage as well as serving to decrease the overall calorific value of the coal. The high oxygen contents of selected low rank coals can, however, be of great value in certain situations, especially with respect to functional groups containing an exchangeable hydrogen ion.

The ability of low rank coals to form stable complexes with several heavy metal ions has long been recognized<sup>(1-8)</sup>. This property has been successfully utilized to estimate the concentration of acidic oxygen functional groups present in low rank coals<sup>(6)</sup> as well as serving as a convenient means of dispersing metal catalysts across a coal surface prior to liquefaction<sup>(9)</sup>. The relatively high ion exchange capacity of several low rank coals studied, coupled with the low overall cost of the bulk material, indicates great potential for the utilization of low rank coals as a means to remove a range of metals from aqueous waste streams.

## Experimental

The lignites chosen for investigation were from A. The Beulah Zap deposit, in Mercer County, North Dakota. B. The Claiborne Deposit in Carlisle County, Western Kentucky and C. The Jackson Group in Atascosa County, Eastern Texas. A sample of brown coal from the Loy Yang coal field in the Latrobe Valley, Victoria, Australia was also included for comparative purposes as its ion exchange properties have been well documented<sup>(1-3)</sup>.

The samples were obtained with a particle size of < 50 mesh and as such no further size reduction was carried out. The samples were received as mined and stored inside double plastic bags to prevent moisture loss from the samples.

Samples of each coal were also petrographically characterized using combined white light and blue light microscopic analysis. Maceral nomenclature was based on descriptions published in Ref.12.

The ion exchange properties of each coal was characterized using batch metal adsorption tests. Metal solutions were made from AR grade reagents and stored in glass volumetric flasks prior to use. No pH adjustment was made to any of the solutions as that would entail the addition of extra competing cations to the solutions and thus interfere with the ion exchange process. Batch ion exchange experiments were performed by shaking 50.0 mL of the metal solution with a pre-weighed mass (equivalent to 2.50 g dry weight) of as-received coal in 125 mL polyethylene bottles. The bottles were shaken for 12 hours on an orbital shaking platform to ensure equilibrium conditions were reached. The samples were allowed to settle for a further 12 hours before the supernatant solution was sampled for metal analysis using Inductively Coupled Plasma Spectrometry.

FTIR spectra were obtained from 0.4% loaded KBr discs using a Nicolet 20SX spectrophotometer. The discs were dried in vacuo over P<sub>2</sub>O<sub>5</sub> to minimize interference due to adsorbed H<sub>2</sub>O.

## Results and Discussion

### Petrographical Analysis

The four Tertiary lignites were analyzed petrographically according to humic maceral nomenclature outlined in Stach et al.<sup>(10)</sup> and through ICCP communications. Previous studies of the petrology of the Kentucky and Texas lignites were done by Hower et al.<sup>(11)</sup> and Mukhopadhyay<sup>(12)</sup>.

Mean reflectance was done on uniform ulminite fragments. No polarizer or stage rotation were employed in the reflectance analysis. The Paleocene Beulah-Zap, Mercer County, North Dakota, lignite has the highest reflectance, 0.33% R<sub>mean</sub>, followed by the Eocene Jackson Group lignite from Atascosa County, Texas, at 0.28% R<sub>mean</sub>. The Eocene Claiborne Formation lignite from Carlisle County, Kentucky, and the Loy Yang lignite from Victoria, Australia, have mean reflectances of about 0.20%. Lower ulminite amounts in

the latter two lignites hindered the reflectance analyses.

The lignites have distinctive maceral compositions. The North Dakota lignite has the highest percentage of relatively "intact" wood-derived macerals: textinite, ulminite, corpohuminite, fusinite, semifusinite versus humodetrinite. The high inertinite concentration of that sample sets it apart from the other samples.

The Texas lignite has over 50% ulminite in contrast to the high humodetrinite concentration in the Kentucky lignite. The Loy Yang lignite has the highest concentration of liptinite macerals with much of the group being liptodetrinite. The Loy Yang lignite appears to have a relatively high concentration of root-derived macerals, particularly suberinite-enclosed rootlets. The contrast between the raw and sized Kentucky and Texas lignites is also distinctive. In both cases much of the relative order of humic maceral percentages is preserved but there is an increase in the percentage of liptinite macerals in the sized fraction. Liptinite contributes to the strength of the particles and tends to be concentrated in the coarser particles. The fine particles would have had a higher percentage of humic macerals, particularly the easily fragmented humodetrinite which was lost in greater proportions than ulminite.

#### **Batch Metal Adsorption Tests.**

Table 2 lists the equilibrium metal concentrations and solution pH's measured after samples of the various lignites were contacted with 1000 ppm solutions of mercury, lead and cadmium at a solid : liquid ratio of 5:100 (measured on a dry coal basis). As expected, equilibrium solution pH was found to be the major factor determining the extent of metal adsorption. Coals that generated the higher solution pH's were found to exhibit the largest metal adsorption capacities. When analyzing solutions that had been treated with either the North Dakota or East Texas lignites, high levels of sodium were detected in the plasma during metal analysis indicating that a large proportion of the carboxylic groups in these coals are naturally present as sodium carboxylates, which explains the relatively high pH's generated in solution. Sodium carboxylates are known to exchange for a divalent cation more readily than protonated groups which accounts for the high level of metal adsorption measured for these lignites. The sample of West Kentucky lignite also displayed a relatively large adsorptive capacity for the metals investigated but did not contain appreciable amounts of sodium (as detected visually in the plasma), although the relatively high pH's generated in solution would indicate that the coal is naturally pre-exchanged with another readily exchangeable cation.

All of the North American lignites investigated showed relatively high adsorptive capacities for each of the metals investigated. Using multi-stage treatments of heavy metal solutions with these lignites, it should therefore be possible to meet EPA discharge limits much more cheaply than using conventional heavy metal treatment processes.

## Infra Red Spectroscopy

The FTIR spectra of the ROM (Run Of Mine) coals is presented in Figure 1. The spectra reveal that Loy Yang has the highest concentration of carbonyl/free carboxyl groups followed by Kentucky whilst the Texas and Nth Dakota coals contain relatively few. The spectrum of the Kentucky coal is dominated by strong adsorptions associated with clays/silicates. The Texas lignite, in addition, features adsorptions commonly associated with carbonates. Loy Yang in accord with its low ash yield contains very little adsorption associated with mineral matter.

Acid washing the ROM Kentucky coal converts the carboxylate salts to their corresponding protonated acids, Figure 2. The broad adsorption associated with carboxylates at  $\sim 1575\text{cm}^{-1}$  is merged with the  $\sim 1600\text{cm}^{-1}$  band in the ROM and metal exchanged spectra. Protonation shifts the carbonyl/carboxyl adsorption band back into the  $\sim 1700\text{cm}^{-1}$  region. Figure 2 reveals that the ROM and metal exchanged spectra are equivalent indicating that the ROM coal is naturally present in its fully exchanged form.

The positive bands in the difference spectrum (Loy Yang-Kentucky) in Figure 3, confirm the greater concentration of free carboxyl groups in the Victorian coal.

## Conclusions

Three North American lignites were studied in order to characterize their ion exchange properties. All three coals were shown to be capable of adsorbing significant quantities of mercury, cadmium and lead from solution. Infra Red spectroscopy confirmed that the metals were ion exchanged with carboxylic acid functional groups to form metal carboxylates on the coal surface. From these results it would appear that low rank coals show great promise as a means of cheaply removing heavy metal contaminants from aqueous streams. Further studies will concentrate on the ion exchange capacity and selectivity of these coals as well as investigating the possible uses of the ion exchanged coals.

## Acknowledgements

The authors thank Bill Schram for his assistance with the metal analyses.

## References

1. Lambert J.D., Lafferty C.J., Perry G.J. and Royston D., 1986, *Proc. Aust. Conf. Coal Sci.* 2, 1, 142.
2. Lafferty C.J. and Hobday M.D., 1990, *Fuel*, 69, 79.
3. Lafferty C.J. and Hobday M.D., 1990, *Fuel*, 69, 84.

4. Stuart A. D., 1986, Fuel, **65**, 1003.
5. Allen S.J., 1987, Fuel, **66**, 1171.
6. Schafer H.N.S., 1970, Fuel, **49**, 197.
7. Schafer H.N.S., 1970, Fuel, **49**, 271.
8. Schafer H.N.S., 1970, Fuel, **56**, 45.
9. Hatswell M.R., Jackson W.R., Larkins F.P., Marshall M., Rash D. and Egers E.R., 1980, Fuel, **59**, 442.
10. Stach, E., Mackowsky, M.-Th., Teichmüller, M., Taylor, G.H., Chandra, D., and Teichmüller, R., 1982, Coal petrology: Berlin, Gebrüder Borntraeger.
11. Hower, J.C., Rich, F.J., Williams, D.A., Bland, A.E., and Fiene, F.L., 1990, Int. Jour. Coal Geology, **16**, 239.
12. Mukhopadhyay, P. K., 1989, Organic petrography and organic geochemistry of Texas Tertiary coals in relation to depositional environment and hydrocarbon generation: Texas Bureau of Economic Geology, Report of Investigations 188.

**Table 1. Petrographic Composition of Lignite Samples.**

	Texas <sup>1</sup>	Texas <sup>2</sup>	Kentucky <sup>1</sup>	Kentucky <sup>2</sup>	N. Dakota	Loy Yang
Textinite	4.5	8.8	4.2	3.8	7.8	11.2
Ullminite	56.9	53.2	18.6	17.0	47.6	14.4
Humodet.	26.1	11.2	50.6	31.8	6.6	22.0
Gelinite			2.0	1.8	0.2	
Corpohum.	3.2	6.6	4.8	7.0	1.4	12.8
Fusinite		0.6	2.2	1.2	19.2	t
Semifusinite	0.6	0.4	1.0	0.2	10.8	
Sclerotinite	0.1	0.2	1.0	1.2		t
Inertodet.					1.2	
Exinite	3.8	4.2	4.6	7.8	2.6	3.2
Resinite	4.6	5.8	2.0	6.8	0.2	10.8
Suberinite	0.1	1.0	0.4	0.2	0.2	3.2
Liptodet.	0.1	7.8	6.4	20.4	2.2	22.4
Alginite			1.2			
R <sub>mean</sub>	0.28		0.20		0.33	0.19

<sup>1</sup> raw sample  
<sup>2</sup> sized sample

**Table 2. Ion Exchange Properties of Selected Lignites.**

<b>Coal</b>	<b>Mass (wet)</b>	<b>Mass (dry)</b>	<b>Metal</b>	<b>[Metal] (ppm)</b>	<b>pH</b>
Blank			Hg	1175	4.97
Loy Yang	6.82	2.32	(Chloride)	566	3.27
North Dakota	3.28	2.62		12	6.53
Blank			Cd	1105	7.11
Loy Yang	6.82	2.32	(Acetate)	128	4.37
North Dakota	3.15	2.52		45	6.55
Blank				1040	
West Ky.	3.49	2.51		116	4.91
East Tx.	3.35	2.48		78	5.64
Blank			Pb	1069	5.98
Loy Yang	6.70	2.28	(Acetate)	30	3.98
North Dakota	2.93	2.34		5	6.72
Blank				1005	
West Ky.	3.47	2.50		7	4.83
East Tx.	3.34	2.47		2	5.74

Coal shaken with 50.0 mL of solution for 12 hours, allowed to settle for approx. 5 hrs and the supernatant sampled for residual metal analysis.

Moistures:	Loy Yang	(Latrobe Valley, Victoria, Australia)	66%
	North Dakota	(Beulah Zap, Mercer Co. ND)	20%
	East Texas	(Jackson Fm, Atascosa Co. Tx)	26%
	West Kentucky	(Claiborne Fm., Carlisle Co., Ky)	28%

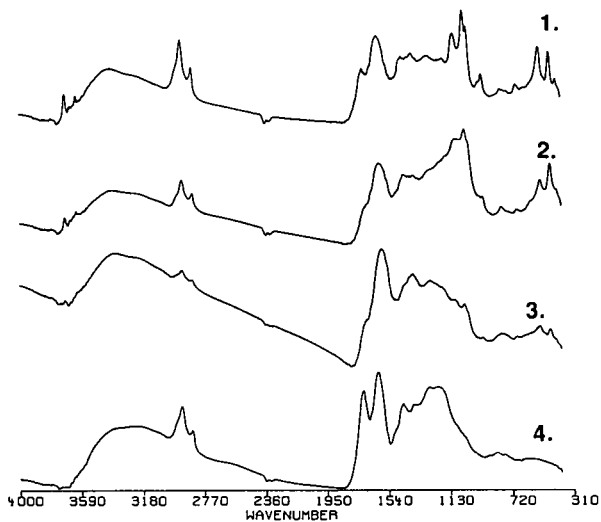


**Figure 1. Infra Red Spectra of As-Received Coals**  
 1. Kentucky 2. Texas 3. North Dakota 4. Loy Yang

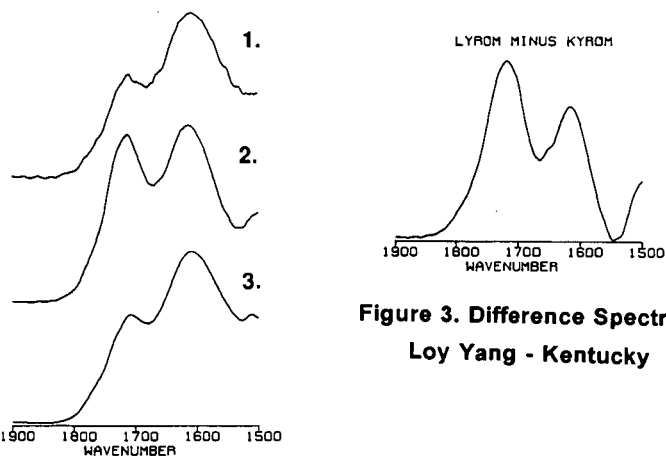


**Figure 2. Infra Red Spectra of Kentucky Lignite**  
 1. As-Received 2. Acid Extracted 3. Metal Exchanged.

## LIQUEFACTION PATHWAYS OF BITUMINOUS AND SUBBITUMINOUS COALS AND THEIR INTERMEDIATES

Robert A. Keogh, Liguang Xu, Scott Lambert,  
and Burtron H. Davis

Center for Applied Energy Research  
University of Kentucky  
3572 Iron Works Pike  
Lexington, KY 40511

**Keywords:** Liquefaction, Pathway, Coal

### ABSTRACT

Thermal liquefaction studies of a number of high volatile bituminous coals suggest that these coals have a common liquefaction pathway. Verification of this pathway was confirmed using a single coal and a number of reaction conditions. The addition of a catalyst did not alter the observed thermal pathway. The thermal and catalytic liquefaction pathway obtained for a subbituminous coal was significantly different from the one obtained for the bituminous coals. To investigate ways to alter the bituminous coal liquefaction pathway, the intermediates, asphaltenes and preasphaltenes, were prepared, isolated and liquefied in batch reactors to determine their conversion pathway.

### INTRODUCTION

Historically, lumped parameter kinetic models have been used successfully to describe industrially significant processes such as catalytic cracking (1), catalytic reforming (1), and condensation polymerization (2). The same approach has been used in the description of the various liquefaction processes (3,4). A physically realistic and technically viable lumped parameter kinetic model for liquefaction would be of considerable value in the development of pathways, mechanism, and the scale-up of the liquefaction processes.

In the work presented here, the solubility classes obtained from the liquefaction products of the coals were lumped into the following parameters: (a) oils plus gases (O+G), (b) asphaltenes plus preasphaltenes (A+P) and (c) insoluble organic matter (IOM). The lumped parameters used for the liquefaction products obtained from the intermediates asphaltenes and preasphaltenes were: (a) O+G, (b) asphaltenes, and (c) preasphaltenes plus IOM. The lumped parameters were plotted on a triangular diagram for interpretation.

### EXPERIMENTAL

The description of the coals used in these study has been given in detail elsewhere (5). All of the liquefaction experiments using the coals were performed in 50 mL batch autoclaves using a hydrogen atmosphere and tetralin as the solvent. Details of the liquefaction runs and the analytical methods used have been described elsewhere (5).

The liquefaction of the intermediates were performed in 25 mL batch autoclaves using the same procedures as those used for the coals.

The intermediates, asphaltenes and preasphaltenes, were obtained from the liquefaction of a Western Kentucky #9 coal and a heavy petroleum resid which contained no asphaltenes. The coal/resid slurry was run in the CAER 1/8 tpd pilot plant using a 1 $\ell$  CSTR, a reaction temperature of 385°C, a 40 minute residence time and a hydrogen pressure of 2000 psig. The products used for the separation of the asphaltenes and preasphaltenes were obtained from the hot, low pressure separator upon reaching steady state conditions. The intermediates were separated into the solubility classes using the same method as was used in the batch microautoclave experiments. The coal conversion obtained during the steady state operation was 76 wt.% (daf).

## RESULTS AND DISCUSSION

The solubility class distributions obtained from the thermal liquefaction of 69 bituminous coals using a single residence time (15 min.) and three reaction temperatures (385°C, 427°C, 445°C) are plotted on a triangle plot in Figure 1. The data suggested a common liquefaction pathway for these coals. The pathway was verified by using a set of reaction temperatures and residence times such that the entire range of conversions were obtained for a single coal (Western Kentucky #6). The data obtained from these experiments are shown in Figure 2. The data in Figure 2 confirmed the thermal pathway suggested from the single residence time data.

The pathway shown in Figure 2 indicates two distinct stages. In the initial coal dissolution stage, the intermediates (asphaltenes plus preasphaltenes) increase with increasing coal conversion. During this stage of coal dissolution, the oil plus gas yields remain fairly constant. It should be noted that the gas produced during this stage of coal dissolution contributes only a small amount to the lumped parameter (O+G). The second stage of the pathway begins after the coal has reached a maximum in conversion (and A+P yield). In this stage the coal conversion remains fairly constant and the major reactions are the conversion of A+P to O+G.

The data obtained from these coals suggest that if a set of conditions could be found which would change the initial stage of the thermal pathway, the process would produce more of the desirable products (oils). One possible method would be to use a catalyst to change the selectivity. A number of catalysts were studied using the Western Kentucky #6 coal. The data obtained from some of these experiments are shown in Figure 3. As can be seen in this figure, the catalytic pathway is similar to the thermal pathway shown in Figure 2. The addition of the catalysts did not change the pathway; however, the catalysts did increase the rate of the production of the intermediates.

Thermal and catalytic data were obtained for a subbituminous Wyodak coal to investigate the effect of rank on the observed pathway. These data are shown in Figure 4. As can be seen in this figure, the pathway obtained is significantly different from the one obtained for the bituminous coals. In the initial and dissolution stage of the pathway, both the A+P and O+G yields increase with coal conversion. In the second stage of the pathway, similar to the pathway of the bituminous coals, the major reaction appears to be

the conversion of A+P and O+G with a small concurrent increase in coal conversion. Also similar to the bituminous coal data, the thermal and catalytic pathway of the Wyodak coal are similar.

The intermediates (asphaltenes and preasphaltenes) were produced, separated and checked for purity to further investigate the pathway of the bituminous coals. The intermediates, both separately and a 50/50 wt.% mixture, were reacted using similar conditions to those used for the coals. The thermal pathway of these samples are shown in Figure 5. The thermal pathway of the coal-derived asphaltenes, as expected, indicates the primary reaction is the conversion of the asphaltenes to oils plus gases. Again, the contribution of the gases to the lumped parameter is small. It appears from these data that the conversion of the asphaltenes follows a similar path both during coal conversion and during the conversion of the isolated intermediate solubility fraction.

The thermal conversion pathway of the preasphaltene intermediate, also shown in Figure 5, was somewhat unexpected. The pathway indicates that the oils are formed slightly faster from the preasphaltenes, presumably through the asphaltene intermediate, than the asphaltenes are formed from the preasphaltenes. However, if the unconverted coal (IOM) is subtracted from the coal conversion products, the points for the conversion of coal and preasphaltenes are similar. Thus, it appears that the conversion of the preasphaltenes follow a similar path during coal conversion and the conversion of the isolated solubility fraction.

The thermal pathway observed for the mixture (50/50 wt.%) of asphaltenes and preasphaltenes is also shown in Figure 5. The pathway defined for the mixture indicates that the two reactants are converted independently. The experimental data and the calculated data based on the conversions of the individual asphaltenes and preasphaltenes runs are similar within experimental error.

## SUMMARY

It has been shown that high volatile bituminous coals have a similar reaction pathway and that the addition of a catalyst does not significantly change the observed thermal pathway. The pathway for the bituminous coals indicate that to obtain a significant oil yield, a maximum in the intermediate (A+P) yield (and coal conversion) must be obtained. The thermal and catalytic pathway obtained for a Wyodak coal is significantly different. For this coal, an increase in the asphaltene plus preasphaltene and oils plus gases yield parallel the increase in coal conversion in the initial stage. The thermal conversion pathways of the isolated intermediate solubility fractions were similar to those obtained during coal conversion.

## ACKNOWLEDGMENT

This work was supported by the Commonwealth of Kentucky and DOE contract No. DE-FC88-PC8806 as part of the Consortium for Fossil Fuel Liquefaction Science (administered by the University of Kentucky).

## REFERENCES

1. V. W. Weekman, *AIChE Monograph Series*, **75** (11), (1979).
2. P. J. Flory, "Principles of Polymer Chemistry", Cornell University Press, New York, NY, 1953.
3. S. Weller, M. G. Pelipetz and S. Friedman, *Ind. Eng. Chem.*, **43** (7), 1575 (1951).
4. D. C. Cronauer, Y. T. Shah and R. G. Ruberto, *Ind. Eng. Chem., Proc. Des. Div.*, **17**, 281 (1978).
5. R. A. Keogh, K. Tsai, L. Xu and B. H. Davis, *Energy & Fuels*, **5** (5), 625 (1991).

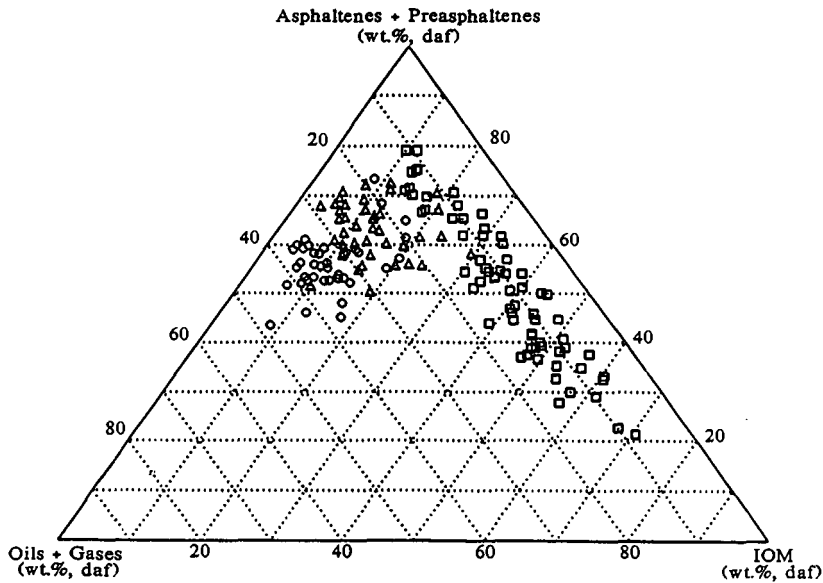


Figure 1. Solubility class distribution of 69 bituminous coals using a 15 minute residence time and three temperatures ( $\square$ , 385°C;  $\triangle$ , 427°C;  $\circ$ , 445°C).

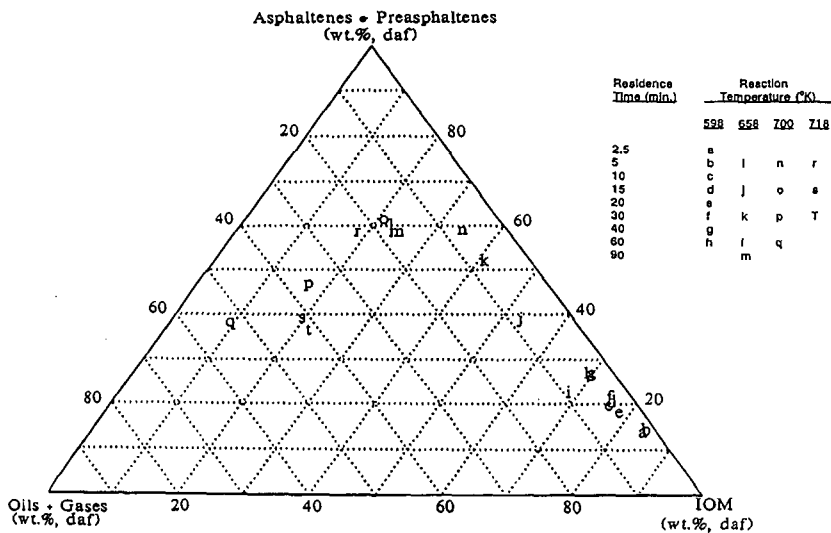


Figure 2. Thermal liquefaction pathway of a Western Kentucky #6 coal.

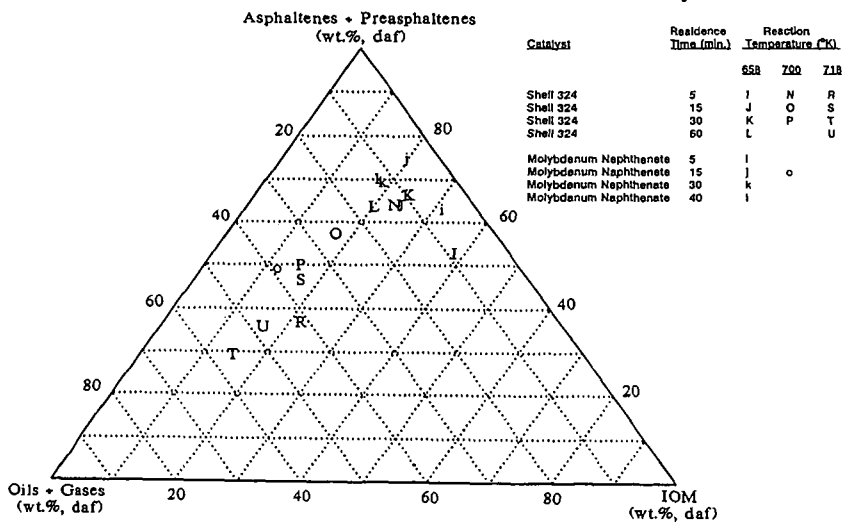


Figure 3. Catalytic liquefaction pathway of a Western Kentucky #6 coal.

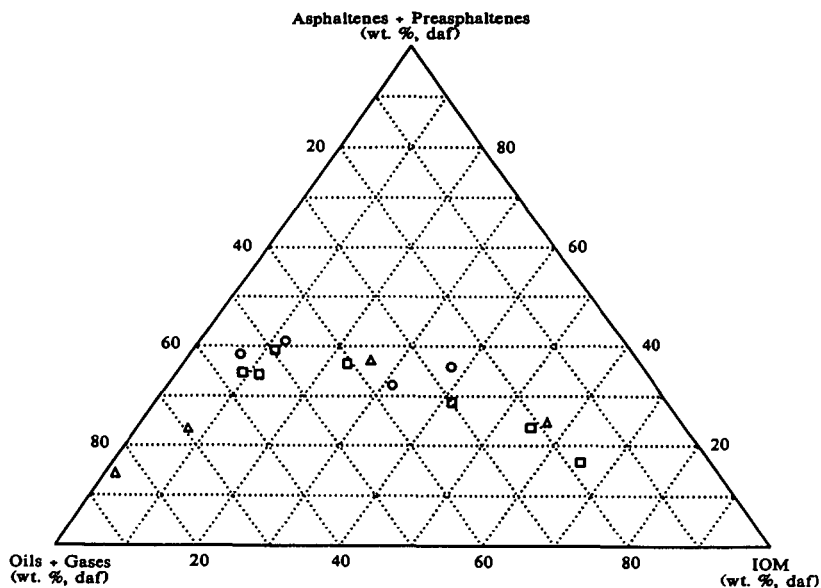


Figure 4. Thermal and catalytic pathway of a Wyodak coal (□, thermal; ○, Fe<sub>2</sub>O<sub>3</sub>; △, molybdenum naphthenate).

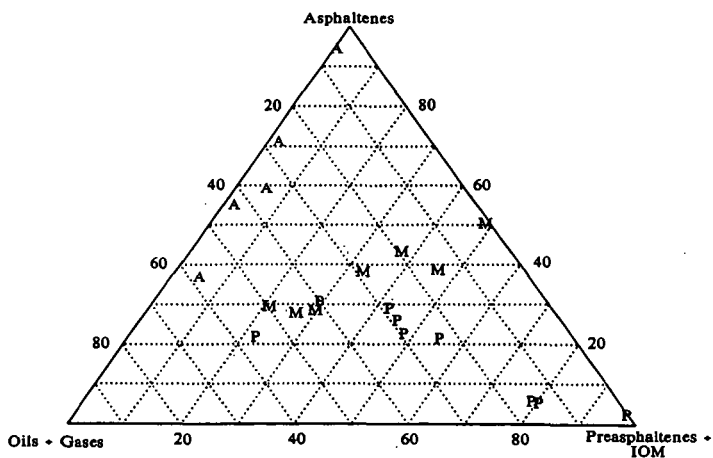


Figure 5. Thermal pathway of bituminous coal-derived asphaltene (A), preasphaltenes (P) and a 50/50 wt.% mixture of asphaltene and preasphaltenes (M).

## NEW DIRECTIONS TO PRECONVERSION PROCESSING OF COAL

M. Nishioka, W. Laird, P. Bendale, and R. A. Zell

*Viking Systems International, 2070 William Pitt Way, Pittsburgh, PA 15238*

Keywords: Coal Liquefaction, High-Temperature Soaking, Coal Associations

### INTRODUCTION

Coal structure should be well understood for the effective development of coal liquefaction. A cross-linked three-dimensional macromolecular model has been widely accepted for the structure of coal. Coal liquefaction is being developed based on this model. Recent studies, however, showed that significant portions (far more than generally believed) of coal molecules are physically associated<sup>1</sup>. If physical association is dominant, all properties and reactivities in coal liquefaction must be a strong function of intra- and intermolecular (secondary) interactions and molecular weight. It is necessary to reinvestigate a coal conversion procedure based on the associated nature of coal.

Many efforts of chemical pretreatments have been made to cleave chemical bonds by using reagents or high pressure of CO and H<sub>2</sub>O etc. Coal changes molecular conformations during soaking/dissolution steps due to relatively strong secondary interactions. This may lead to decrease in dissolution, but this phenomena have often been regarded as retrograde reactions. The stabilization of radical intermediate has been considered to prevent retrograde reactions. These concepts of selective bond cleavages and prevention of retrograde reactions are based on the network model.

If a large portion of coal is associated, coal may be dissolved to a great degree. It is expected that largely dissolved coal can easily be converted to liquid. However, dissolution has not been an easy task, as shown by many researchers for a long time. If coal/coal complexes with high molecular weight are replaced with molecules with low molecular weight, coal may be dissolved to more extent. Associated coal is regarded as material with broad molecular weight distribution. Reactivity of these material may be different. Fractions with different molecular weight may be treated separately to produce desired fractions, if possible. These are the major features considered in this paper based on the associated molecular nature of coal.

In this paper, a new concept of coal preconversion is shown on the basis of these propositions. Two subjects are focused on: (1) maximizing dissolution of associated coal without additional chemicals and (2) step-wise conversion of associated coal with broad molecular weight distribution. For these purposes, the following procedure has been tested: two-step soaking at 350-400°C, followed by isolation of oil, and then liquefaction of residue. This enabled to lower liquefaction severity, to decrease the gas yield, and to increase the oil yield. Some of these results and the future perspective of two-stage liquefaction will be discussed.

### EXPERIMENTAL

Coal samples were obtained from the DOE Coal Bank at Pennsylvania State University.

Illinois no. 6 coal (DECS-2) was used as received, and Smith Roland coal (DECS-8) was washed with 2N HCl<sup>2</sup> and dried before use. A coal liquid derived from Illinois no. 6 coal obtained from the Wilsonville pilot plant<sup>3</sup> was used. All the reagents and solvents were obtained from Aldrich Chemical Co. (Milwaukee, WI) and Fisher Scientific (Pittsburgh, PA), and HPLC-grade solvents were used without further purification.

Two reactors, a 250 ml autoclave (Model 4576; Parr Instrument CO., Moline, IL, USA) and 27 ml microreactors fabricated, were used. These reactors were evacuated and purged with nitrogen five times after charging a coal sample and a solvent. The autoclave was heated approximately at 8°C min<sup>-1</sup> to required temperature, and controlled to  $\pm 3^\circ\text{C}$ , while agitating with the autoclave stirrer (500 rev min<sup>-1</sup>). Microreactors were heated in a fluidized sand bath (Model SBL-2; Techne Corp., Princeton, NJ) which was controlled within  $\pm 1.0^\circ\text{C}$  of the set point. The shaker (Model 75; the Burrell Corp., Pittsburgh, PA) was modified to shake the microreactor horizontally at 320 rev min<sup>-1</sup>. Mixtures in the reactor attained the set point within 5 min, when the reactor was being immersed into the sand bath.

After reactions, the mixtures were filtered and Soxhlet-extracted with cyclohexane, toluene and tetrahydrofuran (THF) for 24 h, respectively, and then these samples were dried under vacuum at 95°C overnight. The amounts of THF solubles (TS), toluene solubles (ToS) and cyclohexane solubles (CyS) were determined from the mass of the respective insolubles. Produced gas was generally included in the CyS yield.

Gas was collected with a sample bag after cooling the autoclave, and analyzed with gas chromatography by the University of Pittsburgh Applied Research Center (Pittsburgh, PA). Approximate gas yields were calculated on the assumption that the amount of nitrogen does not change before and after reactions.

## RESULTS AND DISCUSSION

### *Coal dissolution and liquefaction*

The effect of soaking temperature on liquefaction was compared at 200°C and at 350°C. Illinois no. 6 coal was liquefied at 430°C for 1 h after soaking at these temperatures. The yields of TS were the same for these runs, but the yields of ToS and CyS were 5% higher for the samples soaked at 350°C than for that at 200°C. The coal was mildly refluxed in pyridine for 24 h, followed by the removal of the solvent, and liquefied at 430°C. The conversion was compared to that liquefied under the same condition but using the raw coal. The yield of CyS increased about 10% by soaking in pyridine. Other related results are available. An increase in conversion at 427°C was observed when a coal/coal liquid mixture was soaked at 277-322°C for 10 min<sup>4</sup>. Preswelling with THF and tetraammoniumhydroxide, followed by removal of solvents, enhanced hydroliquefaction yields at 400°C<sup>5,6</sup>. These results show that disintegrated coals lead to high conversions in liquefaction.

Optimum temperature of the high temperature soaking was around 350°C as shown in *Figure 1*. However, the CyS (or oil) yield was still low (35%) at 350°C. The two-step wise soaking was further tested to increase an oil yield. Soaking at 350°C, followed by soaking at 400°C, gave the 50% oil yield (Run 10 in *Figure 2*), but soaking at 200°C, followed by soaking at 400°C, was not effective and led to the yield of more than 100%

because of incorporation of the coal liquid used as a solvent (Run 11).

The effect of radical initiators on the high-temperature soaking and liquefaction were investigated in the recent works<sup>7,8</sup>. Although it has widely been accepted that radicals cause retrograde reactions, the addition of radical initiators did not have the expected negative effect and the slightly positive effect in the high-temperature soaking (350-400°C). The addition of H<sub>2</sub>O<sub>2</sub> at the high-temperature soaking increased the 5% oil yield under low pressure hydrogen gas (Run 12)<sup>8</sup>. The addition of small amount of water alone gave the similar change in conversion in the high-temperature soaking. Therefore, a small amount of water or hydrogen peroxide solution may be added to improve the high-temperature soaking.

The two-step high-temperature soaking at 350°C and 400°C gave the 50% of cyclohexane solubles as shown above. This implies that slow heating is better than fast heating on coal conversion. The autoclave was heated up relatively slowly (at 8°C min<sup>-1</sup>). The effect of heating rate, therefore, was investigated using the microreactor which was relatively fast heated up in the sand bath. The reactor was heated from room temperature to 430°C in 0.5 h and held at 430°C for 2 h (Run 13). For Run 14, the mixture was reacted under the same condition, but heated with a step-wise heating before reaction (at 350°C for 0.5 h and at 400°C for 0.5 h), and then held at 430°C for 1 h. The total heating-up time from room temperature to 350°C, from 350°C to 400°C and from 400°C to 430°C was 0.5 h. So, the total residence time including heating-up was 2.5 h. For Run 15, the mixture was slowly heated from 130°C to 430°C and held at 430°C for 1 h. The total duration of heating-up and reaction time was also controlled to 2.5 h. Although the coal was reacted at 430°C for the longest time for Run 13, coal conversion was the lowest among three Runs. The oil yield was enhanced about 10% by these programmed heatings. These results shows that the programmed heating or step-wise high-temperature soaking was important for coal conversion. Song *et al.*<sup>9</sup> recently reported the effect of the temperature-programmed liquefaction of low rank coals. Montana subbituminous coal was converted to 5-10% more (THF solubles) by slow heating compared to rapid heating.

#### *Coal fractions and liquefaction*

Another important factor to decrease a gas yield is suggested on the basis of the associated molecular nature of coal. Hydrocarbons with lower molecular weight generally produce more gas by thermal pyrolysis. Hydrocarbons with higher molecular weight will be decomposed under more severe conditions under which more gas will be produced from hydrocarbons with lower molecular weight. The associated structural model of coal can be regarded as material with broad molecular weight distribution. Therefore, coal with different molecular weight should be treated separately, if possible.

A low molecular weight fraction may be separated after dissolution of coal, and a remaining high molecular weight fraction may selectively be liquefied. Here, pyridine solubles and insolubles were separately liquefied to compare their conversions under the same condition (Runs 16 and 17). Approximately the same oil yield was obtained from pyridine solubles and insolubles (Figure 3). Furthermore, cyclohexane insolubles from Run 10 was examined. The 50% oil yield was obtained even from this fraction (Run 18).

The liquefaction characteristics of the soluble and insoluble components has recently

been reviewed and studied<sup>10</sup>. The dissolution and hydrogen consumption rates of a pyridine extracted coal and a whole coal were similar for West Kentucky coal (80% carbon, daf)<sup>11</sup>. Whereas, a significant decrease in liquefaction conversions was observed when a coal was extracted with pyridine for Illinois no. 6 coal<sup>12</sup>. Warzinski and Holder<sup>10</sup> found the retrogressive behavior in conversion for pyridine extract part of Illinois no. 6 coal. Although it is difficult to conclude the effect of the soluble and insoluble components from these results, it seems that the reactivity of residues or high molecular weight components is not so poor as that of low molecular weight components.

#### *The associated molecular nature and liquefaction*

It was shown that a large portion of coal can be dissolved by the high-temperature soaking in the coal liquid, and the programmed or step-wise heating is preferred to enhance an oil yield. The highly dissolved coal was liquefied to a larger extent. Further, it was suggested that coal with a broad molecular weight distribution should be separated into an oil fraction after dissolution, and that only residue should be liquefied at the following step. From these results, a new concept is proposed to increase an oil yield and decrease a gas yield as shown in the block diagram (*Figure 4*). Coal is soaked in a recycle oil at 350°C and at 400°C. Gas and oil are recovered by vacuum distillation, and the bottom fraction is fed to a liquefaction section and liquefied under low pressure hydrogen at a relatively low temperature.

The proposed procedure was tested using an autoclave. The DECS-2 coal was soaked in the coal liquid under nitrogen at 350°C and at 400°C for 1 h, respectively. The oil fraction was extracted with cyclohexane, and the cyclohexane insoluble portion was liquefied under low pressure of hydrogen (2.8 MPa) at 430°C for 1 h (Run 20). For comparison, the coal was soaked in the coal liquid at 200°C for 1 h, and then the mixture was liquefied under the same condition for 2 h (Run 19). In these Runs, gas yields were analyzed. *Figure 5* shows these results. It is notable that the CyS (or oil) yield increased 30% and the gas yield decreased 15%.

DECS-8 (subbituminous) coal was also examined with the same procedure. As the ionic forces are relatively strong and abundant in low rank coals<sup>2</sup>, it is an important step to weaken the ionic forces before the high-temperature soaking. Although it has been known that acid washing enhances the conversion of low rank coal<sup>13-16</sup>, the details on acid washing have not clearly been explained. Here, 2N HCl washing<sup>2</sup> was used to weaken the ionic forces in the coal before the high-temperature soaking. The coal was soaked in the coal liquid at 350°C and at 400°C for 1 h, respectively. Cyclohexane insolubles from the soaked coal was similarly liquefied at 430°C for 1 h (Run 22). As the acid washed coal was dried, the dried DECS-8 coal was soaked at 200°C for 1 h and then liquefied at 430°C for 2 h for comparison (Run 21). Again, more than 30% increase in the oil yield and 20% decrease in the gas yield was observed by the procedure (*Figure 5*).

#### CONCLUSIONS

An improved coal liquefaction concept was reinvestigated for the current two-stage process on the basis of the associated molecular nature of coal. Since a significant portion of coal molecules are physically associated as pointed in our recent paper, physical dissolution

should be considered more. The step-wise high-temperature soaking was a simple and effective method for coal dissolution. Larger dissolution made liquefaction severity lower. Broad molecular weight distribution in the associated coal was another important factor. The selective reaction of fractions with high molecular weight which were isolated after the high-temperature soaking made gas yield lower. Tests with using an autoclave by the concept shown in Figure 5 enabled to produce 30% more oil and 15-20% less gas yields. It is expected that the procedure will result in great cost down in coal liquefaction.

#### ACKNOWLEDGEMENT

This work was supported by the U.S. Department of Energy under Contract DE-AC22-91PC91041.

#### REFERENCES

- 1 Nishioka, M. *Fuel* 1992, 71, 941
- 2 Nishioka, M., Gebhard, L. and Silbernagel, B. G. *Fuel* 1991, 70, 341
- 3 Gollakota, S. V., Lee, J. M. and Davies, O. *Fuel Proc. Tech.* 1989, 22, 205
- 4 Wham, R. M. *Fuel* 1987, 66, 283
- 5 Joseph, J. T. *Fuel* 1991, 70, 139
- 6 Joseph, J. T. *Fuel* 1991, 70, 459
- 7 Nishioka, M., Laird, W. and Bendale, P. *Fuel* submitted
- 8 Nishioka, M. and Laird, W. *Fuel* submitted
- 9 Song, C., Schobert, H. H. and Hatcher, P. G. *Energy & Fuels* 1992, 6, 328
- 10 Warzinski, R. P. and Holder, G. D. *Fuel* 1992, 71, 993
- 11 Whitehurst, D. D., Farcasiu, M., Mitchell, T. O. and Dickert, J. J. Jr. Electric Power Research Institute Report EPRI AF-480, Palo Alto, CA, 1077, pp. 7-2-7-10
- 12 Seth, M. PhD Thesis University of California Berkeley, Berkeley, CA, 1980
- 13 Schafer, H. N. S. *Fuel* 1970, 49, 197
- 14 Mochida, I., Shimohara, T., Korai, Y., Fujitsu, H. and Takeshita, K. *Fuel* 1983, 62, 659
- 15 Serio, M. A., Solomon, P. R., Kroo, E., Bassilakis, R., Malhotra, R. and McMillen, D. *Am. Chem. Soc. Div. Fuel Chem. Prepr.* 1990, 35(1), 61
- 16 Joseph, J. T. and Rorrai, T. R. *Fuel* 1992, 71, 75

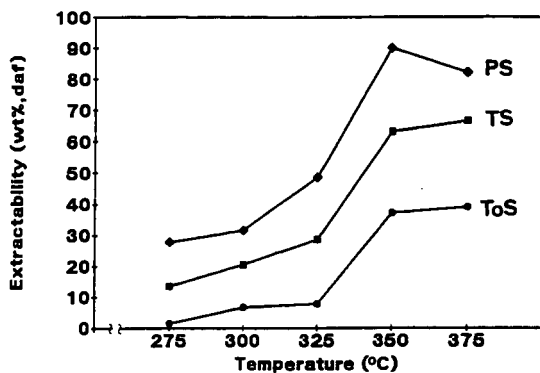


Figure 1 The effect of soaking temperature on extractability (DECS-2 coal, 0.35 MPa  $N_2$ , 1.5h)

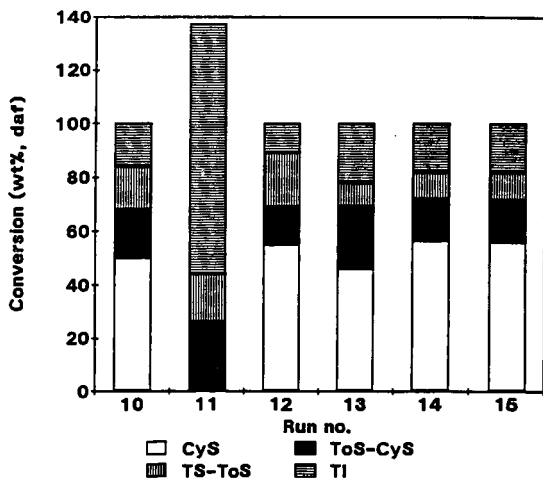


Figure 2 The effect of step-wise soaking on extractability for DECS-2 coal under  $N_2$ , except for Run 12 (Conditions: Run 10; 350°C(1h)/430°C(1h), Run 11; 200°C(1h)/430°C(1h); Run 12; 350°C(1h)/430°C(1h) with  $H_2O_2$  (3000 ppm) and  $H_2$  (1.4 MPa), Run 13; 430°C(2.5h), Run 14; 350°C(0.5h)/400°C(0.5h)/430°C(1h), Run 15; 130°C to 430°C at 3.5°C  $min^{-1}$ , followed by 430°C(1h))

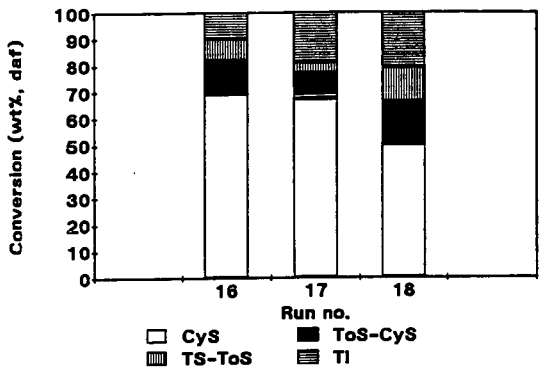


Figure 3 Coal fractions and their conversions at 430°C for 1 h with 2.8 MPa of H<sub>2</sub> ((Run 16; DECS-2/PS, Run 17; DECS-2/PI, Run 18; Cyclohexane insolubles from Run 10)

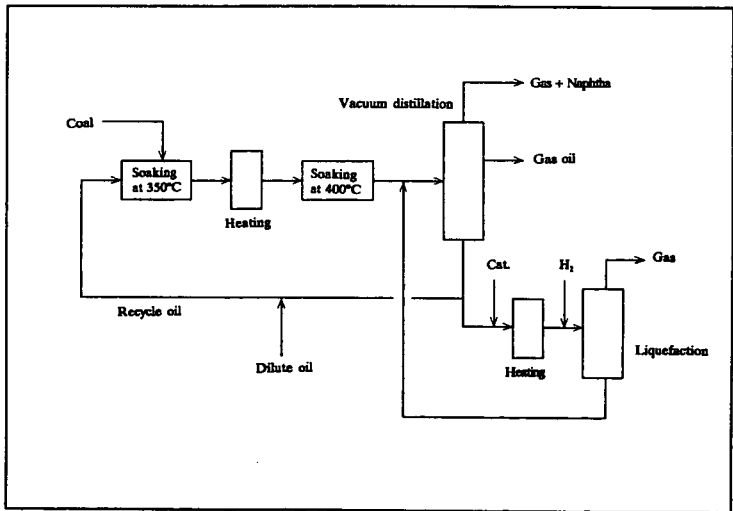
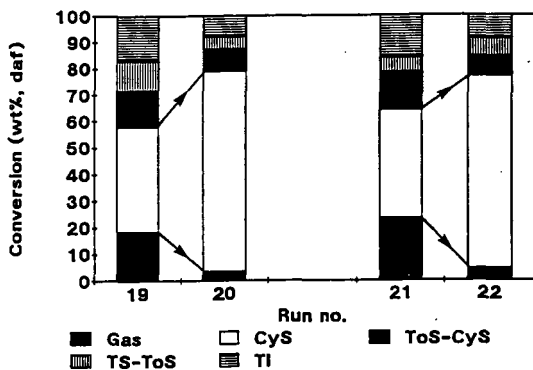


Figure 4 Block diagram of the proposed coal liquefaction concept



**Figure 5** Coal conversion by the proposed procedure for DECS-2 coal (Runs 19 and 20) and DECS-8 coal (Runs 21 and 22) (Run 19; 200°C(1h)/430°C(2h), Run 20; calculation from Runs 10 and 18, Runs 20 and 21 under the same conditions as Runs 19 and 20, see the text in detail)

## Effects of Thermal and Solvent Pretreatments on the Elastic Properties of Coal

Yongseung Yun and Eric M. Suuberg  
Division of Engineering, Brown University  
Providence, RI 02912

(Keywords: Elastic property, Dynamic Mechanical Analysis, Pretreatment)

### INTRODUCTION

It is now well established that thermal pretreatment in a range of temperatures lower than those needed for pyrolysis can significantly affect the penetrability and swellability of coals. This suggests that judicious use of heat together with effective swelling solvents for coal, can affect mass transport of reagents or catalysts into or out of the coal, during the early stages of liquefaction.

The present study is concerned with the effects of heat/solvent pretreatments on the elastic constants of the coal network structure. This, in turn, tells one about how the non-covalent interactions in coal are being broken down. Studies of the elastic properties of coal are nothing new [e.g. 1-10]. Because of the compressibility of coal, the application of mercury porosimetry to pore characterization in coal has involved careful corrections, so that the actual pore size distribution could be calculated [1,11,12]. However, the limitation caused by compressibility of bulk coal structure can be an advantage in revealing the structural changes during pretreatment processes and in establishing a suitable elastic model for macromolecular coal structure.

It is known that dynamic mechanical methods are ca. 1000 times more sensitive for detecting molecular relaxations such as the glass transition temperature,  $T_g$ , than are differential scanning calorimetry (DSC)/differential thermal analysis (DTA) techniques [13]. Weller and Wert [7-10] have extensively applied the torsion pendulum technique, one of the dynamic mechanical methods, for elucidating the elastic properties of coal in the temperature range below 200 °C. They employed square rods cut from whole coal. Since the relevant temperature range for the structural relaxation by heat is generally higher than 200°C, we decided to study the thermal structural relaxation at temperatures higher than 200°C by employing dynamic mechanical analysis (DMA). This technique involves constant amplitude oscillation of the solid to determine stress-strain properties.

### EXPERIMENTAL

A DuPont 982 DMA was employed for mechanical analysis. A detailed description of the equipment has been given elsewhere [13,14]. The sample for the DMA was prepared by pressing the as-received coal powder (-100 mesh) obtained from the Argonne Premium Sample Bank with a press normally used for making FTIR sample pellets, at 15 kpsi for 6-12 hr, which results in a sample of ca. 4 mm thickness with 12.8 mm diameter.

Slippage of the samples from the clamps inside the DMA, especially during oscillation in the high temperature range (>300°C), was noted to be a main cause for irreproducibility, and special care was taken to make certain that the sample was tightly clamped. The pelletizing process used here clearly creates a solid tablet of different macroscopic mechanical properties than the original solid. The choice to work with samples prepared in this way was dictated by a desire to continue to use the Argonne Premium Coal Samples, that are generally only available in powdered form. The gross macroscopic

mechanical properties of such pellets, e.g. tensile modulus, will clearly be different from those of a sample prepared, for example, by cutting a chunk from a virgin block of coal. In fact, any samples cut directly from coal could still be subject to naturally occurring heterogeneities in the coal, and thus mechanical properties are in that case still subject to large variations, depending upon the nature of the tests. This is not important for present purposes, because our goal is not to make use of macroscopic mechanical properties. Rather, we are here only interested in changes on the molecular level that manifest themselves as changes in a particular property.

For purposes of comparison, we examined the changes revealed by DMA in the context of changes earlier noted using thermal techniques, such as DSC and solvent swelling techniques. The detailed procedures for obtaining DSC and solvent swelling results have been reported earlier [15,16].

## RESULTS AND DISCUSSION

Raw DMA results are obtained as the frequency of oscillation and the damping signal. The frequency of oscillation is directly related to an elastic modulus of the sample, whereas the energy needed to maintain constant amplitude oscillation is a measure of damping within the sample [14]. Normally, the modulus is resolved into storage and loss moduli. The storage modulus corresponds to the perfectly elastic component whereas the loss modulus represents the perfectly viscous component. The dimensionless ratio of loss/storage components is defined as the damping factor,  $\tan \delta$ .

The tensile storage modulus, in absolute value, is comparable to what might be encountered in some polymer samples. We caution against placing too much emphasis on this absolute value, because of the issues related to pressing samples from powder. Instead, it is features that are clearly visible in the  $\tan \delta$  or loss modulus spectra that are of significance. It is the changes in storage modulus  $E'$  and loss modulus  $E''$ , and their ratio,  $\tan \delta = E''/E'$  that convey significant information about microscopic change in the material being tested. Both  $E''$  and  $\tan \delta$ , for example, are used to reveal glass transitions as maxima in the spectra. Physically,  $E'$  represents the elastic energy storage capacity of the material, whereas  $E''$  represents the energy lost as heat due to dissipation. Many other transitions, in addition to a glass transition, can cause changes in  $E''$ . Thus this parameter is a sensitive indicator of a change in the ability of molecular segments to move, relative to one another. It is this property we choose to focus on here. It should be also emphasized that in a transition, such as a glass transition, the storage modulus will normally show a slow continuous decline, whereas the loss modulus (and thus  $\tan \delta$ ) will show a distinct peak. This is what makes use of this modulus preferable for detecting transition.

In Figure 1, the first transition is seen near 60°C, for different samples of wet, as-received Pittsburgh high volatile bituminous coal. This transition is normally not visible in DSC, because it is buried beneath the water evaporation peak. The position of this peak is sensitive to the presence of moisture, as is seen from Figure 2. This behavior is typical of the effects of a "plasticizing agent" in a polymer. The molecular motions of the coal chains are enhanced at low temperatures when water is present, and internal hydrogen bonding of the coal itself is suppressed by the opportunity to hydrogen bond with a solvent (in this case, water).

The large peak that is revealed by  $\tan \delta$  above 200°C coincides with a transition shown both by DSC analysis of this coal and by a change in tetrahydrofuran (THF) swellability (see Figure 3). This transition involves an irreversible relaxation of the coal structure [16,17].

Figure 4 illustrates the behavior of Upper Freeport medium volatile bituminous coal in DMA. The tensile storage modulus exhibits a continuous decline with temperature, except for two regions of more

rapid decline in modulus. The loss modulus, and thus  $\tan \delta$ , both suggest that there is a low temperature event, again probably associated with moisture in the coal, at below 100°C. The main relaxation of structure starts to occur from 240°C, as observed in both tensile storage modulus and  $\tan \delta$ . This observation augments the DSC and solvent swelling results (see Figure 5) for the same coal, in that Upper Freeport coal showed the characteristics of a relaxed coal structure such as increased swellability in solvents and endothermic peak. In the DSC, the coal exhibited a distinct endothermic peak centered around 350°C which was started from around 310°C, whereas solvent swellability increased significantly above 250°C. It is thus confirmed by DMA that solvent swelling is a more sensitive indicator of irreversible structural relaxation than is DSC.

## CONCLUSIONS

Two bituminous coals were subjected to DMA analysis and the results were compared our earlier reported DSC and solvent swelling results. Results from different techniques appear to point to the same basic conclusions with regard to transitions, although there are subtle differences between the results of different techniques. The transition related to coal moisture is more visible in DMA and solvent swelling techniques than in DSC analysis. DMA confirms that solvent swellability is a more sensitive index of macromolecular changes than is DSC. The importance of observations made by several different techniques in order to discern transitions accurately has been noted. This study confirms the usefulness of applying different techniques simultaneously for this purpose.

We noticed that good reproducibility in DMA depends upon the reproducibility of forming pellets, in our case. A main problem was small cracks generated while the pellet was released from the press. We are further pursuing these problems in order to obtain a better description of transitions and elastic properties of coal.

**ACKNOWLEDGEMENTS** The work reported here was financially supported by the Department of Energy Contract No. DE-AC22-91PC91027 and grant DE-FG22-90PC90308.

## REFERENCES

1. Van Krevelen, D.W. In *Coal*; Elsevier, New York, 1981; Chapter XX.
2. Hiorns, F.J. *Fuel* **1953**, *32*, 113.
3. Terry, N.B. *Fuel* **1958**, *37*, 309.
4. Morgans, W.T.A.; Terry, N.B. *Fuel* **1958**, *37*, 201.
5. Hall, P.J.; Marsh, H.; Thermas, K.M., unpublished results, University of Newcastle-Upon-Tyne, 1988.
6. Brenner, D. *Prepr. Pap.-Am. Chem. Soc., Div. Fuel Chem.* **1986**, *31(1)*, 17.
7. Weller, M.; Wert, C. *Fuel* **1984**, *63*, 891.
8. Wert, C.A.; Weller, M.; Caulfield, D. *J. Appl. Phys.* **1984**, *56(9)*, 2453.
9. Wert, C.A.; Weller, M. *J. Appl. Phys.* **1982**, *53(10)*, 6505.
10. Weller, M.; Wert, C. *Int. Conf. on Coal Science* **1987**, 65.
11. Toda, Y.; Toyoda, S. *Fuel* **1972**, *51*, 199.
12. Debelak, K.A.; Schrod, J.T. *Fuel* **1979**, *58*, 732.
13. Wetton, R.E. *Polymer Testing* **1984**, *4*, 117.
14. Gill, P.S.; Lear, J.D.; Leckenby, J.N. *Polymer Testing* **1984**, *4*, 131.
15. Yun, Y.; Suuberg, E.M. *Prepr. Pap.-Am. Chem. Soc., Div. Fuel Chem.* **1992**, *37(2)*, 856.
16. Yun, Y.; Suuberg, E.M. *Fuel* **1993**, in press.
17. Yun, Y.; Suuberg, E.M. *Energy & Fuels* **1992**, *6*, 328.

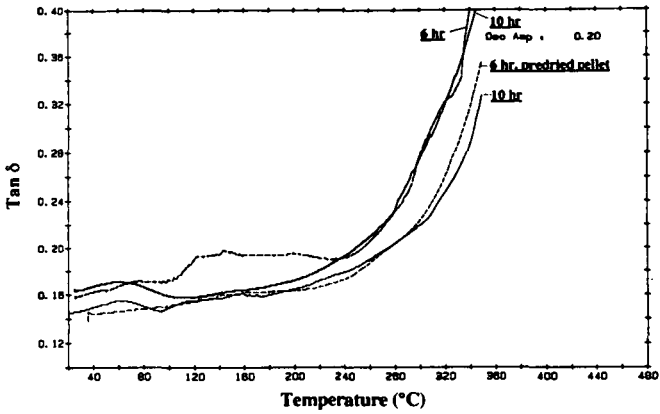


Figure 1. Tan  $\delta$  DMA spectra obtained from 4 °C/min scans of as-received and predried (up to 200°C at 4 °C/min) Pittsburgh No. 8 coal pellet samples. Pellets were made from -100 mesh powder after pressed at 15 kpsi for the duration as specified in the figure.

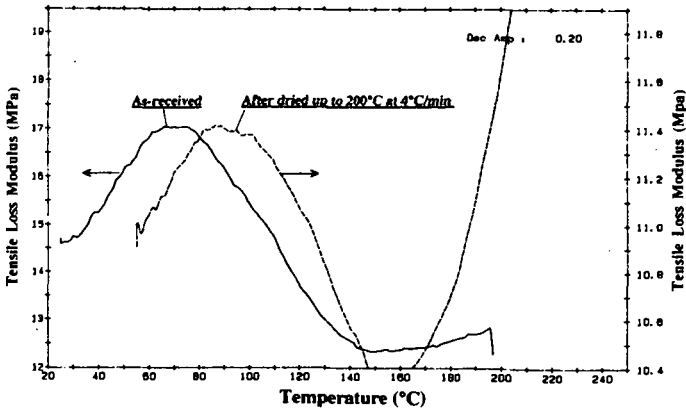


Figure 2. Effect of sample drying on tensile loss modulus obtained at 4°C/min for Pittsburgh No. 8 coal. Sample pellets were made from -100 mesh powder pressed at 15 kpsi for 10 hr.

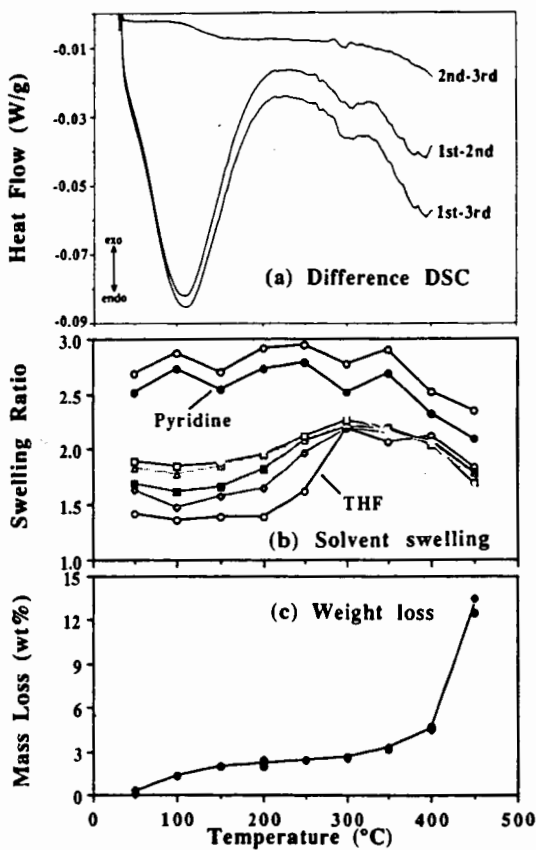


Figure 3. Difference DSC thermograms as well as profiles of solvent swelling ratio and weight loss obtained at 8 °C/min from -100 mesh Pittsburgh No. 8 coal powder (swelling time: ○, 5 hr; □, 1 day; ■, 2 days; ▲, 4 days; ▤, 5 days; ●, 6 days).

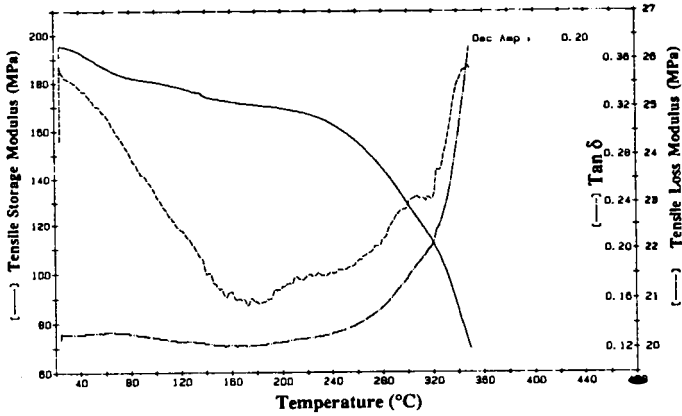


Figure 4. DMA scan of the Upper Freeport medium volatile bituminous coal obtained at 4°C/min. Sample pellet was made from -100 mesh powder pressed at 15 kpsi for 12 hr.

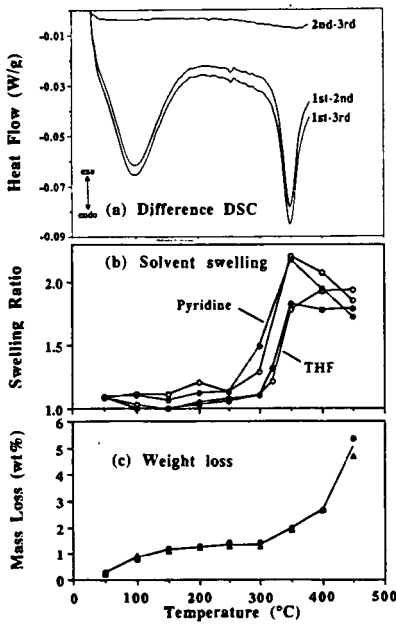


Figure 5. Difference DSC thermograms as well as profiles of solvent swelling ratio and weight loss obtained at 8°C/min from -100 mesh Upper Freeport coal powder (swelling time: ○, 5 hr; ●, 7 days).

## Assessment of Small Particle Iron Oxide Catalyst for Coal Liquefaction

Richard Anderson, Edwin N. Givens and Frank Derbyshire  
University of Kentucky Center for Applied Energy Research  
3572 Iron Works Pike, Lexington, KY 40511-8433

Keywords: Coal liquefaction, iron oxide, catalysis

### Introduction

Current efforts to lower the cost of producing coal liquids are concentrated on the use of low-rank coal feedstocks, and dispersed catalysts to promote coal dissolution in the first stage of a two-stage process. Molybdenum and iron are the most commonly investigated catalyst metals, and precursors of both can be converted to an active sulfide catalyst under liquefaction conditions.<sup>1</sup> Although iron catalysts are less active, they are preferred for reasons of economy. A great deal of research has been spent in attempting to understand the chemistry of liquefaction in the presence of iron catalysts. It has also been demonstrated that the use of powdered iron catalysts has allowed the liquefaction of subbituminous coals which could not otherwise be processed<sup>2</sup>. Nevertheless, the activity of these catalysts is still much less than desired and means to enhance their activity are under investigation.

The catalyst activity is determined principally by its composition and the extent of its dispersion with the coal or coal-solvent slurry. The catalyst dispersion is dependent upon the form and mode of addition of the catalyst precursor. High activities are reportedly favored by catalysts introduced as oil-soluble organometallic precursors such as naphthenates and carbonyls.<sup>3,4,5</sup> The results of some studies, however, indicate that even with these precursors, quite large crystallites or agglomerates can be formed during liquefaction and hence the potentially high dispersion is not maintained. There is some evidence to suggest that, if introduced as fine particulates, there is less tendency for agglomeration. Iron particles of about 50 nm mean diameter synthesized by a flame pyrolysis technique appeared to have retained their particle size and shape during presulfiding and coal liquefaction.<sup>6,7</sup> Other work has shown that FeS is more active as a colloid than in powder form.<sup>8</sup> A number of studies have reported enhanced catalytic activity by using methods of preparation that introduce nanometer size iron catalysts.<sup>9,10,11,12</sup>

The work presented in this paper is concerned principally with a systematic evaluation of the effect of reaction parameters on the catalytic conversion of a subbituminous coal using a commercially produced nanometer size iron oxide catalyst. The work is part of a DOE program to evaluate process concepts that can alone, or in concert, significantly improve process economics. In order to make realistic assessments, studies have been made using process recycle oil from the Wilsonville Advanced Coal Liquefaction Research and Development Facility and Black Thunder subbituminous coal.

### Materials

**Reagents** - Reagents were purchased as follows: Practical grade dimethyl disulfide (DMDS) from Fluka AG; 99% purity UV grade tetralin, high purity tetrahydrofuran (THF), and high purity pentane were Burdick & Jackson Brand from Baxter S/P; UHP 6000# hydrogen was supplied by Air Products and Chemicals, Inc. Coal, coal derived liquids and iron oxide used at the Wilsonville Advanced Coal Liquefaction Research and Development Facility were supplied by CONSOL, Inc.

Coal - Black Thunder subbituminous coal was ground to -200 mesh, riffled and stored under nitrogen at 4°C in a refrigerator.

Recycle oil - A reconstituted recycle oil was used in this program that had been produced at Wilsonville in runs where the plant was in the distillate production mode with all residual materials being recycled to extinction except for the organic matter occluded in the ash reject.<sup>13</sup> The Wilsonville recycle oil, taken from Run 262 while operating on Black Thunder Coal, contained 43.8 wt% 1050°F distillate, 36.6 wt% residual organic material, 9.2 wt% cresol insolubles and 10.4 wt% ash.

The fractions that were used to form the recycle oil contained significant concentrations of both molybdenum and iron which were being added as catalysts in Run 262. The ashy resid contained 3.3 wt% iron plus 300 ppm molybdenum. The distillate contained only 200 ppm of iron and 2 ppm of molybdenum. It is assumed that these metals possess some indeterminate residual catalytic activity. However, in this research, these effects are integrated into the "thermal" baseline.

Catalysts - Two iron oxide catalyst precursors were used in this study. One was a sample of the iron oxide used at Wilsonville in Run 262 (WIO) while the other was a sample of superfine iron oxide (SFIO) provided by MACH I, Inc., King of Prussia, Pennsylvania. The latter has a bulk density 1/26th that of the WIO (.052 vs. 1.37 g/ml), and a very high surface area (318 vs. 9 m<sup>2</sup>/g for WIO).

### Experimental

Equipment and Procedures - In a typical experiment 3 grams of coal, 5.4 grams of recycle oil, catalyst and DMDS (2.4 moles S/mole Fe added as catalyst) were added to the reactor. The reactor was sealed, pressurized with hydrogen to 1000 psig, and leak tested. Reactions were carried out in a fluidized sandbath set at the specified temperature while the reactor was continuously agitated at a rate of 400 cycles per minute. At the termination of the reaction period, the reactor was quenched to ambient temperature in a room temperature sand bath. The gaseous products were collected and analyzed by gas chromatography. A solvent separation technique, which is described in detail elsewhere,<sup>14</sup> was used to separate both reactants and products. The solid-liquid products were scraped from the reactor using THF and the mixture was extracted in a Soxhlet apparatus for 18 hours. The THF insoluble material, which was comprised of IOM and ash, was dried (80°C/25 mm Hg) and weighed. The THF solubles were concentrated by removing excess THF in a rotary evaporator to which a 50:1 excess volume of pentane was added to precipitate the preasphaltenes and asphaltenes (PA+A). The mixture was placed in an ultrasonic bath for 3 minutes to facilitate the precipitation process before filtering off the PA+A. The PA+A fraction was dried and weighed. This then separates the product into oils, PA+A and IOM plus ash.

Material Balance and Product Yield Computational Methods - The calculation of the yield of products differs somewhat from those reported elsewhere, in that the feed is comprised of the multiple individual Wilsonville recycle oil fractions in addition to coal and catalyst. The product distribution was determined using this same fractionation scheme assuming complete recovery of the ash plus catalyst. In this method the iron is presumed to convert to pyrrhotite and the weight of catalyst reporting to the ash fraction is calculated as the corresponding weight of Fe<sub>0.9</sub>S. By this method water produced during liquefaction is included in the oils fraction. Experimentally, complete recovery of ash and catalyst was demonstrated. Net product

yields are calculated by subtracting the amount of material contained in the feed fractions from the corresponding amounts found in the product fractions. The total of the net products equals the amount of maf coal in the feed and reflects the net make (or loss) of each of the solubility fractions while coal conversion equals 100 minus the yield of IOM.

Experimental Design - A major portion of the research reported here has been concerned with a detailed investigation of the influence of the reaction variables during coal liquefaction in the presence of added SFIO. An experimental approach was adopted that would maximize the amount of information gathered in a given series of experiments and provide a data set from which to draw valid comparisons. A full 2<sup>4</sup> factorial experimental design was developed following the method described by Box, Hunter, and Hunter.<sup>15</sup> The main effects and interactions of reaction temperature, catalyst concentration, and sulfur concentration were determined separately for each of several dependent variables including THF conversion, hydrogen consumption, CO+CO<sub>2</sub>, hydrocarbon gas, oil and PA+A yields. This technique is particularly applicable to complex reaction systems, such as coal liquefaction, where the reaction mixture is comprised of recycle oil, which itself is a composite of three process materials, coal, catalyst and hydrogen.

Because of the high concentration of metals in the recycle oil, iron oxide concentrations were selected which could have a clearly discernible effect on coal liquefaction, ranging from 1 to 4 wt% Fe on as-fed coal. Added sulfur was selected to explore a wide range of S/Fe atomic ratios, with the centerpoint at 2:1. The reaction temperatures were 390 and 440°C, centered at 415°C.

## Results

Comparison of Heavy Distillate and Recycle oil - Liquefaction of Black Thunder Coal in Wilsonville heavy 1050°F distillate at 415°C for 60 minutes gave 95 wt% THF conversion and 35.8 wt% oil yield with the addition of 1.1 wt% iron as WIO and excess DMDS for its conversion to pyrrhotite (see Table 1). The added iron catalyst had a significant effect on THF conversion and the yield of pentane solubles. Based upon previous results, distillate would exhibit little reactivity under these conditions and would not complicate the analysis of coal reactivity.<sup>16</sup>

However, coal liquefaction in the Wilsonville recycle oil produced THF conversions which regularly exceeded 100%. In a thermal run, without any added iron oxide, the THF conversion was in excess of 100%, and the oil yield was in excess of the yields observed in the run with distillate alone. The difference between the two solvents was that the recycle oil contained ashy material taken from the vacuum flash unit at Wilsonville and a smaller amount of deashed resid taken from the ROSE-SR deashing unit. The unusually high level of THF conversion and high oil yield indicated that the recycle oil IOM was being converted to soluble product.

Coal Conversion in Wilsonville recycle oil - Liquefaction of Black Thunder coal in the Wilsonville recycle oil, without added catalyst, showed steadily increasing THF conversion, oil and gas make with increasing reaction time at 415°C (see Table 2). The increases parallel the changes in yield obtained with added 1.1 wt% iron as WIO. The main effect of the catalyst was to produce a higher oil yield after 60 minutes. The results are in agreement with experimental data from pilot plant runs at Wilsonville, in which the addition of sulfided iron

oxide caused an appreciable increase in conversion.<sup>17</sup>

In both thermal and catalytic cases, the CO and CO<sub>2</sub> are formed at short times, and the yields increased only slightly between 15 to 60 minutes. In comparison, the hydrocarbon gas yield increased from 0.5 to 1.9 wt%. Much of this increase in hydrocarbon gas yield comes from the conversion of recycle oil.

Influence of Nanometer Size Iron Oxide (SFIO) - Sulfided iron oxide particles in the size range 50-80 nm, that were prepared by high temperature thermal oxidation, have been reported to show high activity for coal liquefaction.<sup>6</sup> The catalytic effect has been attributed to the high surface area and small particle size of the pyrrhotite formed upon sulfiding in the presence of coal where the pyrrhotite particles retain the small particle size of the oxide precursor.<sup>18</sup> The SFIO, whose very high surface area is consistent with nanometer size particles, may also, upon sulfiding, give rise to small particle, high surface area liquefaction catalysts.

The addition of SFIO, at a loading of 2.5 wt% iron on maf coal, produced 11 wt% more oils than in the thermal case (see Table 3). In addition there were slight increases in THF conversion and yield of hydrocarbon gases. These data represent the mid-point of the ranges for each of the three variables. The results of the comparison illustrate the potential advantage of processing with SFIO catalyst.

Impact of Reaction Variables on Liquefaction with SFIO - The R squared values for each dependent variable that was selected indicate the degree of fit by the linear model coefficients as shown in Table 4. Values for the coefficients for each of the simple linear models are summarized in Table 5. The P-value of each coefficient is shown in parentheses.

Of the independent factors, temperature has the strongest overall effect, as seen by the magnitude of the coefficients for THF conversion, hydrogen consumption, and the yields of oil and PA+A; the oil yield increases and PA+A decreases with increasing temperature. Increasing the catalyst concentration produces moderate effects on THF conversion, hydrogen consumption, and enhances the PA+A yield. However, there is no apparent effect of catalyst concentration on oil yield. It must be stressed that only two levels of catalyst concentration have been examined and the zero concentration case is not included: as shown in Table 3, the addition of catalyst significantly improves the oil yield over the thermal case. The effects of added sulfur are small, producing a weak negative coefficient with respect to THF conversion, and a negative coefficient with oil yield.

The average increase in oil yield obtained in the three centerpoint experiments was 11% over the thermal case. This is consistent with the increase of 10 wt% in oil yield predicted by the 2<sup>3</sup> factorial design experiments and lends confidence to the linear model.

The addition of 1.1 wt% added iron as WIO, which was the ratio used in the Wilsonville plant, gave 5% more oil than in the thermal case, which agrees closely with the results observed at Wilsonville.<sup>17</sup> The linear model predicts that SFIO at the lower concentration level (1.1 wt% Fe) will produce 15% higher oil yield than in the thermal case, with a decrease to the observed 11% gain at the center point due to the effect of added sulfur (see Table 6). However, the experimental check of this predicted outcome gave only 8% more oil than the thermal case. The catalytic activity of the SFIO for both oil formation and coal

conversion is greater than the corresponding activity of the WIO.

The negative effect of sulfur on THF conversion and on oil yield was unexpected based upon the results of Das Gupta, et al.,<sup>19</sup> on the liquefaction of an iron deficient Indian coal. They found, through a non-linear parameter estimation procedure, that adding sulfur up to a S/Fe atomic ratio of 8 improved conversion. In this system adding sulfur at a S/Fe atomic ratio between 0.6 to 7.4 was detrimental. This effect could be related to adverse side reactions caused by the presence of excess sulfur.

The negative interaction between temperature and SFIO concentration for oil yield indicates that thermal effects begin to dominate catalytic effects at the higher temperature. Also, in addition to thermal conversion of PA+A, the magnitude of the catalyst coefficient for the PA+A model (4.80 vs. 4.08 for THF conversion) suggests that catalytic TOM dissolution reports mainly to the PA+A fraction.

#### References

1. Derbyshire, F. J., *Catalysis in Coal Liquefaction*, IEACR/08, London, UK, IEA Coal Research, 1988, 69pp.
2. Tomlinson, G. C., Gray, D., Neuworth, M. B. and Talib, A., Report SAND85-7238, Albuquerque, NM, USA, Sandia National Laboratories, 105pp.
3. Hawk, C. O., Hiteshue, R. W., *Hydrogenation of Coal in the Batch Autoclave*. Bulletin 6322 Washington, DC, USA, US Department of the Interior, Bureau of Mines, 1965, 42pp.
4. Watanabe, Y., Yamada, O., Fujita, K., Takegami, Y. and Suzuki T., *Fuel*, 1984, 63, 752-755.
5. Suzuki, T., Yamada, O., Then, J. H., Ando, T. and Watanabe, Y., *Proceedings - 1985 ICCS*, Sydney, NSW, Australia, Pergamon Press, 1985, pp205-8.
6. Andres, M., Charcosset, H., Chiche, P., Davignon, L., Djega-Mariadassou, G., Joly, J-P. and Pregermain, S., *Fuel*, 1983, 62, 69-72.
7. Andres, M., Charcosset, H., Chiche, P., Djega-Mariadassou, G., Joly, J-P. and Pregermain, S., *Preparation of catalysts III* (Eds. G. Poncelet and P. Grange), Elsevier, 1983, pp675-682.
8. Nakao, Y., Yokoyama, S., Maekawa, Y. and Kaeriyama, K., *Fuel*, 1984, 63, 721.
9. Cugini, A. V., Utz, B. R., Krastman, D. and Hickey, R. F., *ACS Div. Fuel Chemistry Preprints*, 1991, 36 (1), 91.
10. Hager, G. T., Bi, X-X., Derbyshire, F. J., Eklund, P. C. and Stencel, J. M., *ACS Div. Fuel Chemistry Preprints*, 1991, 36 (4), 1900.
11. Pradhan, V. R., Tierney, J. W., Wender, I. and Huffman, G. P., *Energy and Fuels*, 1991, 5 (3), 497.
12. Huffman, G. P., Ganguly, B., Taghiei, M., Huggins, F. E. and Shah, N., *ACS Div. Fuel Chemistry Preprints*, 1991, 36 (2), 561.
13. Southern Electric International, Inc., *Technical Progress Report*, "Run 260 with Black Thunder Mine Subbituminous Coal", DOE Contract No. DE-AC22-90PC90033 and EPRI Contract No. RP1234-1-2, Document No. DOE/PC90033-16, January 1992.
14. Derbyshire, F., "Advance Coal Liquefaction Concepts for PETC Generic Bench-scale Unit", DOE/PC/91040-9, May 1992.
15. Box, G. E. P., Hunter, W. G. and Hunter, J. S., *Statistics for Experimenters*, John Wiley and Sons, New York (1978).
16. Anderson, R. R. and Bockrath, B. C., *Fuel*, 1984, 63, 329.
17. Southern Electric International, Inc., *Technical Progress Report*, "Integrated Two-Stage Liquefaction of Subbituminous Coal", DOE Contract No. DE-AC22-82PC50041 and EPRI RP1234-1-2,

EPRI AP-5221, Final Report, June 1987, pp 3-7.

18. Djega-Mariadassou, G., Besson, M., Brodzki, D., Charcosset, H., Huu, T. V. and Varloud, J., Fuel Processing Tech, 1986, 12, 143-145.

19. Das Gupta, R., Mitra, J. R., Dutta, B. K., Sharma, U. N., Sinha, A. K. and Mukherjee, D. K., Fuel Proc Tech, 1991, 27, 35.

**Table 1. Liquefaction of Black Thunder Coal with Wilsonville Oils<sup>a</sup>**

	Distillate <sup>b</sup>	Distillate	Composite <sup>b</sup>	Composite
Added Fe, wt% coal	none	1.1	none	1.1
% Yield, maf coal				
Gases	7.3	7.3	6.9	6.9
Oils	24.9	35.8	48.5	53.8
PA+A	54.5	51.9	52.2	45.3
IOM	13.3	5.0	-7.6	-6.0
THF Conv, wt%	86.7	95.0	107.6	106.0
Run No.	281-1	169-2	139-1/ 167-1	142-2/ 189-1

a. 415° C, 1 hour, 1000 psig H<sub>2</sub> cold, 5.4 grams recycle oil, 3.0 grams coal, 2.4 mole sulfur/mole iron.

b. No DMDS added.

**Table 2. Liquefaction of Black Thunder Coal in Wilsonville Recycle Oil<sup>a</sup>**

Yields, wt %	No Catalyst Added			1.1 wt% Fe Added		
	15 min	30 min	60 min	15 min	30 min	60 min
HC Gases	0.5	1.1	1.9	1.1	1.6	2.1
CO+CO <sub>2</sub>	4.5	5.0	5.0	4.4	4.8	4.8
Oils	21.3	36.4	48.5	20.8	36.0	53.8
PA+A	57.6	56.2	52.2	58.1	59.3	45.3
IOM	16.1	1.3	-7.6	15.6	-1.7	-6.0
Coal Conv, wt %	83.9	98.7	107.6	84.4	101.7	106.0
Run Number	148-2	167-2	139-1/ 167-1	176-1	169-1	189-1/ 142-2

a. 415° C, 1000 psig H<sub>2</sub> cold, 5.4 grams recycle oil, 3.0 grams coal, 2.4 mole sulfur/mole Fe

**Table 3. Effect of Superfine Iron Oxide on Liquefaction<sup>a</sup>**

	Thermal	SFIO	$\Delta$
Iron, wt % coal	None	2.5	
Yields, wt% maf coal			
HC Gases	1.9	2.8	0.9
CO+CO <sub>2</sub>	5.0	4.7	-0.3
Oils	48.5	59.1	10.6
PA+A	52.2	43.3	-8.9
IOM	-7.6	-9.9	-2.3
THF Conversion	107.6	109.9	2.3
Run Number	139-1/167-1	174-2/ 190-1/190-3	

a. 415°C, 1 hour, 1000 psig hydrogen cold, 5.4 grams recycle oil, 3.0 grams coal, 2.0 mole sulfur/mole iron.

**Table 4. Dependent Variables Evaluated**

<u>Effect</u>	<u>Units</u>	<u>R Squared</u>
THF Conv	THF conversion, wt% maf coal	0.926
mg H <sub>2</sub>	H <sub>2</sub> consumption, mg/g maf coal	0.973
HC Gas	Hydrocarbon gas yield, wt% maf coal	0.969
CO+CO <sub>2</sub>	CO and CO <sub>2</sub> gas yield, wt% maf coal	0.944
TGas	Total gas yield, wt% maf coal	0.961
Oils	wt% maf coal	0.880
PA+A	wt% maf coal	0.922

**Table 5. Summary of Estimated Coefficients<sup>a</sup>**

	Intercept	T <sup>b</sup> Coeff (P)	X <sup>b</sup> Coeff	S <sup>b</sup> Coeff	TxX <sup>b</sup> Coeff	TxS <sup>b</sup> Coeff	XxS <sup>b</sup> Coeff
THF Conv	107.40	4.54 (.003)	4.08 (.005)	-1.72 (.097)			-1.62 (.113)
mg H <sub>2</sub>	60.28	9.12 (.001)	2.66 (.014)		1.48 (.097)		-1.13 (.181)
HC Gas	3.50	1.86 (.001)		0.29 (.061)			
CO+CO <sub>2</sub>	5.06	0.84 (.001)		-0.20 (.046)			
TGas	8.57	2.71 (.001)					
Oils	58.61	13.87 (.001)		-5.67 (.054)	-4.60 (.100)		
PA+A	40.23	-12.03 (.005)	4.80 (.085)	3.85 (.141)	3.42 (.179)	3.52 (.169)	

- a. All three way interaction coefficients (TxXxS) are small and set equal to zero. Coefficient estimates are for coded variables (-1,0,+1).
- b. T = temperature; X = wt% Fe in SFIO on coal; S = wt% sulfur in DMDS on coal; TxX = two-way interaction of temperature with wt% Fe in SFIO on coal; TxS = two-way interaction of temperature with wt% sulfur in DMDS on coal; XxS = two-way interaction of wt% Fe in SFIO with wt% sulfur in DMDS on coal.

**Table 6. Comparison of Wilsonville and Superfine Iron Oxide<sup>a</sup>**

	Thermal	WIO	Predicted <sup>b</sup> SFIO	Experimental SFIO
Fe, wt % coal	None	1.1	1.1	1.1
Yields, wt% maf coal				
HC Gases	1.9	2.1	2.6	1.2
CO+CO <sub>2</sub>	5.0	4.8	4.9	5.0
Oils	48.5	53.8	63.7	56.9
PA+A	52.2	45.3	35.1	45.1
IOM	-7.6	-6.0	-6.3	-8.2
THF Conv.	107.6	106.0	106.3	108.2
Run Number	139-1/167-1	142-2/189-1	N/A	272-1

- a. 415°C, 1 hour, 1000 psig H<sub>2</sub> cold, 5.4 grams Wilsonville recycle oil, 3.0 grams coal, 2.4 moles sulfur/mole iron.
- b. Predicted from model parameters. All curvature detected at the mid-range conditions is accounted for as resulting from temperature effects.

## EFFECT OF A CATALYST ON THE DISSOLUTION OF BLIND CANYON COAL

Robert P. Warzinski  
U.S. Department of Energy  
Pittsburgh Energy Technology Center  
Pittsburgh, PA 15236

Keywords: coal liquefaction, dispersed catalyst, molybdenum hexacarbonyl

### INTRODUCTION

The use of catalysts to improve the dissolution and liquefaction of coal dates back to the 1920s. Reviews in this area have been prepared by Weller (1), Derbyshire (2), and Anderson (3). Recently, interest has been renewed in using dispersed catalysts in the early phases of coal liquefaction to improve the quality of the products produced during the initial dissolution and liquefaction of coal. To facilitate the study of dispersed catalysts in laboratory-scale investigations, a particular sample of Blind Canyon coal (denoted DECS-17) that contains very low levels of pyrite (0.04 wt% on a moisture-free basis) has been made available by the Department of Energy through the Penn State Coal Sample Bank. Thus, complications due to inherent catalytic activity associated with pyrrhotites which can be formed from coal pyrite are eliminated and interferences to the characterization of the added catalysts due to native iron and sulfur are reduced.

The purpose of this paper is to define the effects of a molybdenum-containing catalyst on the initial dissolution and conversion of the DECS-17 coal as a function of temperature. To eliminate competing and/or complicating influences of added solvents, the liquefaction tests were performed in the absence of such materials. The catalytic effects on coal conversion and gas uptake were determined by subtraction of thermal data from the corresponding catalytic results at a given temperature. The results provide a picture of the reactivity of the DECS-17 coal and its response to a dispersed liquefaction catalyst.

### EXPERIMENTAL

All of the experiments were performed with the DECS-17 Blind Canyon coal from the Penn State Coal Sample Bank. The coal was minus-60 mesh and was riffled prior to use. The elemental analysis (on a dry basis) provided with the coal was as follows: 76.3% carbon, 5.8% hydrogen, 1.3% nitrogen, 0.4% sulfur, 6.6% ash, and 9.7% oxygen (by difference). The moisture content of the as-received coal was 3.7%.

The liquefaction tests were conducted in 316 stainless-steel microautoclaves. The total internal volume, including connecting tubing, of the microautoclave used in most of this work was 49.0 cm<sup>3</sup>. During the tests, the microautoclave was mounted in a horizontal position and shaken in an arc motion at approximately 360 cycles per minute in a heated, fluidized sand bath.

The microautoclave was charged with 3.3 g of coal and, if used, 0.008 g of molybdenum hexacarbonyl, Mo(CO)<sub>6</sub>. The Mo(CO)<sub>6</sub> was used as received from Strem Chemical Company. Purity was given as 98 + % with moisture being the only major contaminant. No special procedures were used to mix the Mo(CO)<sub>6</sub> with the coal; the compound was simply added from a spatula directly to the microautoclave containing the coal sample.

In all of the tests, an initial charge of 1030 psig (7.20 MPa) hydrogen gas containing 3% hydrogen sulfide was added to the microautoclave after it had been pressure tested and purged with nitrogen.

A series of tests were performed of 60 minutes duration at 325°C, 350°C, 375°C, 400°C, and 425°C. A slow heat-up procedure was employed in which the microautoclave was heated along with the sandbath from room temperature to the desired reaction temperature. The longest heat-up time was approximately 60 minutes to reach the highest temperature of 425°C. The temperature was monitored by a thermocouple placed inside the microautoclave. The pressure was monitored by an electronic pressure transducer connected to the microautoclave by a section of 1/8 inch (3.2 mm) stainless-steel tubing. Time, temperature, and pressure were recorded at ten-second intervals by a PC-based data acquisition system.

At the end of the 60-minute reaction period, the microautoclave was rapidly cooled in water. The gaseous contents of the microautoclave were then measured by water displacement and a gas sample was taken. The microautoclave was then opened and the contents removed with tetrahydrofuran (THF). Sonication was used to facilitate cleaning of the microautoclave and dissolution of the products.

The reaction products were extracted with THF using pressure filtration. The THF conversion was calculated by determining the difference in the weight of the starting coal and the insoluble residue. Cyclohexane conversion was similarly determined by adding the THF-soluble material to cyclohexane and performing another pressure filtration to recover the cyclohexane-insoluble residue. The THF and cyclohexane residues were dried at 110°C under vacuum to constant weight. The conversions are reported on a dry, ash-free basis.

## RESULTS AND DISCUSSION

To determine the effects of a catalyst in coal liquefaction, it is useful to perform the liquefaction tests without added solvents or vehicles. Previous work has shown that fundamental catalyst investigations tend to be confounded if any solvents are present (1,2). In particular, the use of reactive liquids such as tetralin was found to exert a leveling effect on the influence of the catalyst on the initial conversion of coal (4). Using only coal and hydrogen magnifies the effect of the added catalyst.

In most solvent-free liquefaction work, a benefit is noted for impregnating the catalyst precursor on the coal over adding it as a powder (1,2). This is usually evident by higher conversions for the impregnated samples. To make the liquefaction tests as simple as possible, it was desirable to utilize a catalyst precursor that required few, if any, special preparation procedures to produce an active catalyst during the liquefaction test. Compounds commonly used in coal liquefaction research such as ammonium heptamolybdate, ammonium tetrathiomolybdate, and molybdenum trisulfide only perform well when special procedures are employed either to disperse or impregnate them onto the coal or to introduce them as very small particles.

$\text{Mo}(\text{CO})_6$  is not commonly used as a catalyst precursor in coal liquefaction research. While it has been shown to be an effective precursor (5,6), it is not practical for use on a larger scale. However, certain attributes of  $\text{Mo}(\text{CO})_6$  make it desirable for fundamental investigations into catalytic mechanisms relative to coal liquefaction. In particular, the

inherent volatility of  $\text{Mo}(\text{CO})_6$  permits it to form an active liquefaction catalyst ( $\text{MoS}_2$ ) in the presence of sulfur with no special preparation, impregnation, or dispersion techniques (4,6). The reactions involved in the transformation of  $\text{Mo}(\text{CO})_6$  to  $\text{MoS}_2$  appear to take place in the gas phase as the carbonyl sublimates and decomposes. Conversion of  $\text{Mo}(\text{CO})_6$  to  $\text{MoS}_2$  has been observed to occur at temperatures as low as  $100^\circ\text{C}$  in the presence of hydrogen sulfide (7).

Figure 1 shows the effect on the conversion of the DECS-17 coal of simply adding  $\text{Mo}(\text{CO})_6$  powder along with coal to the microautoclave. These tests were performed at  $425^\circ\text{C}$  using a slow heatup to reaction temperature and an initial charge of 1030 psig (7.20 MPa) hydrogen/3% hydrogen sulfide. Duplicate tests were performed with the raw coal (indicated in Figure 1 at 10 ppm) and with 100 ppm added molybdenum. Six replicate tests were performed at a level of 1000 ppm added molybdenum. The bars associated with the data points in Figure 1 indicate the range of values obtained (the results were identical for the tests with raw coal). Good conversions to both THF and cyclohexane-soluble products are noted at catalyst concentrations of 500 ppm Mo (based on daf coal) or above. These conversions are similar to those obtained with this coal when using a hydrogen-donor solvent in conjunction with more conventional catalyst precursors (8). A pronounced catalytic effect is noted even at molybdenum loadings of 50 to 100 ppm. There does not appear to be much additional benefit of using catalyst loadings above 1000 ppm.

To determine the effect of  $\text{Mo}(\text{CO})_6$  on the conversion of DECS-17 coal as a function of temperature, liquefaction tests were performed at  $25^\circ\text{C}$  intervals from  $325^\circ\text{C}$  to  $425^\circ\text{C}$  in the presence and absence of this compound. In the catalytic tests,  $\text{Mo}(\text{CO})_6$  was used at a level of 1000 ppm Mo (based on daf coal). Table I summarizes the number of replicate experiments that were performed in each case.

Table I. Number of Duplicate Tests Performed on the DECS-17 Coal.

Reaction Temperature, $^\circ\text{C}$	Number of Tests Performed	
	Thermal Tests	Catalytic Tests
325	2	2
350	4	4
375	3	2
400	4	2
425	4	6

The conversion data for the thermal and catalytic tests are shown in Figures 2A and 2B, respectively. The symbols represent the average conversion value and the bars associated with the symbols indicate the range of values obtained. No bars imply that the variability was less than two percentage points of conversion (the size of the symbols). The figures reveal that greater variability in conversion values was associated with specific conditions. For example, the greatest variabilities were associated with determinations of cyclohexane conversion for the catalytic tests. It was also noted that

the filtration of the THF solution from the catalytic test at 375°C was much more difficult than for the same product at the other temperatures, resulting in greater variability than for the same determination at the other temperatures.

It is evident from the data in Figure 2B that high conversions of the DECS-17 coal are possible with  $\text{Mo}(\text{CO})_6$  in the absence of any added solvents or vehicles. The THF and cyclohexane conversions at 425°C are over 90% and 60%, respectively. Similar conversions were previously obtained using  $\text{Mo}(\text{CO})_6$  with an Illinois No. 6 coal (6). Both the thermal and catalytic conversions increase with temperature; however, the influence of the catalyst becomes more apparent at higher temperature.

To better illustrate the effect of the catalyst, Figure 3 contains the differences obtained by subtracting the thermal conversions from the corresponding catalytic conversions. Little or no catalytic effect is observed at 325°C. Other data, which are not presented here, show that a catalytic effect is observed at this temperature at longer reaction times. As the reaction temperature increases, there is a corresponding increase in the additional amount of THF conversion due to the effect of the catalyst. The catalytic effect levels as the maximum total conversion is approached (400°C). The greatest increment to the catalytic effect on THF conversion occurs between 350°C to 375°C.

A different trend is observed for cyclohexane conversion. In this case, no activity is observed until the reaction temperature exceeds 375°C, at which point the conversion attributed to the catalyst suddenly increases. In going to 425°C, a smaller increase is noted. Figure 2A shows that the thermal conversion to cyclohexane-soluble materials increases steadily from 325°C to 425°C.

Based on the above data and observations of the resulting products, it appears that the catalyst formed from  $\text{Mo}(\text{CO})_6$  plays two separate roles in the liquefaction of the DECS-17 coal. First, it facilitates the dissolution of the coal to heavy products in a manner that parallels increases in reaction temperature. Second, it improves the conversion of these products to lighter, cyclohexane-soluble material. The onset of catalytic activity occurs at a higher temperature for the latter role. At present, it is not clear whether the difference in onset temperatures for the two catalytic functions is due to differences in activation energies for the catalytic reactions responsible for these two roles, or whether the catalyst itself changes in activity as the reaction temperature is increased. Further experiments would be required to differentiate between these effects. One possibility is that the two roles may be explained on the basis of two different chemical functions. That is, THF conversion is catalytically assisted by prevention of retrogressive reactions while cyclohexane conversion is assisted by catalysis of cracking or deoxygenation reactions.

The conversions noted above are calculated by difference using the weights of the insoluble residues collected and thus do not differentiate between the yields of liquid and gaseous products. Figure 4 shows the average production of gaseous products for the thermal and catalytic tests at the various temperatures. It is apparent that most of the gases produced are the result of thermal chemistry. The largest increase in gas production occurs between 400°C and 425°C. Only the production of butane and, to a lesser degree, propane are influenced by the presence of the catalyst. The increased production of these species again points to increased cracking activity, possibly of hydroaromatic ring structures.

Analysis of the quantity and composition of the gas released when the microautoclave was depressurized permitted calculation of the amount of hydrogen consumed during the reactions. Figure 5 compares the increment in conversion with the increment in hydrogen uptake resulting from the addition of the catalyst. The trends are similar to those in Figure 3 and are consistent with two separate roles of the catalyst. The catalytic promotion of hydrogen uptake is associated with a regular corresponding increase in THF conversion. This is not the case for cyclohexane conversion. This indicates that catalytically promoted hydrogen uptake is insufficient in and of itself to produce lighter or less functional liquefaction products. Catalytic influence on cracking or deoxygenation reactions may require higher temperatures.

The total pressure within the microautoclave was also recorded over time for each test. These data were converted to estimates of the moles of gas in the microautoclave using the ideal gas law and an experimentally derived correlation between measured pressure and reactor temperature. Figure 6 depicts the effect of the catalyst on the rate at which the amount of gas present in the microautoclave changed during the liquefaction tests at the different temperatures. The decreases noted in this figure are primarily due to the uptake of hydrogen. The results are averages of at least two sets of experiments and again are determined by subtracting the thermal data from corresponding catalytic data. The abscissa, time, includes the heat-up period and the one hour reaction time. Little influence of the catalyst on the rate of hydrogen uptake is noted at 325°C. A slightly higher rate is observed at 350°C; however, at even higher temperatures a pronounced increase in the rate of hydrogen uptake is noted. The onset of this pronounced catalytic activity occurs at about 370°C. It also appears that a limit for the catalytic influence on hydrogen uptake of about 0.016 moles is approached at 425°C. This is equivalent to 0.011 grams of hydrogen per gram of coal.

#### SUMMARY

The preliminary work presented here with the DECS-17 Blind Canyon coal shows the importance of utilizing a catalyst in the dissolution and liquefaction of this coal. Under the conditions of the tests reported here, the catalyst appears to have dual roles in the conversion to THF- and cyclohexane-soluble products. The catalyst appears to be active at 350°C with respect to formation of the THF-soluble products; however, no activity is observed with respect to cyclohexane-soluble products until 400°C.

Overall, the data show that high conversions of this coal are possible using only a dispersed catalyst (no added solvents) and hydrogen. In particular, operation at 400°C results in high conversion but with much lower gas production than at 425°C. If one is going to study the effect of a catalyst on the initial dissolution of this coal, it would be advisable to operate at temperatures below 400°C. If interest is in the production of lighter products, then 400°C or higher should be used.

#### ACKNOWLEDGMENTS

The author would like to thank Richard Hlasnik and Jerry Foster for performing the microautoclave work:

## DISCLAIMER

Reference in this report to any specific product, process, or service is to facilitate understanding and does not imply its endorsement or favoring by the United States Department of Energy.

## REFERENCES

1. Weller, S. W. Proc., Fourth International Conference on Chemistry and Uses of Molybdenum, H.F. Barry and P.C.H. Mitchell, eds., 1982, 179-186.
2. Derbyshire, F. J. Catalysis in Coal Liquefaction: New Directions for Research; IEA Coal Research: London, 1988.
3. Anderson, L. L. New Trends in Coal Science, Y. Yürüm, ed.; Kluwer Academic Publishers: Boston, 1988.
4. Warzinski, R. P. Proc., U.S. DOE Direct Liquefaction Contractors' Review Meeting, September 24-26, 1990, 320-336.
5. Suzuki, T; Yamada, H; Sears, P. L.; Watanabe, Y. Energy & Fuels 1989, **3**, 707-713.
6. Warzinski, R. P.; Lee, C.-H.; Holder, G. D. The Journal of Supercritical Fluids 1992, **5**, 60-71.
7. Warzinski, R. P. Proc., U.S. DOE Direct Liquefaction Contractors' Review Meeting, September 22-24, 1992, in press.
8. Personal communication from Anthony V. Cugini, U.S. Dept. of Energy, Pittsburgh Energy Technology Center, Pittsburgh, Pennsylvania.

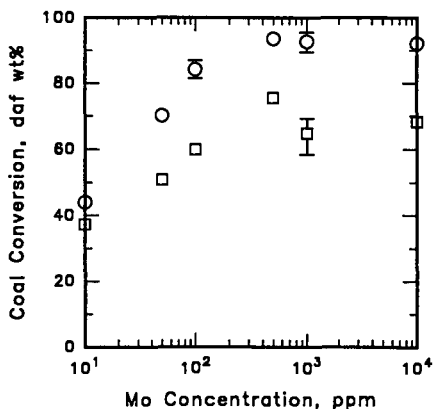


Figure 1. Effect of adding  $\text{Mo}(\text{CO})_8$  on the conversion of DECS-17 coal. (○ THF solubility; □ cyclohexane solubility. Data at 10 ppm are for raw coal.)

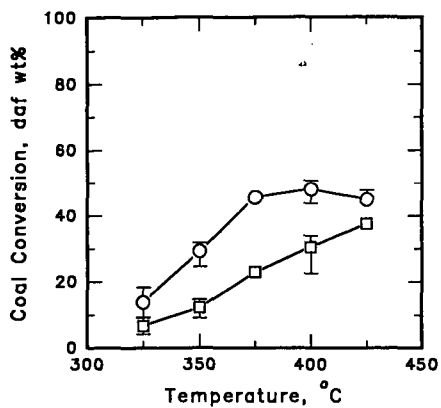


Figure 2A. Conversion results from thermal liquefaction tests. (○ THF solubility; □ cyclohexane solubility)

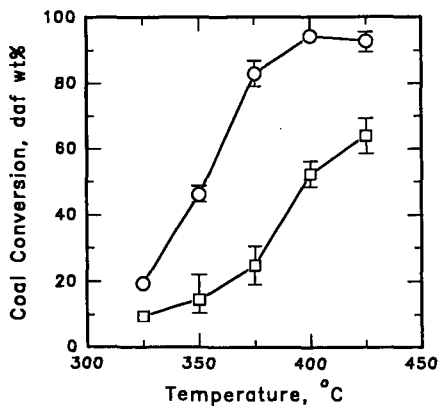


Figure 2B. Conversion results from catalytic liquefaction tests. (○ THF solubility; □ cyclohexane solubility)

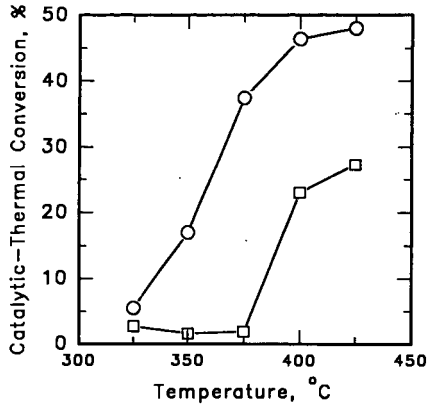


Figure 3. Catalytic-thermal conversions.  
 ( O THF solubility; □ cyclohexane solubility)

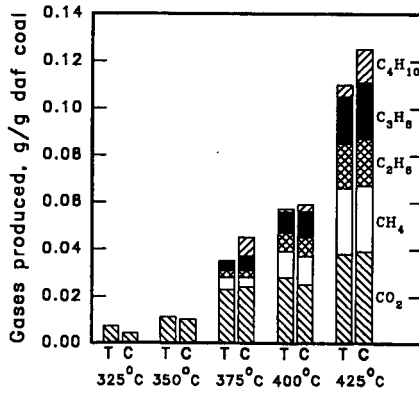


Figure 4. Average gas production for DECS-17 coal for thermal (T) and catalytic (C) tests at different temperatures (shown on abscissa).

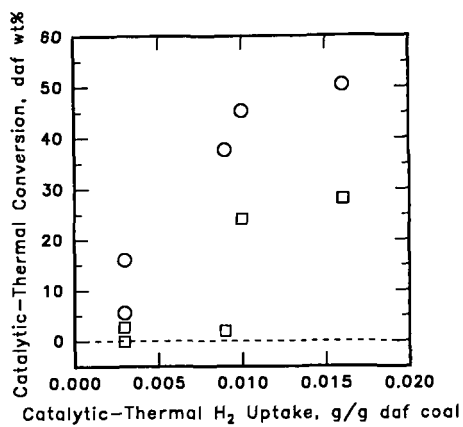


Figure 5. The effect of a catalyst on conversion as a function of the effect of a catalyst on hydrogen uptake. (○ - THF solubility; □ - cyclohexane solubility)

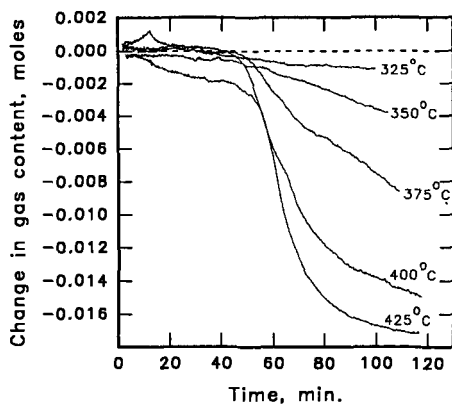


Figure 6. Effect of a catalyst on changes in gas content as a function of time and temperature. Trends are averages of catalytic-thermal data.

## EQUILIBRIUM ADSORPTION OF MOLYBDATE BY COAL

K.T. Schroeder, B.C. Bockrath, and M.L. Tate\*  
U.S. Dept. of Energy, Pittsburgh Energy Technology Center  
P.O. Box 10940, Pittsburgh, PA 15236

**Keywords:** Surface Charge, Catalyst, pH Effects

**Abstract:** To investigate the effect of solution pH on the adsorption of molybdate, two Argonne Premium coals were equilibrated with aqueous solutions of ammonium heptamolybdate at pH 2 and 4. The extent of molybdate adsorption by the coal was calculated from the decreased concentration of molybdate in solution as determined by atomic absorption. The time necessary to reach equilibrium was always less than 24 hours; the majority of the adsorption occurred within the first hour. The Wyodak coal adsorbed more molybdate with better reproducibility than did the Illinois No.6 coal. The amount of Mo adsorbed by both coals increased with a decrease in the pH of the solution and with increased concentrations of molybdate. The increased adsorption under acidic conditions is consistent with increased positive sites on the coal surface at the lower pH.

**Introduction:** Electrokinetic studies of coal-water suspensions demonstrate that the surface charge of the coal particle is dependent upon the pH of the solution.<sup>1</sup> At lower pH values, the coal surface becomes positively charged due to protonation of basic sites. For demineralized bituminous coals, the surface usually becomes positively charged below pH 6. Lower rank and oxidized coals have lower isoelectric points; they develop a net positive charge at lower pH levels.

One would expect that the ability to disperse the negatively charged catalyst precursors, such as molybdenum anions, would be affected by the charge on the coal surface. If the coal surface has a net negative charge, the molybdate anion should tend to aggregate at the small localized positive regions. Increasing the number of the positively charged regions would be expected to provide more sites for the precursor to bind. This could lead to a more evenly dispersed catalyst with a smaller particle size.

Experiments with carbon supports indicate that the mechanisms of dispersion can be related to the carbon surface chemistry.<sup>2</sup> When a number of carbons were treated with molybdate solutions at a pH above their isoelectric points, only small amounts of molybdenum were adsorbed. When the same carbons were treated in the same way at a pH lower than the carbon isoelectric point, considerably larger amounts of molybdenum were adsorbed. The higher molybdenum adsorption at lower pH was taken as evidence that the lower solution pH resulted in a more positively charged carbon particle.

The effect of surface charge on the application of dispersed phase catalysts to coals has been examined only recently.<sup>3</sup> Such effects may be important to the art of catalyst impregnation. To investigate the effect of solution pH on the adsorption of molybdate, two Argonne Premium coals were equilibrated with solutions of ammonium heptamolybdate at pH 2 and 4. The results

---

\* M.Tate was a participant in the Professional Internship Program administered by the Oak Ridge Associated Universities, Oak Ridge, Tennessee.

of these studies indicate that control of the pH during catalyst application may lead to more effective impregnation techniques.

**Experimental:** To a 1 g sample of coal in a 50-mL pyrex centrifuge tube was added 40 mL of a buffered catalyst solution. The slurry was mixed for periods from 0.5 to 24 hours at ambient temperature, then centrifuged. Aliquots (3 mL) were removed for atomic absorption analysis (AA) and the pH was measured. Mixing was then resumed. The solution pH remained relatively constant. The measured pH values over the 3 days of equilibration were  $1.90 \pm 0.06$  for the solution with an initial pH of 1.8 (20 determinations) and  $4.14 \pm 0.05$  for the solution with an initial pH of 4.1 (24 determinations). The average pH of the solutions containing larger amounts of molybdate tended to be slightly higher than those containing lower concentrations, but the difference was always less than 0.1 pH unit.

**Coals:** The Wyodak and Illinois No.6 coals were obtained from the Argonne Premium Coal sample bank'. Vials were tumbled prior to opening in accord with the Argonne instructions. The coals were pre-equilibrated with the same buffers that were used to prepare the catalyst solutions. Although the purpose of the pre-equilibration was to adjust the pH of the coal surface, it also removed all of the alkali and alkaline earth metal cations Na, K, Mg, and Ca. However, no iron was removed. It was also noted that the Illinois #6 coal samples wetted more easily and formed fewer clumps than did the Wyodak samples.

**Catalyst Solutions:** Ammonium heptamolybdate tetrahydrate (Fisher, Certified A.C.S.) was used as received to prepare the various concentrations of molybdate in two buffers listed in Table 1. Concentrations are expressed in ppm molybdenum. An additional solution at 6000 ppm formed a white precipitate, presumed to be  $MoO_3$ , after a couple of days. Because of this instability at higher concentrations, experiments were limited to solutions containing 3000 ppm or less.

**Buffer Solutions:** All solutions were prepared using deionized water which had been deaerated by purging with argon for at least 30 minutes prior to use. An acetate buffer of nominal pH 4 was prepared using acetic acid and sodium acetate. This gave a solution with a measured pH of 4.1. Similarly, a sulfate buffer of nominal pH 2 was prepared using sulfuric acid and sodium sulfate. This gave a solution with a measured pH of 1.8.

**Calculations:** The molybdate on the coal was calculated from the loss of molybdate from solution according to the equation

$$Mo_{coal,i} = Mo_{coal,i-1} + (Mo_{soln,i-1} - Mo_{soln,i}) \frac{V_{soln,i}}{W_{coal}}$$

where  $Mo_{coal}$  is the molybdenum concentration in ppm on the coal,  $Mo_{soln}$  is the molybdenum concentration in the solution in ppm,  $Vol_{soln}$  is the volume of solution remaining in mL, and  $W_{coal}$  is the weight of the coal in grams. It was necessary to take into account the change in volume of the solution with each successive sample  $i$ , because the aliquot size was not negligible in comparison to the solution volume. The concentration of molybdate in solution was measured by AA as described below.

**AA Analysis:** Atomic Absorption (AA) analyses were performed using a Perkin Elmer Model 503 flame atomic absorption spectrophotometer. Ammonium chloride modifier was added to provide a final concentration of 1% in all determinations. The molybdenum

concentration was determined by reference to a linear regression calibration curve derived from four standard solutions ranging from 0 to 10 ppm Mo. Samples which exceeded this range were diluted as needed to fall within the calibrated range.

The agreement of the AA results with the concentrations determined from the weights of molybdate and buffer used in the solution preparations is shown in Table 1. The last column of the Table lists the concentration determined by AA and the fifth column lists the concentration of Mo determined gravimetrically in each of the solutions used in this study. The agreement between the two determinations is very good; the gravimetric determination is always within two standard deviation units of the AA result and is often within one unit. There may be a small bias in one of the methods since the gravimetric determination is always lower than the AA determination, but the difference is considered insignificant for the purpose of these experiments.

The standard deviations and relative standard deviations were derived from a series of control samples analyzed over the several days of the experiment. The magnitudes of the deviations are similar to those found for the AA technique itself. For example, the nominal 600 ppm controls gave a standard deviation of 27 ppm at both pH levels. This compares favorably with the precision of the AA technique of 42 ppm as determined in separate quality assurance experiments. Thus, the solutions themselves were stable with time and precipitation cannot account for the loss of Mo from solution. A false positive was never obtained for blank samples which were also analyzed routinely in single blind experiments.

**Results:** Aqueous solutions of ammonium heptamolybdate containing up to 3000 ppm molybdenum were allowed to equilibrate with samples of the Argonne Premium Wyodak and Illinois No.6 coals. The loss of molybdate from solution was monitored by AA analyses of aliquots of the supernatant solution. The results obtained using the Wyodak coal at a pH of 2 are shown in Figure 1. Molybdate was adsorbed quickly and equilibration occurred within the first 24 hours. At the lowest initial concentration, 60 ppm, the adsorption of Mo was complete; the supernatant solution contained no detectable Mo after the first hour of contact. At 600 ppm, 90% of the Mo was adsorbed resulting in about 2 g of molybdenum being adsorbed per 100 g of as-received Wyodak coal. Increasing the solution concentration by a factor of 2.5 to 1500 ppm resulted in increased adsorption by a factor of about 2. A further doubling to 3000 ppm resulted in an even smaller incremental increase in adsorption, indicating that the amount of molybdate that can be adsorbed is limited. Inspection of the graphs in Figure 1 suggests that under these conditions the limiting value is in the neighborhood of 5%.

Buffering the solution pH to 4 resulted in less molybdate adsorption, as can be seen in Figure 2. Although increasing the initial Mo concentration from 60 through 600 to 3000 ppm resulted in increased amounts of Mo being adsorbed, the equilibrium values are noticeably lower at this higher pH. For the case at 3000 ppm, equilibration at a pH of 4 resulted in the coal adsorbing 3.4% of its weight in Mo; equilibration at a pH of 2 resulted in 4.3% adsorption by coal. Only at 60 ppm where both solutions were depleted in Mo was the amount adsorbed the same. Thus, lowering the pH of the medium effects a larger adsorption of molybdate from solution.

Different levels of adsorption occurred when a bituminous coal was used. Similar experiments using the Argonne Illinois No.6 coal resulted in the data presented in Figures 3 & 4. In contrast to the rather smooth trends discernible at all Mo concentrations for the Wyodak coal, the results for the Illinois coal contained appreciable scatter at the highest Mo concentration. Despite this scatter, some comparisons between the Wyodak and Illinois coals can be made by focusing on the results obtained at the 60 and 600 ppm concentrations. At these lower initial molybdenum concentrations, a rapid equilibration apparent within the first 24 hours was consistent with the rapid equilibration seen for the Wyodak coal. However, the amount of Mo adsorbed was much smaller than was seen for the lower rank coal. At 60 ppm, the molybdenum adsorbed was barely above the detection limits at a pH of 2 and at the detection limits at a pH of 4. By contrast, the Wyodak coal adsorbed all of the available Mo under similar conditions. At an initial Mo concentration of 600 ppm, the amount of Mo adsorbed by the Illinois No.6 coal is only 10% of that adsorbed by the Wyodak coal. Thus, on a weight basis, the Wyodak coal is 10 times more effective at adsorbing molybdenum anions than is the Illinois coal at a pH of 2. Substituting a pH 4 buffer (Figure 4) for the pH 2 buffer (Figure 3) effected an even greater decrease in Mo adsorption for the Illinois No.6 coal than it did for the Wyodak coal. At the 600 ppm level, the higher pH resulted in the coal adsorbing only 0.13% of its weight in molybdate instead of the 0.51% seen at the lower pH. Thus, the Illinois No.6 coal adsorbs less Mo from solution than does the Wyodak coal and the amount adsorbed is more sensitive to the pH of the aqueous solution.

**DISCUSSION:** The results obtained for these two coals appear to be consistent with an adsorption mechanism in which molybdate in solution is in equilibrium with surface-bound molybdate. The extent of surface adsorption is expected to depend on both the concentration of molybdenum in solution and the number of adsorption sites available on the coal surface. Because the coal surface develops more net positive charge at the lower pH, more anion binding sites are expected to become available. Thus, both increasing molybdate concentration and decreasing pH are expected to result in more molybdate being removed from solution.

However, the nature of the molybdenum species in solution changes with changes in total concentration of molybdenum(VI) and pH.<sup>5</sup> For example, at a total Mo(VI) concentration of 50 ppm the predominate species is  $\text{Mo}(\text{OH})_6$  at a pH of 2, but  $\text{MoO}_4^{2-}$  predominates at a pH of 4. At a total Mo(VI) concentration of 2000 ppm the predominate species is  $\text{Mo}_2\text{O}_7^{4-}$  at a pH of 2, whereas  $\text{HMo}_2\text{O}_7^{3-}$  predominates at a pH of 4. This rich chemistry provides alternate explanations to the observed adsorption trends. Each of these species as well as a number of other minor species may all adsorb with different equilibrium constants. Thus, the details of the adsorption mechanism are not clear.

The adsorption sites on the coals are effected by the solution pH. These sites may reside in the organic portion, the mineral portion, or both portions of the coal. Organic functional groups play an important role in the electrokinetic behavior of coal-water suspensions<sup>1</sup> and the adsorption of molybdate by carbon supports can be related, in part, to the degree of surface oxidation.<sup>2</sup> Nitrogen heteroatoms, which become positively charged in acid, may also play an important role. It is interesting to note that an atomic Mo to nitrogen ratio of 1 corresponds to a 5

weight % Mo loading on the Wyodak coal. Thus, it is reasonable to suspect that the extent of molybdate adsorption and the pH dependence are related to the organic heteroatom content. Also, mineral matter may play an important role in the adsorption. The protonation of alumina hydroxyl groups is responsible for the creation of adsorption sites for molybdate on catalyst supports.<sup>6</sup> The clays or other minerals in the coal could behave in a similar fashion.

It is of interest to compare these results with those obtained for some other coal samples. Table 2 compares the results obtained by Abotsi et al.<sup>3</sup> with the results obtained here. Since some of the experimental procedures are different, and the coals are not identical, the results are not strictly comparable. The solution concentration used by Abotsi was 4800 ppm whereas our highest concentration was 3000 ppm. However, the main points are readily discernable. There is a fairly large difference in the % Mo adsorbed between the bituminous and subbituminous coals. This may be due to the higher oxygen content of the latter. However, there are also differences within rank. The Montana Rosebud subbituminous coal (PSOC 1493) adsorbed about half as much Mo as did the Wyodak coal. Thus, the nature of the coal is also important to the adsorption mechanism.

**CONCLUSIONS:** The extent of molybdate adsorption by coal is affected by the nature of the coal and the pH and molybdate concentration of the equilibration solution. Lower pH and higher molybdate concentrations favor molybdate adsorption. Such effects may be important to the art of catalyst impregnation.

**ACKNOWLEDGEMENTS:** The authors thank Ms. Deborah Hreha and Ms. Jodi Schuster who performed the AA analyses reported in this work and José Solar for many helpful discussions.

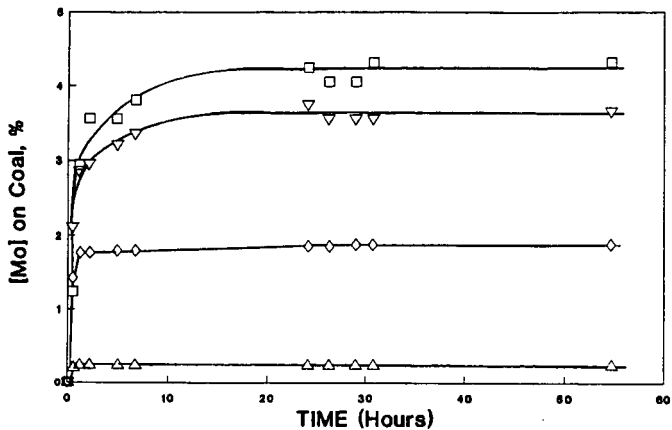
**DISCLAIMER:** Reference in this report to any specific commercial product, process, or service is to facilitate understanding and does not necessarily imply its endorsement or favoring by the U.S. Department of Energy.

#### **REFERENCES**

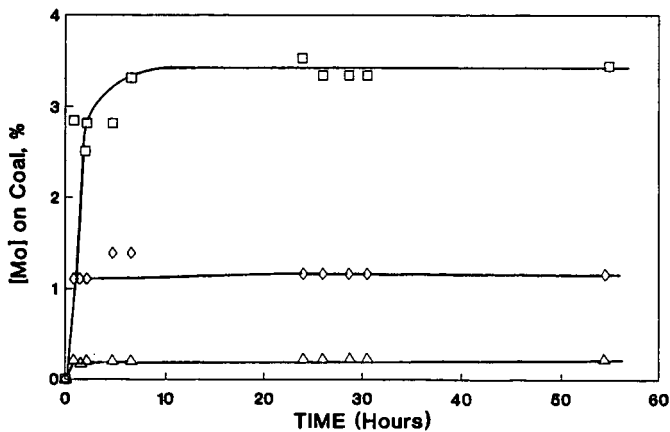
1. Laskowski, J.S.; Parfitt, G.D. *Surfactant Sci. Ser.* 1989, **32**, 279-327.
2. Solar, J.M.; Leon y Leon, C.A.; Osseo-Asare, K. Radovic, L.R. *Carbon* 1990, **28**(2/3), 369-375.
3. Abotsi, G.M.K.; Bota, K.B.; Saha, G. *Energy Fuels* 1992, **6**(6), 779-782.
4. Vorres, K.S. *Energy Fuels* 1990, **4**, 420-426.
5. Cruywagen, J.J.; De Wet, H.F. *Polyhedron* 1988, **7**(7), 547-556.
6. Spanos, N.; Vordonis, L.; Kordulis, Ch.; Lycourghiotis, A. *J. Catal.* 1990, **124**, 301-314.

Table 1. Concentration of Molybdenum in Buffered Solutions					
Nominal pH	Nominal Concentration (ppm Mo)	Ammonium Heptamolybdate (grams)	Amount of Buffer (grams)	Calculated Concentration (ppm Mo)	Concentration Measured by AA (ppm Mo)
4	60	0.0116	100.72	63	66±5 (±8%)
	600	0.1078	100.37	583	598±26 (±4%)
	3000	0.5487	100.20	2960	2968±225 (±8%)
2	60	0.0114	100.60	62	66±5 (±8%)
	600	0.1077	101.46	576	584±27 (±5%)
	1500	0.1325	50.21	1430	1550±71 (±5%)
	3000	0.5484	100.22	2957	3152±175 (±6%)

TABLE 2. Comparison of Molybdate Adsorption for Different Coals			
COAL	pH	% Mo on Coal (Ref. 3)	% Mo on Coal (This Work)
SUBBITUMINOUS	2	2.11	4.1
	4	1.25	3.5
BITUMINOUS	2	0.29	≥0.5
	4	0.19	≥0.3



**FIGURE 1.** Adsorption of Molybdate from Solution by Wyodak Coal at a pH of 2.  $\square$  Initial solution concentration = 3000 ppm.  $\nabla$  Initial solution concentration = 1500 ppm.  $\diamond$  Initial solution concentration = 600 ppm.  $\triangle$  Initial solution concentration = 60 ppm.



**FIGURE 2.** Adsorption of Molybdate from Solution by Wyodak Coal at a pH of 4. Symbols the same as on Figure 1.

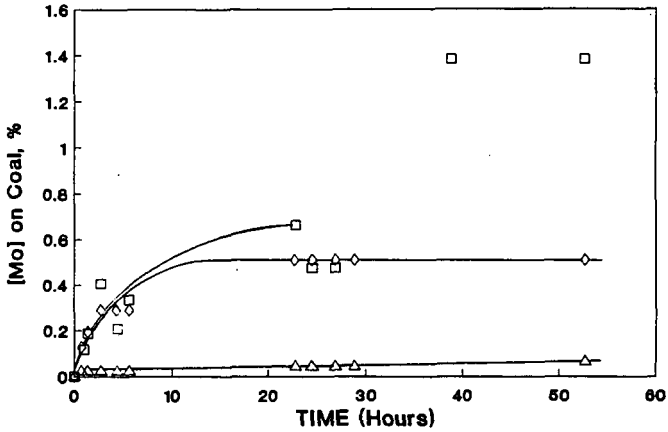


**FIGURE 3.** Adsorption of Molybdate from Solution by Illinois No.6 Coal at a pH of 2. Symbols the same as on Figure 1.

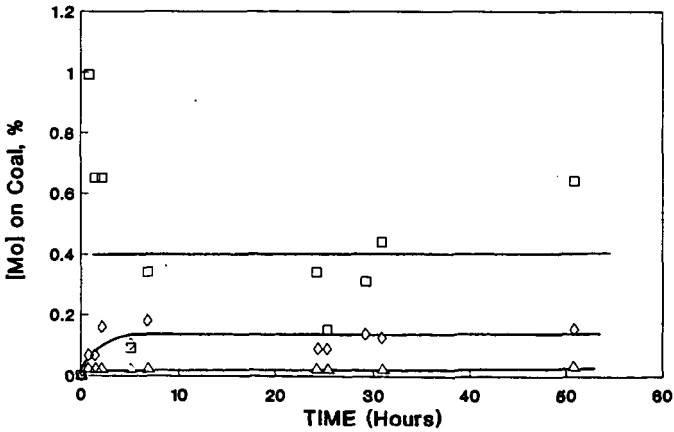


**FIGURE 4.** Adsorption of Molybdate from Solution by Illinois No.6 Coal at a pH of 4. Symbols the same as on Figure 1.

## Empirical Evaluation of Coal Affinity for Various Chemicals

Tetsuo Aida\*<sup>1</sup>, Shuhsaku Suzuki<sup>1</sup>, Masayuki Fujii<sup>1</sup>  
Masakuni Yoshihara<sup>2</sup>, Teijiro Yonezawa<sup>2</sup>

<sup>1</sup>Department of Industrial Chemistry, Faculty of Engineering in Kyushu  
Kinki University

11-6 Kayanomori, Iizuka, Fukuoka 820, JAPAN

<sup>2</sup>Department of Applied Chemistry, Faculty of Science and Engineering  
Kinki University

3-4-1 Kowakae, Higashi-Osaka 577, JAPAN

### INTRODUCTION

Coal is a complicated natural product which has several functional groups in its cross-linked macromolecular structure. Because of this fact the diffusion mechanism of the penetrant molecule into the matrix of a solid coal is not so simple. It is quite important to know the affinity between the penetrant molecule and the macromolecular structure of coal for the coal scientists who are challenging to develop efficient chemical transformations of coal such as liquifaction, gasification and etc.. Nevertheless the reliable methodology to determine the affinity has not yet been developed. One of the most practical approach to this goal will be to use the solvent swelling behaviours of coal. Because as it is mostly true that better solvent makes coal better swelling, the equilibrium swelling value(Q-value) of the penetrant may reasonably reflect its affinity to the coal. However, there are some problems in this idea. One of the most critical problems will be how to determine the Q-value of solvents(chemicals) which used to be a solid(crystal) under the measuring condition. Furthermore the steric bulkiness of the penetrant molecule also will provide an aserious error on the net Q-values(1).

Some years ago, we revealed the steric requirement of coal toward the penetrant molecule is significantly relaxed in binary solvent system which is composed with normal solvent such as methanol or DMF and sterically hindered molecule(i.e., triethylamine or HMPA)(2). The mechanism of the relaxation of the steric requirement of coal is considered as follows; the preferential petration of the normal solvent into solid coal makes the coal-solvent gel. Then, the significant expansion of the cross-linked network of coal is induced and thus it makes the bulky molecule easy to penetrate. These findings hinted us to use this swelling system for evaluating the affinity of various chemicals toward coal.

This paper presents the results of the studies on the new methodology to evaluate the coal affinity of various chemicals.

### EXPERIMENTAL

The swelling measurements were carried out as described into previous paper(3). Coal, Illinois No.6 coal, used in these studies was from the Ames Laboratory Coal Library. Prior to use, the coal was ground, sized, dried at 110°C overnight under vacuum, and stored under a nitrogen atmosphere. The solvents were distilled by ordinary procedures before use.

---

This work was supported by the grant from The Japanese Ministry of Education, during 1989-1992.

## RESULTS AND DISCUSSION

### Swelling of Illinois No. 6 Coal in Various Solvent

Coal swells in the various solvent with the different manners. Figure 1 shows the relation between the equilibrium swelling value of the solvent which were determined by our instrument and its electron donor number(DN). This type of data treatment had been reported by Marzec et al.(4), and they recognized some correlation between them. However as far as the data shown in this Figure, it seems to be quite difficult to find out such correlation. As we discussed before(1), one of the problems in this figure is that the Q-values measured always involve their steric factor, that is, the sterically hindered solvents are restricted the penetration into the macromolecular structure of coal by the steric requirement, probably due to the cross-linking density. If in this Figure we can pick up only the solvents which are not sterically bulky and also have relatively high dielectric constant(>20), the correlation becomes very clear and almost linear as shown in Figure 2. It is quite interesting that the dielectric constant of the penetrant also seems to be one of the key parameters controlling the coal affinity. This fact may suggest that there are the significant contribution to the macromolecular cross-linking structure of coal from relatively weak bonding interactions such as van der Waals, hydrogen bonding, charge transfer bonding and  $\pi$ - $\pi$  bonding.

### Introduction of Coal Affinity Parameter

Although these data shown above suggest the possibility to use the equilibrium swelling value(Q-value) as a convenient scale for evaluating the affinity to the coal, there seems to be at least two big problems, that is, the first of all is how to determine the Q-value of solid chemicals(crystal) by means of the solvent swelling measurement, and the second of all is how to eliminate the steric factor from the observed Q-value.

Table 1 summarizes the swelling behaviours of Illinois No.6 coal in the steric isomers of butylamine. It is obvious that there is a significant steric requirement on their swelling which is reflected not only on the swelling rate(V-value), but also on the Q-value. Thus, the Q-value measured in the neat solvent always involves the contribution from the steric factor. Namely, in order to use the Q-value as a tool for evaluating the coal affinity, we have to find out the methodology to extract the net Q-value from the observed one.

Figure 3 demonstrate the swelling behaviour of Illinois No.6 coal in the binary mixture of the butylamine and methanol. In the case of n-butylamine-methanol system, the observed Q-values have a nice linear relationship versus the concentration. Meanwhile in the mixed system of more sterically bulkier isomers such as sec- and tert-amine a kind of the synergistic effect were observed. It is particularly interesting that the values obtained by the extrapolation(dotted line on the Figure) from the Q-value at the lower concentration region seems to reasonably reflect their own values. We had revealed this phenomena as the relaxation of the steric requirement by the coa-gel formation(2). Now, we may be able to define for the extrapolated values obtained on the Figure to be their potential Q-value( $Q_{pot}$ ) which used to be hidden by the steric factor.

If these speculation are correct, we can use this swelling system as a general procedure for evaluating the coal affinity. Namely, as far as the chemicals are soluble in the solvent (reference solvent), gas, liquid even solid or crystal, the potential Q-value( $Q_{pot}$ ) must be empirically determined by this method. Furthermore, very fortunately, because of the binary solvent system the steric factor in the observed Q-value can be minimized.

Based on these considerations, we propose a new empirical parameter to evaluate the affinity to the macromolecular structure of coal, as the Coal Affinity Parameter( $\kappa_Q$ ) which is calculated following equation.

$$\kappa_Q = Q_{pot} / Q_{DMF}$$

In this study we have adopted N,N'-dimethylformamide(DMF) as the reference solvent. The reason is that it has a powerful ability to solve many kinds of chemicals even inorganic compounds and it is also easy to purified.

Table 2 summarizes the typical example of Coal Affinity Parameter( $\kappa_Q$ -value) determined for various chemicals. In these data it is particularly interesting that the  $\beta$ -naphthol(mp 122-123°C), nitrobenzene and maleic anhydride(mp 54-56°C) have higher  $\kappa_Q$ -values than pyridine. These compounds have long been assumed to have reasonably good affinity to coal, but their relative abilities were never compared.

Figure 5 shows the relation between Coal Affinity Parameter( $\kappa_Q$ -value) and the electron donor number(DN). Surprisingly, a good correlation was observed towards wide range of organic compounds. particularly, a solid(crystal) compound such as ethylenecarbonate(mp.35°C) and a sterically hindered compound such as hexamethylphosphoramide(HMPA) in which coal used to give very small degree of swelling, probably because of the steric hindrance. As previously discussed there seems to be reasonable relationship between coal affinity and electron donor number(DN), and now we can see a similar relation between the Coal Affinity Parameter( $\kappa_Q$ -value) and DN. Although this methodology proposed may not be a perfect one to evaluate the affinity to coal, but as far as the results shown in this Figure and Table 2, we are very much encouraged to use the  $\kappa_Q$ -value for the study on the chemical transformations of coal.

It will be also interesting to examine the dependency of  $\kappa_Q$ -value on the coal rank or the nature of the reference solvent, which are now underway in our laboratory.

#### ACKNOWLEDGEMENTS

This research was supported by the grant from the Japanese Ministry of Education(Kagaku Kenkyuho Hojokin, Juhten Ryouiki Kenkyu) during 1989-1992.

#### REFERENCES

- (1) T. Aida, K. Fuku, M. Fujii, M. Yoshihara, T. Maeshima, T. G. Squires, *Energy & Fuels*, **5**, 79(1991)
- (2) T. Aida, Y. Shimoura, N. Yamawaki, M. Fujii, T.G. Squires, M. Yoshihara, T. Maeshima, *Prepr. Pap.-Am. Chem. Soc., Div. Fuel Chem.*, **33**, 968(1988)
- (3) T. Aida, T.G. Squires, *Prepr. Pap.-Am. Chem. Soc., Div. Fuel Chem.*, **30**, 95(1985)
- (4) J. Szeliga, A. Marzec, *Fuel*, **62**, 1229(1983)

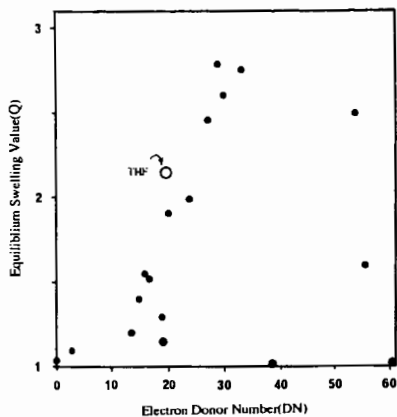


Figure 1 Correlation between Q-value and Electron Donor Number(DN)  
(Illinois No. 6 Coal: 60-100mesh; at 20°C)

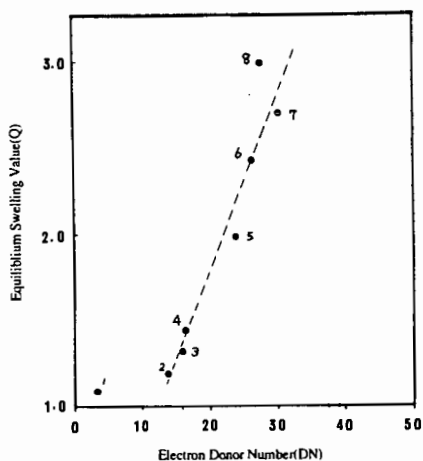


Figure 2 Correlation between Q-value and Electron Donor Number(DN)  
(Illinois No. 3 Coal: 60-100mesh; at 20°C)  
SOLVENT: 1 nitroethane, 2 acetonitrile, 3 n-butylamine, 4 acetone,  
5 trimethylphosphane, 6 DMF, 7 DMSO, 8 N-methylpyrrolidone

Table 1 Solvent Swelling of Illinois No. 6 Coal<sup>a</sup> in  
Butylamines at 20.0 ± 0.5 °C

amine	$V_{ret}^b$	$Q^c$	$\eta_{20}^d$ cP	CSA <sup>e</sup>
n-butylamine	1.0	2.56	1.54	32.7
isobutylamine	11.9	2.57		32.8
sec-butylamine	5.4	2.41	1.37	33.2
tert-butylamine	599	1.96 <sup>e</sup>	1.48	34.1

<sup>a</sup>100-200 US mesh. <sup>b</sup> $V_{ret} = V_{n-Bu} / V_{isomer}$ ;  $V_{n-Bu} = 3.7 \times 10^{-1}$  min<sup>-1</sup>. <sup>c</sup>Measured after 10 days' swelling. <sup>d</sup>Determined by means of Ubbelohde viscometer at 20.00 ± 0.02 °C. <sup>e</sup>Swelling is still continuing.

<sup>e</sup> Cross-sectional Area( Å<sup>2</sup> )

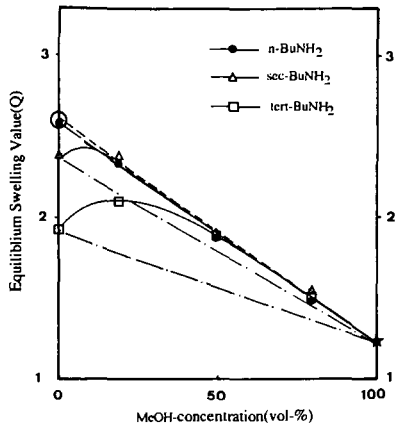


Figure 3 Coal Swelling in Binary mixture (Illinois No. 6 Coal; 60-100mesh; at 20°C)

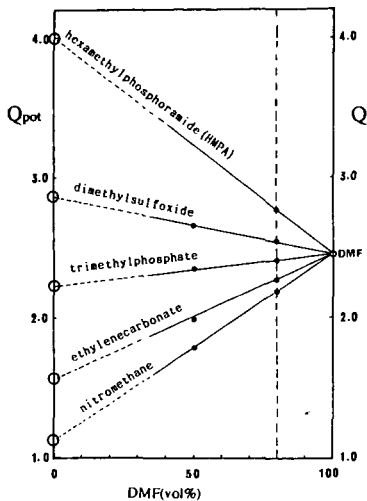


Figure 4 Determination of Potential Q-value ( $Q_{pot}$ ) (Illinois No. 6 Coal; 60-100mesh; at 20°C)

Table 2  $\kappa_Q$ -values of various Chemicals (Illinois No. 6 Coal; 60-100mesh; at 20°C)

Chemicals	$^{\circ}\kappa_Q$
nitromethane	0.43
acetonitrile	0.41
n-butyronitrile	0.52
ethylenecarbonate	0.61
acetone	0.68
trimethylphosphate	0.88
DMF	1.00
pyridine	1.08
DMSO	1.14
N-methylpyrrolidinone	1.21
HMPA	1.62
nitrobenzene	1.13
b-naphthol	1.22
maleic anhydride	1.30
benzoic acid	0.80

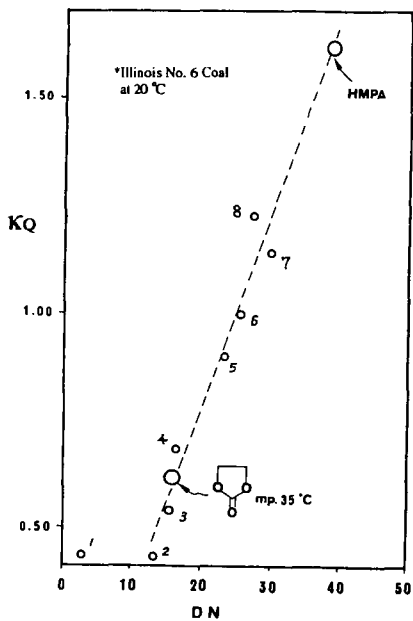


Figure 5 Correlation between  $K_Q$ -value and Electron Donor Number(DN)  
(Illinois No. 6 Coal; 60-100mesh; at 20°C)

SOLVENT : 1 nitromethane, 2 acetonitrile, 3 n-butyl nitrile, 4 acetone,  
5 trimethylphosphate, 6 DMF, 7 DMSO, 8 N-methylpyrrolidone

PROMOTION OF DEUTERIUM INCORPORATION FROM D<sub>2</sub> INTO  
COAL MODEL COMPOUNDS BY BENZYLIC RADICALS

Robert D. Guthrie  
Buchang Shi  
Rustem Sharipov  
Department of Chemistry  
University of Kentucky  
Lexington, KY 40506

Burtron H. Davis  
Kentucky Center for Applied Energy Research  
3572 Iron Works Pike, Lexington, KY 40511

Keywords: D<sub>2</sub>, hydroliquefaction, diphenylethane

INTRODUCTION

A large number of revealing mechanistic investigations have been carried out dealing with the thermolysis of coal and compounds which model its structure. Perhaps because of experimental difficulties, much less attention has been given to the reaction with molecular hydrogen. It seems fair to say that the detailed mechanism by which molecular hydrogen, separately or in combination with "donor solvents", is able to effect the reductive simplification of coal is not completely understood. An obvious approach to following the reaction with H<sub>2</sub> is to substitute D<sub>2</sub>. The literature contains ample evidence that deuterium is incorporated into reaction products when thermolysis of coal and coal models is carried out under D<sub>2</sub> gas.<sup>1</sup> It has also been shown that D-labeled substrates, such as tetralin-d<sub>12</sub>, transfer D atoms back to dihydrogen such that HD is produced from H<sub>2</sub>.<sup>2</sup>

Similarly it is clear that once incorporated into a molecule of organic substrate, transfer of D atoms between molecules is often facile.<sup>3</sup> Several mechanisms can be involved in the scrambling process. Molecule-induced homolysis and symmetry-allowed, pericyclic mechanisms have been documented by Brower and Pajak.<sup>4</sup> A demonstration of radical-promoted exchange was provided by King and Stock<sup>5</sup> who showed that the presence of species which undergo facile homolysis increases the rate of transfer of deuterium between benzylic positions in different molecules. The mechanisms suggested seem reasonable, however, most of the proposed schemes do not address the question of how the initial transfer from H<sub>2</sub> occurs.

The facility of the scrambling reactions makes the question of how the hydrogen is transferred from H<sub>2</sub> gas into the coal structure in the first place, a particularly difficult one to answer because the initial landing site of the hydrogen atoms is rendered uncertain. Because the H-H bond is quite strong, this initial step would seem likely to be a major obstacle to the process of interest and slower than subsequent events. A scheme put forward by Vernon<sup>6</sup> proposes hydrogen abstraction from H<sub>2</sub> by benzyl-type radicals. This suggestion was later supported by Shin.<sup>7</sup> Vernon's suggestion is based on the observation that the cleavage of 1,2-diphenylethane, DPE, gives an increased yield of benzene when the reaction is carried out under H<sub>2</sub>. The phenomenon is more pronounced when the reactions are run in the absence of a hydrogen atom donor (tetralin or 9,10-dihydrophenanthrene). It is suggested that benzyl radicals react with dihydrogen, producing toluene and

hydrogen atoms. The hydrogen atoms thus generated are responsible for the hydrogenolysis of the DPE to give benzene. In the presence of hydrogen donor solvents, the benzyl radicals react to give toluene and the production of H atoms is reduced. The latter part of this scheme seems quite reasonable based on the observed facility of reaction between benzyl radicals and compounds with structures similar to donor solvents.<sup>8</sup> Likewise, the reaction of hydrogen atoms with the aromatic ring of DPE seems reasonable both on energetic grounds and in consideration of the results of Price<sup>9</sup> who showed that H-atoms generated in the thermolysis of toluene above 500 °C react with toluene to produce CH<sub>3</sub> and H<sub>2</sub> with nearly equal rates. The reaction between benzyl radicals and H<sub>2</sub> seems the most uncertain part of the scheme in that the C-H bond energy of toluene is 85 kcal/mole where as that of H-H is 104 kcal/mole.<sup>10</sup> The reaction of benzyl radical with dihydrogen to form toluene and hydrogen atoms is thus likely to have an activation enthalpy of more than 20 kcal/mole. This would seem to make it an unlikely competitor with various other potential reactions of benzyl radicals which are possible in the system studied.

An additional uncertainty regarding these reactions, is that most of the reported exchange studies using D<sub>2</sub> as a source of deuterium had utilized metal reactor vessels. This raised the question of whether the initial process for introduction of D atoms into the thermolysis milieu might be metal catalyzed. Either the walls of the reaction vessel or metal species contained in common reactor vessel sealants are possible stopover points for D atoms prior to their introduction at the seminal sites for the scrambling process. If these were involved, the well-precedented process of double bond reduction by metal-bound deuterium would then be a likely entry route for D atoms. In cases where liquefaction is accomplished by the deliberate addition of hydrogenation catalysts, this would be the expected mechanism.<sup>11</sup> As we wished to understand the noncatalyzed reaction and to use it as a base line for further studies of catalytic agents, we designed and employed a suitable glass reaction vessel.

## RESULTS AND DISCUSSION

Using the glass reactor vessel described in the experimental section, we have carried out the thermolysis of 1,2-diphenylethane, DPE, under 2000 psi of D<sub>2</sub> gas at 450 °C. DPE disappeared following a first order rate law as shown in Figure 1. The resultant mixture showed products reported earlier by Poutsma<sup>12</sup> for this reaction in the absence of D<sub>2</sub>: toluene, benzene, ethylbenzene, stilbene, 1,1-diphenylethane, phenanthrene and diphenylmethane. We also found what appeared to be diphenylpropane and trace amounts of other materials. For comparison, we carried out the reaction at the same pressure of N<sub>2</sub> and found most of the same products except, as reported by Vernon,<sup>6</sup> greatly reduced relative amounts of stilbene, benzene and ethylbenzene. These results are shown in Table I.

Representative GC/MS data on the mixture obtained from the D<sub>2</sub> reaction are shown in Table II. The data suggest that deuterium introduction is taking place both at aliphatic positions and in the aromatic rings (note both benzene-d<sub>1</sub> and -d<sub>2</sub> are formed.) To assess the relative amounts of aromatic and aliphatic substitution, the reaction mixture was subjected to gas chromatographic separation and the individual components analyzed by both <sup>2</sup>H-NMR and <sup>1</sup>H-NMR. Typical results are shown in Table III.

Interestingly, as seen in Table II, the pattern is very similar for

deuterium distribution in toluene and DPE at low conversion. Later in the reaction, the amount of deuterium in DPE is significantly greater than in toluene. Surprisingly, despite the fact that hydrogen atoms must be supplied in order for DPE to be converted to toluene, the toluene formed at low conversions (in the 8 minute run, ca. 20% of the bibenzyl has been converted to products and about half of this is toluene) contains only about 20% of one atom of D by GC/MS. This can only mean that at least 80% of the benzyl radicals reacting to give toluene do so by removing H atoms, presumably from DPE, rather than D atoms from D<sub>2</sub>. Moreover, the fact that at short reaction times, there is already a substantial amount of D in the starting DPE, demands that at least some of the D-substituted toluene arises because it is formed from D-substituted DPE. This strongly suggests that DPE molecules can pick up D atoms without first undergoing homolysis.

If this reasoning is correct, it suggests that the most prominent reaction of the R· + D<sub>2</sub> → R-D + D· type, is that in which R· = 1,2-diphenylethyl radical rather than benzyl radical. This is somewhat surprising in that more highly-substituted radicals are normally viewed as being more stable and consequently less reactive. On the other hand, in the equilibration of species present during reaction conditions, the diphenylethyl radical will achieve higher concentration<sup>13</sup> which will compensate for its possibly lower reactivity. Further, results to be described later for a new substrate suggest that viewing more highly-substituted radicals as less reactive, may be an oversimplification.

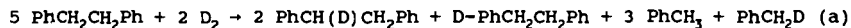
It will be noted that the deuteration pattern for ethylbenzene as seen in Tables I and II, is distinctly different from those of toluene and DPE. If, as is generally accepted,<sup>6</sup> ethylbenzene is formed by the reaction of 2-phenylethyl radical with a hydrogen source, the results suggest that, being a more reactive radical, the 2-phenylethyl radical is less selective and therefore reacts directly with D<sub>2</sub> to a greater extent than do the more stable benzylic radicals present. Even after only 10% conversion of DPE, about 50% of the ethylbenzene molecules present contain deuterium. A similar situation exists for 1,1-diphenylethane which is believed to arise from 2,2-diphenylethyl radical, believed to be formed by rearrangement.<sup>12</sup> (See Table II.) Unfortunately, we have not yet been able to get reliable GC/MS data for benzene at low conversion because of the problem of getting it cleanly separated from solvent on the GC. We are still working on this.

It has been possible to isolate the more abundant products by preparative GC. We have then determined both <sup>2</sup>H and <sup>1</sup>H NMR spectra using DCO<sub>2</sub>Me as an internal standard for both spectra. This has allowed us to calculate the relative amounts of GC/MS-determined D atoms which are located at aliphatic vs aromatic sites. These data are shown in Table III for toluene, DPE and ethylbenzene. It is immediately apparent that deuterium is being incorporated at both aliphatic and aromatic sites. Moreover, the D-atom populations at the two types of location would appear to be similar in magnitude. This is consistent with a mechanism in which each aliphatic D atom introduced via R· + D<sub>2</sub> → R-D + D· results in D-atom incorporation in an aromatic ring. More detailed analysis of the recovered DPE suggests that the number of aromatic D atoms exceeds the number of aliphatic D atoms by a factor of between 1.2 and 1.5 (average = 1.4). This would suggest that there is some mechanism for D incorporation at aromatic sites which does not require an aliphatic radical precursor. There are a variety of possibilities, but one of the simplest is the displacement of H atoms by D atoms (probably a two step process such as reactions 4 and 9 in Figure 3). The H atoms thus generated could then react with

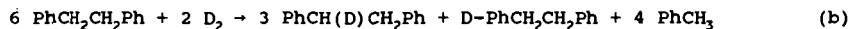
D<sub>2</sub> to generate more D atoms. It is reasonable to expect that if D atoms can displace alkyl radicals from the aromatic ring, the same can happen for H atoms with a five to one statistical advantage. Seeing that the amount of ethylbenzene produced is roughly 10% of the total conversion, it is perhaps reasonable to find a substantial excess of D at aromatic sites.

By computer simulation, we have tried to match the product distribution (including deuterated products) using only the first 8 reactions shown in Figure 3. These account only for the introduction of deuterium into starting DPE and the formation of toluene. We felt if we could get close to an accommodation of the data with this simple scheme, we could then approach the full set of products by elaboration and fine tuning. It will be noticed that the reaction of benzyl radicals with molecular deuterium ( $\text{PhCH}_2\cdot + \text{D}_2 \rightarrow \text{PhCH}_2\text{D} + \text{D}\cdot$ ) has been omitted.

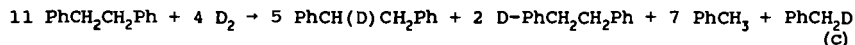
The assumption that only the reactions 1 through 8 are involved leads to the conclusion that the stoichiometry for formation of the major products should be between:



and

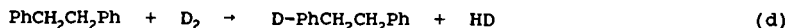


Eq (b) represents the limit in which reaction 2 (Figure 3) becomes so preferred relative to reactions 7 and 8 that all of the toluene formed arises via reaction 2 and thus would contain no D. Eq (a) results from the limit wherein reactions 5 and 6 become unimportant relative to reaction 3 thus maximizing the amount of PhCH<sub>2</sub>D produced. If reactions 5, 6, 7 and 8 all participate equally in consuming the adduct, then the intermediate stoichiometry of eq (c) should be found.



Clearly none of these options nor any gradation in between can explain the observed facts. The observed ratio of PhCH<sub>2</sub>D and PhCH<sub>3</sub> is not far from the stoichiometry of eq (c), but the experimentally observed ratio of aromatically deuterated DPE to aliphatically deuterated DPE is found experimentally to be rather constant at a value of 1.4. The stoichiometries of eqs (a), (b), or (c) demand that the ratio be between 0.25 and 0.40. Even if a huge isotope effect were assumed favoring reaction 5 over reaction 6, the maximum possible ratio would be 1.0.

Reactions 9 and 10 coupled with reaction 4, constitute a kinetic chain sequence for the introduction of aromatic D without producing aliphatically deuterated DPE. The stoichiometry of this sequence, taken in isolation from the other reactions is simply:



It therefore seems that it should be possible to combine reactions 1 through 10 to approximately match the experimental data by selecting an appropriate set of relative rates. We are working on this proposition at the present time and preliminary results indicate that it will be possible to match the distribution of the major products.

## EXPERIMENTAL SECTION

**Reaction Procedure.** The device shown in Figure 2 (a) consists of a thick glass reaction bulb with a long capillary neck. The reactor is inverted and several glass beads are added followed by solid reactants through the end opposite to the capillary. The reactor is sealed at the constriction Figure 2 (b). The vessel is then suspended in glass wool in the interior of a stainless steel reaction tube having a long neck to house the capillary section of the vessel. The entire apparatus is evacuated, pressured with D<sub>2</sub> gas, closed off and shaken at the desired temperature in a fluidized sand bath. When the reaction is complete, carbon disulfide is added and products removed for analysis using a long syringe needle. In the absence of gas generation within the tube, our observation has been that little or no material is lost from the interior of the bulb. Control experiments in which a hydrogenation catalyst was deliberately added showed complete saturation of aromatic compounds under the reaction conditions.

## REFERENCES

1. a. Skowronski, R. P.; Ratto, I. B.; Goldberg, I. B.; Heredy, L. A. Fuel **1984**, 63, 440-448. b. Ratto, J. J. ACS Fuel Chem. Preprints **1979**, 24, 155. c. Goldberg, I. B.; Crowe, H. R.; Ratto, J. J.; Skowronski, P. R.; Heredy, L. A. Fuel **1980**, 59, 133. d. Noor, N. S.; Gaines, A. F. Abbott, J. M. Fuel **1986**, 65, 67-73. e. Kershaw, J. R.; Barrass, G. Fuel **1977**, 56, 455.
2. Cronauer, D. C.; McNeil, D. C.; Ruberto, R. G. Fuel **1982**, 61, 610-619.
3. a. Franz, J. A.; Camaioni, D. M. Fuel **1984**, 63, 213-229. b. Franz, J. A. Fuel **1979**, 58 405-412. c. Aulich, T. R.; Knudson, C. L.; Hawthorne, S. B. Preprints Div. of Fuel Chem., Am. Chem. Soc. **1988**, 33, 368-379. d. Benjamin, B. M.; Douglas, E. C.; Mesmer, S. ibid. **1982**, 27, 1-5.
4. a. Pajak, J.; Brower, K. R. J. Org. Chem. **1986**, 50, 2210-2216. b. Brower, KR.; Pajak, J. ibid., **1984**, 49, 3970-3973.
5. King, H. H.; Stock, L. M. Fuel **1982**, 61, 257-264.
6. Vernon, L. W. Fuel **1980**, 59, 102.
7. Shin, S.-C.; Baldwin, R. M.; Miller, R. L. Energy and Fuels **1989**, 3, 71-76.
8. Bockrath, B.; Bittner, D.; McGrew, J. J. Am. Chem. Soc. **1984**, 106, 135-138.
9. Price, S. J. Can. J. Chem. **1962**, 40 1310.
10. Benson, S. W. J. Chem. Ed. **1965**, 42, 502.
11. a. Chien, P.-L.; Sellers, G. M.; Weller, S. W. Fuel Processing Technology **1983**, 2, 1-9. b. Brammer, S. T.; Weller, S. W. ibid. **1979**, 2, 155-159. c. Patxer, J. F.; Farrauto, R. J.; Montagna, A. A. Ind. Eng. Chem. Process Des. Dev. **1979**, 18, 625-630. d. Davis, K. P.; Garnett, J. L. J. Phys. Chem. **1971**, 75, 1175-1177. e. Davis, K. P.; Farnett, J. L.; O'Keefe, J. H. Chem. Communications **1970**, 1672-1673.

12. a. Poutsma, M. L.; Dyer, C. W. J. Org. Chem. **1982**, *42*, 4903. b. Buchanan, A. C.; Dunstan, T. S. J.; Douglas, E. C.; Poutsma, M. L. J. Am. Chem. Soc. **1986**, *108*, 7703.

13. Livingston, R.; Zeldes, H.; Conradi, M. S. J. Am. Chem. Soc. **1979**, *101*, 4312-4319.

**Table I.** Product Distribution in the Thermolysis of Diphenylethane at 450° C for 30 Minutes

	Mole % Under D <sub>2</sub>	Wt. % Under D <sub>2</sub>	Mole % Under N <sub>2</sub>	Wt% Under N <sub>2</sub>
1,2-Diphenylethane	23.5	36.6	36.1	47.1
Toluene	47.8	37.1	47.1	31.1
1,2,3,4-Triphenylbutane	0.25	0.8	<0.1	<0.1
Benzene	17.2	9.3	0.9	0.5
Ethylbenzene	8.6	7.7	--	--
1,1-Diphenylethane	1.5	2.3	0.9	1.2
Stilbene	1.3	1.9	12.2	15.8
Phenanthrene	0.8	1.2	<0.3	<0.5
Triphenylpropane	0.8	1.8	0.7	1.9
Diphenylpropane	0.44	0.73	--	--
Diphenylmethane	0.36	0.52	1.4	1.7

**Table II.** Deuterium Distribution in Products from Thermolysis of Diphenylethane at 450 °C Under D<sub>2</sub>

Compound	After 8 min					After 30 min				
	%d <sub>0</sub>	%d <sub>1</sub>	%d <sub>2</sub>	%d <sub>3</sub>	%d <sub>4</sub>	%d <sub>0</sub>	%d <sub>1</sub>	%d <sub>2</sub>	%d <sub>3</sub>	%d <sub>4</sub>
1,2-Diphenyl-ethane	66	28	6	1	-	14	29	29	17	7
Toluene	78	20	2	-	-	45	36	14	4	1
Benzene	54	39	7	-	-	46	41	12	2	-
Ethylbenzene	42	45	12	1	-	18	34	29	14	4
1,1-Diphenyl-ethane	40	43	15	3	-	9	24	30	22	11
Stilbene	70	23	6	-	-	36	33	20	8	3
Phenanthrene						25	34	25	12	4
Diphenyl-methane	67	27	6	-	-	30	33	22	10	4

**Table III.** Aliphatic vs. Aromatic Deuterium in Products from Thermolysis of 1,2-Diphenylethane under  $D_2$  at  $450^\circ C$  by NMR.

Compound	Time (min)	Aromatic D /molecule	Aliphatic D	
			/molecule $CH_2$	$CH_3$
1,2-Diphenyl-ethane	8	0.13	0.09	
	30	0.91	0.65	
Toluene	8	0.17		0.18
	30	0.65		0.39
Benzene	30	0.66		
Ethylbenzene	15	0.36	0.18	0.54
	30	0.50	0.28	0.44
	45	1.32	0.54	0.71

**Figure 1.** First-Order Plot for Conversion of 1,2-Diphenylethane Under  $D_2$  at  $450^\circ C$ .

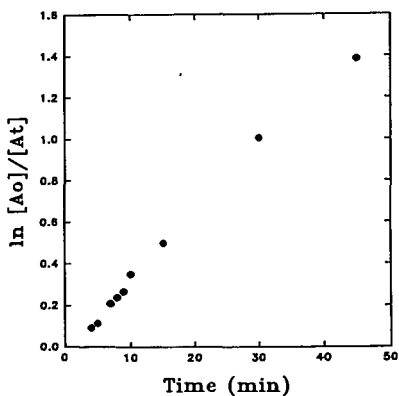


**Figure 2.** Glass Reaction Vessel for Thermolysis Under  $D_2$ .

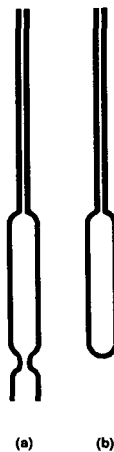
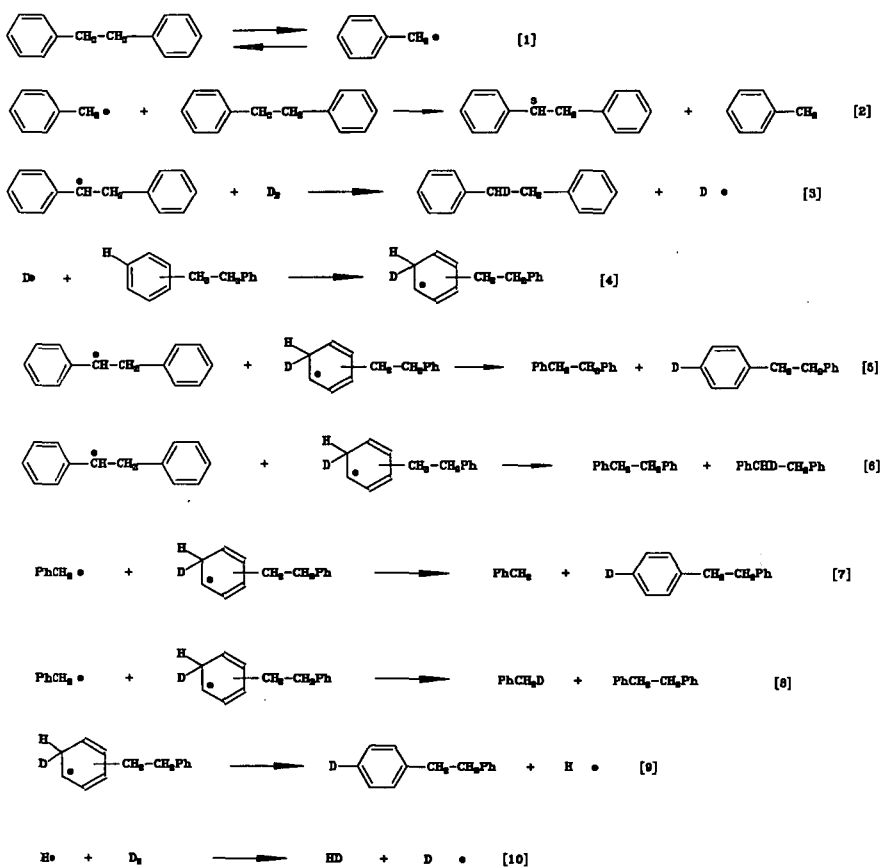


Figure 3. Minimum Steps to Explain Deuterium Distribution Pattern



## COAL LIQUEFACTION USING DONOR SOLVENTS HYDROGENATED AT LOW TEMPERATURES\*

R.J. Kottenstette and H.P. Stephens  
Process Research Department 6212  
Sandia National Laboratories  
P.O. Box 5800  
Albuquerque, NM 87185

**Keywords:** Hydrogen Donor, Coal Liquefaction, Solvent Quality

### Introduction

Direct coal liquefaction proceeds initially through a complex series of bond breaking and hydrogen transfer reactions involving coal and a donor solvent. When the recycle solvent contains high amounts of donor solvent, the requirement for high hydrogen gas pressure in the initial stage of liquefaction is reduced and coal conversion is augmented. Effective tests for hydrogen donating ability of coal derived solvents often consist of GC/MS, proton NMR, catalytic dehydrogenation, as well as microautoclave coal liquefaction testing [1,2,3]. Microautoclave testing is an empirical measure of solvent quality for hydrogen donation using coal, a donor solvent and an inert gas instead of hydrogen. Previous studies [4] have investigated the hydrogen transfer cycle for direct liquefaction using Illinois #6 high volatile bituminous coal and a distillate (650°F-770°F) derived from a coal liquefaction process solvent. The objective of this work is to determine the effects of donor solvent on coal conversions in microautoclave liquefaction experiments performed at 400°C with Wyodak coal. These tests used a heavy distillate solvent that had been hydrogenated with a synthesis gas (50% carbon monoxide:50% hydrogen) mixture and steam at low temperatures (300°C-325°C). The in situ water-gas shift (WGS) reaction provides an alternate source of hydrogen and has the potential of eliminating the need for high purity high pressure hydrogen for solvent hydrogenation. Hydrogenation at low temperatures can lead to increased donor content since larger amounts of hydroaromatics are produced at equilibrium with any given hydrogen pressure. Distillate solvents were hydrogenated at various weight hourly space velocities, using two different catalysts, and used in microautoclave coal liquefaction tests to evaluate solvent pretreatment effects on coal solubility.

### Experimental

**Materials** - Because solvent quality is favorably affected by increasing the aromatic nature of the solvent being fed to the catalytic hydrotreater, and solvent dewaxing has been shown to be an effective means of increasing the aromatic nature of the solvent [5], a heavy distillate and a dewaxed heavy distillate were used. Heavy distillate sample (V1074) from the Wilsonville, Alabama Advanced Integrated Two Stage Liquefaction Facility was provided by CONSOL Inc., Library PA. Dewaxed V1074 distillate was prepared by CONSOL at -5°C from the V1074 heavy distillate using an acetone dewaxing procedure. 1,2,3,6,7,8 hexahydropyrene was purchased from Aldrich Chemical Company with a 99% purity. Reagent grade tetrahydrofuran (THF), pentane, and heptane were purchased from Fischer Scientific. Wyodak subbituminous coal was used as -100 mesh from the Argonne Premium Coal Sample Bank. The NiMo catalyst, was Shell 324M and the platinum catalyst was a hydrous titanium oxide (HTO) compound synthesized in our lab. Hydrogen, carbon monoxide, and nitrogen were UHP grade.

\*This work was supported by the U. S. Department of Energy at Sandia National Laboratories under contract DE-AC04-76DP00789.

### Apparatus and Procedure

**Microflow Reactor Experiments** - A fixed bed microflow reactor consisting of liquid and gas feed systems and a stainless steel reactor containing the catalyst bed (0.5" O.D.) was used to hydrogenate heavy distillate and dewaxed heavy distillate. The reactor had an internal volume of 23 cm<sup>3</sup> and typically held a 20 gram catalyst charge. These distillate pretreatment experiments consisted of three days of testing for each catalyst and feed combination. The first two days of experiments used the in situ water-gas shift reaction to hydrotreat the distillate. Reactions on the third day used solely hydrogen to test the effect of varying the partial pressure of hydrogen gas upon solvent hydrogen uptake. The reactor tube was first packed with catalyst and then presulfided with a 9% H<sub>2</sub>S in hydrogen mixture for four hours at 390°C for the commercial nickel molybdenum on alumina catalyst (NiMo), or pre-reduced in hydrogen at 200°C for the platinum (Pt HTO) catalyst. After catalyst pretreatment, the reactor was pressurized to 1000 psig with a 50:50 mixture of carbon monoxide and hydrogen. The reactor temperature was increased to the operating value while the distillate and a 1:1:1 molar mixture of CO:H<sub>2</sub>:H<sub>2</sub>O was fed the top of the reactor. Distillate was pumped into the reactor with an Eldex A-30 liquid chromatograph pump and the synthesis gas was metered into the reactor with two Brooks 5850 mass flow controllers. The liquid weight hourly space velocities were varied between 0.4 hr<sup>-1</sup> and 0.8 hr<sup>-1</sup>. Water was fed to the reactor with a Beckman 114M microflow liquid chromatography pump. All reactants flowed downward over the packed bed into a reservoir to separate the gases and liquids. Solvent and gas products were taken from the sample reservoir at the bottom of the reactor during operation. Reactor pressure was maintained with a Circle Seal BPR-7A back pressure regulator, which was located downstream from the liquid separator. Distillates and hydrotreated distillates were also analyzed by high resolution gas chromatography using a Hewlett Packard 5890 GC to qualitatively measure hydrogenation of aromatic compounds.

**Microautoclave Experiments** - Coal liquefaction tests were used to evaluate donor solvent quality. Hydrogenated solvent was tested in a microautoclave consisting of a 0.75" O.D. Swagelok tubing tee with 40 cm<sup>3</sup> of gas volume. Pressure and temperature were measured in the microflow and batch microautoclave reactors with Entran pressure transducers and internal reactor thermocouples. Data acquisition for both the flow and batch reactor systems was accomplished with a personal computer using Labtech Notebook software.

Coal and pretreated solvents representing various hydroprocessing conditions were weighed into the microautoclave reactor. The microautoclaves were sealed and pressurized with nitrogen to 100 psig cold charge to facilitate post reaction gas analysis. The pressurized microautoclaves were then fastened to a wrist-action shaker and immersed in a fluidized sand bath while being shaken at 200 cycles per minute. After a rapid heat up (< 2min.) the microautoclaves were maintained at 400°C for 30 minutes. Following reaction the microautoclaves were cooled to room temperature in water, then depressurized into gas sample bottles and dismantled to recover the reaction products. The gas samples were analyzed for hydrogen, carbon monoxide, carbon dioxide and C<sub>1</sub>-C<sub>2</sub> hydrocarbons using a Carle series 400 Gas Chromatograph. Liquid and solids were recovered from the reactor with THF and the THF insolubles were determined by pressure filtration. The THF insolubles were dried and weighed while the THF solubles were rotoevaporated to remove most of the THF. Pentane was then added to these samples to precipitate the preasphaltene/asphaltene material. These solutions were pressure filtered to remove the pentane insolubles. The pentane insolubles were then dried and weighed.

All microautoclave tests were performed with a solvent to coal ratio of 1.5:1. Solvent samples A, B, C and D, shown in Table 1, were produced in the microflow reactor using various catalysts, temperatures and weight hourly space velocities (WHSV). Hydrogen donor (H<sub>6</sub>PY) was added to comprise 20 % of the solvent charge for experiments that were designed to test the effect of adding a known amount of a good hydrogen donor. Donor hydrogen was effectively increased in this "composite" solvent by 0.6 wt% (see Table 1).

**Model Compound Test** - In a series of donor solvent tests which examined the effects of using different levels of hexahdropyrene (H<sub>6</sub>PY) alone as the solvent, heptane was used instead of pentane as the precipitating solvent, as shown in Figure 5.

### Results and Discussion

The extent of distillate hydrogenation is given in Table 1, which shows elemental analysis results for baseline distillates and hydrotreated products from the microflow reactor. A comparison of samples A and B (from the same reactor run) shows that sample B was hydrogenated to a greater extent than sample A which had a slower space velocity. This is due in part to catalyst deactivation since sample B was obtained earlier in the run when the catalyst bed was fresher. The hydrogenated dewaxed distillates labeled samples C and D compare solvents hydrogenated with different catalysts. The maximum amount of hydrogen increase was 1.0 wt% in the dewaxed distillate (sample D); this distillate was produced at 325°C with the Pt HTO catalyst using only hydrogen gas. This catalyst deactivated to a lesser degree than the NiMo catalyst and was more effective using hydrogen only rather than the in situ water-gas shift reaction. It is believed that the more aromatic dewaxed solvent could be hydrogenated to a greater degree, and this was true for our tests. Figures 1 and 2 show capillary gas chromatograms of the -5°C dewaxed distillate and the hydrotreated distillate. The hydrotreated sample shows a reduction in parent aromatic compounds with an emergence of hydroaromatic products.

Figure 3 shows the product distributions for microautoclave experiments with V1074 (feed), two hydrogenated V1074 distillates (samples A and B), and V1074 + donor solvent (H<sub>6</sub>PY) addition. Overall the coal conversion (100-%IOM, Insoluble Organic Matter) increased from 57% to 63% with sample B. Sample B, which had an additional 0.7 wt% hydrogen (over the V1074 amount), gave an increase in pentane solubles from 14% to 25%. The experiment that contained added H<sub>6</sub>PY gave 33% pentane soluble material.

Figure 4 shows the product distributions for microautoclave experiments with -5°C dewaxed V1074 (feed), two hydrogenated dewaxed distillates (samples C and D) and dewaxed V1074 with H<sub>6</sub>PY addition. The coal conversions increased from 64% to 69% with solvent C. Most notable, however was the increase in pentane solubles with samples C and D. These increased from 0% to 22% and 23% respectively using the hydrotreated solvent. These results show that unhydrogenated dewaxed solvent produced a higher coal conversion than V1074 but little or no oil. The small oil yield for the -5°C dewaxed distillate shows that it is necessary to hydrogenate the more reactive dewaxed solvents to avoid potentially retrogressive conditions that occur when solvent hydrogen is limited. Sample D which had an increase of 1 wt% hydrogen did not perform as well as the H<sub>6</sub>PY doped solvent even though the doped solvent had only 0.6 wt% hydrogen. The increase in hydrogen, in sample D, could possibly have been in alicyclic compounds which are poorer donors than hexahdropyrene. Increasing the liquid space velocity could adjust the hydrogenation extent to enhance production of hydrogen donor species in the product when the Pt HTO catalyst is used.

### Model Compound Test

Figure 5 shows the product distributions for donor solvent tests which used only hexahydropyrene as the solvent. Coal conversion increases dramatically from 52% to 87% when the hexahydropyrene amount was increased from 0.5g to 1.0g. These addition rates amounted to 10 and 20 mg hydrogen / g dmmf coal respectively. Further addition of H6PY (1.75g H6PY or 35mg H / g dmmf coal) showed little improvement in conversion or heptane solubility over the 1g H6Py addition. This could possibly be due to the relatively mild liquefaction temperature. For comparison the -5°C dewaxed solvent with H6PY addition (Figure 4.) had 15mg of hydrogen / g dmmf coal from the H6PY giving 77% coal conversion.

### **Conclusions**

At 400°C for 30 minutes, coal conversions and pentane/heptane soluble yields increase with increasing solvent hydrogen content during liquefaction using Wyodak coal. Dewaxed V1074 heavy distillate gives higher coal liquefaction conversions than V1074 without dewaxing, yet very little pentane soluble product compared to the V1074 heavy distillate. Hydrogenation of dewaxed heavy distillate is necessary to avoid potentially retrogressive conditions with this solvent since it is a good physical solvent yet produces very little pentane soluble material at these conditions. There is of course a potential to over hydrogenate the solvent by forming alicyclic and naphtheno compounds which would add hydrogen without the benefit of increasing solvent quality. These concerns are especially valid when using low rank coals and solvents with limited hydrogen donating capacity.

### **Acknowledgments**

The authors gratefully acknowledge R. A. Winschel and M. S. Lancet from CONSOL inc. for providing dewaxed solvents for the hydrotreating studies. Experimental contributions from W. K. Hollis of Sandia National Laboratories are also gratefully acknowledged.

### **References**

- 1) C. E. Snape, H. P. Stephens, R. J. Kottenstette and S. R. Moineiro. Proceedings of the 1989 Conference of Coal Science, Vol. 2, p 739.
- 2) J. Delpuech, D. Nicole, M. Le Roux, P. Chiche and S. Pregerman. Fuel, 1986, Vol.65, p 1600.
- 3) R. A. Winschel, G. A. Robbins, and F. P. Burke. Fuel, 1986, Vol.65, p 526.
- 4) H. P. Stephens and R. J. Kottenstette. Preprints of Papers, Amer. Chem. Soc. Div. Fuel Chem. 32 (3), p 377 (1987)
- 5) R. A. Winschell, G. A. Robbins and F. P. Burke. Fuel, 1987, Vol.66, p 654.

Table 1. Elemental analysis of V1074 and -5°C dewaxed hydrotreated distillates

Distillate	WHSV (hr <sup>-1</sup> )	Catalyst	Hydrotreating Temp(°C)	%C	% H	Increase in Hydrogen (wt%)
V1074 (feed)	-	-	-	89.5	9.9	-
Sample A	0.46	NiMo	300	88.5	10.1	0.2%
Sample B	0.61	NiMo	300	88.9	10.6	0.7%
V1074+H6PY	-	-	-	-	-	0.6%
-5C Dewax (feed)	-	-	-	90.2	8.6	-
Sample C	0.78	NiMo	325	90.2	8.9	0.3%
Sample D	0.78	Pt HTO	325	89.9	9.6	1.0%
-5C Dewax+H6PY	-	-	-	-	-	0.6%

**Figure 1. High resolution gas chromatogram of -5°C dewaxed heavy distillate V1074**

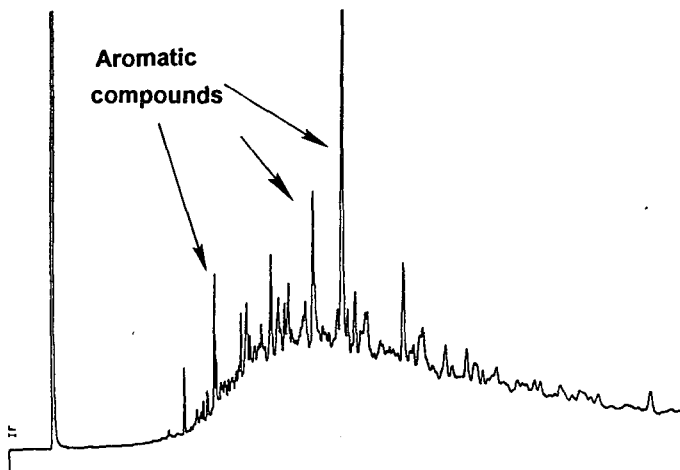


**Figure 2. High resolution gas chromatogram of Sample D**

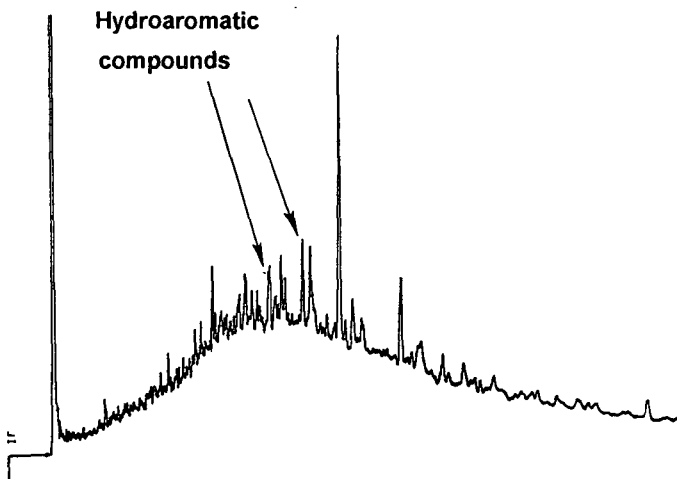


**Figure 3. Product distribution for V1074 heavy distillate experiments (Wyodak, 400C, N2, 30 min.)**

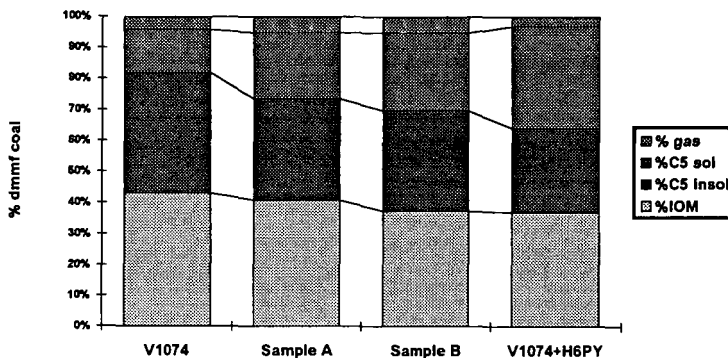


**Figure 4. Product distribution for dewaxed V1074 heavy distillate (Wyodak, 400C, N2, 30 min.)**

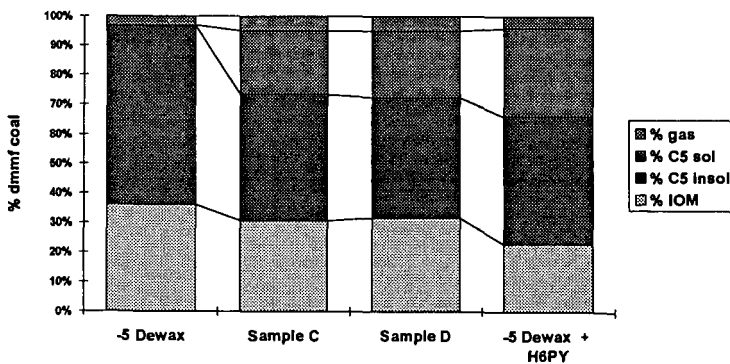
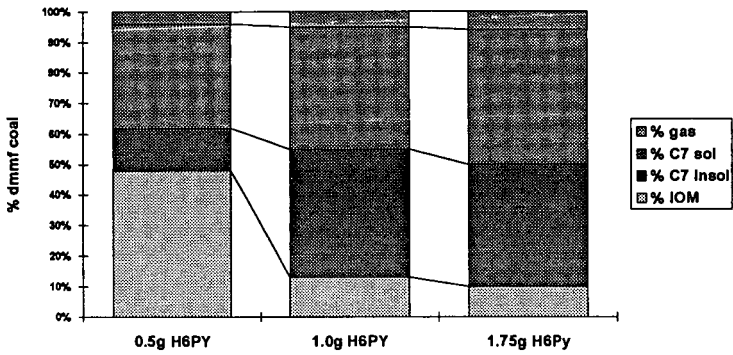


**Figure 5. Product distribution for hexahydroprylene donor solvent (Wyodak, 400C, N2, 30 min.)**



## Bimetallic Ru/Mo Catalyst Particles for HDN of Tetrahydroquinoline

Daniel B. Ryan, Thomas Hinklin, Gregory Reuss, S.-M. Koo<sup>†</sup> and Richard M. Laine, Contribution from the Departments of Materials Science and Engineering, and Chemistry, University of Michigan, Ann Arbor, MI 48109-2136, <sup>†</sup>Depart. of Chemistry and Eng., Hanyang University Seoul, Korea

**KEY WORDS:** Unsupported RuMo Bimetallic Catalysts, Tetrahydroquinoline Hydrodenitrogenation, Heteropolyanion Catalyst Precursors

### ABSTRACT:

Ethanol solutions of the heteropolyanion  $H_3PMo_{12}O_{40} \cdot xH_2O$ , (Mo-HPA) mixed with  $RuCl_3$  were decomposed, at 180°C in the presence of  $CS_2$  and  $H_2$  to form small multimetallic catalyst particles. Previous efforts have demonstrated the synergistic effect of these catalyst systems for Quinoline hydrogenation to THQ and alkylation of THQ by ethanol. The current study extends these efforts to the HDN of THQ in hexadecane.

### INTRODUCTION

We have previously shown that alumina supported RuMo and RuCoMo bi- and trimetallic catalysts provide catalytic activities and product selectivities during quinoline (Q) and tetrahydroquinoline (THQ) hydrodenitrogenation (HDN) that are not normally observed with alumina supported,  $M'Mo$  ( $M' = Co, Ni$ ) or single metal Mo or Ru catalysts.<sup>1-7</sup> The RuMo combination of metals appears to offer synergistic behavior during Q and THQ HDN. In particular, the catalysts are sulfur tolerant, even showing enhanced activities in the presence of sulfur compounds. Their activities are 5 to 10 times higher than corresponding  $M'Mo$  catalysts for similar weight loadings on identical supports. Moreover, their selectivity towards the formation of propylbenzene vs. propylcyclohexane during Q or THQ HDN is much higher (1:3 product ratios at temperatures of 350°C and  $H_2$  pressures of 400-600 psig at RT).

In an effort to completely delineate this synergistic behavior, we have examined the catalytic activity of RuMo catalysts with Q and THQ under a variety of conditions. Furthermore, we have examined the feasibility of preparing these heterogeneous bimetallic catalysts directly from soluble precursors based on ethanolic solutions of molybdenum heteropolyanion,  $H_3PMo_{12}O_{40}$  (Mo-HPA) and  $RuCl_3 \cdot xH_2O$  (Ru-Cl).

We find that 1:9 Ru:Mo atomic ratio solutions consisting of 1.0 ml ( $5.7 \times 10^{-3}$  M,  $5.7 \times 10^{-3}$  mmol) of  $RuCl_3 \cdot xH_2O$  in EtOH with 4.0 ml of  $1.1 \times 10^{-3}$  M in Mo-HPA ( $4.38 \times 10^{-3}$  mmol) in EtOH, when heated with 5.0 ml (42 mmol) Q or THQ and 50  $\mu$ l of  $CS_2$  for 3 h at 175-200°C decompose uniformly to give 0.3-1.5  $\mu$ m dia. RuMo catalyst particles (surface areas typically of 5-9  $m^2/g$ ).<sup>6,7</sup> These bimetallic particles appear to be more catalytically active for Q hydrogenation to THQ than similar particles generated either from Mo-HPA or Ru-Cl under identical conditions.<sup>7</sup> Furthermore, efforts to promote HDN of

THQ at somewhat higher temperatures in EtOH solutions leads to the N-ethylation of THQ rather than HDN.<sup>6</sup> Again, the RuMo catalyst is much more effective for N-ethylation than either of the metals alone. N-ethylation was also observed when THQ HDN was attempted in acetonitrile solutions of RuMo. We have now determined that it is possible to conduct THQ HDN to the exclusion of extraneous reactions through the use of hexadecane as solvent. We describe here preliminary efforts to study this reaction.

#### EXPERIMENTAL

HDN catalysis studies were conducted using hexadecane as solvent and using 1:9 RuMo catalyst particles generated under conditions identical to the Q hydrogenation reactions, at 175°C, but in the absence of Q.<sup>7</sup> Particle surface areas were 5-6 m<sup>2</sup>/g. Studies were done with two 250 mg batches of catalyst which were mixed to obtain a uniform catalyst.

Product analyses for all the kinetic studies were performed on a temperature programmed Hewlett-Packard 5890A reporting GC equipped with FID using a 12 m x 0.53 mm x 2.65 μm capillary column packed with 100 % dimethyl polysiloxane gum. The column heating schedule was initiated with a hold at 35°C (2 min) followed by ramping at 7°C/min to 250°C. The eluting gas mixture was H<sub>2</sub>/He.

GC-MS studies were performed using an HP 5890 Series II GC, an HP 5970 mass spectrometer, and the HP 5940 MS Chemstation. The capillary column used for product separation was a 12 m x 0.12 mm x 0.33 μm film thickness HP-5 (crosslinked 5% phenyl methyl silicone) capillary column. The temperature for the analysis was held at 50°C for 5 min, then ramped at 4°C/min to 275°C. The eluting gas used was H<sub>2</sub>/He.

#### THQ HDN Kinetic Runs

Typically, 18-20 mg of catalyst are added to a solution of 5.0 ml (42.3 mmol) of THQ mixed with 5.0 ml of hexadecane and 50 μl of decane as internal standard in a quartz lined, Parr General Purpose Bomb reactor with a 34 ml internal volume. The reaction solution is then pressurized to 400 psig with N<sub>2</sub> at RT and depressurized. The process is repeated and then 400 psig with H<sub>2</sub> at RT is added and the reaction is heated, with magnetic stirring, to the desired temperature, e.g 370°C for the studies shown below. At the appropriate times (typically 3, 6, 9, 12 and 15 h) the reactor is cooled in flowing water, depressurized and a sample is taken for GC analysis. The reactions are run to less than 5% conversion so that the initial rates of product formation correspond essentially to zero order in reactant concentration.

#### RESULTS AND DISCUSSION

Figure 1 shows the standard reaction network for Q HDN.<sup>8</sup> Propylcyclohexene may arise both from hydrogenation of propylaniline and from deamination of aminopropylcyclohexane, presumed to be an intermediate in DHQ HDN. Propylaniline and DHQ are presumed to derive directly from catalytic reactions of THQ, and propylbenzene and propylcyclohexane are presumed to arise from the catalytic reactions of propylaniline and DHQ respectively; although propylcyclohexane could also derive from propylbenzene.

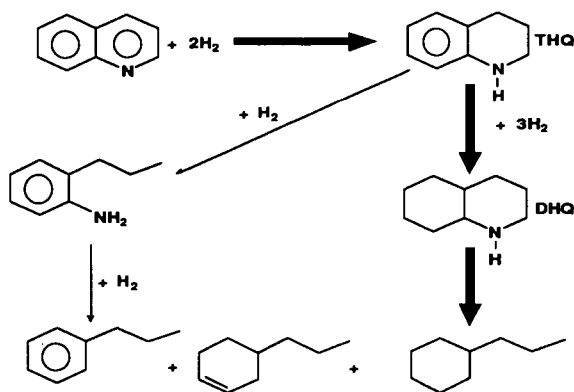


Figure 1. Quinoline HDN Reaction Network

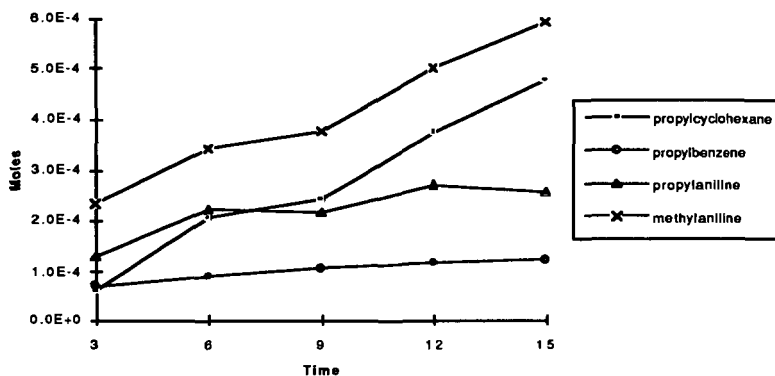
Figure 2 shows a plot of the major bond cleavage products observed at  $370^\circ\text{C}$  during RuMo catalyzed HDN of THQ, as a function of time. In Figure 2, the quantities of propylaniline initially produced are not significantly higher than the propylbenzene. Furthermore, [propylcyclohexane] increases significantly with time whereas [propylbenzene] does not. Given that the amount of products produced during the course of the reaction all fall in the 0.1 to 0.8 mmol range and the starting amount of THQ is on the order of 42 mmol, the percent conversion of THQ is of the order of 1%. Normally, the sequential formation of products, as depicted in Figure 1, should not lead to the formation of significant amounts of secondary products such as propylbenzene or propylcyclohexane at conversions of 1%. Thus, these results are rather surprising.

We offer two explanations for these observations, the first is that the catalyst particles are highly porous and that much of the catalysis occurs in the particles' interiors. In this case, the actual concentration of reactants at the catalyst surface would be much higher than it is in solution and secondary products might be expected to escape from the porous body at about the same rate as primary products. Hence the relative concentrations of the two types of products seen by GC would be representative of the mixture in the particle rather than in solution.

The second possibility is that once THQ is bound to the active catalytic site in these unsupported catalyst particles, it remains bound for sufficient periods of time to undergo more than one type of catalytic reaction. This would mean that the site would have a higher affinity for the reaction products and would be able to perform several different types of catalytic operations.

At this point, it is not possible to distinguish between the two possibilities; however, the surface

areas of the particles and the SEM micrographs<sup>6,7</sup> bely the possibility of a very porous catalyst particle. But the conversions are sufficiently low that it may be that some of this type of porosity exists and is responsible for most of the catalytic activity. Further studies will be required to differentiate between these, or other, possible explanations.



Finally, the appearance of significant quantities of methylaniline, a product of C-C rather than C-N bond hydrogenolysis suggests that there are Ru rich regions on the catalyst particles as this product is more typical of bulk Ru catalyzed HDN of THQ.<sup>5</sup>

#### ACKNOWLEDGEMENTS

We wish to thank the Department of Energy and the Pittsburgh Energy and Technology Center for generous support of this work through contract no. DE-FG22-90PC90313.

#### REFERENCES

- Hirschon, A. S.; Wilson, Jr., R. B.; Laine, R. M.; *New J. Chem.*, **1987**, *11*, 543-547.
- Hirschon, A. S.; Wilson, Jr., R. B.; Laine, R. M.; in *Adv. in Coal Chemistry*, Theophrastus Publ, Athens **1988**, p 351.
- Hirschon, A. S.; Wilson Jr., R. B.; Laine, R. M.; *J. Appl. Cat.*, **1987**, *34*, 311-316.
- Laine, R. M.; Hirschon, A. S.; Wilson Jr., R. B.; U.S. Pat. No. 4,716,142 **1987**.
- Hirschon, A. S.; Laine, R. M.; *J. Energy and Fuels*, **1988**, *2*, 292-295.
- Koo, S-M.; Ryan, D. B.; and Laine, R. M.; *Appl. Organomet. Chem.*, **1992**, *6*, 437-448.
- Hoppe, M. L.; Koo, S-M.; Ryan, D. B.; and Laine, R. M.; submitted to *Energy and Fuels*.
- a. Satterfield, C.N.; and Cocchetto, J.F.; *AIChE J.*, **1975**, *21*, 1107-1111. b. Yang, S. H. and Satterfield, C.N., *J. Catal.* **1983**, *81*, 168-178.

# Temperature-Programmed Liquefaction of Coals Using Bimetallic Dispersed Catalysts from Organometallic Complexes

Chunshan Song\*, Derrick S. Parfitt, and Harold H. Schobert

Fuel Science Program, 209 Academic Projects Building,  
The Pennsylvania State University, University Park, PA 16802

**Keywords:** Bimetallic catalysts, coal, temperature-programmed liquefaction

## Introduction

It has been recognized recently that dispersed catalysts are superior to supported catalysts for primary coal liquefaction. Most previous work involved dispersed molybdenum sulfide from a water-soluble salt [Derbyshire, 1988]. Some organometallic compounds including metal carbonyls and naphthenates have also been tested as catalyst precursors [Suzuki et al., 1987; Herrick et al., 1990; Swanson, 1992], which often requires the addition of sulfur compounds [Yamada et al., 1985]. There are some unique advantages of organometallic compounds as catalyst precursors. First, most organometallic compounds are soluble in hydrocarbon solvents and may be used as oil-soluble precursors. Second, as has been demonstrated by Hirschon and Wilson [1991, 1992], some organometallic compounds can be easily decomposed to metal sulfides at low temperatures. The present work is concerned with organometallic precursors which can directly produce metal sulfides upon thermal decomposition.

Little work on bimetallic dispersed catalyst for coal liquefaction has appeared, although previous work on multicomponent catalysts has involved the mixture of two or more inorganic salts [Garg and Givens, 1984; Song et al., 1986, 1991; Sommerfeld et al., 1992]. Related to this work is a general observation from previous investigations that there could be synergistic effects between different metals, and an organometallic precursor may be better than an inorganic one. Our interest in the heteronuclear organometallic compounds was stimulated by the recent book on metal clusters published by Mingos and Wales [1990]. It seemed to us that highly active catalysts might be prepared from some clusters containing metal-metal bonds, especially the "thiucubane" clusters containing two metals such as Fe or Co and Mo in a single molecule.

Two different metals bound together in a single compound should have a more systematic spatial arrangement in the resulting catalytic phase upon thermal decomposition than if two separate compounds were used to introduce the two different metals to a catalytic system. The present work is an exploratory study of bimetallic dispersed metal sulfide catalysts for coal liquefaction, involving the synthesis of the organometallic thiucubane clusters that contain Mo and Co as well as sulfur in a single molecule, and liquefaction of coal impregnated with the precursors under non-programmed and temperature-programmed (TPL) conditions, where the programmed heat-up serves as a step for both catalyst activation and coal pretreatment or preconversion. The advantages of temperature-programmed conditions have been demonstrated in our recent work [Song et al., 1992; Song and Schobert, 1992; Huang et al., 1992].

## Experimental

### Catalyst Precursors and Coal Samples

Three bimetallic thiocubanes were used as catalytic precursors:  $\text{Mo}_2\text{Co}_2\text{S}_4(\text{S}_2\text{CNEt}_2)_2(\text{CH}_3\text{CN})_2(\text{CO})_2$  [MoCo-TC1],  $\text{Mo}_2\text{Co}_2\text{S}_4\text{Cp}_2(\text{CO})_2$  [MoCo-TC2], and  $\text{Mo}_2\text{Co}_2\text{S}_4(\text{Cp}^{\prime\prime})_2(\text{CO})_2$  [MoCo-TC3], in which Et, Cp and Cp<sup>''</sup> represent ethyl group, cyclopentadiene, and pentamethylcyclopentadiene, respectively. These thiocubanes were synthesized in our laboratory based on the procedures of Brunner and Watcher [1982] and Halbert et al. [1985]. For comparative examination, bimetallic metal sulfide complex, cobalt bis-tetrathiomolybdate trianion was also synthesized based on the procedure of Pan et al. [1985]. The trianionic compound,  $(\text{PPh}_4)_3\text{Co}(\text{MoS}_4)_2$ , is designated as MoCo-S.

The U.S. Department of Energy Coal Samples (DECS, #9 and #12) were obtained from the Penn State/DOE Coal Sample Bank. The Montana subbituminous coal (DECS-9, PSOC-1546, < 60 mesh) has the following composition: 24.7% moisture, 4.8% ash, 33.5% volatile matter, and 37.1% fixed carbon on an as-received basis; 76.1% carbon, 5.1% hydrogen, 0.9% nitrogen, 0.3% organic sulfur, and 17.5% oxygen on a dmmf basis. The Pittsburgh #8 bituminous coal (DECS-12, PSOC-1549, < 60 mesh) has the following composition: 2.4% moisture, 10.0% ash, 35.2% volatile matter, and 52.4% fixed carbon on an as-received basis; 84.8% carbon, 5.7% hydrogen, 1.4% nitrogen, 0.7% organic sulfur, and 6.5% oxygen on a dmmf basis. The coals were dried for two hours at 100°C in a vacuum oven before use.

### Incipient Wetness Impregnation of Catalyst Precursors

The catalytic precursors were dispersed on to the coal by the incipient wetness impregnation (IWI) method using organic solvents. IWI method was applied to coal in a previous work [Huang et al., 1992]. Because of the difference in the solubility of the organometallic precursors, several solvents including toluene, THF,  $\text{CHCl}_3$  and acetonitrile were used for dissolving them. The organic solution of a precursor was intermittently added dropwise to the dried coal in a 100 mL beaker, in a fashion that the wet spots over the coal particles do not touch each other, followed by manual stirring with a glass rod until all signs of wetness disappeared. In order to keep the metal loading from different precursors at a constant level, we first estimated the incipient wetness volume prior to the catalyst impregnation with a given solvent, which means the total volume of the solvent needed to reach the point of incipient wetness: the point when the solution drops begin to remain on the external surface of the coal. The loading for the bimetallic thiocubanes was 0.5-0.6 wt% of molybdenum on the basis of dmmf coal. The impregnated coal sample was dried at 100°C for 2 h in a vacuum oven. IWI method is often used for loading inorganic salts from their aqueous solution on to a catalyst support without [Solar et al., 1991]. It should be noted that the IWI method used in our work is different from conventional one in that we only use certain amount of solution defined by the estimated incipient wetness volume to achieve a constant metal loading.

### Liquefaction under SSL and TPL Conditions

All reactions were carried out in 25 mL tubing bomb microautoclaves in a temperature-controlled fluidized sandbath. Each reaction used approximately 3 g dried coal. 1-Methylnaphthalene was used as the reaction solvent (3 g) unless otherwise mentioned. In several experiments tetralin was also used as a hydrogen-donor solvent (3 g) for comparison. The initial  $\text{H}_2$  pressure was 7 MPa at room temperature for all the runs. For catalyst screening, single-stage liquefaction (SSL) was performed, where the tubing bomb was rapidly heated to the prescribed temperatures (400-425. °C) for 30 minutes (plus a three minute heat-up period) followed by a rapid quench in cold water bath. Temperature-programmed liquefaction (TPL) had the tubing bomb rapidly heated up to a low temperature (275°C in all the catalytic runs, 200°C in the thermal

runs) and soaked at that temperature for 30 minutes before the temperature was gradually increased (5-7°C/min) to a higher temperature (400°C-425°C) and held there for 30 minutes before rapid quenching with cold water bath. These procedures were established in our recent work [Song and Schobert, 1992; Huang et al., 1992].

The gaseous product was vented after the reaction was complete and the liquid and solid products were washed into a tared ceramic thimble with hexane. The products were separated under a N<sub>2</sub> atmosphere by Soxhlet-extraction using hexane, toluene, and THF in succession. Solvents were removed by rotary evaporation, and the products were dried in vacuum at 100°C for 6 h except for the hexane-solubles. The asphaltene (toluene soluble, but hexane insoluble), preasphaltene (THF soluble, but toluene insoluble), and residue were weighed and the conversion and product distribution were calculated based on dmmf coal. All the runs were repeated at least once or twice to confirm the reproducibility. In most cases, the experimental errors were within ± 2 wt% for conversion, and the average data are reported here.

## Results and Discussion

### Effects of Precursor Type and Solvents for Impregnation

Table 1 shows the results of liquefaction of the Montana subbituminous coal at 400°C for 30 min. We first prepared and tested Mo<sub>2</sub>Co<sub>2</sub>S<sub>4</sub>(S<sub>2</sub>CNEt<sub>2</sub>)<sub>2</sub>(CH<sub>3</sub>CN)<sub>2</sub>(CO)<sub>2</sub> [MoCo-TC1], which was first synthesized and used recently by Halbert et al. [1991] in preparing MoCo hydrotreating catalyst. Using MoCo-TC1 impregnated on to DECS-9 coal from acetonitrile, however, showed little catalytic effect for increasing conversion. Replacing CH<sub>3</sub>CN with THF for impregnating MoCo-TC1 increased coal conversion relative to the thermal run by 14 wt%, but did not improve oil formation to any significant extent. It seems that the acetonitrile solution and the dithiocarbamate and acetonitrile ligands in MoCo-TC1 can poison the resulting catalyst under the conditions employed. This observation prompted us to prepare the thiocubane which contains no nitrogen in the ligands, leading to the synthesis of Mo<sub>2</sub>Co<sub>2</sub>S<sub>4</sub>Cp<sub>2</sub>(CO)<sub>2</sub> [MoCo-TC2], and Mo<sub>2</sub>Co<sub>2</sub>S<sub>4</sub>(Cp'')<sub>2</sub>(CO)<sub>2</sub> [MoCo-TC3]. The basic difference between these three thiocubanes is the type of ligands to the Mo [ Cp = C<sub>5</sub>H<sub>5</sub>, Cp'' = C<sub>5</sub>Me<sub>5</sub>; all the five (ring) carbon atoms are equidistant from the metal atom].

MoCo-TC2 impregnated from toluene afforded much higher conversion and oil yield; it appears to be much more active than MoCo-TC1. MoCo-TC3 exhibited slightly lower catalytic activity compared to MoCo-TC2. It was expected that MoCo-TC2 would afford greater conversion when THF was used as the impregnating solvent, since THF is a better swelling solvent and can penetrate the coal structure, which would improve the dispersion of the resulting Co-Mo bimetallic sulfide catalyst. Surprisingly, the catalytic liquefaction using MoCo-TC2 gave both higher oil yields and total conversion when toluene was used rather than THF. The structure and ligands of MoCo-TC3 and MoCo-TC2 are of the same nature, except that cyclopentadiene in MoCo-TC2 is substituted by pentamethylcyclopentadiene in MoCo-TC3. There was a small increase in the oil yield coupled with a decrease in preasphaltene yield when MoCo-TC3 was used in temperature-programmed liquefaction. Table 2 presents the results of catalytic runs of DECS-9 coal at 425°C. The order of catalytic activity at 425°C is the same as that observed from runs at 400°C: MoCo-TC2 > MoCo-TC3 > MoCo-TC1.

In an attempt to examine the role of bonding between Co and Mo, we further prepared and tested heterometallic cluster of the form Co(MoS<sub>4</sub>)<sub>2</sub><sup>3-</sup> which has distinctly different structure than the above-mentioned thiocubanes. Comparing results in Table 1 and Table 2 reveal that MoCo-S is more active than MoCo-TC1 at both 400 and 425°C but is much less active compared to MoCo-TC2, regardless of the

impregnating solvent.

Table 3 shows the effect of using the catalytic precursors on liquefaction of DECS-12 Pittsburgh #8 bituminous coal. At 400°C, the catalytic effects appear to be enhanced coal conversion to preasphaltene and asphaltene, with little increase in oil production relative to thermal run. At 425°C, using MoCo-TC2 increased total conversion significantly compared to the thermal run; it also promoted oil production moderately. However, increasing temperature from 400°C to 425°C caused decrease in total conversion both in thermal run and catalytic runs. In both cases, MoCo-TC2 was much more active than MoCo-TC1, although the latter was used under better conditions (TPL) than the former (SSL), as we further describe below. This again points to the negative impact of the CH<sub>3</sub>CN and S<sub>2</sub>CNEt<sub>2</sub> ligands in MoCo-TC1 upon the resulting catalyst in coal liquefaction. Therefore, it appears that an active MoCo bimetallic sulfide catalyst is generated in-situ from MoCo-TC2 during liquefaction. Under comparable conditions the catalyst from MoCo-TC1 is much less active, although an active catalyst could be generated also from this precursor if first decomposed at low temperature followed by venting and purging to remove poisonous compounds and followed by re-charging H<sub>2</sub> gas and heat-up.

By combining Tables 1, 2 and 3 it becomes very clear that MoCo-TC2 is the best precursor and MoCo-TC1 is the worst precursor among the three thiocubanes which differ from each other only in the type of ligands to Mo. Bimetallic sulfide complex MoCo-S also produces a catalyst whose activity is lower than that from MoCo-TC3 at 400°C and close to MoCo-TC3 at 425°C. In MoCo-S, the Co and Mo are bound through sulfur-bridge bonding, but in MoCo-TC2 or TC3, there are direct metal-metal bonds between Co-Mo, Co-Co, and Mo-Mo in addition to the sulfur-bridges. The superiority of MoCo-TC2 over MoCo-S may suggest the importance of direct metal-metal bonding; the differences between the three thiocubanes clearly indicate the importance of ligand type. The solvents used for loading the precursors are also influential. Both toluene and THF were tested for impregnating MoCo-TC2 but the non-polar solvent seems to be better in terms of higher oil yield; the optimum solvent and method for loading catalyst are not known yet. In summary, the above results indicate that both the ligands to the metal species and the type of bonding between the two metals affect the activity of the resulting bimetallic MoCo sulfide catalyst significantly. For a given precursor, the solvent used for catalyst impregnation also affects coal conversion, although the impregnating solvent was removed before reaction.

#### Effects of Temperature-Programming

The second major task in this study is to optimize the performance of promising catalysts selected from screening tests described above. As a means to increase conversion, the liquefaction of coals impregnated with the precursors was carried out under temperature-programmed (TPL) conditions, where the programmed heat-up serves as a step for both catalyst activation (precursor decomposition to active phase) and coal pretreatment or preconversion.

Table 4 shows the effects of temperature-programming on the catalytic and thermal runs of both DECS-9 and DECS-12 coals. In the presence of either MoCo-TC2 or MoCo-TC3, TPL runs in 1-MN always give higher conversions and higher oil yields than the corresponding SSL runs. At a final reaction temperature of 425°C with 1-MN solvent, TPL runs of both DECS-9 and DECS-12 coals using MoCo-TC2 or TC3 gave 13-15 wt% higher conversions and 5-11 wt% higher oil yields than the corresponding SSL runs. Most of the trends observed from Table 4 can be rationalized based on a general reaction model for liquefaction presented in recent papers [Song et al., 1989, 1991].

The first question that arises is why programmed heat-up is better than rapid heat-up? The superiority of TPL over SSL in catalytic runs with 1-MN solvent could be due to 1) more products from coal after longer residence time irrespective of catalyst, since a programmed heat-up is included in TPL but SSL only involves a very rapid heat-up in about three minutes followed by reaction at 400 or 425°C; 2) due to reactions including precursor decomposition and catalytic reactions during programmed heat-up. The first is not the case, as demonstrated by the fact that in the non-catalytic runs in 1-MN, using temperature programmed heat-up had essentially no impact on the liquefaction of DECS-9, neither on total conversion nor on product distribution, as can be seen from Table 4. The desirable effects of TPL, therefore, are associated with low-temperature catalytic hydrogenation reactions during programmed heat-up.

It is interesting to note from Table 4 that under TPL conditions using 1-MN solvent, increasing final temperature of all the catalytic runs from 400 to 425°C further increased coal conversions and oil yields considerably. In distinct contrast, under SSL conditions, increasing temperature of the catalytic runs (using MoCo-TC<sub>2</sub>, TC<sub>3</sub>) from 400 to 425°C caused marked decrease in the total conversions, which is a remarkable sign of significant retrogressive reactions. As pointed out in Song et al. [1989], the rate of coal thermal fragmentation is influenced by temperature and heating rate; very fast heating to high temperature would lead to extremely rapid fragmentation of coals that may exceed the capacity or rate of hydrogenation (H-donation) of the system, leading to significant retrogressive crosslinking. It is also likely that under SSL conditions (heating rates,  $\geq 100^\circ\text{C}/\text{min}$ ) very fast radical formation occurs before transformation of MoCo-TC<sub>2</sub> into active phase is completed, resulting in an imbalance between the rate of radical formation and the rate of radical-capping by H from catalyst surface, especially at higher temperature. In TPL runs, however, the catalyst precursor decomposes to form active bimetallic sulfide and the weak linkages are broken and stabilized during programmed heat-up, so that at the time the radical formation becomes considerable at high temperature (425°C), the catalyst is already activated and can provide dissociated hydrogen atom to cap the thermally generated radicals. These mechanistic considerations account for why using MoCo-TC<sub>2</sub> or TC<sub>3</sub> affords further increased conversion and oil yield under TPL conditions but gives decreased conversion under SSL conditions when the final reaction temperature is increased from 400 to 425 °C.

In regards to the catalytic effects associated with solvent, the increases in conversion and oil yield due to catalyst are much higher when using a non-donor 1-MN solvent as compared to the runs using a H-donor tetralin (Table 4). For example, for SSL runs of DECS-9 coal at 400°C, using MoCo-TC<sub>2</sub> increased coal conversion from about 32 to 75 wt% [(75-32)/32 = 134% increase] with 1-MN, and from about 71 to 88 wt% [(88-71)/71 = 24% increase] with tetralin. In the presence of H-donor solvent, the catalytic effects relative to thermal runs appear to be higher in SSL runs than under TPL conditions, as can be seen by comparing the thermal and catalytic runs with tetralin in Table 4.

## Conclusions

This work provides a fundamental approach to developing novel bimetallic dispersed catalysts and optimum conditions for coal conversion. We have synthesized and tested several heterometallic complexes consisting of two transition metals [Co, Mo] and sulfur as precursors of bimetallic dispersed catalysts for liquefaction of a subbituminous and a bituminous coal. The results revealed that both the ligands to the metal species and the type of bonding between the two metals affect the activity of the resulting catalyst significantly. Among the M-M' type precursors tested, Mo-Co thiocubane cluster,  $\text{Mo}_2\text{Co}_2\text{S}_4(\text{Cp})_2(\text{CO})_2$  [MoCo-TC<sub>2</sub>], produced the best catalyst. Loading

of MoCo-TC2 at the level of 0.5 wt% Mo can increase the conversion of the subbituminous coal from 32 to as high as 80 wt%. The performance of the Mo-Co bimetallic catalyst was further enhanced by using temperature programmed heat-up (TPL) conditions. For a final temperature of 425°C, using the programmed conditions with MoCo-TC2 significantly increased the conversions by about 12-13 wt% for both coals, as compared to the non-programmed runs. Further work is now in progress.

### Acknowledgements

This project was supported by the US DOE Pittsburgh Energy Technology Center and the US Air Force Wright Laboratory/Aero Propulsion and Power Directorate. We are pleased to thank Mr. W. E. Harrison III and Dr. D. M. Storch of WL, and Dr. S. Rogers of PETC for their support. We gratefully acknowledge Mr. J. McConnie for his assistance in the non-catalytic SSL and TPL experiments. We also wish to thank Dr. A. Davis and Mr. D.C. Glick of PSU for providing the samples and data of the coals from the sample bank, and Dr. A.S. Hirschon of SRI International for providing recent literature information.

### References

- Brunner, H.; Wachter, J., *J. Organomet. Chem.* 1982, 240, C41-44.  
Derbyshire, F.J.; *Catalysis in Coal Liquefaction*, IEACR/08, IEA Coal Research, London, 1988, 69 pp.  
Garg, D.; Givens, E.N.; *Fuel Process. Technol.*, 1984, 8, 123-134.  
Halbert, T. R.; Cohen, S. A.; Stieffel, E. I., *Organometallics* 1985, 4, 1689-1690.  
Halbert, T.R.; Ho, T. C. Stieffel, E. I.; Chianelli, R. R., Daage, M., *J. Catal.* 1991, 130, 116-119.  
Herrick, D. E.; Tierney, J. W.; Wender, I.; Huffamn, G. P.; Huggins, F. E., *Energy & Fuels* 1990, 4, 231-236.  
Hirschon, A.S.; Wilson, R.B.; *Am. Chem. Soc. Sym. Ser.*, 1991, 461, 273-283.  
Hirschon, A.S.; Wilson, R.B.; *Fuel*, 1992, 71, 1025-1031.  
Huang, L.; Song, C.; Schobert, H. H., *Am. Chem. Soc. Div. Fuel Chem. Prepr.*, 1992, 37(1), 223-227.  
Mingos, D.M.P.; Wales, D.J., "Introduction to Cluster Chemistry", Prentice Hall: Englewood Cliffs, New Jersey, 1990, 318 pp.  
Solar, J.M.; Derbyshire, F.J.; de Beer, V.H.J.; Radovic, L.R.; *J. Catal.*, 1991, 129, 330-342.  
Sommerfeld, D.A.; Jaturapitpornsakul, J.; Anderson, L.; Eyring, E.M.; *Am. Chem. Soc. Div. Fuel Chem. Prepr.*, 1992, 37(2), 749-755.  
Song, C.; Nomura, M.; Miyake, M.; *Fuel*, 1986, 65, 922-926.  
Song, C.; Hanaoka, K.; Nomura, M.; *Fuel*, 1989, 68, 287-292.  
Song, C.; Nomura, M.; Ono, T., *Am. Chem. Soc. Div. Fuel Chem. Prepr.* 1991, 36(2), 586-596.  
Song, C.; Schobert, H. H.; Hatcher, P. G., *Energy & Fuels*, 1992, 6, 326-328.  
Song, C.; Schobert, H. H.; *Am. Chem. Soc. Div. Fuel Chem. Prepr.* 1992, 37(2), 976-983.  
Suzuki, T.; Ando, T.; Watanabe, Y., *Energy & Fuels* 1987, 1, 299-300.  
Swanson, A.; *Am. Chem. Soc. Div. Fuel Chem. Prepr.* 1992, 37(1), 149-155.  
Yamada, O.; Suzuki, T.; Then, J.; Ando, T.; Watanabe, Y.; *Fuel Process. Technol.*, 1985, 11, 297-311.

**Table 1.** Liquefaction of DECS-9 Montana Subbituminous Coal at 400°C for 30 min

Catalyst precursor	Solvent for catalyst impregn <sup>a</sup>	Reaction solvent <sup>b</sup>	Reaction condition	Oil + Gas dmmf wt%	Asphalt dmmf wt%	Preasph. dmmf wt%	Tot Conv dmmf wt%
None	None	1-MN	SSL	16.0	9.4	6.8	32.2
MoCo-TC1	CH <sub>3</sub> CN	1-MN	SSL	22.8	4.8	5.2	32.8
MoCo-TC1	THF	1-MN	SSL	18.7	12.8	14.8	46.3
MoCo-TC2	Toluene	1-MN	SSL	32.4	18.0	24.2	74.6
MoCo-TC2	THF	1-MN	SSL	25.8	17.9	23.7	67.4
MoCo-TC3	Toluene	1-MN	TPL	33.8	17.8	19.9	71.5
MoCo-S	CHCl <sub>3</sub>	1-MN	SSL	21.3	12.6	16.0	49.8

a) The impregnating solvent was removed by evaporation in vacuum before reaction.

b) 1-MN was added as reaction solvent after the impregnating solvent was removed.

**Table 2.** Liquefaction of DECS-9 Montana Subbituminous Coal at 425°C for 30 min

Catalyst precursor	Solvent for catalyst impregn	Reaction solvent	Reaction condition	Oil + Gas dmmf wt%	Asphalt dmmf wt%	Preasph. dmmf wt%	Tot Conv dmmf wt%
None	None	1-MN	SSL	16.7	16.4	13.8	46.9
MoCo-TC1	THF	1-MN	SSL	20.3	9.9	5.7	35.9
MoCo-TC2	Toluene	1-MN	SSL	42.3	14.9	14.8	72.0
MoCo-TC2	THF	1-MN	SSL	36.5	15.5	18.0	70.0
MoCo-TC3	Toluene	1-MN	SSL	36.7	11.9	13.2	61.4
MoCo-S	CHCl <sub>3</sub>	1-MN	SSL	34.9	11.1	13.2	59.2

**Table 3.** Liquefaction of Pittsburgh #8 Bituminous Coal in 1-MN at 400-425°C

Catalyst precursor	Solvent for catalyst impregn	Reaction temp °C	Reaction condition	Oil + Gas dmmf wt%	Asphalt dmmf wt%	Preasph. dmmf wt%	Tot Conv dmmf wt%
None	None	400	SSL	13.7	20.4	26.8	60.9
MoCo-TC1	THF	400	TPL	9.8	21.9	34.0	65.7
MoCo-TC2	Toluene	400	SSL	14.5	27.8	34.3	76.6
None	None	425	SSL	16.2	19.1	16.1	51.4
MoCo-TC1	THF	425	TPL	16.9	24.6	19.4	60.8
MoCo-TC2	Toluene	425	SSL	21.8	27.7	23.8	73.3

**Table 4.** Effect of Temperature Programming on Coal Liquefaction Using Bimetallic Thiocubane Precursors MoCo-TC2 and MoCo-TC3\*\*

Catalyst precursor	Solvent for catalyst impregn	Reaction solvent	Reaction condition	Oil + Gas dmmf wt%	Asphalt dmmf wt%	Preasph. dmmf wt%	Tot Conv dmmf wt%
<b>DECS-9 Montana Subbit Coal</b>							
None	400	1-MN	SSL	16.0	9.4	6.8	32.2
None	400	1-MN	TPL	18.9	8.2	7.0	34.1
MoCo-TC2	400	1-MN	SSL	32.4	18.0	24.2	74.6
MoCo-TC2	400	1-MN	TPL	37.0	19.8	22.0	78.7
None	425	1-MN	SSL	16.7	16.4	13.8	46.9
MoCo-TC2	425	1-MN	SSL	42.3	14.9	14.8	72.0
MoCo-TC2	425	1-MN	TPL	46.7	19.5	15.0	81.1
MoCo-TC3	425	1-MN	SSL	36.7	11.9	13.2	61.4
MoCo-TC3	425	1-MN	TPL	46.3	17.5	12.9	76.6
None	400	Tetralin	SSL	29.4	20.6	21.4	71.4
None	400	Tetralin	TPL	34.4	21.1	23.7	79.2
MoCo-TC2	400	Tetralin	SSL	44.1	22.9	21.0	88.1
MoCo-TC2	400	Tetralin	TPL	46.4	25.4	17.4	89.2
<b>DECS-12 Pittsburgh #8 Bitum Coal</b>							
None	400	1-MN	SSL	13.7	20.4	26.8	60.9
MoCo-TC2	400	1-MN	SSL	14.5	27.8	34.3	76.6
MoCo-TC2	400	1-MN	TPL	15.8	28.7	35.4	79.9
None	425	1-MN	SSL	16.3	17.6	16.1	51.4
MoCo-TC2	425	1-MN	SSL	21.8	27.6	23.9	73.3
MoCo-TC2	425	1-MN	TPL	33.1	31.5	23.4	87.9
MoCo-TC2	400	Tetralin	SSL	18.8	32.6	31.0	82.4
MoCo-TC2	400	Tetralin	TPL	21.9	34.2	33.0	89.1

\*\* Impregnated from toluene solution using incipient wetness method.

## MILD PRETREATMENT METHODS FOR IMPROVING THE LOW SEVERITY REACTIVITY OF ARGONNE PREMIUM COALS

S. Kelkar, K. Shams, R. L. Miller, and R. M. Baldwin  
Chemical Engineering and Petroleum Refining Department  
Colorado School of Mines  
Golden, Colorado 80401

### ABSTRACT

This paper describes results from an on-going coal pretreatment study with the goal of developing simple, inexpensive treatment options to enhance low severity coal dissolution reactivity. Data are presented for two pretreatment methods: 1) ambient treatment with methanol and hydrochloric acid, and 2) aqueous carbonic acid treatment. We have found that ambient pretreatment of eight Argonne coals using methanol and a trace amount of hydrochloric acid improves THF-soluble conversions by 24.5 wt% (maf basis) for Wyodak subbituminous coal and 28.4 wt% for Beulah-Zap lignite with an average increase of 14.9 wt% for liquefaction of the eight coals at 623 K (350°C) reaction temperature and 30 min. reaction time. Pretreatment with methanol and HCl separately indicated that both reagents were necessary to achieve maximum liquefaction improvement. The extent of calcium removal correlated well with reactivity enhancement in these experiments. This effect is attributed to the role of calcium as a catalyst for retrogressive reactions during the initial stages of dissolution. Preliminary treatment results using CO<sub>2</sub>/H<sub>2</sub>O suggest that the reactivity of bituminous coals such as Illinois #6 can be significantly enhanced with this method but that less improvement is seen for low rank coals such as Wyodak or Beulah-Zap.

### INTRODUCTION

Much of the recent research in direct coal liquefaction seeks to develop methods for dissolving coal at lower reaction severity [often defined as temperatures below 623 K (350°C) and pressures in the range of 6.9-10.3 MPa (1000-1500 psi)]. The incentives for developing a viable low severity liquefaction process are numerous; they include: 1) reduced hydrocarbon gas production resulting in reduced feed gas consumption and enhanced hydrogen utilization efficiency; 2) suppressed retrogression of primary coal dissolution products resulting in enhanced distillate and residuum product quality; 3) production of high boiling residuum which is less refractory and thus more amenable to catalytic upgrading in a conventional second-stage hydrocracker; 4) substitution of less expensive off-the-shelf vessels, piping, valves, pumps, etc. in place of expensive, custom-designed units; and 5) less severe slurry handling and materials of construction problems as a result of lower operating temperatures and pressures.

However, as shown schematically in Figure 1, lowering the reaction severity reduces coal conversion reaction rates and liquid product yields unless the intrinsic coal reactivity can be sufficiently enhanced using some method of physical or chemical pretreatment prior to dissolution. Possible methods for reactivity enhancement include: 1) dispersed homogeneous or heterogeneous catalysts, 2) promoters such as basic nitrogen compounds, 3) physical pretreatment of the coal structure, or 4) chemical pretreatment of the coal's inorganic and organic fractions. Generally these methods all improve low severity coal liquefaction reactivity, but for various reasons (use of exotic, expensive, and sometimes hazardous chemical feedstocks; long pretreatment times; and the potential for incorporating undesirable chemical constituents into the coal), none have been seriously considered as a process step in coal liquefaction. The objective of the research described in this paper has been to develop simple, inexpensive coal pretreatment methods using readily available commodity chemicals to enhance low severity liquefaction reactivity of lignites, subbituminous, and bituminous coals.

In the past, chemical treatments including reductive and non-reductive alkylation (1,2), acylation (3), partial oxidation (4), alkali hydrolysis (5), and solvent swelling (6) have been used to disrupt the coal's organic structure, increase solubility in selected solvents, and improve liquefaction reactivity. Selected coal demineralization has also been studied as a method for enhancing liquefaction reactivity. Mochida (7) reported that hydrochloric acid can be used to destroy cationic bridges present in low rank coals, thereby reducing coordination between oxygen-containing functional groups and allowing better contacting between coal and solvent during the initial stages of dissolution. Joseph (8) used ion exchange techniques to remove various cations from Wyodak subbituminous coal and North Dakota lignite. He found that removal of calcium, magnesium, sodium, and potassium from each low rank coal improved high severity [673 K (400°C), 3.5 MPa (500 psig) H<sub>2</sub>, 60 min.] liquefaction conversion and product quality. This result was attributed to inhibited hydrogen transfer in the presence of alkaline and alkaline earth cations. Serio (9) also found that ion-exchanged and demineralized low rank coals were more reactive at high reaction severity. He attributed his results to reduced cross-linking of the treated coals during the initial stages of dissolution.

The objective of this paper is to present experimental results from a study in which two pretreatment methods were used to improve intrinsic coal reactivity at low severity liquefaction conditions. Possible explanations for the observed reactivity enhancement will also be discussed.

#### EXPERIMENTAL PROCEDURE

The entire suite of eight coals from the Argonne Premium Coal Sample Bank was used as the source of feed coals for this study. Ultimate analysis (10) and calcium content (11) data for each coal are listed in Table I. Additional chemical and physical properties of the Argonne coals have been reported (12).

Two methods of coal pretreatment were used in this study. The first method employed a liquid phase technique we developed based on the gas phase alkylation chemistry reported by Sharma (13). Coal was pretreated by suspending 5 g of undried coal in 40 cm<sup>3</sup> of methanol and 0.2 cm<sup>3</sup> (0.5 vol%) of concentrated hydrochloric acid in a 100 cm<sup>3</sup> round bottom flask and continuously stirring the coal/methanol slurry on a magnetic stirring plate for the desired pretreatment time (usually 3 hrs.). The flask was connected to a cooling water condenser to reduce solvent losses by evaporation. Treated coal samples were washed with 500 cm<sup>3</sup> aliquots of methanol and centrifuged to remove excess acid and soluble mineral species.

The second pretreatment method was based on a CO<sub>2</sub>/H<sub>2</sub>O treatment technique reported by Hayashi, et al. (14). Five gram samples of coal were pre-dried at 50°C in vacuum [1.3-2.6 Pa (10-20 millitorr)] for 1 hour and then placed in a 300 cm<sup>3</sup> autoclave reactor. Distilled water (100 g) was added to the reactor which was then sealed, flushed with CO<sub>2</sub>, and finally pressurized with CO<sub>2</sub> to 600 KPa (87 psig) pressure at ambient temperature. The coal/water slurry was agitated at 1000 rpm for the desired treatment time (usually 2 hours). At the end of each pretreatment run, the reactor was depressurized and the moist coal sample recovered from the slurry by centrifugation. Each sample was washed with 500 cm<sup>3</sup> aliquots of distilled water to remove any water-soluble species present in the treated coal.

Coal samples from each pretreatment method were vacuum dried at 298 K (25°C) under 1.3-2.6 Pa (10-20 millitorr) pressure for 24 hrs. Untreated coal samples were vacuum dried at the same conditions prior to use. After drying, all treated and untreated coal samples were stored at room temperature in a vacuum desiccator at 13.3 Pa (0.1 torr) before analysis or liquefaction. Reactor runs were scheduled so that each coal sample was stored for less than 12 hours before use. Portions of each untreated coal and pretreated coal were subjected to elemental analysis and ash analysis, as well as <sup>1</sup>H CRAMPS NMR, <sup>13</sup>C CP/MAS NMR, FTIR, Mossbauer, and XRD spectroscopy.

Liquefaction experiments were conducted in a 20 cm<sup>3</sup> tubing bomb reactor system attached to an agitator and immersed in a fluidized sandbath. Low severity liquefaction conditions were set at 350°C reaction temperature, 6.9 MPa (1000 psig) initial cold hydrogen pressure, and 30 minutes reaction time. Dihydrophenanthrene (DHP) was used as hydrogen donor solvent (2/1 solvent/coal wt. ratio) in these runs. Coal conversion was monitored using THF extraction data corrected for the intrinsic THF solubilities of treated and untreated coals. Solubility measurements were conducted at ambient conditions and consisted of three steps: 1) sonicating the liquid products from the tubing bomb reactor (or feed coal sample) in excess THF for 10 min., 2) centrifuging the mixture at 2000 rpm for 20 min., and 3) decanting THF-soluble products and excess THF from the THF-insoluble residuum. This procedure was repeated at least two times or until no additional THF-soluble products were recovered. Remaining THF-insolubles were dried at 373 K (100°C) for 24 hours to remove residual THF, weighed, and finally ashed. Coal conversion to THF-soluble products was computed on a moisture and ash-free basis correcting for the intrinsic solubility of each feed coal sample. Thus reported changes in coal conversion levels can be attributed solely to inherent differences in low severity coal liquefaction reactivity and not to changes in intrinsic solubility.

## RESULTS AND DISCUSSION

Several sets of experiments were completed to evaluate the effectiveness of our pretreatment method in enhancing low severity liquefaction reactivity. In each set of runs, individual reactor experiments were duplicated and in some cases triplicated. Results shown in this paper represent average values of replicated runs; conversion differences of 2.1 wt% or greater (maf basis) represent statistically significant differences in liquefaction reactivity at the 95% confidence level.

Baseline low severity liquefaction reactivity data for the untreated Argonne coals are summarized in Figures 2 and 3. At the conditions studied, three of the high volatile bituminous coals [Illinois #6 (75.0 wt%), Blind Canyon (69.9 wt%), and Pittsburgh #8 (57.0 wt%)] gave the highest THF conversions. Wyodak subbituminous coal was the next most reactive coal (42.0 wt%), while Pocahontas low volatile bituminous coal was the least reactive sample studied (15.6 wt%). These reactivity data follow the generally accepted trends reported for thermal conversion of the Argonne coals (15).

Pretreatment with methanol and 1.5 vol% HCl for three hours at ambient conditions using the procedure described earlier enhanced low severity liquefaction reactivity for all eight Argonne coals. The absolute increase ranged from 24.5 wt% for Wyodak coal and 28.4 wt% for Beulah-Zap lignite to 5.2 wt% for Blind Canyon coal, and averaged 14.9 wt% for the eight coals. No simple trends in reactivity improvement with chemical or physical properties of the coals were obvious, although reactivity of the pretreated low rank coals (Wyodak and Beulah-Zap) increased much more than reactivity of the six bituminous coals.

Although Sharma (13) showed that vapor phase methanol/HCl mixtures would partially alkylate bituminous coals, elemental analyses of the treated coals indicated that little methylation (fewer than 0.1 methyl groups/100 C atoms) had occurred during liquid phase methanol/HCl pretreatment; no evidence of methylation was observed from NMR and FTIR measurements on untreated and treated coal samples. This result was confirmed by replacing methanol with hexane during coal pretreatment; reactivity of hexane/HCl pretreated coals was also enhanced. Since hexane cannot participate in the proposed alkylation chemistry, other effects must also contribute to the observed reactivity enhancement. Several pretreatment experiments were conducted using acetone in place of methanol or hexane and similar reactivity results were obtained. Throughout this portion of the study, we found no obvious trends relating reactivity enhancement, pretreatment solvent properties, and coal properties. Our general conclusion is that any simple organic solvent may be used to conduct the liquid phase pretreatment step.

The effect of CO<sub>2</sub>/H<sub>2</sub>O pretreatment on low severity liquefaction of the Argonne coals is also shown in Figures 2 and 3. With the exception of Blind Canyon coal, CO<sub>2</sub>/H<sub>2</sub>O pretreatment significantly enhanced low severity reactivity of each Argonne coal. Interestingly, the extent of enhancement for the two low rank coals (Wyodak and Beulah-Zap) was significantly lower than the enhancement observed using MeOH/HCl pretreatment. Conversely, CO<sub>2</sub>/H<sub>2</sub>O pretreatment of each bituminous coal except Blind Canyon and Lewiston-Stockton provided greater reactivity enhancement than MeOH/HCl pretreatment.

At this point, we can only speculate on the contrast in reactivity behavior between the two pretreatment methods. We have previously reported (16) that reactivity enhancement using MeOH/HCl pretreatment can be correlated with the extent of calcium removal and that HCl destroys calcium dicarboxylate bridging structures. We also presented model compound evidence (16) that calcium can directly catalyze retrogressive reactions involving coal-derived free radical intermediates during the initial stages of coal dissolution. Thus, it appears that given the reactivity enhancement data shown in Figures 2 and 3, we can tentatively conclude that CO<sub>2</sub>/H<sub>2</sub>O pretreatment more efficiently removes calcium from coals such as Illinois #6 in which calcium exists predominately as part of a discrete mineral phase, while MeOH/HCl pretreatment more efficiently removes calcium from dicarboxylate bridging structures which predominately occur in low rank coals. Further analyses of pretreated coals and additional model compound experiments are currently underway to help elucidate pretreatment effects on low severity coal liquefaction reactivity.

#### ACKNOWLEDGMENT

We wish to acknowledge financial support from the U.S. Department of Energy under Contract Nos. DE-AC22-88PC88812 and DE-FG22-90PC90289. Jenefer R. Olds performed the intrinsic solubility analyses for untreated and treated coal samples.

#### LITERATURE CITED

1. Sternberg, H. and Delle Donne, C.L. *Fuel* 1974, **53**, 172.
2. Liotta, R. *Fuel* 1979, **58**, 724.
3. Hodek, W. and Kolling, G. *Fuel* 1973, **52**, 220.
4. Hessley, R.K. 'Co-Oxidative Depolymerization of Coal,' Final Report for Electric Power Research Institute Project No. 2383-2, June 1985.
5. Mirza, Z.B., Sarkar, M.K. and Sharma, D.K. *Fuel Proc. Tech.* 1984, **2**, 149.
6. Sanada, Y. and Honda, H. *Fuel* 1986, **65**, 295.
7. Mochida, I., Shimohara, T., Korai, Y., Fujitsu, H. and Takeshita, K. *Fuel* 1983, **62**, 659.
8. Joseph, J.T. and Forrai, T.R. *Fuel* 1992, **71**, 75.
9. Serio, M.A., Solomon, P.R., Kroo, E., Bassilakis, R., Malhotra, R., and McMillen, D. *Am. Chem. Soc. Div. Fuel Chem. Prepr.* 1990, **35**(1), 61.
10. Vorres, K.S. *Energy & Fuels* 1990, **4**, 420.
11. Doughten, M.W. and Gillison, J.R. *Energy & Fuels* 1990, **4**, 426.
12. Vorres, K.S. "Users Handbook for the Argonne Premium Coal Sample Program," Argonne National Laboratory, Argonne, Illinois, October 1989.
13. Sharma, D.K., Sarkar, M.K., and Mirza, Z.B. *Fuel* 1985, **64**, 449.
14. Hayashi, J., Takeuchi, K., Kusakabe, K., and Morooka, S. *Fuel* 1990, **70**, 1181.
15. Shin, S.C., Baldwin, R.M. and Miller, R.L. *Energy & Fuels* 1989, **3**, 193.
16. Shams, K., Miller, R.L., and Baldwin, R.M. *Fuel* 1992, **71**, 1015.

**Table I**  
**Analysis of Feed Coals**

Ultimate Analysis (wt% maf coal)	Wyodak	Beulah-Zap	Ill. #6	Pittsburgh #8
Carbon	68.4	65.9	65.7	75.5
Hydrogen	4.9	4.4	4.2	4.8
Nitrogen	1.0	1.0	1.2	1.5
Sulfur	0.6	0.8	4.8	2.2
Oxygen	16.3	18.2	8.6	6.7
Ash	8.8	9.7	15.5	9.3
Calcium content (wt% maf coal)	1.20	1.54	0.96	0.21
Coal Rank	Subbit.	Lignite	HVB	HVB
Symbol	WY	ND	IL	PITT

**Table I (cont.)**  
**Analysis of Feed Coals**

Ultimate Analysis (wt% maf coal)	Blind Canyon	Lewiston- Stockton	Upper Freeport	Pocahantas
Carbon	76.9	66.2	74.2	86.7
Hydrogen	5.5	4.2	4.1	4.2
Nitrogen	1.5	1.3	1.4	1.3
Sulfur	0.6	0.7	2.3	0.7
Oxygen	10.8	7.8	4.8	2.3
Ash	4.7	19.8	13.2	4.8
Calcium content (wt% maf coal)	0.41	0.06	0.45	0.45
Coal Rank	HVB	HVB	MVB	LVB
Symbol	UT	WV	UF	POC

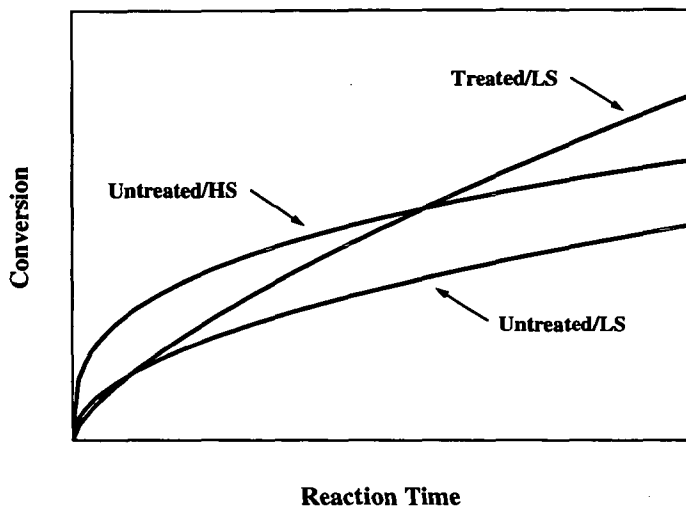


Figure 1 - Schematic Representation of Reactivity Enhancement Using Coal Pretreatment (LS = low reaction severity, HS = high reaction severity)

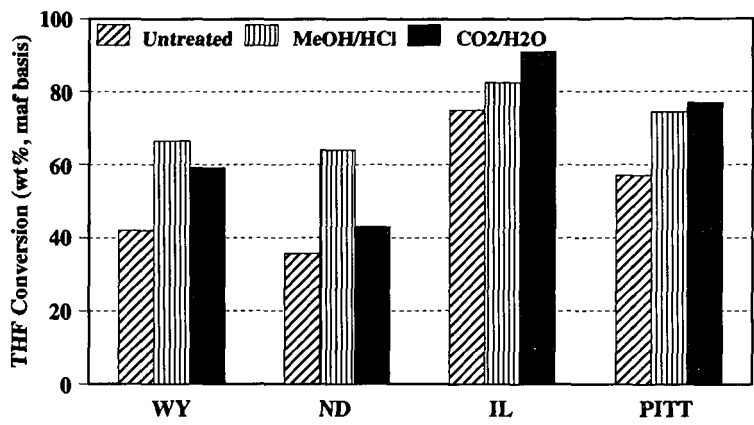


Figure 2 - Effect of Pretreatment with Methanol/Hydrochloric acid and Carbon Dioxide/Water on Low Severity Liquefaction Reactivity of Argonne Coals

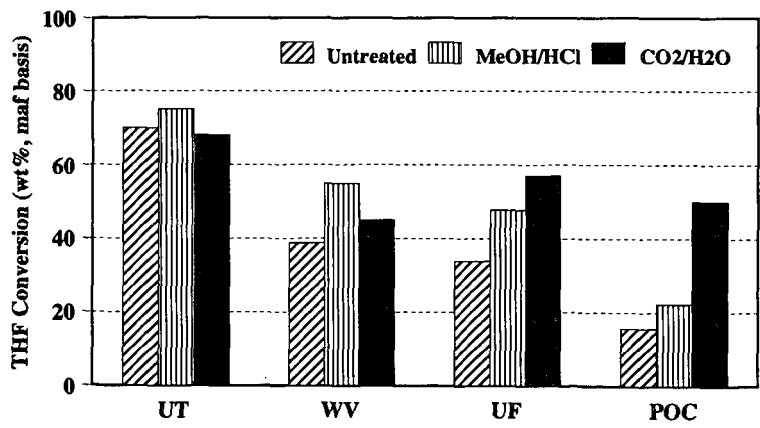


Figure 3 - Effect of Pretreatment with Methanol/Hydrochloric acid and Carbon Dioxide/Water on Low Severity Liquefaction Reactivity of Argonne Coals

DISSOLUTION OF THE ARGONNE PREMIUM  
COAL SAMPLES IN STRONG BASE\*

R. E. Winans, R. L. McBeth, and J. E. Hunt  
Chemistry Division, 9700 S Cass Avenue  
Argonne National Laboratory, Argonne, IL 60439

Keywords: Solubilization, Base Hydrolysis, Premium Coals

INTRODUCTION

The objective of this study is to solubilize the Argonne Premium Coal Samples in order to facilitate analysis by mass spectrometry, FTIR and NMR. Earlier, in a search for relatively mild methods for solubilizing coal, we discovered that treating coals with potassium hydroxide in ethylene glycol at 250°C to be quite an effective approach.<sup>1</sup> Under these conditions, secondary reactions which may obscure the distribution of the basic building blocks of the coal structure are not expected to occur. At higher temperatures, such as those used in more traditional liquefaction processes (> 400 °C), secondary reactions such as the formation of polycyclic aromatic and heteroaromatic compounds dominate.

A focus of our approach to characterization of coals is desorption-pyrolysis high resolution CI and EI mass spectrometry and laser desorption mass spectrometry (LDMS). It has been shown by PyMS that the yields and the distribution of products is superior for coal extracts compared to the original whole coals.<sup>2,3</sup> There appears to be few secondary reactions occurring and many molecules, which are released in analysis of the extract, are trapped in the solid matrix of the coal and never observed. In addition, soluble materials are more amenable to LDMS.<sup>4</sup>

The glycol/KOH system was chosen since in early work up to 93% of the product was soluble for lower-rank bituminous coals.<sup>1</sup> Others have solubilized coals under basic conditions. Ouchi and co-workers<sup>5</sup> used ethanolic - NaOH at temperatures ranging from 260 °C to 450 °C. More recently, Stock and co-workers have discussed the use of Lochmann's base (potassium tert-butoxide, n-butyl lithium in heptane at reflux) which is especially effective for the higher rank coals.<sup>6,7</sup> Also, a base hydrolysis is included in a low severity liquefaction scheme devised by Shabtai and co-workers.<sup>8</sup>

Table VII-1. Elemental analyses for the coal samples.

Sample	Name	%C (dmmf)	H	Per 100 Carbons		
				N	S	O
8	Beulah-Zap Lignite	74.1	79.5	1.35	0.36	20.9
2	Wyodak-Anderson SubB	76.0	85.6	1.28	0.23	18.0
3	Herrin hvCB	80.7	77.2	1.51	1.15	13.0
6	Blind Canyon hvBB	81.3	85.7	1.67	0.17	10.8
4	Pittsburgh hvAB	85.0	76.7	1.69	0.40	7.96
7	Lewiston-Stockton hvAB	85.5	76.3	1.62	0.30	8.93
1	Upper Freeport mvB	88.1	66.0	1.55	0.32	6.59
5	Pocahontas lvB	91.8	58.5	1.25	0.21	2.04

## EXPERIMENTAL

The following procedure was applied to all eight of the Argonne Premium Coal Samples. Approximately 20 g of coal was stirred in 100 ml concentrated HCl and 100 ml 48% HF under a N<sub>2</sub> atmosphere in a teflon container for at least 48 hours. After dilution to 1.5 l with distilled water, it was filtered through acid-hardened filter paper, the residue was washed off the paper and, subsequently, filtered through a sintered glass funnel, washed acid-free and vacuum dried at 100 °C for 16 hours. An ash determination was made on the dried product.

The demineralized coal was refluxed in pyridine for 10 hours. After cooling, the residue was separated by centrifuging and decantation. The residue was stirred in 5% HCl heated to 80°C for 2 hours, filtered, washed acid-free with distilled water, then methanol and, finally, vacuum dried at 100 °C for 16 hours. The pyridine solution was roto-evaporated to dryness and the pyridine soluble material was treated in the same manner as the insoluble; hot 5% HCl but no methanol rinse.

Ten grams of the pyridine extracted residue was added to a 100 ml solution of 10 g KOH and dissolved in ethylene glycol in a 300 ml stirred Parr reactor. The reaction mixture was heated to 250 °C for 2 hours and cooled. After dilution to 1 l, the mixture was heated to 60 °C and filtered, washed alkaline-free, and the residue vacuum dried at 100 °C for 16 hours.

The residue was then successively extracted by refluxing for 2 hours in hexane, 1:1 benzene-methanol, and pyridine. The filtrates were roto-evaporated to dryness and vacuum dried at 60 °C for 16 hours. The pyridine soluble and insoluble residues were washed as described above with 5% HCl and vacuum dried at 100 °C for 16 hours.

## RESULTS AND DISCUSSION

The solubility yields from the KOH in glycol reaction are shown in Figure 1. The pyridine soluble yields are a combination of the yield of pyridine solubles prior to the reaction added to the pyridine solubles produced during the reaction of the extracted coal. This reaction produces (typically less than 1%) of very small, non-polar molecules which would be soluble in hexane. Indigenous molecules of this type would have been removed prior to the reaction by the initial pyridine extraction. Apparently, the extensive bond breaking which occurs at higher temperatures such as in pyrolysis and liquefaction is not taking place under those reaction conditions. In addition, the recovery weights were very close to 100% for all of the samples. Very little sample weight was lost to small molecules or gained from the addition of the solvent to the products.

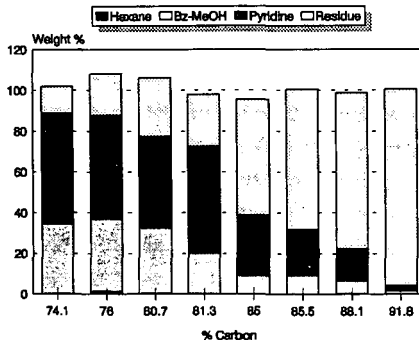


Figure 1. Yields from the ethylene glycol-KOH treatment of the Argonne Premium Coals.

A much more definitive trend is seen for the decrease in soluble product yields as a function of increasing rank than in the previous study.<sup>1</sup> In the original study, surprisingly, only 60% of the lignite products were soluble. However, this lignite coal was highly oxidized and had not been stored under premium conditions as is the case with the present samples. This procedure is obviously very effective for the lower rank coals. There are significant yields of benzene/MeOH solubles in the three lowest rank coals. These mixtures are typically much more amenable to characterization than the pyridine extracts.

There is good correlation with oxygen content as is shown in Figure 2. This is expected since it is likely that cleavage of ether linkages is one of the important mechanisms of solubilization. The Utah coal is much more reactive than expected from its oxygen content. However, this coal tends to be much more reactive than one would expect from its rank, such as in vacuum pyrolysis.<sup>2</sup> Also, this result implies that oxygen functionality is only partially responsible for the mechanisms of solubilization for this reaction.

The Lochmann's base reaction yields the opposite rank trend compared to the KOH/glycol approach. For the subbituminous coal, which has been methylated, the pyridine solubility increases only to 44% from 35%,<sup>6</sup>

while for the high rank Pocahontas coal (APCS 5), pyridine solubility increases dramatically from 2.5% to 55% upon treatment with the base.<sup>7</sup> These results suggest that these two different base treatments can be used in parallel to produce a very soluble set of samples for the complete set of Argonne Premium Coal Samples. Mass spectral data from both LDMS and DCIMS, along with FTIR data, are being analyzed for this complete set of samples from the KOH glycol solubilization.

#### ACKNOWLEDGMENT

This work was performed under the auspices of the Office of Basic Energy Sciences, Division of Chemical Sciences, U.S. Department of Energy, under contract number W-31-109-ENG-38.

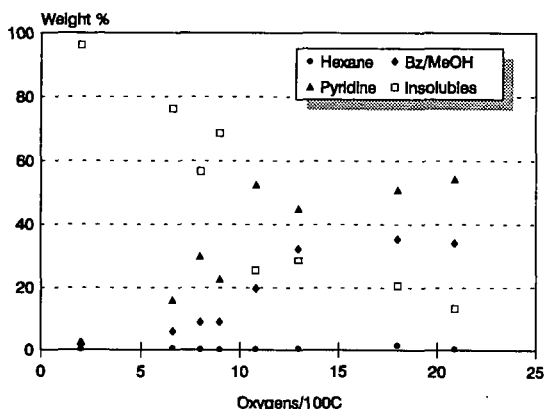


Figure 2. Yields as a function of oxygen content for the ethylene glycol-KOH reaction.

## REFERENCES

1. Winans, R.E.; Hayatsu, R.; McBeth, R.L.; Scott, R.G.; Moore, L.P.; Studier, M.H. In *Coal Structure*, Gorbaty and Ouchi, K. Eds.; Adv. Chem. Series 192, ACS, 1981, 161-178.
2. Winans, R.E.; Melnikov, P.E.; McBeth, R.L. *Preprint, Div. Fuel Chem., ACS, 1992, 37(2)*, 693-698.
3. Cagniant, D.; Gruber, R.; Lacordaire-Wilhem, C.; Shulten, H.-R. *Energy Fuels*, 1992, 6, 702-708.
4. Hunt, J.E.; Lykke, K.R.; Winans, R.E. *Preprint, Div. Fuel Chem., ACS, 1992, 36(3)*, 1325-1329.
5. Ouchi, K.; Hosokawa, S.; Maeda, K.; Itoh, H. *Fuel*, 1982, 61, 627-630.
6. Chatterjee, K.; Miyake, M.; Stock, L.M. *Energy Fuels*, 1990, 4, 242-248.
7. Chatterjee, K. Ph.D. Dissertation, The University of Chicago, 1991.
8. Shabtai, J.; Saito, I. *U.S. Patent 4,728,418* (1988).

## EFFECT OF CHLOROBENZENE TREATMENT ON THE LOW-SEVERITY LIQUEFACTION OF COALS

Carol A. McArthur, Peter J. Hall and Colin E. Snape

University of Strathclyde, Dept. of Pure & Applied Chemistry, Thomas Graham Building, 295 Cathedral Street, Glasgow G1 1XL, UK

Keywords: Conformational changes, tetralin extraction, hydrogen transfer.

### ABSTRACT

Chlorobenzene has the advantage of extracting virtually no organic matter from coals and it has been reported previously, that for the Pittsburgh No. 8 Argonne Premium Coal Sample (APCS), chlorobenzene treatment significantly improved the oil yield as measured by dichloromethane (DCM-solubles) from short contact time hydrogen-donor liquefaction with tetralin (400°C, 15 min.). Similar effects with tetralin have been found for two UK bituminous coals, Point of Ayr and Bentinck, where the yields of DCM-solubles also increased. In contrast, for Wyodak sub-bituminous coal (APCS), pretreatment reduced the yield of DCM-solubles reflecting the vast differences in both liquefaction chemistry and pore structure with bituminous coals. The amounts of hydrogen transferred are broadly similar for the initial and chlorobenzene treated coals strongly suggesting that the improved oil yields arise from limiting char-forming retrogressive reactions rather than cleaving more bonds *per se*. The effect was still evident for Point of Ayr coal when the extraction time was increased from 15 to 60 min., although conversions were considerably higher underlying the importance of the initial contact between coal and solvent. A similar improvement in the oil yield for Point of Ayr coal to that found with tetralin was achieved with hydrogenated anthracene oil which has a boiling range of *ca* 250-450°C and, unlike tetralin, is largely in the liquid phase at 400°C.

### INTRODUCTION

Much of the recent literature on the effects of pre-swelling and pre-extracting coals in both polar and non-polar solvents on liquefaction and pyrolysis behaviour<sup>(1-10)</sup> was briefly reviewed by the authors in an earlier article<sup>(11)</sup>. In cases where improved liquefaction yields are achieved, the accessibility of solvents within the highly porous macromolecular structure of coals is undoubtedly improved, particularly during the initial stages of liquefaction where retrogressive reactions need to be avoided. However, unambiguous interpretation of these phenomena in terms of changes in the macromolecular structure of coals is complicated by the fact some organic matter is invariably removed at the same time that conformational changes may be occurring and, in the case of polar solvents and pre-treatments at elevated temperatures, hydrogen bonds are being disrupted. Chlorobenzene has the advantage of extracting virtually no organic matter from coals<sup>(12)</sup> but it is non-polar and does not significantly disrupt hydrogen bonds at relatively low temperatures (<150°C). Previous work by one of the authors (PJH)<sup>(13)</sup> demonstrated that chlorobenzene treatment markedly

affect mass transfer phenomena in both the Pittsburgh No.8 and Upper Freeport Argonne Premium Coal Samples (APCS) and this prompted an investigation into the effects of the treatment on tetralin extraction and dry hydrogenation (70 bar, with and without a dispersed sulphided molybdenum (Mo) catalyst) for the Pittsburgh No.8 APCS <sup>(11)</sup>.

Tetralin was selected because, although it is clearly not representative of process-derived liquefaction solvents as it can be largely in the vapour phase at 400°C, mass transfer effects may be particularly prevalent for this very reason. Further, a relatively short contact time of 15 min. was used as any conformational effects are likely to be most pronounced during the initial stages of conversion. Indeed, the chlorobenzene treatment significantly improved the oil yields as measured by dichloromethane (DCM)-solubles from both tetralin extraction and non-catalytic dry hydrogenation presumably due to improved accessibility of the tetralin and the hydrogen gas. In marked contrast, reduced yields were obtained in catalytic hydrogenation. However, this was probably due to the macromolecular conformation of the coal being further altered by the procedure used for catalyst addition which involved contacting the coal with methanol before drying at ca 100°C.

The yield of pyridine-solubles from the tetralin extraction was also improved by the chlorobenzene treatment. This finding would appear to be contrary to the recent communication by Larsen and co-workers <sup>(14)</sup> who found that the chlorobenzene treatment reduced the yield of pyridine-insolubles in tetralin for the Illinois No. 6 APCS. However, the extraction was conducted at 350°C where the conversions and level of hydrogen transfer are going to be considerably less than at 400°C. Further, only the yield of pyridine-solubles was determined which is less sensitive than the yield of DCM-solubles to hydrogen utilisation as high conversions to pyridine/quinoline-solubles can be achieved with non-donor polynuclear aromatic compound, such as pyrene for some bituminous coals <sup>(4)</sup>.

In the continuing investigation into the effects of chlorobenzene treatment on coal conversion phenomena, liquefaction experiments have been conducted on two UK bituminous coals and the Wyodak APCS to address whether the effects of the chlorobenzene treatment found for Pittsburgh No. 8 coal <sup>(11)</sup> are general and, in cases where improved conversions are achieved with hydrogen-donor solvents, whether more hydrogen transferred. Further, are similar effects likely to occur with other hydrogen-donor and non-donor solvents, for example, hydrogenated anthracene oil (HAO) which, unlike tetralin, is largely in the liquid phase at 400°C?

## EXPERIMENTAL

The two UK coals, Point of Ayr (87% dmmf C) and Bentinck (83% dmmf C), and the Wyodak APCS were treated in ca 10 g batches with chlorobenzene under nitrogen for 1 week in a Soxhlet apparatus. The treated coals were then dried *in vacuo* at 50°C as were the original coals prior to the liquefaction experiments. For Point of Ayr coal, the treatment was also carried out with the time reduced from 1 week to 3 hours.

The tetralin extractions were conducted in duplicate on the original and chlorobenzene treated samples, using 1 g of coal and 2 g of tetralin at 400°C for 15 min. as described previously <sup>(11)</sup>, the yields of DCM and pyridine-solubles being determined. In addition, extractions on Point of Ayr coal were carried out with HAO and naphthalene using the

same conditions and an extraction time of 60 min. with tetralin. The amounts of hydrogen donated to the coals from the tetralin during the extractions were calculated from the gas chromatographic-determined mass ratios of tetralin to naphthalene in the recovered DCM solutions.

## **RESULTS AND DISCUSSION**

### **Tetralin extractions**

Tables 1 and 2 list the yields of DCM-solubles, pyridine-solubles/DCM-insolubles and pyridine-insolubles from the tetralin, HAO and naphthalene experiments. For comparison, the results reported previously for Pittsburgh No. 8 coal are included in Table 1. The duplicate tetralin and naphthalene extractions indicate that the repeatability is  $ca \pm 1\%$  daf coal. The mean values are presented in Figure 1, together with the concentrations of hydrogen donated for the 15 min. extractions.

The results indicate that chlorobenzene treatment has significantly improved the yield of DCM-solubles for the two UK bituminous coals as found previously for Pittsburgh No.8 coal<sup>(11)</sup>. Similarly, the yield of pyridine-insolubles for Bentinck coal has also been reduced (Table 1). It would appear that for the 3 bituminous coals investigated, the increase in the yield of DCM-solubles decreases with increasing rank being smallest for Point of Ayr coal (Figure 1). In contrast, the conversions to DCM and pyridine-solubles for the Wyodak APCS have been reduced considerably (Table 1 and Figure 1). This striking difference in behaviour for the one low-rank coal investigated thus far is attributed to the fact that the macromolecular structures of sub-bituminous coals and lignites are swollen to a considerable extent by the water present and its removal during the chlorobenzene treatment and subsequent drying could well lead to a collapse of the pore structure giving much poorer access to hydrogen-donor solvents. Further, the liquefaction chemistry for bituminous and low-rank coals is quite different during the initial stages of conversion, particularly retrogressive reactions involving coupling of dihydric phenolic moieties being more prevalent in low-rank coals<sup>(15)</sup>.

The concentrations of hydrogen transferred during the tetralin extractions are similar for the initial and the treated coals (Figure 1, expressed on a % daf coal basis). This important finding strongly suggests that the improved oil yields are due to changes in the conformational structure of the bituminous coals allowing better solvent access. This limits the extent of char-forming retrogressive reactions rather than cleaving more bonds *per se* which would result in a greater demand for hydrogen. Indeed, the effect is still evident for Point of Ayr coal with an extraction time of 60 min. (Table 1) although the yield of DCM-solubles and the amount of hydrogen donated are considerably higher underlining the importance of the initial contact achieved between the coal and solvent

Reducing the chlorobenzene treatment time from 1 week to 3 hours had little effect on the conversions indicating that the conformational changes in the macromolecular structure of the coals brought about by the treatment occur on a fast timescale to that of *ca* 3-7 days usually associated with the removal of low temperature solvent extractable material.

### HAO and naphthalene extractions

Table 2 indicates that the effect of the chlorobenzene treatment upon HAO extraction of Point of Ayr coal is similar to that for tetralin with the yield of DCM-solubles increasing by *ca* 10% daf coal. The fact that HAO is largely in the liquid rather than the vapour phase at 400°C suggests that mass transfer limitations on controlling the initial rate of conversion are still severe.

The oil yields obtained with non-hydrogen-donor aromatic compounds, such as naphthalene are obviously much lower than with effective donor solvents and this is reflected in the DCM-soluble yields in Table 2. However, as discussed earlier, aromatic compounds can give high conversions to pyridine/quinoline-solubles (*ca* 80% daf basis) for some bituminous coals<sup>(3)</sup> probably with the aid of hydrogen shuttling or radical mediated hydrogen radical transfer in the case of a number of 4 and 5 ring systems, such as pyrene. Table 2 indicates that the chlorobenzene treatment has reduced the yield of pyridine-insolubles for Point of Ayr coal with naphthalene but has had little effect for the lower rank UK bituminous coal, Bentinck. It was reported previously<sup>(3)</sup> for a different sample of Point of Ayr coal that THF extraction lead to significant improvements in primary conversions to pyridine-solubles with both naphthalene and pyrene. In the case of Bentinck coal, it could well be that the primary conversion is limited by the lack of available hydrogen rather than by solvent accessibility.

### General discussion

This investigation has reinforced other recent work<sup>(1-7)</sup> which has indicated that pre-treatments can greatly enhance liquefaction yields, particularly in relatively low-severity regimes. However, much of the other work was concerned with pre-swelling coals in polar solvents where the dominant effect is undoubtedly the disruption of hydrogen bonding. The increases in oil yield obtained here of 20-25% upon chlorobenzene treatment for the two bituminous coals of lowest rank (Pittsburgh No.8 and Bentinck) are somewhat greater than that of 14% reported by Joseph<sup>(3)</sup> for tetralin extraction (with a hydrogen over-pressure) of an Illinois No.6 coal pre-treated with tetrabutylammonium hydroxide (TBAH). Increases of only 5% were obtained for THF and methanol, but, nonetheless, pre-swelling with both these weakly-basic solvents increased the overall conversions to THF-solubles more than with TBAH. However, their boiling points are considerably lower than that of 132°C for chlorobenzene and, although some disruption of the hydrogen-bonding network in coals would undoubtedly have occurred as the coal swells to a significant extent in these polar solvents, it is uncertain whether the glass transition temperature would have been lowered sufficiently to allow the coal to adopt a lower energy configuration as with chlorobenzene. The nature of the conformational changes have yet to be fully elucidated and are currently being investigated in our laboratory by a combination of DSC, surface area measurements, broadline <sup>1</sup>H NMR and electron microscopy. However, they are clearly different to those induced by polar solvents and could well involve the disruption of non-covalent bonding between aromatic moieties.

There would appear to be considerable scope for improving conversions with process-derived solvents through pretreatments. Although it is clearly impractical to consider the chlorobenzene treatment in terms of a liquefaction process, the fact that it has been shown that the conformational changes can be brought about with a relatively short treatment time (3 hours, Table 1) provides a basis for exploiting such treatments above the glass transition temperatures of bituminous coals with actual process solvents.

## ACKNOWLEDGEMENT

The authors thank the British Coal Utilisation Research Association (Contract No. B18) for financial support.

## REFERENCES

1. R.M. Wham, *Fuel*, 1987, **66**, 283.
2. N.R. Pollack, G.D. Holder and R.P. Warzinski, *Prepr. Am. Chem. Soc. Div. Fuel Chem.*, 1991, **36(1)**, 15.
3. J.T. Joseph, *Fuel*, 1991, **70**, 139 and 459.
4. C.E. Snape, F.J. Derbyshire, H.P. Stephens, R.J. Kottenstette and N.W. Smith, *Fuel Process. Technol.*, 1990, **24**, 119.
5. J.M. Rincon and S. Cruz, *Fuel*, 1988, **67**, 1162.
6. N.K. Narain, H.R. Appell and B.R. Utz, *Prepr. Am. Chem. Soc. Div. Fuel Chem.*, 1983, **28(1)**, 161.
7. L. Artok, H.H. Schobert, G.D. Mitchell and A. Davis, *Prepr. Am. Chem. Soc. Div. Fuel Chem.*, 1991, **36(1)**, 36.
8. C. Riemer and C.E. Snape *GB Patent No. 2,204,877A*, 1988.
9. J.W. Larsen, T.L. Sams and B.R. Rogers, *Fuel*, 1980, **59**, 666.
10. R.J. O'Brien, J.R. Gibbons and R. Kandiyoti, *Fuel Process. Technol.*, 1987, **15**, 71.
11. C.A. McArthur, S. Mackinnon, P.J. Hall and C.E. Snape, *Prepr. Am. Chem. Soc. Div. Fuel Chem.*, 1992, **37** (San Francisco meeting).
12. M. Nishioka and J.W. Larsen, *Energy and Fuels*, 1990, **4**, 100.
13. P.J. Hall and J.W. Larsen, *Energy and Fuels*, 1991, **5**, 228.
14. J.W. Larsen, M. Azik and A. Korda, *Energy & Fuels*, 1992, **6**, 109.
15. D.S. Ross, B.H. Loo, D.S. Tse and A.S. Hirschon, *Fuel*, 1991, **70**, 289.

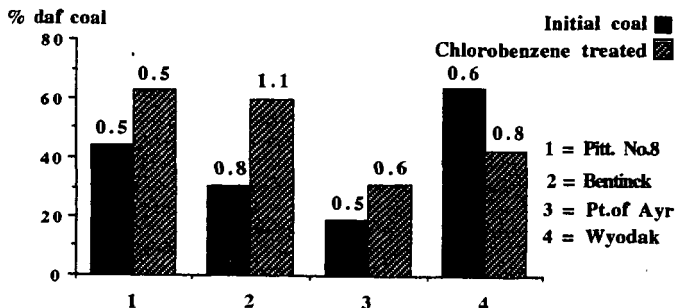


**FIGURE 1 YIELDS OF DCM-SOLUBLES FROM TETRALIN EXTRACTIONS INDICATING %H TRANSFERRED (daf BASIS)**

**Table 1 Tetralin Extraction Results**

Coal	DCM-solubles*	% daf coal Pyr sols/DCM- insols	Pyr. insols
<b>Pitt. No. 8 (a) (15 min.)</b>			
Initial coal	43.9	52.4	3.7
CB treated coal	62.8	31.0	6.2
<b>Bentinck (15 min.)</b>			
Initial coal	31.5	49.9	18.6
	28.9	46.9	24.4
CB treated coal	59.9	25.2	14.9
	56.6	28.9	14.5
<b>Pt. of Ayr, 15 min.</b>			
Initial coal	18.0	52.9	29.1
	20.1	48.8	31.1
CB treated coal	28.9	27.9	43.2
-one week	33.6	25.1	41.3
-3 hours	29.2	22.3	48.5
<b>Pt. of Ayr, 60 min.</b>			
Initial coal	37.3	36.2	26.5
CB-treated coal	46.7	29.7	23.6

\* = 100 - %DCM-insols, includes DCM soluble liquid product + gas + water.

(a) = mean of duplicate runs from ref. 11.

**Table 2 HAO and Naphthalene Extraction Results**

Solvent/coal (15 min. extraction time)	DCM-solubles*	% daf coal Pyr sols/DCM- insols	Pyr. insols
<b>HAO, Pt. of Ayr</b>			
Initial coal	18.5	31.1	50.4
CB-treated coal	29.9	30.2	39.9
<b>Naphthalene, Pt. of Ayr<sup>(a)</sup></b>			
Initial coal	13.6	15.9	70.5
CB-treated coal	21.0	19.2	57.8
<b>Naphthalene, Bentinck<sup>(a)</sup></b>			
Initial coal	21.7	24.8	53.5
CB-treated coal	22.1	20.6	57.3

(a) = mean of duplicate runs

## THE STRUCTURAL ALTERATION OF HUMINITE BY LOW SEVERITY LIQUEFACTION

Kurt A. Wenzel, Patrick G. Hatcher, George D. Cody, and  
Chunshan Song

Fuel Science Program  
The Pennsylvania State University  
University Park, Pa 16802

Keywords: low severity liquefaction, coal structure, huminite

### **Introduction**

Hydrous pyrolysis experiments were performed on low-rank coalified wood to investigate the chemical transformations that occur in huminite (vitrinite) during low severity liquefaction. The coal chosen for the experiments was of lignite rank. It consists of a single maceral huminite which consists predominantly of guaiacol- and catechol-like structures. These structures are believed to be responsible for many of the retrogressive reactions during liquefaction (1). Tubing bomb reactions were varied with reaction times ranging from 30 minutes to 240 hours and temperatures ranging from 100°C to 350°C. Structural characterization of the reacted residues were quantified by solid state <sup>13</sup>C NMR and flash pyrolysis/gas chromatography/mass spectrometry. The combined analytical techniques show there is a progressive loss of oxygen which corresponds with the loss of catechols and guaiacols with increasing thermal stress. Further, dehydration of these catechol structures involves the transformation to phenol, and alkyl phenol structures that make up the macromolecular structure of the altered coalified wood. Dealkylation is also a dominant reaction pathway, as revealed by a decrease in alkyl substituents in the residue.

Detailed studies using NMR spectroscopic and pyrolysis GCMS techniques indicate that the natural evolution of humic coals proceeds through several fundamental stages (2-6). The transformation of huminite to vitrinite is characterized by reactions which result in complete demethylation of methoxy phenols to catechols and a concomitant reduction in catechols (and alkylated catechols), presumably through reaction, to form phenols and cresols; the details of the catechol reaction are so far unknown. Low severity hydrous pyrolysis of lignite parallels many of the natural coalification reactions.

Recently, Siskin et al. (7) have demonstrated that many of the reactions which typify coalification are facilitated, if not initiated, in the presence of water. They recognized that since coalification occurs in a water saturated system, water may play an integral role in the geochemistry of coalification. From their study of an enormous number of reactions with model compounds, several mechanisms with direct bearing on the chemical structural evolution of coal during liquefaction under hydrous conditions are clear. The demethylation reaction, for example, has been shown to be acid catalyzed yielding phenol as the predominant product (8). The mechanism by which the alkyl-aryl ether linkage (beta-0-4) of the modified lignin is rearranged to the beta-C-5 linkage may reasonably be expected to parallel the mechanism that Siskin et al. (7) demonstrated for their model compound study of the aquathermolysis of benzyl phenyl ether in which they observed significant yield of 2 benzyl phenol; this product is a perfect analog for the rearrangement necessary to yield the beta-C-5 linkage.

To date there is no mechanism proposed for the reduction of catechols and their alkylated analogs, through conversion, to phenol and cresols. This reaction appears to be a principal means by which the oxygen content of coal is reduced during the transformation through the subbituminous range (2-6). Although Siskin et al. (7) have not investigated the chemistry of catechols specifically, it appears reasonable to assume that the reactions of catechols may be ionic as well as thermolytic.

### **Experimental**

A crushed sample of a coalified log described previously as the Patapsco lignite (2) was heated under hydrous conditions in a 22 ml autoclave reactor. The reactor was charged with approximately 1 gram of coal and 7 milliliters of deionized, deoxygenated water following a procedure similar to that of Siskin et al. (7). The tubing bomb reactor was consecutively pressurized to 1000 psi and depressurized with nitrogen three times to ensure all the oxygen was removed from the reactor. Finally it was depressurized to atmospheric pressure before heating. The bomb was inserted into a heated fluidized sand bath for different reaction periods, ranging from 30 min. to 10 days, and at various temperatures, ranging from 100°C to 350°C. After the elapsed heating times the reactor was removed and immediately quenched in water and then allowed to cool to room temperature. The liquids and solids were collected and analyzed. Only trace amounts of gases were detected. The bombs were opened and the liquid content pipetted off. The organic matter dissolved in the water was separated by extraction with diethyl ether. The residual lignite was removed, extracted in a 50:50 mixture of benzene:methanol, dried in a vacuum oven at 45° C for 24 hours, and then weighed.

The original lignite and solid residue from the reactors were analyzed by flash pyrolysis and by solid state NMR. The flash pyrolysis technique used was that published by Hatcher et al. (4). Solid-state <sup>13</sup>C NMR spectra were obtained by the method of cross polarization and magic angle spinning (CPMAS) using the conditions previously given (2). The spectrometer was a Chemagnetics Inc. M-100 spectrometer operating at 25.2 MHz carbon frequency. Cycle times of 1 sec and contact times of 1 msec were chosen as the optimal conditions for quantitative spectroscopy.

### **Results and Discussion**

Aquathermolysis of the Patapsco lignite was conceived as a means to trace the chemical changes that occur to the dominant maceral in low rank coals during liquefaction. Accordingly, our goal was to examine the coal before and after thermal treatment and to infer liquefaction pathways. Conversions ranged from 29 to 40 percent for the different experiments (Table I). This mass loss probably reflects low molecular weight products formed, water, and partial solubilization of lignitic structures originally of low molecular weight. The GC/MS analysis of the water soluble materials indicates the presence of lignin phenols and catechols, all of which are components of the lignite prior to thermolysis. Cleavage of a few bonds on the macromolecule could conceivably produce a catechol or methoxyphenol which would be soluble in water. Another water soluble product identified was acetic acid. This product is most likely derived from thermolysis of the side-chain carbons associated with the original lignin and coalified lignin in the sample. The content of evolved gases was not measured, because the amount of gas evolved was negligible.

The NMR data of the thermolysis residues (Figure 1) indicates clearly the evolutionary path during thermolysis. Comparing the NMR data for the residues with the original lignite and with gymnospermous wood coalified to higher rank (2) there appear to be several changes which describe the average chemical alteration. First, the most obvious change is the loss of aryl-O carbons having a chemical shift at 145 ppm. From previous studies (2) this peak has been assigned to aryl-O carbons in catechol-like structures in the coalified wood, based on chemical shift assignments and pyrolysis data. These are thought

to be originally derived from demethylation of lignin during coalification (2-6). The NMR spectrum of the aquathermolysis residue has clearly lost most of the intensity at 145 ppm but now shows a peak at 153 ppm which is related to aryl-O carbons in monohydric phenols. These are the primary constituents of subbituminous and high volatile bituminous coalified wood as depicted in the NMR spectra for such woods. It is obvious that the catechol-like structures of the lignitic wood have been transformed to phenol-like structures somewhat similar to those in higher rank coal. Thus, the aquathermolysis has reproduced, to some degree, the coalification reactions acting on aromatic centers.

The second most apparent change to occur during aquathermolysis is the loss of aliphatic structures. The methoxyl groups at 56 ppm are lost from the lignitic wood as are the other alkyl-O carbons at 74 ppm, consistent with demethylation reactions and dehydroxylation of the three carbon side chains of lignin which occur naturally during coalification of woods. However, the loss of alkyl-C carbons (those aliphatic carbons not substituted by oxygen) is the most significant change in the aliphatic region in the aquathermolysis residue. Loss of substantial amounts of aliphatic carbon is not observed during coalification of wood from lignite to high volatile bituminous coal. In fact, in most coalified wood samples, loss of alkyl-C carbon occurs only at higher ranks, above that of medium volatile bituminous coal. The lack of retention of aliphatic carbon during aquathermolysis is an indication that this treatment probably does not reproduce well the low-rank coalification reactions associated with aliphatic structures. It is important to note that the alkyl-C carbons in the aquathermolysis residues become dominated by methyl carbons with increasing thermal stress.

The pyrolysis data (Figure 2) provide confirmation for the average changes in structure observed by NMR. The loss of catechol-like structures is documented with the significant diminution of catechols in the pyrolyzate of the aquathermolysis residue compared to that of the original lignite. This loss of catechols is the singular most significant change in pyrolysis products. The pyrolyzate of the residue mimics somewhat the pyrolysis data for subbituminous coalified wood (3), being dominated by phenol and alkylphenols. Another difference between aquathermolysis residues and the original lignitic wood is in the abundance of methoxyphenols derived from lignin-like structures. The aquathermolysis has apparently reduced the relative yields significantly, consistent with the NMR data showing loss of methoxyl carbons. Some of the methoxyphenols may have been transformed to water soluble phenols and washed out of the residue in the aqueous phase; others may have undergone demethylation reactions, converted to catechols and then transformed to phenols.

The pyrolysis of the residue yields mostly phenol and the cresol isomers; other alkylated phenols, the C<sub>2</sub> and C<sub>3</sub> phenols, are not as abundant relative to phenol and cresols as the C<sub>2</sub> and C<sub>3</sub> phenols are in the pyrolysis of original lignite or the subbituminous log. This is probably related to the fact that alkyl substituents are not as abundant in the residue and the alkyl substituents are probably mostly methyl substituents as was deduced from the NMR data. Thus, the lack of significant relative amounts of C<sub>2</sub> and C<sub>3</sub> phenols in the thermolysis residue's pyrolyzate further supports the conclusion that thermolysis does not reproduce coalification reactions with regard to the aliphatic structures in the residue. The relatively high temperatures used in this study may force proportionally more thermolytic pathways over ionic pathways. The potential for such a situation has been recognized by Siskin et al. (7).

#### **Acknowledgments**

Financial support for this work was provided by the U. S. Department of Energy, Pittsburgh Energy Technology Center, under contract No. DE-AC22-91PC91042.

### References

- 1) Song, C.; Schobert, H. H.; Hatcher, P.G.; *Am. Chem. Soc. Div. Fuel Chem. Prepr.* **1992**, *37*, 638.
- 2) Hatcher, P. G.; *Energy Fuels* **1988**, *2*, 40
- 3) Hatcher, P. G.; Lerch, H.E.; Verheyen, T. V.; *Int. Jour. Coal. Geol.* **1989**, *13*, 65.
- 4) Hatcher, P. G.; Lerch, H. E.; Kotra, P.K.; Verheyen, T. V.; *Fuel* **1988**, *67*, 106.
- 5) Hatcher, P. G.; Wilson, M.A.; Vassallo, A. M.; *Int. Jour. Coal. Geol.* **1989**, *13*, 99.
- 6) Hatcher, P. G.; Lerch, H. E.; Bates, A. L.; Verheyen, T. V.; *Org.Geochemistry* **1989**, *14*, 145.
- 7) Siskin, M.; Brons, G.; Vaughn, S.N.; Katritzky, A.K.; Balasubramanian, M.; *Energy & Fuels* **1990**, *4*, 488.
- 8) Katritzky, A. K. and Siskin, M. *Energy Fuels*, **1990**, *4*, 475-584.
- 9) Katritzky, A.K.; Murugan, R.; Balasubramanian, M.; Siskin, M.; *Energy Fuels* **1990**, *4*, 482.
- 10) Hatcher, P. G.; *Org. Geochem.* **1990**, *16*, 959.

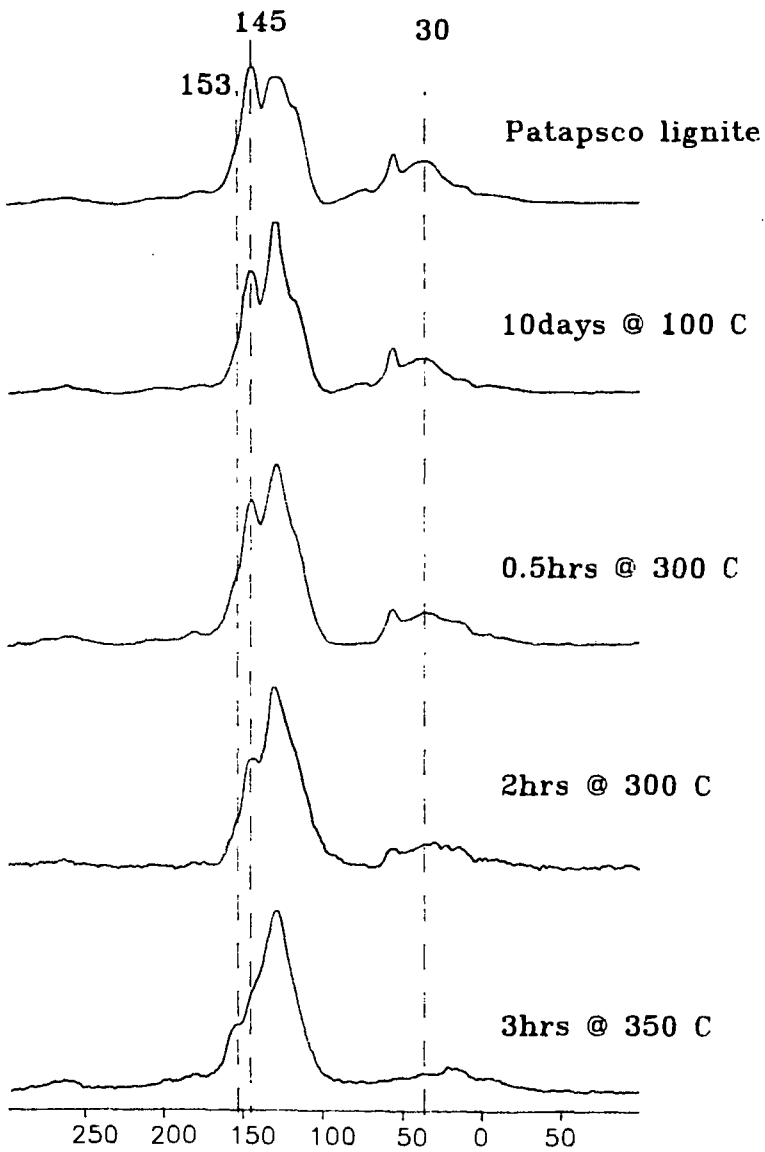


Figure 1. CPMAS  $^{13}\text{C}$ NMR of the Patapsco lignite and the thermally altered residues.

Table I. Conversion data for hydrous pyrolysis experiments.

#	time	temperature	conversion, %
1	240 hrs	100°C	29.3
2	.5 hrs	300°C	29.8
3	2 hrs	300°C	30.6
4	3 hrs	350°C	39.7

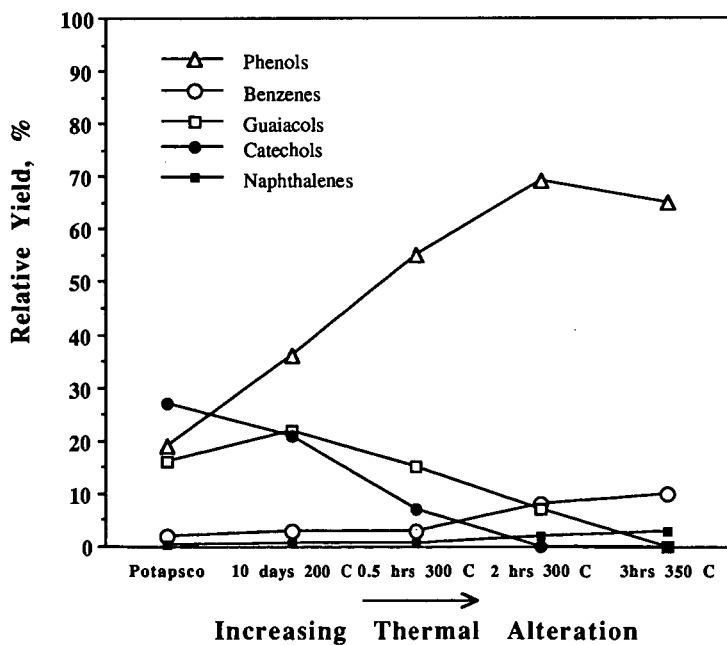


Figure 2. Relative Yields of Flash Pyrolysis Products from Aquathermolysis Residues

## THE EFFECTS OF MOISTURE AND CATIONS ON LIQUEFACTION OF LOW RANK COALS

M.A. Serio, E. Kroo, H. Teng, and P.R. Solomon  
Advanced Fuel Research, Inc.  
87 Church Street  
East Hartford, CT 06108

**Keywords:** Coal liquefaction, Cations, Low rank coals

### INTRODUCTION

The role of calcium in reducing liquefaction yields from low rank coals has been suggested in previous work by Whitehurst et al. (1) and Mochida et al. (2). It is also consistent with work which shows an effect of calcium on reducing pyrolysis tar yields (3-7). The role of calcium may be to provide a nascent crosslink site in the coal by allowing coordination of groups like carboxyl and hydroxyl which are prone to such reactions. Otherwise, these sites would be more likely to coordinate with water (through hydrogen bonding) than with each other. There have been no studies of the effects of cation type and the associated moisture on liquefaction yields.

Studies were done on samples of Argonne Zap Lignite and Wyodak subbituminous coals which have been demineralized and then exchanged with calcium, barium or potassium cations. Two sets of samples were prepared: 1) vacuum-dried; 2) exposed to water vapor until an equilibrium moisture content was reached. The samples were characterized by FT-IR transmission analysis in KBr pellets, programmed pyrolysis in a TG-FIR system and liquefaction in donor solvent. The pyrolysis and liquefaction results are discussed in the current paper.

### EXPERIMENTAL

In order to subject coals to a variety of modifications and avoid exposure to the ambient air, an apparatus for continuous-flow, controlled-atmosphere demineralization and controlled pH ion-exchange of coals was designed and constructed. A closed system is used, where instead of stirring the batch reactor contents, a continuous flow of solvent through the sample is used. By utilizing valves, it is possible to change solvents without opening the reactor. The different solvents are held in separate reservoirs which are all equipped with sparge valve systems to deoxygenate the solvents before use (with N<sub>2</sub> or He as needed).

**Demineralization** - The procedure is similar to that described in the work of Bishop and Ward (8). The coal samples used in this study are the Zap lignite and Wyodak subbituminous coals from the Argonne premium sample bank (9). The sample sizes were all -100 mesh. Before starting the acid treatment, the samples were thoroughly wetted by mixing with de-ionized water under a nitrogen environment. Demineralization involved washing the coal with a flow of 2M HCl for 45 minutes, 50% HF for 45 minutes, 2M HCl for 45 minutes, and de-ionized water for 120 minutes. The process was performed at 80 °C. After demineralization, the sample was dried in vacuum for at least 20 hours at room temperature. The vacuum dried samples were kept in a nitrogen box for subsequent analysis and liquefaction experiments.

**Ion-Exchange of Carboxyl Groups with Metal Cations** - The acidity constant ( $k_a$ ) of carboxylic acids is around  $10^{-5}$ , and that of phenols is around  $10^{-10}$ . Theoretically, almost all carboxyl OH can be exchanged with cations at pH 8, whereas the phenolic-OH can remain in the acid form, according to the equation:  $[A^-] / [HA] = k_a / [H^+]$ , where HA is either the carboxyl or phenolic group in acid form. At pH 8,  $[A^-] / [HA]$  would be a value of order  $10^3$  for carboxyl groups, and  $10^2$  for phenols. Schafer's experimental results also suggest that the carboxyl groups in coal can be completely exchanged with cations at pH around 8-8.5, along with ortho-dihydroxy groups (10). In the case of barium, a 1N barium acetate solution, which has a pH value around 8.2, was used for ion-exchange with carboxyl groups. Roughly 3 g of demineralized coal was

mixed with 300 ml of 1N barium acetate in a cell under a nitrogen environment. After 5 minutes of mixing, the pH value of the mixture dropped to less than 7.5. The mixture was filtered through a Teflon membrane by increasing the nitrogen pressure, and the mixing cell was refilled with another 300 ml of barium acetate. The pH value of the solution dropped again after mixing. The filtration and refilling procedure was repeated, usually 15-20 times, until the pH value of the mixture in the cell reached  $8.0 \pm 0.1$  and remained constant with mixing. The drop of the pH value was probably due to the release of  $H^+$  from carboxylic acids in the coal.

The mixture was kept under continuous mixing conditions in a nitrogen environment for at least 20 hours before the acetate solution was purged out, and the cell was refilled with a final 300 ml charge of 1N barium acetate. After 10 minutes of mixing, the acetate solution was purged out, and the coal sample was washed with 150-200 ml of de-ionized water. The coal sample was then removed from the cell for vacuum drying, which lasted for at least 20 hours. The sample was kept in a nitrogen box after drying. A similar procedure was used for exchanging calcium and potassium cations, starting with the metal acetate.

**Ion-Exchange of Phenolic and Carboxyl Groups with Metal Cations** - In theory, both phenolic and carboxyl groups can be totally exchanged with cations at pH around 12.5. Schafer (10) also reported that the exchange of -OH groups was complete at pH 12.6. In this study, a solution, recommended by Schafer, of 0.8 N  $BaCl_2$  and 0.2 N  $Ba(OH)_2$  having a pH of 12.7, was used for ion-exchange of barium cations. A similar procedure was used for calcium and potassium cations.

Approximately 3 g of a demineralized coal sample was stirred with 300 ml of the pH 12.7 solution in a nitrogen environment. After 5 minutes of mixing, the mixture was filtered through a membrane and the cell was refilled with another 300 ml of the pH 12.7 solution. The purging and refilling procedure was repeated 3 times, and the pH value of the final mixture was around 12.6. The mixture was continuously mixed under a nitrogen environment for at least 20 hours for exchange. After this long-time exchange period, the solution was purged out, and the cell was refilled with the pH 12.7 solution.

After 10 minutes of mixing, the solution was purged out, and the coal sample was washed with a solution of 0.1 N  $BaCl_2$  and 0.03 N NaOH, which has a pH around 12.7, to avoid hydrolysis of the exchanged coal. The coal sample was then removed from the cell for vacuum drying. After drying, the sample was kept in a nitrogen box for further study.

It was noticed, in the process of ion-exchange that part of the coal structure was dissolved in the high pH value solution, since the filtrate had a yellowish color. This is most likely due to hydrolysis of the ester linkage in coal. The amount of the coal structure (so called humic acids) dissolved in the high pH value solutions during complete ion-exchange was estimated to be about 6.6 wt% daf of the demineralized Zap and 17 wt% daf of the demineralized Wyodak.

**Preparation of Moisturized Coal Samples** - A procedure for restoring the moisture level of modified coal samples was developed. The moisturized samples were prepared by enclosing the vacuum-dried modified samples in a box with a nitrogen purge of 100% humidity. The sample exposure to moisture was performed for several days (~6 days) until no further moisture uptake was observed.

## RESULTS AND DISCUSSION

The modified coal samples were characterized by FT-IR transmission analysis in KBr pellets, programmed pyrolysis in a TG-FTIR system and liquefaction in donor solvent. The results are discussed below.

**Effect of Cations on Pyrolysis Tar and Liquefaction Yields** - The results of sample analysis by programmed pyrolysis in the TG-FTIR are shown in Figures 1 and 2, and summarized in Table

1 for the Zap lignite. These results show that demineralization tends to increase the tar yield, whereas both the gas and char yields were reduced. Similar results were observed for the Wyodak coal (11). Table 1 also shows a decrease of the tar yield with the extent of ion-exchange with the metal cations, and a corresponding increase in the total amount of gas evolution. The liquefaction results for different samples are shown in Table 2. The data in Tables 1 and 2 show that the yields of both the pyrolysis tar and toluene solubles from liquefaction decrease with the extent of ion-exchange, i.e., in the order of (demineralized) > (ion-exchanged at pH 8) > (ion-exchanged at pH 12.5). This result indicates that having the carboxyl or phenolic groups in the salt form makes it easier to crosslink the coal structure during pyrolysis or liquefaction reactions.

It is realized that this is a more difficult comparison for the samples exchanged at pH 12.5, since considerable amounts of humic acids were observed to dissolve in the high pH value solutions. The dissolution of coals in the aqueous alkaline solutions may be due to the breaking of ester bonds in coal, i.e.,  $\text{RCOOR}' + \text{OH}^- \rightarrow \text{RCOO}^- + \text{R}'\text{OH}$ . This coal dissolution mechanism was also proposed by other workers (12). The solubility of coal in alkaline solutions varies with the cations contained in the solution. The color difference of the calcium and potassium solutions after ion-exchange at high pH is striking, in that the potassium solution has a much darker color, indicating much more coal dissolved in the monovalent cation ( $\text{K}^+$  here) solution than the bivalent cation ( $\text{Ca}^{++}$  here) solution. The results also show that the barium solution extracted more coal than the calcium solution, but not as much as the potassium solution. A possible reason is the fact that  $\text{Ca}^{++}$  and  $\text{Ba}^{++}$  ions can act as cross-links between two acid groups of different coal fragments (12), whereas  $\text{K}^+$  can only interact with one acidic site. The ability of bivalent cations to act as initial crosslinks in the structure at high pH is supported by data on the pyridine volumetric swelling ratios (VSR) and pyridine extractables, shown in Table 3. The values of the VSR are lower for the bivalent cations at high pH for both the dry and moist coals. It can be seen in Table 1, for the pyrolysis of vacuum dried samples, that the tar yield was higher for the potassium-exchanged coals than the calcium and barium-exchanged samples at high pH, suggesting that bivalent cations tighten the coal structure by cross-linking coal fragments and making it more difficult for tar molecules to form (7). At pH 8; the values of the tar yield and VSR for the monovalent and bivalent cations are more similar, though lower than the values for either the raw or demineralized coals. Consequently, it appears that the monovalent cations help to hold the structure together, although this must occur through electrostatic rather than covalent interactions. It makes sense that valency would be less important in the normal state of the coal or at pH=8 since, for steric reasons, cations are unlikely to be exchanged on more than one carboxyl or ortho-dihydroxy site.

It is likely that coal solubility in aqueous alkaline solutions increases with the size of the cations of the same valence. If this is true, the dissolution of coal in sodium solution would be expected to be less than that in the potassium solution. Preliminary results show that this is the case. However, this requires further confirmation. In summary, at similar pH values (~12.5), the amounts of Zap lignite extracted by 1 liter of the cation solutions in 20 hours increases in the order of  $\text{Ca}^{++} < \text{Ba}^+ < \text{K}^+$ .

In considering the size effect of the cations on the pyrolytic tar and liquefaction yields, one should compare the data for the barium- and calcium-exchanged samples. It is interesting that the size of the cations has an opposite effect on the tar and liquefaction yields. In pyrolysis, the tar yield for the barium-exchanged samples is lower than that of the calcium-exchanged samples, while in liquefaction, the yield was higher for the barium-exchanged samples. This could be due to increased extraction of tar precursors during ion-exchange in the case of barium which subsequently makes the coal more accessible to the liquefaction solvent.

**Effect of Cations on Gas Yields from Pyrolysis and Liquefaction** - It is of interest to note that the gas yields from liquefaction and pyrolysis do not always follow the same trend. Table 1 shows that, in pyrolysis, the total yield of oxygen-containing gases (i.e.,  $\text{CO}_2$ ,  $\text{CO}$ , and  $\text{H}_2\text{O}$ ) always increases with decreasing tar yield. Table 2 shows the expected increase of the

liquefaction yields with tar yield. However, the gas yields in liquefaction show an irregular variation with pH and with cation type. For example, the CO<sub>2</sub> yield is high for the partially barium exchanged Zap lignite, and is significantly reduced for the completely barium exchanged sample. The Wyodak subbituminous coal shows the opposite trend. For the ion-exchanged Zap lignite, the decrease of the CO<sub>2</sub> yield in liquefaction can be explained by the loss of some organic components, which contain CO<sub>2</sub>-forming functions, during the barium exchange at high pH. Some of these variations could be due to catalysis of secondary gas-phase or gas-solid reactions.

For CO evolution in pyrolysis, the demineralized samples show the major evolution at temperatures between 400 and 800 °C. CO evolution also occurs in a similar temperature range for fresh and ion-exchanged samples. However, the evolution is depressed at temperatures lower than about 750 °C, but elevated above this temperature by comparing with that of the demineralized samples. It was also noted that the fraction of CO evolving before 750 °C increases with increasing tar yield, as shown in Fig. 3a for the Zap lignite. This observation is significant. The higher CO evolution at temperatures lower than 750 °C for demineralized samples could be due to more oxygen functions evolving as CO without crosslinking. For ion-exchanged samples, the depressed CO evolution at lower temperatures is probably caused by oxygen retention through crosslinking between oxygen functions, and the CO evolved at 750 °C or above, is likely from the decomposition of the metal carboxylate groups which can produce carbonates as a decomposition product. The raw and cation exchanged samples have a sharp evolution peak in the TG-FTIR analysis, as shown in Figs. 1 and 2. This occurs in the same temperature range as the decomposition of carbonates and could be the result of catalytic gasification of the CO<sub>2</sub> produced to CO. The correlation of the total CO evolution in coal pyrolysis with pyrolytic tar and liquefaction yields was studied, as shown in Fig. 3b for the Zap lignite. The data shows that both tar and liquefaction yields increase with decreasing total (pyrolysis) CO yield. Therefore, both the relative amount of CO evolved before 750 °C and the total CO evolution are indicators of the extent of crosslinking.

Figures 1 to 2 also show that CO<sub>2</sub>, H<sub>2</sub>O, and low temperature CO evolve in a similar temperature range. This might imply that these products are derived from a consecutive mechanism. The CO<sub>2</sub> evolution curve does not show as much shape variation with changes in cation content. However, the yield is basically a decreasing function of tar yield. In previous work, the relationship between CO<sub>2</sub> evolution and crosslinking events has been noted (13-15). This has been explained by the mechanism that elimination of CO<sub>2</sub> would create aryl radicals to enhance crosslinking. The CH<sub>4</sub> yield also showed a trend opposite to that of the tar yield for the ion-exchanged samples. This has been generally reported in coal pyrolysis studies. By reincorporation into the solid matrix by more stable bonds, the tar precursors can yield volatiles only by cracking off of small side groups, hence the increased CH<sub>4</sub> yields with decreasing tar yields.

One aspect of the H<sub>2</sub>O evolution data revealed in Figs. 1 and 2 merits further comment. For samples which contain acidic functions in the salt form, including fresh and barium exchanged samples, there is always a water evolution peak present at around 200 °C. This 200 °C peak is obscure for demineralized samples. It is very likely that this peak is due to the evolution of moisture which is ionically bonded on the salt structure. For vacuum dried samples, it can be seen that the moisture content increases with the amount of barium in the samples, as shown in Table 3. This indicates that the acidic functions in the salt forms attract polar water molecules. These attracted water molecules cannot be removed by vacuum drying, but only by raising the temperature of the sample.

**Analysis of Carboxyl and Phenolic Groups by Barium Titration** - In theory, all of the carboxyl groups of demineralized samples can be exchanged with barium at pH 8. Consequently, it follows that one could determine the concentration of carboxyl groups in coal by knowing the amount of barium ion exchanged at pH 8. The chemical composition of ash formed by combustion of the barium exchanged sample is predominantly BaO. Therefore, from the ash

content of the samples ion-exchanged at pH 8, one can estimate the concentration of carboxyl groups in the coal. Similarly, the total concentration of carboxyl and phenolic groups can be determined by the ash content of the sample ion-exchanged at pH 12.6. The concentration of phenolic groups can be obtained from the difference of the above two measurements. The concentrations of carboxyl and phenolic groups determined in this manner for Zap and Wyodak are shown in Table 4. The results shown in Table 4 are similar to those determined by Schafer (10, 16) for Australian low-rank coals, using barium titration methods. However, our FT-IR results indicate that not all of these groups can be exchanged and that the cations can interact with additional sites in the coal. This will be the subject of a separate publication.

**Pyrolysis and Liquefaction of Moisturized Coal Samples** - Remoisturization of vacuum dried Zap and Wyodak was done in the attempt to understand if moisture uptake for low rank coals is a reversible process and to see if moisture influences the role of the cations. The remoisturized samples were analyzed by programmed pyrolysis with TG-FTIR. Preliminary results show that the moisture content can reach that of the raw samples by remoisturization for Zap, but not for Wyodak. The results for the Zap lignite are shown in Table 3. Furthermore, the chemical structure of the coal samples seems to have been changed by remoisturization, since different CO<sub>2</sub> evolution behaviors were observed. A comparison of the CO<sub>2</sub> evolution behavior for raw and remoisturized coal samples is given in Fig. 4. The detailed liquefaction and pyrolysis results are presented in Ref. 11.

In almost every case, the asphaltene yield was increased with moisturization except for the pH 8 Zap, in which case the asphaltene yield was slightly reduced. Interestingly enough, the oil yield was reduced for most of the modified samples with moisturization, except for the demineralized Zap and the pH 12.6 Wyodak. The indication from the above results is that moisturization favors the formation of the larger molecular weight asphaltenes in liquefaction, while the formation of the smaller molecular weight oils is less favored.

It is usually shown that the trends for improved liquefaction yields parallel those for improved tar yields in pyrolysis. However, it was found in this study that the influences of moisturization on the yields of pyrolytic tars and liquefaction toluene soluble yields are different in that moisturization does not appear to have a significant effect on pyrolysis tar yields. This indicates that moisture plays different roles for the formation of tars in pyrolysis and coal liquids in liquefaction. A possible explanation for the difference is that most of the moisture is depleted early in the pyrolysis process, whereas the moisture is retained in the reactor during liquefaction and can exist in a liquid phase. This aspect requires further investigation.

The results also show that the moist samples have higher gas yields in liquefaction than the vacuum dried samples. The increase in gas yield is mainly from CO<sub>2</sub> and CO (especially CO<sub>2</sub>), whereas the yields of hydrocarbon gases decrease with moisturization. One possible explanation for this result is that moisture may react with side chain structures in coal, which are the sources for the formation of oils and hydrocarbon gases during liquefaction, to form oxygen functions. The subsequent reaction of these oxygen functions produces more CO<sub>2</sub>, CO and asphaltenes in the liquefaction of moist coals.

## CONCLUSIONS

The conclusions from this study are as follows:

- The tar yields and liquefaction yields are reduced for all three cations tested (K<sup>+</sup>, Ca<sup>++</sup>, Ba<sup>++</sup>) and are lower for the fully exchanged coals. The ability of cations to act as initial crosslinks is an important aspect of their role in retrogressive reactions.
- The previously observed correlation between pyrolysis tar and liquefaction yields for coals and modified coals appears to hold for the vacuum-dried cation-exchanged coals, but not always for the re-moisturized coals.

always for the re-moisturized coals.

- The total evolution of CO<sub>2</sub> and CO from pyrolysis is changed significantly by cation-exchange. However, only in the case of CO does the evolution profile change significantly.
- After careful demineralization, a calcium form Zap or Wyodak coal can be prepared at pH = 8, which is similar to the raw coal with regard to pyrolysis and liquefaction behavior.
- At pH=8, cations are most likely to be coordinating multiple oxygen functionalities around themselves through electrostatic type interactions, which diminishes the importance of valency.
- Some of the moisture in a coal is associated with the cations. The moisture content has a larger role in liquefaction than in pyrolysis because it is present for a longer period of time.

#### ACKNOWLEDGEMENTS

This work was supported by the U.S. D.O.E. Pittsburgh Energy Technology Center under Contract No. DE-AC22-91PC91026.

#### REFERENCES

1. Whitehurst, D.D., Mitchell, T.O., and Farcasiu, M., Coal Liquefaction, The Chemistry and Technology of Thermal Processes, Academic Press, NY (1980).
2. Mochida, I., Shimohara, T., Korai, Y., Fujitsu, H., and Takeshita, K., *Fuel* **62**, 659, (1983).
3. Tyler, R.J. and Schafer, H.N.S., *Fuel*, **59**, 487, (1980).
4. Morgan, M.E. and Jenkins, *Fuel*, **65**, 757, (1986).
5. Morgan, M.E. and Jenkins, *Fuel*, **65**, 764, (1986).
6. Morgan, M.E. and Jenkins, *Fuel*, **65**, 769, (1986).
7. Wornat, M.J., and Nelson P.F., *Energy and Fuel*, **6** (2) (1992).
8. Bishop, M., and Ward, D.L., *Fuel*, **37**, 191, (1958).
9. Vorres, K.S., *Energy and Fuel*, **4** (5), 420 (1990).
10. Schafer, H., *Fuel*, **49**, 197, (1970).
11. Serio, M.A., Kroo, E., Teng, H., Charpenay, S., and Solomon, P.R., "The Dual Role of Oxygen Functions in Coal Pretreatment and Liquefaction: Crosslinking and Cleavage Reactions," Fifth Quarterly Report, U.S. DOE Contract No. DE-AC22-91-PC91026 (1992).
12. van Bodegom, B., van Veen, J.A., van Kessel, G.M.M., Sinnige-Nijssen, M.W.A., and Stuiver, H.C.M, *Fuel*, **63**, 346 (1984).
13. Suuberg, E.M., Lee, D., and Larsen, J.W., *Fuel*, **64**, 1668, (1985).
14. Suuberg, E.M., Unger, P.E., and Larsen, J.W., *Energy & Fuels*, **1**, 305, (1987).
15. Solomon, P.R., Serio, M.A., Deshpande, G.V., and Kroo, E., *Energy & Fuels*, **4** (1), 42, (1990).
16. Schafer, H., *Fuel*, **51**, 4, (1972).

Table 1. Pyrolysis Results of Vacuum Dried Modified Zap Samples.

Coal (type/preparation)	Pyrolysis Products (wt.% daf)					
	Tars	CO <sub>2</sub>	CO	H <sub>2</sub> O	CH <sub>4</sub>	Char
Fresh	7	8.9	14.7	14.3	2.2	57
Demin.	20	4.8	10.4	8.4	2.7	54
Demin. + K <sup>+</sup> (pH8)	11	8.6	9.9	16.0	1.9	57
Demin. + Ca <sup>++</sup> (pH8)	10	8.6	13.5	10.3	2.4	58
Demin. + Ba <sup>++</sup> (pH8)	6	11.7	15.8	18.6	2.6	55
Demin. + K <sup>+</sup> (pH12.5)	5	9.9	12.4	13.5	1.6	57
Demin. + Ca <sup>++</sup> (pH12.5)	4	8.2	22.6	12.6	2.0	51
Demin. + Ba <sup>++</sup> (pH12.5)	3	10.5	24.1	15.5	2.6	52

Table 2. Liquefaction Results of Vacuum Dried Modified Zap Samples.

	Toluene Solubles			Gas		
	Total	Oils	Asphaltenes	CO <sub>2</sub>	CO	CH <sub>4</sub>
Fresh	26	12	14	4.3	0.24	0.25
Demin.	52	26	26	1.1	0.43	0.27
Demin. + K <sup>+</sup> (pH8)	30	11	19	7.7	0.27	0.17
Demin. + Ca <sup>++</sup> (pH8)	25	13	12	2.7	0.30	0.22
Demin. + Ba <sup>++</sup> (pH8)	37	25	12	7.3	0.40	0.20
Demin. + K <sup>+</sup> (pH12.5)	17	5	12	5.0	0.24	0.27
Demin. + Ca <sup>++</sup> (pH12.5)	*	*	3	0.7	0.04	0.08
Demin. + Ba <sup>++</sup> (pH12.5)	15	15	0.5	0.3	0.27	0.02

\* Yields Calculated by Difference were Negative. Solvent Incorporation is Suspected.

Table 3. Characterization of Cation-Exchanged Zap Samples.

Coal Type	Dry			Moist			
	V.S.R	P <sub>s</sub>	Moisture	V.S.R.	P <sub>s</sub>	Moisture	
Zap Raw	2.7	5	NM	1.9	15	32	
Zap Demin.	3.1	20	4	2.6	22	16	
pH 8	K <sup>+</sup>	2.0	10	6	1.9	9	20
	Ba <sup>2+</sup>	1.8	3	5	1.5	4	22
	Ca <sup>2+</sup>	2.1	6	5	1.6	6	21
pH 12	K <sup>+</sup>	1.7	2	6	1.4	2	29
	Ba <sup>2+</sup>	1.1	2	7	1.2	2	22
	Ca <sup>2+</sup>	1.1	1	9	1.2	1	25

Notes: V.S.R. = Volumetric Swelling Ratio in Pyridine; P<sub>s</sub> = Pyridine Solubles (daf)  
Moisture was Determined by TG-FTIR and is Reported on an As-received Basis.  
NM = Not Measured.

Table 4. The Carbonyl and Phenolic Contents of Zap and Wyodak Coals Determined by Barium Titration. (meq g<sup>-1</sup> daf basis)

	Carboxyl Groups	Phenolic Groups	Total Acidity
Zap Lignite	2.52	6.74	9.26
Wyodak Sub.	2.40	5.76	8.16

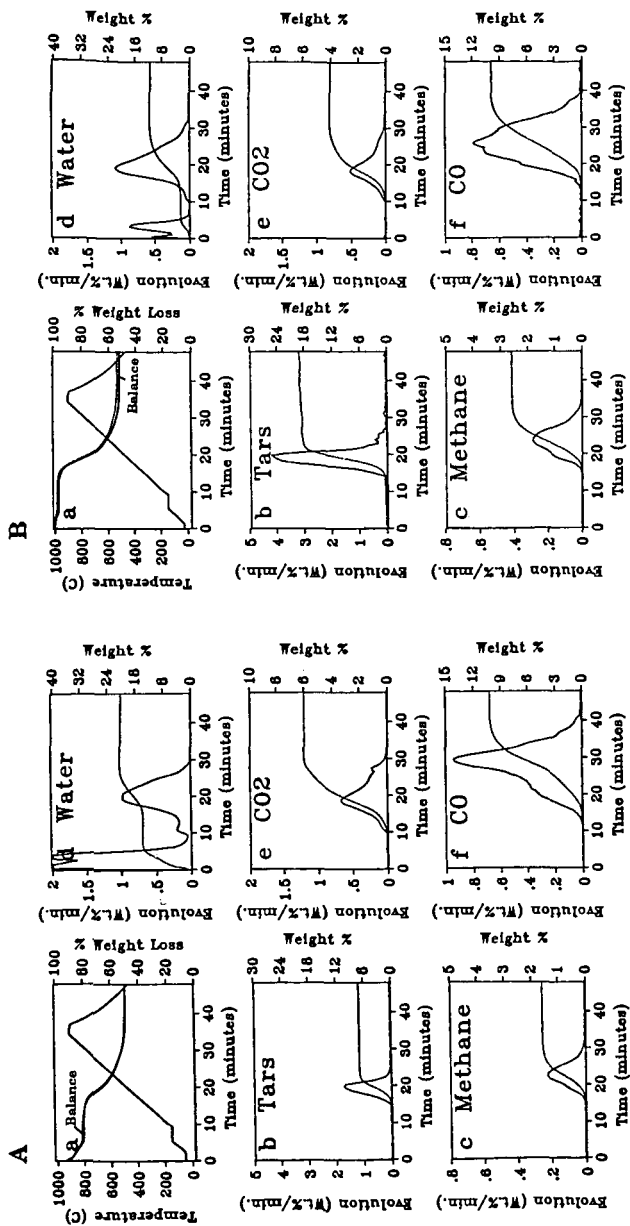


Figure 1. TG-FTIR Analysis of A) Raw and B) Demineralized Argonne Zap Lignite.

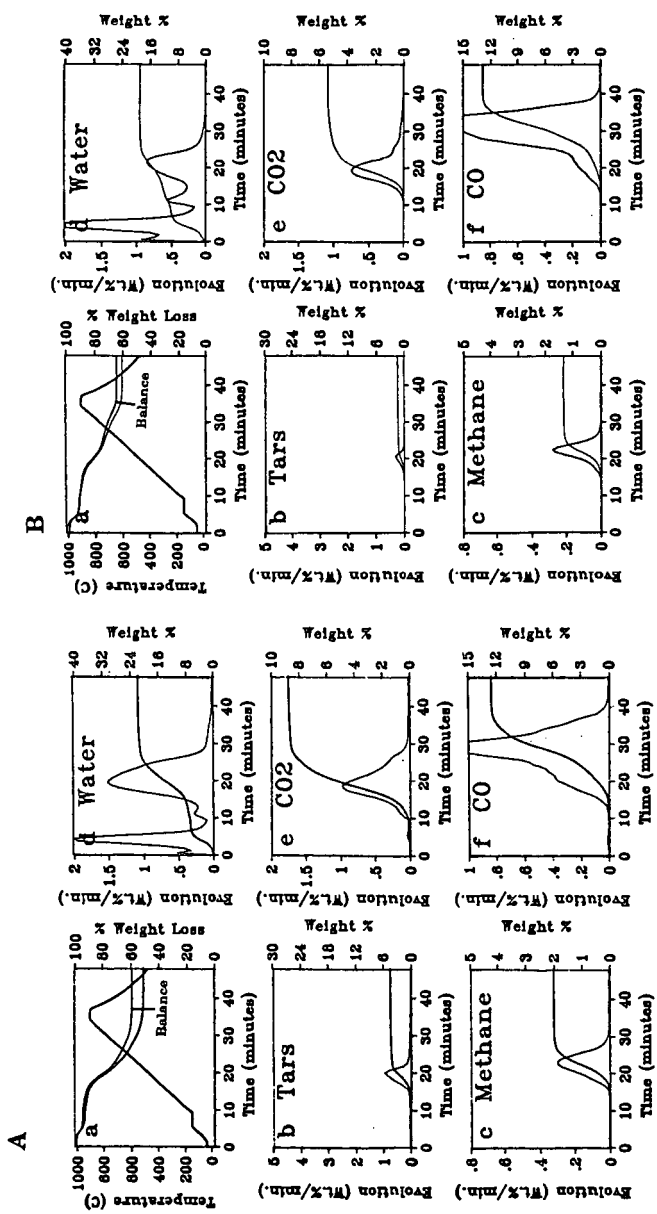


Figure 2. TG-FTIR Analysis of Zap Samples which A) have had Carboxyl Groups Exchanged with Barium; B) have had Carboxyl and Phenolic Groups Exchanged with Barium.

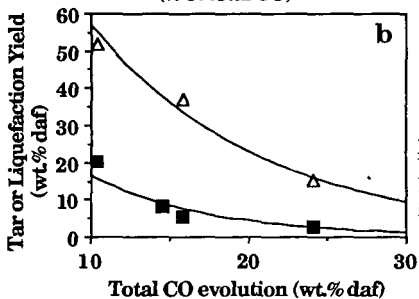
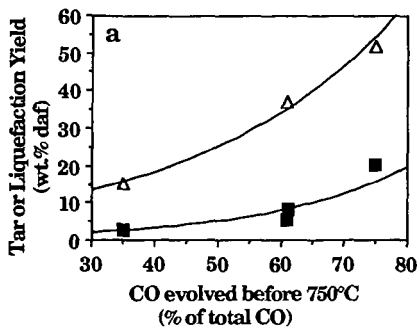


Figure 3. Correlation of Pyrolysis Tar Yield (■) and Toluene Solubles from Liquefaction (Δ) for Zap Lignite with a) Pyrolysis CO Evolution Before 750°C; b) Total Pyrolysis CO Evolution.

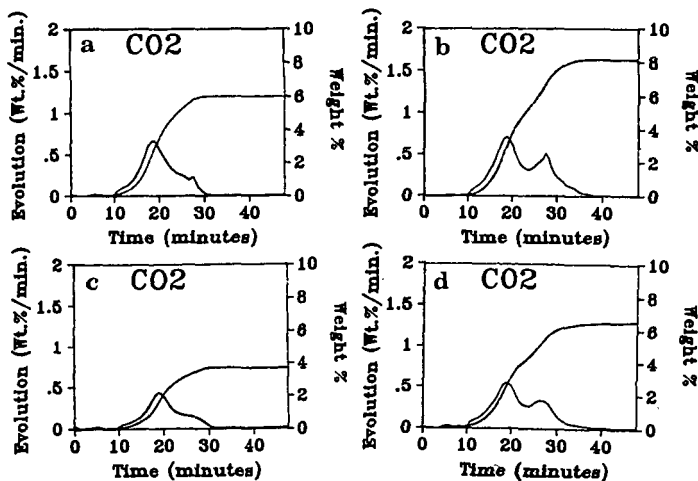


Figure 4. CO<sub>2</sub> Evolution During Coal Pyrolysis. a) Raw Zap; b) Remoisturized Zap; c) Raw Wyodak; d) Remoisturized Wyodak.

**EFFECT OF TEMPERATURE, SAMPLE SIZE AND GAS FLOW RATE ON  
DRYING OF BEULAH-ZAP LIGNITE AND WYODAK SUBBITUMINOUS COAL**

Karl S. Vorres  
Chemistry Division, Building 211  
Argonne National Laboratory  
Argonne, IL 60439

Keywords: drying, liquefaction, TGA

**ABSTRACT**

Beulah-Zap lignite and Wyodak-Anderson (-100 and -20 mesh from the Argonne Premium Coal Sample Program) were dried in nitrogen under various conditions of temperature (20-80°C), gas flow rates (20-160 cc/min), and sample sizes (20-160 mg). An equation relating the initial drying rate in the unimolecular mechanism was developed to relate the drying rate and these three variables over the initial 80-85% of the moisture loss for the lignite. The behavior of the Wyodak-Anderson subbituminous coal is very similar to that of the lignite. The nitrogen BET surface area of the subbituminous sample is much larger than the lignite.

**INTRODUCTION**

Economical production of synthetic coal liquids suitable for transportation fuels is a continuing goal of a number of coal conversion programs. The vast reserves of low rank coals in the western part of the U. S. provide a plentiful supply of input for potential processes. The low rank coals generally possess a high reactivity in many chemical reactions which also make them attractive feedstocks. One of the major detractors, however, is the high moisture content associated with many of these fuels, ranging up to 40%. An economical means of removing the moisture without sacrificing the reactivity or oil yields would be desirable.

A number of studies have been carried out on the drying behavior of coals from a fundamental viewpoint (1,2,3,4,5). The drying behavior has been found (1,2,3,4) to follow a unimolecular mechanism in a flow of dry gas (nitrogen or carbon dioxide) over a range of temperatures, gas flow rates and sample sizes). The mechanism proceeds through two stages. The initial stage accounts for about 80-85% of the moisture loss, while the second accounts for all but about 1% of the rest of the loss.

**EXPERIMENTAL**

Coal drying was done with a modified Cahn model 121 thermobalance or thermo-gravimetric analyzer (TGA) attached to an IBM PC/XT microcomputer. Vendor-supplied software was used to monitor the progress of individual runs, and convert data files to a form that could be further studied with Lotus 123.

The data were obtained as files of time, temperature and weight at 10 second intervals. Run times varied from 7-23 hours. Sample sizes typically started at about 80 mg, but varied from

20-165 mg. Runs were typically isothermal, with temperatures selected from 20 to 80°C. The gas velocity moving upward past the sample was typically 80 cc/min (but ranged from 20 to 160) in the 25 mm diameter tube. The thermobalance was modified so that all of the gas flow passed around the sample, rather than partly through the weighing mechanism. The sample was placed in a quartz flat bottom bucket about 10 mm internal diameter. The samples were the -100 mesh Argonne Premium Coal Samples: Beulah-Zap lignite and Wyodak-Anderson subbituminous (6).

Samples were quickly transferred from ampoules which had been kept in constant humidity chambers with water at room temperature (20°C or 293 K). In the thermobalance system a period of about 5 minutes was used to stabilize the system and initiate data acquisition. A condenser was made to replace the usual quartz envelope and furnace that surrounds the sample. Water was circulated from a constant temperature bath through the condenser to maintain constant temperature during the experiments. This was more stable than the original furnace and provided uniform temperature control during the experiments.

The atmosphere for the nitrogen gas runs was cylinder nitrogen (99.99%) or "house" nitrogen from the evaporation of liquid nitrogen storage containers used without further purification.

Data were analyzed on a separate microcomputer as reported earlier (1-4). Regression analysis was used to obtain the kinetic constants in terms of mg of water lost/gm sample per 10 second time interval. Lotus 123 was used for analysis of individual run data. In some runs, approximations to a first and second derivative of the rate expressions were made in Lotus 123 by averaging over a number of the 10 second time intervals before and after the point of interest. These derivatives were plotted with the rate data to aid in identifying the beginning of the transitions from an initial phase of drying to a second, slower phase. The initial drying kinetic data from a run at a temperature different from room temperature were collected over a time in which the sample was reaching the temperature of the system. These runs indicated that the initial rate increased for about 10-30 minutes until a constant value for the first phase was reached. Figure 1 indicates typical weight changes over the duration of a run for the Beulah Zap lignite and the Wyodak-Anderson subbituminous samples. Note that the lignite has a higher initial moisture content and therefore can lose more water.

Surface area measurements were carried out to complement the drying kinetic runs. The surface area was assumed to be important in that it determines the amount of exposure to the gaseous phase. The greater the surface area the greater the overall reaction rate will be, assuming a similar reactivity per unit of surface and comparable access to exterior and interior surface.

The Quantasorb Jr. instrument was used for nitrogen BET (Brunauer-Emmett-Teller) measurements of the surface. A series of values were obtained on samples which were prepared by drying in the vacuum oven at a range of temperatures as well as a set of nitrogen dried samples, prepared both in the vacuum oven with a flow of nitrogen at atmospheric pressure, and also the products

of some of the thermobalance runs. The typical run gives the data from the desorption cycle. Samples of nitrogen in helium (10, 20 and 30% nitrogen) were allowed to interact with the surface of the sample. Adsorption was carried out at liquid nitrogen temperatures. The amount of adsorbed nitrogen was determined by calibration of a thermal conductivity bridge.

## RESULTS AND DISCUSSION

A typical run indicates a rapid initial moisture loss, followed by significantly reduced rates. A plot of the logarithm of the water left as a function of time gives two straight line segments followed by a downward slope for the loss of the last 1%. See Figure 2 for typical lignite and subbituminous coal runs. The first line segment has been correlated with the loss of "freezable" water, while the latter has been associated with "non-freezable" water as identified by Mraw and co-workers (7,8). The rate constants for the initial rate loss can be correlated with an Arrhenius plot to give an activation energy for the initial stage of water loss, but the second stage could not be correlated. A multiple regression analysis of the initial rate with the values of the absolute temperature, gas flow and sample weight was carried out with the data from 51 runs made with -100 mesh material in dry nitrogen. For an equation of the form:

$$\text{Log Initial Rate (mg water left/gm sample/10 second interval)} = c_1 * \text{Temperature (K)} + c_2 * \text{Gas flow (cc/min)} + c_3 * \text{Sample Weight (mg)} + c_4$$

The best fit was given for:

$$\begin{aligned} c_1 &= .0248 & c_2 &= .00376 \\ c_3 &= -.00528 & c_4 &= -3.295 \end{aligned}$$

with an  $R^2$  value of .867. These values cover experiments in the range of 20-80°C, 20-160 cc/min gas flow and 20-169 mg sample weight.

A smaller series of runs (6) made with the -100 mesh Wyodak subbituminous sample at gas flow rates of 80 cc/min were analyzed with multiple regression. The best fit over the range of 20-60°C and weight of 40-80 mg were given by:

$\log k_1$  (initial rate in mg water left/gm sample /10 second interval) = .0242 \* Temperature (K) - .00673 \* Sample weight (mg) - 9.315. The  $R^2$  value = .983. There is a similarity in the coefficients for the temperature and the weight for the two coals. The similarity in the two curves in Figure 2 would also indicate this.

The surface area measurement data are given in Table 1.

Table 1, Surface Area Measurements

Run #	Drying Method	Temp. °C.	Surface area m <sup>2</sup> /gm
ND173	Nitrogen	22	1.993

RM-59-1	Vacuum	22	3.221	
RM-59-1	Vacuum	22	2.889	reproducibility check
RM-68-2	Vacuum	22	2.969	repro. different sample
ND175	Nitrogen	40	1.811	
RM-67-1	Vacuum	40	2.141	
ND177	Nitrogen	60	1.887	
ND178	Nitrogen	70	1.286	Questionable value
RM-62-1	Nitrogen	110	1.819	
RM-63-1	Vacuum	110	1.768	
RM-65-1	Nitrogen	150	1.865	
RM-65-1	Vacuum	150	1.900	
RM-66-1	Vacuum	150	1.764	repeat above after heating overnight in N2 at 150°C.

For comparison a run was made using Wyodak subbituminous coal:

RM-68-1 Vacuum 25 10.61

Clearly the subbituminous coal has a much larger surface area, reflecting a greater order in the coal particles, and better developed pore structure.

## CONCLUSIONS

### Generalizations on Lignite Drying

1. A complete understanding of the rate of lignite drying must include the effects of a number of variables. Some of these are inherent in the material itself, others depend on the processing given to the material, and still others have to do with mass transfer effects.

2. The rate of drying is affected by the temperature, gas flow, sample thickness and history. For the experiments conducted in this study the rate of drying from the 10 mm diameter container can be expressed by:

$$\text{Log rate} = .0248 * \text{Temp. (K)} + .00376 * \text{gas flow (cc/min)} - .00528 \text{ sample wt (mg)} - 3.295.$$

3. There is a unimolecular mechanism for the initial 60-85% of the weight loss. A transition occurs to a slower mechanism until about 1% of the water remains.

4. There are at least two kinds of water present in the low rank coals. The terms "freezable" and "non-freezable" have been applied to these. The kinetic data support this concept, and extend the perception to exchange between the two forms. The initial water loss corresponds to "freezable" water, while the later loss corresponds to "non-freezable" water.

### Generalizations on Subbituminous Drying

1. The behavior of subbituminous coal on drying is very similar to that of lignite.

2. The mechanism of drying is a unimolecular process. There is a transition after about 80% of moisture loss to a slower unimolecular process.

3. The rate of drying is affected by the temperature, sample thickness or weight and history. For the experiments conducted in this study the rate of drying from the 10 mm diameter container can be expressed by:

$$\text{Log rate} = .0242 * \text{Temp. (K)} - .00673 \text{ sample wt (mg)} - 9.315.$$

4. The subbituminous coal has a larger nitrogen BET surface area, but the rate of drying is not enhanced by this larger area.

#### ACKNOWLEDGMENTS

The author is grateful for the support of the Office of Fossil Energy, U. S. Department of Energy in this work.

#### REFERENCES

1. Vorres, K. S., R. Kolman, and T. Griswold, Am. Chem. Soc. Preprints Fuel Chem. Div. 33 (2), 333 (1988).
2. Vorres, K. S. and R. Kolman, Am. Chem. Soc. Preprints Fuel Div. 33 (3), 7 (1988).
3. Vorres, K. S., Wertz, D. L., Malhotra, V. M., Dang, Joseph, J. T. and Fisher, R. Fuel, 71 (9) 1047-1053 (1992)
4. Vorres, K. S. Am. Chem. Soc. Preprints Fuel Chem. Div. 37 (2), 928 (1992). See also Vorres, K. S., Wertz, D., Joseph, J. T., and Fisher, R., Am. Chem. Soc. Preprints Fuel Chem. Div. 33 (3), 853 (1991) and Vorres, K. S., Molenda, D., Dang, Y., and Malhotra, V. M. Am. Chem. Soc. Preprints Fuel Chem. Div. 36 (1), 108 (1991).
5. Abhari, R. and L. L. Isaacs, Energy & Fuels 4, 448 (1990).
6. Vorres, K. S. Energy & Fuels 4 (5) 420-426 (1990)
7. Mraw, S. C. and B. G. Silbernagel, Am. Inst. Physics Proceedings 70, 332 (1981).
8. Mraw, S. C. and Naas-O'Rourke, D. F., Science, 205 901 (1979) and J. Coll. Int. Sci., 89 268 (1982)

Fig. 1: Wyodak and Beulah-Zap Dried in N<sub>2</sub>, 40 C.  
 WY13 & ND86, -100 mesh, 80 cc/min, 80 mg, fbb

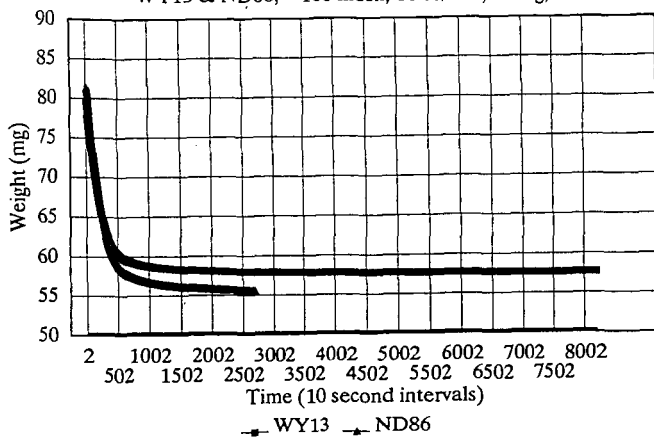
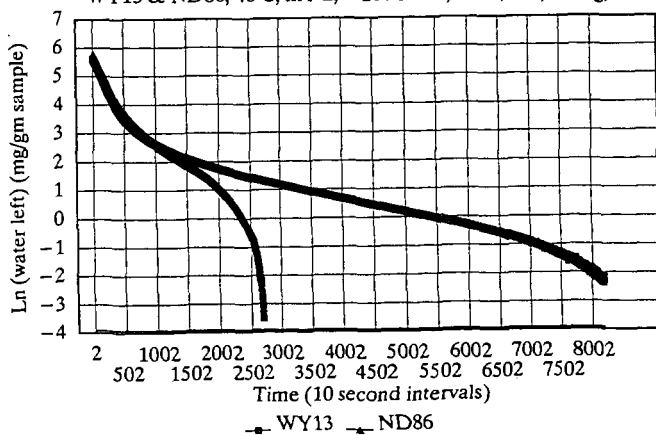


Fig. 2 Wyodak & Beulah-Zap Dried in N<sub>2</sub>, 40 C.  
 WY13 & ND86, 40 C, in N<sub>2</sub>, -100 mesh, 80 cc/min, 80 mg, fbb



## Influence of Drying and Oxidation of Coal on its Catalytic and Thermal Liquefaction. 1. Coal Conversion and Products Distribution.

Ajay K. Saini, Chunshan Song and Harold H. Schobert

Department of Material Science and Engineering, 209 Academic Projects Building, Fuel Science Program, The Pennsylvania State University, University Park, PA 16802.

Keywords: Drying, Oxidation, Coal liquefaction.

### INTRODUCTION

Most of the subbituminous coals contain more than 25 wt % of moisture and it is considered an economic necessity to dry these coals prior to liquefaction. The drying of coal can have significant effect on the conversion reactivity of coal. Atherton (1) reported that the drying of low rank subbituminous coal in a gas atmosphere did not effect the total conversion except in air. The air-drying gave somewhat lower conversion, which may be a result of the adverse effect of preoxidation. The best conversion was obtained by vacuum and microwave drying. The oxidation of coal has been known to have an adverse effect on the coal conversion. Neavel (2) reported a significant reduction in the yield of benzene soluble products from hvc bituminous coal as a result of oxidation. Cronauer et al. (3) reported that partial drying of subbituminous coal in a mixture of nitrogen and oxygen or even in nitrogen alone reduced the conversion as compared to that of the raw coal. On the other hand, Vorres et al. recently reported that drying improves the oil yield in liquefaction of lignite samples (4)

In the present study we report the influence of drying Wyodak subbituminous coal in air and vacuum on the THF-conversion in thermal and catalytic liquefactions. From our results it appears that the drying of coal in air to some extent, which has been considered to be worse for liquefaction, may give a better conversion with dispersed Mo catalyst compared to the vacuum-dried coal in the presence of a liquefaction solvent. The raw coal was also subjected to liquefaction. Best conversion was obtained from the raw coal in the thermal and catalytic solvent-free run. In presence of solvents during catalytic runs the raw coal did not show any improvement over the thermal runs.

### EXPERIMENTAL

The coal used was Wyodak subbituminous coal (DECS-8). This coal contains 32.4 % volatile matters, 29.3% fixed carbon, 9.9 % ash and 28.4 % moisture, on as-received basis; 75.8% C, 5.2% H, 1.0% N, 0.5% S and 17.5% O, on dmmf basis. The coal was dried under vacuum for 2 h at 100 °C. The drying of coal in air was done in an oven maintained at 100 and 150 °C with the door partially open. At 100 °C the coal was dried for 2, 20 and 100 hours and at 150 °C it was dried for 20 hours. The liquefaction was carried out at 350 °C for 30 minutes under 7 MPa (cold) H<sub>2</sub> in 25 ml tubing bomb. Ammonium tetrathiomolybdate (ATTM) was used as precursor for molybdenum sulfide catalyst. It was loaded on to coal by incipient wetness impregnation method from aqueous solution with 1 wt % Mo on dmmf basis. The impregnated coal samples were dried in a vacuum oven at 100 °C for 2 h. The experimental details about the liquefaction and the product work up is given elsewhere (5). The total conversion (TC) of the coal into soluble products have been calculated on the basis of the THF-insoluble residues. The analysis of the gases evolved during liquefactions at 350 °C show that the major components of the gases are CO and CO<sub>2</sub>. The total yield of the hydrocarbon gases produced is less than 1 wt % dmmf coal, in all the liquefaction runs.

### RESULTS AND DISCUSSION

#### Solvent-free Liquefaction

The products distribution for the solvent-free thermal liquefactions are given in Table 1. As compared to the vacuum-drying the air-drying of coal at 100 °C for up to 100 h did not effect the total conversion on the basis of THF-insoluble residue. But the total gas yield increased with the drying time in air. This increase is mainly due to the increase in the CO and CO<sub>2</sub> yields (Table 3) at the expense of other products which is undesirable. The drying in air, oxidizes the coal, increasing the carboxylic and carbonyl functionalities which upon thermolysis produce CO<sub>2</sub> and CO gases. Upon excessive oxidation at 150 °C for 20 h the coal conversion slightly decreased but the gas yield increased considerably, which was accompanied by the decrease in the oil, asphaltene and preasphaltene yields. Since the main constituent of the gas is CO<sub>2</sub> which is associated with air-oxidation, it would be more appropriate to see the effect of drying on the desirable products. Figure 1 shows the distributions of the liquid and solid products in the

solvent-free thermal liquefaction experiments. It is clear that compared to the vacuum-drying, the air-drying of coal at 100 °C for up to 20 h increases the oil yield with no significant effect on the total conversion into THF-soluble products in thermal runs. But oxidative drying for the extended period of time decreases the total conversion as well as the oil yield because of the extensive degradation of the coal.

As with the vacuum-dried coal, the presence of catalyst in the solvent-free runs of the air-dried coal increases the total conversion compared to that of the thermal runs on the basis of THF-insoluble residues (Table 2). Similar to the thermal runs, in catalytic liquefactions the drying of coal in air at 100 °C for up to 100 h does not show any significant effect on the total conversion as compared to that of the vacuum-dried coal. The gas yields in the catalytic runs are lower than in the corresponding thermal runs with the most contribution from CO<sub>2</sub> and also increases with the drying time. If the conversion is calculated excluding the gas yield, the air-dried coal at 100 °C for up to 20 h does not show any effect but for the drying time of 100 h and at 150 °C for 20 h there is a considerable decrease in the conversion compared to that of the vacuum-dried coal (Figure 1). Over all, the increase in total conversion for the air-dried coal in catalytic runs over the thermal runs is similar to that for the vacuum-dried coal (Table 2 and Figure 1).

As-received coal (raw) was also subjected to thermal and catalytic liquefactions. The products distribution is given in Tables 1 and 2. Surprisingly, best values for the total conversions are obtained in the solvent-free thermal (25.0 wt%) and catalytic (43.3 wt%) runs on the basis of THF-insoluble residue compared to the vacuum- (12.5 and 29.8 wt%, respectively) and air-dried coal (14.8 and 29.2 wt%, respectively, for 2 h drying time). Significant increase in the oil yield is also observed from the raw coal compared to the dried coal. There is also a higher gas yield from the raw coal in thermal run compared to the vacuum- and air-dried coal at 100 °C for upto 20 h (Table 3). The increase in the gas yield is mainly due to the remarkable increase in the CO and CO<sub>2</sub> yields. The increase in the CO and CO<sub>2</sub> gases is due to the presence of water in the coal. It has been reported that the presence of water in the oxidized coal may enhance the removal of oxygen-containing groups (6). It appears that the presence of water during liquefaction removes the carbonyl functionalities from the coal network which makes the coal less refractory for liquefaction and hence improved conversion. The total-conversions excluding the gas yield shown in Figure 1, are the best in the case of the raw coal both in the solvent-free thermal and catalytic runs.

#### Liquefaction in Presence of Tetralin

It is known that the presence of a hydrogen donor solvent during liquefaction, enhances the total conversion of a coal to THF-soluble products as compared to the solvent-free runs. In the presence of tetralin during thermal runs the increase in total conversion of the vacuum-dried and air-dried coal is quite remarkable but, relatively, air-dried coal shows more increase in conversion (Table 1 and 2). The vacuum-dried coal shows an increase of 13.4 % (12.5% excluding gas yield) while the total conversion for the air-dried coal for 2 h at 100 °C increases by 20.3 % (19.9% excluding gas yield). The coal dried in air for 20 and 100 h at 100 °C also show a remarkable increase in conversion in the presence of tetralin but the increase is not as much as for the coal dried for 2 h. The oil yield for the air-dried coal for 2 h at 100 °C increases from 3.3 % to 11.7% with an increase of 8.4% in presence of tetralin, correspondingly, the increase in the oil yield for the vacuum-dried coal is only 2.0%. The oil yield for the coal dried at 100 °C in air for 20 h is also better than that of the vacuum-dried coal. The increase in the asphaltene and preasphaltene yields in presence of tetralin as compared to that of the solvent-free runs for the air-dried for 2 h and vacuum-dried coal are not significantly different. As the coal was dried in air for longer periods of time at 100 °C the increase in the oil production declined. The coal dried in air for 20 h at 150 °C showed only an increase of 1.5%. These results show that in thermal runs with tetralin the air-dried coal at 100 °C for up to 20 h gives better conversion and oil yield compared to the vacuum-dried coal (Figure 2). This suggests that the oxidation of a coal to some extent may enhance the oil yield and the total conversion but excessive oxidation of coal may have a negative effect.

The total conversion for the raw coal is 43.3% (37.5%, excluding gases) in thermal liquefaction in the presence of tetralin (Table 1). This conversion is undoubtedly better than the air-dried or vacuum-dried coal runs. Raw coal liquefaction gives an oil yield of 15.8% with an increase of 10.4% over the solvent-free run. Increasing the oil yields in liquefaction experiments is most desirable. Compared to the air-dried or vacuum-dried coal the oil yield is better in the case of raw coal run (Figure 2).

In the catalytic liquefactions also there is a remarkable increase in the total conversion from that of the solvent-free runs in presence of tetralin. This increase is similar to that in the thermal runs for the air-dried coal at 100 °C and vacuum-dried coal (Tables 1 and 2). In the catalytic runs in presence of tetralin the air-dried coal at 100

°C gives better total conversion compared to the vacuum-dried coal, on the basis of THF-insoluble or the total yields of oil, asphaltene and preasphaltene (Table 2 and Figure 2). It seems that the extent of drying at 100 °C also does not decrease the total conversion. Unexpectedly, the liquefaction of the raw coal in presence of tetralin does not show any significant catalytic improvement in total conversion (Figure 2). In the catalytic liquefaction in presence of tetralin of the raw coal the total conversion is 42.2% (39.4% excluding gas yield) and is 43.3% (37.5% excluding gas yield) in the thermal runs with tetralin. The products distribution of the raw coal experiments are also quite similar. As seen before in the thermal runs the raw coal showed a remarkably higher conversion in presence of tetralin, compared to the air-dried coal (Table 1). In the catalytic runs the raw coal and the air-dried coal showed a very similar conversions (Table 2 and Figure 2). It seems that during liquefaction of the raw coal in presence of tetralin the catalyst is less active. The decrease in the H<sub>2</sub>-consumption by the raw coal during catalytic liquefaction in presence of tetralin from that in the solvent-free run is much higher than that for the dried coal (Figure 4).

#### Liquefaction in the Presence of 1-Methylnaphthalene

It has been seen before that the presence of a non-donor solvent such as 1-methylnaphthalene (1-MN) also enhances the total conversion to some extent compared to that of the solvent-free runs. In the thermal liquefaction of the vacuum-dried coal the total conversion increases from 12.5% in the solvent-free run to 18.3% with 1-MN (Table 1). The difference is significantly high. The liquefaction of the air-dried coal in presence of 1-MN also show a considerable increase as compared to that of the solvent-free runs. Total conversions for the coal dried at 100 °C for 2 and 20 h in air increases from 14.8 and 15.5% to 22.4 and 24.1% respectively, in presence of 1-MN. These conversion figures are better than that of the vacuum-dried coal (Table 1). Even after excluding the gas yields, the conversion is better if the coal was dried at 100 °C for up to 20 h in air. (Figure 3). Upon drying coal for 100 h at 100 °C in air the total conversion decreases and it is worse for the extensively oxidized coal at 150 °C for 20 h.

The total conversion of the raw coal in the thermal liquefaction increases from 25.0% (17.3% excluding gas) in solvent-free run to 39.9% (34.0%, excluding gas) with 1-MN (Table 1). This increase is significantly higher than that of the air- or vacuum-dried coal. In the thermal runs with 1-MN the raw coal gives 19.7% more THF-soluble products excluding gas yield, compared to the vacuum-dried coal, which is remarkably higher than that of the air-dried coal. The most importantly the increase in the total conversion of the raw coal is due to the significant increase in the yield of the most desirable product, oil. The oil yield increases from 1.1% in the vacuum-dried coal to 15.9% in the raw coal.

The catalytic liquefaction of vacuum- or air-dried coal in presence of 1-MN improves the conversion. The best conversion is obtained in the case of air-dried coal at 100 °C. The extent of drying at this temperature does not seem to make any considerable difference in the conversion (Table 2 and Figure 3). The catalytic liquefaction of the raw coal in presence of 1-MN gives a total conversion of 35.9% on the THF-insoluble residue basis. This conversion is rather lower than that of the thermal liquefaction under similar conditions. The unusual decrease in the oil yield for the raw coal in the catalytic run compared to that in the thermal run may be an artifact which needs to be reconfirmed. As in the presence of tetralin, the liquefaction of the raw coal in the presence of 1-MN in the catalytic runs there is no improvement in the total conversion compared to the thermal runs. In the catalytic liquefaction in presence of 1-MN the best conversion obtained is with the coal-dried in air at 100 °C with a significantly higher oil yields compared to the vacuum-dried coal.

#### Hydrogen Consumption

Figure 4 shows the H<sub>2</sub>-consumption profile for the thermal and catalytic liquefactions from H<sub>2</sub>-gas and from tetralin.. There is a significant decrease in the H<sub>2</sub>-consumption during thermal liquefaction if the coal is pre-dried. In the solvent-free thermal run the H<sub>2</sub>-consumption increases with the drying time in air at 100 °C and also the consumption increases as the coal is dried at 150 °C for 20 h. With tetralin and 1-MN there is an initial decrease in the H<sub>2</sub>-consumption from 2 h to 20 h drying time and then it increases with the increased oxidative drying of coal. This suggests that the oxidative drying of coal increases the H<sub>2</sub>-consumption during liquefaction and the consumption is higher if no solvent is used. In the catalytic runs the oxidative drying of coal at 100 °C for up to 100 h does not seem to have any significant effect on H<sub>2</sub>-consumption. When the coal is dried at 150 °C for 20 h a slight decrease in the H<sub>2</sub>-consumption in the solvent-free catalytic liquefaction is observed otherwise in presence of a solvent the H<sub>2</sub>-consumption is essentially the same. These results suggest that the H<sub>2</sub>-consumption increases with the extent of oxidation in thermal liquefaction and in catalytic liquefactions the oxidation does not make any considerable difference.

The vacuum-dried coal shows a similar H<sub>2</sub>-consumption value as that of the coal dried in air for 2 h in thermal as well as catalytic runs. But during thermal liquefaction of the raw coal the H<sub>2</sub>-consumption is higher than that of the vacuum- and air-dried coal for 2 h. In the catalytic liquefaction of the raw coal in presence of solvents the H<sub>2</sub>-consumption is not much different from that of the vacuum- or air-dried coal for 2 h, but in the solvent-free catalytic run the H<sub>2</sub>-consumption is remarkably higher. These results may account for the better conversions in the case of raw coal liquefaction compared to that of the vacuum- or air-dried coal.

Hydrogen-transfer from tetralin (Figure 4) increases (in the thermal liquefactions) with the extent of oxidation of coal. Vacuum-dried and the raw coal show a lower H-transfer compared to that of the air-dried coal. In the catalytic runs the H-transfer from tetralin is relatively lower than that in the corresponding thermal run and does not make any noticeable difference as the coal is dried at 100 °C in air up to 100 h. When the coal is dried at 150 °C for 20 h the H-transfer is slightly higher. The vacuum-dried coal shows a lowest value for the H-transfer from tetralin in the catalytic run.

#### CONCLUSIONS

The air-dried coal at 100 °C for up to 20 h gave similar conversions as the vacuum-dried coal in the solvent-free thermal and catalytic liquefactions. In the presence of solvents, better conversions were obtained from the coal dried in air at 100 °C for 2 h compared to the vacuum-dried coal. The extensive oxidation of coal decreased the coal conversions in thermal as well as catalytic runs. These results suggests that air-drying of coal to some extent may be beneficial for liquefaction. The raw coal gave the best conversions in the solvent-free runs. The improved conversion seems to be due to the presence of water, which enhances the removal of carbonyl functionalities during liquefaction making coal network less refractory for liquefaction.

#### ACKNOWLEDGEMENTS

This work was supported by the U.S. DOE Pittsburgh Energy Technology Center.

#### REFERENCES

1. Atherton, L.F.; Proc. 1985 Int. Conf. Coal Sci., p.553.
2. Neavel, R.; Fuel 1976, 55, 237.
3. Cronauer, D.C., Ruberto, R.G., Silver, R.S., Jenkins, R.G., Davis, A., and Hoover, D.S.; Fuel, 1984, 63, 77.
4. Vorres, K.S., Wertz, D.L., Malhotra, V., Dang, Y., Joseph, J.T., and Fisher, R.; Fuel, 1992, 71, 1047.
5. Saini, A.K., Song, C., Schobert, H.H., and Hatcher, P.G.; ACS Fuel Chem. Div. Prepr. 1992, 37(3), 1235.
6. Petit, J.C.; Fuel, 1991, 70,1053.

**Table 1.** Products distributions (dmmf wt %) for the thermal liquefactions of the raw and dried coal at 350 °C with different solvents.

Drying Conditions.	Gas*	Oil	Asphal.	Preasp.	Total Conv.
<b>Solvent-free</b>					
Raw-undried	7.7 (9.5)	5.4	2.8	9.1	25.0
Air-dried,2h,100°C	5.0 (6.3)	3.3	0.7	5.8	14.8
Air-dried,20h,100°C	5.7 (7.3)	6.0	0.6	3.2	15.5
Air-dried,100h,100°C	8.5 (12.0)	1.2	0.7	3.3	12.7
Air-dried,20h,150°C	9.8 (13.2)	0.6	0.2	0.4	10.9
Vac.-dried,2h,100°C	3.3 (5.9)	2.1	2.6	4.5	12.5
<b>Tetralin</b>					
Raw-undried	5.8 (7.7)	15.8	9.3	12.4	43.3
Air-dried,2h,100°C	5.4 (6.3)	11.7	7.4	10.6	35.1
Air-dried,20h,100°C	5.9 (8.7)	11.1	6.5	8.9	32.4
Air-dried,100h,100°C	8.7 (11.6)	6.1	6.3	9.7	30.8
Air-dried,20h,150°C	11.8(16.6)	2.1	2.8	3.2	19.9
Vac.-dried,2h,100°C	4.2 (5.4)	4.1	7.6	10.0	25.9
<b>1-Methylnaphthalene</b>					
Raw-undried	5.9 (8.4)	15.9	6.6	11.4	39.9
Air-dried,2h,100°C	5.1 (7.6)	4.2	4.0	9.4	22.7
Air-dried,20h,100°C	6.2 (7.5)	8.0	5.6	4.7	24.5
Air-dried,100h,100°C	9.0 (12.7)	1.7	4.1	6.3	21.1
Air-dried,20h,150°C	11.4(16.5)	1.8	2.2	2.5	18.0
Vac.-dried,2h,100°C	4.0 (5.7)	1.1	5.8	7.4	18.3

\* The figures in parenthesis give the total gas yields calculated from GC analysis.

**Table 2.** Products distributions (dmmf wt %) for the catalytic liquefactions of the raw and dried coal at 350 °C with different solvents.

Drying Conditions.	Gas*	Oil	Asphal.	Preasp.	Total Conv.
<b>Solvent-free</b>					
Raw-undried	2.2 (4.3)	16.9	9.2	14.9	43.3
Air-dried,2h,100°C	3.3 (6.2)	12.6	3.2	10.1	29.2
Air-dried,20h,100°C	4.8 (6.8)	14.6	3.1	8.7	31.2
Air-dried,100h,100°C	7.6 (9.3)	13.3	2.4	5.1	28.4
Air-dried,20h,150°C	11.2(11.2)	5.1	0.5	1.7	18.5
Vac.-dried,2h,100°C	3.0 (2.9)	10.0	5.4	11.4	29.8
<b>Solvent Tetralin</b>					
Raw-undried	2.8 (4.9)	16.0	11.5	11.9	42.2
Air-dried,2h,100°C	3.9 (5.5)	15.7	11.1	14.9	45.6
Air-dried,20h,100°C	5.6 (7.4)	18.6	8.6	10.7	43.5
Air-dried,100h,100°C	6.7 (9.7)	16.5	10.8	11.0	45.0
Air-dried,20h,150°C	11.8(13.2)	9.6	2.3	5.7	29.4
Vac.-dried,2h,100°C	3.0 (2.9)	10.2	12.9	10.6	36.4
<b>Solvent 1-MN</b>					
Raw-undried	3.2 (5.0)	10.4	10.4	11.9	35.9
Air-dried,2h,100°C	3.0 (5.8)	10.3	8.1	16.0	37.4
Air-dried,20h,100°C	6.4(10.0)	14.1	8.7	10.5	39.7
Air-dried,100h,100°C	5.2(10.3)	14.4	8.7	11.1	39.4
Air-dried,20h,150°C	12.1(13.0)	5.3	2.8	4.3	24.5
Vac.-dried,2h,100°C	2.6 (3.7)	6.1	10.1	12.3	31.1

\* The figures in parenthesis give the gas yields calculated from GC analysis.

**Table 3.** Gas yields (dmmf wt %) for the thermal and catalytic liquefactions.

Drying Conditions.	Thermal				Catalytic			
	CO	CO <sub>2</sub>	C <sub>1</sub> -C <sub>4</sub>	Total	CO	CO <sub>2</sub>	C <sub>1</sub> -C <sub>4</sub>	Total
<b>Solvent-free</b>								
Raw-Undried	0.37	8.90	0.25	9.52	0.24	3.52	0.35	4.26
Air-dried,2h,100°C	0.26	5.93	0.14	6.33	0.38	5.18	0.59	6.15
Air-dried,20h,100°C	0.39	6.70	0.16	7.25	0.42	5.67	0.71	6.79
Air-dried,100h,100°C	0.66	11.18	0.17	12.01	0.65	8.01	0.63	9.29
Air-dried,20h,150°C	0.80	12.32	0.09	13.21	0.94	9.76	0.54	11.24
Vac.-dried,2h,100°C	0.24	4.50	0.19	5.93	0.19	2.30	0.29	2.88
<b>Tetralin</b>								
Raw-Undried	0.11	7.41	0.19	7.72	0.14	4.45	0.35	4.94
Air-dried,2h,100°C	0.24	5.91	0.19	6.35	0.21	4.83	0.43	5.47
Air-dried,20h,100°C	0.28	7.18	0.28	8.74	0.17	6.86	0.36	7.39
Air-dried,100h,100°C	0.46	10.95	0.22	11.63	0.36	8.80	0.51	9.67
Air-dried,20h,150°C	0.59	15.87	0.11	16.58	0.41	12.43	0.38	13.20
Vac.-dried,2h,100°C	0.19	4.10	0.15	5.44	0.13	2.58	0.28	2.99
<b>1-Methylnaphthalene</b>								
Raw-Undried	0.14	7.02	0.18	8.45	0.14	4.48	0.34	4.96
Air-dried,2h,100°C	0.25	6.18	0.15	7.59	0.19	5.23	0.37	5.79
Air-dried,20h,100°C	0.28	7.04	0.15	7.48	0.18	9.26	0.51	9.95
Air-dried,100h,100°C	0.50	11.95	0.21	12.67	0.32	9.50	0.44	10.26
Air-dried,20h,150°C	0.65	15.69	0.12	16.47	0.33	12.36	0.32	13.01
Vac.-dried,2h,100°C	0.16	4.34	0.16	5.66	0.11	3.37	0.25	3.73

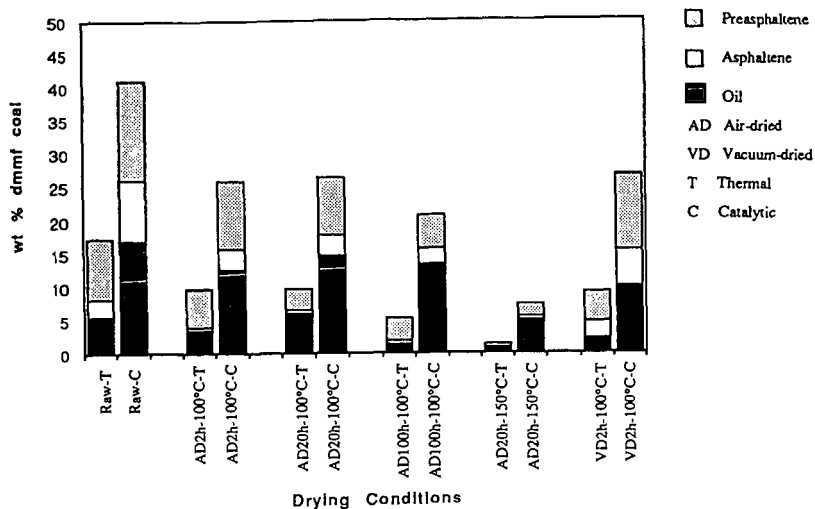


Figure 1. Products distribution from solvent-free thermal and catalytic liquefactions at 350 °C of the raw and coal dried in different conditions.

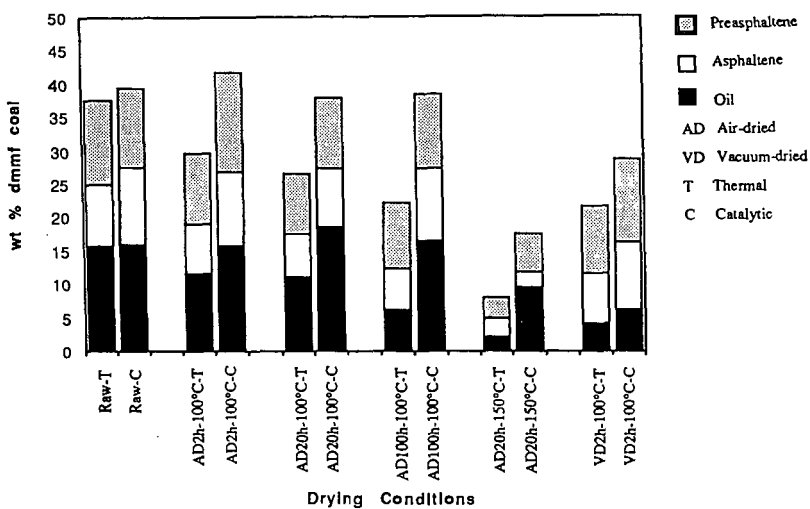


Figure 2. Products distribution from the thermal and catalytic liquefactions in the presence of tetralin at 350 °C of the raw and coal dried in different conditions.

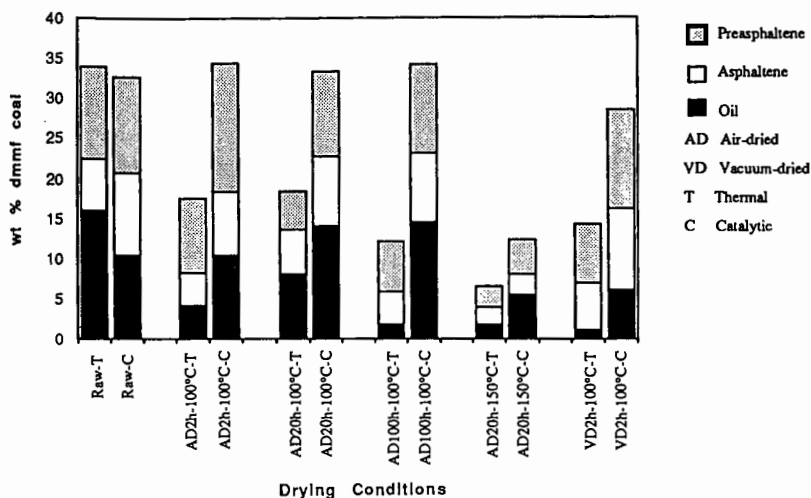


Figure 3. Products distribution from the thermal and catalytic liquefactions in the presence of 1-methylnaphthalene at 350 °C of the raw and coal dried in different conditions.

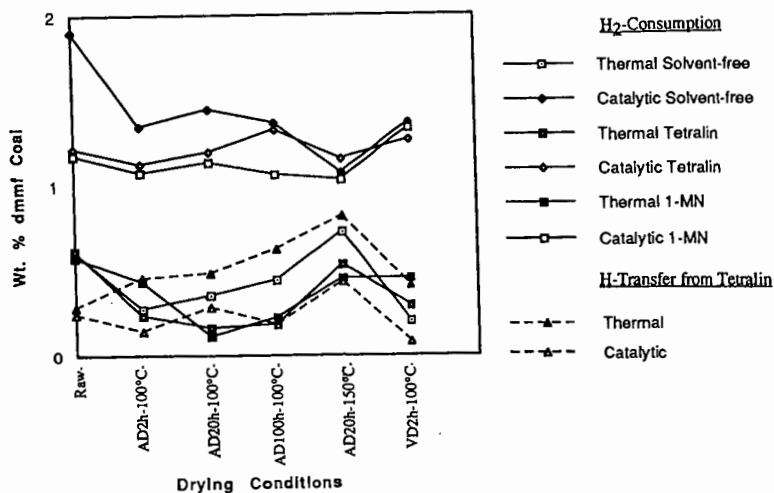


Figure 4. Hydrogen consumption profiles during thermal and catalytic liquefactions from H<sub>2</sub> and tetralin.

## Influence of Drying and Oxidation of Coal on Its Catalytic and Thermal Liquefaction. 2. Characterization of Dried and Oxidized Coal and Residues.

Ajay K. Saini, Chunshan Song and Harold H. Schobert

Department of Material Science and Engineering, 209 Academic Projects Building, Fuel Science Program, The Pennsylvania State University, University Park, PA 16802.

Keywords: Drying, Oxidation, Structural characterization.

### INTRODUCTION

Because of the high moisture content of the low rank coals it is desirable to dry coal before liquefaction. It has been recognized that drying of coal could adversely affect the reactivity of subbituminous coal for liquefaction (1,2). This study has been carried out with a view to understand the effect of low temperature oxidative and non-oxidative drying on coal structure and liquefaction residues. In the preceding paper the impacts of coal drying on the liquefaction have been discussed (3).

Several papers have been devoted to understanding the oxidation of coal (4-10) but very little has been reported on the effect of oxidation on the structures of liquefaction residues which could lead to an insight of the oxidative effect on liquefaction. In the present work we have analyzed the residues from thermal as well as catalytic liquefactions of the raw and dried coal under vacuum and in air. The analysis of the residues reveal that although there is a significant decrease in the aliphatics upon oxidative drying of coal compared to the vacuum dried coal the residues from the air-dried coal are more aliphatic rich, and as the oxidation proceeds more longer-chain aliphatics are lost during liquefaction. The raw coal shows an enhanced loss of carbonyls during liquefaction, which may be the cause of its higher conversion.

### EXPERIMENTAL

The coal used was Wyodak subbituminous obtained from the Penn State Sample Bank (DECS-8). The characteristics of coal are given elsewhere (11). For the raw coal liquefaction it was used as received. For the drying experiments the coal was dried under vacuum at 100 °C for 2 h and in air at 100 °C for 2, 20 and 100 h. At 150 °C coal was dried for 20 h. The air-drying of coal was done in a preheated oven at desired temperature with the door slightly open to ensure the sufficient air supply. The thermal and catalytic liquefactions of coal were carried out at 350 °C under 6.9 MPa (cold) H<sub>2</sub> pressure for 30 minutes. Ammonium tetrathiomolybdate (ATTM) was used as catalyst. It was loaded on to coal by incipient wetness impregnation method from aqueous solution, with 1 wt % Mo on dmmf coal. After the reaction, the liquid and solid products were separated by sequential extraction with hexane, toluene and THF. After the extraction the THF-insoluble residues were washed first with acetone and then pentane in order to remove all the THF, followed by drying at 110 °C for 6 h under vacuum. The coal and residues were analyzed by Py-GC-MS, solid state CPMAS <sup>13</sup>C NMR and FTIR techniques discribed elsewhere (12, 13).

### RESULTS AND DISCUSSION

#### Characterization of the Raw and Dried Coal

#### CPMAS <sup>13</sup>C NMR

Figure 1 compares between the CPMAS <sup>13</sup>C NMR spectra of the raw coal and the vacuum and air-dried coal. The raw coal and the dried coal show similar NMR features. The region between 0-80 ppm consists of aliphatic carbons which may include methoxy carbons and the second region between 90 to 170 ppm is due to the aromatic carbons including two shoulders due to catechol-like and phenolic carbons (11). The carboxylic band appears at 170-190 ppm and carbonyl group between 190-230 ppm. Upon drying coal under vacuum there was no noticeable difference in the NMR spectrum as compared to that of the raw coal. When the coal was dried in air a slight difference seems to be apparent but not very significant until the coal was dried at 100 °C for 100 h or at 150 °C for 20 h. It appears that as the coal was dried under oxidative conditions there was a decrease in the intensity of the catechol shoulder. The other change seems to be the broadening in the carboxyl and carbonyl bands. These changes in the coal structure becomes apparent when the coal was dried in air under severe conditions. After drying coal at 150 °C for 20 h the CPMAS <sup>13</sup>C NMR shows a complete disappearance of the catechol peak and the

carboxyl and carbonyl peaks also show significant broadening, seems to be merging into the aromatic band. The oxidation of coal significantly decreases the aliphatics from the coal. From NMR the decrease in aliphatics is not apparent when coal is dried at 100 °C, but after drying at 150 °C the aliphatic band shows a significant decrease.

#### FTIR

Obvious difference in the FTIR spectrum of the dried coal compared to that of the raw coal is the decrease in the broad water band between 3000-3600  $\text{cm}^{-1}$  which is apparent from the direct comparison of the spectra. The drying of coal in air is known to oxidize the coal causing increase in the ketone, carboxyl and ester type functionalities and decrease in the aliphatic groups. Such changes in the functionalities of the coal upon oxidation at 100 °C were not apparent from direct comparison of the spectra. The difference FTIR technique was utilized to detect the minute spectroscopic changes in the coal structure. Vacuum-dried coal was used as a reference for the difference spectra. The differences in coal structure arising due to oxidative drying of coal apparent from the difference FTIR spectra are consistent with the literature (4-10). The difference spectra show a prominent peak at 1720  $\text{cm}^{-1}$  due to carbonyl which increases in intensity with the severity of drying. There is another shoulder on the high energy side of the 1720  $\text{cm}^{-1}$  band near 1770  $\text{cm}^{-1}$  which also increases with the severity of drying. This band could be assigned to the ester groups. The band at 1640  $\text{cm}^{-1}$  in the difference spectra can be assigned to the highly conjugated carbonyls formed by the oxidation of the methylene bridges linking aromatic units (Ar-CH<sub>2</sub>-Ar) which are highly susceptible to autooxidation forming Ar-CO-Ar groups. As the oxidative drying at 100 °C proceeds the band at 1720  $\text{cm}^{-1}$  due to carboxyl carbonyls seem to be increasing at a faster rate than 1640  $\text{cm}^{-1}$  band. This band may also contain carbonyls in unconjugated ketones. After drying coal at 150 °C for 20 h in air the 1720  $\text{cm}^{-1}$  band becomes more intense relative to the 1640  $\text{cm}^{-1}$  band. A broad band between 1500 and 1590  $\text{cm}^{-1}$  also becomes apparent in the difference spectra of the dried coal. This band is assigned to the carboxylate (COO-) groups which increase upon oxidative drying of coal. After drying coal at 150 °C the broad band at 1550  $\text{cm}^{-1}$  in the difference spectrum due to the carboxylate carbonyls (-COO-) which is just a broad shoulder in the case when coal was dried at 100 °C, becomes an independent peak. The increase in the intensity of the 1550  $\text{cm}^{-1}$  band could be related to the increase in the carboxylic functional groups upon oxidation followed by exchange with cations present in the coal to give COO. The region between the range 1000 and 1300  $\text{cm}^{-1}$  consists of the bands due to C-O type of linkages in ethers, esters and phenols. Upon oxidative drying at 100 °C there is a slight increase in the intensity of the ether region.

#### Pyrolysis-GC-MS

The major aromatic components of wyodak subbituminous coal obtained upon pyrolysis have been reported previously (3). Low rank coals are known to have higher oxygen functionalities. The major oxygen compounds are phenol, methylphenol, ethylphenol, C<sub>2</sub>-phenols and catechol and these are the most abundant components in the pyrogram of the raw coal. Among the alkylbenzenes the most abundant compounds identified are toluene, xylenes and C<sub>3</sub>-benzenes. The other aromatic compounds such as naphthalene and alkyl-naphthalenes are also found but in a very low concentrations. There are many other peaks appearing over the whole pyrogram of the raw coal. These peaks have been identified as alkanes and alkenes ranging from C<sub>4</sub>-C<sub>31</sub>. The most abundant of these are C<sub>4</sub>-C<sub>6</sub> alkanes and alkenes which appear in the early part of the pyrogram and are not very well resolved.

Upon drying coal under vacuum or in air the pyrogram is similar to that of the raw coal from which one can find identical peaks. The only difference is in the relative intensities of the peaks. Table 1 shows the ratios between the total area of the major phenolic and the alkylbenzene compounds in the pyrograms of the raw and the dried coal samples. The vacuum drying of coal did not change the phenolics to alkylbenzene ratio but oxidative drying of coal seems to have a significant effect on these ratios. For first two hours of drying coal in air at 100 °C the change is not very significant but as the extent of drying increases the ratio seems to be decreasing as if the phenolic structures are being consumed from the coal as the air-drying proceeds. After drying coal at 150 °C for 20 h the phenolic to alkylbenzene ratio decreases remarkably.

Using the selective ion chromatogram (SIC) technique for the 71 m/z ion the pattern of the abundances of the alkanes and alkenes can be recognized in the pyrogram of the coal. The SIC for the raw and the vacuum-dried coal using 71 m/z ion show a similar pattern. The most abundant are the C<sub>4</sub>-C<sub>6</sub> alkanes and alkenes. Upon air-drying, coal shows a decrease in the intensities of the short chain aliphatic compounds. The extent of air-drying did not change overall pattern of the aliphatics, the SIC of aliphatics for all the air-dried samples looked similar.

## Characterization of the Liquefaction Residues

### *FTIR*

To investigate the differences in the structure of the residues from the raw and air-dried coal and to understand the liquefaction behavior of the coal dried under different conditions, the residues from the vacuum dried coal were used as reference for the FTIR difference spectra. The vacuum dried coal residues were subtracted from that of the raw and the air-dried coal. The subtraction factors were calculated on the basis of the amount of organic matters left in the residues after liquefactions and calculated by the ratio of the amount of dmmf coal per mg of the pellet keeping the diameter of the pellet constant. Before discussing the differences in coal structure using difference technique, it should be noted that the frequencies of the bands in the difference spectra are not well defined and also the apparent frequencies of different bands can often be affected by the degree of subtraction and residual band overlap (8).

The difference spectra of the residues from the thermal runs show a significant differences in the coal structure as a consequence of air-drying (Figure 2). The major differences are in the carbonyl region (1500-1800  $\text{cm}^{-1}$ ). The raw coal shows a negative band at 1740  $\text{cm}^{-1}$  which could be assigned to the ester and ketone groups. This band is negative, also in the case when tetralin or 1-methylnaphthalene was used as solvent suggesting that during liquefaction the raw coal losses more of carbonyl structures compared to the vacuum-dried coal. The enhanced loss of carbonyls from the raw coal can also be accounted by the relative increase in the  $\text{CO}_2$  and CO gas yields compared to the vacuum-dried coal. The residues from the air-dried coal also show a significantly higher loss of ester groups as indicated by the negative dip in the ester region of the difference spectra. But, there is also a positive band at 1700  $\text{cm}^{-1}$  which could be assigned to the carboxylic groups. The carboxylic band increases with the extent of oxidation. The increase in the carboxylic functionalities in the residues could also be noticed by the broad band centered at 1590  $\text{cm}^{-1}$ . This band is assigned to the carboxylate ( $\text{COO}^-$ ) groups. The increase in these functionalities is the consequence of increase in the carboxylic groups upon oxidation of coal. This band may also have slight contribution from the aromatic  $\text{C}=\text{C}$  stretching which appears at 1610  $\text{cm}^{-1}$ .

In the aliphatic region between 2700-2950  $\text{cm}^{-1}$  the raw coal shows no significant change in the band (Figure 2). But, relative to the vacuum-dried coal the residues from the air-dried coal show a significantly higher aliphatic content shown by the positive aliphatic bands. This is only true when coal was dried in air at 100 °C but for the coal dried at 150 °C for 20 h the aliphatic region shows a negative change. The increase in the aliphatics in the residues from air-drying at 100 °C is interesting because the unreacted air-dried coal show a decrease in the aliphatics because of the oxidation of some of the aliphatic groups. It appears that during liquefaction, the air-dried coal at 100 °C has retained more of the aliphatic components of the network as compared to that of the vacuum-dried coal. The negative aliphatic band in the case of the coal dried at 150 °C could be due to the extensive loss of these groups initially during air-drying. In the presence of tetralin or 1-MN also the air-dried coal showed an increase in the aliphatics.

Same criteria was adopted, as for the thermal runs, to obtain the FTIR difference spectra for the residues from the catalytic runs. Compared to the thermal runs, the difference spectra for the catalytic runs did not show any significant differences. Similar to the thermal runs, the residues from the air-dried coal at 100 °C were found to be more aliphatic and carbonyl rich compared to the vacuum dried coal. The residues from the tetralin and 1-MN runs also showed similar difference spectra except that the raw coal seemed to be aliphatic richer in the catalytic runs.

More significant differences in the thermal and catalytic runs were observed when the difference spectra were obtained between the residues from thermal and catalytic runs (Figure 3). The FTIR spectra of the catalytic runs were subtracted from that of the thermal runs. The negative mineral matter bands (1010 and 1035  $\text{cm}^{-1}$ ) in the difference spectra of the thermal and catalytic runs are the signs for more conversion of coal during catalytic runs. In the case of the raw coal the mineral matter bands are negative only in the solvent free runs may be because in the presence of solvents the raw coal did not show any significant difference in conversions between thermal and catalytic runs. The negative aliphatic bands in the difference spectra of the solvent-free runs clearly showed that during thermal runs more aliphatic compounds were lost in all the cases except when coal was oxidized at 150 °C. The differences in the aliphatic contents in the solvent runs were not very clear probably due to the differences in the adduction of solvents during liquefaction. In the carbonyl region positive bands near 1700 and 1550  $\text{cm}^{-1}$  were observed in the solvent-free as well as solvent runs. The first band could be due to ketone and carboxylic groups and the second band could be assigned to the carboxylate ions. It suggests that the residues from the thermal runs are

richer in such functionalities. The ether region between 1100-1300  $\text{cm}^{-1}$  also showed significantly intense positive bands which clearly suggests that more of ether type bonds are broken during catalytic liquefaction compared to that of the thermal runs. At the high oxidation level the ether region did not show any noticeable difference in the ether contents of the thermal and catalytic residues. The most significant difference was observed in the coal dried at 100 °C.

#### *Pyrolysis-GC-MS*

Compared to the raw coal the residues from the thermal solvent-free liquefactions show similar pyrolysis compounds, that is one can identify the same compounds in the raw coal as well as in residues. The differences in the pyrograms appear to be in the relative abundances of the compounds. Table 1 gives the ratios between phenolic and alkylbenzene compounds. For these ratios same compounds have been used as for the raw coal mentioned above. These ratios indicate the variations in the chemical composition of the aromatic compounds in the coal network as a consequence of different treatments to coal. After solvent-free thermal liquefaction of the raw coal the phenolic to alkylbenzene ratio decreases remarkably compared to that of the unreacted coal. Similar decrease is observed for the air-dried coal at 100 °C for 2 h and the vacuum-dried coal. For the coal dried at 100 °C for 20 and 100 h and dried at 150 °C there is no significant change in this ratio. From the catalytic solvent-free liquefaction the phenolic to alkylbenzene ratios of the residues are slightly higher than that of the corresponding residue from the thermal run but it is still lower than that of the unreacted coal. It appears that as the oxidative drying proceeds the difference in the phenolic to alkylbenzene ratio between the unreacted coal and the liquefaction residue decreases. Eventually at extensive oxidation of coal this ratio becomes same for the unreacted coal and its liquefaction residue.

Figure 4 compares of the pattern of the aliphatics present in the pyrogram of the residues from solvent-free thermal runs. Noticeable differences can be seen in the relative intensities of the aliphatics compared to that of the corresponding unreacted coal. In the residues from the raw and vacuum dried coal there is an appreciable decrease in the intensities of the shorter chain relative to the longer chain aliphatics, which has been noticed before with different coals too. For the air-dried unreacted coal, as mentioned before the pattern of the aliphatics in the pyrogram remains similar with the extent of drying, but for the residues the pattern is quite different. By comparing the residues from the air-dried coal at different extent of oxidation it appears that as the extent of oxidation increases more and more of longer chain aliphatics are lost during thermal liquefaction (Figure 4). It seems that for the air-dried coal the shorter chain aliphatics are strongly retained upon liquefaction. This phenomena was not observed for the catalytic runs.

All the pyrolysis compounds found in the pyrogram of the raw coal can also be identified in the pyrogram of the residues from the liquefactions in presence of solvents. Besides, there are several new bands which are known to have come from the adduction of solvent used during liquefaction (11). Some of these compounds are in most abundances. From the liquefaction runs in presence of tetralin the peaks due to the solvent are tetralin, dihydronaphthalene, naphthalene and 1 and 2-methylnaphthalenes. C2-naphthalenes may also be due to tetralin but are in a very low abundances. From the runs with 1-methylnaphthalene two solvent adduction bands are observed, naphthalene and 1-methylnaphthalene. In our previous work (11) we reported that the adduction of solvents could be either due to the formation of chemical bond between the solvent molecules and coal network or the solvent molecules could be physically entrapped in the micropores. From Figure 5 the adduction of solvent is apparent by the presence of tetralin, dihydronaphthalene, naphthalene and 1 and 2-methylnaphthalene peaks. It is clear that the extent of adduction of the solvents is remarkably effected by the extent of initial oxidation of the coal. Apparently, as the oxidation proceeds the relative intensities of the adducted compounds increases. Similar trend was observed in the case when 1-MN was used as solvent. The residues from the catalytic runs also show a similar trends in the adduction of solvents with the drying of coal but during catalytic runs the adduction seems to be lower as compared to the thermal run.

Not much difference is observed between the pyrograms qualitatively in Figure 5. All the pyrograms for the raw and dried coal under different conditions have the same compounds but there relative intensities are significantly different. Table 1 gives the phenolic to alkylbenzene ratios. These ratios have increased significantly for residues from the raw coal and for the coal dried in air at 100 °C for 2 h and under vacuum, compared to that of the solvent-free runs. But, for the 1-MN runs these ratios seems to be similar to that of the thermal runs. It seems that during solvent-free runs or in the presence of 1-MN more phenolic type units which produce phenolic compounds upon pyrolysis are lost. This phenomena seems to be true for raw, vacuum-dried coal and for the coal dried in air at 100 °C for 2 h. At the higher oxidative drying of coal the change in the ratios of the phenolic to alkylbenzene is not significant.

## CONCLUSIONS

The characterization of the liquefaction residues reveal that the residues from the air-dried coal are more aliphatic and carbonyl rich compared to the vacuum-dried coal. The increase in the carbonyls is due to the oxidation of the coal upon air-drying. It appears that upon oxidation of coal at 100 °C more shorter chain aliphatics are retained in the coal network as compared to the vacuum-dried coal. The enhanced conversion of the unoxidized raw coal may be due to the enhanced loss of carbonyls upon reacting with water. The enhanced loss of carbonyls with water can make coal less refractory for liquefaction. The Py-GC-MS analysis of the residues suggests that the extent of oxidation can enhance the solvent adduction during liquefaction.

## ACKNOWLEDGEMENTS

This work has been supported by the U.S. Department of Energy, Pittsburgh Energy Technology Center. We wish to thank Dr. P. G. Hatcher, Mr. K. Wenzel and Mr. L. Hou for their instrumental support with Py-GC-MS and CPMAS <sup>13</sup>C NMR instruments and Dr. M. Sobkowiak for her help with FTIR instrument.

## REFERENCES

1. Cronauer, D.C., Ruberto, R.G., Silver, R.S., Jenkins, R.G., Davis, A., and Hoover, D.S.; *Fuel*, 1984, 63, 71-77.
2. Atherton, L.F.; *Proc. 1985 Int. Conf. Coal Sci.*, p.553.
3. Saini, A.K., Song, C., and Schobert, H.H.; *ACS Fuel Chem. Prepr.*, 1993, Preceding Paper.
4. Cronauer, D.C., Ruberto, R.G., Jenkins, R.G., Davis, A., Painter, P.C., Hoover, D.S.; Starsinic, M.E., and Schlyer, D.; *Fuel*, 1983, 62, 1124-1132.
5. Calemma, V., Iwanski, P., Rausa, R., and Girardi, E.; *ACS Fuel Chem. Prepr.* 1992, 730.
6. Calemma, V., Rausa, R., Margarit, R., and Girardi, E.; *Fuel*, 1988, 67, 764.
7. Clemens, A.H., Matheson, T.W., and Rogers, D.; *Fuel*, 1991, 70, 215.
8. Rhoads, C.A., Senftle, J.T., Coleman, M.M., Davis, A., and Painter, P.C.; *Fuel*, 1983, 62, 1387.
9. Painter, P.C., Snyder, R.W., Pearson, D.E., and Kwong, J.; *Fuel*, 1980, 59, 283.
10. Chamberlain, E.A.C., Barrass, G., and Thirlaway, J.T.; *Fuel*, 1976, 55, 217.
11. Saini, A.K., Song, C., Schobert, H.H., and Hatcher, P.G.; *ACS Fuel Chem. Prepr.*, 1992, 37(3), 1235.
12. Sokowiak, M. and Painter, P.; *Fuel*, 1992, 71, 1105.
13. Song, C., Schobert, H.H. and Hatcher, P.G.; *ACS Fuel Chem. Prepr.*, 1992, 37(2), 638-645; *Energy & Fuels*, 1992, 6, 326-328.

Table 1. Ratios of the amounts of the phenolic compounds to the alkylbenzenes.

Drying Conditions	Unreacted Coal	Residues	
		Thermal	Catalytic
<b>Solvent-Free</b>			
Raw			
Air-dried, 2h, 100	3.8	1.9	2.8
Air-dried, 20h, 100°C	3.5	2.0	2.8
Air-dried, 20h, 100°C	2.5	2.4	2.6
Air-dried, 100h, 100°C	2.3	2.0	2.2
Air-dried, 20h, 150°C	1.1	1.2	1.6
Vacuum-dried	3.6	2.2	2.4
<b>Tetrahn</b>			
Raw		2.5	2.9
Air-dried, 2h, 100		3.3	3.7
Air-dried, 20h, 100°C		2.8	3.3
Air-dried, 100h, 100°C		2.2	2.6
Air-dried, 20h, 150°C		1.4	1.5
Vacuum-dried		3.1	3.1
<b>1-Methylnaphthalene</b>			
Raw		2.2	2.0
Air-dried, 2h, 100		2.4	2.7
Air-dried, 20h, 100°C		2.4	2.8
Air-dried, 100h, 100°C		1.5	2.3
Air-dried, 20h, 150°C		1.3	1.1
Vacuum-dried		1.8	2.3

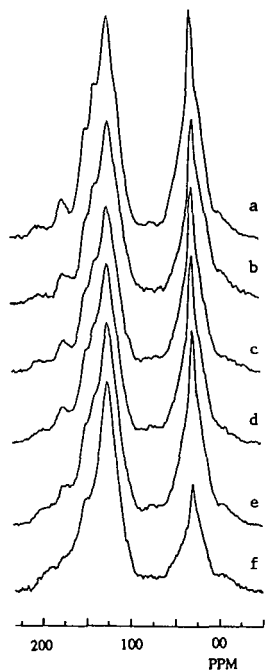


Figure 1. CPMAS  $^{13}\text{C}$  NMR spectra of the coal a) raw, b) vacuum-dried at  $100^\circ\text{C}$ , dried in air at  $100^\circ\text{C}$  for c) 2 h, d) 20 h, e) 100 h, and f) dried at  $150^\circ\text{C}$  for 20 h.

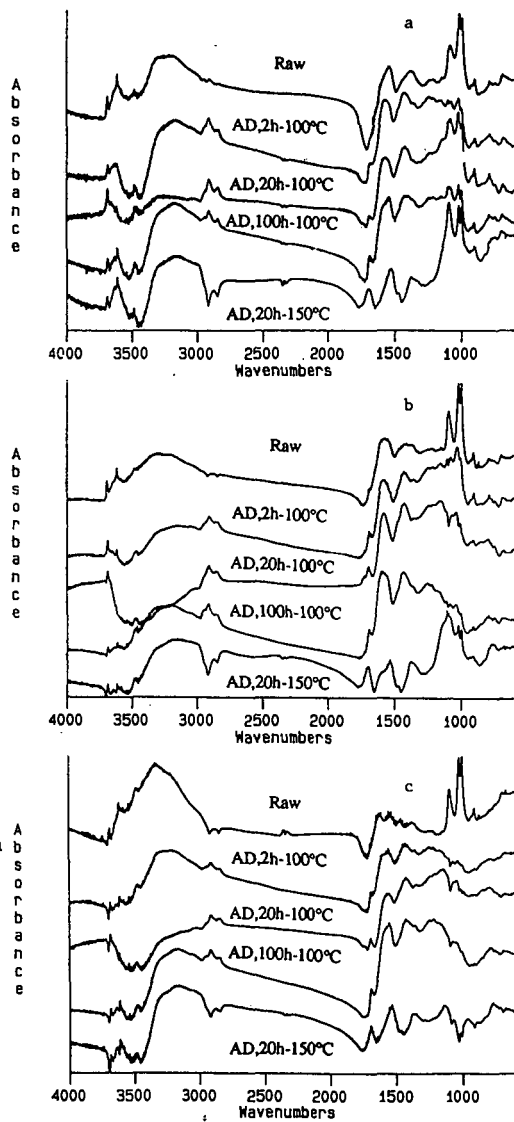
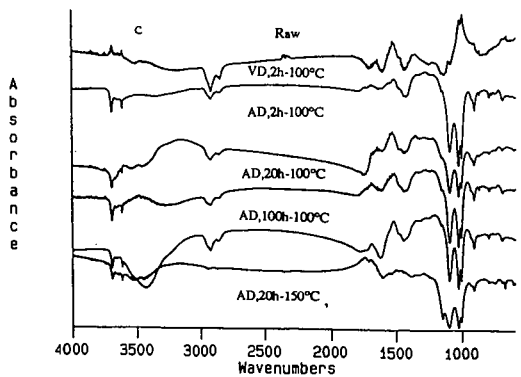
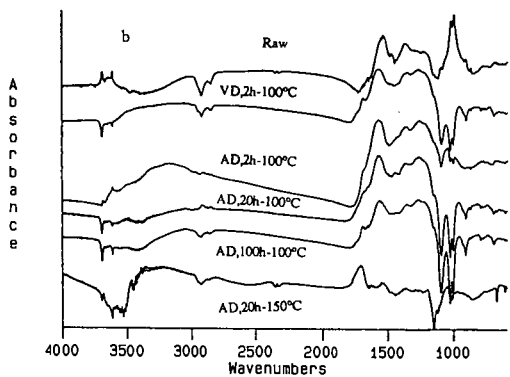
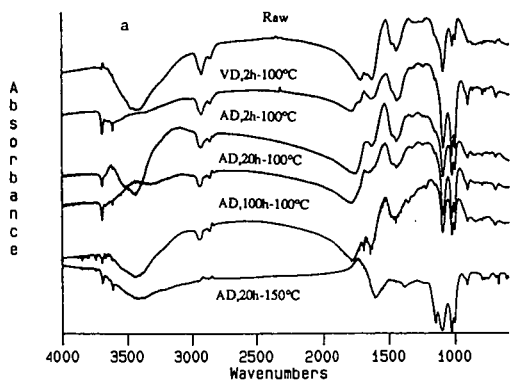
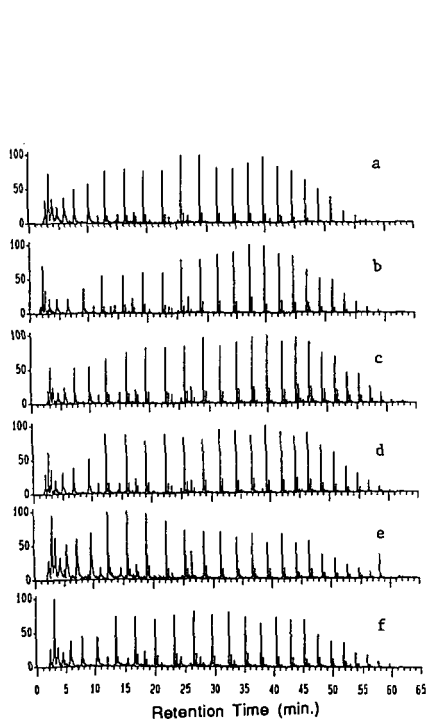


Figure 2. FTIR difference spectra for the residues from thermal liquefactions in a) solvent-free, b) tetralin, and c) 1-methylnaphthalene runs for the raw and air-dried (AD) coal.



**Figure 3.** FTIR difference spectra between the residues from the thermal and catalytic a) solvent-free, b) tetralin and 1-methylnaphthalene runs for the raw, vacuum-dried (VD) and air-dried (AD) coal.



**Figure 4.** Selective ion monitoring of paraffins at  $m/z$  71 from Py-GC-MS profiles of residues from thermal liquefactions of the coal a) raw, b) vacuum-dried at 100°C, dried in air at 100°C for c) 2 h, d) 20 h, e) 100 h, and f) dried at 150°C for 20 h.

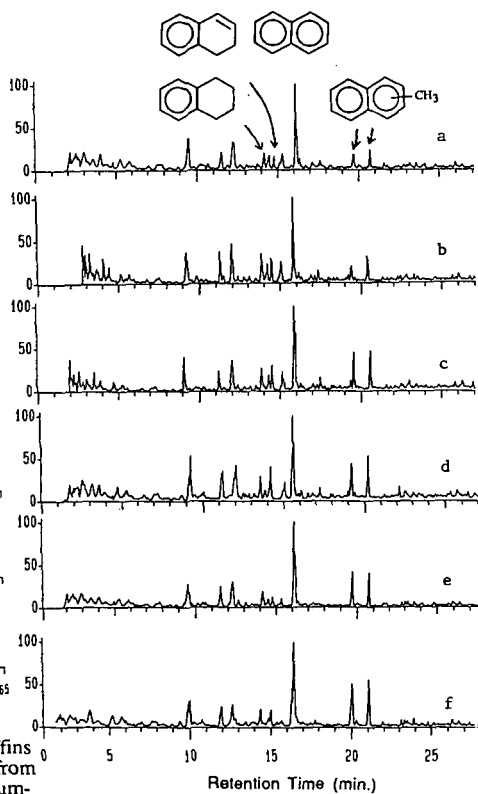


**Figure 5.** Py-GC-MS profiles of the residues from the thermal liquefactions in presence of tetralin of the coal a) raw, b) vacuum-dried at 100°C, dried in air at 100°C for c) 2 h, d) 20 h, e) 100 h, and f) dried at 150°C for 20 h.

## **An NMR Investigation of the Effects of Different Drying Methods on Coal Structure.**

Francis P. Miknis, Daniel A. Netzel and Thomas F. Turner,  
Western Research Institute, Box 3395, Laramie, WY 82071-3395

**Keywords:** Microwave and chemical drying, solid-state NMR, subbituminous coals

### **INTRODUCTION**

One area for improvement in the economics of coal liquefaction is coal drying. This is particularly true for subbituminous coal and lignites of which the US reserves are huge. These coals contain significant amounts of water so that simply drying these materials before transportation to their final destination can represent a sizable reduction in cost. There is considerable evidence to show that drying has a detrimental effect on the liquefaction behavior of coals (1,2,3). As coals have both a physical and chemical structure, it is conceivable that drying affects one, the other, or both of these structures.

There do not appear to have been any systematic studies of different methods of coal drying on coal structure, and the role that water plays in enhancing, or lessening coal reactivity toward liquefaction. The overall objectives of this work are to investigate the effects of different drying methods on the liquefaction behavior of coal. Different methods for coal drying are being investigated to determine if drying can be accomplished without destroying coal reactivity toward liquefaction, thereby making coal drying a relatively economical and efficient method for coal pretreatment. Coal drying methods include conventional thermal and microwave drying at elevated temperatures, and chemical drying at low temperature. Solid-state nuclear magnetic resonance (NMR) techniques of cross polarization with magic-angle spinning (CP/MAS) are employed to measure changes in coal structure brought about by the different methods of drying and by low temperature oxidation. The initial work on the project has focused on development of standardized procedures for thermal, microwave, and chemical methods of coal drying. Results of this aspect of the project are reported in this paper.

### **EXPERIMENTAL**

#### **Coal Preparation**

In order to study the effects of different methods for drying coal on moisture removal, a master batch sample (~500 g) of Eagle Butte subbituminous coal from the Powder River Basin, Wyoming was prepared by grinding and screening to -20, +100 mesh particle size. This sample was placed in a wide mouth jar and allowed to equilibrate in an oven with a beaker of water at 40°C for 24 hrs. The sample was then removed from the oven and placed in a humidifier until aliquots were taken for the different drying tests. The moisture values for all the coal drying tests were determined from the weight loss at 105°C for 24 hrs. The

moisture values for 2-gram aliquots from the master batch of Eagle Butte coal were 18-20% using this method.

### Thermal Drying

Samples of the Eagle Butte subbituminous coal were heated to different final temperatures in order to determine at what temperature, significant structural changes begin to occur that might affect the liquefaction behavior. These heating experiments are referred to as ballistic heating experiments. The ballistic heating experiments were performed with a small, vertically aligned furnace. The furnace has a 12-centimeter long heated section which accepts a 1.4-centimeter i.d. quartz liner. A stainless steel screen provides support for the coal and a steel wool pack heats the nitrogen sweep gas which is introduced at the bottom of the quartz liner. In a typical experiment, the furnace is preheated to about 10°C above the desired final coal temperature. A 2-gram coal sample is then poured into the quartz liner and a thermocouple is inserted into the coal sample bed. When this thermocouple reaches the desired temperature, the quartz liner is removed from the furnace and allowed to cool. Nitrogen flow is maintained at all times. When the sample temperature is below 60°C the coal is poured into a sample vial, capped with nitrogen, and sealed. Heatup times with this system are typically from 15 to 20 minutes.

### Microwave Drying

A number of microwave drying experiments were conducted using Eagle Butte subbituminous coal. The experiments were conducted using a CEM model MDS 81-D laboratory microwave oven that is equipped with facilities to introduce different gaseous environments, or using a commercially available microwave oven. Microwave drying tests were conducted in the following manner: ~ 2 grams of coal were placed in 25 mL beakers, and the beakers placed at the center of the microwave oven. Samples were exposed to microwave radiation for different periods of time and at different power levels, after which the samples were removed from the oven and a thermocouple inserted into the coal bed to determine an average temperature.

### Chemical Drying

Chemical drying experiments were conducted on the Eagle Butte subbituminous coal, and also a Usibelli subbituminous coal from Alaska using 2,2-dimethoxypropane as a drying agent. One-half gram of coal was weighed into a 10 mL centrifuge tube followed by 2 mL of 0.2 N  $\text{CH}_3\text{SO}_3\text{H}$  in  $\text{CH}_3\text{OH}$  and 1 mL of the reference standard cycloheptane. Four mL of dimethoxypropane were then added to the mixture. The total mixture was stirred, then centrifuged for 10 minutes. After 2, 4, 6, and 8 hours, one-half mL aliquots were removed, diluted with one-half mL  $\text{CDCl}_3$ , and the  $^1\text{H}$  NMR spectrum recorded. The solution was stirred and centrifuged prior to removing the aliquots.

A  $^1\text{H}$  NMR method was developed to rapidly measure the amount of water in coal. The  $^1\text{H}$  NMR spectra of the reaction products, methanol and acetone, give single resonances for the methyl groups, which are easily identified. These resonances do not overlap the hydrogen NMR resonances of DMP. Integration of the methyl resonances from acetone is used to measure directly the moles of water reacted. The average relative error using the  $^1\text{H}$  NMR method is < 3% for standard solutions with a known amount of water. A curve-fitting routine

for determining the area of the peaks increases the precision and accuracy of the NMR method by eliminating instrumental and other artifacts which contribute to the peak shape.

## RESULTS AND DISCUSSION

### Thermal Drying

Samples of the Eagle Butte coal were ballistically heated to final temperatures of 100, 150, 200, and 250 °C. Solid-state <sup>13</sup>C NMR measurements were made on the heated samples, and are shown in Figure 1 for the starting coal, and coal heated to 150, and 250 °C. The spectra indicate that under this method of heating, there are no significant changes in carbon functionality up to temperatures of 250 °C, except for some deterioration in resolution of branched aromatic carbons (~140 ppm), phenolic carbons (~155 ppm), and carboxyl carbons (~180 ppm).

### Microwave Drying

Microwave drying is an alternative thermal method of drying coals. However, the mechanism of drying with microwaves is different from that of simply heating the coal. In order for a substance to absorb microwaves and become heated, it must have a permanent dipole moment. Therefore, the functional groups that are the most efficient absorbers of microwaves are those that are highly polar, such as the -OH group in water.

When a substance containing water molecules is exposed to microwaves of the proper frequency (2,450 MHz) the water molecules attempt to align and realign with the alternating electric field of the microwaves. This causes friction at the molecular level, which becomes manifested as heat. Because the water in coals can be distributed on the surface, in pores, or as part of the coal structure as in a gel, depending on rank, microwaves might be used to provide some selectivity for coal drying without appreciably affecting the overall coal structure and liquefaction behavior of the coal.

The objective of the microwave drying subtask is to determine whether microwave drying alters the structure and composition of the coal, and hence its behavior toward liquefaction. This work was prompted by earlier work of Silver and Frazee (1) that showed that drying coal with microwaves beyond ~75% moisture removal actually had a detrimental effect on the reactivity toward liquefaction. However, there has not been a systematic study of changes in coal structure induced by microwave drying.

At full power (600 watts), 75 % or greater of the moisture was removed in ~2 min., and removal of the remaining moisture caused the temperatures to increase rapidly (Figure 2). Because of the rapid moisture removal at full power, different levels of microwave power were used in order to obtain a more complete drying curve. At power levels of 300 watts, 25 -75 % moisture could be removed for irradiation times of up to 15 min.

The general features of the coal drying curves using microwave radiation are shown in Figure 2. In general, there is a very rapid temperature rise after ~10 % of the moisture is removed. This is followed by removal of the bulk of the moisture (10-80%) at temperatures close to the

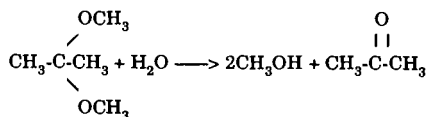
boiling point of water, which is ~ 93 °C at the 7,200 ft elevation in Laramie, WY. The rapid increase in temperature after >75% of the moisture is removed seems to be a general characteristic of microwave heating of subbituminous coals. This behavior was also observed by Silver and Frazee (1), who also noted a decreased reactivity toward liquefaction for greater than 75% moisture removal. We speculate that beyond this level of moisture removal, the additional moisture that is removed is an integral part of the gel or pore structure of the coal. These water molecules have a more difficult time aligning and realigning with the radiation field, and thus would cause heating to higher temperature, and possible disruption of part of the coal matrix enabling some retrograde reactions to take place that diminish the reactivity toward liquefaction.

It was possible to remove greater amounts of moisture than that determined by thermal drying, by microwave drying for extended periods of time (180 min) using lower power levels (300 watts). These results are shown in Figure 3. Solid-state <sup>13</sup>C CP/MAS NMR spectra of the microwave heated coals are shown in Figure 4. The spectra do not show any significant carbon structural changes as a result of moisture removal using microwaves, even though the temperatures were greater than 100 °C and greater than 100% of the moisture removable by thermal drying at 105 °C was removed using microwaves. In general, there is a slight degradation in the resolution of some of the carbon functionality during heating, as evidenced by the smoothing of the resonance bands at -140, 155, 180 ppm, similar to what was observed in the ballistically heated samples (Figure 1).

### Chemical Drying

Chemical drying of coals is a relatively unexplored technique for removing water at low temperature. Thermal methods of drying can alter the physical structure of coal as well as promote undesirable chemical reactions. Low-temperature drying of coal, on the other hand, should preserve the structural integrity, reduce retrograde reactions, reduce thermal degradation, and provide information on nonbonded, chemisorbed, and physisorbed water. This method of dehydrating coal should provide a baseline for studying initial stages of retrograde/condensation reactions. That is, decarboxylation and low-temperature oxidation reactions can then be studied in the presence and absence of water and gases and as a function of temperature.

Pore water and surface adsorbed water on coal can be effectively removed by the use of chemical dehydration agents which react with water to form volatile reaction products. We are investigating the use of a unique chemical dehydrating agent, 2,2-dimethoxypropane (DMP), for chemically drying coals. The reaction of DMP with water is as follows:



This reaction is rapid (<10 min) and endothermic. The use of DMP to dehydrate coal accomplishes two things: (1) the removal of water at ambient temperature by chemical means rather than by physically forcing exchange by mass action preserves the structural integrity

of the coal components and (2) the reaction products can easily be measured quantitatively to determine the amount of water in coal.

The results of the chemical drying experiments are summarized in Figure 5. As expected, the measured moisture content increased with time and reached a maximum after about 8 hrs. The data suggest that two types of water are removed sequentially. Free or surface sorbed water is rapidly removed upon contact with the drying agent, followed by removal of more tightly bound water as the reagents diffuse into the micropore structure. There appears to be an induction period of about 4 hrs for the Eagle Butte coal before the moisture content increases more rapidly due to removal of the more tightly bound water.

The chemical drying experiment was repeated twice for the Usibelli subbituminous coal. In the first experiment, aliquots were removed sequentially, and in the second experiment, separate coal samples were prepared and allowed to stand until the appropriate time for acquisition of the  $^1\text{H}$  NMR spectrum. The data show excellent reproducibility.

Both coals were thermally dried at 110°C for 1 hour. The moisture content was determined by weight loss. Eagle Butte coal had an as determined moisture content of 16.6 wt% and the Usibelli had an as determined moisture content of 14.1 wt%. These values are close to the early time moisture contents determined by chemical drying.

#### ACKNOWLEDGMENT

This work was supported by DOE contract DE-AC22-91PC91043 and DOE grant DE-FG22-91PC91310. The solid-state NMR analyses were provided, in part, by a DOE University Research Instrumentation grant No. DE-FG05-89ER75506. Such support does not, however, constitute endorsement by DOE of the views expressed in this paper.

#### REFERENCES

1. Silver H.F., W.S. Frazee, Integrated Two-Stage Coal Liquefaction Studies, University of Wyoming, Laramie, WY, August 1985, EPRI report AP-4193, 460 p.
2. Silver H., P.J. Hallinan, W.S. Frazee, Amerf. Chem. Soc. Div. Petrol. Chem. Preprints, 1986, 31(3), 755.
3. Serio M.A., P.R. Solomon, E.Kroo, R. Bassilakis, R Malhotra, D. McMillen, Amer. Chem. Soc. Div. Fuel Chem. Preprints, 1990, 35(1), 61.

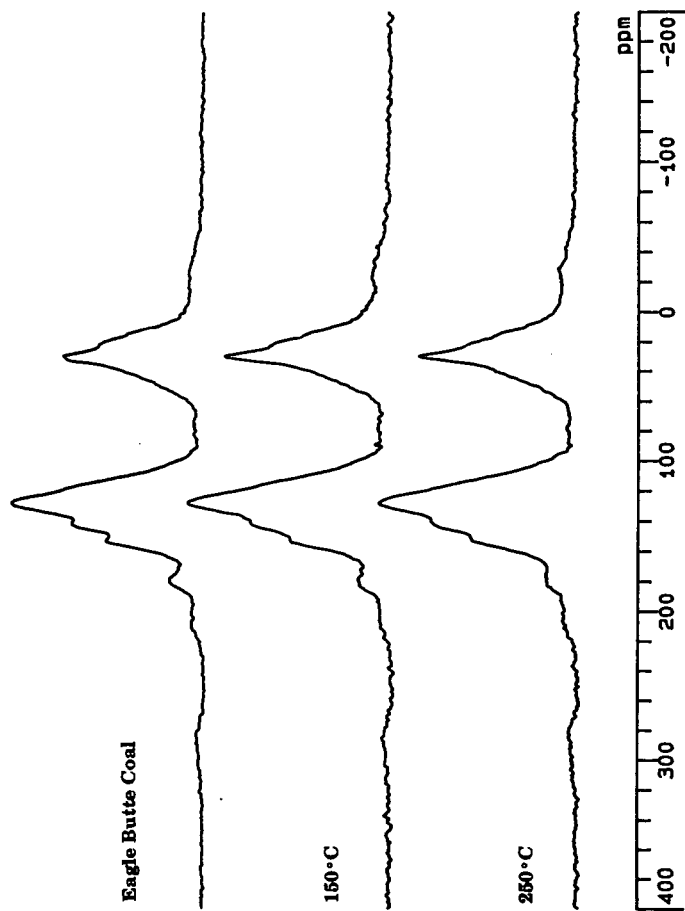


Figure 1. CP/MAS  $^{13}\text{C}$  NMR spectra of ballistically-heated Eagle Butte subbituminous coal.

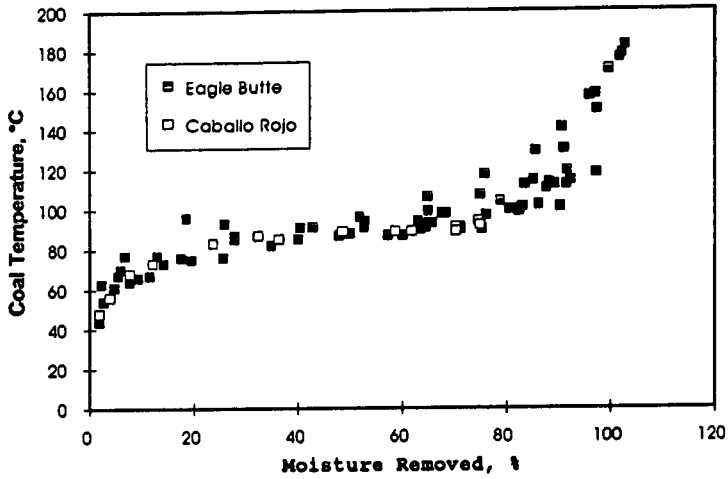


Figure 2. Coal temperature as a function of moisture removal for microwave drying.

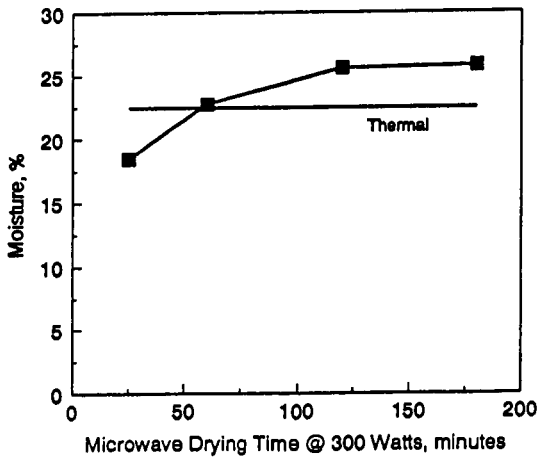


Figure 3. Moisture removal as a function of microwave drying time at 300 watts.

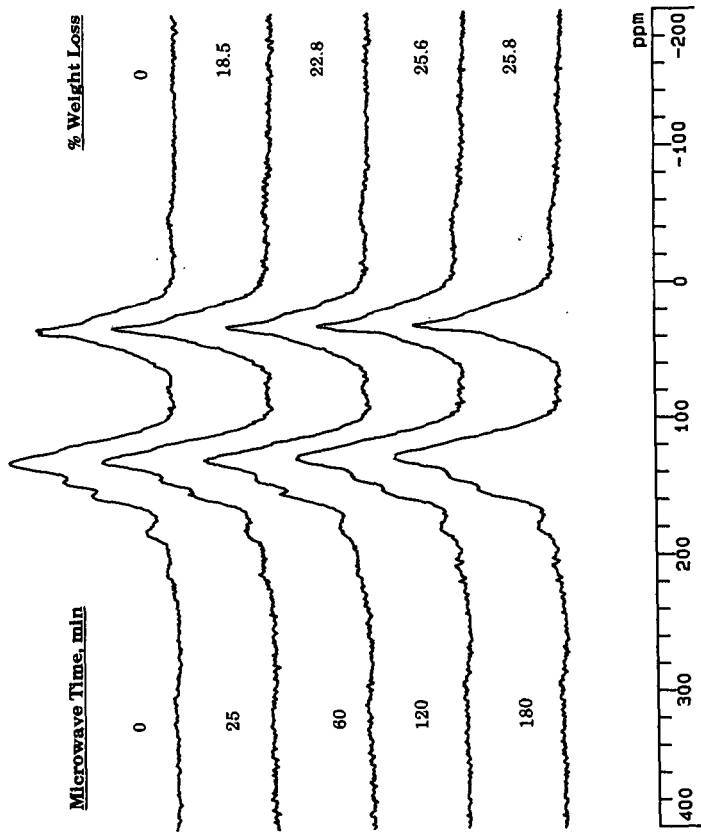


Figure 4. CP/MAS  $^{13}\text{C}$  NMR spectra of microwave-dried Eagle Butte coal (weight loss from thermal drying = 22.5%).

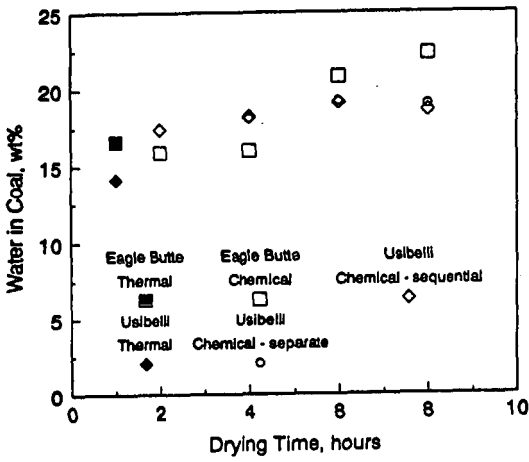


Figure 5. Moisture removal as a function of time for chemical drying.

## CO PRETREATMENT AND LIQUEFACTION OF SUBBITUMINOUS COAL

S. C. Lim, R. F. Rathbone, E. N. Givens and F. J. Derbyshire,  
University of Kentucky Center for Applied Energy Research,  
3572 Iron Works Pike, Lexington, KY 40511-8433.

Keywords: Coal liquefaction, Pretreatment, Carbon Monoxide, Water

### Abstract

A Wyodak subbituminous coal was pretreated at 300°C at various CO partial pressures in aqueous NaOH. Up to one-third of the oxygen is removed both in the presence and absence of CO. Oxygen-rich, water soluble humic acids are formed in the absence of or at low CO pressures; at 800 psig CO, water soluble product is absent. Higher CO conversions to hydrogen via the water gas shift (WGS) reaction was observed at lower pressures with higher H<sub>2</sub> consumption occurring at the higher pressures. Pyridine solubility and optical microscopy of the pretreated material indicate major reconstruction of the coal structure. Liquefaction of the pretreated material at 400°C in hydrogen/tetralin indicates that pretreated coal reacts faster giving higher conversion and lower hydrogen consumption than raw coal.

### INTRODUCTION

Pretreating coal prior to liquefaction has been shown to result in higher yields of product through a net reduction of retrograde reactions. The methodology can vary from treatment of coal through demineralization,<sup>1,2</sup> acid-washing, solvent swelling,<sup>3,4</sup> alkylation,<sup>5-7</sup> dissolution with strong acids and bases,<sup>8,9</sup> catalytic reactions,<sup>10</sup> or by the presence of hydrogen.<sup>11</sup> Solomon et al.<sup>12</sup> identified at least two distinct cross-linking events when coals are heated; one applies primarily to low-rank coals and occurs at lower temperatures simultaneous with CO<sub>2</sub> and H<sub>2</sub>O evolution<sup>13</sup> that correlates with loss of carboxyl groups and occurs prior to bridge breaking or depolymerization reactions. A second event that is exhibited by higher rank coals occurs at moderate temperatures simultaneous with methane formation subsequent to the initial bridge breaking reactions and correlates best with methane formation. For lignites, these cross-linking reactions begins at about 200°C while the corresponding reaction for higher rank coals begin at temperatures above 400°C.<sup>12</sup>

Aqueous treatment around the supercritical temperature of water, i.e. ~372°C, is also known to cause significant changes in coal which enhance coal conversion under a variety of process conditions.<sup>14,15</sup> Illinois No. 6 coal, pretreated with steam at 50 atm between 320-360°C, provided a two fold increase in liquid yields and a 20% increase in total volatile yields when pyrolyzed at 740°C.<sup>16</sup> Pretreated coal had lower oxygen content, exhibited reduced hydrogen bonding, had increased pore volume,<sup>17</sup> and had twice as many hydroxyl groups than the starting coal.<sup>18</sup> Steam inhibited retrograde reactions of the phenolic groups that were evolved.<sup>17,19</sup>

Generally, coal conversion in aqueous systems to which CO and base are added, is higher than in straight aqueous systems or in hydrogen/donor solvent,<sup>20</sup> especially for lower rank coals.<sup>21-25</sup> In the CO/H<sub>2</sub>O/base system the water-gas shift conversion occurs<sup>26</sup> (CO+H<sub>2</sub>O→H<sub>2</sub>+CO<sub>2</sub>) which involves the intermediacy of the formate anion, HCO<sub>2</sub><sup>-</sup>.<sup>27</sup> In the study reported here the effect of this reaction system on subbituminous coal at temperatures around 300°C has been investigated. Substantial changes to the coal

substructure have been identified and the liquefaction of the pretreated coal in hydrogen donor solvent has been evaluated.

#### EXPERIMENTAL

**Materials** - Reagents were purchased as follows: 99% purity UV grade tetralin, high purity tetrahydrofuran (THF), and high purity pentane were Burdick & Jackson Brand from Baxter S/P; UHP 6000# hydrogen was supplied by Air Products and Chemicals, Inc. A sample of Wyodak Clovis Point coal was supplied by the Wilsonville Advanced Coal Liquefaction Research and Development Facility and had been ground to -200 mesh, riffled and stored in a tightly sealed container. Analysis of the coal is presented in Table 1.

**Procedures** - Pretreatment experiments were conducted by adding the specified amounts of coal, distilled water, and NaOH to a 25 ml vertical reactor which was sealed and pressurized with CO. The pH of the starting solution was between 13-14. After leak testing, the reactor was submerged in a fluidized sandbath at 300°C and shaken at a rate of 400 cycles per minute. At the end of the reaction period, the reactor was rapidly quenched to room temperature. Gaseous products were vented into a collection vessel and analyzed by gas chromatography. Solid and liquid products were scrapped and washed from the reactor using water and then filtered, and 'freeze dried'. The pH of the aqueous layer was between 5 and 6. Subsequently the sample was dried at 80°C/25 mm Hg for 60 min. In several experiments the insoluble material was placed in a Soxhlet thimble, extracted with THF for 18 hours, and dried overnight at 80°C/25 mm Hg. Ashing of the water and THF insolubles indicated >95% of the Na fed as NaOH reported to the aqueous layer. Soluble material was concentrated by removing excess THF to which was added a 50:1 excess volume of pentane and the mixture placed in an ultrasonic bath for 3 min. The insolubles were removed by filtering and the solubles recovered after evaporating the pentane. The water soluble fraction was acidified with HCl to precipitate humic acids which were centrifuged, collected and dried. The aqueous layer was extracted with ether. Recoveries and products are reported on an maf basis calculated by subtracting the coal ash from the total THF insolubles. Na product is assumed to report completely to the aqueous phase.

Liquefaction experiments were performed by placing raw or pretreated coal and tetralin (2:1 tetralin:coal) in the reactor described above and submerging the reactor in a sandbath at 400°C for periods from 15 to 60 min in 800 psig (cold) H<sub>2</sub>. The reactor was rapidly cooled and gaseous products collected. The solid/liquid products were separated into THF insoluble (IOM plus ash), THF soluble/pentane insoluble (PA+A) and pentane soluble (oils) fractions. Conversions and product yields are reported on an maf basis by assuming complete recovery of the ash in the THF insolubles.

**Analyses** - FTIR transmittance spectra were obtained on a Nicolet Model 20SXC spectrometer using KBr pellets of the parent and demineralized coals. Carbon, hydrogen and nitrogen were determined on a Leco Model 600 combustion analyzer. Total sulfur was determined according to ASTM D4239-84 with a Leco Model SC32 combustion-IR analyzer.

**Optical Microscopy** - Samples of coal, pretreated coal, and liquefaction residues were prepared for microscopical examination by mixing with epoxy resin, placing the mixture into a small cylindrical mold, and allowing the epoxy to harden. A sample surface was then ground and

polished on a polishing wheel using a series of SiC grits and alumina polishing compounds. Microscopical observations were conducted using a Leitz MPV Compact polarizing microscope-photometer. As a qualitative measure of the acidic oxygen functional groups in the feedstock and pretreated coal, a freshly polished surface of the coal-epoxy pellet was immersed in aqueous KOH (pH = 13), rinsed, and then placed in a Safranin-O (a cationic dye) water solution. This procedure has been used as a petrographic method for detecting weathering in coals.<sup>28,29</sup> This provides a measure of the number of carboxyl and phenolic groups in the coal; the more intense the staining of the polished coal surface, the greater the proportion of acidic oxygen functional groups.

#### RESULTS AND DISCUSSION

**CO Pretreatment of Coal** - The yields on an maf basis ranged from 75-92 wt% for water insoluble products and up to 7 wt% for water soluble products as presented in Table 2. All of the unaccounted for organic matter plus water and CO+CO<sub>2</sub> produced from the coal is lumped into Oil+Gas+Water. Total elemental recoveries based upon analysis of the water-insoluble material, or the subdivided PA+A and THF insoluble fractions, and humic acids indicate generally complete carbon recovery, especially at the higher CO pressures. The minor amounts of carbon associated with direct elimination of CO and CO<sub>2</sub> from the coal, which would be less than 1 wt%, plus the ether extract, which was formed only at the lower CO pressures, are not included in these values. Combined hydrogen recoveries ranged from 81% in the absence of CO to greater than 100% at higher CO pressures, and parallel the higher H<sub>2</sub> gas consumptions. Because of the small magnitude of the nitrogen and sulfur contents in the coal these numbers show greater scatter. A rather uniform 40 ± 4 wt% oxygen loss was observed. Based upon ash measurements, Na, added as NaOH, reported exclusively to the water phase.

The highest yield of water soluble product occurs in the complete absence of added CO with its yield steadily decreasing as CO concentration increases. At 800 psig it is completely absent. On the other hand, water insoluble product, as well as the PA+A portion of that product, is higher at higher CO pressures. Significantly, in the absence of CO, the PA+A fraction is completely absent. The yield and H/C atomic ratios of water insoluble product increase simultaneously.

The WGS reaction was approximately 80% complete at the lower CO concentrations versus only 39-53% complete at the higher pressures. Based upon the 4 fold greater CO concentration present at the higher pressure, twice as much H<sub>2</sub> is present at this concentration at which much higher levels of H<sub>2</sub> are consumed. At the lower CO concentrations the observed lower PA+A yields, the higher water insoluble product yields, and the generally higher oil+gas+water yields may be due, in part, to pyrolysis processes which dominate the competing hydrogenation reactions in the more hydrogen deficient environment. Data from the run in the complete absence of CO, where PA+A is absent and the highest yield of water soluble product was obtained, supports this view.

In each of the runs sufficient water is present to maintain a liquid phase at reaction temperature. The results suggest that increasing water concentration gives higher coal conversion at both 200 and 800 psig CO. The WGS reaction appears to show no sensitivity to water concentration in these runs probably because of similar water partial pressures. At this point whether water concentration affects the reaction remains unclear.

Pyridine extraction showed that 60 wt% of pretreated coal prepared at 800 psig CO pressure was soluble versus only 4.5 wt% solubility of the starting coal (Table 3). Pyridine solubility was lower for water insoluble products prepared either at low CO concentrations or in the absence of CO. Pyridine solubility qualitatively reflects the degree of cross-linking in the sample. This value plus the increased H<sub>2</sub> consumption and the absence of any significant reaction in a H<sub>2</sub> environment under these conditions,<sup>30</sup> suggest that coal depolymerizes into smaller fragments which are stabilized by the *in-situ* hydrogen generated during the WGS reaction. The poorer result observed at lower CO concentrations suggest rapid depletion of the CO which converts to CO<sub>2</sub> and H<sub>2</sub> before any significant coal upgrading takes place. This is consistent with a reaction path in which the coal structure is stabilized and hydrogenated by the active WGS intermediate.

Optical microscopy showed significant morphological changes in the coal structure of the water insoluble product prepared at the higher CO pressure (Run 45). The structure was completely melted and agglomerated to form large, coherent masses as compared to the original coal (Figure 1). The treated material contained abundant pores ranging from submicron to tens of microns in size, some of which were filled with solid homogeneous bitumen-type material which was fluorescent under ultraviolet illumination, suggesting a high-hydrogen content. The reflectance of the surrounding more abundant altered vitrinite (0.43%) was close to the original coal (0.39%) and showed no visible fluorescence. Staining of the samples with Safranin-O indicates that some of the oxygen functional groups were removed during pretreatment which agrees with the elemental analysis.

FTIR data indicate partial decarboxylation occurred during pretreatment. The intensity of the carbonyl absorption, which appears as a shoulder at 1703 cm<sup>-1</sup> on the relatively intense aromatic stretching vibration at 1600 cm<sup>-1</sup>, is reduced in the pretreated coal.

**Liquefaction of Pretreated Coal** - THF conversions for liquefaction of pretreated coal in hydrogen and tetralin were 60.8 wt.% at 15 min and 83.2 wt.% at 60 min. The corresponding values for raw coal were higher: 49.4 wt.% at 15 min and 74.8 wt.% at 60 min (see Table 4). The increase in THF conversion at 15 min reported mainly to the PA+A fraction while in the 60 min run the improvement in conversion reported to the oil fraction. The CO+CO<sub>2</sub> yields for pretreated coal were significantly reduced for both 15 and 60 min runs suggesting significant elimination of carbon oxides during pretreatment.

Both gaseous H<sub>2</sub> and total hydrogen consumption, the latter which includes the sum of gaseous H<sub>2</sub> and hydrogen from tetralin, were determined. Hydrogen consumed in liquefaction of the pretreated coal over the reaction period from 15 to 60 min is nearly constant even though THF conversion increases by 22 wt%. By contrast, raw coal showed a larger increase in total hydrogen consumption over the period.

#### CONCLUSIONS

Low temperature CO pretreatment of coal promotes formation of a material through hydrogenation and modification of the coal structure which is more reactive than the starting coal. Retrogressive reactions competing for hydrogen during liquefaction apparently have been quenched leading to a more effective utilization of hydrogen.

#### REFERENCES

1. Serio, M. A., P. R. Solomon, E. Kroo, R. Bassilakis, R. Malhotra and D. McMillen, Preprints, Am. Chem. Soc. Div. of Fuel Chem., 1990, 35(1), p. 61.
2. Deshpande, G. V., P. R. Solomon and M. A. Serio, Preprints, Am. Chem. Soc., Div. of Fuel Chem. 1988, 33(2), p. 310.
3. Matturo, M. G., R. Liotta, and R. P. Reynolds, Energy and Fuels, 1990, 4, p. 346.
4. Warzinski, R. P., and G. D. Holder, Preprints, Am. Chem. Soc., Div. of Fuel Chem. 1991, 36(1), p. 44.
5. Schlosberg, R. H., R. C. Neavel, P. S. Maa and M. L. Gorbarty, Fuel, 1980, 59, p. 45.
6. Baldwin, R. M., O. Nguanpraesert, D. R. Kennar, and R. L. Miller, Preprints, Am. Chem. Soc. Div. of Fuel Chem. 1990, 35(1), p. 70.
7. Solomon, P. R. and K. R. Squire, Preprints, Am. Chem. Soc. Div. of Fuel Chem. 1985, 30(4), p.346
8. van Bodegom, B., J. A. Rob van Veen, G. M. M. van Kessel, M. W. A. Sinnige-Nijssen and H. C. M. Stuiiver, Fuel, 1984, 63, p. 346.
9. Kasehegen, L., Ind. Eng. Chem., 1937, 29, p.600
10. Solomon, P. R., M. A. Serio, G. V. Deshpande, E. Kroo, H. Schobert, and C. Burgess, Preprints, Am. Chem. Soc. Div. of Fuel Chem. 1989, 34(3), p. 803.
11. Bockrath, B.C., E. G. Illig and W. D. Wassell-Bridger, Energy and Fuels, 1987, 1, p.227.
12. Solomon, P. R., M. A. Serio, G. V. Deshpande and E. Kroo, Energy and Fuels, 1990, 4, p.42.
13. Suuberg, E.M., D. Lee, and J. W. Larson, Fuel, 1985, 64, p.1669.
14. Towne, S. E., Y. Shah, G. D. Holder, G. V. Deshpande and D. C. Cronauer, Fuel, 1985, 64, p883.
15. Bienkowski, P. R., R. Naragan, R. A. Greenkorn, K. C. Chao, Ind. Eng. Chem., 1987, 26, 202.
16. Graff, R. A., S. D. Brandes, Energy and Fuels 1987, 1, p 84.
17. Tse, D. S., A. Hirschon, R. Malhotra, D. F. McMillan and D. S. Ross, Preprints, Am. Chem. Soc., Div. of Fuel Chem., 1991, 36(1), p. 23.
18. Khan, M. R., W, Y, Chen, and E. Suuberg, Energy and Fuels 1989, 3, p. 223.
19. Trehwella, M. J. and A. Grint, Fuel, 1988, 67, p.1135.
20. Lim, S.C., Ph.D Thesis, Monash University, 1990.
21. Appell, H. R. et al., Preprints, Am. Chem Soc., Div. of Fuel Chem., 1968, 12(3), p. 220.
22. Appell, H. R. , Energy, 1976, 1(4), p.24.
23. Jackson, W. R. et al., 1987 International Conference on Coal Science, Maastricht, Coal Science and Technology 11 (J. A. Moulijn, K.A. Nater, H.A.G. Chermin. Eds.), p.45.
24. Oelert, H.H et al., Fuel, 1976, 55, p.39.
25. Takemura, Y. et al., Fuel, 1983, 62, p.1133.
26. D. C. Elliott and L. J. Sealock, Jr., Ind. Eng. Chem. Prod. Res. Dev. 1983, 22, p 426.
27. Ross, D. S., in "Coal Science," (M.L. Gorbarty, J.W. Larsen and I. Wender, Eds. ) Academic Press, Inc., New York, NY.
28. Gray, R. J., A. H. Rhoads and D. T. King, Trans. Society Mining Engineers, 1976, 260, p. 334.
29. Marchioni, D. L., Int. J. Coal Geol., 1983, 2, p. 231.
30. D. S. Ross, J. E. Blessing, Q. C. Nguyen and G. P. Hum, Fuel, 1984, 63, p 1206.

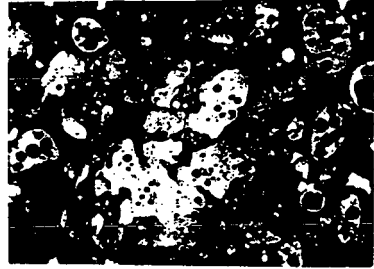


Figure 1. Reflected white-light photomicrographs of Wyodak coal (left) and CO-pretreated coal (right), at 625X. Width of each field of view is approximately 165 microns.

Table 1. Analysis of Wyodak Clovis Point Coal

Composition, wt % maf	
Carbon	71.0
Hydrogen	4.9
Nitrogen	1.3
Sulfur	1.1
Oxygen (by difference)	21.7
Ash, wt% dry coal	6.94
H/C Ratio	0.83

Table 2. Product Distribution from CO Pretreatment of Coal<sup>a</sup>

CO, psig cold	200	200	400	800	800	800 <sup>b</sup>
Added water, ml	2	6	4	2	6	6
Products, wt% maf coal						
Water Insoluble	80.8	74.7	90.0	91.7	89.7	80.0
PA+A <sup>c</sup>	2.2	5.5	17.2	17.6	18.0	-
THF Insoluble	78.6	69.2	72.8	74.1	71.7	80.0
Water Soluble						
Humic Acids <sup>d</sup>	5.1	5.5	2.7	-	-	7.0
Ether Extract <sup>e</sup>	1.1	0.5	-	-	-	-
Oil+Gas+Water <sup>f</sup>	13.0	19.3	7.3	8.3	10.3	13.0
Elemental Recovery <sup>g</sup>						
Carbon	93	-	101	101	97	97
Hydrogen	84	-	99	103	107	81
Nitrogen	79	-	120	99	91	115
Sulfur	62	-	60	67	97	51
Oxygen <sup>h</sup>	64	-	66	60	59	56
WGS Conversion <sup>i</sup>	78	82	47	39	53	-
H <sub>2</sub> Gas Consumed <sup>j</sup>	-	8	13	22	26	-
H/C Atomic Ratio <sup>k</sup>	0.75	-	0.83	0.85	0.92	0.71
Run Number	52	48	46	49	45	69

<sup>a</sup> 2 g dry coal, 4.4 wt% NaOH on maf coal

<sup>b</sup> 100% Nitrogen

<sup>c</sup> THF soluble-pentane insoluble

<sup>d</sup> Precipitated from acidified aqueous phase

<sup>e</sup> Ether extract from acidified aqueous phase

<sup>f</sup> Oil+Gas+Water=100-[water soluble (maf)+water insoluble (maf)]

<sup>g</sup> Total in combined water soluble + water insoluble

<sup>h</sup> Oxygen analysis by difference

<sup>i</sup> WGS = H<sub>2</sub>O gas shift; % WGS Conv =  $[(CO_{in}-CO_{out})/CO_{in}] \times 100$

<sup>j</sup> H<sub>2</sub> Consumed is [mg H<sub>2</sub>(from WGS)-mg H<sub>2</sub>(final)]/g maf coal

<sup>k</sup> Ratio for water insoluble product.

Table 3. Pyridine Extraction

Sample <sup>a</sup>	Pyridine Soluble, wt% maf
Wyodak Coal	4.5
N <sub>2</sub> /6 ml H <sub>2</sub> O/NaOH	6.4
200 psi CO/6 ml H <sub>2</sub> O/NaOH	9.0
800 psi CO/6 ml H <sub>2</sub> O/NaOH	60.0

a. 1.0 g water insoluble product extracted with 300 ml of pyridine in Soxhlet apparatus for 18 hours.

Table 4. Liquefaction of Raw and CO Pretreated Coal<sup>a,b</sup>

Coal	Raw	Pretreated	Raw	Pretreated
Time, min	15	15	60	60
THF Conv, wt% maf coal	49.4	60.8	74.8	83.2
Products, wt% maf coal				
PA+A	34.3	47.0	42.8	41.8
Oils+Water	9.9	11.6	26.3	38.9
CO+CO <sub>2</sub>	5.0	2.0	5.4	1.9
HC Gases	0.2	0.2	0.3	0.6
H <sub>2</sub> Gas Consumed <sup>c</sup>	11	19	17	18
Total H <sub>2</sub> Consumed <sup>d</sup>				
Run Number	79	81/82	85	86

a. Pretreatment: 800 psig CO cold, 6 ml water, 4.4 wt% NaOH on dry coal, 300°C, 1 hr.

b. Liquefaction conditions: 400°C, 800 psig H<sub>2</sub> cold, 2 g pretreated coal, 2 g tetralin.

c. H<sub>2</sub> Gas Consumed =  $[H_{2\text{ in}} - H_{2\text{ out}}]/\text{coal}$  (mg/g maf coal); excludes H<sub>2</sub> consumed by tetralin.

d. Includes both gaseous H<sub>2</sub> and hydrogen consumed from tetralin.

## REACTOR SYSTEM DEVELOPMENT TO REDUCE COAL LIQUEFACTION SEVERITY

H.G. Sanjay, Arthur R. Tarrer  
Department of Chemical Engineering  
Auburn University, Auburn, ALA 36849

**Keywords:** Loop Reactors, Coal Liquefaction, Hydrogenation

### INTRODUCTION

The hydrogenation of aromatic hydrocarbons is of interest not only because of the commercial interest of the reaction, but also because the liquefaction of coal and the subsequent product upgrading involves the hydrogenation of aromatic rings [1]. A number of reactions of industrial importance, such as the hydrogenation of various organic compounds and the hydrodesulfurization of petroleum fractions, involve reactions between two fluids in the presence of a solid catalyst. Coal liquefaction is one such reaction in which coal slurried in a solvent reacts with hydrogen to yield liquid products. The goal in a coal liquefaction process is to convert coal into a clean liquid fuel by increasing the hydrogen content of coal derived liquids and removal of heteroatoms such as sulfur, nitrogen and oxygen.

The efforts to improve yield and selectivity from coal liquefaction have focussed on the development of improved catalysts [2-4] and the use of different hydrogen donors [5-7]. These attempts have met with limited success due to the autocatalytic nature of the free radical propagation. The hydrogen supply rates are not sufficient to saturate the free radicals generated at longer residence times used in conventional reactors such as tubing bomb microreactors and stirred autoclaves. The development of new and improved reactor systems with better reaction control and improved mass transfer rates will reduce some of the problems associated with coal liquefaction.

### REACTOR DESIGN CONCEPT

Coal liquefaction reactions proceed via a free radical propagation mechanism. The free radical propagation increases exponentially and very high gas-liquid mass transfer rates are necessary to saturate the free radicals and prevent retrogressive reactions. Commercial gas-liquid contactors are not capable of providing sufficiently high gas-liquid mass transfer rates to prevent hydrogen starvation and thus retrogressive reactions from occurring. An alternative approach to increase the yield and improve the product selectivity in free radical type reactions is to control the rate of free radical propagation so that only practically achievable mass transfer rates would be required. The reactor system used in this study is based on this alternative approach.

The approach used in developing the reactor system was two-fold: 1) a reactant flow pattern was developed which would allow versatility in reaction rate controllability and 2) a gas-liquid contactor design was sought that would provide the highest mass transfer rates per unit volume. The higher the mass transfer rate can be made per unit reactor volume via gas-liquid contactor design, the farther the operational range of the reactor system over which the rate of retrogressive reactions would be low.

A bang-bang control strategy was used to regulate the reaction rate. A cyclic switching from high to low reaction temperatures was used to control the free radical propagation rate. The adjustable control parameter selected was the frequency of the cyclic switching of the reaction temperature. Physically, this was accomplished using a recycle loop type reactor in which the temperature in part of the loop was kept high (reaction zone) and that in the remainder of the loop it was lower (quenching zone). The frequency of cyclic switching of the reactant temperature could be varied simply by changing the reactant recycle flow rate. The mass transfer requirements per reaction cycle could be maintained within a range that could be satisfied by practical gas-liquid contactors, simply by optimizing the recycle flow rate. This type of reactor flow arrangement is similar to jet loop type reactors, which have been employed when reaction rates are very high and the reactions are mass transfer limited.

#### REACTOR SYSTEM

The conventional slurry reactor designs are modified in industrial reactors to achieve specific objectives such as higher heat and mass transfer capabilities, higher catalyst efficiency, better reactor performance and selectivity, etc [8]. The high heat and mass transfer rates, easy control over the degree of backmixing, and simple design have made loop reactors very attractive for both industrial and academic purposes. A jet loop type reactor was designed and used in this study.

Jet loop reactors with hydrodynamic jet flow drive are suitable for gas-liquid-solid processes which require rapid and uniform mass distribution and high mass transfer rates. The reactor system developed for this study operates in a semi-batch mode with the gas being supplied continuously. The liquid and the solid constituting the slurry are recycled through the reactor system.

The reactor system employs stainless steel columns measuring eight inches in length and one inch in outer diameter (O.D.) as reactors. The reactors were connected with 0.5 inch O.D. tubing and were placed in a fluidized sand bath for efficient temperature control. The reactor tubes were filled with stainless packing rings, as heat transfer in a packed column with metal rings is highly efficient due to a large surface area per unit volume of liquid. The slurry was recycled through the closed loop reactor system by a pump. The slurry passes through a preheater before entering the reactor system. The slurry is heated to the desired temperature in the preheater by using ethylene glycol as the heating fluid. The glycol was heated in a cylindrical tank fitted with three electric heaters. A centrifugal pump was used to circulate the ethylene glycol between the preheater and the tank. The slurry passes through the preheater into the reactor tubes and through the reactors into a chiller. The slurry is cooled in the chiller using tap water as the coolant. A gas-liquid decoupling chamber separates the gas and the liquid coming out of the chiller. The liquid flows into the suction side of the pump to be recycled. The gas flows into a gas recirculation unit. The unit consists of three gas-liquid separators and an air driven gas compressor. The gas is drawn from the decoupling chamber into the separators in succession. The gas is fed to the compressor and pumped into the slurry along with fresh gas at the gas-liquid contactor on the discharge side of the pump. Any vapors in the gas condense in the separators and are drained after the run.

The reactant gas is fed into the reactor system through a gas-liquid contactor before the slurry enters the preheater. A number of gas-liquid contacting devices are available to increase the gas-liquid mass transfer rates. These include motionless mixers, column packings, high shearing mechanical agitators and different kinds of nozzles. An improvement in the gas-liquid mass transfer will result in stabilization of free radicals and could result in improved product selectivity.

Different types of nozzles are being used increasingly to enhance mass transfer during gas-liquid contacting. Two phase nozzles, where both the phases come into contact inside the nozzle, were used in this study due to their high mass transfer capabilities and their ease of use in a closed system. A very efficient type of two phase nozzle employed in the present study is the slot injector introduced by Zlokarnik [9]. In a slot injector, the mixing chamber which is circular becomes slot shaped gradually keeping the cross-sectional area constant. The slot shape results in a lower pressure drop, because the shear rate increases along the convergent surface. This produces a fine gas dispersion with the free jet retaining a large portion of its kinetic energy. In addition, the free jet leaves as a flat band and mixes rapidly with the surrounding liquid, reducing bubble coalescence. The reactor system is shown in Figure 1.

#### EXPERIMENTAL

Naphthalene hydrogenation experiments in the reactor system were conducted using tetralin as the solvent. A predetermined quantity of naphthalene and catalyst (5% Pd on carbon) was mixed with the solvent in a beaker. The mixture was sonicated for about ten minutes to effectively disperse the catalyst. The slurry was charged into the reactor system when the desired reaction temperature was reached (130-160°C). The system pressure was then increased to 125 psig by feeding in hydrogen. The pressure was monitored and the system was charged back to 125 psig after a 10 psig drop. A sample was withdrawn for analysis approximately a minute after gas recharging. The reaction was allowed to proceed until no drop in pressure was observed. The system was then drained and the product mixture was filtered before sampling for analysis. The system was flushed with toluene or tetralin after every run.

#### RESULTS AND DISCUSSION

The model reaction used in the present study to evaluate the reactor system was the hydrogenation of naphthalene. This is a very important reaction during the liquefaction of coal to regenerate the hydrogen donor solvent (tetralin). The catalyst used in the study was a commercial 5% Pd on carbon. Palladium is the most active hydrogenation catalyst, but is strongly inhibited by the presence of sulfur compounds [10]. However, the use of palladium in model compound studies (without the presence of sulfur) will facilitate evaluation of new and improved reactor systems under conditions which are not severe. This helps to reduce the "bugs" in the reactor system and, in addition, will also demonstrate improvements in conversion and selectivity.

The results of naphthalene hydrogenation in the present reactor system and in tubing bomb microreactors (TBMR) are shown in Tables 1 & 2. It appears from the tubing bomb results that the catalyst is deactivated very rapidly when the temperature is

increased from 120°C to 135°C, resulting in no conversion. The catalyst requirement in the tubing bomb was very high (35% based on naphthalene) at 120°C to obtain 93% conversion. There was no conversion in the TBMR at 165°C with 10% catalyst loading, but when the tubing bomb experiments were conducted with repeated heating and cooling every three minutes, 86% conversion was obtained in 7.5 minutes. The repeated heating and cooling is similar to the conditions in the reactor system, where the reactants are exposed to the high temperature for a very short time (6-10 seconds). The naphthalene conversion in the reactor system was nearly complete (Table 1) under similar conditions with much lower catalyst loading and less time. In the TBMR, the reactants are exposed to high temperature throughout the reaction time resulting in an exponential increase of free radicals. The mass transfer rates are not adequate to saturate all the radicals and this leads to polymerization of free radicals resulting in the deactivation of the catalyst. In the reactor system however, the reactants are subjected to high temperature for a very short time per pass, reducing the probability of free radical polymerization.

The effect of catalyst loading on naphthalene hydrogenation in the reactor system (Table 1) was used to determine if gas-liquid mass transfer was controlling the reaction. A plot of reciprocal reaction rate vs reciprocal catalyst loading indicated that gas-liquid resistance is about 25% of the total resistance at the lowest catalyst loading and about 50% at the highest loading, indicating that the reactor is operating in a regime where gas-liquid mass transfer is only partially controlling. The mass transfer coefficient  $K_a$  determined from the experimental results was 6.0/min.

A limitation of the reactor system for use with severe reaction conditions was the performance of the mechanical pump. The pump was not capable of handling slurries under these conditions and suitable custom made pumps were prohibitively expensive. To overcome this limitation, a gas driven pumping system was developed and integrated to the reactor system. The reactor system with the gas-driven pumping system has been used for naphthalene hydrogenation under elevated pressures (800-1000 psig). Attempts are being made at present to use the system for coal liquefaction.

## CONCLUSIONS

A loop reactor system has been developed for use with reaction systems such as coal liquefaction that are gas-liquid mass transfer limited. The reactor system has the ability to process slurries and permits better control of free radical generation/reaction and provides higher mass transfer rates than conventional reactors. The reactor system was tested using naphthalene hydrogenation as a model reaction and performed much better than the conventional tubing bomb microreactors. The amount of catalyst required was considerably less than that required in the microreactors. A unique gas-driven pumping system was developed and integrated to the system because of the prohibitive cost of a suitable mechanical pump that could withstand coal liquefaction conditions. The reactor system will be used to coprocess coal with waste oil. Improvements in coal conversion/selectivity will be compared with those obtained in conventional reactors.

## REFERENCES

1. Satterfield, C.N., *Heterogeneous Catalysis in Industrial Practice*, McGraw Hill, Inc, New York, 1991.
2. Pradhan, V. R., Tierney, J. W., Irving, W., *Energy & Fuels* 1991, 5, 497-507.
3. Suzuki, T., Yamada, O., Takehaski, Y., Watanabe, Y., *Fuel Process. Technol.* 1985, 10, 33-43.
4. Zielke, C. W., Struck, R. T., Evans, J. M., Costanza, C. P., Gorin, E., *I & EC Process Des. Dev.* 1986, 5(2), 151, 158.
5. Bedell, M. W., Curtis, C. W., *ACS Fuel Div. Preprints* 1990, 2, 577.
6. Curtis, C. W., Guin, J., Kwon, K., *Fuel* 1984, 63, 1404.
7. Neavel, R. C., *Fuel* 1984, 63, 237.
8. Chaudhari, R.V., et al *Catalysis Review-Science and Engineering* 1986, 28(4)
9. Zlokarnik, M., *Chemical Engineering Science* 1979, 34, 1265
10. Boitiaux, J.P., et al., *Hydrocarbon Processing* 1985, 3, 51,

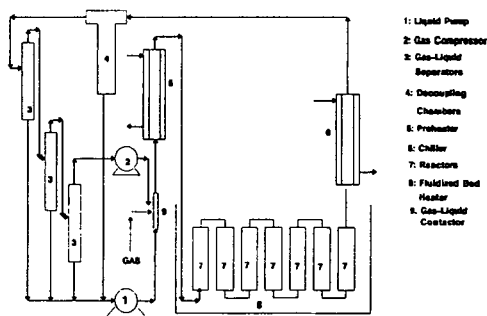


**Figure 1. Jet Loop Reactor System**

Table 1. Naphthalene hydrogenation (Reactor system)			
Catalyst (5.0%) <sup>*</sup>		Catalyst (7.5%) <sup>*</sup>	
Time (min)	Conversion (%)	Time (min)	Conversion (%)
7.0	17.07	3.5	24.75
9.0	31.20	6.5	33.13
14.0	47.22	9.0	45.14
20.0	64.30	10.75	54.50
27.0	85.44	15.0	69.62
37.0	98.81	20.50	88.88
		30.0	99.21
Catalyst (10.0%) <sup>*</sup>		Catalyst (15.0%) <sup>*</sup>	
Time (min)	Conversion (%)	Time (min)	Conversion (%)
4.0	35.34	3.5	39.92
6.5	40.18	5.0	44.55
8.75	54.14	7.25	63.94
11.25	70.82	9.50	78.89
14.50	86.57	15.0	99.14
19.00	98.41		

\* wt% based on the amount of naphthalene used

Tetralin: 750 ml

Naphthalene : 129.9 gm (18% of Tetralin)

Average reactor inlet Temperature: 123°C;

Average reactor outlet Temperature: 153°C;

Pressure: 120 psig

Table 2.  
Naphthalene Hydrogenation (Tubing bomb reactor)

10% Naphthalene*, 10% Catalyst**			
Temperature (°C)	Pressure (psig)	Time (min)	Conversion (%)
90	150	30	0
105	300	60	20
120	300	60	36
126	300	60	0
18% Naphthalene*, 10% Catalyst**			
Temperature (°C)	Pressure (psig)	Time (min)	Conversion (%)
90	150	30	0
165	150	30	0
165	300	30	0
10% Naphthalene*, 35% Catalyst**			
Temperature (°C)	Pressure (psig)	Time (min)	Conversion (%)
120	300	30	93
18% Naphthalene*, 14.57% Catalyst**, Cooling frequency 3 min			
Temperature (°C)	Pressure (psig)	Time (min)	Conversion (%)
165	100	3.0	38.26
165	100	6.0	73.85
165	100	7.5	86.09

\* Wt% based on the amount of tetralin used

\*\* Wt% based on the amount of naphthalene used

## Use of Biocatalysts for the Solubilization/Liquefaction of Bituminous Coal in a Fluidized-Bed Bioreactor

Eric N. Kaufman, Charles D. Scott, Timothy C. Scott, and Charlene A. Woodward

Chemical Technology Division  
Oak Ridge National Laboratory  
Oak Ridge, TN 37831

**Keywords:** coal liquefaction, enzymes, fluidized-bed reactor

### Abstract

Biocatalysts allow the solubilization/liquefaction of coal at near-ambient temperatures. This research has focused on the chemical modification of enzymes to enhance their solubility and activity in organic media and on optimal reactor design for a biocatalyst coal-liquefaction process. Modification of hydrogenase and cytochrome *c* using dinitrofluorobenzene has effected increased solubilities up to 20 g/L in organic solvents ranging from dioxane to benzene. Use of these modified enzymes in a small fluidized-bed reactor (with H<sub>2</sub> sparge) resulted in greater than 35% conversion of coal. A new class of continuous columnar reactors will be necessary to achieve the high throughput and low inventory necessary for biocatalyst processes. The controlling mechanisms in fluidized-bed systems using very small coal particulates are being studied. This investigation has included the hydrodynamic modeling of coal segregation in fluidized-bed reactors, with direct microscopic visualization using fluorescence microscopy.

### Introduction

Biocatalysts allow the solubilization/liquefaction of coal at near-ambient temperatures. In such applications, it is apparent that enzymes must retain solubility and activity in organic media. This work summarizes our previous efforts on the modification of enzymes using dinitrofluorobenzene (DNFB) to enhance enzyme solubility and activity in organic media.<sup>1</sup> The ability of DNFB-modified hydrogenase and cytochrome *c* to solubilize lignite and bituminous coals in a fluidized-bed bioreactor is demonstrated. Optimal reactor design and scaleup will require detailed knowledge of coal segregation in the fluidized-bed bioreactor. A fluorescence visualization method is introduced to enable direct *in situ* observation of coal particles in operating fluidized bed reactors.<sup>2</sup> This information will be combined with a predictive mathematical model of coal fluidization<sup>3</sup> to enable efficient reactor design and operation.

## Methods

### Techniques for Enzyme Modification

Modification of hydrogenase and cytochrome c with DNFB was achieved by a significant revision of the method originally developed by Sanger.<sup>4-7</sup> Typically, the reaction solution was a mixture of water and ethyl alcohol, with the ethanol fraction varying from 28 to 65% that contained 0.1 to 3 vol% DNFB buffered to a pH of approximately 8.5 with a 7 mM phosphate buffer and/or NaHCO<sub>3</sub>. The reaction was carried out in shake flasks at ambient temperature ( $25 \pm 1^\circ\text{C}$ ) in the presence of air for reaction times of 0.5 to 2 h. After the primary reaction, the pH was reduced to 7 by the addition of HCl, and the reaction mixture was dialyzed overnight against 50 times the volume of the same ethanol-water-buffer mixture (without DNFB) at a pH of 7, using a cellulose membrane. After dialysis, the modified enzymes were converted to the reduced state by the addition of 5 mg/mL sodium dithionite and then lyophilized and stored under N<sub>2</sub> until used.

### Fluidized-Bed Tests

Tests with coal were made with a small, tapered fluidized-bed bioreactor that was fabricated from glass. The reaction chamber was a 15-cm-long column in the form of an inverse cone with a diameter varying from 1.25 cm at the entrance to 2.5 cm at the exit, and the reactor was temperature-controlled at 30°C by circulating fluid in a surrounding jacket. The 0.5- to 1.0-g samples of coal particles (North Dakota lignite and Illinois No. 6 bituminous coal, -270+325 mesh fraction) were fluidized by pumping the reaction fluid containing the biocatalyst through the column at the rate of 2 to 3 mL/min. The system operated with continuous liquid recycle, and there was a H<sub>2</sub> sparge in the upper part of the column. The course of the reaction was followed by periodically measuring the spectrophotometric properties of the liquid phase. There appears to be a broad increase in light absorption in the range of 250 to 450 nm as the coal disappears, although it is usually convenient to choose a single wavelength for the presentation of results. At the end of tests for coal conversion, the solid residue was removed by successive centrifugation and washing. The first wash solution was the same solvent as that used in the tests, and this was followed by acetone and, finally, water. The supernatants were removed by siphoning, and spectral measurements were made. Coal conversion was reported on a moisture and ash-free basis.

## Results

### Enzyme Modification with Dinitrofluorobenzene

Modification of enzymes with DNFB resulted in higher solubilization in organic solvents, which increased as the hydrophobicity of the solvent decreased. The solubility of the unmodified enzyme also increased as the hydrophobicity of the solvent decreased, but it varied from undetectable in benzene and toluene to barely detectable in pyridine and dioxane. Appreciable enzyme deactivation was noted in the solvent of lowest hydrophobicity, dioxane, although significant enzyme solubilization occurred in that solvent.

The degree of dinitrophenylation affects the solubilization of the modified enzyme in organic solvents. For example, with a 0.5-h reaction time, as the concentration of DNFB in the reaction solution was increased from 0 to 0.67 vol %, there was a corresponding increase in the dinitrophenyl (DNP) content and solubilization in benzene that reached a maximum value of 9.2 mg/ml.<sup>7</sup> However, there was also a corresponding decrease in the enzyme activity, presumably due to the addition of DNP in the region of the active sites. At the higher DNFB concentration, the activity was only 40% of the original value.<sup>7</sup> This could be partially alleviated by the adsorption of an appropriate substrate, such as benzyl viologen, to the enzyme mixture prior to the addition of the DNFB. For example, when 0.17% DNFB was used to react with hydrogenase for 30 min, the biocatalytic activity was only 86.5% that of the starting material. But, when 20 mM benzyl viologen was added to the reaction mixture, the resulting activity of the modified hydrogenase was increased to the original value. The preadsorption of the substrate apparently partially protected the active site from interaction with the phenylizing reagent.

### Coal Liquefaction/Solubilization Tests in Fluidized Beds

Two types of tests were made in small fluidized bed reactors: one in which the initial charge was maintained throughout the test, with periodic measurements of spectrophotometric changes in the organic solution, and one in which the solvent with modified enzymes was periodically replenished while the coal residue was maintained in the reactor. The latter type of test was somewhat representative of a continuous system in which some fresh biocatalyst was continuously introduced. Tests were made with pyridine as the solvent in contact with either bituminous or lignite coal.

In fluidized-bed tests with a single charge of the solvent containing DNP-enzymes, an apparent rapid conversion of the coal occurred during the first few hours, followed by a more gradual process throughout the remaining 24 h. This observation could be due to an initial use of the included reducing agent (DNP-cytochrome c) for the hydrogenation reaction, followed by the use of molecular H<sub>2</sub> for the succeeding hydrogenation at a lower rate. Without treatment for removing enzyme precipitation, the liquefaction/solubilization of the lignite was 23.9% and that of bituminous coal was 8.5%. The results were

somewhat higher than comparable shake-flask tests for both types of coal without HCl treatment.<sup>1</sup> Thus, the fluidized bed appears to be a more efficient contacting system.

One test was made with bituminous coal in pyridine in which the solvent containing DNP-mixed enzymes was replaced after 4 and 8 h in order to determine whether appreciable interaction could be induced throughout the course of the 24-h run. This was apparently the case since there was a significant increase in absorbance at 376 nm throughout a greater portion of the 24-h test. Apparent coal conversion without acid leaching of the residue to remove precipitated enzymes was 35.3%. This is the largest amount of biocatalyzed liquefaction/solubilization of a higher-rank coal that has been observed; it is a threefold increase over the fluidized-bed test in which there was a single charge of the solvent mixture.

#### Fluorescence Visualization of Coal Particles in a Fluidized Bed

Effective modeling, design and implementation of fluidized-bed reactors rely upon knowledge of bed expansion and segregation tendencies with particles of varying size and density. We have recently introduced a fluorescence method for the visualization of coal particles within a fluidized bed-reactor.<sup>2</sup> In this method, the dye fluorescein is added to the liquid phase and serves as a contrast agent. A modified fluorescence microscope abuts the column and is used to image the fluorescence emission in response to epi-illumination. The resulting image (dark particles on a bright field of fluorescent liquid) may be digitized and analyzed by using edge-detection algorithms to provide particle-area fraction and size distributions. The microscope may be positioned at any height relative to the column, thus producing particle segregation and expansion statistics as a function of bed height. Unlike previous attempts to visualize segregation in fluidized beds which require direct sampling, use of a modified ultra-thin column, low particle volume fraction, or radiation, the proposed method is non-invasive and may be conducted in an operational reactor at standard flow rates and particle loading. Further, unlike our previous attempts to directly label a bimodal distribution of coal particles,<sup>8</sup> the current method may be applied to any distribution of particle sizes and densities, without possible alteration of particle hydrodynamics.

Preliminary results have been obtained on a small (1-ft) column in which a bimodal distribution (53-63 and 150-250  $\mu\text{m}$ ) of coal was fluidized. Digitized images clearly show that particle segregation is occurring and that both large and small particles are present throughout the column. Figure 1 demonstrates the current abilities in bed visualization. Figure 1a is a view near the top of the column while Figure 1b displays conditions near the bottom. In these figures, the round, darker regions are coal particles fluidized by fluorescein/water. Even from these preliminary data, it is evident that more large particles reside at the bottom of the column. Digital filtering and edge-detection algorithms have been developed to convert such images into particle area fraction and size distribution data as a function of axial position. These data will be of use in the development of predictive mathematical models of bed expansion and segregation<sup>3</sup>, and will also be useful in assessing the accuracy of current models.

## Conclusions

Reducing enzymes can be chemically modified by the addition of dinitrophenyl groups so that they will be soluble in organic solvents while still maintaining biocatalytic activity. A hydrogenase has been shown to enhance the liquefaction/ solubilization of bituminous and lignite coals in both pyridine and benzene at 30°C when a reducing reagent such as reduced cytochrome c and/or molecular H<sub>2</sub> is used. A less polar organic solvent such as benzene may be more effective, and a small fluidized-bed has been shown to be an efficient contactor, especially with sequential addition of the reaction liquids. Coal conversions of up to 35.3% have been observed. A fluorescence method has been introduced to enable the visualization of coal-particle segregation and degradation in a fluidized bed-reactor. This technique will greatly enhance the ability to design and efficiently utilize this reactor scheme.

## Acknowledgments

Research supported by the Fossil Energy Advanced Research and Technology Program, managed in part by the Pittsburgh Energy Technology Center, U.S. Department of Energy, under contract DE-AC05-84OR21400 with Martin Marietta Energy Systems, Inc. "The submitted manuscript has been authored by a contractor of the U.S. Government under contract DE-AC05-84OR21400. Accordingly, the U.S. Government retains a nonexclusive, royalty-free license to publish or reproduce the published form of this contribution, or allow others to do so, for U.S. Government purposes."

## REFERENCES

- 1 Scott, C. D., Scott, T. C. and Woodward, C. A., *Fuel*. In Press
- 2 Kaufman, E. N. and Scott, T. C., *Powder Technology*. Submitted for Publication.
- 3 Asif, M., Petersen, J. N., Scott, T. C. and Cosgrove, J. M., *Fuel*. In Press.
- 4 Scott, C. D., Faison, B. D., Woodward, C. A., and Brunson, R. R. in "Proceedings: 1991 Second International Symposium on the Biological Processing of Coal," (Ed. S. Yunker), Electric Power Research Institute, Palo Alto, CA, 1991, pp. 4-29 - 4-39.
- 5 Sanger, F. *Biochem. J.* 1945, **39**, 507.
- 6 Sanger, F. *Biochem. J.* 1949, **45**, 563.
- 7 Scott, C. D., Scott, T. C., and Woodward, C. A. *Appl. Biochem. Biotechnol.* In Press.
- 8 Scott, T. C., Cosgrove, J. M., Asif, M. and Petersen, J. N., *Fuel*. In Press.

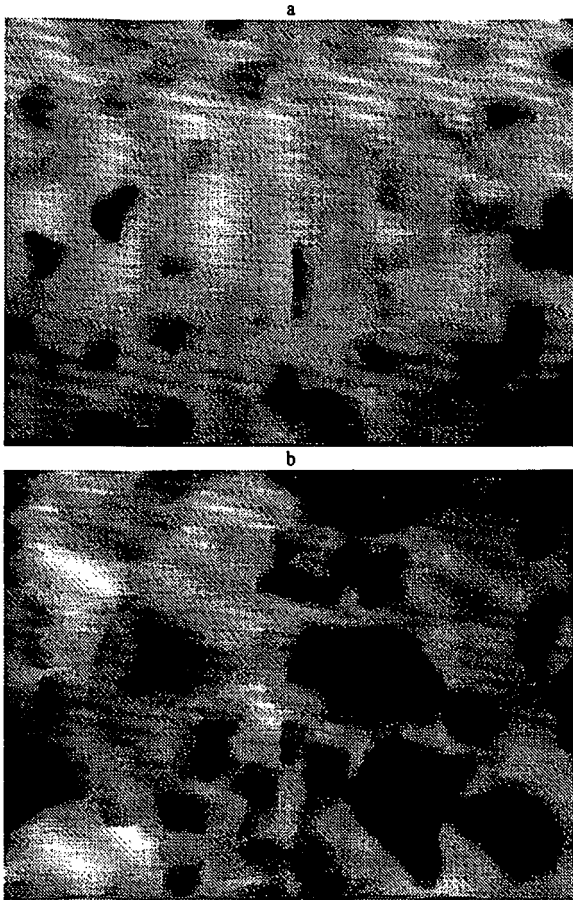


**Figure 1:** Visualization of fluidized coal particles using fluorescence microscopy. Coal particles appear dark on the otherwise bright background of fluorescent liquid. (a) Near top of column, the bed consists of only smaller particles (b) near bottom of column, the bed is a mixture of large and small coal particles. Video digitization, filtering and edge detection algorithms will be implemented to provide area fraction and particle size information from such images.

**Dynamics of the Extract Molecular-Weight Distribution  
in Supercritical Thermolysis of Coal:  
Continuous-Mixture Kinetics**

Chunjie Zhang, Ming Wang,  
J. M. Smith, Ben J. McCoy

Department of Chemical Engineering  
University of California  
Davis, CA 95616

Keywords: coal, thermolysis, kinetics

**Introduction**

In this paper experimental molecular-weight distribution data for coal thermolysis at 340 °C and 360 °C in a differential flow reactor are interpreted by assuming that decomposition reaction rate expressions are continuous with molecular weight. Three groups of chemical species, representing polyaromatic compounds bound in the coal network by one, two, or more chemical linkages, are extracted simultaneously during the thermolysis reaction. The three groups are gamma distributions in molecular weight (Darivakis et al., 1990). The data support the hypothesis that the first-order rate coefficient is independent of molecular weight, and that as a consequence the MWD has a similar shape during the time of extraction.

When the number of chemical species involved in a chemical process reaches a large number, e.g.,  $10^2$ - $10^3$ , it is convenient to consider a property of the components to be a continuous variable. For example, the molecular weight, the number of carbon or oxygen atoms, or the boiling point of the different species can be considered a continuum of values, rather than discrete numbers. One line of inquiry is to formulate and solve the equations governing the chemical kinetics, or thermodynamics, of the continuous mixture, and to test the theory by experimentally measuring the frequency of occurrence of the continuous variable (e.g., the molecular weight distribution). Another possible program is to average the governing equations to obtain relations for lumped variables that can be measured experimentally for the bulk mixture. Both these approaches have been explored for continuous-mixture thermodynamics. The theoretical issues of continuous mixture and lumping kinetics for chemical reactions have been addressed in numerous mathematical studies, but their use to interpret experimental data has been limited. In the present work we wish to apply concepts from continuous-mixture kinetics to thermolytic coal extraction.

Some essential ideas of continuous-mixture kinetics provide a framework for the theoretical analysis of the data given below. The averaging, or lumping procedure shows how the kinetics governing the MWDs can lead to overall, lumped rate expressions used in most earlier studies of coal thermolysis. The overlapping groups of extractable compounds in the coal matrix present, in some cases, complications for lumping mathematics. The low temperature data ( $T \leq 360$  °C) are readily explained by first-order expressions with rate coefficients that are independent of molecular weight and identical for the three groups of extractable compounds. The lumping in this case provides overall first-order rate expressions with the same rate coefficient.

### Theory

In the present continuous-mixture approach the MW is considered to be a continuous variable. If  $x$  is the MW then the MWD is  $c_i(x,t)$ , where at time  $t$ ,  $c_i(x,t)dx$  is the concentration in the MW interval  $(x, x+dx)$ . The integral over all  $x$  is the lumped concentration, expressed in units of mass (kg) of extractables per mass (kg) of coal sample.

A central question of continuous-mixture kinetics is whether the reaction order is preserved by the lumping procedure. We follow Aris (1989) in answering this question for kinetics that describe coal thermolytic extraction when secondary reactions are negligible. For the flow reactor used here the residence time is too short for further (secondary) reactions of the extract molecules to occur. We generalize the earlier development by considering that several groups of chemical species are extracted simultaneously from the coal. If the process consists of parallel reactions of  $n$ th-order at each molecular weight,  $x$ , then the governing differential equation for the differential coal batch is

$$dc_i(x,t)/dt = -k_i(x) [c_i(x,t)]^n \quad (1)$$

with initial condition  $c_i(x,t=0) = c_{i0}(x)$ . The rate coefficient is  $k_i(x)$  and the subscript  $i$  refers to the  $i$ th group of compounds that react. The solution is

$$c_i(x,t) = c_{i0}(x) [1 + (n-1) c_{i0}(x)^{n-1} k_i(x)t]^{1/(n-1)} \quad (2)$$

where in the limit as  $n \rightarrow 1$ ,  $c_i(x,t)$  approaches an exponential. The averaged, or lumped, concentration is given by

$$C(t) = \sum_i \int_0^\infty c_i(x,t) dx \quad (3)$$

and

$$C_0 = \sum_i \int_0^\infty c_{i0}(x,t) dx \quad (4)$$

The lumped  $n$ th-order kinetics equation corresponding to this system,

$$dC(t)/dt = -K [C(t)]^n \quad (5)$$

with initial condition  $C(t=0)=C_0$  has the solution

$$C(t) = C_0 [1 + (n-1) C_0^{n-1} Kt]^{1/(n-1)} \quad (6)$$

where  $K$  is the rate constant. The solutions for  $C(t)$  and the lumped expression of  $c_i(x,t)$  are identical when

$$c_{i0}(x)^{n-1} k_i(x) = K C_0^{n-1} \quad (7)$$

Thus for first-order kinetics ( $n=1$ ) we must have  $k_i(x) = K$ , independent of molecular weight, for the lumped expression to be first-order. If the rate coefficient is not constant with  $x$ , then the resulting lumped kinetics can be other than first-order.

Ho and Aris (1987) showed how lumping first-order continuous-mixture kinetics can lead to any reaction order between one and two, depending on the initial condition. We apply their reasoning here to the chemical groups extracted from coal. Consider that the rate coefficient is proportional to MW, i.e.,  $k_i(x) = k_{1i}x$ , where  $k_{1i}$  is independent of  $x$ . A general initial MWD that covers many possible forms for  $c_{i0}(x)$  is the gamma distribution (or Pearson Type III distribution; see Abramowitz and Stegun, 1968),

$$c_{i0}(x) = m_{oi} Y_i^{\alpha_i - 1} \exp(-Y_i) / \beta_i \Gamma(\alpha_i) \quad (8)$$

where  $Y_i = (x - x_{i0}) / \beta_i$ . The zero moment of the distribution is  $m_{oi}$ . The average position of the peak,  $x_{ai} = x_{oi} + \alpha_i \beta_i$ , and its variance,  $\sigma_i^2 = \alpha_i \beta_i^2$ , are the first and second moments. The position of the peak maximum is  $x_{pi} = x_{oi} + \beta_i(\alpha_i - 1)$ . The distribution is equivalent to that used by Ho and Aris (1987) if  $\beta = 1/\alpha$  and  $m_{oi} = 1$ . In the limit as  $\alpha_i \rightarrow \infty$ ,  $c_{i0}(x) = m_{oi} \delta(x - x_{i0})$ , so that only components having a single molecular weight are reacting, and the rate coefficient has a constant value at that MW.

With the solution for  $c_i(x, t)$ , i.e., the case when  $n=1$  in Eq. (2) above, we can integrate to obtain the lumped concentration,

$$C(t) = \sum \int_0^\infty c_{i0}(x) \exp(-k_{1i} x t) dx = \sum C_i(t) \quad (9)$$

with

$$C_i = m_{oi} (1 + \beta_i k_{1i} t)^{-\alpha_i} \quad (10)$$

The rate expression is obtained by differentiation,

$$dC/dt = \sum dC_i/dt \quad (11)$$

where

$$dC_i/dt = -m_{oi} \alpha_i \beta_i k_{1i} (C_i / m_{oi})^{\alpha_i + 1} / \alpha_i \quad (12)$$

In the special case that only one species group is reacting, this last equation simplifies to a power-law rate expression,

$$dC/dt = -K C^\phi \quad (13)$$

where  $\phi = (1 + \alpha)/\alpha$ . As  $\alpha$  increases from one to infinity, the order of the lumped kinetics expression decreases from two to one. For the more general case when several groups react independently, however, no simple kinetics expression appears. One can perform the lumping operation numerically, and determine a reaction expression empirically.

For our experimental procedure, the extractable component MWD and concentration of coal,  $c(x, t)$  and  $C(t)$ , are not measured directly. Rather, the concentrations of solubilized extract (both MWDs and lumped concentrations) in the solvent leaving the reactor are monitored with time. The time evolution of these concentrations is described by mass balances written for the reactor. The use of a differential bed of fine coal particles allows the reactor analysis to be simplified considerably. The convective term in the mass balance can be approximated as the volumetric flow rate multiplied by the gradientless concentration in the fixed bed. For the experimental conditions the residence time in the heated zone of the reactor is much less than the characteristic reaction time (reciprocal of the rate coefficient). Thus the accumulation term can be neglected, and the mass balance becomes simply

$$u_i(x, t) = k_{1i}(x) f[c_i(x, t)] / Q \quad (14)$$

where  $u_i(x, t)$  is the MWD of extract in the solvent,  $Q$  is the volumetric flow rate of solvent, and  $f[c_i(x, t)]$  represents the rate expression. The lumped extract concentration is

$$U(t) = \sum \int_0^\infty u_i(x, t) dx \quad (15)$$

Various rate expressions can be hypothesized for  $f[\ ]$  and substituted into the equation for  $U(t)$ . Similar to the discussion above of the coal batch extraction, one concludes that only for special cases

will simple lumped mass balance expressions be found for  $U(t)$ . For example, at temperatures 360 °C and below, the rate is first-order with rate coefficients,  $k_0$ , independent of  $x$  and identical for the extractable groups. For this case it is straightforward to demonstrate that the lumped rate is first-order with rate coefficient equal to  $k_0$ ; thus,

$$u(x,t) = k_0 c_0(x) \exp(-k_0 t)/Q \quad (16)$$

and

$$U(t) = k_0 C_0 \exp(-k_0 t)/Q \quad (17)$$

which can be compared with the lumped reactor exit concentration.

### Experiments

The experimental apparatus and procedure have been described previously (Zhang et al., 1992). Supercritical fluid thermolysis of Illinois No. 6 coal is conducted in a fixed-bed reactor with flowing solvent. The lumped, reactor-exit concentration is measured by spectrophotometric absorbance in a flow cuvette. Thus we select t-butanol as the solvent, since it does not interfere with the uv absorbance of aromatic coal extraction products. The thermolysis process is carried out at constant pressure, 6.8 MPa, and constant flow rate, 0.17 cm<sup>3</sup>/sec. Coal particles are small enough that intraparticle diffusion resistance is not significant, and the solvent flow rate is large enough that external mass transfer resistance is negligible (Zhang et al., 1992). The coal is pretreated by supercritical extraction at 300 °C to remove physically extractable constituents. Coal extract samples of 100 ml were collected during the thermolysis process, and concentrated by evaporation of t-butanol under vacuum. The MWDs of these samples, based on polystyrene molecular-weight standards, are determined by gel permeation chromatography with the uv detector set at 254 nm (Bartle et al. 1984).

### Discussion of Results

The time evolution of extract MWDs for the temperatures 340 and 360 °C are provided in Figures 1. The two temperatures show MWDs whose shapes are similar at the different times, i.e., the ratio of peak heights, the position of peaks, and the average molecular weight are invariant with time. Such behavior can be described by assuming that the rate coefficient for the MWDs is independent of MW. The values of the first-order rate coefficients at the two temperatures, displayed in Table 1, give an energy of activation  $E_1 = 58$  kJ/mol. The gamma distribution parameters, provided in Table 2, show that increasing the temperature changes only the zero moments. The concentrations for each group of extractable compounds,  $m_{0i}$ , shift due to the greater extraction at the higher of the two temperatures.

The comparison of the calculated and experimental MWDs is shown in Figure 2 for two samples. Only time changes during the course of the evolution of the MWDs; the parameters for the initial MWD in the coal and the rate coefficients are constant. The agreement between the experimental data and the model calculations is consistently good for all samples during the course of a run.

Figure 3 shows experimental data for total, lumped extract concentrations for the thermolytic extractions at two temperatures. The lumped concentrations are determined by the flow-through spectrophotometer at the reactor exit. The model calculations shown in Figure 3 are based on Eq. (17) and the same rate constant values (Table 1) determined from the time evolution of the MWDs. The

satisfactory agreement between theory and experiment, for both the lumped and MWD data, supports the validity of the explanation of coal thermolytic extraction that we have proposed.

#### Conclusion

A continuous-flow thrmolysis reactor, in which supercritical t-butanol contacts a differential bed of coal particles, provides sequential coal-extract samples that are analyzed by HPLC gel permeation chromatography to obtain time-dependent MWD data. The coal thermolysis experimental data support an interpretation of the results based on considering the molecular weight of extraction products as a continuous variable. This continuous-mixture theory suggests that three groups of coal components are extracted independently. At temperatures 340 °C and 360 °C the MWDs maintain a similar shape during the semibatch extraction. This indicates that first-order kinetics dominate, and that the rate coefficient is independent of molecular weight. The lumped extract concentration is monitored at the reactor exit by continuous uv-absorbance spectrophotometry. Both MWD and lumped concentration data are described by consistent expressions based on the same rate coefficient.

#### Acknowledgements

The financial support of Pittsburgh Energy Technology Center Grant No. DOE DE-FG22-90PC90288, and the University of California UERG is gratefully acknowledged.

#### References

- R. Aris, "Reactions in Continuous Mixtures," AICHE J. **35**, 539 (1989).
- Abramowitz, M. and I. A. Stegun, Handbook of Mathematical Functions, NBS, Chap. 26 (1968).
- Bartle, K. D., M. J. Mulligan, N. Taylor, T. G. Martin, C. E. Snape, "Molecular Mass Calibration in Size-Exclusion Chromatography of Coal Derivatives," Fuel, **63**, 1556 (1984).
- Darivakis, G. S., W. A. Peters, J. B. Howard, "Rationalization for the Molecular Weight Distributions of Coal Pyrolysis Liquids," AICHE J. **36**, 1189 (1990).
- Ho, T. C., R. Aris, "On Apparent Second-Order Kinetics," AICHE J. **33**, 1050 (1987).
- Zhang, C., J. M. Smith, B. J. McCoy, "Kinetics of Supercritical Fluid Extraction of Coal: Physical and Chemical Processes," ACS Symposium on Supercritical Fluids, in press (1992).

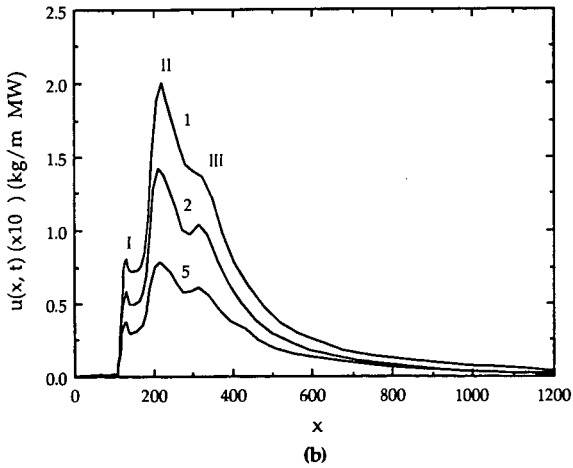
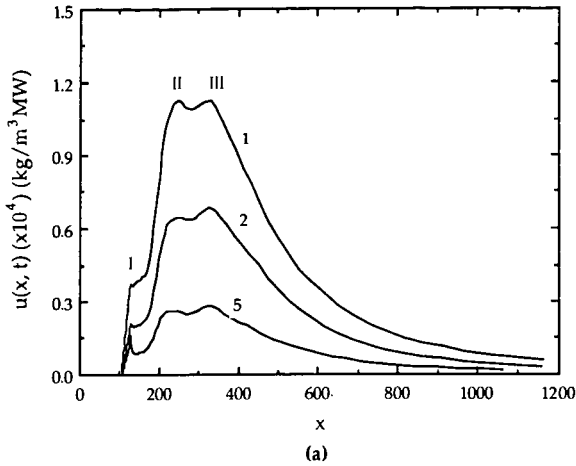


**Figure 1. Time evolution of MWDs for thermolytic extractions of coal at 340 °C (a) and 360 °C (b). Samples 1, 2, and 5 were collected at the reactor effluent at times 30, 56, and 145 min for runs at 340 °C and 10, 30, and 70 min for runs at 360 °C.**

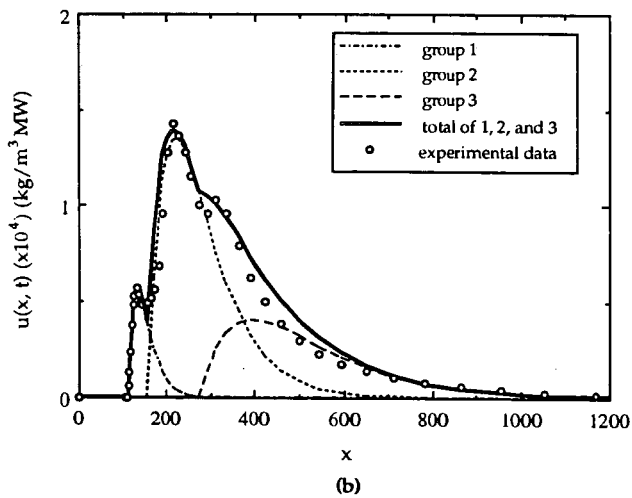
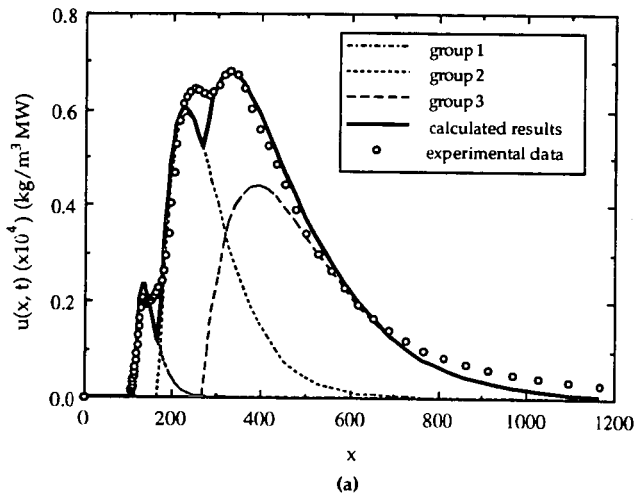


Figure 2. Comparison of model calculations and experimental data for MWDs for Sample 2 of runs at 340 °C (a) and 360 °C (b), respectively.

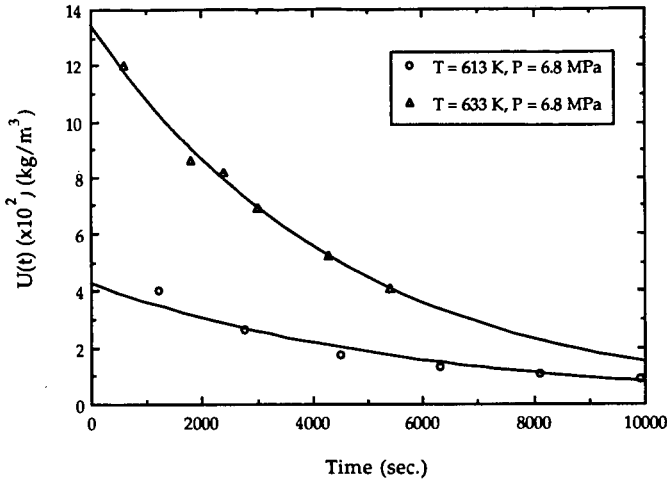


Figure 3. The experimental data of total extract concentrations at 613 K and 633 K and their exponential fit based upon kg of initial coal sample mass.

Table 1. The values of the first-order rate constants from the model

Temperature (K)	Rate Constant, $k_i$ , sec <sup>-1</sup>	Activation Energy, kJ/mol
613	0.00015	58
633	0.00022	

Table 2. The parameter values for the gamma distributions

T = 613 K	$m_{01} = 0.0033$ kg/kg coal	$\alpha = 2$	$x_{01} = 120$
	$m_{02} = 0.032$ kg/kg coal	$\beta_1 = 20$	$x_{02} = 170$
	$m_{03} = 0.029$ kg/kg coal	$\beta_2 = 62$	$x_{03} = 275$
T = 633 K	$m_{01} = 0.0080$ kg/kg coal	$\beta_3 = 120$	$x_{01} = 120$
	$m_{02} = 0.049$ kg/kg coal	$\alpha = 2$	$x_{02} = 170$
	$m_{03} = 0.041$ kg/kg coal	$\beta_1 = 20$	$x_{03} = 275$

## The Use of Solid State C-13 NMR Spectroscopy to Study Pyridine Extracted and Extraction Residues in the Argonne Premium Coals

**R.J. Pugmire,\* M.S. Solum,\*\* S. Bai, +  
T.H. Fletcher,\*\* S. Woods,+ and D.M. Grant\*\***  
**Departments of Chemical & Fuels Engineering\* and Chemistry\*\***  
**University of Utah, SLC, UT 84112**  
**and**  
**Departments of Chemistry+ and Chemical Engineering\*\***  
**Brigham Young University, Provo, UT 84602**

### INTRODUCTION

The relationship between coal structure and combustion behavior is a matter of on-going research in our laboratories. A great deal of effort has gone into obtaining data that is used for modeling studies of devolatilization behavior.<sup>1</sup> We have also carefully studied the process of char formation.<sup>2-3</sup> Our past work has focused on trying to understand the relationship between coal/char/tar formation<sup>2</sup> as they relate to the devolatilization and char oxidation phenomena. The formation of metaplast during pyrolysis was studied by Fong and Howard<sup>5</sup> in terms of extractable material obtained at different stages of the devolatilization process. We have recently turned our attention to metaplast formation in devolatilization and plan to conduct a series of experiments that will help define the formation and chemical structure of metaplast in coals of different rank.

Howard and Fong used pyridine extraction methods to quantify the amount of metaplast formed during pyrolysis of a Pittsburgh #8 coal. These experiments demonstrated that pyridine extractable material initially increased with pyrolysis temperature, passed through a maximum, and then decreased as retrogressive reactions became dominant at the higher temperatures. We have completed an initial study of the pyridine extraction of the Argonne Premium coal samples and the detailed study of the carbon skeletal structure of the extracts and the extraction residues from these coals. The <sup>13</sup>C NMR data obtained from these extracts and extraction residues will be compared with the extracts and extraction residues formed at different stages of the pyrolysis process in these coals as our pyrolysis work develops.

### EXPERIMENTAL

It is well known that a considerable amount of material is extracted by pyridine from bituminous coals. However, a significant part of the extract seems to form colloidal dispersions that can be disruptive to analytical techniques such as proton and carbon NMR spectroscopy. It is also known that pyridine is imbibed into the structure of coal and is very difficult to remove. This imbibed pyridine makes it difficult to quantify the structural features of coals. We adopted the technique of Buchanan<sup>6</sup> in an effort to minimize the formation of colloidal dispersions. Extractions were carried out at room temperature after the manner of Buchanan's procedure with the extraction process taking as much as three days to complete. It was judged that extraction was complete at the point that the pyridine recycle solvent in the Aberhalden extraction apparatus was colorless. The samples were then washed as described by Buchanan and dried at room temperature in a vacuum to remove solvents. Proton NMR spectra were then obtained on the extract to determine the level of incorporation of pyridine into the extract material. In all cases only minor traces of pyridine were observed in the proton NMR spectra.

The carbon-13 NMR spectra of all extracts and extraction residues were obtained according to the procedure of Solum, et al.<sup>7</sup> High resolution NMR data was obtained on a Varian VXR-500 spectrometer using dimethyl sulfoxide as solvent. It was noted that the solubility of the extracts varied with the coal and that solubilization was not complete for any of the coals. The NMR spectra exhibited the characteristics of high resolution with line widths that would be typical of compounds with molecular weights of several hundred daltons.

## RESULTS

The amount of extract obtained from each of the 8 Argonne Premium coals is given in Table 1. The duplicate extractions were run in parallel and the reproducibility of the results appears to be quite adequate. It is noted that a mass closure of at least 94% was obtained on each sample. Figure 1 portrays the extract yield together with the fraction of total carbons that are protonated aromatic carbons in the pyridine extracts and residues. In each case this parameter is found to be higher in the extract than in the residue, indicating that the residue contains a higher fraction of substituted carbons than the extract. In Figure 2, the coordination number of the residues is higher than the extracts with the single exception of the Illinois #6 in which no distinction can be made. The number of bridges and loops in the residues and extracts are shown in Figure 3. This parameter is a measure of the cross link structure that exists between individual aromatic clusters. As one might expect, the residues exhibit a greater number of bridges than are found in the extracts. The single exception, again, is the Illinois #6 coal in which no distinction can be made between the two. In Figure 4, the average aromatic cluster size is given and in each case the size of the extract is less than that of the residue, with the single exception of Illinois #6 where no clear distinction can be made. Figure 5 portrays the number of side chains per cluster in the extracts and residues. From this data no consistent trend can be observed. Figure 6 contains the aromatic characteristics of the extracts from the Argonne coals. As expected, both the carbon and proton aromaticity of the extracts increase with rank with the single exception of the Pocahontas extract. The carbon aromaticity of the residue is also plotted for comparison purposes. Using the proton structural definitions reported by Fletcher, et al.,<sup>2</sup> it is possible to approximate the contributions 1, 2, and 3-ring aromatic species in the coal extracts. These data are also shown in Figure 6. In Figure 7, the contributions of total  $\alpha$ -hydrogens,  $\alpha$ -methyls,  $\alpha$ -CH<sub>2</sub> groups, and  $\gamma$ -methyls for the pyridine extracts are given. It is interesting to note that the total  $\alpha$ -hydrogen and  $\alpha$ -CH<sub>2</sub> groups pass through a maximum, as a percent of the total hydrogen in the samples, in the high volatile bituminous coal. As expected, the contributions of  $\gamma$ -methyl groups decrease from lignite through the high volatile bituminous coal range and then increase slightly in the Upper Freeport and Pocahontas extracts.

## CONCLUSIONS

Comparing the <sup>13</sup>C NMR data on the extracts and residues, it becomes apparent why material is extracted from the parent coal. While the CP/MAS spectra of both the extracts and residues are quite similar, an examination of the details of the structure provide the subtle differences in structural detail that are important in describing the extraction process. While one must recognize that we are observing the averages of all the components present in the extracts, the extracted material appears to have many of the structural features that are observed in the macromolecular structure of the coal. The

differences lie in the fact that the number of cross links is reduced and the number of substituents on the aromatic rings is lower in the extracts than in the residues. Hence, these data are consistent with the fact that this material can be extracted since it is not extensively incorporated by means of covalent bonds into the macromolecular structure. The proton NMR data shows that the amount of 2- and 3-ring components present in the extracts increases with the rank of the coal. The aliphatic region of the proton NMR data indicates that: a) the amount of  $\alpha$ -methyl groups is essentially the same in all extracts, b) the amount of  $\gamma$ -methyl groups decreases with rank, and c) the amount of  $\alpha$ -hydrogen goes through a maximum at the high volatile bituminous rank range.

These data on the extracts will be used to compare the pyridine extractable material that is obtained as these coals are pyrolyzed. Experiments that are now underway in our laboratories together with the results presented herein will be useful in our future work on modeling the transformation that occur during devolatilization and char formation.

#### ACKNOWLEDGMENT

This work was supported by the National Science Foundation through the Advanced Combustion Engineering Research Center at Brigham Young University and the University of Utah.

#### REFERENCES

1. T.H. Fletcher, A.R. Kerstein, R.J. Pugmire, and D.M. Grant, A Chemical Percolation Model for Devolatilization: 3. Chemical Structure as a Function of Coal Type, *Energy & Fuels*, 1992, 6, 414.
2. T.H. Fletcher, M.S. Solum, D.M. Grant, S. Critchfield, and R.J. Pugmire, Solid State  $^{13}\text{C}$  and  $^1\text{H}$  NMR Studies of the Evolution of the Chemical Structure of Coal Char and Tar During Devolatilization, 23rd Symposium (International) on Combustion, The Combustion Institute, 1990, 1231.
3. R.J. Pugmire, M.S. Solum, D.M. Grant, S. Critchfield, and T.H. Fletcher, Structural Evolution of Matched Tar/Char Pairs in Rapid Pyrolysis Experiments, *Fuel*, 1991, 70, 414.
5. W.S. Fong, W.A. Peters, and J. Howard, *Fuel*, 1986, 65, 251.
6. D.H. Buchanan, *Am. Chem. Soc., Div. of Fuel Preprints*, 32, No. 4, p. 293.
7. M.S. Solum, R.J. Pugmire, and D.M. Grant,  $^{13}\text{C}$  Solid State NMR of the Argonne Premium Coals, *Energy & Fuels*, 1989, 3, 187.

**Table 1**  
**Pyridine Extraction Yields**

Coals	Extractable Yield (%) <sup>a</sup>	Residue Yield (%) <sup>a</sup>	Total Recovery
Stockton	13.8	80.2	94.0
	15.6	80.5	96.1
Pittsburgh #8	26.0	69.1	95.2
	27.0	70.5	97.5
Blind Canyon	31.1	65.3	96.4
	33.1	64.6	97.5
Illinois #6	27.3	67.3	94.6
	28.5	65.1	93.6
Upper Freeport	14.8	81.8	96.6
	15.0	82.7	97.7
Wyodak	6.1	92.4	98.5
	6.3	91.7	98.0
Zap	3.0	94.5	97.5
	3.2	94.7	97.9
Pocahontas	0.5	96.8	97.3
	0.5	97.2	97.7

<sup>a</sup> Weight percent on a dry basis.

**PROTONATED AROMATIC CARBONS IN  
PYRIDINE EXTRACTS AND RESIDUES FROM  
ARGONNE COALS**

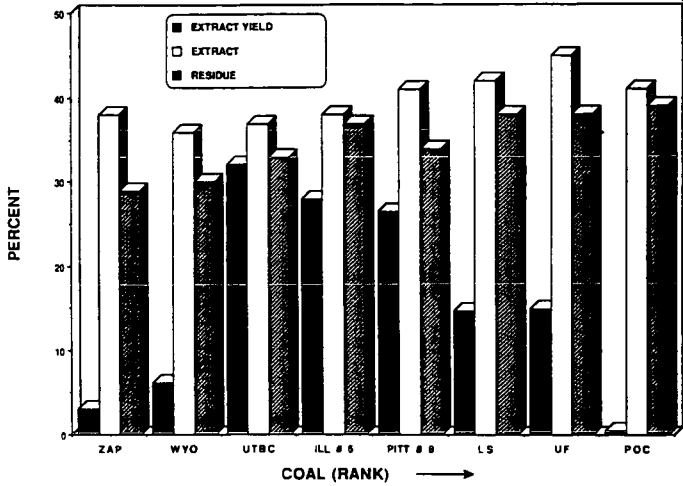


Figure 1. Extract yields and fraction of total aromatic carbons that are protonated ( $f_aH$ ) in pyridine extracts and residues of the APCS coals.

**COORDINATION NUMBER IN PYRIDINE  
EXTRACTS AND RESIDUES IN ARGONNE COALS**

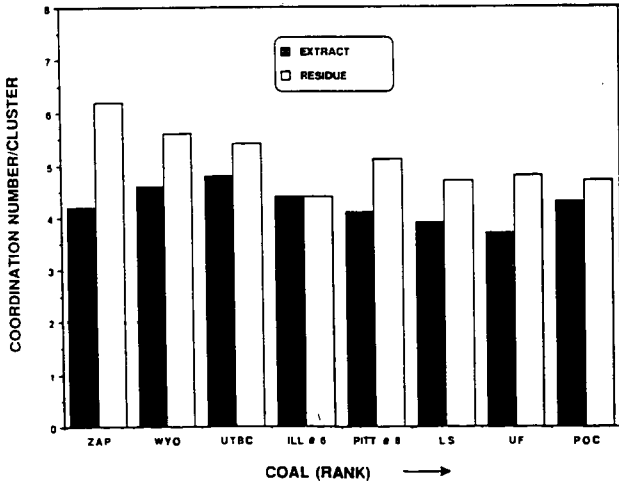


Figure 2. Coordination number in pyridine extracts and residues of the APCS coals.

**BRIDGES AND LOOPS IN PYRIDINE EXTRACTS  
AND RESIDUES FROM ARGONNE COALS**

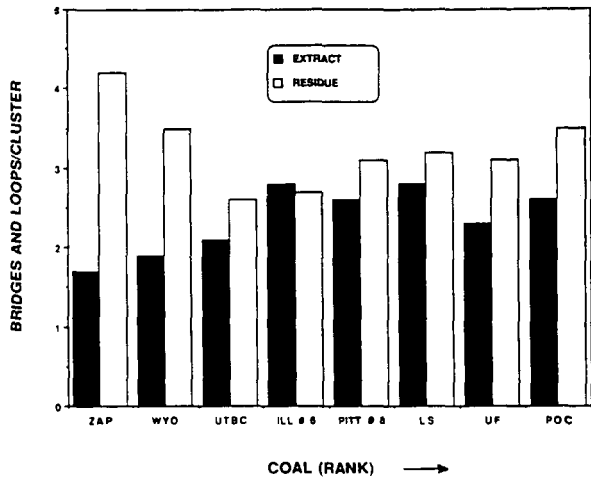


Figure 3. Number of bridges and loops per cluster in pyridine extracts and residues of the APCS coals.

**AVERAGE AROMATIC CLUSTER SIZE IN  
PYRIDINE EXTRACTS AND RESIDUES  
FROM ARGONNE COALS**

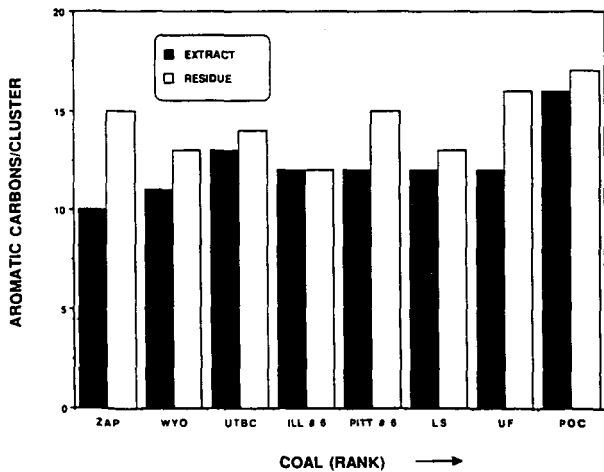


Figure 4. Average aromatic cluster size in the extracts and residues of the APCS coals.

### SIDE CHAINS IN PYRIDINE EXTRACTS AND RESIDUES FROM ARGONNE COALS

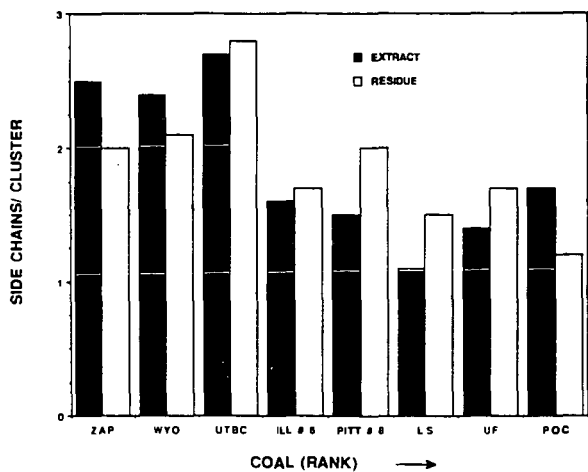


Figure 5. Number of side chains per cluster (coordination number) in the extracts and residues of the APCS coals.

### AROMATIC CHARACTERISTICS OF PYRIDINE EXTRACTS FROM ARGONNE COALS

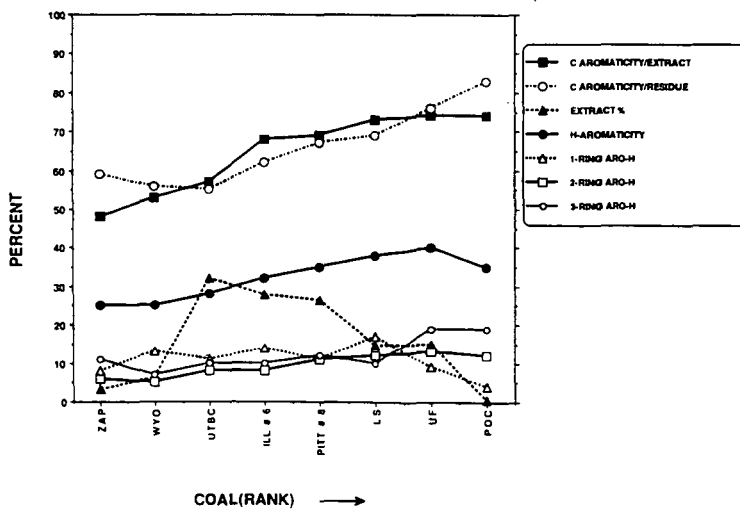


Figure 6. Aromatic characteristics in the extracts and residues of the APCS coals.

**ALIPHATIC PROTON STRUCTURAL PARAMETERS  
IN PYRIDINE EXTRACTS FROM ARGONNE COALS**

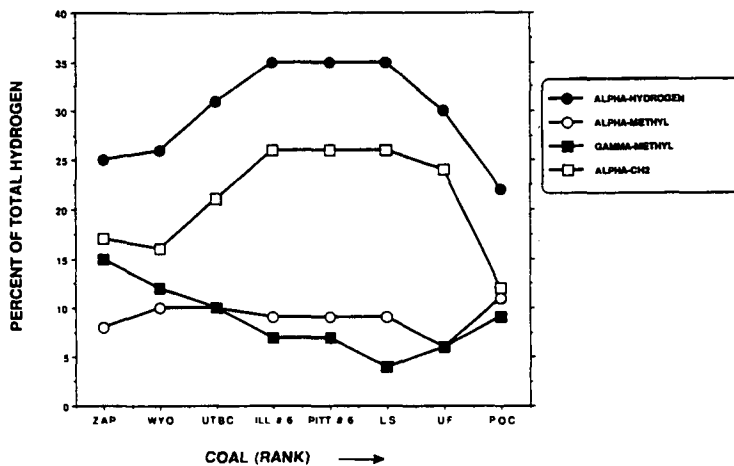


Figure 7. Aliphatic proton structural parameters of the APCS coals.

## ORGANIC VOLATILE MATTER AND ITS SULFUR-CONTAINING COMPOUNDS PRODUCED BY COAL PYROLYSIS

M.-J.M. Chou, C.W. Kruse, and J.M. Lytle, Illinois State Geological Survey, Champaign, IL 61820  
K.K. Ho, Illinois Clean Coal Institute, Carterville, IL 62918-0008

Keywords: coal, pyrolysis, volatile matter

### INTRODUCTION

The types and distributions of the major components in the volatile matter produced from two types of coal pyrolysis were examined. Batch pyrolysis was used to produce coal tars for fractionation and characterization. Flash pyrolysis, in combination with gas chromatography (GC) analysis, showed a broad distribution of the volatile organics, including sulfur-containing compounds. Further characterization of these volatile sulfur compounds should provide the understanding needed of coal's behavior during thermal processing, an understanding critical for cleaning coal through flash pyrolysis or thermal pre-treatment processes.

### EXPERIMENTAL

**Tar Collection, Separation, and Characterization - Batch Pyrolysis:** About 100 g of coal was pyrolyzed at 450 °C or 600 °C in a Parr reactor (1). The tar was delivered through a heated quartz tube to a collection flask containing a mixture of tetrahydrofuran and dimethoxypropane at -30 °C. After evaporation of the solvents, the tar was fractionated into acid, base, neutral-nitrogen, saturates, and aromatic fractions by ion-exchange, coordination, and adsorption chromatography (SARA) (2). The *n*-paraffins, separated from the saturates by a molecular sieve method (3), were analyzed by GC. Three solvents (5% benzene in pentane, 15% benzene in pentane, and 20% benzene/20% ethyl ether/60% methanol) were used to separate aromatic fractions into three subfraction by column chromatography on alumina. The fractions were designated monoaromatics, diaromatics and polyaromatics, and identified as SAF-1, SAF-2, and SAF-3, respectively (4). Elemental analyses were performed on each subfraction.

**On-line Analysis of Volatile Matter from Flash Pyrolysis:** A Perkin-Elmer 3920B gas chromatograph (GC) with a flame photometric detector (FPD) and a flame ionization detector (FID) and a Dexsil-300 column (programmed for 8 °C/min from 50 °C to 280 °C) was used. Coal volatile matter was produced by a Chemical Data System pyroprobe 190 pyrolyzer in the GC's injection port. Pulverized coal (5 mg to 15 mg) in a 25 mm by 2.4 mm quartz tube was heated at 75 °C/msec in the GC's helium carrier gas flowing at 30 mL/min. Samples were preheated at 100 °C for 30 seconds prior to the first analysis. A given sample was analyzed at 300 °C, 400 °C, 500 °C, 600 °C, 700 °C, and 800 °C. The pyroprobe temperature was held at each temperature for 20 seconds and then it was allowed to return to the injection port temperature during the 37 minutes required for the GC analysis of the volatile matter from each step using the FID. A new coal sample was analyzed at 600 °C with FPD for sulfur compounds.

### RESULTS AND DISCUSSION

**Batch Pyrolysis Products:** The amount of tar obtained from the pyrolysis of six coals (Table 1) varied from 3 to 15 weight percent of the raw coal and the yields were approximately proportional to the H/C atomic ratio of the raw coal. Yields of fractions separated from each coal by the SARA method are also listed in Table 1. The aromatic fraction was generally the largest fraction in the tars. Elemental analysis of the SARA fractions from one coal sample (Table 2) showed most of the nitrogen to be in the base fraction. Sulfur was more evenly distributed but it too was highest in the base fraction.

The C, H, N, and S contents of the three aromatic subfractions are listed in Table 3. The H/C ratio decreased as expected for a progression of increasing aromaticity from monoaromatics (SAF-1) to the polyaromatics (SAF-3). Sulfur in the aromatic fractions was detected only in the polyaromatic subfractions, and this trend was observed both at 450 °C and 600 °C. The nitrogen content within the aromatic subfractions varied in a similar fashion, especially at 600 °C. The lack of sulfur and nitrogen in the monoaromatics and diaromatics fractions may be due a higher ratio of the functional group(s) to carbon atoms in the hydrocarbon portion of the molecule, or to having both sulfur and nitrogen in the same small molecule. Either factor might result in the partitioning of these aromatics into earlier SARA fractions,

possibly the basic fraction. Further study is needed to identify the S and N functional groups and learn more about their positions in the structure of molecules in order to understand the solvent partitioning properties seen in this study and other studies (3, 5). GC/FPD chromatograms of two SAF-3 fractions show most of the sulfur-containing compounds to be in the GC retention time range starting with dibenzothiophene and beyond as expected of a polyaromatic fraction. They also indicated that the distribution of sulfur-containing compounds of the high-sulfur Illinois coal (Figure 1, B) was much more complex than those of the low-sulfur Alabama coal (Figure 1, A).

Patterns among tars for the distribution of  $n$ -paraffins are indicated in Figure 2. The effect of different pyrolysis temperatures (450 and 600 °C) on  $n$ -paraffins distribution of the same coal sample was minor. Calkins et al. (6) who studied flash pyrolysis of pure  $n$ -paraffins and also low-temperature tar showed that  $n$ -paraffins in low temperature tar (<600 °C) were the precursors of light hydrocarbon gases, such as ethylene and propylene, that were produced when the low temperature tar was further subjected to a much higher temperature (700-800 °C) heating. The current results indicated that there was not much more cracking of  $n$ -paraffins at 600 °C than at 450 °C. The distribution of chain lengths appeared to be related to coal rank. As indicated in Figure 2, the major  $n$ -paraffins from lignite were distributed between C<sub>14</sub> and C<sub>21</sub>. The distributions of the major  $n$ -paraffins produced from high volatile bituminous (hvCb) and medium volatile bituminous (mvb) coals were in a relatively narrow carbon number band compared to the broad band obtained from the lignite sample, and they peaked at C<sub>17</sub>. The two pyrolysis temperatures (450 and 600 °C) appeared to induce a similar thermal extraction of  $n$ -paraffins in coal (7,8). The lower rank, less mature LigA contains more longer chain  $n$ -paraffins than the higher rank, relatively more mature hvCb and mvb coals.

Cross Polarization/Magic Angle Spinning (CP/MAS) solid state <sup>13</sup>C NMR has been used to determine the aliphatic and aromatic compositions of the raw coals (9). In this study, three raw coals were analyzed by the CP/MAS NMR. The analysis condition and peak assignment are described elsewhere (10). The percent of total carbon in aliphatic positions was 48% for LigA coal, 54% for the hvCb, and 34% for the mvb coal. Comparison of the NMR data with the  $n$ -paraffins data from batch pyrolysis suggests that more paraffin, algae/resins-derived material (11) is found during the relatively early stages of coalification, and perhaps more branch/cyclic or aromatic associated aliphatic material occurs in coal at later stages of coalification. The NMR analysis does not distinguish among these aliphatic types.

**Flash Pyrolysis Products:** Typical step wise pyrolysis GC/FID chromatograms of LigA, hvCb and mvb coals are shown in Figure 3. The chromatograms of these coals indicated that volatilization of heavy hydrocarbons in coal took place mainly between 500 °C and 700 °C. The maximum production appears to be rank dependent. The maximum volatility appears to be lower than 600 °C for lignite, at 600 °C for hvCb coal, and higher than 600 °C for mvb coal (Figures 3a, 3b, and 3c, respectively). These observations are consistent with those of Barker (12) on programmed-temperature pyrolysis of vitrinite of various rank coals. His programs, showing the GC detector response as a function of temperature, indicated a single maximum at 660 °C for higher rank samples and 420 °C for lignite samples.

In the present study, through GC fingerprint analysis, volatile organics were examined in more detail in the C<sub>15</sub>+ region. The components in this region appeared to be less branched for the lignite. The proportion of the long straight chain aliphatic components decreased as the rank of the coal increased from ligA, hvCb, to mvb. These results are consistent with the earlier suggestion that the low-rank coal contained a greater degree of longer chain aliphatic hydrocarbons.

GC chromatograms of volatile organic sulfur compounds produced from flash pyrolysis of three coals at 600 °C were compared. As indicated in Figure 4, the GC fingerprint of products from the high-sulfur Illinois coal (hvCb) was much more complex than those of the low-sulfur Alabama coal (mvb) and the low-sulfur North Dakota lignite (LigA). The GC chromatogram of sulfur compounds from high sulfur Illinois hvBb coal has material with retention times expected of aliphatic sulfides, thiophene, and alkylthiophene isomers. The large envelop fraction at 15 minutes to 40 minutes retention time corresponds to retention times expected of benzothiophene and dibenzothiophene having an array of side chains. Additional high-sulfur Illinois coals were analyzed. Their fingerprints (not shown) indicate that the types of volatile organic sulfur compounds in other Illinois coals were quite similar. They were present in a much greater variety and in larger quantities than those of either the Alabama coal or the North Dakota lignite. The GC/FPD chromatograms obtained from the flash pyrolysis of raw coal were consistent with those of SAF-3 fractions

(Figure 1). They indicated that the distribution of sulfur-containing compounds of the high-sulfur Illinois coal was much more complex than that of the low-sulfur coal. Flash pyrolysis of raw coal with on-line GC/FPD analysis of sulfur volatile matter (Figure 4) showed sulfur-containing compounds as a broad peak in the region corresponding to retention times for benzothiophene (two aromatic rings) and dibenzothiophene (three aromatic rings). The sulfur compounds in the SAF-3 fractions (Figure 1) are better resolved. The absence of sulfur in SAF-1 and SAF-2 (Table 3), despite the presence sulfur compounds in pyroprobe products corresponding to their molecular weight range (Figure 1), suggests that sulfur in this molecular weight range may be in basic nitrogen molecules separated by the SARA method into another fraction.

### SUMMARY AND CONCLUSION

With one exception, the aromatic fraction was the largest fraction isolated. The sulfur-containing compounds were observed to concentrate in the polyaromatic subfraction of the three aromatic subfractions, and this tendency was observed for both 450°C and 600°C samples. This study indicated that the distribution of sulfur-containing organic compounds in the tar produced from the high-sulfur Illinois coal was much more complex than that of the low-sulfur coal. Although there are numerous sulfur compounds in flash pyrolysis products having molecular weights up through those of benzothiophene and dibenzothiophene, sulfur compounds did not appear in the monoaromatics and diaromatics subfractions. We postulate that sulfur in the molecular weight compounds below dibenzothiophene may be in compounds having a basic nitrogen as well. Sulfur as well as nitrogen were the highest in the SARA base fractions as would be expected by this postulate. This would account for the absence of this molecular weight range of sulfur compounds in the SARA aromatic fraction. The nitrogen compounds in batch pyrolysis tars partitioned mainly into the base fraction of the tar, whereas the sulfur-containing compounds were more evenly distributed between the base, neutral-nitrogen, and aromatic fractions. This study also indicated that flash pyrolysis in a pyroprobe is a fast method to screen and compare sulfur-containing compounds produced during thermal treatment of coals of different rank.

The observation that the distributions of *n*-paraffins in tars produced at 450°C or 600°C from a given coal were essentially the same supports the view that these *n*-paraffins are thermal extraction products, not cracking products. The variations in the distributions of the *n*-paraffins from coals of different rank show that the lower rank, less mature LigA contained more longer chain *n*-paraffins than the higher ranks. The NMR spectra of raw coal together with the batch pyrolysis *n*-paraffins GC analysis support the view that algae/resins-derived *n*-paraffinic material occurring during the relatively early stages of coalification may have been converted to branched/cyclic material and ultimately either eliminated as light hydrocarbons or converted to aromatics as coalification progressed toward anthracite. The preponderance of relatively long chain aliphatic hydrocarbons in low-rank coal was also seen in the GC spectra of flash pyrolysis products.

### ACKNOWLEDGMENTS

Support for this research was provided by the Illinois State Geological Survey and the U.S. Environmental Protection Agency, Fuel Process Branch, Research Triangle Park, North Carolina, under Contract 68-02-2130 to the University of Illinois: "Characterization of Coal and Coal Residues." The current publication and continued research on coal desulfurization are supported by the Illinois Clean Coal Institute (ICCI). The authors are indebted to D.R. McKay, and J.S. Frye of the Colorado State University for NMR analysis and to two members of the ISGS staff, R.H. Shiley for coal tar generation by batch pyrolysis and D.D. Dickerson for the technical assistance in coal tar fractionation.

### REFERENCES

1. Cahill, R.A., R.H. Shiley, and N.F. Shimp, 1982, "Forms and Volatiles of Trace and Minor Elements in Coal," Illinois State Geological Survey, EGN 102:6.
2. Jewell, D.M., J.H. Weber, J.W. Bunker, H. Plancher, and D.R. Latham, 1972, "Ion-Exchange, Coordination, and Adsorption Chromatographic Separation of Heavy-Petroleum Distillates," *Anal. Chem.*, 44:1391-95.
3. O'Connor, J.G., F.H. Burow, and M.S. Norris, 1962, "Determination of normal paraffins in C<sub>20</sub> to C<sub>32</sub> paraffins waxes by molecular sieve chromatography," *Anal. Chem.*, 34(1):82-85.
4. Selucky, M.L., Y. Chu, T. Ruo, and O.P. Strausz, 1977, "Chemical Composition of Athabasca Bitumen," *Fuel*, 56: 369-381.

5. Farcasiu, M., 1977, "Fractionation and Structural Characterization of Coal Liquid," *Fuel*, 56:9-14.
6. Calkins, W.H., and R.J. Tyler, 1984, "Polymethylene Compounds in Low-Temperature Flash Pyrolysis Tars," *Fuel*, 63:1119-1124.
7. Given, P.H., A. Marzec, W.A. Barton, L.J. Lynch, and B.C. Gerstein, 1986, "The Concept of a Mobile or Molecular Phase Within the Macromolecular Network of Coals: A Debate," *Fuel*, 65:155-164.
8. Yun, Y., H.L.C. Meuzelaar, N. Simmleit, and H.-R. Schulten, 1991, "Mobile Phase in Coal Viewed from a Mass Spectrometric Perspective," In *ACS Symposium Series*, 461:89-110.
9. Solum, M.S., R.J. Pugmire, and D.M. Grant, 1989, "<sup>13</sup>C Solid-State NMR of Argonne Premium Coals," *Energy and Fuels*, 3(2):187-193.
10. Chou, M.-I.M., D.R. Dickerson, D.R. McKay, and J.S. Frye, 1984, "Characterization of Coal Chars from a Flash Pyrolysis Process by Cross Polarization/Magic Angle Spinning <sup>13</sup>C NMR," *Liquid Fuels Technology*, 2(4):375-384.
11. Colin, E.S., W.R. Landner, and K.D. Bartle, 1985, "Fate of Aliphatic Groups in Low-Rank Coals During Extraction and Pyrolysis Processes," *Fuel*, 64:1394-1400.
12. Barker, C., 1974, "Programmed-Temperature Pyrolysis of Vitrinites of Various Rank," *Fuel*, 53:176-177.

Table 1. Yields of pyrolysis products from six coal samples

Coal	(seam)	Blue Creek	Herrin (No. 6)	Herrin (No. 6)	Herrin (No. 6)	Springfield (No. 5)	Ft. Union Formation
Coal Sample Number		C-18848	C-18857	C-16501	C-18560	C-16264	C-18440
State		Alabama	Illinois	Illinois	Illinois	Illinois	N. Dakota
Rank		mvb	hvBb	hvBb	hvCb	hvCb	ligA
H/C Atom Ratio (mf)		0.67	1.05	0.85	0.85	0.85	0.78
Type of sample		composite face channel	face channel	composite face channel	column	composite face channel	face channel
Tar Yield (wt %)	450°C	3.2	14.5	10.4	12.1	11.9	7.3
	600°C	3.1	14.6	15.8	12.2	13.8	8.3
Tar Sample No.	450°C	T-18848	T-18857	T-16501	T-18560	T-16264	T-18440
Tar fraction recovered from chromatography (wt%)							
	Acid	10.4	11.7	26.0	11.1	52.2	10.4
	Base	2.5	2.7	1.0	8.6	2.3	5.1
	Neutral-Nitrogen	--	2.4	2.0	10.5	--	3.4
	Saturate	3.9	5.4	9.0	5.7	8.6	8.2
	Aromatic	57.1	24.9	35.0	46.9	27.6	29.9
Tar Sample No.	600°C	T-18848	T-18557	T-16501	T-18560	T-16264	T-18440
Tar fraction recovered from chromatography (wt%)							
	Acid	27.5	10.3	--	9.3	47.9	12.2
	Base	2.0	5.2	--	7.4	4.0	5.1
	Neutral-Nitrogen	--	5.4	--	0.5	--	3.9
	Saturate	3.5	5.6	--	6.1	7.5	14.5
	Aromatic	57.6	39.1	--	49.0	27.6	46.8

-- not determined

Table 2. Elemental analyses acid, base, and neutral-nitrogen, saturate, and aromatic fractions derived from coal sample C18440.

Fraction	Carbon	Hydrogen	Nitrogen	Sulfur	H/C Atom Ratio
Acid	78.75	7.81	0.12	0.56	1.18
Base	77.29	7.73	3.85	1.13	1.21
Neutral-Nitrogen	78.42	8.18	0.38	0.90	1.25
Saturate	79.75	12.22	--	--	1.84
Aromatic	79.50	9.22	0.30	1.05	1.39

-- not determined

Table 3. Elemental analysis of aromatic subfractions

Coal (seam)		Blue Creek	Herrin (No.6)	Springfield (No. 5)
Tar Sample Number		T-18848-450 °C	T-16501-450 °C	T-16264-450 °C
Aromatic Subfraction 1 monoaromatics (eluted with 5% benzene in n-pentane)	Carbon	89.64	87.06	84.24
	Hydrogen	9.77	10.70	11.60
	Nitrogen	trace	0.18	0.21
	Sulfur	--	--	--
	H/C Atom Ratio	1.30	1.46	1.64
Aromatic Subfraction 2 diaromatics (eluted with 15% benzene in n-pentane)	Carbon	89.97	87.26	84.91
	Hydrogen	8.02	8.21	9.03
	Nitrogen	0.23	0.07	0.25
	Sulfur	--	--	--
	H/C Atom Ratio	1.14	1.12	1.27
Aromatic Subfraction 3 polyaromatics (eluted with mixed solvent: 20% benzene, 20% ethyl ether and 60% methanol)	Carbon	85.81	82.48	84.41
	Hydrogen	7.30	7.32	7.44
	Nitrogen	0.53	0.14	0.24
	Sulfur	1.10	2.37	2.37
	H/C Atom Ratio	0.97	1.06	1.05
<hr/>				
Tar Sample Number		T-18848-600 °C	T-16501-600 °C	T-16264-600 °C
Aromatic Subfraction 1 monoaromatics (eluted with 5% benzene in n-pentane)	Carbon	87.25	87.74	86.71
	Hydrogen	9.55	10.20	10.70
	Nitrogen	--	--	--
	Sulfur	--	--	--
	H/C Atom Ratio	1.30	1.39	1.47
Aromatic Subfraction 2 diaromatics (eluted with 15% benzene in n-pentane)	Carbon	90.55	86.14	85.45
	Hydrogen	7.71	7.25	8.01
	Nitrogen	--	--	--
	Sulfur	--	--	--
	H/C Atom Ratio	1.01	1.01	1.12
Aromatic Subfraction 3 polyaromatics (eluted with mixed solvent: 20% benzene, 20% ethyl ether and 60% methanol)	Carbon	86.88	81.90	80.92
	Hydrogen	7.04	6.90	7.81
	Nitrogen	0.35	0.34	0.90
	Sulfur	0.80	3.93	4.29
	H/C Atom Ratio	0.97	1.01	1.15
-- not detectable				

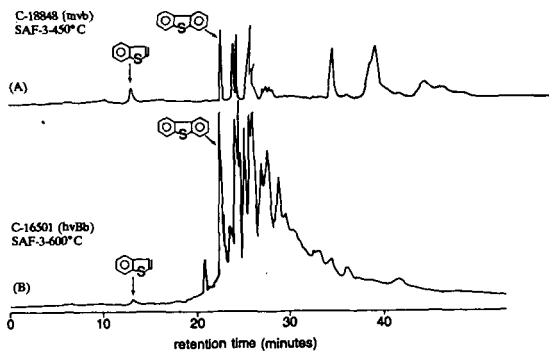


Figure 1. Typical GC/FPD chromatogram of SAF-3 fraction from a low-sulfur Alabama coal (A) and a high-sulfur Illinois coal (B).

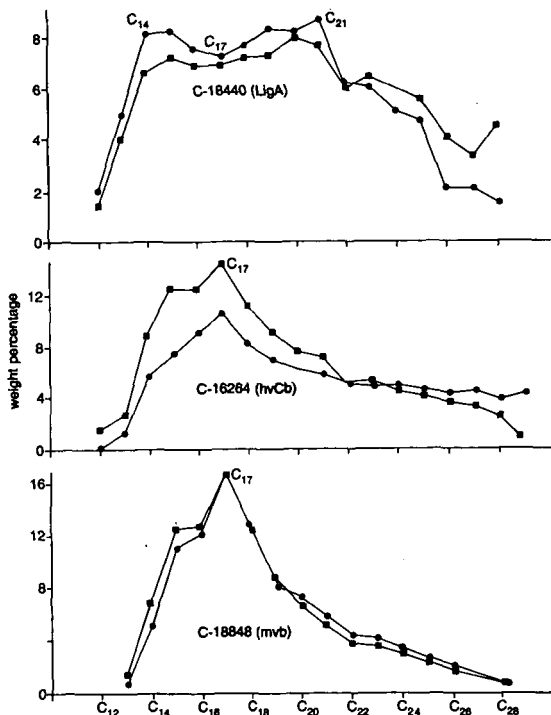


Figure 2. Distribution of n-paraffins obtained from batch pyrolysis three different ranks of coal at 450°C (●) and 600°C (■).

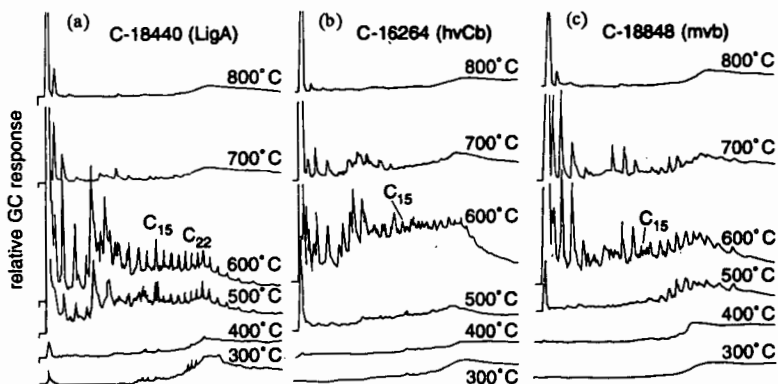


Figure 3. GC/FID chromatogram of organic compounds produced from stepwise flash pyrolysis of three different ranks of coal.

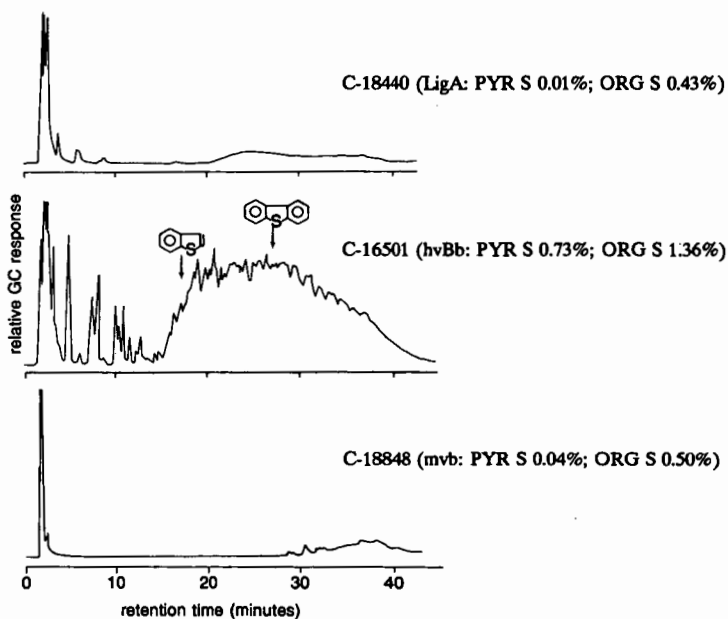


Figure 4. GC/FPD chromatogram of volatile sulfur compounds produced from flash pyrolysis of three different ranks of coal at 600°C.

## DEVELOPMENT OF PROCESS TO SIMULTANEOUSLY SCRUB $\text{NO}_2$ AND $\text{SO}_2$ FROM COAL-FIRED FLUE GAS

A.B. Evans, R.K. Lyon, J.N. Pont, G.C. England, W.R. Seeker  
Energy and Environmental Research  
18 Mason  
Irvine, CA 92718

V. Zamansky  
Research Cottrell  
P.O. Box 1500  
Somerville, N.J. 08876

Key Words:  $\text{NO}_2$  scrubbing, Combi $\text{NO}_x$ , Na/Ca based scrubbers.

### INTRODUCTION

The Combi $\text{NO}_x$  process is being developed to provide a low-cost method of controlling the  $\text{NO}_x$  emissions of coal-fired utility boilers to very low levels. This process incorporates a family of  $\text{NO}_x$  reduction technologies including staged combustion, Advanced Reburning (i.e. reburning combined with selective non-catalytic reduction) and methanol injection to convert  $\text{NO}$  to  $\text{NO}_2$  which can then be removed by wet scrubbing. While individually these technologies are limited in their  $\text{NO}_x$  reducing capabilities, in combination they are capable of reducing  $\text{NO}_x$  emissions to extremely low levels at a fraction of the cost of selective catalytic reduction.

The methanol injection step, however, is subject to the limitation that one must have a scrubber that will remove  $\text{NO}_2$ . The removal of  $\text{SO}_2$  and  $\text{NO}_2$  by sodium-based wet scrubbers is a well-established technology, but the majority of wet scrubbers currently in use are calcium based. Accordingly, this study was undertaken to determine whether or not the chemistry which occurs in calcium based scrubbers could be modified to allow removal of  $\text{NO}_2$  as well as  $\text{SO}_2$ .

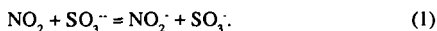
Bench-scale experiments were performed in conjunction with chemical computational modeling to evaluate the effect of scrubbing solution composition on  $\text{SO}_2$  and  $\text{NO}_2$  scrubbing efficiency. In addition, potential by-products were identified. Finally, larger pilot-scale tests were performed with a packed tower scrubber to address scale-up issues and confirm the bench-scale results.

### BENCH-SCALE STUDIES

The bench-scale  $\text{NO}_2$  scrubbing apparatus is displayed in Figure 1. A simulated flue gas containing variable amounts of  $\text{NO}_2$  and  $\text{SO}_2$  was flowed through a constant temperature, 80 cubic centimeter, bubbler containing the scrubbing solution to be evaluated. After passing through the "scrubber", the gas was analyzed for  $\text{O}_2$ ,  $\text{NO}_x$ ,  $\text{N}_2\text{O}$ , and  $\text{SO}_2$  to determine removal efficiencies.

Figure 2 graphically summarizes the bench-scale results. The numbers symbolize various cases that were performed while varying slurry composition, the lines show the resulting performance as a

function of time. A  $\text{Ca}(\text{OH})_2$  solution (2 percent  $\text{Ca}(\text{OH})_2$  by weight) achieved 99+ percent  $\text{SO}_2$  reduction, indicating that the scrubber provides good mass transfer. However, only 50 percent of the  $\text{NO}_2$  was removed. Reference 1 indicates that the crucial reaction for  $\text{NO}_2$  scrubbing is:



With pure  $\text{Ca}(\text{OH})_2$  solution, the necessary sulfite ion ( $\text{SO}_3^{2-}$ ) tends to precipitate out as calcium sulfite, instead of reacting, as desired, with  $\text{NO}_2$ .

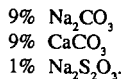
Since sodium sulfite ( $\text{Na}_2\text{SO}_3$ ) can provide the necessary sulfite ions for  $\text{NO}_2$  absorption, a 2 percent solution was evaluated. 99+ percent  $\text{SO}_2$  and 89 percent  $\text{NO}_2$  capture was obtained initially, however, this performance decreased after approximately 2 minutes of run time. After these 2 minutes,  $\text{SO}_2$  reduction became negative and  $\text{NO}_2$  reduction dropped to 17%.  $\text{SO}_2$  is captured via the reaction



and  $\text{NO}_2$  via reaction (1). Unfortunately, the  $\text{SO}_3^-$  generated by  $\text{NO}_2$  removal is a chain carrier in the oxidation of sulfite and bisulfite ions to sulfate and bisulfate ions. Oxidation of the bisulfite ion to the bisulfate ion acidifies the solution, forcing  $\text{SO}_2$  back into the gas phase.

Adding  $\text{Ca}(\text{OH})_2$  to the  $\text{Na}_2\text{SO}_3$  scrubbing solution eliminates the problem of  $\text{SO}_2$  rejection by keeping the solution basic, however the  $\text{NO}_2$  capture remains poor and short lived. Replacing the highly soluble  $\text{Ca}(\text{OH})_2$  with very low solubility  $\text{CaCO}_3$  increases the concentration of sulfite ion that stays in solution. This improves  $\text{NO}_2$  absorption, but the sulfite ion quickly oxidizes to sulfate, hampering  $\text{NO}_2$  removal. Experiments were conducted under conditions which inhibited the oxidation of sulfite to sulfate (i.e. decreasing reaction temperature and/or flue gas oxygen content). Even though these conditions can not be applied to a real application, they did show that if sulfite ion stays in solution,  $\text{NO}_2$  capture improves and can be sustained for a longer period of time.

Sodium thiosulfate ( $\text{Na}_2\text{S}_2\text{O}_3$ ) has been proposed as a method of inhibiting the oxidation of sulfite to sulfate (2). We found that by adding this compound to the scrubbing solution (1% by weight), 95%  $\text{NO}_2$  capture was achieved and this capture was sustained for the duration of the test. Based on these results, the recommended slurry solution to achieve 99+ percent  $\text{SO}_2$  and 95 percent  $\text{NO}_2$  at bench-scale level is:



This scrubbing mixture was studied computationally using the mechanism of Chang et al. (1). For the batch experiments, the reaction was found to proceed in three stages. During the first stage, carbonate ion concentration falls while the concentrations of sulfate, bisulfate and sulfite ion increase. This first stage ends when the ratio of carbonate to sulfite ion becomes so low that calcium carbonate starts to dissolve while calcium sulfite precipitates. During the second stage, the ratio of the concentrations of carbonate and sulfite ion are constant and the pH remains fairly steady. The

concentration of sulfate ion increases until calcium sulfate starts to precipitate. The second stage ends when the calcium carbonate is exhausted. When this happens the pH begins to rise until it reaches a level at which  $\text{SO}_2$  absorption fails and scrubbing solution is spent.

The model predicts that  $\text{NO}_2$  capture will remain effective through these three stages of the process, but the fate of absorbed  $\text{NO}_2$  changes. During the first and second stages nearly all of the absorbed  $\text{NO}_2$  will be present as nitrite ion, with only trace amounts of the complex nitrogen sulfur ions being formed. During the third stage, however, the nitrite ion is converted to complex nitrogen sulfur ions, chiefly the aminetrisulfonate ion. Near the end of the third stage the aminetrisulfonate ions are hydrolyzed to sulfate ion and sulfamic acid.

While the model contains reactions which are capable of forming  $\text{N}_2\text{O}$  and nitrate ions, these reactions are only significant at very low pH. During the bench-scale experiments samples were taken of the bubbler's exhaust and, consistent with the models predictions, no significant  $\text{N}_2\text{O}$  production was observed. Measurements were also made with EM Quant test strips on spent scrubbing solution. As one would expect from the model, nitrite ion was found in fresh solution but not in solution which had been allowed to age. Nitrate ions were not detected in the spent solution.

#### PILOT-SCALE STUDIES

Scale-up effects were investigated in two different pilot-scale facilities corresponding nominally to heat inputs of 2 MMBtu/hr and 10 MMBtu/hr. The small pilot-scale scrubber tests were performed by Research Cottrell using the facility illustrated in Figure 3. The small pilot-scale scrubber consists of a propane combustor, absorber tower, absorber feed tank, analytical train, and solid disposal system. To simulate a coal-fired flue gas, variable amounts of  $\text{SO}_2$  and  $\text{NO}_2$  were doped into the exhaust upstream of the absorber tower. At the absorber tower exit,  $\text{NO}_x$ ,  $\text{SO}_2$ ,  $\text{CO}$ , and  $\text{O}_2$  were measured. The absorber tower is a vertical, stainless steel, 16 inch diameter tube, approximately 20 feet in height. The simulated flue gas enters the tower from the bottom, travels through five sections to the top, and exits to the gas sample conditioning systems and analyzers. The first two sections can be packed with a light packing material to provide improved gas/liquid contact. Sections of the tower may also be removed, if desired, to reduce absorber tower residence time. The scrubber slurry is continually being mixed with dry limestone, sodium salts, and water in the absorber feed tank. From the 200-gallon feed tank, the slurry is pumped to the top of the absorber tower and dispensed in counter flow to the flue gas with a single slurry nozzle. The slurry solution is drained by gravity from the bottom of the tower back to the feed tank.

The first tests were performed to verify that  $\text{SO}_2$  removal was possible on the pilot-scale scrubber. For a 6 percent limestone slurry, flue gas flow rates were varied between 127 - 140 cfm, and slurry flow rates were maintained at 12 gpm. Up to 99 percent  $\text{SO}_2$  removal was obtained indicating satisfactory mass transfer.

Simultaneous scrubbing of  $\text{NO}_2$  and  $\text{SO}_2$  was evaluated using scrubbing salts consisting of 49.5 percent  $\text{CaCO}_3$ , 49.5 percent  $\text{Na}_2\text{CO}_3$ , 1 percent  $\text{Na}_2\text{S}_2\text{O}_3$ . Note this is approximately 1/5 of the concentration of  $\text{Na}_2\text{S}_2\text{O}_3$  utilized in the bench-scale tests. During this test series, the following parameters were varied: liquid/gas ratio (liquid flow and gas flow were independently varied),

concentration of sodium carbonate in slurry, concentration of sodium thiosulfate in slurry, and initial  $\text{NO}_2$  concentration.  $\text{NO}_2$  removal efficiency ranged between 65 and 90 percent while maintaining 97 - 99 percent  $\text{SO}_2$  removal.

The ratio of slurry flow rate to flue gas flow rate is defined as the liquid to gas ratio (L/G), and is expressed here in units of (gallons of slurry)/(1000 cubic feet of gas). The slurry flow and gas flow were varied independently of one another. Figure 4 summarizes the effects of L/G ratio on  $\text{NO}_2$  scrubbing efficiency. As would be expected, a larger L/G ratio results in higher  $\text{NO}_2$  removal. Even though not depicted in the figure, data indicate that gas flow rate has a larger affect on the  $\text{NO}_2$  scrubbing efficiency than slurry flow rate. By decreasing the gas flow rate by a small fraction (from 135 to 115 cfm), efficiency increased from 77 to 84 percent. However, when the slurry flow rate was nearly doubled (11.4 to 20 gpm), the efficiency only increased by approximately the same amount, 77 to 85 percent.

Experiments were performed to determine the effect of initial  $\text{NO}_2$  concentration on  $\text{NO}_2$  scrubbing efficiency. Slurry flow rate remained approximately constant as inlet  $\text{NO}_2$  concentration was varied by adjusting the doping gas flow rate. Results are displayed in Figure 5. The general trend shows that scrubbing effectiveness drops as initial  $\text{NO}_2$  concentrations increase.

The effect of  $\text{Na}_2\text{CO}_3$  concentration on  $\text{NO}_2$  and  $\text{SO}_2$  scrubbing efficiency was evaluated by diluting the scrubbing solution by a factor of two, while continuing to add limestone to maintain pH and ion concentration. Figure 6 shows that even though scrubbing efficiency was initially hampered by the dilution that occurs 200 minutes into the test, with time the  $\text{NO}_2$  removal efficiency rose again to approximately the same level as before the dilution. Even after diluting the slurry a second time, the  $\text{NO}_2$  scrubbing efficiency returned to almost the original value. These data indicate that  $\text{NO}_2$  removal efficiency is not sensitive to  $\text{Na}_2\text{CO}_3$  concentration in this range.

The effect of sodium thiosulfate concentration was tested by adding an additional 3.8 mmol of sodium thiosulfate per liter of solution. As expected,  $\text{NO}_2$  removal efficiency jumped from 65 percent to 89-90 percent within 15 minutes, and  $\text{SO}_2$  removal efficiency remained at 99+ percent. The thiosulfate inhibits oxidation of sulfite to sulfate, sustaining the presence of sufficient sulfite ions for  $\text{NO}_2$  capture.

Throughout the experiments discussed above, scrubbing solution composition measurements were periodically taken. In general, these observations were consistent with the model and the assumption that the scrubber was operating in the second stage (see previous discussion). The model is, however, limited in its ability to account for sulfite ion oxidation, therefore, not surprisingly, sulfite to sulfate conversion was much higher than predicted. The small pilot-scale studies also show nitrate ion as a major product, contradicting both model's prediction and the bench-scale results.

A single test was performed in EER's large pilot-scale facility. The large pilot-scale scrubber facility consists of a simple spray tower with a pad-type demister. The spray tower is 6 ft in diameter and 16 ft high, with an array of 16 spray nozzles. Natural gas combustion products were doped with  $\text{NO}_2$  to a concentration of 74 ppm.  $\text{SO}_2$  was not added. The test was conducted at an L/G ratio of approximately 30 gal/1000 acf and the scrubbing solution was 9 percent  $\text{CaCO}_3$ /9 percent  $\text{NaOH}$ /1

percent  $\text{Na}_2\text{S}_2\text{O}_3$ . The test results are also shown in Figure 4. Much higher  $\text{NO}_2$  removal was achieved than was expected based on the small pilot-scale results. This may have been due to the much higher concentration of sodium thiosulfate used in the large pilot-scale test. However, additional tests are necessary to validate this hypothesis. The results do indicate that high  $\text{NO}_2$  removal efficiencies can be achieved even with a relatively primitive scrubbing system operating at L/G ratios similar to that of large commercial scrubbers.

## DISCUSSION

The primary goal of this research, demonstration of efficient  $\text{NO}_2$  and  $\text{SO}_2$  scrubbing in a calcium based wet limestone scrubber, has been achieved. Two important questions, however, remain with respect to the disposability of the products produced by this modified scrubber. First, there is the question of whether or not using sodium compounds in the scrubbing solution will result in unacceptable sodium contamination of the calcium sulfate/sulfite product. Since wet scrubbers require considerable amounts of makeup water, it is theoretically possible to solve this problem by washing the calcium sulfate/sulfite with the makeup water, but this option would require an engineering design study which has not been done.

The second question of disposability regards the formation of nitrate ion seen in the pilot-scale experiments. This ion formation was not detected during bench-scale or computer modeling studies. One possible explanation for this discrepancy is that as the scrubbing liquid passes downward through the absorber tower, it reaches a point at which its ability to absorb  $\text{SO}_2$  is completely exhausted. This low pH condition was not considered in the modeling study, yet it may be responsible for the increase in nitrate concentration. Mechanisms within the computer model do, in fact, show nitrate ion formation at low pH levels.

While the possible formation of nitrate ion will require further research, there are a number of ways in which this problem might be solved. Adjustment of scrubbing conditions so that the solution is prevented from over-reacting may prevent nitrate formation. Alternatively, if nitrate forms by oxidation of nitrite ion, the removal of nitrite ion by reaction with  $\text{NH}_2\text{SO}_3\text{H}$  may prevent nitrate formation, or, all else failing, nitrate ion could be removed by selective reduction with scrap aluminum (3). In a brief study the authors found that this method works quite well with shredded soda cans as the source of aluminum.

## ACKNOWLEDGMENTS

This work was funded under DOE Contract No. DE-AC22-90PC90363, Development of Advanced  $\text{NO}_x$  Control Concepts for Coal-Fired Utility Boilers. Mr. Charles E. Schmidt of Department of Energy Program Coordinator. The small pilot-scale experimental scrubbing studies were conducted by Research Cottrell under subcontract to EER.

## REFERENCES

1. S.C. Chang, D. Littlejohn and N.H. Lin, *Flue Gas Desulfurization*, ACS Symposium Series 188, American Chemical Society, p. 128 - 152, (1982)
2. E. Gorin, M.D. Kulik, R.T. Struck, U.S. Patent 3,937,788 (1976).
3. A.P. Murphy, *Chemical Removal of Nitrate from Water*, Nature 350, 223-225, (1991).

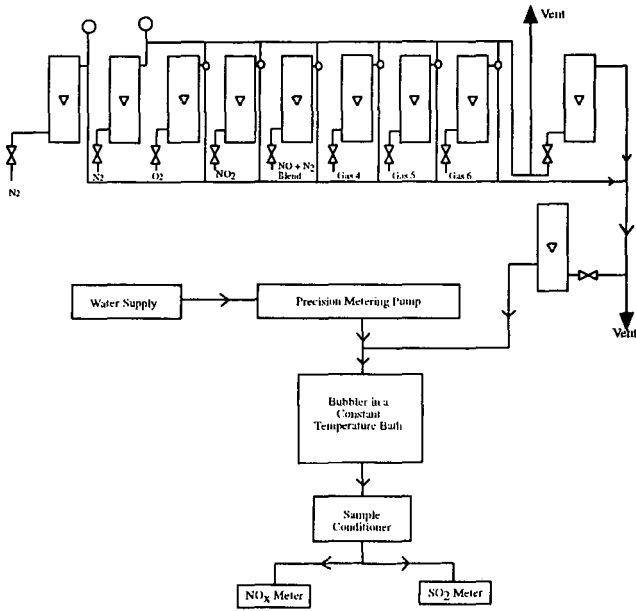


Figure 1. Experimental set-up for  $\text{NO}_2/\text{SO}_2$  scrubbing experiments.

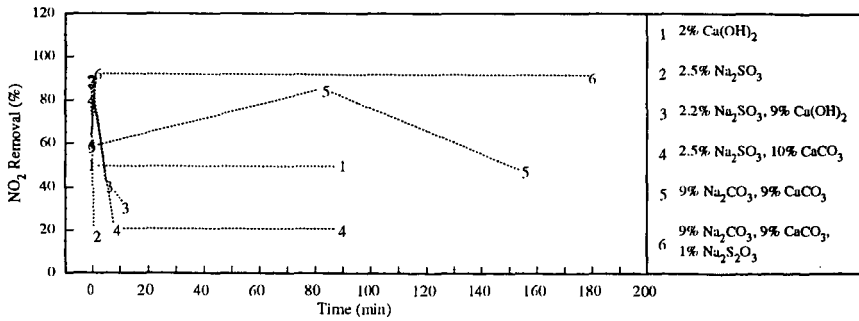


Figure 2. Bench-scale scrubbing studies results.

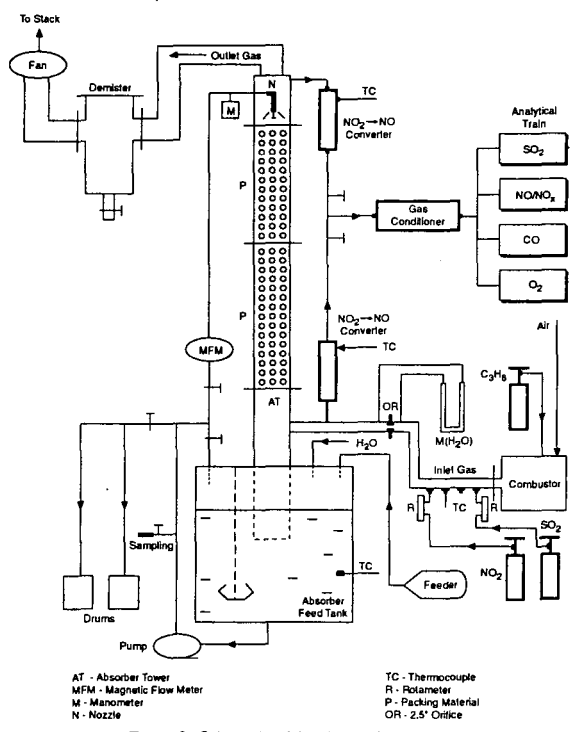


Figure 3. Schematic of the pilot-scale scrubber.

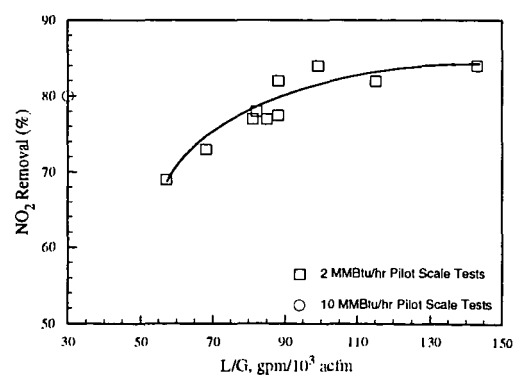


Figure 4. Effect of liquid to gas ratio on NO<sub>2</sub> removal.

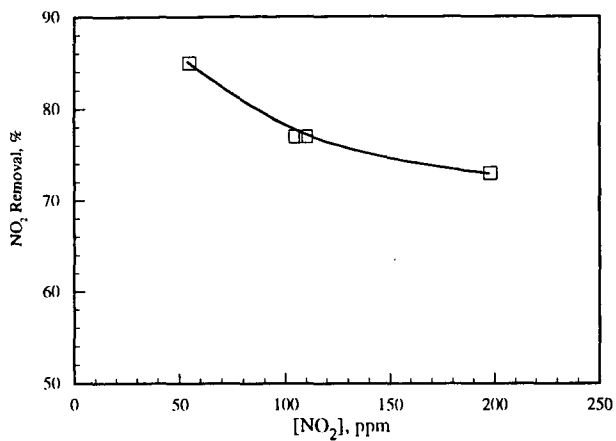


Figure 5. Effect of initial NO<sub>2</sub> concentration on NO<sub>2</sub> removal.

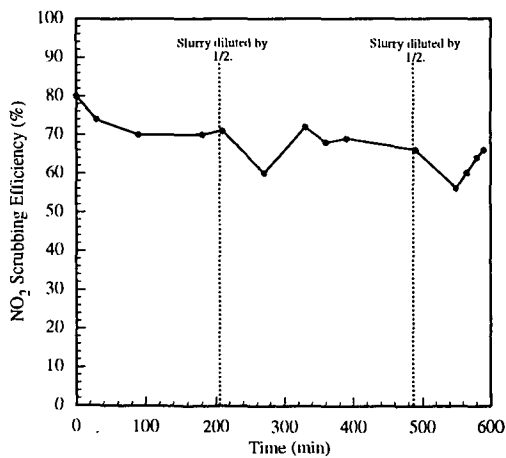


Figure 6. Effect of Na<sub>2</sub>CO<sub>3</sub> dilution on NO<sub>2</sub> scrubbing performance.

THE CHEMISTRY OF  
ELECTROSTATIC PRECIPITATION

P. L. Feldman and K. S. Kumar  
Research-Cottrell  
Somerville, NJ

Keywords: Electrostatic precipitation; corona; electrical  
breakdown; resistivity; chemical conditioning

ABSTRACT

Electrostatic precipitation is a leading means of particulate emissions control for large industrial and utility plants. It effects collection of the particulate matter by charging the particles in a corona discharge and causing them to migrate to a grounded collecting surface under the influence of an electric field. At first it may appear that this process is strictly electrical in nature, but in reality the chemistry of the process is just as important, if not moreso, as the electrical aspects are to the efficiency of the process. The important chemical effects are seen primarily in the gas phase chemistry as it influences electrical breakdown, or sparking, and particle surface chemistry as it influences conductivity and cohesivity. This paper presents examples of the use of chemical methods to enhance the precipitation process including the use of chemical conditioning agents to improve particle conductivity or cohesivity or to increase gas breakdown strength. Also discussed are specific effects of sulfur, sodium, carbon and various metals in determining the viability of electrostatic precipitation in a given application. A section is also devoted to a discussion of the use of corona discharge to promote chemical reactions for air pollution control.

THE ELECTROSTATIC PRECIPITATION PROCESS

Electrostatic precipitation is a leading means for the control of particulate emissions from large industrial and power generation sources. It is capable of very high particulate removal efficiencies, including the control of the submicron particulate fraction. The electrostatic precipitation process is different from other mechanical means of particulate control, such as filters and cyclones, in that it uses electrical forces to separate the particles from the gas stream. These electrical forces are applied by exposing the particles to a corona discharge, thereby charging them electrically, and then placing them in a zone of high electric field strength. The resultant electrical force, proportional to the product of the particle charge and the field strength, moves the particles towards a grounded collecting surface where they are held until periodically rapped into hoppers for disposal. Modern industrial precipitators use the single-stage design which accomplishes the corona discharge and electric field functions simultaneously in a single geometry consisting of high voltage discharge electrodes placed between grounded collecting plates. The discharge polarity in these precipitators is negative. The discharge electrodes themselves are either small-diameter wires or more rigid bodies with points or sharp edges. A sharp radius of curvature

is necessary to concentrate electric field strength to allow corona discharge.

Although electrostatic precipitation is electrophysical in nature, the process efficiency and viability are strongly influenced by other scientific disciplines, especially gas and surface chemistry. In fact much of the original development work of the precipitator was carried out by chemists and metallurgists. Dr. Frederick Cottrell is credited with developing the first practical electrostatic precipitator in the early 1900's. The importance of chemistry in electrostatic precipitation can be understood by looking more closely at some of the performance-limiting aspects of the process, namely gas-phase breakdown, dust layer breakdown and particle reentrainment. Enhancement of the precipitation process can then be achieved by altering the system chemistry toward more favorable conditions.

#### ELECTRICAL BREAKDOWN OF THE GAS PHASE

Electrical breakdown of the gas phase as manifested by sparking limits the operation of the precipitator by imposing a maximum to the voltage which can be applied to the discharge electrodes, thereby limiting the power input to the precipitator as well as the field strength and the supply of corona-generated ions necessary to the process. Since precipitator efficiency can be correlated with power input, this limitation is very important. The levels of voltage and corona current at which sparking will occur is determined by gas density and electrode spacings as well as the chemistry of the gas flowing through the precipitator. In the corona zone, electrons are emitted from the discharge points and move toward the grounded electrode under the influence of the electric field between the discharge electrode and the collecting plate. As they lose their initial energy they tend to attach to gas molecules they encounter on the way, forming negative ions which then travel at much lower velocities toward the grounded electrode, resulting in a more controlled corona current. Gas molecules differ in their receptiveness to attachment of electrons. Nitrogen for example is not receptive. Therefore in pure nitrogen no ions are formed and the current is totally electronic, resulting in high current (because of the high electron velocities) and breakdown at voltages only slightly above corona start. The precipitation process is not practical under these circumstances.

For effective electrostatic precipitation, small amounts of electronegative gases must be present in the gas stream to attach the electrons and, through their lower ionic mobility, provide controlled corona current over a wide range of voltage before breakdown occurs. Such gases include oxygen, water, ammonia, sulfur dioxide, many organic vapors and others. Normal industrial flue gases contain adequate amounts of electronegative gases so generation of stable corona is not usually a problem. However, there are situations in which gas conditioning can be employed to reduce the net ion mobility and achieve more stable operation. An important example is precipitation at low gas density. Such applications include high temperature operations such as precipitators on fluid cat cracker exhaust in the petroleum industry. These precipitators normally operate at about 700°F and

frequently are limited by premature breakdown because of the low gas density. Addition of ppm amounts of ammonia is found to remedy the situation and allow operation at higher power input levels, thereby restoring efficient operation.

In other applications the addition of percentage amounts of water vapor can have significant benefits to electrostatic precipitation by allowing operation at higher voltage and power input levels because of the net reduction of ionic mobility. Practical increases in power input of 20% or more can be achieved in this way.

#### ELECTRICAL BREAKDOWN OF THE DUST LAYER

Another important performance limitation encountered by electrostatic precipitators is the electrical breakdown of the dust layer deposited on the collecting electrode. This condition arises when the resistivity of the dust layer is high. Generally when the resistivity is above  $10^{11}$  ohm-cm, electrical breakdown of the dust layer occurs before gas-phase breakdown. Dust layer breakdown is caused by the development of a high voltage gradient across the dust layer which exceeds the breakdown strength of the gas in the interstices of the dust layer. The voltage gradient is due to current flow through the layer, and is equal to the product of resistivity and current density. As resistivity increases, the allowable current before breakdown decreases, and, in extreme cases, operation of the precipitator is seriously impaired. Dust layer breakdown may manifest itself as premature sparking or as back corona. Back corona is a phenomenon in which a stable discharge of positive ions originates from the dust layer because of the high voltage gradient present there. The positive ions then tend to neutralize the negative particle charge achieved by the forward corona and thereby defeat the particle collection process.

Dust layer resistivity is dependent on the chemical composition of the dust and its temperature. For coal combustion flyash, several models and rules-of-thumb exist for relating flyash resistivity to ash composition, gas chemistry and temperature. For example a computer model developed by Southern Research Institute uses a large database to derive correlations for resistivity with virtually all the constituents of flyash. In addition there are many indices which have been published in the literature for relating various key components to resistivity. Examples include the alkali-silicate index relating resistivity to the ratio of sodium + potassium to silica + alumina; the Soviet index which uses the ratio of silica + alumina times ash content to moisture + hydrogen times sulfur content; the Bureau of Mines oxide index which uses the ratio of calcium + magnesium oxides to sodium oxide + sulfur trioxide; and many more. Also it is generally true that coals high in sulfur content produce ashes which are not of high resistivity. The point to be made is that the chemical composition of the dust to be precipitated determines its resistivity, and therefore determines whether or not the precipitator will have difficulty in operating effectively.

Temperature determines the mode of electrical conduction through the layer; at higher temperatures, e.g. above 400°F, volumetric

conductivity of the particles is controlling, and, at lower temperatures, e.g. below 300°F surface conductivity is controlling. In the transition range between about 300°F and 400°F a maximum in resistivity usually occurs. For power generation applications, flue gas temperature is normally around 300°F and, depending on ash composition, may be subject to high resistivity problems. Although it may appear that an easy solution is to either raise or lower the temperature of operation of the precipitator, this is not necessarily a practical solution. Lowering the temperature may result in acid dew point problems, and operation at higher temperature, though sometimes effective, carries with it other problems including the possibility of the sodium depletion phenomenon. Sodium depletion refers to the migration of sodium out of a thin sublayer of ash next to the collecting surface under the influence of the electric field at high temperature. The resulting sodium-poor layer, for many ashes, is itself highly resistive and presents the same high resistivity limitation the high temperature operation was intended to solve. The sodium depletion problem, however, has been found to be treatable by the addition of sodium compounds to the coal feed, although this is objectionable to many boiler operators.

An effective remedy for high resistivity and one that is practiced widely is chemical conditioning of the flyash. Chemical conditioning is effective in enhancing the surface conductivity of the ash and is thus generally used at temperatures of 300°F and below. Sulfur trioxide is the most used conditioning agent. The addition of ppm levels of sulfur trioxide to the flue gas can reduce resistivity out of the problem range by depositing a conductive layer of sulfuric acid on the ash surface. Not all ashes are easily conditioned by SO<sub>2</sub>, however. For example the acidic Eastern bituminous ashes are more difficult to condition, often requiring higher levels of SO<sub>2</sub> to be effective. On the other hand the alkaline Western coal ashes are easily conditioned by low ppm of SO<sub>2</sub>. To improve the conditionability of the Eastern ashes it has become common to consider the use of dual conditioning, using low ppm levels of ammonia injection in the flue gas in addition to the SO<sub>2</sub>. The effect of the ammonia is probably to increase the pH of the ash surface so that it is more receptive to the acid.

Although most commonly used, sulfur trioxide is not the only conditioning agent found effective for reducing resistivity. Others include sulfonic acid, sulfamic acid, ammonium sulfate and bisulfate, sodium carbonate, triethylamine, and various proprietary chemicals. In some cases moisture addition alone is effective.

#### PARTICLE REENTRAINMENT

Proper operation of an electrostatic precipitator involves periodic rapping of the collecting plates to jar loose the collected dust and allow it to fall into the hoppers for subsequent removal. Before the collected dust is finally removed from the precipitator, however, it is subject to reentrainment back into the gas stream by three mechanisms: scouring of the dust off the collecting surface by the gas flow itself; electrical reentrainment caused by inductive reversal of charge on the

collected dust because of inadequate electrical current; and reentrainment induced by the rapping blow itself. The effect of reentrainment is to reduce the net collection efficiency of the precipitator. This can be a serious limitation in achieving modern high efficiency particulate control requirements in a reasonably sized precipitator.

The reentrainment problem can be greatly reduced by agglomeration of the particles on the collecting surface. This is because the agglomerates will tend to cake and fall to the hoppers more readily than the non-agglomerated fine particles. Also the agglomerates, because of their larger size, are more easily recaptured in the remaining precipitator than the fine particles. It has been found that certain chemical additives are effective in promoting this desired agglomeration by enhancing the surface cohesivity of the particles. Some of these are ammonia, dual injection of ammonia and sulfur trioxide, moisture, sodium sulfate and others. Through use of these chemicals, reduction of reentrainment results in a marked decrease in emissions from the electrostatic precipitator. It is interesting to note that the precipitator's chief rival for high-efficiency particulate control, the fabric filter, also benefits from conditioning to increase particle cohesivity; the benefits to the fabric filter include higher collection efficiency and reduced pressure drop because of the formation of a more porous filter cake.

#### CORONA CHEMISTRY

The region immediately surrounding the corona discharge point on the precipitator's discharge electrode is a region of intense electron activity. Electrons are emitted with high enough energy to create reactive species such as OH and O radicals when colliding with the constituent gas molecules. These radicals in turn can initiate reactions leading to the production of ozone and the oxidation of various flue gas components, e.g. NO and SO<sub>2</sub>, therefore presenting the possibility of gaseous pollutant control by corona initiated reactions. Various investigators have realized this potential and work is ongoing to develop practical corona systems for the control of SO<sub>2</sub> and NO. EPA and others are investigating the use of corona for VOC destruction, claiming destruction of benzene, toluene and other organics at very high efficiencies.

Normal electrostatic precipitator configurations are far from optimum for taking advantage of corona chemistry. The active corona region occupies only a small fraction of the volume of the interelectrode space. Therefore the opportunity and time for exposure of the gaseous components to the active species is not adequate for good removal. Changes away from normal precipitator design have to be made to evolve into a practical contactor for the purpose of gaseous pollutant control. Electrode spacings have to be reduced to increase the fraction of volume occupied by the active species; very sharp discharge points have to be used to concentrate the electric field strength and deliver high energy electrons; and pulse energization should be used to maximize the applied discharge voltage.

Further work is needed to develop the use of corona initiated reactions for gaseous pollutant control. It will not be done in a conventional precipitator design. Attention will also have to be paid to the energy requirement for achieving high levels of pollutant removal. Some of the reported work indicates that this requirement may be high depending on the pollutant to be removed.

## INVESTIGATION INTO THE DISCREPANCY BETWEEN MWI AND MWC CDD/CDF EMISSIONS

W. Steven Lanier, T. Rob von Alten, and Richard K. Lyon  
Energy and Environmental Research Corporation  
Irvine, California 92718

### INTRODUCTION

On February 11, 1991, the EPA promulgated standards of performance for new municipal waste combustors (MWC's) and emission guidelines for existing MWC's with a unit capacity greater than 250 tons/day of waste. These standards included limitations on total dioxins (tetra- through octa-chlorinated dibenzo-p-dioxins or CDD) and dibenzofurans (tetra- through octa-chlorinated dibenzofurans or CDF). For new units the CDD/CDF stack emission limit was set at 30 nanograms/dry standard cubic meter (ng/dscm) (12 gr/billion dscf), corrected to 7 percent oxygen (dry basis), and was based on use of a spray dryer/fabric filter (SD/FF) emission control system. For existing systems the CDD/CDF emission guideline was established at 125 ng/dscm (50 gr/billion dscf) and was based on use of a dry sorbent injection/fabric filter (DSI/FF) emission control system. In the Federal Register, the EPA concludes that "all types of existing MWC's . . . applying . . . a . . . DSI/FF system can meet a dioxin/furan emission level of . . . 50 gr/billion dscf at 7 percent [oxygen]." Based on limited emissions test data, it was believed that this emission level reflected a nominal 75 percent reduction in CDD/CDF emissions.

The EPA is currently developing emission standards for new and existing medical waste incinerators (MWIs). An initial belief was that MWIs and MWCs equipped with similar air pollution control devices (APCDs) would have similar CDD/CDF emission reductions and stack CDD/CDF removal being effected. This paper compares available CDD/CDF emission data from MWCs and MWIs and examines various parameters which could potentially contribute to higher emissions from MWIs. Based on this examination, a possible explanation was developed involving the partitioning of CDD/CDF between the stack gases and the captured fly ash. Data is then presented from subsequent testing which supports the hypothesis.

This study was funded by the U.S. Environmental Protection Agency through a subcontract to EER from Mid West Research Institute. The effort was coordinated by Mr. Ken Durkee at EPA and Mr. Roy Neulicht at MRI.

### EMISSION COMPARISON: MWI vs. MWC

In the discussion that follows it is important to establish that with similar APCDs, stack CDD/CDF concentrations from MWIs are greater than from MWCs. To accomplish this objective, it is important to institute a frame of reference and a set of terminology reflecting the potential for formation of CDD/CDF in APCDs. Figure 1 illustrates the various chemical processes and the bifurcation of material within the APCD. Both solid and gas phase material exit the furnace (either MWI or MWC) and enter the APCD. CDD and CDF may be in either the gas phase or may be directly associated with solid phase material. Both phases of materials entering the APCD may also provide precursor materials or catalytic surfaces for formation of CDD/CDF in the APCD.

Within the APCD, many complex processes may occur. Surface catalyzed reactions can cause formation of CDD/CDF with key constituents supplied from either the gas phase or from material associated with the particulate or both. When the CDD/CDF, is formed it may be retained on the particle surface or desorbed to the gas phase. Any gas phase CDD/CDF entering the APCD may pass directly through the control device or may be absorbed on solid surfaces. From a mass balance perspective, there is a flow of CDD/CDF into the APCD with additional CDD/CDF formed in the control device. The inflow plus generated CDD/CDF will exit the APCD through the stack or with the collected fly ash. CDD/CDF in the gas phase will exit the APCD with the flue gas while the majority of the solid phase CDD/CDF will exit with the collected fly ash.

Historically, the effectiveness of APCD systems to "control" CDD/CDF emissions has been based on concentration measurements in the stack and at the APCD inlet, ignoring the quantity of CDD/CDF associated with the collected fly ash. The current study examines the available data from MWC and MWI

facilities within the broader framework and attempts to identify process parameters that could be responsible for apparent differences in emission performances between the two classes of incinerators.

#### APCD INLET CONCENTRATIONS

The initial point of comparison between MWCs and MWIs is to compare the CDD/CDF concentration in the gases leaving the incinerator -entering the APCD system. Figure 2 provides a compilation of inlet CDD/CDF data for a variety of MWIs<sup>1-5</sup> and MWCs<sup>6,7,8</sup>. A relatively wide variation in inlet CDD/CDF concentration is observed indicating differences in equipment design and possibly mode of operation. The important issue, however, is that no trend is observed indicating significantly higher CDD/CDF concentrations coming from either type of combustion equipment.

#### APCD OUTLET CONCENTRATIONS

There is a relatively small body of data defining the CDD/CDF emission performance of MWIs with APCDs and an even smaller body for units equipped with dry sorbent injection and a fabric filter. One such facility is the MWI at the Borgess Medical Center in Michigan. The Borgess Medical Center incinerator uses dry hydrated lime injection upstream of a baghouse for control of acid gas and particulate matter. A complete description of the Borgess facility and the test program is given in Volume II of the *Michigan Hospital Incinerator Emissions Test Program*<sup>1</sup>.

The initial expectation was that CDD/CDF emission rates and APCD collection efficiency for the Borgess facility would be generally consistent with emissions from MWC facilities equipped with DSI/FF. Figure 3 illustrates outlet CDD/CDF concentrations for Borgess<sup>1</sup> and various MWCs<sup>6,7,8</sup> with DSI/FF. The CDD/CDF concentration from all the MWCs tested were under 60 ng/dscm while the outlet concentration measurements at the Borgess MWI ranged between 250 and 650 ng/dscm. Clearly the stack CDD/CDF emission concentrations from Borgess are significantly higher than emissions from MWCs with similar APCDs. Moreover, comparison of the data in Figures 2 and 3 indicates that the "Control Efficiency" of the DSI/FF at Borgess was extremely low and, on certain tests, was negative.

#### CDD/CDF FORMATION IN APCDs

The above comparisons indicates that stack CDD/CDF emissions from MWIs are higher than from MWCs. Two obvious explanations include the potential that more CDD/CDF is formed in the APCD system of MWIs or that DSI/FF is less effective on MWIs than on MWCs. The following section discusses the possibility that more CDD/CDF is formed in the APCD of medical waste incinerators.

**APCD Temperature** Formation of CDD/CDF can occur in the APCD and the formation rate generally increases with increasing temperature. Several laboratory studies suggest that peak formation rates occur when the reaction temperature is on the order of 300°C (572°F)<sup>9</sup>. Figure 4 presents the stack outlet CDD/CDF concentration versus APCD temperature for various MWI and MWC facilities utilizing PM control both with dry sorbent injection (DSI) and without acid gas control. The clearly illustrates the trend of increased CDD/CDF emission at higher APCD operating temperature. More importantly, the data tend to fall into two distinct groups. At any given APCD operating temperature, MWIs emit higher CDD/CDF concentrations than MWCs. Based on this comparison the APCD temperature does not provide a reasonable basis for explaining why MWIs have higher CDD/CDF stack emissions.

**Surface Area** Numerous process parameters have been suggested as key variables influencing low temperature formation of CDD/CDF. Since the basic formation reaction process is believed to be catalytic, one of the key parameters should be the amount of surface area provided by the fly ash. In general, the uncontrolled (inlet to the APCD) particulate matter (PM) loading from an MWC will be about an order of magnitude higher than from a MWI (1-2 gr/dscf for MWCs<sup>10</sup> vs. ~0.1 gr/dscf for MWIs<sup>1,3</sup>). However, the PM emitted by typical MWIs tends to be highly skewed toward submicron particles. Thus, it is possible that the shift in size distribution could more than offset the reduced mass loading.

Only limited size distribution data is available from either MWC or MWI<sup>11</sup> units. By combining actual or typical particle size distribution data with mass loading data it was possible to broadly PM surface area

variation. This process indicated that there is not major difference between MWCs and MWIs as regards the amount of PM surface area available for low temperature formation of CDD/CDF.

**Presence of Chlorine and Catalysts** The low temperature reactions to form CDD/CDF clearly involve surface reactions, but there is more than one way in which the surface could potentially participate. Researchers have shown a significantly greater formation of chlorinated organics when passing concentrations of  $\text{Cl}_2$  rather than HCl over synthetic ash<sup>12</sup>. In these tests, the organic precursor to CDD/CDF was supplied by the particulate, but tests suggest an additional role for the particulate. Specifically, one of the standard processes for forming  $\text{Cl}_2$  is to pass HCl over a copper catalyst. Copper or other catalysts in the particulate could enhance formation of  $\text{Cl}_2$  and thereby increase CDD/CDF formation. Laboratory experiments using synthetic fly ash have shown that increasing the quantity of copper increased CDD/CDF formation<sup>9</sup>. Further studies examining fly ash from many incinerators found a moderate correlation between copper in ash and CDD/CDF<sup>13</sup>.

Based on the above studies, there is at least a possibility that MWIs produce greater quantities of CDD/CDF because of enhanced formation of  $\text{Cl}_2$ . Medical waste incinerators typically have double the uncontrolled HCl emission compared to MWCs. The difference is due to the higher chlorine content of medical waste. The limited data on the amount of Cu in fly ash is not sufficient to draw conclusions on the comparative role of chlorine and catalysts in the formation of CDD/CDF. Although it remains possible that the higher chlorine content of medical waste (in conjunction with a catalyst) may influence the formation of CDD/CDF, there is a strong opinion that this is not the source of the observed variation in MWI and MWC CDD/CDF emissions. The HCl concentration from MWIs is probably no more than a factor of 2 greater than that from MWCs, and yet the CDD/CDF emissions are increased by a factor of 5 to an order of magnitude.

#### SYSTEM MASS BALANCE

The preceding evaluation, though not exhaustive, provides no explanation for the observed higher CDD/CDF concentration in MWI stack gases. Those evaluations, however, tend to focus on comparison of inlet and stack outlet CDD/CDF concentrations and do not include consideration of the CDD/CDF associated with the collected fly ash. For a limited number of facilities it is possible to estimate the actual formation of CDD/CDF in APCDs. The calculation requires that a mass balance be performed for the APCD. The amount formed equals the total CDD/CDF leaving the system (both in solid residue and in stack gases) minus the quantity entering the system. While portions of this data are available for many facilities, very few data sets contain all the required data. Three data sets which did contain all the necessary information are Borgess (MWI)<sup>1</sup>, Montgomery County (MWC)<sup>6</sup>, and Quebec City pilot study<sup>8</sup> (MWC).

For the three facilities with sufficient data, the total CDD/CDF generated is determined by adding all of the exit streams and subtracting the inlet concentrations. Data for all streams were normalized by the volumetric flow rate of flue gas for that facility, corrected to 7%  $\text{O}_2$ . Results are presented in Figure 5 and show that CDD/CDF formation is consistent between the comparable APCD systems at Borgess (MWI) and Quebec City (MWC) as well as with the DSI/ESP equipped Montgomery County facility. By comparing total CDD/CDF formation in the APCD the broad groupings of data observed in Figure 4 is collapsed into a single line.

#### GAS/SOLID CDD/CDF SPLIT IN APCDs

The preceding discussion has first shown that there is no significant difference between MWCs and MWIs relative to the concentration of CDD/CDF exiting the incinerator. Next it has been shown that there is no significant difference MWCs and MWIs relative to the mass of CDD/CDF formed in similar APCD systems. Thus, it is strongly suggested that the source of the discrepancy between MWC and MWI stack concentrations is the split between CDD/CDF captured with the fly ash and CDD/CDF which escapes with the flue gas. In general, it is expected that CDD/CDF in the gas phase within the APCD will be released with the flue gas while that associated with the PM (fly ash and sorbent) will likely be captured and exit the APCD with the solid residue. This section examines the issue of CDD/CDF partitioning in MWIs and MWCs.

A common perception is that under the low temperature conditions in an APCD, CDD and CDF will condense onto fly ash or onto injected sorbent material. A brief examination of the CDD/CDF vapor pressure characteristics shows that, in fact, condensation is not the controlling process. Figure 6 illustrates the variation in tetra and octa CDD vapor pressure as a function of temperature<sup>14</sup>. As shown, at 300°F the vapor pressure of octa CDD is  $> 10^{-3}$  atmospheres and the vapor pressure of tetra CDD is about  $10^{-4}$  atmospheres. Thus, at 300°F, if the concentration of octa CDD is less than 1000 parts per million, it will remain in the vapor phase or be evaporated if it is a free liquid on the surface of a particle. By comparison, 1000 ng/Nm<sup>3</sup> of tetra CDD is equivalent to a concentration of about 50 parts per trillion.

Based on the above data, it is clear that within APCDs, CDD/CDF does not condense onto the surface of particles and remains as a free liquid or solid. It is also a fact, however, that substantial concentrations of CDD/CDF are found in fly ash collected from MWCs and MWIs. For this to occur it is necessary that the CDD/CDF be chemically or physically bonded to the PM. The implications of this requirement will be examined below.

If CDD/CDF is chemically bound to the surface of particulate matter (chemisorption), one would expect that bonding to be influenced by temperature and by the nature of the particle surfaces. As regards temperature, one would anticipate that the bonds would tend to break as the temperature increases. This possibility is evaluated by examining experimental data from the MWC in Montgomery County, Ohio where CDD/CDF concentrations were determined in both the collected fly ash and stack gas at several different APCD operating temperatures. These data are important in that tests were conducted both with and without sorbent injection. Further, the Montgomery County MWC is equipped with a water quench upstream of the ESP which tends to remove most of the large diameter particulate. In fact, this MWC has a PM size distribution entering the ESP which is quite similar to an MWI controlled-air system.

Table 1 and Figure 7 illustrate data from the Montgomery County MWC. The data have been converted such that both the fly ash and stack CDD/CDF concentrations are normalized to the volume of dry flue gas, corrected to 7% oxygen. These data illustrate that greater amounts of CDD/CDF are formed at higher temperatures but also show how temperature impacts the bifurcation. As shown in Figure 7, all of the data without duct injection of sorbent exhibit a linear relationship. As APCD temperature increases, there is a substantial increase in the fraction of the total CDD/CDF which escapes with the stack gas. This is precisely the anticipated trend discussed earlier. Test point TC-5 was the only condition in the Montgomery County test series where hydrated lime was injected into the duct leading to the ESP. Table 1 and Figure 7 illustrate two important trends. First, the total quantity of CDD/CDF leaving the ESP (both gas and solid phase) was significantly reduced relative to the tests without duct sorbent injection at an equivalent temperature (test point TC-4). Additionally, however, of the total CDD/CDF from test TC-5, a much larger fraction was released to the gas phase. In test condition 5, 57% of the total CDD/CDF was released with the stack gas as compared to 22% in test condition 4.

The above described Montgomery County MWC data make two very important suggestions. Reducing APCD temperature will decrease the total quantity of CDD/CDF formed and will also reduce the fraction of that organic which will be released to the gas phase. The other key indication from this single test point is that hydrated lime injection greatly reduces total CDD/CDF formation. Further, the presence of hydrated lime appears to increase the percentage of total CDD/CDF released to the gas phase. The increase in percent released with stack gas was not nearly significant enough to offset the decrease in total formation and, hence, a reduction in stack gas concentration was observed.

Measurements similar to those discussed above for Montgomery County were taken at several other facilities. The Borgess MWI facility tests provide both ash and stack data but the testing covered only a relatively narrow band of fabric filter temperature. For the series of five tests at Borgess, the average CDD/CDF concentration at the APCD inlet, in the stack, and in the ash were 459, 452, and 355 ng/dscm of flue gas respectively. Thus, the ratio of CDD/CDF in the fly ash to CDD/CDF in the stack gas is 0.78. Since the APCD temperature at Borgess was nominally 320°F, the tendency for CDD/CDF to be retained with the ash is almost identical to that observed at Montgomery County (with duct sorbent injection).

The other facility for which there is a large body of data is the Quebec City MWC which was tested as part of Environment Canada's NITEP program. Table 2 presents the CDD/CDF data in ng/dscm of flue gas basis at several locations in the pilot scale DSI/FF tests. In all cases, there was a substantial concentration of CDD/CDF leaving the fabric filter but essentially all of the organic was retained with the collected

solids. Note that even with the fabric filter operating at 408°F, only 7.3 ng/dscm were in the stack gas as compared to 2383 ng/dscm of total CDD/CDF exiting the fabric filter in the ash and stack gas combined. When compared to the previously described results, the data in Table 2 suggest that perhaps there is something different about the Quebec City Data. Duct injection of sorbent certainly did not significantly suppress the total CDD/CDF formation in the fabric filter. In fact, much more CDD/CDF was formed in the bag house at Quebec City than was formed at Borgess. What is totally different, however, is the fraction of that CDD/CDF that is released to the gas phase.

### CARBON LOADING

The current study is unable to prove why the Quebec City MWC retained nearly all of its CDD/CDF with the collected solids. We can, however, suggest that carbon in the fly ash could be a controlling parameter and suggest that this parameter is the key difference between MWCs and MWIs.

Several field tests have demonstrated that injection of small quantities of activated carbon can have a significant impact on the emission of CDD/CDF from both MWC's and MWI's. Activated carbon injection is currently used at a few incinerators for mercury and volatile organic control. Typically, a small amount of carbon is injected into the flue gas and adequately mixed. Effort is made to assure good mixing prior to a moisturizing environment since water is believed to plug the pores and reduce the reactivity of the activated carbon. The small amounts of carbon (typically 20-400 mg/Nm<sup>3</sup> with an average of ~70 mg/Nm<sup>3</sup>) are believed to provide a large amount of active surface area for chemisorption of CDD/CDF. Results from a hospital incinerator test in Sweden showed that activated carbon reduced outlet CDD/CDF emissions by 76 to 92% over tests without activated carbon<sup>16</sup>. A full scale MWC in Zurich reduced outlet CDD/CDF by 57 to 93%.

The relevance of the above data to the Quebec City MWC is that the pilot scale tests described in Table 2 were performed prior to completing extensive hardware modifications to improve combustion performance. In fact, personnel from the facility and from Environment Canada described the plume for the Quebec City MWC as containing many "black birds" -- thin, large diameter pieces of black material escaping the ESP. The carbon content of the particulate from this MWC (prior to the facility modification) is not reported in the various Environment Canada (EC) documentation. It is safe to assume, however, that the carbon in the uncontrolled ash was at least at the upper end of the range observed for other MWCs tested in recent years (1 to 5%). EC does report the uncontrolled PM concentration for the pilot scale DSI/FF tests. The average concentration reported was 6700 mg/Nm<sup>3</sup>. If the carbon in ash was only 5%, then the total solid phase carbon loading entering the Quebec City pilot-scale fabric filter would be 335 mg/Nm<sup>3</sup>. Thus, the "naturally occurring" carbon concentration is, as a minimum, consistent with the level of activated injected into the above MWI in Sweden or the MWC in Zurich.

In contrast to the situation at Quebec City, controlled air incinerators such as the Borgess facility have very low uncontrolled PM concentrations. At Borgess the average carbon content of the fly ash was approximately 5% (not including injected sorbent) and the average PM loading was 253 mg/dscm. Thus, at Borgess the solid phase carbon flow into the fabric filter is only 13 mg/dscm. That is significantly less than at Quebec City. There may be several phenomena which can explain the CDD/CDF retention discrepancy between Borgess and Quebec City, but clearly the flow of solid carbon to the particulate control device is a leading contender. In fact, it is the only phenomena uncovered thus far which can explain the observed discrepancy between MWC and MWI stack CDD/CDF emissions.

### TESTING

The Borgess incinerator was retested to evaluate the impact of activated charcoal injection. The system was modified to inject activated carbon upstream of the fabric filter. Eight tests were completed. Three tests were run without carbon injection, two tests with carbon injection at 1 lb/hr, and three tests with carbon injection at 2.5 lb/hr. The test condition averages are illustrated in Figure 8. Carbon injection at 1 lb/hr reduced stack emissions by 88% from baseline average. With carbon injection at 2.5 lb/hr, stack emissions were reduced by 95% from baseline average. The results support the hypothesis that the amount of unburned carbon influences CDD/CDF stack emissions. The complete data set was not yet available to analyze the impacts of carbon injection on the split between captured fly ash and stack gases.

However, it is believed that the observed reduction is due to the carbon adsorbing the CDD/CDF from the gases and transferring it into the captured fly ash stream.

## SUMMARY

The preceding material has examined a variety of phenomena in an attempt to explain a major inconsistency between CDD/CDF emissions from MWCs and MWIs utilizing similar pollution control systems and operating under similar conditions. The available data indicates that a larger portion of the CDD/CDF formed in the APCD of MWIs is released with the flue gas. For MWCs the larger fraction appears to be retained with the collected fly ash. The data also indicates that CDD/CDF leaving the APCD with the solid material is chemisorbed to the surface and not merely condensed on the surface. Increasing APCD temperature weakens those bonds and causes more of the CDD/CDF to be released to the gas phase. Further, it was shown that the strength of this bonding appears to depend on the nature of the particulate surface. Injected sorbent material tends to reduce the total quantity of CDD/CDF formed but the sorbent apparently does not provide a strong bonding between the CDD/CDF and the surface.

The issue of surface bonding led to a reexamination of DSI/FF pilot tests at the Quebec City MWC. The data shows three important trends. First, the total amount of CDD/CDF formed in the APCD system at Quebec City is greater than the quantity formed at the Borgess MWI. Secondly, almost all of this CDD/CDF was retained on the particulate matter and not released with the flue gas. This is very different than the situation with MWIs or with the Montgomery County MWC. Finally, it was shown that the Quebec City pilot-tests had a quite high concentration of carbon in the fly ash. In fact, the carbon levels are at least as high as in tests conducted in Europe where activated carbon was injected into the APCD. Those European tests showed major reduction in exhaust CDD/CDF concentration. In contrast to the Quebec City pilot test, typical MWIs (and the MWC test at Montgomery County) have very low solid carbon loading entering the APCD. The carbon in fly ash levels for MWIs are on the same order or less than in MWCs but the total particulate loading in MWIs is about a factor of 10 to 20 less than for MWCs. The low concentration of solid carbonaceous material, with strong bonding to gaseous hydrocarbons like CDD/CDF, could result in more of the formed CDD/CDF being released to the gas phase.

This theory was evaluated by retesting the Borgess incinerator. Tests were conducted with and without activated carbon injection. The results showed that the injection of activated carbon did reduce CDD/CDF stack concentrations to less than 20 ng/dscm @ 7% O<sub>2</sub>. Those concentrations are approximately what is expected for a MWC with dry sorbent injection. Therefore, it is believed that the higher CDD/CDF stack emission concentrations observed at MWIs utilizing similar control technologies as a MWC, is due to the lower amount of unburned carbon loading in an MWI. The lower carbon loading in an MWI results in a greater fraction of the CDD/CDF escaping with the flue gas rather than be adsorbed and collected with the fly ash as in an MWC.

## References

1. England, G., D. Hansell, J. Newhall and N. Soelberg. Draft Report "Michigan Hospital Incinerator Emissions Test Program Volume II: Site Summary Report, Borgess Medical Center Incinerator." April 15, 1991.
2. Radian Corporation. Draft Report "Medical Waste Incineration Emission Test Report, Volume 1 Jordan Hospital, Plymouth, Massachusetts." May 1991.
3. England, G., D. Hansell, J. Newhall, and N. Soelberg. Draft Report "Michigan Hospital Incinerator Emissions Test Program, Volume III: Site Summary Report, University of Michigan Medical Center Incinerator." April 25, 1991
4. Jenkins, Al, C. Castronovo, G. Lindner, P. Ouchida, and D. C. Simeroth. "Evaluation Test on a Hospital Refuse Incinerator at Cedars Sinai Medical Center, Los Angeles, CA." Test Report. April 1987.
5. Jenkins, Al, P. Ouchida, and G. Lew. "Evaluation Test on a Refuse Incinerator At Stanford University Environmental Safety Facility." California Air Resources Board, ARB/ML-88-025, August 1988.

6. Radian Corporation. "Draft Emissions Test Report for the Parametric Test Program at the Montgomery County South Facility, Unit 3, Dayton Ohio Volume I: Summary of Results." October, 1989.
7. P.J. Schindler. "Municipal Waste Combustion Assessment: Combustion Control at Existing Facilities." EPA Report No. 600/8-89-058. August 1989.
8. Environment Canada. "The National Incinerator Testing and Evaluation Program: Air Pollution Control Technology, Summary Report." EPS 3/UP/2. September 1986.
9. Stieglitz, L. and H. Vogt. "New Aspects of PCDD/PCDF Formation in Incineration Processes." Formation and Decomposition of Polychlorodibenzodioxins and -furans in Municipal Waste Incineration. February 1988.
10. Radian Corporation. "Municipal Waste Combustors - Background Information for Proposed Standards: Post-Combustion Technology Performance." EPA Report No. 450/3-89-27c. August 1989.
11. Brady, Jack. "Submicron Aerosol Generation and Aerosol Emission Control in Infectious Waste Incinerators." Presented at the Second International Conference on Municipal Waste Combustion. Tampa, Florida. April 16-19, 1991.
12. Gullet, Brian, K. Bruce, and L. Beach. "Formation of Chlorinated Organics During Solid Waste Combustion." Waste Management and Research, Vol. 8, pp. 203-214 (1990).
13. Hinton, W. S. and A.M. Lane. "Characteristics of Municipal Solid Waste Incinerator Fly Ash Promoting the Formation of Polychlorinated Dioxins." Chemosphere, Vol. 22, pp. 473-483 (1991).
14. Rordorf, Berchtold. "Prediction of Vapor Pressures, Boiling Points and Enthalpies of Fusion for Twenty-Nine Halogenated Dibenzo-p-Dioxins and Fifty-Five Dibenzofurans by a Vapor Pressure Correlation Method." Chemosphere, Vol. 18, pp. 783-788 (1989).
15. Brown, B. and K.S. Felsvang. "Control of Mercury and Dioxin Emissions From United States and European Municipal Solid Waste Incinerators By Spray Dryer Absorption Systems." Presented at Second International Conference on Municipal Waste Combustion. Tampa, Florida. April 16-19, 1991.
16. Skovde Hospital Waste Incinerator. Performance Test Data.

**Table 1 Montgomery County CDD/CDF Behavior**

\* (ng/dscm) corrected to 7% O<sub>2</sub>

	Test Condition 1	Test Condition 2	Test Condition 3	Test Condition 4	Test Condition 5	Test Condition 6
Flue gas flow rate (dscm/min)	713	756	922	859	805	779
Oxygen concentration (%)	13.09	13.50	13.61	13.43	12.47	14.50
ESP temperature (°F)	571	396	394	298	306	534
Fly ash collection rate (g/min)	548	398	994	955	2270	436
Fly ash CDD/CDF conc. (ng/g)	2539	1761	2323	1179	9	4399
Fly ash CDD/CDF (ng/min)	1390220	700856	2309592	1125379	20433	1918123
CDD/CDF in fly ash *	3449	1731	4743	2424	42	5304
Stack CDD/CDF emissions *	17109	866	1480	673	57	14517
Total CDD/CDF out *	20558	2596	6223	3097	99	19821
Uncontrolled CDD/CDF conc.*	252	33	38	14	5	214
Total CDD/CDF Generated*	20306	2563	6185	3083	94	19607

**Table 2 Complete CDD/CDF Behavior at Quebec City Pilot Study**

\* (ng/Nm<sup>3</sup>) corrected to 7% O<sub>2</sub>

Uncontrolled CDD/CDF *	880	2340	2300	1590
Fly ash CDD/CDF*	2076	2589	2576	2376
Stack CDD/CDF*	2.5	0.2	1.1	7.3

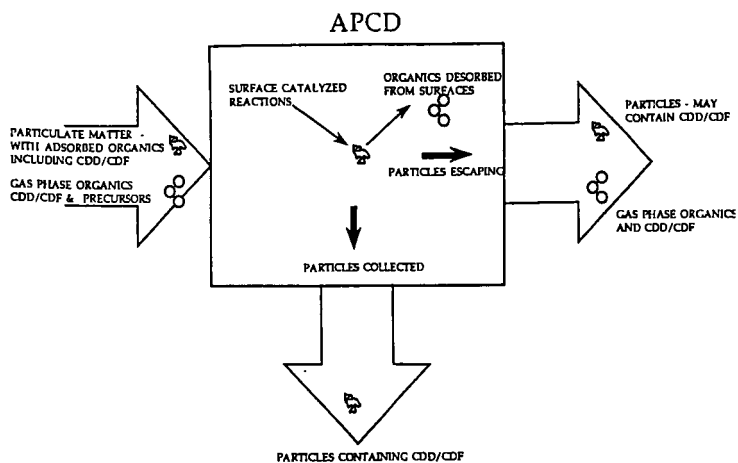


Figure 1 CDD/CDF Behavior in an APCD

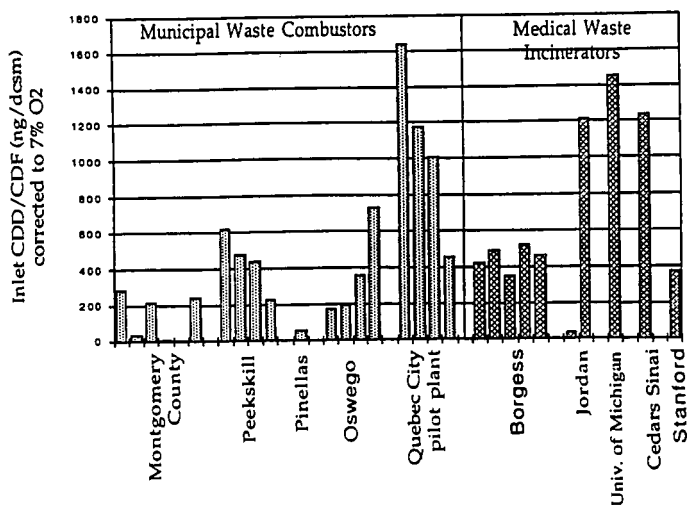
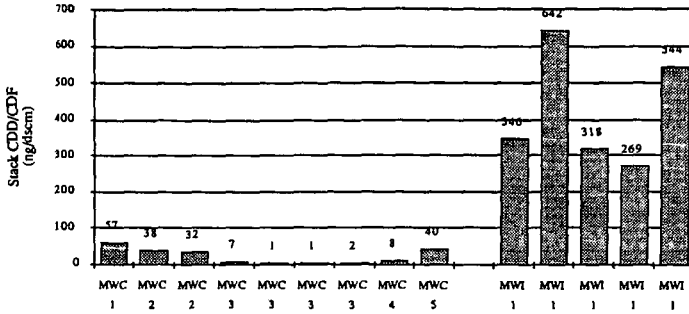


Figure 2 APCD Inlet CDD/CDF Concentrations



values corrected to 7% O<sub>2</sub>

Facility code

Facility code	Facility name	combustor type	APCD
MWC1	Montgomery County, OH	rotary kiln	WQ/DSI/ESP
MWC2	Claremont	mass burn	DSI/FF
MWC3	Quebec City pilot test	mass burn	WQ/DSI/FF
MWC4	St. Croix	MOD/EA	DSI/HE/FF
MWC5	Wurzberg	mass burn	WQ/DSI/FF
MWI1	Borgess	MOD/SA	DSI/FF

Figure 3 Comparison of Outlet CDD/CDF Concentrations for an MWI and MWCs with Dry Sorbent Injection

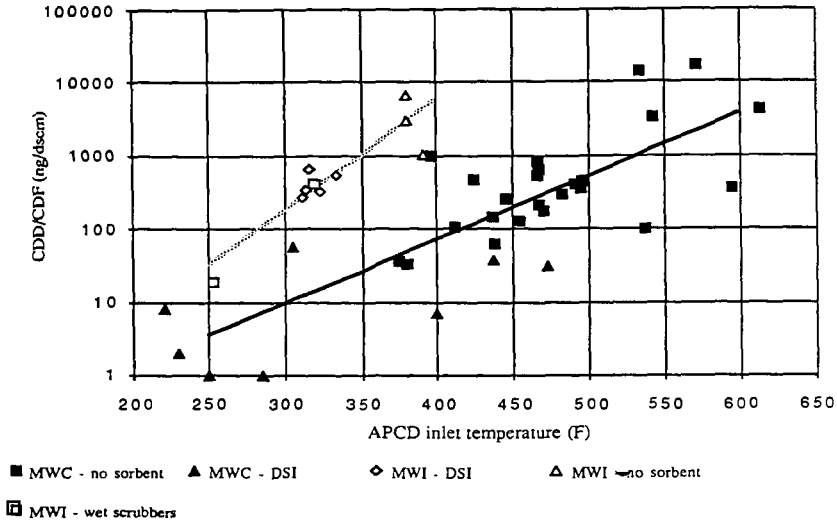


Figure 4 Effect of APCD Temperature on CDD/CDF Outlet Concentration

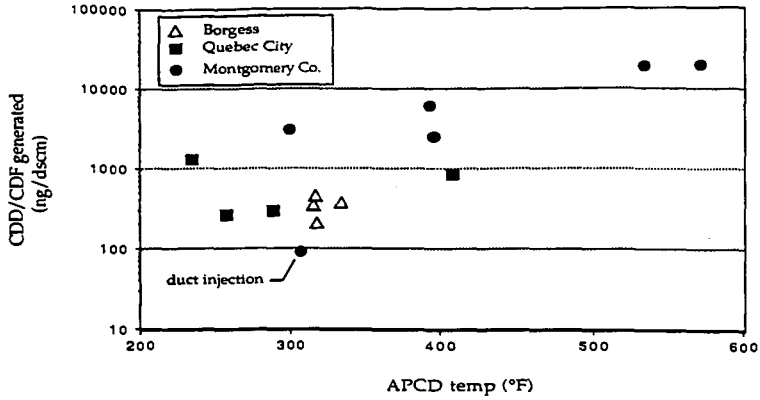


Figure 5 Comparison of Total CDD/CDF Generated in APCDs

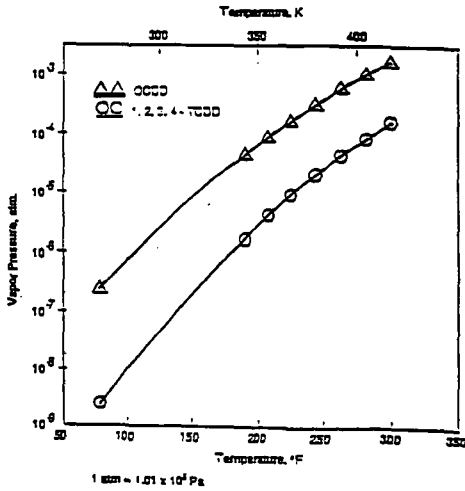


Figure 6 Vapor Pressure of Octa- and Tetra-chlorodibenzo-(p) dioxins

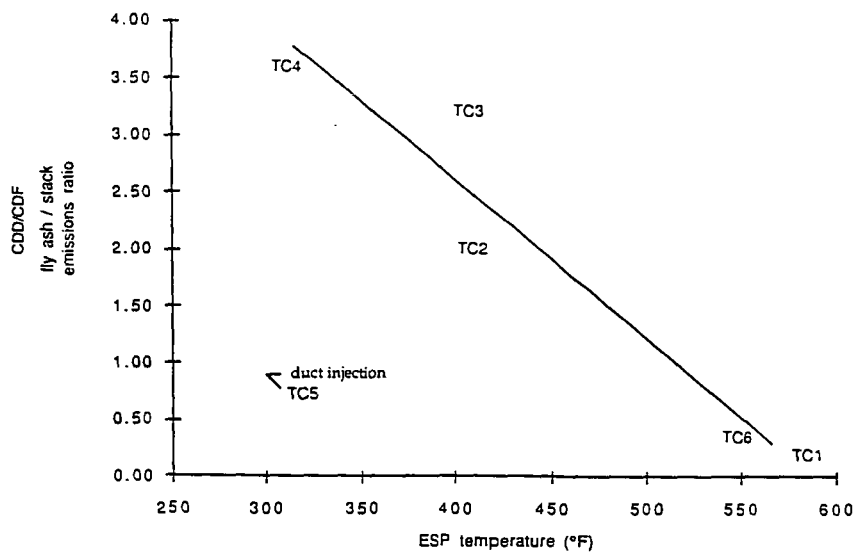


Figure 7 Effect of Temperature on Bifurcation of CDD/CDF in an ESP

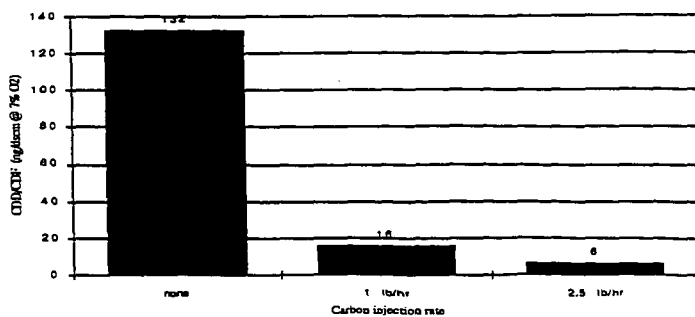


Figure 8 Effect of Activated Carbon on CDD/CDF Stack Concentration

UNMIXED COMBUSTION: A NEW TECHNOLOGY FOR PREVENTION  
OF PUFFING BY ROTARY KILN INCINERATORS AND OTHER APPLICATIONS

Richard K. Lyon  
Energy and Environmental Research Corp  
18 Mason  
Irvine, CA. 92718

Key words: copper oxide, puffing, incinerator

INTRODUCTION

**The Problem of Puffing in Civilian Incinerators** The United States currently produces 265 million tons per year of hazardous waste. In most instances the toxicity of this waste come from toxic organic materials which, in principle, can be completely destroyed by incineration. Since all other disposal technologies involve the risk that some of the toxic materials will return to the environment incineration is, in principle, the ideal solution to the problem. Presently available incinerator technology is subject to a number of limitations, one of the most important of these limitations being the puffing problem of rotary kiln incinerators, i.e. these incinerators are observed to occasionally emit puffs of toxic organic materials. This is a serious failure since as discussed by Oppel (1) rotary kiln incinerators are a substantial fraction of total U. S. incineration capacity. Detailed mathematical models of this puffing phenomenon has been presented in references 2, 3, and 4. As these references discuss rotary kiln incinerators handle both solid and liquid wastes. For combustible liquid wastes the practice is to mix the liquid waste with a sorbent, which is then placed in a container (typically a cardboard, plastic, or steel drum), and feed to the rotary kiln incinerator. These large closed containers are heated until the vapor pressure of the liquid is sufficient to cause them to rupture. This results in a sudden discharge of a large amount of combustible vapors into the incinerator. The supply of combustion air can be much less than sufficient for complete oxidation of these suddenly released vapors and this can cause substantial amounts of these toxic organic vapors to be discharged from the incinerator into the environment.

**Disposal of Chemical Weapons** A problem very similar to puffing is likely to occur during the U.S. Army's planned incineration of its stockpile of chemical weapons. If during the unpacking of these weapons a live munition were inadvertently included in the packing material sent to the dunnage incinerator most of the nerve agent it contains would be discharged to the environment. A risk analysis by GA Technologies (5) estimates a probability of 0.01 per year per site for such a mishap. Since there are nine sites and the destruction of the munitions will require a number of years, the probability of such an accident happening at least once is significant.

**Puffing Control via CuO** In both civilian and military incinerators the fundamental problem is that organic matter can go into the combustion chamber in slugs while combustion air is supplied continuously. It occurred to the author that this problem of mismatch between the supplies of fuel and air could be solved by using a bed of copper oxide. Organic matter passing through copper oxide at elevated temperatures is rapidly oxidized and air readily reoxidizes the copper to copper oxide. Thus a bed of copper oxide can, in effect, provide a means of storing an inventory of combustion air.

**The Concept of Unmixed Combustion** The research reported herein was initiated to test on a laboratory scale the feasibility of this method of controlling puffing. During the course of this work, however, it was recognized

that the use of copper oxide to maintain an inventory of combustion air make s possible a novel type of combustion system, one in which the fuel and air do not mix. Such an unmixed combustion system would be unique in that in all other combustion systems the stoichiometric ratio (i.e. the fuel/air ratio) is a critical parameter but in unmixed there are two stoichiometric ratios each of which is important, the ratio of the amount of fuel passed through the bed during a cycle to the maximum capacity of the bed to oxidize fuel and the ratio of the amount of air passed through the bed during a cycle to the maximum capacity of the bed to reduce  $O_2$ .

Preliminary experiments were done to examine the properties of such an unmixed combustor and are reported below.

#### APPARATUS AND EXPERIMENTAL PROCEDURES

Three sets of experiments were done, two to demonstrate puffing control with a fixed bed and and fluid bed CuO on high surface area alumina and one to explore unmixed combustion.

**Fixed Bed Experiments for Puffing Control** In the former experimental setup rotameters were used to prepare a flowing gas mixture containing oxygen and nitrogen in known proportions. For experiments involving volatile organic compounds a third rotameter was used to send a measured flow of nitrogen through a bubbler partially filled with the volatile organic compound and this stream of nitrogen saturated with the volatile organic was added to the flow of the oxygen/nitrogen mixture. A fourth rotameter was then used to take a measure portion of this flowing mixture and the rest was sent to vent via a back pressure regulator. For experiments with materials which are not readily volatile, i.e. phosphonoacetic acid, a precision metering pump send a flow of an aqueous solution of the material to the top of the fixed bed where the temperature was high enough to cause it to vaporize.

From the fourth rotatmeter the flowing gas mixture was sent to a three way valve and thence either went downward through the fixed bed and then to the analytical instruments or went directly to the analytical instruments. In these experiments the fixed bed was housed in a 1" OD stainless steel tube inside an electrically heated furnace. Two type K thermocouples were used to monitor and control its temperature.

The analytical instruments used were a Beckmann 400 Hydrocarbon analyzer (i.e. a flame ionization detector) and a Teledyne O2 analyzer.

The fixed bed consisted of 25.5 wt% CuO supported on 5/16" alumina rings and was prepared by the incipient wetness method. In this method a solution of copper nitrate was added to the alumina with constant stirring until the bed could not absorb more without becoming macroscopically wet. The alumina rings were then heated to 800°C to drive off water and decomposed copper nitrate to copper oxide. Manufacturer's specifications on these alumina rings list them to have a surface area of 2B4  $M^2/gm$ , total pore volume,  $H_2O$ , of 1.10 cc/gm, total pore volume, Hg, of 1.038 cc/gm, and a median pore diameter of 0.009 microns.

In doing these experiments the following procedure was used: an oxygen/nitrogen mixture without organic matter was passed through the bed and the oxygen level measured for the gas exiting the bed. Initially the concentration of oxygen in the gas going out of the bed could be extremely low because all the input oxygen was reacting will copper metal formed in the previous experiment. The oxygen level in the output gas would remain very low until virtually all of the metallic copper was consumed then would rise rapidly to equal the input level. Once the level of oxygen in the output gas was stable organic matter could

be added via either the bubbler or the metering pump and the change in the oxygen level of the exit gas noted. Since flame ionization detector was limited to concentrations less than 1000 ppmC, the change in the oxygen content which occurred when organic matter was added was used to calculate the input concentration of the organic matter. After making these observations the oxygen content of the gas going into the bed was reduced to zero and the flame ionization detector was used to measure the amount of organic matter which survived passage through the copper oxide bed as a function of time.

**Fluid Bed Experiments for Puffing Control** For fluid bed experiments the experimental apparatus and procedures were the same the following exceptions. The fluid bed was housed in a 26mm ID, 91 cm long, quartz tube which was placed inside an electric furnace with a 30 cm. heated length. The bed had a settled height of 13 cm. It operated in a slugging mode with a height of 30cm. Gases flowing out of the quartz tube went directly into a laboratory hood. Sample gas for the analytical instruments was obtained by a probe. The material in the fluid bed was 16.8 wt% CuO supported on Alcoa type F-1 activated alumina, 28-48 mesh. A single batch of this material was prepared, loaded into the fluid bed reactor, and used for all fluid bed experiments.

**Examination of Unmixed Combustion** For these experiments a setup was used in which flows of methane and air were measured by two rotameters and then each went to the common inlet of an electrically activated three way valve. (The use of three way valves allowed the flow through the rotameters to be continuous and hence more accurately measurable.) One of the flows was passed through the three way valve to vent while the other was passed through a 0.902 ID steel tube in an electric furnace, the heated length of this tube having a volume of 160cc and containing 87grams of 25.5% copper oxide on alumina rings. An electrical cycle timer was used to switch the three way valve at predetermined intervals.

## RESULTS

**Demonstration of Puff Suppression** Figure 1 shows raw data from a packed bed experiment, i.e. in this experiments a mixture of 2520ppm  $C_5H_5N$ , 3.6%  $O_2$ , balance  $N_2$ , the  $O_2$  was shut off, and the flame ionization detector is used to measure the amount of  $C_5H_5N$  surviving passage through the bed as a function of time. From the known initial and observed final concentrations of the  $C_5H_5N$  one can calculate as a function of time both the DRE and the extent to which the bed's oxidation capacity have been used. Figure 2 shows the data from Figure 1 recalculated in this manner. Using this procedure the experimental results from the fixed bed and fluid bed experiments were reduced to determine the initial DRE and the extent to which the oxidation capacity of copper oxide can be used before the DRE falls below some predetermined value. Capacity of the copper oxide bed is conveniently expressed in terms of the volume of combustion air a volume of the bed is equivalent to. The results of these calculations are shown in Table 1.

The following observation is also to be reported: when oxygen was present in the gas going into the hot copper oxide bed the amount of organic matter surviving passage through the bed was zero within the noise level of the FID. This was found in all experiments with one exception: during the experiments with  $CCl_3F$  76% of the input  $CCl_3F$  survived passage through the bed both in the presence and absence of oxygen.

Using the unmixed combustion setup the bed of CuO was subjected to approximately 5400 puffs of pure  $CH_4$  and showed no signs of mechanical deterioration or of its losing chemical activity. On completion of this test a

series of experiments was done to examine the operational characteristics of the unmixed combustor. Figure 3 shows the variations in the oxygen level of the postcombustion gases when the bed was operated at a fuel to capacity ratio less than one but an air to capacity ratio much greater than one. Figure 4 also shows oxygen level but with the combustor operating at fuel to capacity and air to capacity ratios which are both less than one. Figure 4 also shows the amount of NOx being produced by unmixed combustion.

A series of experiments was done in which the variations of levels of NOx and oxygen in the postcombustion gases was measured over a range of overall fuel to air stoichiometric ratios with the results shown in Figures 5 and 6

In another experiment the electrical furnace was shut off and the combustor was allowed to operate autothermally with a  $\text{CH}_4$  input of 3212 cc/min for 2 seconds, off for 15 seconds, and an air input of 3000cc/min for 15 seconds, off for 2 seconds. Initially the bed temperature in this experiment was 775°C. After dropping to 635°C the bed temperature wandered, slowly rising to 681°C. At 2.8 hours after shutting off the electric furnace the run was voluntarily terminated.

#### DISCUSSION

**Laboratory Scale Demonstration of Puffing Control** The results in Table 1 show that for a considerable variety of compounds (i.e. hydrocarbons and organic compounds containing nitrogen, phosphorous, chlorine and sulfur) copper oxide can provide both the DRE and the capacity needed in a practical method of puffing control. While the results for  $\text{C}_2\text{H}_2\text{F}_2$  were not as good, they still indicate that this technique may be useful for fluorine containing hydrocarbons. Similarly the results for  $\text{CCl}_3\text{F}$  were arguably positive. Freons are extremely refractory materials and even in the absence of puffing would normally be expected to pass unchanged through an incinerator. Thus in addition to providing a solution to the occasional problem of puffing, the use of a copper oxide bed also provides a means of substantially reducing the continuous emission of freons from incinerators.

**Controlling NOx production by Unmixed Combustion** The data reported above show that it is in principal possible to use supported CuO as the basis for a novel combustion system, one in which the fuel and air are largely unmixed. During unmixed combustion the production of NOx was found to be extremely low. Given the generally accepted mechanisms for NOx production this result is not surprising. For fuels which do not contain chemically bound nitrogen it is generally agreed that NOx is chiefly thermal NOx, i.e. most of the NOx is produced by the "extended" Zeldovitch mechanism,  $\text{O} + \text{N}_2 = \text{NO} + \text{N}$ ,  $\text{N} + \text{O}_2 = \text{NO} + \text{O}$ ,  $\text{OH} + \text{N} = \text{NO} + \text{H}$ . The other source of NOx is the prompt NOx mechanism, i.e. the attack of hydrocarbon radicals such as CH on  $\text{N}_2$  to produce HCN which is then oxidized to NO. Both these mechanisms are strongly disfavored at lower temperatures and both depend on the superequilibrium concentrations of free radicals which conventional combustion produces. By eliminating direct contact between the fuel and air both the extremely high temperatures normally associated with combustion and the high free radical concentrations are avoided and thus NOx production is suppressed.

**Controlling CO<sub>2</sub> emissions by Unmixed combustion** The problem of global warming due to the emissions of CO<sub>2</sub> during combustion has recently begun to receive a great deal of serious attention. In many locations pure CO<sub>2</sub> could economically be used in tertiary oil recovery or put to other use but the possibility of recovering dilute CO<sub>2</sub> from combustion gases have been given little consideration because the expense and large energy consumption involved. In an unmixed combustion system, however, the fuel is converted to CO<sub>2</sub> and water without being diluted with nitrogen. Thus unmixed combustion may, in favorable situations, be the basis of burning fuel without CO<sub>2</sub> emissions.

ACKNOWLEDGMENT The author gratefully acknowledges the support of the U. S. Environmental Protection Agency under the SBIR program, contract 68D20093.

REFERENCES

- 1 E. T. Oppelt, J. Air Poll. Cont. Assoc., 37, 558 (1987)
- 2 J. O. L. Wendt, W. P. Linak, Combust. Sci. and Tech, 61, 169-185, (1988)
- 3 J. O. L. Wendt, W. P. Linak, and P. M. Lemieux, HAZARDOUS WASTE & HAZARDOUS MATERIALS, 7, 41-53, (1990)
- 4 P. M. Lemieux, W. P. Linak, J. A. McSorley, J. O. L. Wendt, and J. E. Dunn, Submitted to Combust. Sci. and Tech
- 5 Risk Analysis of the Disposal of Chemical Munitions at National or Regional Sites, ADA 193355

TABLE 1 SUMMARY OF FIXED BED EXPERIMENTS

Puff being Oxidized	Reaction Conditions	Initial DRE	DRE as a function of Bed Oxidation Capacity, Equivalent cc of air per cc of bed
1974 ppmC of C <sub>6</sub> H <sub>5</sub> Cl	802°C for 0.53sec.	99.9985%	99.99% at 37.3cc/cc
3683 ppmC of C <sub>6</sub> H <sub>5</sub> Cl	812°C for 0.53sec.	>99.999%	99.9% at 136cc/cc 99% at 207cc/cc
10,000 ppmC of C <sub>6</sub> H <sub>6</sub>	811°C for 0.53sec.	99.997%	99.9% at 118cc/cc 99% at 197cc/cc
19,000 ppmC of C <sub>5</sub> H <sub>4</sub> S	814°C for 0.53sec.	99.9999%	99.9% at 186cc/cc 99% at 373cc/cc
7,800 ppmC of C <sub>6</sub> H <sub>5</sub> F	815°C for 0.53sec.	99.3%	
7,800 ppmC of C <sub>6</sub> H <sub>5</sub> F	991°C for 0.45sec.	99.94%	99.9% at 2.8cc/cc 99.3% at 59cc/cc
2,520 ppmC of C <sub>5</sub> H <sub>5</sub> N	817°C for 0.53sec.	99.9968%	99.99% at 99cc/cc
6000 ppmC of CCl <sub>3</sub> F	821°C for 0.53sec.	76%	
3110 ppmC of (HO) <sub>2</sub> POCH <sub>2</sub> COOH	818°C for 0.53sec.	99.993%	99.9% at 29cc/cc 99% at 54 cc/cc

SUMMARY OF FLUID BED EXPERIMENTS

8000 ppmC of C <sub>6</sub> H <sub>6</sub>	806°C for 0.75sec.	>99.994%	99.9% at 43cc/cc 99% at 73cc/cc
3900 ppmC of C <sub>6</sub> H <sub>5</sub> Cl	805°C for 0.75sec.	>99.95%	99.9% at 169cc/cc 99% at 215 cc/cc

## Oxidation of C<sub>5</sub>H<sub>5</sub>N by CuO

Run 7

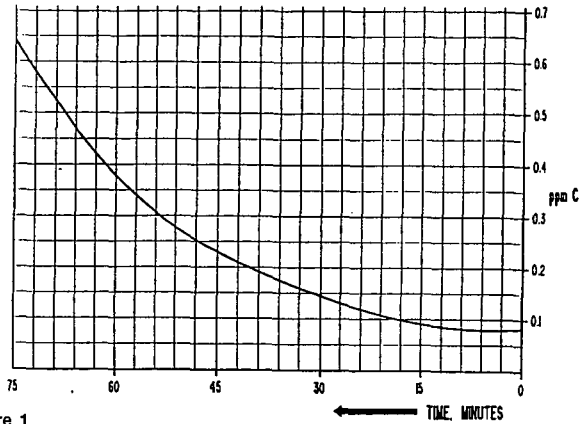
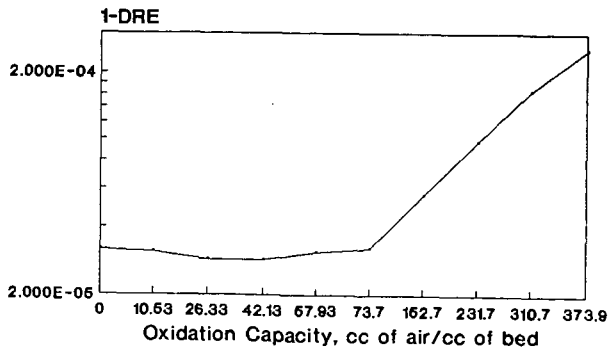


Figure 1

## Destruction and Removal Efficiency for Oxidation of C<sub>5</sub>H<sub>5</sub>N by CuO



Run 7  
Figure 2

### Unmixed Combustion

CH<sub>4</sub> and Air feed alternately to a bed of CuO on alumina, long pulses of air

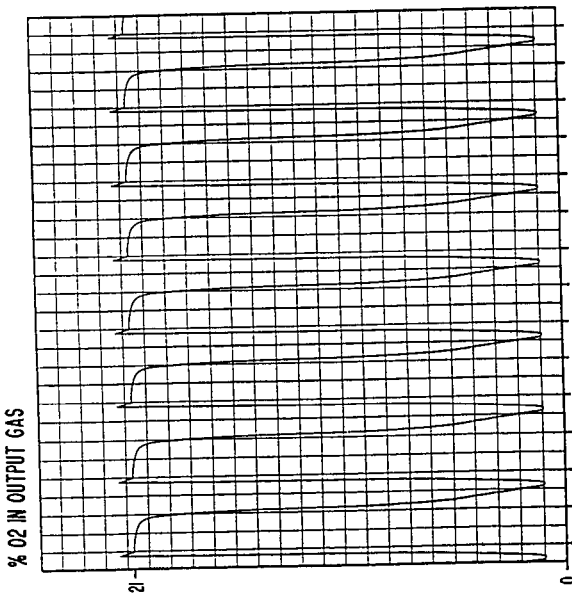


FIG. 3

STOICHIOMETRIC RATIO = 0.315  
 B5C. 87g OF 25.5 WT% CuO IN A 160 cc BED  
 AIR = 3470 cc/MIN FOR 1/5 SEC. OFF FOR 5 SEC.  
 CH<sub>4</sub> = 2513 cc/MIN FOR 5 SEC. OFF FOR 1/5 SEC.

### Unmixed Combustion

CH<sub>4</sub> and Air feed alternately to a bed of CuO on alumina, short pulses of air

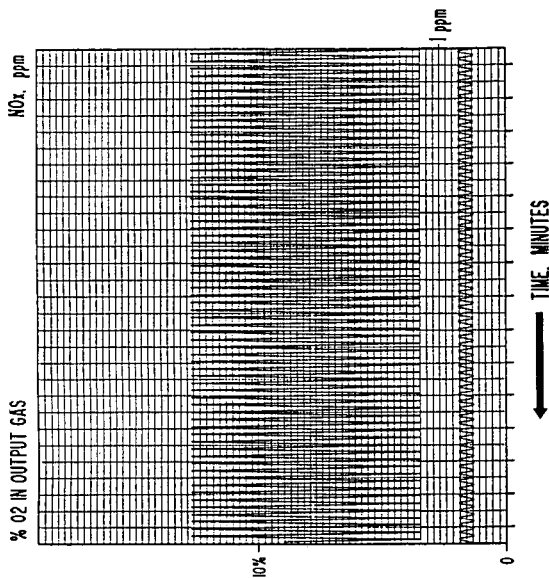
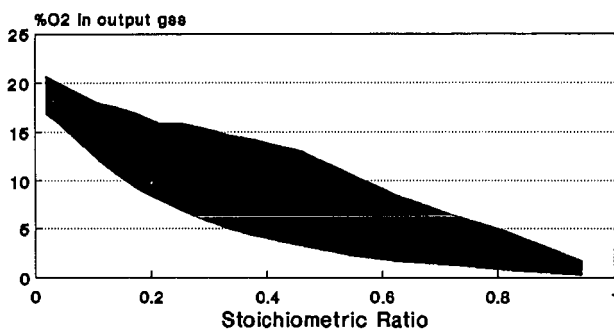


FIG. 4

STOICHIOMETRIC RATIO = 0.458  
 AIR = 3660 cc/MIN FOR 1/5 SEC. OFF FOR 1 SEC.  
 CH<sub>4</sub> = 1 SEC ON, 1/5 SEC OFF

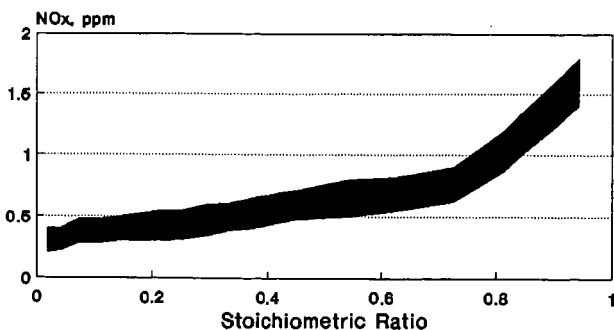
### Effect of Stoichiometric Ratio on the variance of O<sub>2</sub> in the output gas from unmixed combustion



816C, 87g of 25.5wt% CuO in a 180 cc bed  
Air - 3660cc/min for 16 sec, 1 sec off  
CH<sub>4</sub> - 1 sec on, 15 sec off,

Figure 5

### Effect of Stoichiometric Ratio on the variance of NO<sub>x</sub> in the output gas from unmixed combustion



816C, 87g of 25.5wt% CuO in a 180 cc bed  
Air - 3660cc/min for 16 sec, 1 sec off  
CH<sub>4</sub> - 1 sec on, 15 sec off,

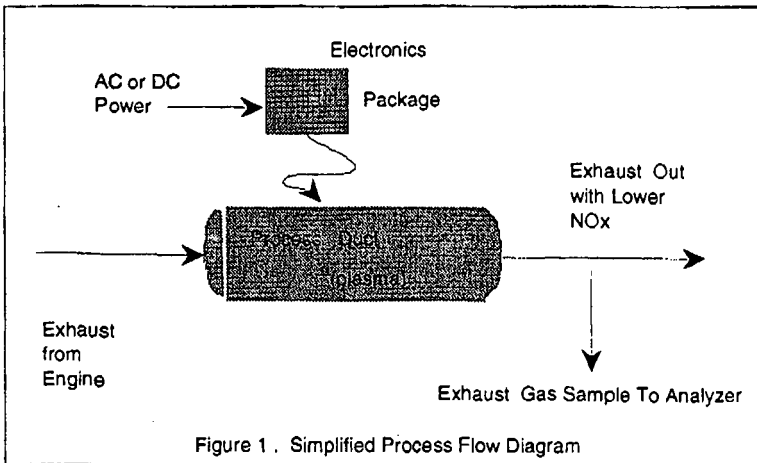
Figure 6

## ENOX, AN ELECTRONIC PROCESS FOR NOx ABATEMENT

Michael P. Manning  
PlasMachines Inc.  
11 Mercer Road  
Natick MA 01760

Recent revisions of the Clean Air Act have mandated increasingly stringent controls on NOx emissions. Combustion of fuel in engines for transportation and in boilers for electric utility and industrial power generation produce over 90 percent of all NOx emissions. ENOX, a recently discovered electronic process, shows significant promise for reducing NOx emissions from mobile sources such as cars and trucks in the near term and large stationary sources such as boilers in the long term.

The key to PlasMachines ENOX emission control process is the use of a **plasma**, that is an **electronically excited gas**, to cause the decomposition of NO and NO<sub>2</sub>. A simplified process diagram is shown in Figure 1. Electrical power feeds a proprietary electronics package which provides the excitation to the process duct. The duct is basically an open chamber with special electrodes and operates at atmospheric pressure or the combustion exhaust stream pressure. The process plasma is an alternating current, discontinuous, multifrequency, non-equilibrium discharge. During operation,



exhaust gas flows through the process duct and constituents of the exhaust stream are activated by collision or ionization with plasma electrons under the influence of the electronic excitation. Molecules of NO and NO<sub>2</sub> are thermodynamically unstable with respect to decomposition back to the elements, nitrogen and oxygen. Hence, after activation by plasma processes, NO and NO<sub>2</sub> undergo decomposition and their concentrations in the exhaust are reduced.

Three engines have been tested using this exhaust treatment process: a 5 hp Briggs and Stratton gasoline engine, an 8 hp Kubota diesel electrical generator set, and a 40 hp Ford multi-fuel industrial engine. The Ford Model VSG-411 is a multi-fuel four cylinder, four stroke, 1.1 liter engine. The engine will accept either gasoline or methanol as liquid fuels and with an IMPCO carburetor will also burn natural gas. Natural gas was used as the fuel for the testing during this experimental work.

PlasMachines current facilities include a complete test facility for dynamometer and emissions testing of engines of all types up to 1000 hp. A Superflow 901 Dynamometer utilizes a water brake to load and measure the output torque of engines, including the Ford engine used in this development work, operating on a test stand under computer control. A photograph of the Ford engine mounted on the dynamometer is shown in Figure 2

Samples of exhaust gas are drawn continuously by vacuum pumps from the engine exhaust line, through a teflon transfer line, and into the emissions analyzers. A small refrigerator with collection trap was used to prevent condensation from the exhaust sample line from entering and interfering with the analyzers.

Emissions monitoring equipment utilized include a Thermo Electron Model 10S NO/NO<sub>x</sub> Chemiluminescent Analyzer capable of measuring either NO or total NO<sub>x</sub> concentrations from 1 to 10,000 ppm. An Horiba Model MEXA-554GE NDIR automotive emission analyzer provides capability of continuous or spot monitoring of O<sub>2</sub>, CO<sub>2</sub>, CO, unburned hydrocarbons (UHC), and calculated air to fuel (A/F) ratio.

The four parallel reactors were each assembled from two stainless steel tees and a single straight length of 1.5 inch tube which were clamped together and clamped to the inlet and outlet manifold. Adapters clamped to each end of the reactor tube served to coaxially locate and support a one inch diameter electrode. Each reactor was connected electrically to a PlasMachines electronic source with two leads - the ground lead was connected to the stainless steel reactor shell while the electronic signal was connected to the electrode. A front view of the parallel reactor array are shown photographically in Figure 3.

The engine and reactors were tested using the following protocol. The Ford natural gas engine was started and run for approximately twenty minutes to ensure that all operating components and fluids including engine oil, cooling and dynamometer water were up to normal operating temperatures. The surface temperatures on the exhaust lines and reactor exterior surfaces were measured. The reactor exterior

surfaces were found to be between 250 and 280 F. The engine was operated at 830 and 1600 rpm with a torque load of 7 ft-lbs. With the PlasMachines electronic sources turned off, the uncontrolled levels of NO and NOx were measured as 300 and 320 respectively. When the electronic sources were turned on, the resulting ENOX process plasma reduced the NO and NOx levels to 60 and 180 respectively. This demonstrates an 80% reduction in NO and a 44% reduction in NOx. Power consumption by the electronic unit was 200 W.

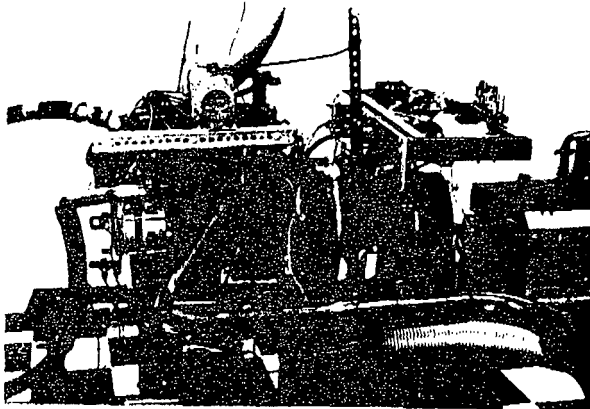


Figure 2. Ford industrial engine mounted on Superflow 901 Dynamometer

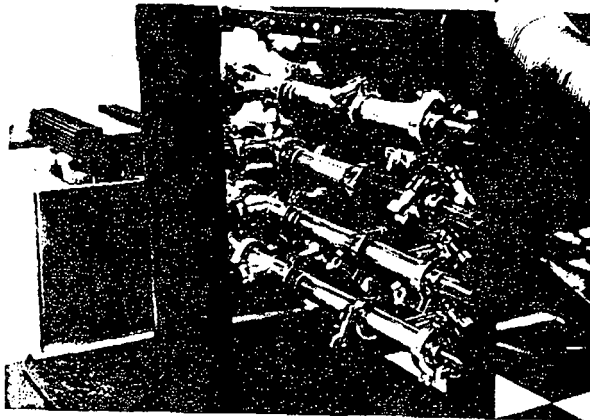


Figure 3. Front view of four parallel reactor units

THE EFFECT OF INITIAL NO<sub>x</sub> LEVELS  
ON SELECTIVE NON-CATALYTIC NO<sub>x</sub> REDUCTION PERFORMANCE

Greg C. Quartucy  
Tami A. Montgomery  
Dr. Lawrence J. Muzio  
Fossil Energy Research Corp.  
23342-C South Pointe  
Laguna Hills, CA 92653

Keywords: Selective Non-Catalytic Reduction, Initial NO<sub>x</sub>

ABSTRACT

The primary parameters affecting NO<sub>x</sub> reduction performance of SNCR processes include injection temperature and the chemical N/NO<sub>x</sub> molar ratio. Previous work showed that SNCR performance was also dependent upon initial NO<sub>x</sub> levels. This is of concern for future applications to oil- and gas-fired systems, where initial NO<sub>x</sub> levels of 30 to 100 ppm may be anticipated after combustion modifications are implemented.

To quantify the effect of these low initial NO<sub>x</sub> (NO<sub>x</sub>) levels on SNCR performance, a pilot-scale test program was performed to investigate the effect of NO<sub>x</sub> levels with both urea and ammonia injection. This pilot test program evaluated the effect of NO<sub>x</sub> levels ranging from 30 to 200 ppm on process performance. A range of temperature and N/NO<sub>x</sub> ratios was evaluated for each SNCR chemical. The laboratory effort was supported by chemical kinetic modeling of the SNCR process. Test results included characterization of both the ammonia and urea injection processes. The effect of process parameters on NO<sub>x</sub> reduction, and secondary emissions including NH<sub>3</sub>, N<sub>2</sub>O, and CO emissions was characterized. The laboratory data revealed important information regarding the implementation of SNCR processes at low initial NO<sub>x</sub> levels.

INTRODUCTION

Since NO<sub>x</sub> plays a major role in the formation of photochemical smog (Ref. 1), regulations requiring NO<sub>x</sub> emissions reductions have been enacted in many areas. For example, NO<sub>x</sub> emissions from utility boilers in the South Coast Air Quality Management District have been reduced significantly from their baseline, uncontrolled levels through the implementation of combustion modification techniques.

To meet upcoming regulations, which mandate further NO<sub>x</sub> emission reductions, alternate control methods may be required. One approach under consideration involves the use of selective non-catalytic NO<sub>x</sub> reduction (SNCR) techniques in conjunction with advanced combustion modification techniques. Both urea and ammonia injection have been shown to provide NO<sub>x</sub> reductions at full-scale for a variety of combustion devices.

The primary parameters affecting NO<sub>x</sub> reduction performance of SNCR processes are the injection temperature and N/NO<sub>x</sub> molar ratios. Previous work (Ref. 2) also showed the dependence of process performance on initial NO<sub>x</sub> levels. This is a concern for future applications to oil- and gas-fired systems, where initial NO<sub>x</sub> levels of 30 to 100 ppm may be anticipated after combustion modifications are implemented.

In order to quantify the effect of these low initial  $\text{NO}_x$  ( $\text{NO}_y$ ) levels on SNCR performance, a test program investigating the effect of  $\text{NO}_y$  levels with both ammonia and urea injection was performed. This laboratory test program evaluated the effect of  $\text{NO}_y$  levels ranging from 30 to 200 ppm on process performance for both urea and ammonia injection. Urea injection tests were performed over a temperature range of 1600 to 2075°F at varying reagent injection rates. Ammonia slip was measured, using wet chemical techniques at selected urea injection conditions. Ammonia injection tests were performed over a temperature range of 1470 to 1900°F. The laboratory experimental effort was supported by chemical kinetic modeling of the urea injection process using CHEMKIN.

#### FACILITY DESCRIPTION

The tests were performed using a natural gas-fired pilot-scale combustor facility. This facility has a design heat input of 300,000 Btu/hr, and a combustion product flowrate of 47 SCFM. This provides a nominal residence time of 0.5 second in the test section at 1800°F. Combustion gas temperatures entering the test section are controlled by adjusting the firing rate and with a series of adjustable water-cooled probes. Heat removal is controlled by varying the number and insertion depth of individual probes. The unit has a temperature gradient of 400-500°F/second over the test section length. While this is relatively high compared to other laboratory facilities, it was designed to match the temperature gradients typical of utility boiler environments.

Liquid and/or gaseous reagents were injected into the combustion products using water-cooled injectors. Gaseous  $\text{NH}_3$  was injected using diametrically opposed injectors. The liquid urea solution was injected using a single small water-cooled atomizer.

A suction pyrometer was used to measure true gas temperatures at the entrance to the test section. For this test program, all gas analysis sampling was performed at the test section exit. A portion of the sample was taken from the sample probe exit and transported to the gas analysis instrumentation by a heated Teflon sample line. Before passing through the analyzers, the sample was dried in a refrigerated dryer. The dried sample was analyzed for  $\text{NO}$ ,  $\text{NO}_x$ ,  $\text{O}_2$ ,  $\text{CO}$ ,  $\text{CO}_2$ ,  $\text{N}_2\text{O}$  and  $\text{O}_2$ , using continuous electronic gas analyzers. Ammonia concentrations were determined by passing a gas stream through an impinger train containing a dilute sulfuric acid solution. The ammonia concentration was subsequently determined using a specific ion electrode.

#### $\text{NH}_3$ INJECTION TEST RESULTS

The ammonia injection tests were performed using initial  $\text{NO}_x$  levels ranging from 30 to 200 ppm. Injection temperatures ranged from nominally 1470 to 1900°F. The  $\text{N}/\text{NO}_x$  ratio, the molar ratio of nitrogen in the SNCR chemical to the inlet  $\text{NO}_x$ , characterizes the amount of chemical injected.  $\text{N}/\text{NO}_x$  molar ratios of 1.0 and 2.0 were evaluated during these tests.

Figure 1 shows  $\text{NO}_x$  reduction data plotted versus temperature for tests performed at  $\text{N}/\text{NO}_x$  ratios of 1.0 and 2.0, and varying initial  $\text{NO}_x$  levels. A number of observations can be made from the data in Figure 1. First, the level of  $\text{NO}_x$  reduction decreases as the initial  $\text{NO}_x$  level decreases. Also, the optimum injection temperature appears to shift to higher temperatures as the initial  $\text{NO}_x$  level increases. Conversely, operation at low initial  $\text{NO}_x$  levels appears to require injection at reduced temperatures to obtain optimum results. This trend was observed for tests performed at both  $\text{N}/\text{NO}_x$  molar ratios. This temperature shift increases as the  $\text{N}/\text{NO}_x$  ratio increases. A final observation can be made about the effect of initial  $\text{NO}_x$  level at low injection temperatures. Over the majority of the temperature range, decreasing the initial  $\text{NO}_x$  level decreased  $\text{NO}_x$  reduction. However, as can be seen in Figure 1, at temperatures below nominally 1500°F, decreasing the initial  $\text{NO}_x$  level results in an increase in  $\text{NO}_x$  removal (albeit the overall levels of  $\text{NO}_x$  reduction are small).

## UREA INJECTION TEST RESULTS

The urea injection tests were conducted using an aqueous urea solution. Solution flow rates were held constant for these tests to maintain a constant thermal environment in the injection zone. To change the N/NO<sub>x</sub> ratios, the concentration of the urea solution was varied.

For the urea injection tests, gaseous emissions measurements were made over a temperature range of 1600 to 2075°F. Initial NO<sub>x</sub> levels were varied from 30 to 200 ppm, while molar ratios of N/NO<sub>x</sub> were varied from 0.5 to 4.0. Byproduct ammonia emission measurements, performed in conjunction with urea injection, were made over a more limited matrix. A temperature range of 1600 to 1940°F was used for performance of the subsequent byproduct NH<sub>3</sub> emissions (NH<sub>3</sub> slip) tests. NH<sub>3</sub> measurements were not made at temperatures in excess of 2000°F, since previous tests have shown that ammonia emissions are negligible at these high temperatures. Molar N/NO<sub>x</sub> ratios of 0.5, 1.0 and 2.0 were evaluated during these tests for initial NO<sub>x</sub> levels of 30, 70 and 200 ppm (in the present paper, only the results obtained for a N/NO<sub>x</sub> molar ratio of 2.0 are shown).

Figure 2 shows NO<sub>x</sub> reduction as a function of injection temperature for urea injection tests performed at a N/NO<sub>x</sub> molar ratio of 2.0. The results are similar to the ammonia test results shown in Figure 1. These data also show that NO<sub>x</sub> reductions decreased with decreasing initial NO<sub>x</sub> levels. This trend was evident for all injection temperatures. It was also evident that the optimum injection temperature decreased as initial NO<sub>x</sub> levels decreased. Also note that at low temperatures (i.e., less than 1600°F), decreasing the initial NO<sub>x</sub> level increased NO<sub>x</sub> reduction.

Ammonia slip data are plotted in Figure 3, which shows NH<sub>3</sub> concentration versus temperature as a function of initial NO<sub>x</sub> level at a N/NO<sub>x</sub> molar ratio of 2.0. As expected, the data show that NH<sub>3</sub> emissions increase with initial NO<sub>x</sub> level and decrease with temperature.

N<sub>2</sub>O has been found to be a product of the reaction between urea and NO<sub>x</sub>. N<sub>2</sub>O production is plotted as a function of temperature for operation at a N/NO<sub>x</sub> molar ratio of 2.0 in Figure 4. The data show that, below 2010°F, N<sub>2</sub>O emissions increased with increasing temperature, regardless of initial NO<sub>x</sub> level or N/NO<sub>x</sub> ratio. At temperatures above 2010°F, the N<sub>2</sub>O emissions decreased. N<sub>2</sub>O emissions also increased with both the N/NO<sub>x</sub> and initial NO<sub>x</sub> levels, as expected. Comparison with data reported previously show that N<sub>2</sub>O production peaks at approximately the same temperature as NO<sub>x</sub> reduction.

The slope of the N<sub>2</sub>O versus temperature curves increased as initial NO<sub>x</sub> levels increased for all of the N/NO<sub>x</sub> ratios. This change in sensitivity likely reflects the quantity of reagent available to react at the differing injection rates.

## CHEMICAL KINETICS MODELING RESULTS

In support of the laboratory urea injection tests, a series of chemical kinetic calculations were performed to investigate the effect of initial NO<sub>x</sub> level upon the urea temperature and NO<sub>x</sub> reduction, in particular, the behavior of the initial NO<sub>x</sub> level at low temperatures. The chemical kinetics calculations were performed over a temperature range of 1472 to 1992°F at initial NO<sub>x</sub> levels of 30, 70 and 200 ppm. Urea injection rates were set to give a N/NO<sub>x</sub> molar ratio of 2.0. Combustion products were set at a stoichiometry comparable to the pilot-scale work. The urea was assumed to decompose as NH<sub>3</sub> and HNCO.

The chemical kinetics calculations were performed using a PC version of SANDIA's CHEMKIN program. The mechanism used was that of Miller and Bowman (Ref. 3). A residence time of 2.0 seconds was used in the calculations.

Calculated  $\text{NO}_x$  reductions,  $\text{NH}_3$  slip and  $\text{N}_2\text{O}$  production for a  $\text{N}/\text{NO}_x$  ratio of 2.0 are plotted as a function of temperature at three initial  $\text{NO}_x$  levels (30, 70, and 200 ppm) in Figure 5. For an initial  $\text{NO}_x$  level of 200 ppm, the calculated chemical kinetics data show that a peak  $\text{NO}_x$  removal of approximately 100 percent occurred at 1740°F. At an initial  $\text{NO}_x$  level of 70 ppm, the maximum  $\text{NO}_x$  removal decreased to approximately 90 percent and occurred at a temperature of 1605°F. When the initial  $\text{NO}_x$  was decreased to 30 ppm, the maximum  $\text{NO}_x$  removal decreased to 80 percent and occurred at approximately 1520°F. The calculations indicate that decreasing the initial  $\text{NO}_x$  concentration shifts the temperature window and reduces the maximum achievable  $\text{NO}_x$  reduction. In spite of the shift in optimum temperature and maximum reduction, the shape of the window appears to remain essentially the same over the range of conditions evaluated. At low temperatures, the calculated results also show an increase in  $\text{NO}_x$  reduction with decreasing initial  $\text{NO}_x$  level (Figure 5).

The model predicts higher  $\text{NO}_x$  removals and slightly different temperature windows than were seen experimentally. However, the experimental results follow the same trends predicted by the model calculations. As initial  $\text{NO}_x$  levels decrease, the temperature window shifts to lower temperatures and the maximum amount of  $\text{NO}_x$  removal decreases.

The  $\text{NH}_3$  slip and  $\text{N}_2\text{O}$  levels predicted by the model also support the experimental results (Figure 5). The model predicts the increase in  $\text{NH}_3$  and  $\text{N}_2\text{O}$  with increasing  $\text{NO}_x$  levels, and their decrease with increasing injection temperatures. However, the model predicts lower levels of  $\text{NH}_3$  and  $\text{N}_2\text{O}$  than observed experimentally; in addition, the model predicts  $\text{N}_2\text{O}$  production at temperatures lower than those observed experimentally. Part of these differences can be ascribed to the thermal profiles. The calculations were done assuming isothermal conditions while the experimental combustor exhibits a temperature gradient of 400-500°F/second.

## CONCLUSIONS

Based on the data presented above, the following conclusions can be drawn for both urea and ammonia injection:

- Reducing initial  $\text{NO}_x$  levels results in 1) a decrease in  $\text{NO}_x$  reduction performance, and 2) a decrease in optimum injection temperatures.

The following conclusions can be drawn for urea injection:

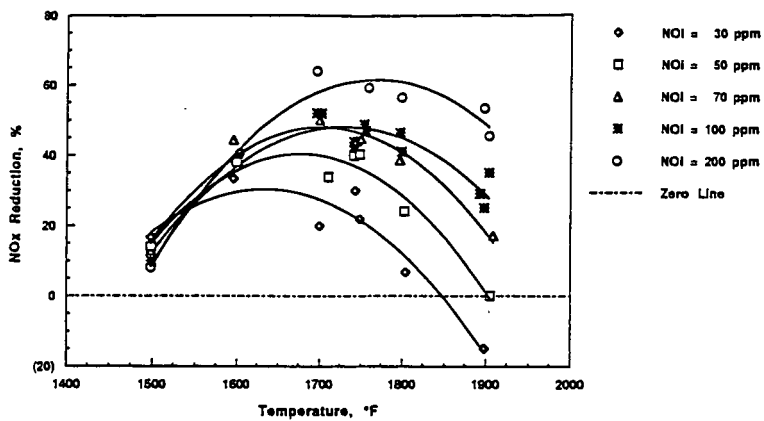
- Decreasing temperatures result in increasing  $\text{NH}_3$  emissions.
- Below 2010°F, increasing urea injection rates result in increasing  $\text{N}_2\text{O}$  emissions. However,  $\text{N}_2\text{O}$  emissions decrease at temperatures above 2010°F.

Chemical kinetic modeling of the urea injection process showed trends similar to those seen during performance of the laboratory tests.

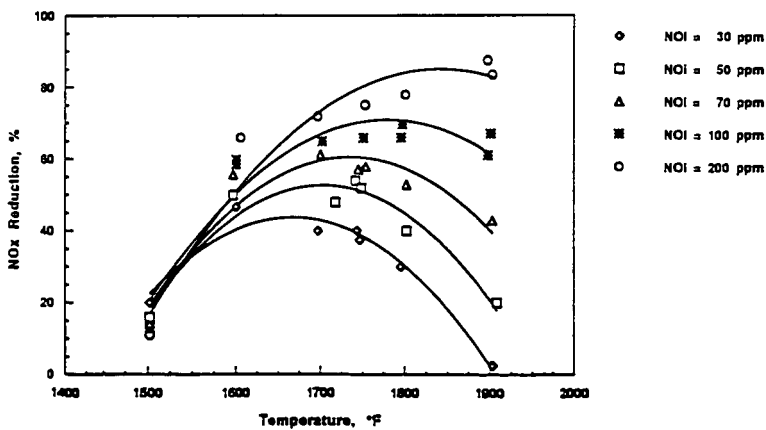
## REFERENCES

- (1) Seinfeld, J. H., Air Pollution-Physical and Chemical Fundamentals, McGraw Hill, NY, 1975.

- (2) Muzio, L. J. and Arand, J. K., "Homogeneous Gas Phase Decomposition of Oxides of Nitrogen," Electric Power Research Institute Report No. EPRI 461-1, July 1976.
- (3) Miller, J. A. and Bowman, C. T., "Mechanisms and Modeling of Nitrogen Chemistry in Combustion," Paper Number WSS/CI 88-63, presented at the Fall Meeting of the Western States Section/The Combustion Institute, Dana Point, CA. October 1988.



(a)  $N/NO_x = 1.0$



(b)  $N/NO_x = 2.0$

Figure 1. Laboratory test results with NH<sub>3</sub> injection. Effect of injection temperature on NO<sub>x</sub> removal at variable initial NO<sub>x</sub> levels

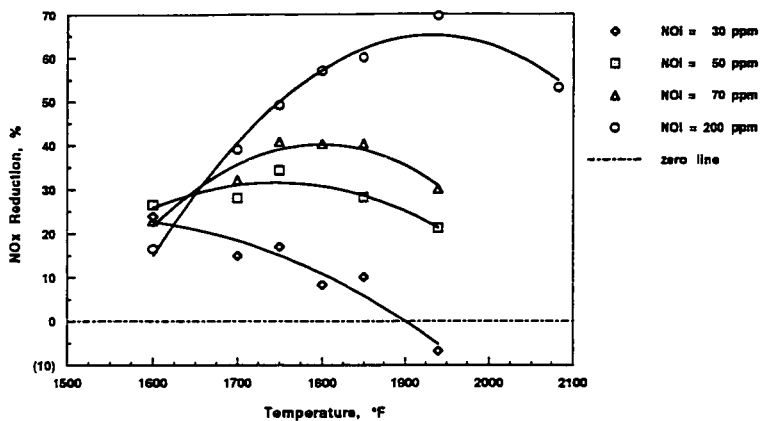


Figure 2. Laboratory test results with urea injection. Effect of injection temperature on  $\text{NO}_x$  removal at variable initial  $\text{NO}_x$  levels

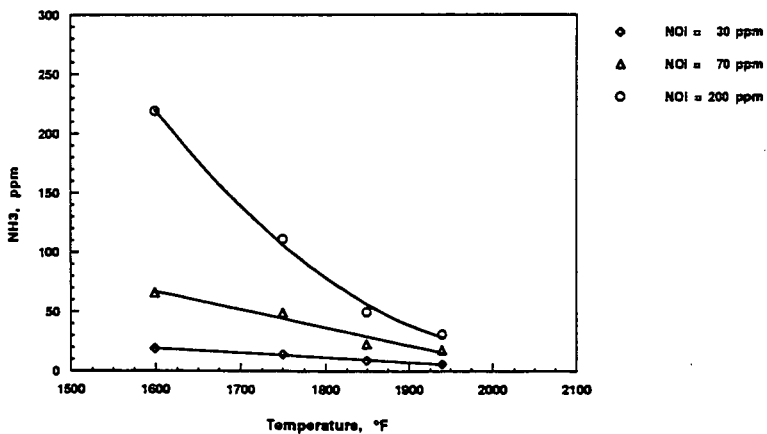


Figure 3. Laboratory test results with urea injection. Effect of injection temperature on  $\text{NH}_3$  emissions at variable initial  $\text{NO}_x$  levels,  $\text{N}/\text{NO}_x = 2.0$ .

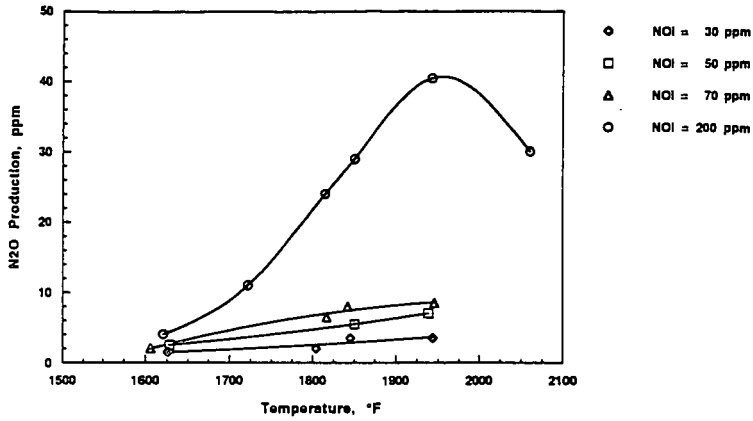
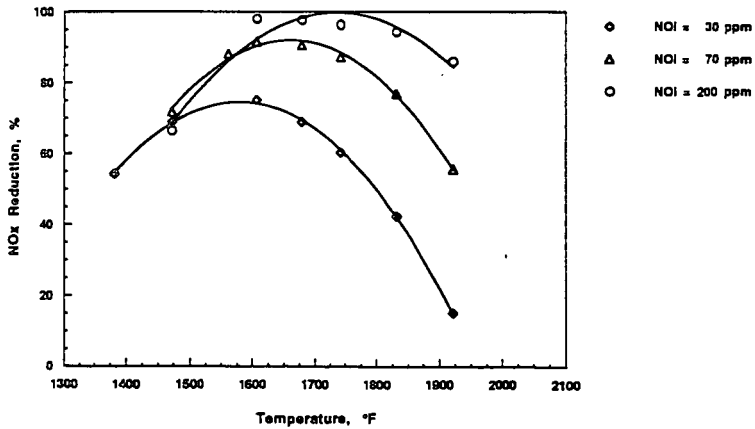
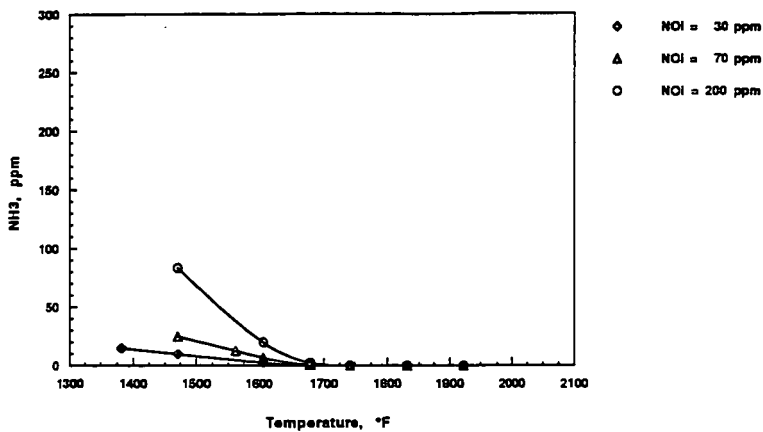


Figure 4. Laboratory test results with urea injection. Effect of injection temperature on  $N_2O$  emissions at variable initial  $NO_x$  levels,  $N/NO_x = 2.0$ .

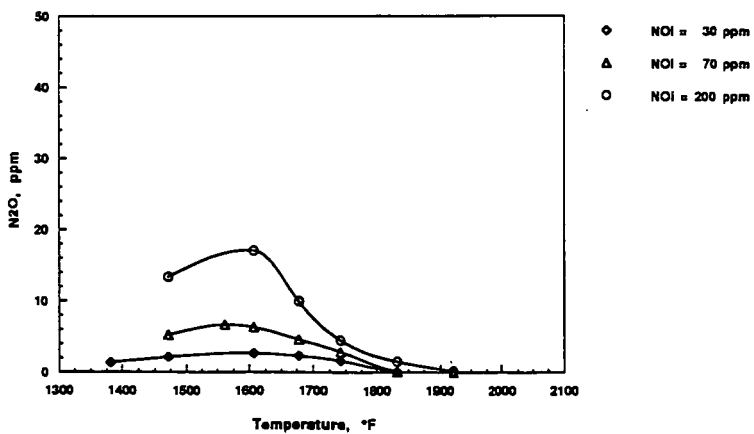


(a)  $NO_x$  Reduction

Figure 5. CHEMKIN chemical kinetics modeling results showing the predicted effect of temperature on  $NO_x$  reduction with urea injection.



(b)  $\text{NH}_3$  Emissions



(c)  $\text{N}_2\text{O}$  Production

Figure 5. CHEMKIN chemical kinetics modeling results showing the predicted effect of temperature on  $\text{NO}_x$  reduction with urea injection.

## LIMITS TO NO<sub>x</sub> REDUCTION BY NH<sub>3</sub> INJECTION

John H. Pohl  
Energy International  
Laguna Hills, CA 92653

Shyh-Ching Yang  
Energy and Resources Laboratory  
Hsinchu, Taiwan

William A. Sowa and James W. Dill  
University of California  
Irvine, CA 92717

Keywords: NO<sub>x</sub> Reduction by NH<sub>3</sub>

### INTRODUCTION

The process to reduce NO<sub>x</sub> by NH<sub>3</sub> was patented by Lyon (1975). The process initially found limited use to control NO<sub>x</sub> in oil- and gas-fired boilers in Japan. The process was experimentally investigated by Muzio, et al. (1976) and Lyon (1978). Typically the NO<sub>x</sub> reduction cited in small scale studies or practical application was 40-70 percent. Recently, NH<sub>3</sub> injection systems have been installed on a number of incinerators and fluid bed combustors. The measured emission of NO<sub>x</sub> from some of these operating combustors is below 10 ppm (d, 3% O<sub>2</sub>). These results implied that better reduction could be achieved than had been thought based on previous small scale results and from field trials.

This paper describes experiments and calculations aimed at establishing the maximum NO<sub>x</sub> reduction that can be achieved in the absence of mixing limitations and to determine how gas composition, operating parameters, and additives affect the reduction of NO<sub>x</sub> and the slip of NH<sub>3</sub>.

### EXPERIMENTS

Experiments were designed to be controllable, free of mixing constraints and catalytic influence, and capable of investigating the range of operation of commercial systems. The experimental apparatus, Figure 1., delivers gas from analyzed bottles, mixes and meters the flow through rotometers, adds water vapor as desired from a saturated bath, and passes the gases through a quartz coil reactor in a temperature controlled oven. The bottled gases are mixed to represent the range of flue gases to be treated or the gases after treatment. The gases are analyzed before and after the oven using continuous monitors for NO, NO<sub>2</sub>, O<sub>2</sub>, CO, and CO<sub>2</sub> and an ion specific electrode for NH<sub>3</sub> concentration.

The conditions investigated were ( baseline conditions are underlined):

- o residence time: 0.1, 0.2, 0.5, 1.0 seconds
- o temperature: 1061, 1116, 1144, 1172, 1200, 1228, 1255, 1283, and 1311 K
- o NO: 100, 200, 300, 400, 600, 800 ppm
- o CO: 0, 100, 200, 400, 600, 700 ppm

- o H2O: 0, 6 %
- o CO2: 15 %
- o O2: 3 %
- o NH3/NO: 1, 1.5, 2.0, 3.0, 4.0

Calculations were used to interpret and extend the results of the experimental. Calculation were made using the Sandia National Laboratories SENKIN and the extended mechanism of Miller and Bowman (1989). Selected results from the calculations were fit with mathematical expressions. These expressions allow the data to be easily interpolated and possibly to be extended slightly.

## RESULTS

The influence of the above conditions on NOx reduction and NH3 slip were determined by experiment and calculations and were compared with previous experimental data. The following conclusions were derived from the range of conditions studied.

### Residence Time

Longer residence times generally resulted in slightly increased reduction of NOx and less NH3 slip. However, shorter residence time, occasionally produced slightly greater NOx reductions and the maximum NOx reduction occurs at lower temperatures for shorter residence times.

### Temperature

We find an optimum temperature for the reduction of NOx in the range of 1175- 1225 K and the minimum temperature for nearly complete destruction of NH3 to be greater than 1300 K as shown in Figure 2. and in agreement with other literature values. However, our experimental results show much higher reduction of NOx and much greater NH3 slip compared with the measurements of Muzio, et al. (1976). Our results agree with those reported by Lyon (1979) and calculations made using the unaltered Miller and Bowman Mechanism. The differences between our results and those of Muzio, et al. (1976) may result from their injection of aqueous NH4OH solutions instead of gaseous NH3, mixing limitations in their pilot scale combustor compared to our plug flow reactor, temperature gradients in their reactor compared to our constant temperature reactor, and their use of 100 ppm NO compared to our use of 400 ppm.

### H2O

The influence of H2O in the range of 0-6 percent was found to be small on NOx reduction and NH3 slip.

### CO

Increased concentrations of CO were found to reduce the NOx reduction and create a peak in the NH3 slip as shown in Figure 3. Our results show that increasing CO concentration from 0 to 700 ppm causes a relative small decrease in NOx reduction, where as the results of Teixeira et al. (1991) show a large increase. Conversely, our results show that increasing

the CO concentration from 0 to 100 ppm can result in a four fold increase in NH<sub>3</sub> slip: higher concentrations of CO reduce the NH<sub>3</sub> slip until the slip reaches a low level at 600 ppm CO. The results of Teixeira et al. show low NH<sub>3</sub> slips at all levels of CO. Again, our experimental results agree with calculations obtained from the unaltered Miller and Bowman Mechanism and the difference between our results and those of Teixeira et al. may result from the difference in experimental conditions particularly any imperfect mixing in their experiment.

## NO

The fractional NO reduction decreases with decreased levels of initial level of NO concentration below 400 ppm as shown in Figure 4. Conversely, the level of NH<sub>3</sub> slip increases with increased level of initial NO concentration. The influence of initial NO concentration on NO reduction and NH<sub>3</sub> slip agrees with the results of Muzio, et al. (1976) and the results from calculation based on the Miller and Bowman Mechanism.

## NH<sub>3</sub>/NO

The level of NO reduction increases as the NH<sub>3</sub>/NO level increases to 1.7 as shown in Figure 5. The amount of NH<sub>3</sub> slip increases at NH<sub>3</sub>/NO ratios greater than 1.0 to 1.5. The results of our experiments agree with those of Teixeira, et al. (1991) and results of calculations made using the Miller and Bowman Mechanism.

## Additives

Calculations on the effect of H<sub>2</sub>, H<sub>2</sub>O<sub>2</sub>, and CH<sub>4</sub> additives injected after the NH<sub>3</sub> injection zone were done to determine the effects of these additives on NO<sub>x</sub> reduction and NH<sub>3</sub> slip. The results of these calculations shown in Figure 6. are based on the effluent from the NH<sub>3</sub> reaction zone with a concentration of 8 ppm NO and 81 ppm NH<sub>3</sub>. The NO reductions reported in Figure 6. is based on the fractional reduction from an original NO concentration of 400 ppm. Therefore, values greater than 0.02 indicate production of NO after the reaction zone. At the temperatures required to reduce NH<sub>3</sub> to 5 ppm, injection of H<sub>2</sub> and H<sub>2</sub>O<sub>2</sub> both result in increases in NO concentration.

Calculations predict injection of CH<sub>4</sub> at a temperature 100 K below the NH<sub>3</sub> injection temperature of 1200 K has little effect on NO<sub>x</sub> emission while reducing the NH<sub>3</sub> slip to about 5 ppm. Figure 7. experimentally confirms that CH<sub>4</sub> can reduce NH<sub>3</sub> slip, although not to the levels predicted by the calculations.

## ACKNOWLEDGMENTS

The work reported in this paper was sponsored by the Energy Resources Laboratories in Hsinchu, Taiwan and managed through Energy International of Laguna Hills, California. The work was performed at University of California at Irvine, California.

## REFERENCES

Lyon, R.K., "Method for the Reduction of the Concentration of NO in Combustion Effluents Using Ammonia," U.S. Patent 3,900554 (1975).

Lyon, R.K., "Thermal DeNOx: How it Works", Hydrocarbon Processing, October (1979).

Miller, J.A. and C.T. Bowman, "Mechanisms and Modeling of Nitrogen Chemistry in Combustion", Prog. Energ. Comb. Sci., 15, pp. 287-338 (1989).

Muzio, L.J., J.K. Arand, and D.P. Teixeira, "Gas Phase Decomposition of Nitric Oxide in Combustion Products", Sixteenth Symposium ( International ) on Combustion, pp. 199-207 (1976).

Teixeira, D.P., L.J. Muzio, and T.A. Montgomery, "Effect of Trace Combustion Species on SNCR Performance", International Conference on Environmental Control of Combustion Processes, Joint Meeting of the American Flame Research Committee and the Japanese Flame Research Committee, Honolulu, HI, October (1991).

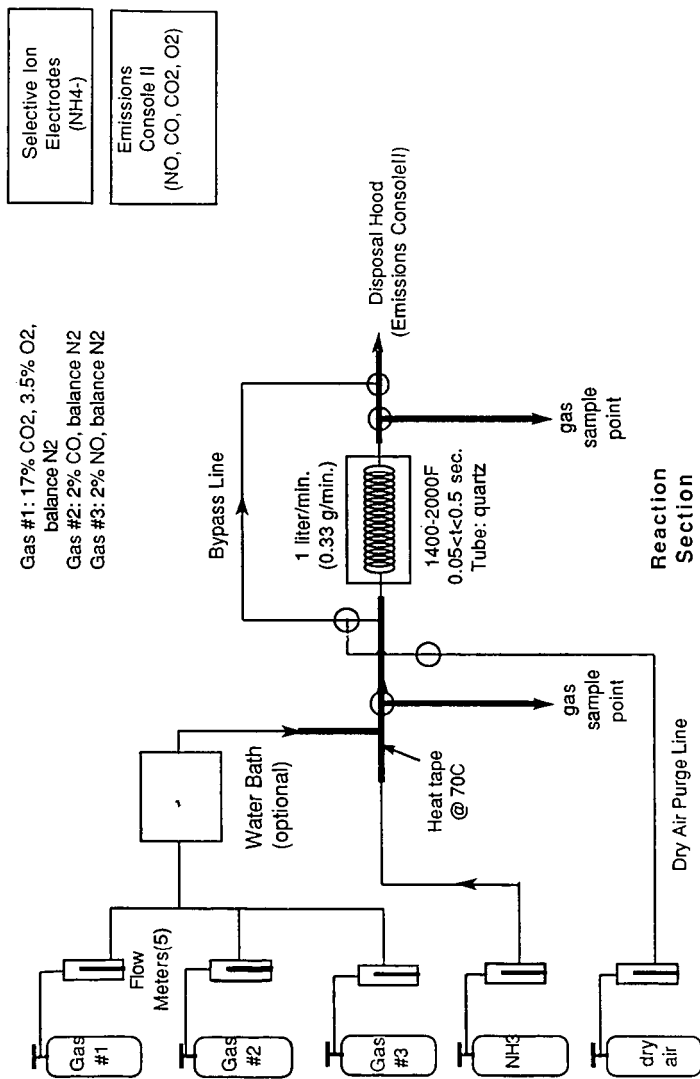
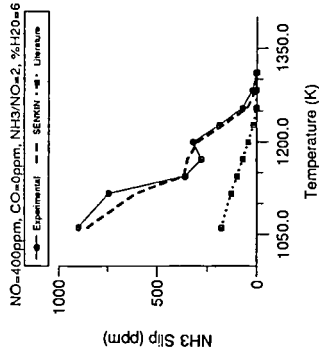
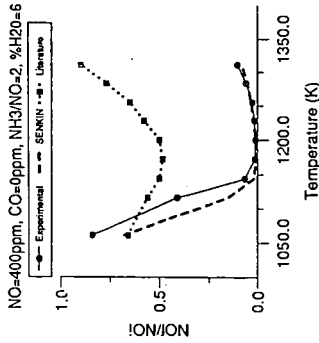


Fig. 1. Experimental Apparatus.

a.) NO Reduction, Experimental Results b.) Residual NH<sub>3</sub>, Experimental Results



c.) NO Reduction, Modelled (ppm out/in) d.) Residual NH<sub>3</sub>, Modelled (ppm)

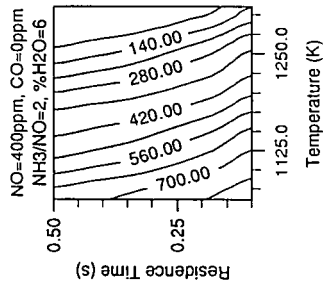
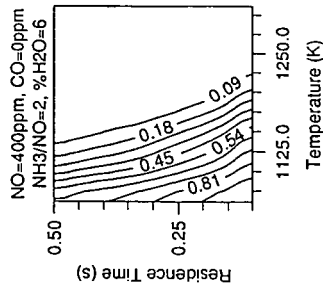
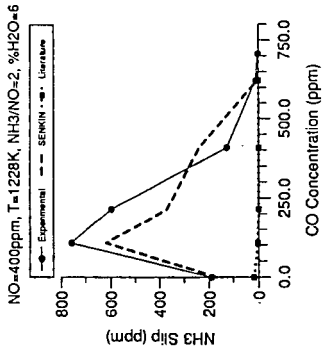
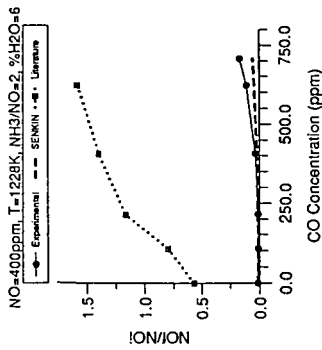


Fig. 2. Effect of Temperature on NO<sub>x</sub> Reduction and NH<sub>3</sub> Slip.

a.) NO Reduction, Experimental Results b.) Residual NH<sub>3</sub>, Experimental Results



c.) NO Reduction, Modelled (ppm out/in) d.) Residual NH<sub>3</sub>, Modelled (ppm)

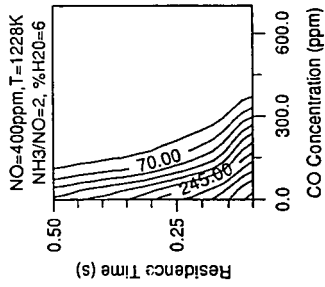
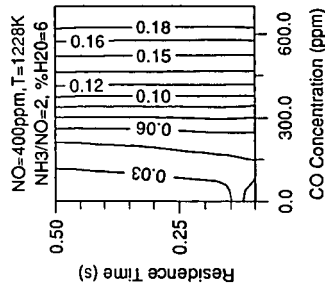
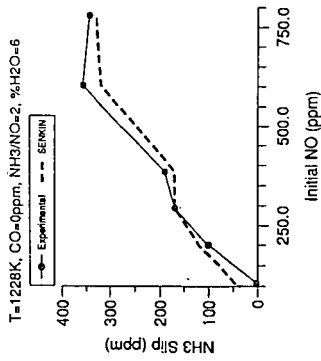
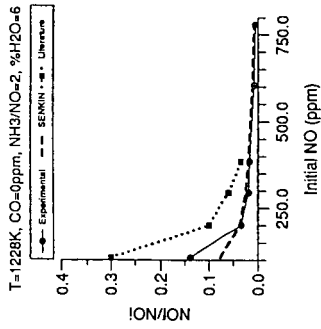


Fig. 3. Effect of CO Concentration on NO<sub>x</sub> Reduction and NH<sub>3</sub> Slip. Teixeira, et al. (1991).

a.) NO Reduction, Experimental Results      b.) Residual NH<sub>3</sub>, Experimental Results



c.) NO Reduction, Modelled (ppm out/in)      d.) Residual NH<sub>3</sub>, Modelled (ppm)

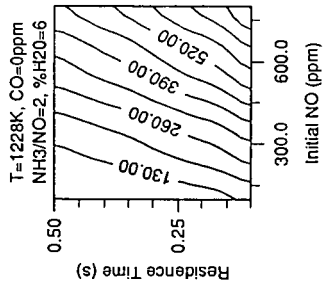
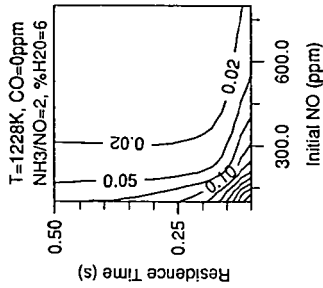
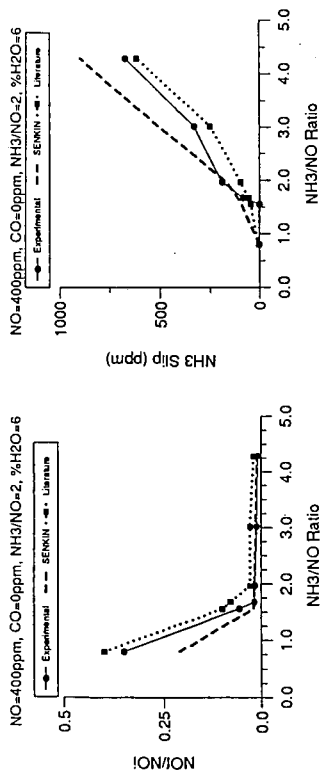


Fig. 4. Effect of Initial NO Concentration on NO<sub>x</sub> Reduction and NH<sub>3</sub> Slip. Muzio, et al. (1976).

a.) NO Reduction, Experimental Results b.) Residual NH<sub>3</sub>, Experimental Results



c.) NO Reduction, Modelled (ppm out/in) d.) Residual NH<sub>3</sub>, Modelled (ppm)

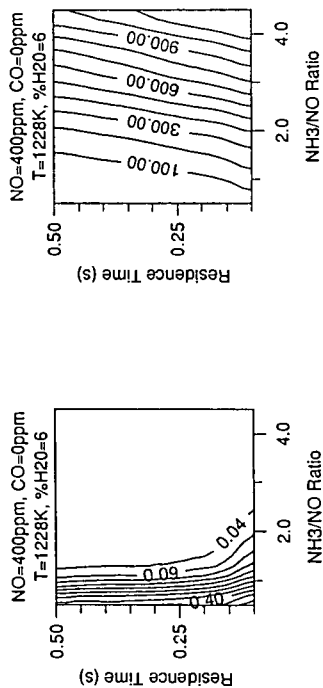


Fig. 5. Effect of NH<sub>3</sub>/NO Ratio on NO<sub>x</sub> Reduction and NH<sub>3</sub> Slip. Teixeira, et al. (1991).

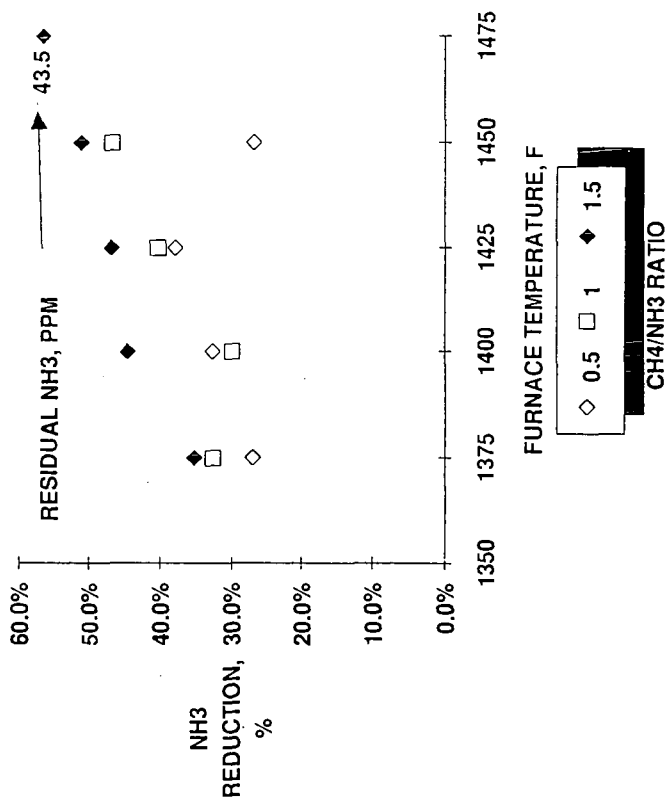


Fig. 6. Effect of CH4 Additive on NH3 Slip.

## RESULTS FROM A MODELING AND EXPERIMENTAL EVALUATION OF THE COMBINO<sub>x</sub> PROCESS

J.N. Pont, A.B. Evans, R.K. Lyon, G.C. England, D. K. Moyeda, W.R. Seeker  
Energy and Environmental Research Corporation  
18 Mason  
Irvine, CA 92718

**Key Words:** CombiNO<sub>x</sub>, NO<sub>x</sub> Reduction Technology, Advanced Reburning

### INTRODUCTION

Control of emissions of oxides of nitrogen, or NO<sub>x</sub>, from fossil-fuel fired combustion systems is becoming of increasing interest due to the role of atmospheric nitrogen oxide species in the formation of acid rain and photochemical oxidant or smog. High levels of NO<sub>x</sub> removal are typically only achievable with expensive post-combustion technologies employing catalyst beds. This paper describes a process, called "CombiNO<sub>x</sub>", which is capable of achieving high levels of NO<sub>x</sub> reduction at costs significantly below those of catalytic technologies. The CombiNO<sub>x</sub> process consists of three NO<sub>x</sub> control technologies—reburning, selective non-catalytic reduction ("agent injection"), and NO<sub>2</sub> scrubbing—which have been integrated and optimized in a manner which takes advantage of the chemical reactions involved in each process to achieve NO<sub>x</sub> reduction approaching 90 percent.

The CombiNO<sub>x</sub> process has been studied experimentally using two pilot-scale furnaces. The first series of tests were conducted in a one million Btu/hr down-fired furnace. At this facility, each component of the CombiNO<sub>x</sub> process was parametrically evaluated. Results from these studies have been reported elsewhere [1]. Pilot-scale tests at 10 million Btu/hr were also conducted to address process scale-up issues. This paper presents selected results of both series of experimental studies as well as kinetic modeling studies performed to aid in interpretation of the experimental results.

### BACKGROUND

The technologies involved in the CombiNO<sub>x</sub> process have been extensively studied in small scale combustion tests and demonstrated in a wide range of industrial applications. In general, the global chemical mechanisms involved in the processes are considered relatively well-known. The three technologies used in the CombiNO<sub>x</sub> process are described in the following.

**Reburning.** The reburning concept was first investigated nearly two decades ago [2]. This process consists of injecting a portion of fuel downstream of the primary combustion zone to drive the flue gas stoichiometry slightly fuel rich. In this "reburning zone", the NO<sub>x</sub> generated in the primary zone is reduced to molecular nitrogen. Downstream of the reburning zone, additional air is injected to complete combustion of the unburnt products from the reburning zone. Bench and pilot scale studies have identified the general requirements for applying the process to industrial combustion systems [3-4]. Recently, demonstrations of the reburning process employing natural gas as a reburning fuel have been performed on coal-fired utility boilers [5-6].

**Agent Injection.** Selective non-catalytic reduction, or agent injection, technologies consist of the injection of amine-producing agents into post-combustion flue gases. Typical agents include ammonia

and urea. These agents must be injected into a narrow temperature window generally centered about 1850°F. Injection of the agent at too high of a temperature can cause oxidation of the agent resulting in increased NO<sub>x</sub> emissions, while injection of the agent at too cold of a temperature can lead to excessive by-product emissions, such as unreacted NH<sub>3</sub>. The fundamentals of the process have been described in the literature [7-8]. Reagent injection for NO<sub>x</sub> control has been applied to full-scale utility boilers [9-10]. The results of these and similar tests have shown that the process is extremely sensitive to the gas temperature and that broad temperature distributions at the point of injection of the agent can limit performance.

**NO<sub>2</sub> Scrubbing.** Studies have shown that it is possible to scrub NO<sub>2</sub> with conventional SO<sub>2</sub> scrubber solutions provided that the solution is slightly modified [11]. The CombiNO<sub>x</sub> process exploits this phenomena by injecting methanol into the flue gas downstream of the reburning and agent injection processes to convert any remaining NO to NO<sub>2</sub> and then scrubbing the NO<sub>2</sub> in a conventional wet limestone SO<sub>2</sub> scrubber operating with a modified scrubbing liquor. Although methanol injection has been evaluated at full utility boiler scale as a means of reducing ammonia slip from SNCR systems [12], the integrated NO<sub>2</sub> scrubbing process has yet to be demonstrated in a practical system.

#### ADVANCED REBURNING

In practice, agent injection performance is extremely sensitive to flue gas temperature at the injection point. However, in the presence of oxidizing CO, the dependence of the process on injection temperature is significantly reduced [12]. The CombiNO<sub>x</sub> process furnishes oxidizing CO by injecting reburning fuel upstream of the reducing agent. The EER patented combination of reburning and agent injection, called Advanced Reburning, comprises the first two steps of the CombiNO<sub>x</sub> process.

Figure 1 shows schematically how Advanced Reburning was experimentally evaluated. A high-volatile bituminous coal was used as the primary fuel, while natural gas was used as the reburning fuel. The process can be divided into three zones: the region between the top of the furnace and the reburn fuel injectors is referred to as the primary zone, the region between the reburn fuel injectors and the burnout air ports is the reburning zone, the region downstream of the burnout air ports is referred to as the burnout zone. In these experiments, urea was injected within the reburning zone. The Advanced Reburning parameters evaluated included: reburning zone stoichiometry (or CO level), urea injection temperature, and burnout air injection location.

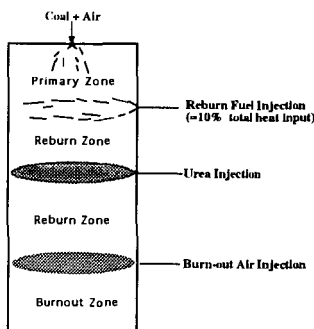
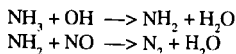
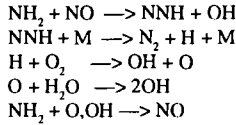


Figure 1. Advanced reburning pilot scale testing schematic.

The effect of reburn zone stoichiometry on urea performance was evaluated to determine the impacts of CO oxidation on the optimal temperature window and achievable NO<sub>x</sub> reductions. The chain branching de-NO<sub>x</sub> reactions of importance are summarized below [13]:





The rate limiting step is the oxidation of ammonia to form  $\text{NH}_2$ . The reducing agent needs to be injected at high enough temperatures to allow the reaction to proceed fast enough to generate sufficient radicals to oxidize  $\text{NH}_2$ . If temperatures are too hot, the reaction intensity will be too high, and  $\text{NH}_2$  will be oxidized rather than react with NO to form molecular nitrogen. If temperatures are too low, the ammonia will not oxidize, and will show in the emissions as ammonia slip. Therefore, there is an optimum agent injection temperature. At temperatures above and below approximately 1850°F, NO reduction efficiency drops off.

The addition of CO has been shown to shift the reaction window to lower temperatures because carbon monoxide oxidizes and generates additional radicals [13] that support further oxidation of  $\text{NH}_2$  in the process. Figure 2 shows predicted NO reduction versus injection temperature using a chemical kinetic model which incorporates a plug flow/stirred reactor algorithm [15]. The plot compares injection of urea without CO to injection of urea with the equivalent of 3000 ppm CO for a stoichiometric ratio (SR) of 1.2. The addition of CO generates additional radicals, which shifts the cold side of the window to lower temperatures. The hot side of the window also shifts to the left, but to a lesser degree because the incremental amount of OH radicals contributed by this small amount of CO is not as great as that from ammonia alone. The net result of these effects is a broader reaction window.

Figure 2 also shows the predicted effect of co-injecting urea with the equivalent of 3000 ppm CO into two different stoichiometric environments. At higher stoichiometries, CO will oxidize more readily and generate more radicals, improving urea performance at lower temperatures, but worsening performance at higher temperatures. At the lower stoichiometry, fewer additional radicals are generated and the curve is not shifted as far to cooler temperatures. An interesting point is that the SR=1.2 curve is broader at the bottom, but rises more steeply as injection temperature increases than the SR=1.02 curve. The explanation may be that the increase in radicals at the high temperature side is relatively less for the SR=1.02 case than for the SR=1.2 case, resulting in relatively less oxidation of  $\text{NH}_2$ .

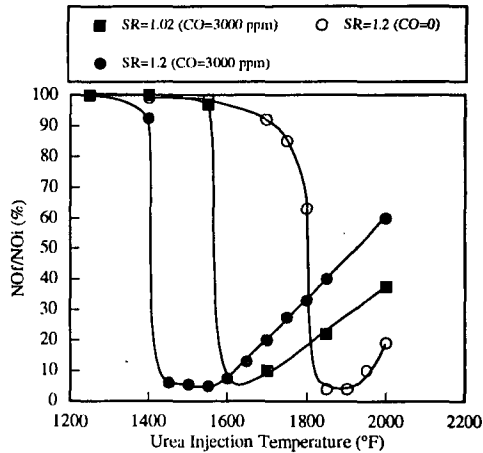


Figure 2. Predicted effect of CO on urea injection performance.

The design and operating conditions of a particular actual combustion system will significantly influence the amount of CO produced at a given stoichiometry. In the pilot-scale tests, the reburning zone stoichiometry was varied to evaluate the impact of reburning zone CO and O<sub>2</sub> levels on urea performance. Figure 3 shows the effect of reburn zone stoichiometry on the urea temperature window for the small (one million Btu/hr) pilot-scale tests. As the reburn zone stoichiometry drops, CO increases and O<sub>2</sub> decreases and the temperature window broadens with the optimum injection temperature at 1850°F. For a reburn zone stoichiometry of 1.02, the window not only broadens, but deepens as well, indicating that this unique combination of CO and O<sub>2</sub> provides an optimum amount of radicals. When SR<sub>2</sub> was more fuel-rich than this optimum, the curve shifted to the left rather than broadening. This result is believed to be due to an overabundance of radicals at the high temperature level.

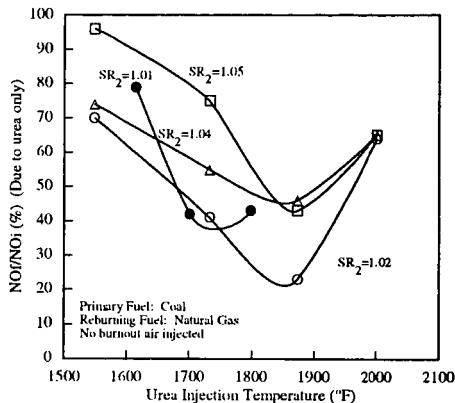


Figure 3. Effect of local CO concentration (SR) on urea performance at small pilot scale.

Because the flue gas flow in the small pilot-scale furnace is laminar, the mixing properties are not representative of a boiler. Also, flue gas temperature quench rates are much lower than on an actual full-scale boiler. Therefore, the 10 million Btu/hr tests were designed to provide information on advanced reburning performance in the presence of large scale turbulent mixing phenomena and at more realistic quench rates. Urea was injected at various temperatures for reburning zone stoichiometries from 1.05 to 0.99, which produced CO concentrations in the reburning zone ranging from 1,500 to 15,000 ppm, respectively. These results are presented in Figure 4. Contrary to the small pilot-scale results, the stoichiometry of the reburning zone did not appear to have a large effect on either the optimum injection temperature or NO reduction. It is hypothesized that the CO enhancement relies on mixing to distribute OH radicals to the SNCR agent uniformly. At large scale, bigger pockets of CO and O<sub>2</sub> co-exist, yielding non-uniform concentrations of radicals, and ultimately failing to promote the deNO<sub>x</sub> chemistry as well. It may be stated however, that the SR =

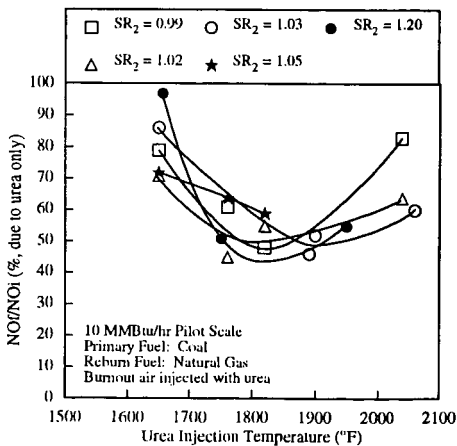


Figure 4. Effect of reburn zone stoichiometry on urea performance at large pilot scale.

1.20 case where no reburning is performed (no CO promotion) upstream of urea injection yielded the narrowest temperature window.

The final Advanced Reburning parameter of interest is the location of burnout air injection to complete combustion of the reburning fuel. Figure 5 shows overall  $\text{NO}_x$  reduction (due to reburning and urea injection) as a function of burnout air injection temperature (location) for optimum reburn zone stoichiometry and urea injection temperature. At small pilot-scale,  $\text{NO}_x$  reduction improves as the burnout air is moved away from the urea injection point. This is probably because downstream air prolongs the urea residence time in the "optimum" radical environment. Also shown in the figure are the large pilot-scale data.  $\text{NO}_x$  reduction did not vary with burnout air location at large scale. From an application standpoint, this is important in that it is less expensive to retrofit Advanced Reburning to a boiler if the burnout air and reduction agent can be injected through the same openings.

Figure 6 presents Advanced Reburning  $\text{NO}_x$  reduction levels as a function of reburn zone stoichiometry and urea injection temperature at large pilot-scale. Compared to traditional agent injection, the Advanced Reburning process offers a wider range of urea injection temperatures and significantly improved reduction performance up to 84 percent.

### METHANOL INJECTION

The third step of the Combi $\text{NO}_x$  pro-

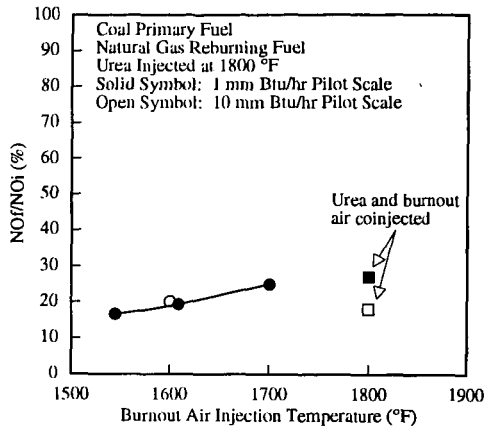


Figure 5. Effect of burnout air injection temperature on Advanced Reburning performance.

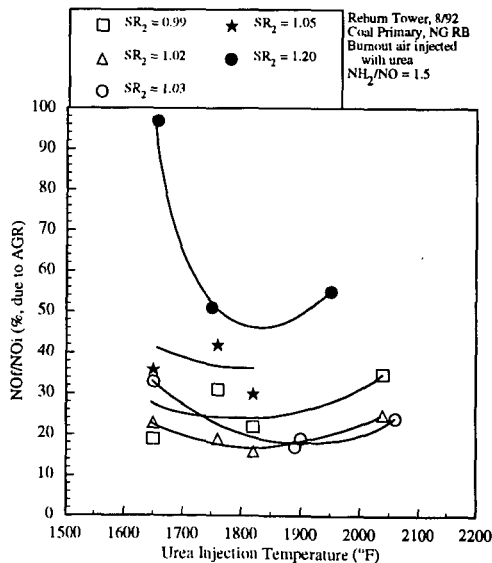


Figure 6. Large pilot scale Advanced Gas Reburning performance

cess, methanol injection, is performed downstream of the Advanced Reburning process. The methanol is intended to convert the NO remaining after Advanced Reburning to  $\text{NO}_2$ . Since  $\text{NO}_2$  is very water soluble, it can subsequently be removed in wet  $\text{SO}_2$  scrubber operating with modified liquor. Based on previous kinetic studies, the reaction mechanism for the methanol step is [16]:

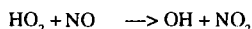
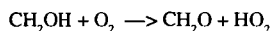
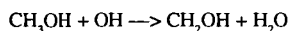


Figure 7 summarizes the effect of methanol injection temperature on the conversion efficiency of NO to  $\text{NO}_2$ . Depending on residence time and temperature, the model predicts an optimum injection temperature of between 1500 °F and 1800 °F. Complete conversion was shown to be theoretically possible, with an optimum injection temperature of 1550 °F and a residence time of 0.1 seconds.

Experiments were conducted to verify the modeling results at bench- and one million Btu/hr pilot-scale. At bench-scale, a simulated flue gas was combined with vaporized methanol and introduced into a quartz tube reactor. The reactor temperature and residence times were varied to evaluate their impact on NO conversion. At pilot-scale, methanol was injected into natural gas combustion products at various locations (temperatures) and the resulting NO and  $\text{NO}_x$  levels were recorded. The residence time at the optimum injection temperature ( $\pm 50^\circ\text{F}$ ) is approximately 600 msec. Figure 8 shows that the pilot-scale result for natural gas combustion products and the bench-scale data for the same residence time agree quite well.

The experimentally-determined opti-

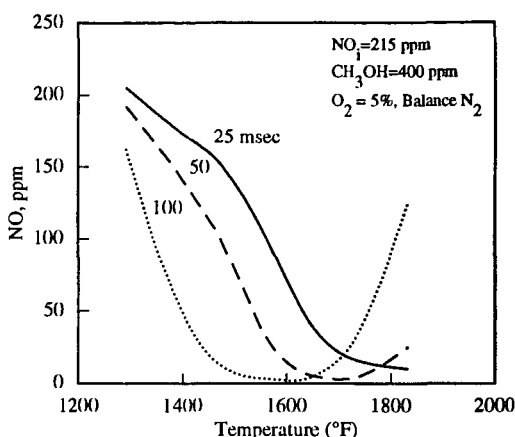


Figure 7. Predicted effect of temperature and residence time on methanol performance.

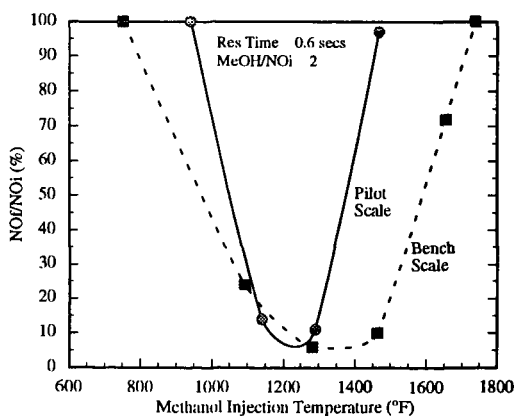


Figure 8. Bench vs Pilot scale methanol performance.

imum methanol injection temperature ranged from 1150°F to 1300°F, which is significantly lower than that predicted by the model. However, the experimental data were obtained at a residence time of 0.6 second residence time, while the predictions were performed for 0.1 second residence time. Additional modelling is planned to determine if increasing the residence time available for methanol reactions shifts the optimum injection temperature to lower levels.

## CONCLUSIONS

These studies have shown the influence of the main parameters controlling performance of the Advanced Reburning process. Close coupling of the CO level in the reburning zone and the temperature at which the agent is injected is needed to optimize NO<sub>x</sub> reduction. Studies of the methanol injection step in bench- and pilot-scale reactors have shown that conversion of the NO remaining from the Advanced Reburning process to NO<sub>2</sub> is feasible.

In conclusion, the CombiNO<sub>x</sub> process, consisting of Advanced Reburning and methanol injection combined with NO<sub>x</sub> scrubbing, is a promising retrofit technology for coal fired utility boilers. The Advanced Reburning portion has been demonstrated at 10 millionBtu/hr pilot scale to reduce NO<sub>x</sub> emissions by 84 percent. The complete process has the potential to reduce NO<sub>x</sub> emissions by 90 percent.

## ACKNOWLEDGMENTS

This work was funded under Department of Energy Contract No. DE-AC22-90PC90363, Development of Advanced NO<sub>x</sub> Control Concepts for Coal-Fired Utility Boilers. Mr. Charles E. Schmidt is the DOE Program Coordinator.

## REFERENCES

1. Pont, J. N., et al. *Evaluation of the CombiNO<sub>x</sub> Process at Laboratory and Pilot Scales*. Presented at the AIChE 1992 Summer National Meeting, Minneapolis, Minnesota, August 1992.
2. Wendt, J. O. L. et al. *Reduction of Sulfur Trioxide and Nitrogen Oxides by Secondary Fuel Injection*. Fourteenth Symposium (International) on Combustion, pp. 897-904, The Combustion Institute, 1973.
3. Greene, S. B., et al. *Bench Scale Process Evaluation of Reburning and Sorbent Injection for In-Furnace NO<sub>x</sub> Reduction*. ASME Paper No. 84-JPGC-APC-9, 1984.
4. Seeker, W. R., et al. *Controlling Pollutant Emissions from Coal and Oil Combustors Through the Supplemental Use of Natural Gas*. Final Report, GRI Contract 5083-251-0905, 1985.
5. Borio, R. W., et al. *Reburn technology for Boiler NO<sub>x</sub> Control*. Presented at the ASME Winter Annual Meeting, San Francisco, California, December 1989.
6. Moyeda, D. K., et al. *Demonstration of Combined NO<sub>x</sub> and SO<sub>2</sub> Emission control Technologies Involving Gas Reburning*. Presented at the 1991 AIChE Annual Meeting, Pittsburgh, Pennsylvania, August 1991.

7. Lyon, R. K. Thermal DeNO<sub>x</sub>, *Controlling Nitrogen Oxides Emissions by a Noncatalytic Process*. Environmental Science and Technology, Volume 21, No. 3, pp. 231-236, 1987.
8. Muzio, L. J., J. K. Arand and D. P. Teixeira. *Gas Phase Decomposition of Nitric Oxide in Combustion Products*. Presented at the Sixteenth Symposium (International) on Combustion, Cambridge, Massachusetts, August 1976.
9. Bartok, W. and G. M. Varga. *Applicability of the Thermal DeNO<sub>x</sub> Process to Coal Fired Utility Boilers*. Presented at the American Flame Research Committee International Symposium on NO<sub>x</sub> Reduction in Industrial Boilers, Heaters and Furnaces, Houston, Texas, October 1979.
10. Abele, A. R., et al. *Performance of Urea NO<sub>x</sub> Reduction Systems on Utility Boilers*. Presented at the 1991 Joint EPA/EPRI Symposium on Stationary Combustion NO<sub>x</sub> Control, Washington, D. C., March 1991.
11. Evans, A. B., et al. *Development of Process to Simultaneously Scrub SO<sub>2</sub> and NO<sub>2</sub> from Coal-Fired Boiler Flue Gas*. ACS Spring Symposium, Denver, Colorado, March 1993.
12. Irons, M. A., et al. *Tailoring Ammonia-Based SNCR for Installation on Power Station Boilers*. 1991 Joint Symposium on Stationary Combustion NO<sub>x</sub> Control, Washington D.C., March 25-28, 1991.
13. Chen, S. L., et al. *Advanced NO<sub>x</sub> Reduction Processes Using -NH and -CN Compounds in Conjunction with Staged Air Addition*. Twenty-Second Symposium (International) on Combustion, pp. 1135-1145, The Combustion Institute, 1988.
14. Lyon, R.K.: *Kinetic and Mechanism of Thermal DeNO<sub>x</sub>: A Review*. Preprints: ACS Division of Fuels Chemistry, ACS, 32 (4), 433 (1987).
15. Kau, C.J. and Tyson, T.J. *A Computer Program for General Flame Analysis*. U.S. Environmental Protection Agency Report No. EPA-600/7-87-027 (1987).
16. Lyon, R.K., et al. *The Selective Reduction of SO<sub>2</sub> to SO<sub>3</sub> and the Oxidation of NO to NO<sub>2</sub> by Methanol*. Combustion and Flame, 81, pp. 30-39, 1990.

SYMPOSIUM ON CHEMISTRY OF FLUE GAS CLEANUP PROCESSES  
FOR PREPRINTS OF THE FUEL CHEMISTRY DIVISION  
AMERICAN CHEMICAL SOCIETY  
DENVER, CO MEETING, MARCH 28-APRIL 2, 1993

ACTIVATED CARBON FOR SELECTIVE REMOVAL OF NITROGEN OXIDE  
FROM COMBUSTION FLUE GAS

By

A.M. Rubel, J.M. Stencel, S. N. Ahmed  
University of Kentucky, Center for Applied Energy Research  
3572 Iron Works Pike, Lexington, KY 40511-8433

**Keywords:** NO, selective adsorption, activated carbons

## INTRODUCTION

A new concept for non-catalytic NO removal from combustion flue gas is being developed at the University of Kentucky Center for Applied Energy Research (CAER). Flue gas cleanup would be achieved through the use of activated carbons for the selective capture of NO<sub>x</sub> at stack temperatures between 70-120°C followed by desorption of a concentrated stream of NO<sub>x</sub> at elevated temperatures, near 140-150°C. Processing would involve repeated NO<sub>x</sub> adsorption/desorption cycles using the same adsorbent carbon.

Previous work on the removal and adsorption of NO over carbaceous materials has focused on the heterogeneous reduction of NO by carbon to CO, CO<sub>2</sub>, and N<sub>2</sub><sup>1-6</sup>. The proposed reaction mechanisms involve the chemisorption of NO on carbon at temperatures near 200°C resulting in the formation of a carbon-NO complex which rearranges to form a carbon-oxygen complex and molecular nitrogen<sup>2</sup>. The amount of NO adsorbed was less than 2 wt% of the carbon and, upon desorption, 40-50 wt% of the carbon is gasified<sup>2,6</sup>. Some work has been done toward the use of activated carbon to remove NO<sub>x</sub> from moist off-gases in nitric acid plants at ambient temperatures and in the presence of O<sub>2</sub>. The NO adsorptive capabilities found were low and near 0.16 to 0.7 mg NO/g carbon<sup>7</sup>. No information has been found in the literature concerning NO/NO<sub>2</sub> adsorption on active carbon under conditions found in combustion flue-gases.

During this study, the mechanisms and kinetics of NO<sub>x</sub> adsorption/desorption on activated carbon under conditions typical to combustor stacks were investigated by thermogravimetry/mass spectrometry (TG/MS). Information was obtained concerning the requirements for NO<sub>x</sub> capture, the NO<sub>x</sub> adsorption capacity of an activated carbon, the effect of repeated adsorption/desorption cycles on NO<sub>x</sub> adsorption, and the mechanism of adsorption.

## EXPERIMENTAL

### Instrumentation

NO<sub>x</sub> adsorption/desorption profiles were obtained using a Seiko TG/DTA 320 coupled to a VG Micromass quadrupole MS. The two instruments were coupled by a heated (170°C)

fused silica capillary transfer line leading from above the sample pan in the TG to an inert metrasil molecular leak which interfaced the capillary with the enclosed ion source of the MS. The TG was connected to a disk station which provided for programmable control of the furnace, continuous weight measurements, sweep gas valve switching, data analysis, and export of data to other computers. The MS has a Nier type enclosed ion source, a triple mass filter, and two detectors (a Faraday cup and a secondary emissions multiplier). The MS was controlled by a dedicated personal computer which was also used to acquire and review scans before export to a spreadsheet for data manipulation.

#### TG-MS procedures

The TG conditions kept constant during the acquisition of adsorption/desorption profiles were: sweep gas flow rate of 200 ml/min metered at room temperature and pressure and a constant carbon sample volume weighing approximately 20 mg. The MS was scanned over a 0-100 amu range with measurement intervals of approximately 30 seconds. NO (mass 30) or NO<sub>2</sub> (mass 30 and 46) were identified by comparing amu 30/46 ion ratios. These ratios were determined for all combinations of gases flowing through the TG-MS system both with and without carbon in the TG sample pan.

The TG heating regime used to produce NO<sub>x</sub> adsorption/desorption profiles incorporated segments for outgassing, cooling, adsorption, desorption, and temperature-induced desorption. Table I shows a typical heating program for a single adsorption/desorption cycle. During outgassing and subsequent cooling of the carbon sample to an adsorption temperature (segments a and b, Table I), an inert (He) gas sweep was usually used. However, O<sub>2</sub> and CO<sub>2</sub> pretreatments of the carbon were also done during these steps for some experiments. Maximum outgassing temperature was always the same as the maximum used during temperature programmed desorption (step e). After preconditioning of the carbon, NO or NO<sub>2</sub> was introduced in a simulated flue gas atmosphere containing either O<sub>2</sub> or CO<sub>2</sub>, or both O<sub>2</sub> and CO<sub>2</sub>. After completion of an adsorption interval (30 or 60 minutes), He was again used to purge the system during segments d and e. Two maximum desorption temperatures were used, 300 and 400°C. Multiple and consecutive adsorption/desorption cycles were performed by recycling the temperature programmer to segment b.

#### Materials and simulated flue gas composition

A commercially (Carbo Tech) produced coal-based carbon was used. This carbon was produced by physical activation and had a N<sub>2</sub> BET surface area of 450 m<sup>2</sup>/g.

During this study, the concentrations of gases used during adsorption and pretreatments were: 2% or 0.3% NO or NO<sub>2</sub>; 5% O<sub>2</sub>, 15% CO<sub>2</sub> and He as the balance. NO adsorption capacity of the activated carbon studied was determined for the following combinations of gases: 2% NO with O<sub>2</sub> and CO<sub>2</sub>; 2% NO in He alone; 0.3% NO in O<sub>2</sub> and CO<sub>2</sub>; 0.3% NO in either O<sub>2</sub> or CO<sub>2</sub>; 0.3% NO in He with carbon presaturated with either O<sub>2</sub> or CO<sub>2</sub>; 0.3% NO in He alone; and 0.3% NO<sub>2</sub> in O<sub>2</sub> and CO<sub>2</sub>.

## RESULTS AND DISCUSSION

#### Capacity of activated carbon to selectively capture NO<sub>x</sub>

Both single cycle and repeated cycles TG-MS adsorption/desorption profiles were used to show effective and rapid removal of NO from simulated flue gas by activated carbon.

During a single NO adsorption/desorption cycle using a simulated flue gas with a high NO concentration (2% NO, 15% CO<sub>2</sub>, and 5% O<sub>2</sub> with a balance of He), 0.14 g NO/g carbon was adsorbed in 30 minutes as evidenced by the increased weight of the carbon (Figure 1). Increasing the adsorption time to 60 minutes only marginally increased NO capture to 0.16 g NO/g carbon. Desorption of NO<sub>x</sub> from the carbon through both physisorption and temperature programmed desorption was confirmed by the mass spectra showing a major peak in the ion intensity of amu 30 (the primary ion mass for both NO and NO<sub>2</sub>) coinciding with the TG monitored weight loss. A small peak was also observed for amu 46, a secondary ion mass for NO<sub>2</sub>. The temperature of maximum desorption occurred at 140°C.

Repeated cycling of the same carbon through three NO<sub>x</sub> adsorption/desorption cycles, resulted in a 15% total loss of adsorptive capacity (Figure 2). The maximum desorption temperature (400°C) used during this experiment was higher than the 250-300°C required for complete NO<sub>x</sub> desorption. Since the loss in adsorptive capacity of the carbon coincided with a 0.5-1.0 wt% loss of carbon, possibly through oxidation/gasification, lowering the desorption temperature should reduce this already small loss in adsorptive capacity.

#### Effect of flue gas constituents on NO<sub>x</sub> adsorption

To determine the effect of typical flue gas constituents on the kinetics of NO adsorption, a parametric study was done using 0.3% NO in various combinations with O<sub>2</sub> (5%), CO<sub>2</sub> (15%), and He (balance) (Figure 3). Adsorption time for all experiments was kept constant at 60 minutes. NO capture was dependent on the presence of O<sub>2</sub> but was not significantly affected by the presence of CO<sub>2</sub>. Presaturation of carbon with O<sub>2</sub> followed by NO adsorption in He increased adsorption from 1 wt% using He alone to 6 wt% suggesting a carbon surface reaction mechanism. Control experiments without NO present during adsorption showed that 1% or less of the weight gain during NO adsorption resulted from O<sub>2</sub>, CO<sub>2</sub>, or He adsorption on the carbon (Figure 3).

#### Possible reaction mechanism

The dependency of NO adsorption on the presence of O<sub>2</sub> suggests that NO must be converted to a surface species similar to NO<sub>2</sub> during the adsorption step. Simultaneous differential thermal analyses (DTA) conducted during these experiments supported such conversion. A significant exotherm accompanied NO adsorption (Figure 4) whereas, no heat of reaction was associated with NO<sub>2</sub> adsorption (Figure 5).

A comparison of MS ion ratios for masses (30/46) for all combinations of NO or NO<sub>2</sub> and O<sub>2</sub> or CO<sub>2</sub> flowing through the TG-MS system with and without activated carbon in the sample pan shows the differences obtained in these ratios (Figure 6). These differences were used to identify the form of NO<sub>x</sub> desorbed from the carbon. Since the (30/46) ion ratios for all combinations of NO or NO<sub>2</sub> with O<sub>2</sub> or CO<sub>2</sub> were less than 20, an experiment where desorption occurred in a He sweep with low baseline levels of O<sub>2</sub> and CO<sub>2</sub> was necessary. This requirement was met by presaturating carbon with O<sub>2</sub> followed by adsorption and desorption in He. The ion ratio during desorption for this experiment was 94 and most closely matched the ion ratio for NO<sub>2</sub> in He (Figure 7). For comparison, the desorption ion ratio for a NO, CO<sub>2</sub>, O<sub>2</sub> experiment is also shown.

## **SUMMARY AND CONCLUSIONS**

The data presented provides evidence for the selective capture of NO<sub>x</sub> by activated

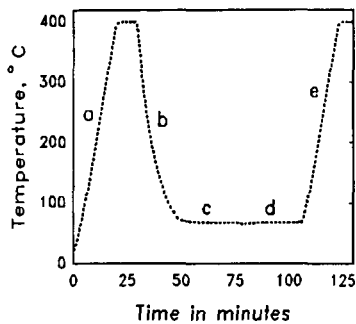
carbons in the presence of typical flue gas components. The NO adsorption capacities approached 0.16 g NO/g carbon. Adsorption of NO was rapid only in the presence of O<sub>2</sub>, was not influenced by the presence of CO<sub>2</sub>, and involved the exothermic conversion of NO to NO<sub>2</sub>-like species at the surface of the carbon. The capacity for NO adsorption was only slightly diminished by repeated adsorption/desorption cycles. At desorption temperature as high as 400°C, the capacity after three cycles decreased to about 85% of the original value with a coincident loss of 0.5-1.0 wt% of the carbon. The results suggested that activated carbon can be used for NO<sub>x</sub> flue gas clean-up and would provide a simple alternative to more expensive and complex methods such as selective catalytic reduction.

#### REFERENCES

1. Smith, R.N., J. Swinehart, and D. Lesnini. *J. Physical Chem.* 63(1959)544.
2. DeGroot, W.F., T.H. Osterheld, G.N. Richards. *Carbon* 29(1991)185.
3. Teng, H., E.M. Suuberg, J.M. Calo, and P.J. Hall. *Proc. 19th Conf. on Carbon*, (1989)574.
4. Suuberg, E.M., H. Teng, and J.M. Calo. *23rd Symposium (International) on Combustion*, The Combustion Institute (1990)1199.
5. Teng, H., E.M. Suuberg, and J.M. Calo. *Preprints of the 200th ACS National Meeting*, Washington, DC, 35,3(1990)592.
6. Gray, P.G., N.J. Desai, and D.D. Do. *Recent Trends in Chem. Rxn Engr.*, B.O. Kulkarni, R.A. Mashelkar, and M.M. Sharma, eds., Wiley Eastern Ltd., 1(1987)383.
7. Richter, E., R. Kleinschmidt, E. Pilarczyk, K. Knoblauch, and H. Juntgen. *Thermochemica Acta* 85(1985)311.

**Table I.** Typical TG heating regime for acquisition of NO<sub>x</sub> heating profile.

Step	Temp C	Rate C/min	Hold min
a	0-400	20	10
b	400-70	50	10
c	70 (1)	0	30-60
d	70 (2)	0	30
e	70-400	20	10



<sup>1</sup>Adsorption step  
<sup>2</sup>Physidesorption step

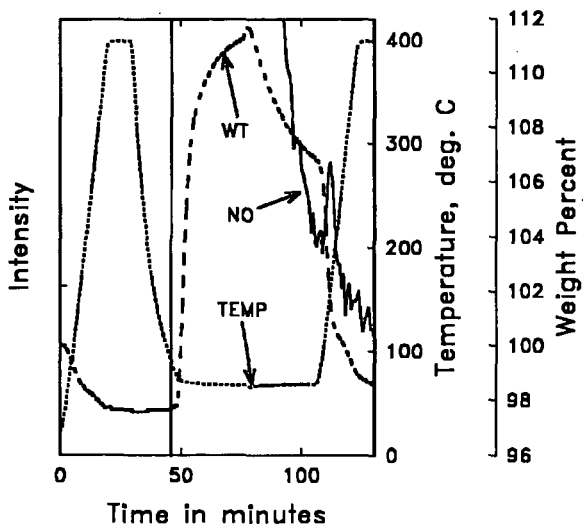


**Figure 1.** Single adsorption/desorption profile. Adsorption atmosphere: 2% NO, 5% O<sub>2</sub>, 15% CO<sub>2</sub>, and He balance; adsorption time: 30 min.

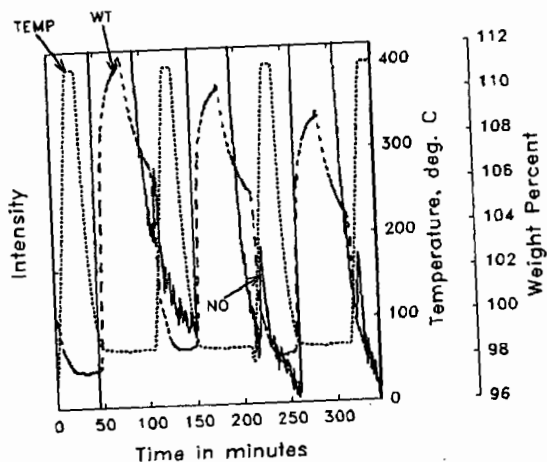


Figure 2. Three consecutive adsorption/desorption cycles using the same carbon sample. Adsorption atmosphere: 2% NO, 5% O<sub>2</sub>, 15% CO<sub>2</sub>, and He balance; adsorption time: 30 min.

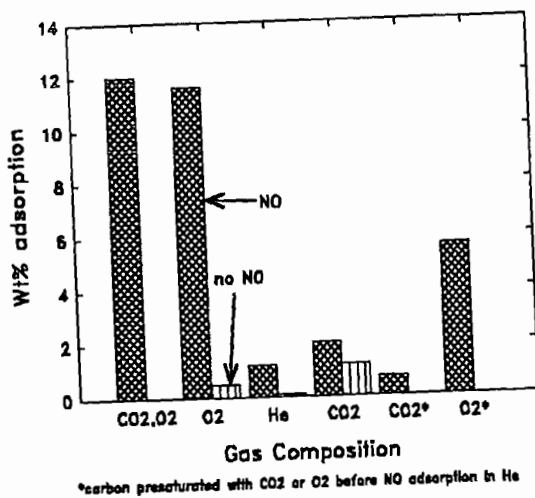


Figure 3. Study of the effect of O<sub>2</sub> and CO<sub>2</sub> on NO adsorption on activated carbon. Gases: 0.3% NO, 5% O<sub>2</sub>, 15% CO<sub>2</sub>, and He balance; adsorption time: 60 min.

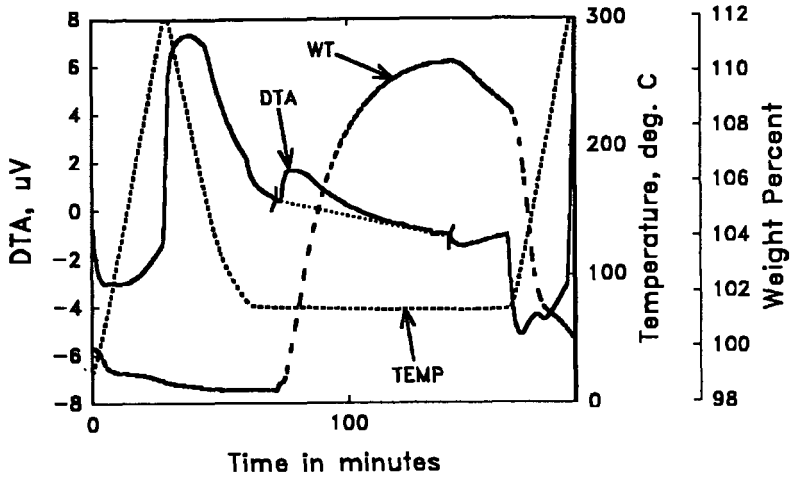


Figure 4. Simultaneous TG/DTA of NO adsorption on activated carbon. Adsorption atmosphere: 0.3% NO, 5% O<sub>2</sub>, 15% CO<sub>2</sub>, and He balance; adsorption time: 60 min.

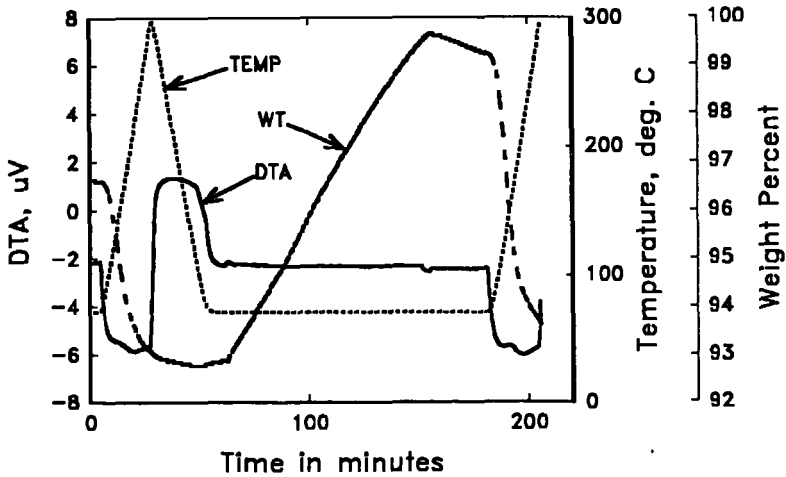


Figure 5. Simultaneous TG/DTA of NO<sub>2</sub> adsorption on activated carbon. Adsorption atmosphere: 0.3% NO<sub>2</sub>, 5% O<sub>2</sub>, 15% CO<sub>2</sub>, and He balance; adsorption time: 60 min.

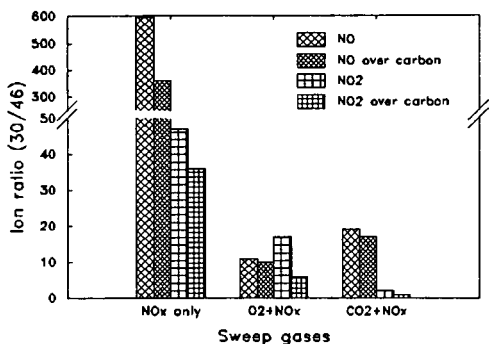


Figure 6. Mass (30/46) ion ratio for various combinations of NO or NO<sub>2</sub> and O<sub>2</sub> or CO<sub>2</sub> with and without the presence of carbon in the TG sample pan as determined by MS.

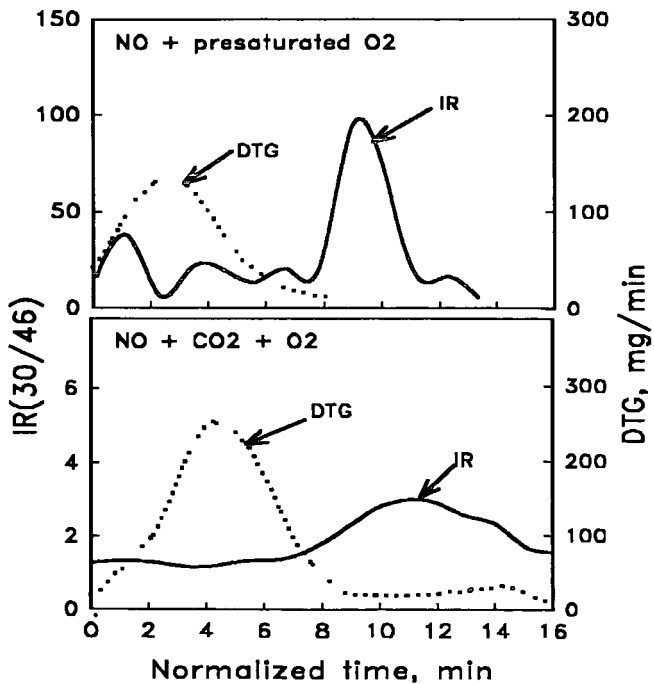


Figure 7. Mass (30/46) ion ratios during desorption of NO<sub>x</sub> from activated carbon.

Reaction Kinetics of Selective Non-Catalytic  
NO<sub>x</sub> Reduction with Urea

William H. Sun, Penelope Stamatakis, John E. Hofmann  
Nalco Fuel Tech  
Naperville, Illinois, U.S.A.

Abstract

Selective Non-Catalytic Reduction (SNCR) of NO<sub>x</sub> with urea has proven to be an effective method in controlling NO<sub>x</sub> from various stationary combustion sources. The chemistry of this process that is marketed under the name of NO<sub>x</sub>OUT<sup>®</sup>, was modelled to identify major pathways, limitations, and important parameters. The chemical kinetic model includes over 90 elementary radical reactions among various stable and radical species. The developed model has been validated with data generated from a pilot facility.

The model provided understanding of the effects of residence time, treatment rate and baseline NO<sub>x</sub>, oxygen and CO concentrations. In addition, the lowest achievable NO<sub>x</sub> concentration, referred as 'Critical NO<sub>x</sub>', has been identified. This limit is the result of the chemical reaction kinetics. The existence of such limit is explained through reaction chemistry and validated with laboratory and field data.

Introduction

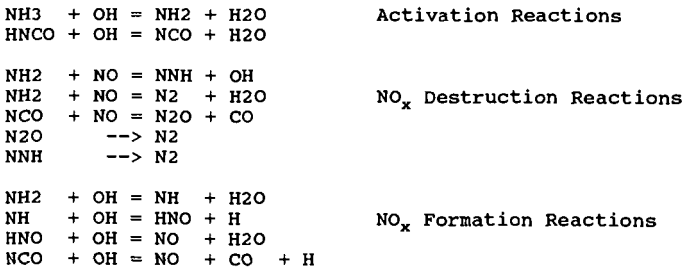
Post combustion NO<sub>x</sub> control methods reduce NO<sub>x</sub> after its formation is completed. Other methods such as flue gas recirculation and staged combustion limit the formation of NO<sub>x</sub> by lowering combustion temperature or by limiting oxygen for N<sub>2</sub> oxidation. Once NO<sub>x</sub> is formed, post combustion control methods take advantage of the highly selective reactions between ammonia and NO<sub>x</sub> or urea and NO<sub>x</sub>. These reactions occur at temperatures between 850 - 1100 °C without a catalyst and are called selective noncatalytic reactions (SNCR). Ammonia injection is an Exxon process and has been called the Thermal DeNO<sub>x</sub> Process [1,2] while the urea injection was patented by EPRI [3,4]. Nalco Fuel Tech is EPRI's exclusive licensing agent, and the technology is being marketed as NO<sub>x</sub>OUT Process. At lower temperatures (300 - 500 °C), various metal and ceramic catalysts are required to reduce NO<sub>x</sub> by reacting with ammonia (SCR)[5].

NO<sub>x</sub>OUT Kinetic Model

As part of a development effort, a chemical kinetic model has been developed to understand the basic chemistry, to determine important factors and to define the limits of process capability. This model describes an ideal plug flow, i.e., no temperature or species concentration gradient in radial direction and no back-mixing. Chemical reactions along an ideal plug flow can be described by a set of ordinary differential equations. Reaction rates, density, and thermodynamic information are supplied through a library of

gas-phase subroutines called CHEMKIN developed at the Sandia National Laboratories [6]. The CHEMKIN requires a user supplied chemical reaction set and a thermodynamic data set. The resulting set of equations is integrated simultaneously with a numerical integrator called LSODE [7]. The enthalpy equation is neglected in the model. Instead, measured or calculated temperature profiles are required as an input to the model. Computational fluid dynamics modelling is extensively used to provide temperature and residence time relationships for the kinetic model [8]. Initial conditions are the equilibrium concentrations at flue gas temperatures and excess O<sub>2</sub> as measured. Measured NO<sub>x</sub> and CO concentrations are also inputs.

The reaction set is adopted from the work of Miller and Bowman [9]. From this set, reactions involving hydrocarbons were neglected. The wet CO oxidation reactions, ammonia oxidation reactions, and HCN oxidation reactions make up the set. Urea decomposition is modelled as a rapid and one step breakdown to NH<sub>3</sub> and HNCO. The reaction set consists of 92 reactions describing interactions among 31 species. The major pathway of urea breakdown and reaction with NO<sub>x</sub> is shown in Fig. 1. Ammonia and HNCO, the assumed breakdown products of urea, must react with chain carrier radicals, O, OH, and H, before reacting with NO. Under oxygen rich conditions, OH concentrations are several orders of magnitude higher than O or H. Therefore, reactions involving OH radicals are more important than those involving O or H. Reaction products of NH<sub>3</sub> and HNCO with OH are NH<sub>2</sub> and NCO. These compounds reduce NO<sub>x</sub> or react with OH to form NO<sub>x</sub> according to reactions listed below. The balance between formation and destruction of NO<sub>x</sub> hinges on concentration of OH and temperature.



#### Model Validation

Results from a pilot scale combustor are compared with results from the developed model. A schematic of the pilot combustor and the analytical setup is shown in Fig. 2. The test zone of the combustor was kept isothermal by electrical heating. The residence time at this zone was about 0.7 seconds. This is the average residence time between the injection point and the end of the isothermal zone. Urea solution was injected co-flow with an air

atomized nozzle located along the axis of the test zone. Temperature was varied from 700 °C to 1070 °C, baseline  $\text{NO}_x$  at 300 ppm, and a treatment rate at NSR of 2. NSR is defined as the actual mole ratio of urea to  $\text{NO}_x$  divided by the theoretical stoichiometric ratio, which is 0.5 for the reaction between urea and  $\text{NO}_x$ . Comparison of the model and experimental results is shown in Fig. 3. The available chemical reaction time is less than the residence time because part of the residence time is used to distribute and evaporate droplets. Because of these delays, model results for reaction times of 0.1, 0.3, 0.5, and 0.7 seconds are compared to the experimental results. As shown, the trend and the shape of the experimental results are well modelled.

A range of temperature where significant  $\text{NO}_x$  reductions are obtained is called the temperature window as indicated on Fig. 3. Within this window, controlled  $\text{NO}_x$  versus temperature curve consists of three zones: left side, right side and plateau. This shape is a result of competing reactions (formation vs. destruction) on the right side and a limitation of reaction time due to slow reaction rates on the left side. On the plateau zone, destruction reaction rates are sufficiently fast while formation reactions are slow, yielding optimum  $\text{NO}_x$  reductions. Although the reduction is less than the maximum, operation on the right side is practiced and recommended since byproduct emissions are low on the right side [10].

#### Treatment Rate

Increasing NSR has a diminishing return in  $\text{NO}_x$  reduction. In Fig. 4, model results of  $\text{NO}_x$  concentration as a function of NSR are presented at several temperatures.  $\text{NO}_x$  decreases with increasing NSR at temperatures within the window; increasing NSR increases  $\text{NO}_x$  at higher temperatures. At temperatures between 900 and 1200 °C,  $\text{NO}_x$  reaches a limit at an NSR of about 2. A further increase from NSR of 2 increases  $\text{NO}_x$  for 1200 °C case but has no effect at lower temperatures.

#### Residence Time

The temperature window becomes wider with an increase in residence time. As shown in Fig. 5, the window is about 150 °C wide at 0.1 second but the window increases to 300 °C at one second. This widening occurs on the left side only and has virtually no effect on the right side. On the plateau region, reactions are essentially complete after 0.6 seconds and even shorter (0.2 seconds) at temperatures above 1100 °C.

#### Baseline $\text{NO}_x$

The controlled  $\text{NO}_x$  is unaffected by the baseline  $\text{NO}_x$  at the plateau zone, while  $\text{NO}_x$  increased at higher baselines on the left and right sides. Fig. 6 shows  $\text{NO}_x$  concentration versus temperature at 100, 200, and 500 ppm baseline  $\text{NO}_x$ . NSR is kept constant at 2 and residence time is 1 second. At 1200 °C,  $\text{NO}_x$  increased from 100 ppm

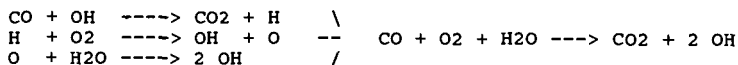
to 120 ppm, but decreased from 500 ppm down to ~300 ppm. This indicates that  $\text{NO}_x$  can be reduced even at high temperatures provided that baseline  $\text{NO}_x$  concentrations are also high. In terms of reduction, the temperature window widens toward the higher temperature side with increases in baseline  $\text{NO}_x$  as shown in Fig. 7.

#### Excess Oxygen

The effect of excess oxygen is studied by modelling at several levels of excess oxygen and substoichiometric conditions. The fuel equivalence ratio was 1.1 for the substoichiometric case. As shown in Fig. 8, temperature windows are affected slightly as oxygen increased beyond 3%. However, at less than 3%  $\text{O}_2$ , the temperature window shifted about 80 °C for a change in excess oxygen from 0.5 to 0.1%. Under a substoichiometric condition, the window shifted to temperatures above 1200 °C. This shift to higher temperatures is the result of reduction in OH concentration. Under a typical oxygen rich condition, OH concentrations are not strongly affected by  $\text{O}_2$ . Near the stoichiometric condition, however, a slight decrease in excess oxygen directly reduces OH radicals, which in turn, slows the activation reactions and shifts the window to higher temperatures. Experimental investigation of urea injection under oxygen starved condition by Arand and Muzio also indicates that the window exists at much higher temperature under fuel rich conditions [4]. The present reaction set does not address hydrocarbon reactions and therefore the modelling of stoichiometric and fuel rich conditions needs further work. Nevertheless, very low excess oxygen conditions shift a temperature window to higher temperatures.

#### Carbon Monoxide Concentration

Carbon monoxide oxidizes to generate H, O, and OH radicals through reactions listed below. Overall, one mole of CO generates two moles of OH radicals.



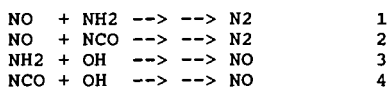
This additional source OH increases rates of the activation reactions and the  $\text{NO}_x$  formation reactions. A net result is shifting of temperature windows to lower temperatures with CO concentration as shown in Fig. 9. Therefore, CO enhances the process performance when operating on the left side, but degrades reductions on the right side.

#### Critical $\text{NO}_x$

On Fig. 5, part of the curve that represents the controlled  $\text{NO}_x$  concentrations at 1 second residence time and at temperatures between 900 and 1300 °C is the lowest achievable  $\text{NO}_x$  concentration curve. Increases in residence time or NSR do not lower  $\text{NO}_x$  below this curve. On Fig 10,  $\text{NO}_c$  concentrations are plotted for the

equilibrium concentration of CO at three baseline NO<sub>x</sub> concentrations. At temperatures below 900 °C, 10 seconds of residence time are required to determine the lowest achievable concentration. This minimum achievable NO<sub>x</sub> concentration through urea injection, is termed as 'Critical NO<sub>x</sub>', as first indicated by Fenimore [11] for the Thermal DeNO<sub>x</sub> process. Neither an increase in residence time nor treatment rate above a certain value will lower the controlled NO<sub>x</sub> below this critical NO<sub>x</sub> concentration.

The existence of critical NO<sub>x</sub> and its lack of dependencies to residence time and treatment rate are understood through a simplified chemical kinetic analysis. The change of NO concentration with respect to time for following reactions is formulated as equation 1.



$$\frac{d[\text{NO}]}{dt} = -k_1[\text{NH}_2][\text{NO}] - k_2[\text{NCO}][\text{NO}] + k_3[\text{NH}_2][\text{OH}] + k_4[\text{NCO}][\text{OH}] \quad (1)$$

With urea injection, NO<sub>x</sub> concentration will change from its baseline value to a steady state value. At this point, the lefthand side of the above equation becomes zero. After rearranging, an expression for critical NO<sub>x</sub>, [NO]<sub>c</sub>, is arrived as equation 2.

$$[\text{NO}]_c = \frac{[\text{OH}]\{k_3[\text{NH}_2] + k_4[\text{NCO}]\}}{\{k_1[\text{NH}_2] + k_2[\text{NCO}]\}}; \frac{d[\text{NO}]}{dt} = 0 \quad (2)$$

This equation is further simplified for cases where NH<sub>2</sub> is comparable to NCO, NH<sub>2</sub> is in large excess of NCO, and NCO is in large excess of NH<sub>2</sub>.

$$[\text{NO}]_c = [\text{OH}] \frac{(k_3 + k_4)}{(k_1 + k_2)} \quad \text{NH}_2 \sim \text{NCO}$$

$$[\text{NO}]_c = [\text{OH}] \frac{k_3}{k_1} \quad \text{NH}_2 \gg \text{NCO}$$

$$[\text{NO}]_c = [\text{OH}] \frac{k_4}{k_2} \quad \text{NCO} \gg \text{NH}_2$$

These three cases show that NO<sub>c</sub> is only a function of OH concentration at a given temperature and does not dependent on residence time or NSR. However, chemicals that generate CO and consequently increase the OH concentration will affect the critical NO<sub>x</sub>.

The critical  $\text{NO}_x$  limits the process on the right side of the window. As shown in Fig. 10, the critical  $\text{NO}_x$  concentrations are less than 40 ppm at 1050 °C and even lower at temperatures below 1000 °C. These low levels usually do not limit process applications. Instead, the critical  $\text{NO}_x$  limits achieving low controlled  $\text{NO}_x$  concentrations at high temperatures where  $\text{NO}_x$  increases sharply with temperature and baseline  $\text{NO}_x$ . Finally, reductions are achievable as long as a baseline  $\text{NO}_x$  is higher than the critical  $\text{NO}_x$  concentration.

#### Laboratory and Field Verification

The model study indicates that achievable  $\text{NO}_x$  concentrations are limited by critical  $\text{NO}_x$  and this limit is mainly affected by temperatures. Case 1 and case 2 exhibit the process limitation due to  $\text{NO}_c$  while case 3 shows that reductions are possible even at high temperatures if baseline  $\text{NO}_x$  is greater than the  $\text{NO}_c$ .

##### Case 1.

A  $\text{NO}_x$ OUT Process testing on a coal fired boiler revealed that  $\text{NO}_x$  reduction increased with decreasing boiler load, as shown in Fig. 11. At full load,  $\text{NO}_x$  reduction remained essentially unchanged in spite of a series of injection optimization tests. However, a slight reduction in boiler load from 100% to 90% increased  $\text{NO}_x$  reduction. At full load, reaction is occurring at the steep part of the  $\text{NO}_c$  curve, and therefore,  $\text{NO}_x$  reduction improved rapidly with decreasing load under an essentially identical injection configuration. The controlled  $\text{NO}_x$  curve on Fig. 10 virtually represents the critical  $\text{NO}_x$  curve for this boiler.

##### Case 2.

During a process demonstration at an ethylene cracker,  $\text{NO}_x$  reduction was limited regardless of the  $\text{NO}_x$ OUT Process parameters. The cracker unit operated steadily at a temperature of approximately 1050 °C. When the unit operated at a higher  $\text{NO}_x$  baseline,  $\text{NO}_x$  reduction increased, but the lowest achievable  $\text{NO}_x$  concentration remained the same, as shown in Fig. 12. Increasing NSR or other methods to optimize chemical distribution had no effect on the lowest controlled  $\text{NO}_x$ . This showed the existence of critical  $\text{NO}_x$  that is unaffected by NSR, chemical distribution, or baseline  $\text{NO}_x$ .

##### Case 3.

An increase in  $\text{NO}_x$  baseline shifts the right side of the temperature window to a higher temperature. To verify this, a pilot scale combustor was operated at 1200 °C and the baseline  $\text{NO}_x$  concentration was increased from 150 to 750 ppm. At baseline  $\text{NO}_x$  below about 200 ppm,  $\text{NO}_x$  increased with urea injection, while at higher than 200 ppm,  $\text{NO}_x$  decreased as shown in Fig. 13. Comparison with ammonia injection showed that urea is more effective in reducing  $\text{NO}_x$  at high temperatures than ammonia.

## Conclusions

The reaction kinetic model has proven to be a valuable tool in the development of the NO<sub>x</sub>OUT Process. Model predictions with respect to the temperature window, the effect of residence time and CO, the effect of very low excess oxygen, and the phenomenon of critical NO<sub>x</sub>, which limits NO<sub>x</sub> reduction at the high end of the temperature window, have all been verified in laboratory and field tests. The temperature window is defined primarily by residence time at the low temperature (left) side and by baseline and critical NO<sub>x</sub> at the high temperature (right) side of the window.

The model is now used to define temperature/residence time requirements for specific applications and to predict maximum achievable NO<sub>x</sub> reduction. The model has also shown that the NO<sub>x</sub>OUT Process can be applied at higher temperatures than previously thought applicable provided that the NO<sub>x</sub> baseline is sufficiently high.

## References

1. Lyon, R.K., U.S. Patent 3,900,559, 1975.
2. Lyon, R.K., "Thermal DeNO<sub>x</sub>: Controlling Nitrogen Oxides Emissions by a Noncatalytic Process", Environ. Sci. Technol., Vol. 21, No. 3, p.231, 1987.
3. Arand, J.K., and Muzio, L.J., U.S. Patent 4,208,386, 1980.
4. Arand, J.K., Muzio, L.J., Teixeira, D.P., U.S. Patent 4,325,924, 1982.
5. Benson, C.E., Chittick, G.D., and Wilson R.P., Selective Catalytic NO<sub>x</sub> Reduction Technology for Cogeneration Plants, Arthur D. Little Report, Prepared for New England Cogeneration Association, November 1988.
6. Kee, R.J., Miller, J.A., Jefferson, T.H., "CHEMKIN: A General Purpose, Problem-Independent, Transportable, Fortran Chemical Kinetics Code Package", Sandia Laboratories Report #SAND80-8003, Livermore, CA, 1980.
7. Hindmarsh, A.C., "ODEPACK, A Systematized Collection of ODE Solvers", Scientific Computing, R.S. Stepleman et al. (eds.), Vol.1 of IMACS Transactions on Scientific Computation, p.55, North-Holland, Amsterdam, 1983.
8. Sun, W.H., Stamatakis, P., Michels, W.F., Comparato, J.R., Hofmann, J.E., "Selective Non-Catalytic NO<sub>x</sub> Control with Urea: Theory and Practice, Progress Update", AFRC 1992 Fall International Symposium, October 1992.
9. Miller, J.A., Bowman, C.T., "Mechanism and Modeling of Nitrogen Chemistry in Combustion", Fall Meeting of the Western States Section/The Combustion Institute, Dana Point, California, October, 1988.
10. Epperly, W.R., O'Leary, J.H., Sullivan, J.C., U.S. Patent 4,780,289, 1988.
11. Fenimore, C.P., "Destruction of NO by NH<sub>3</sub> in Lean Burnt Gas", Combustion and Flame, 37, 245, 1980.

# POST COMBUSTION NO<sub>x</sub> REDUCTION with UREA

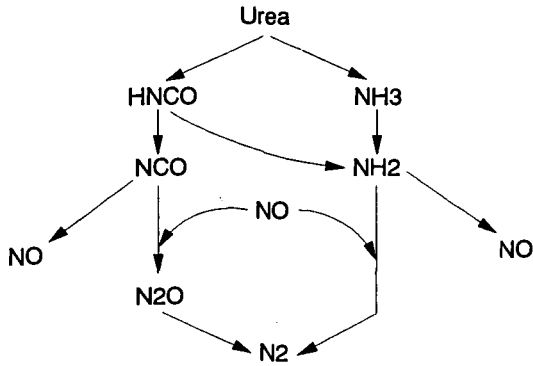


Fig. 1

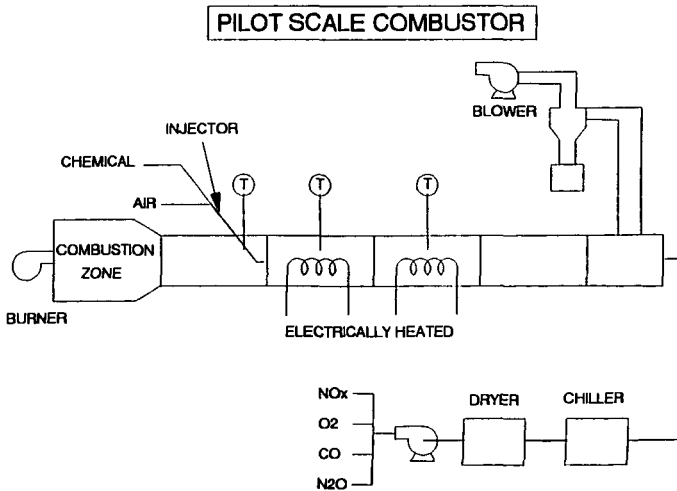


Fig. 2

## Effect of Temperature on NOx Reduction

Urea Injection, NSR = 2, NOxI = ~300ppm  
Comparison of Model vs. Experimental

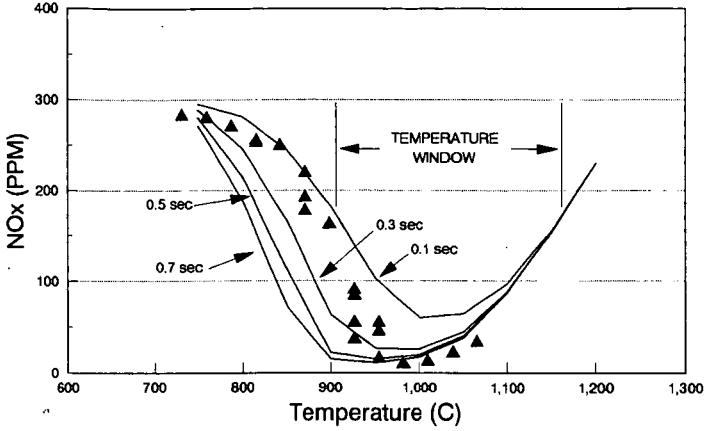


Fig. 3

## Effect of NSR on NOx Reduction

Residence Time = 1 sec, NOxI = 200 ppm  
NOxOUT Kinetic Model

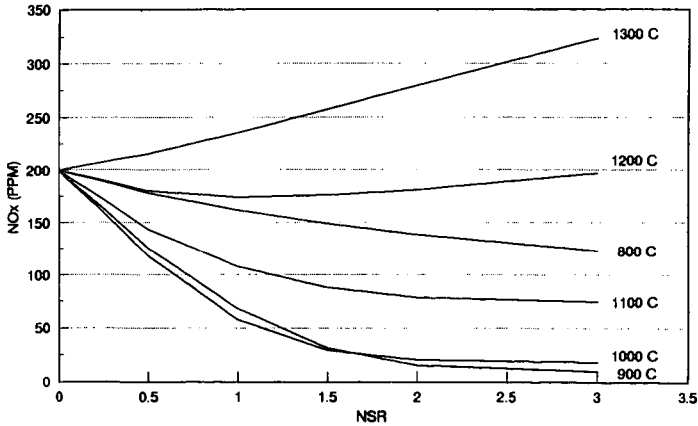


Fig. 4

### Effect of Residence Time on NOx Reduction

NSR = 2, NO<sub>x</sub>i = 200 ppm  
NO<sub>x</sub>OUT Kinetic Model

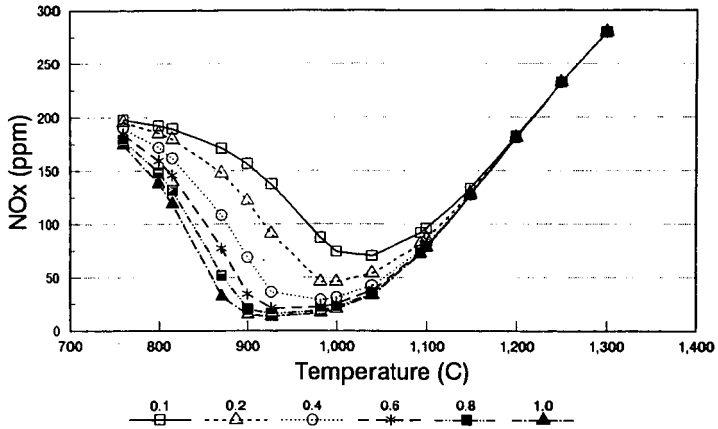


Fig. 5

### Effect of Baseline NOx

NSR = 2, O<sub>2</sub> = 3%, Residence Time = 1 sec.  
NO<sub>x</sub>OUT Kinetic Model

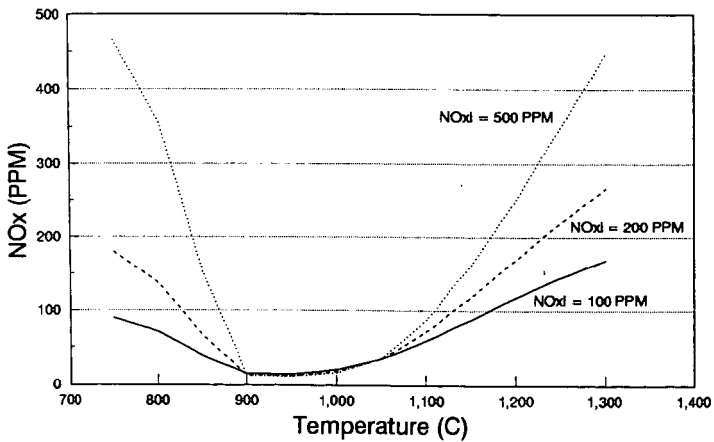


Fig. 6

## Effect of Baseline NOx on Temperature Window

NSR = 2, Residence Time = 1 sec.  
NOxOUT Kinetic Model

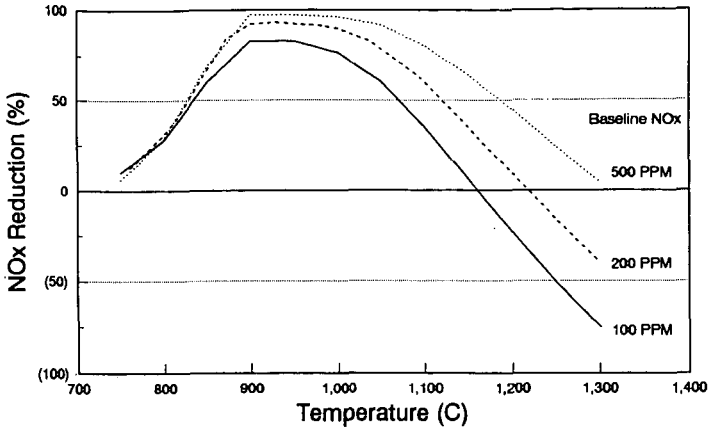


Fig. 7

## Effect of O2 Concentration on NOx Reduction

NSR = 2, Residence Time = 1 sec., NOx = 200 ppm  
NOxOUT Kinetic Model

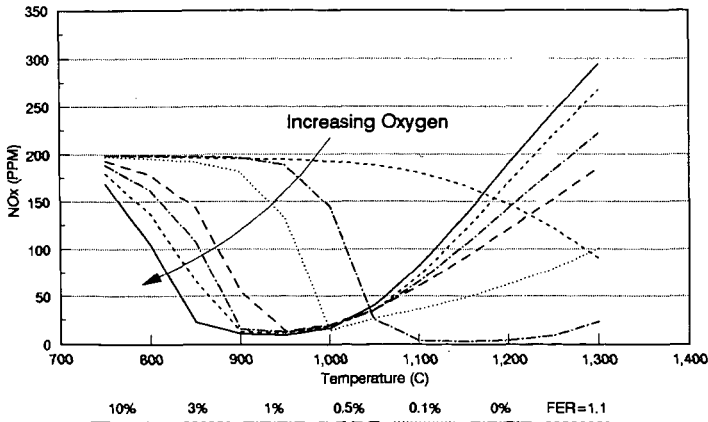


Fig. 8

### Effect of CO Concentration on NOx Reduction

NSR = 2, Residence Time = 1 sec., NOxI = 200 ppm  
NOxOUT Kinetic Model

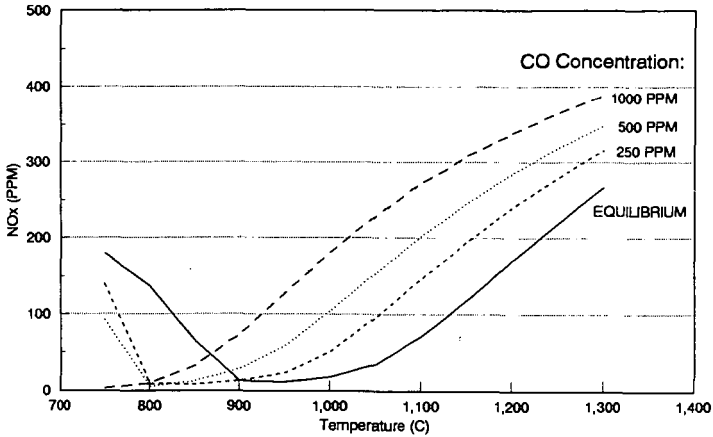


Fig. 9

### Critical NOx Concentration

3% Excess Oxygen, Equilibrium CO Concentration  
NOxOUT Kinetic Model

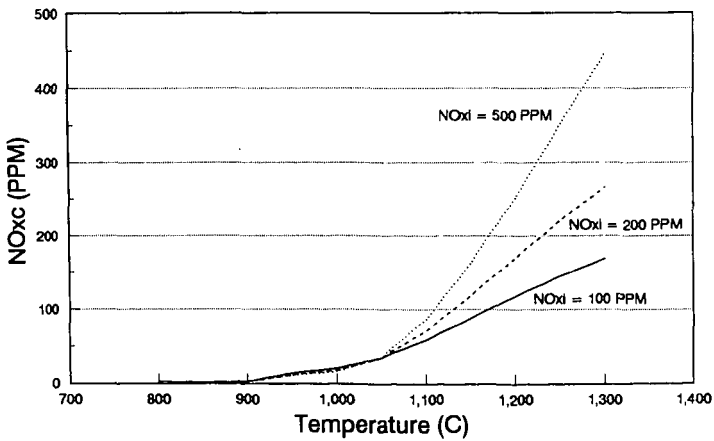


Fig. 10

## Effect of Boiler Load on Controlled NOx

NOxOUT Process Testing on a Coal-Fired Boiler

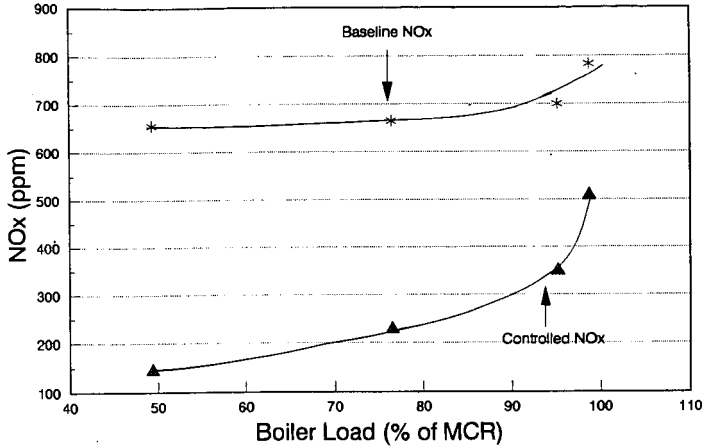


Fig. 11

## NOx REDUCTION AT ETHYLENE CRACKER

Temperature - approximately 1050 C

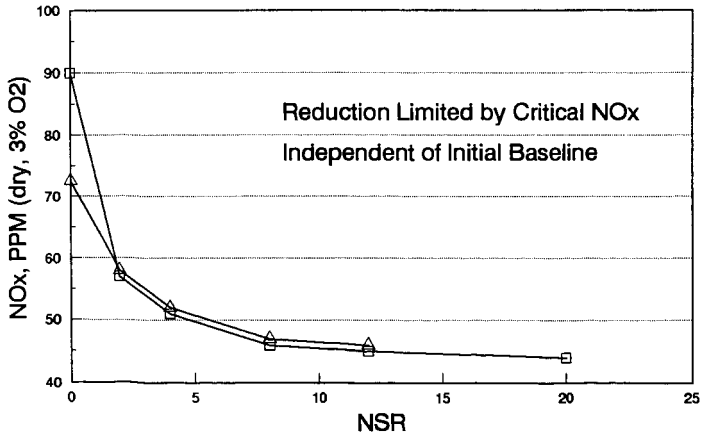


Fig. 12

### Effect of Baseline on NOx Reduction

Result from Pilot Scale Combustor, NSR = 2

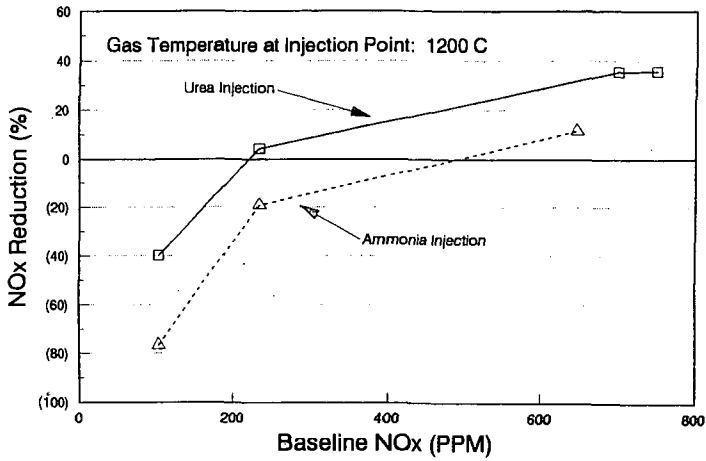


Fig. 13

## N<sub>2</sub>O DECOMPOSITION CATALYZED IN THE GAS PHASE BY SODIUM

S. L. Chen, R. Seeker, R. K. Lyon, and L. HO  
Energy and Environmental Research Corp  
18 Mason  
Irvine, CA. 92718

Key words: N<sub>2</sub>O, sodium atom, fluid bed combustion, urea injection

### INTRODUCTION

The concentration of N<sub>2</sub>O in the atmosphere is observed to be increasing at a rate of 0.18% to 0.26% annually. This increase in the N<sub>2</sub>O concentration is presumably the result of one or more human activities, though the activities responsible have not been identified with certainty. Whatever the source of the N<sub>2</sub>O its increase in the atmosphere is a matter of concern both because N<sub>2</sub>O is a greenhouse gas and because it has a major and unfavorable influence on the ozone layer (1,2,3).

Until recently it was believed that in additions to its problems with NO, NO<sub>2</sub>, and SO<sub>2</sub> emissions pulverized coal firing also had a severe problem with N<sub>2</sub>O emissions. Weiss and Craig (4), Pierotti and Rasmussen (5), Hae et al (6), and C. Castaldinin et al (7), have all reported measurements of N<sub>2</sub>O emissions by pulverized coal fired utility boilers (8). N<sub>2</sub>O levels of approximately 25% of the NO emissions were found. If one accepted this 25% correlation between N<sub>2</sub>O and NOx emissions, the observed increase in N<sub>2</sub>O concentration could be accounted for with reasonable accuracy as coming from pulverized coal firing (5). Thus in addition to its problems with NO, NO<sub>2</sub> and SO<sub>2</sub> emissions pulverized coal firing appeared to be an unacceptable technology because of its N<sub>2</sub>O emissions.

Lyon and coworkers (9) have, however, shown that when samples of combustion gases are allowed to stand for periods of hours, chemical reactions occur which form N<sub>2</sub>O. Since the studies mentioned above all involved taking samples for later analysis, they were all subject to this artifact and it was possible that the N<sub>2</sub>O which was apparently present in gases from pulverized coal firing was in fact absent. Later measurements of N<sub>2</sub>O emissions for numerous pulverized coal fired utility boilers and other large combustion systems confirmed this expectation, i.e. none of the long established combustion technologies were found to produce significant quantities of N<sub>2</sub>O (10). Given N<sub>2</sub>O is unstable at extremely high temperatures and that all the long established combustion technologies involve extremely high temperatures, this result is not surprising.

For the much lower temperatures involved in fluid bed combustion, however, N<sub>2</sub>O production is quite high (11) and this may be a barrier to extending the industrial use of this technology.

N<sub>2</sub>O emissions are also a problem in the NOxOUT and RAPRENOx technologies for controlling NOx emissions, but not in the Thermal DeNOx process. In the latter NH<sub>3</sub> is injected into hot flue gas, and NO is reduced by the

$\text{NH}_3 + \text{NO}$  reaction. In RAPRENOx, however, HNCO is injected, the NCO radical can be formed, and  $\text{N}_2\text{O}$  can be formed via the  $\text{NCO} + \text{NO} = \text{N}_2\text{O} + \text{CO}$  reaction. Since the urea injected in the NOxOUT process decomposes to equimolar amounts of  $\text{NH}_3$  and HNCO this technology also has a problem with  $\text{N}_2\text{O}$  production.

This paper reports the discovery of a promising new method of controlling the emissions of  $\text{N}_2\text{O}$ . This discovery has been demonstrated on a 0.9 MBTU/hr natural gas fired research combustor and has been examined by computer modeling.

#### APPARATUS, EXPERIMENTAL PROCEDURES AND COMPUTER MODELING PROCEDURES

Experiments were done in a 15.2 centimeter diameter by 2.4 meter long refractory lined tunnel furnace which has been described in detail elsewhere (12).

Computer modeling experiments were done using the reaction mechanism shown in Table 1 with the PC version of Chemkin. While this program is nominally limited to gas phase specie, the presence of liquid phase materials such as  $\text{Na}_2\text{CO}_3$  was easily handled by assuming a fictional gas phase specie with thermodynamic properties such that at equilibrium it produced the same gas phase species in the same amounts as does the vaporization of the liquid phase material.

#### EXPERIMENTAL RESULTS

A series of experiments was done in which the effects of various additives on the reduction of NO by urea injection was examined. Figure 1 shows the results of an experiment comparing NO reduction by urea and by urea mixed with monosodium glutamate (MSG). The urea-MSG mixture achieves a deeper reduction of NO over a wider temperature range than did pure urea. While results similar to this were obtained with other mixtures of urea with organic compounds, as shown in Figure 2 the addition of MSG was also found to greatly decrease the production of  $\text{N}_2\text{O}$ .

Figure 3 shows the effect on  $\text{N}_2\text{O}$  production during NO reduction by urea of adding  $\text{Na}_2\text{CO}_3$  and  $\text{Na}_2\text{SO}_4$ .

Figure 4 shows the results of an experiment in which solid  $\text{Na}_2\text{CO}_3$  was injected into the post combustion gases at a point at which their temperature was  $2150^\circ\text{F}$  and  $\text{N}_2\text{O}$  was injected at a downstream point for which the temperature was  $1800^\circ\text{F}$ . Not only do these results show that  $\text{Na}_2\text{CO}_3$  injection is an effective method for  $\text{N}_2\text{O}$  removal, they show that in some manner the  $\text{Na}_2\text{CO}_3$  acts as a catalyst for  $\text{N}_2\text{O}$  removal, many  $\text{N}_2\text{O}$  molecules being removed for each injected  $\text{Na}_2\text{CO}_3$ .

Figure 5 shows computer modeling calculations which will be discussed later and experimental data for the temperature dependence of  $\text{Na}_2\text{CO}_3$  catalyzed  $\text{N}_2\text{O}$  decomposition. It is interesting to note that within experimental error the rate of  $\text{N}_2\text{O}$  decomposition is independent of whether 50 or 100ppm  $\text{Na}_2\text{CO}_3$  is used to catalyze the decomposition.

Figure 6 shows the effect of  $\text{SO}_2$  on the  $\text{Na}_2\text{CO}_3$  catalyzed decomposition of  $\text{N}_2\text{O}$ . While the presence of  $\text{SO}_2$  does to some extent reduce the ability of  $\text{Na}_2\text{CO}_3$  to catalyze the decomposition of  $\text{N}_2\text{O}$ , even high ratios of  $\text{SO}_2$  to  $\text{Na}_2\text{CO}_3$  are not able to completely inhibit this catalyzed reaction.

#### COMPUTER MODELING RESULTS

At high temperatures the thermodynamically most favorable path for  $\text{Na}_2\text{CO}_3$  vaporization is the reaction  $\text{Na}_2\text{CO}_3 = 2\text{Na} + 1/2\text{O}_2 + \text{CO}_2$ . Figure 7 shows the calculated equilibrium for this reaction. The rate of the reaction between sodium atom and  $\text{N}_2\text{O}$  has been measured by a number of investigators and is relatively well established as are all of the other reactions shown in Table 1 with the exception of  $\text{Na} + \text{Na}_2\text{O} = \text{NaO} + \text{NaO}$ . Since this reaction is analogous to a number of reactions which are known to be extremely rapid, it is assumed to occur with a rate equal to the three body collision rate.

In doing these calculations it was also assumed that the vaporization of  $\text{Na}_2\text{CO}_3$  achieves equilibrium instantaneously.

The predictions of this computer model agree with experiment in that the model shows that  $\text{Na}_2\text{CO}_3$  can cause rapid  $\text{N}_2\text{O}$  decomposition, that this  $\text{N}_2\text{O}$  decomposition is catalytic, and that it occurs only above a threshold temperature which the model approximately predicts.

In qualitative terms this reaction mechanism also explains the fact that  $\text{SO}_2$  inhibited  $\text{Na}_2\text{CO}_3$  catalyzed  $\text{N}_2\text{O}$  decomposition, i.e.  $\text{SO}_2$  reacts readily with  $\text{Na}_2\text{CO}_3$  converting it to nonvolatile  $\text{Na}_2\text{SO}_4$ . Once the  $\text{Na}_2\text{CO}_3$  becomes coated with a layer of  $\text{Na}_2\text{SO}_4$  its ability to exert its vapor pressure would be reduced.

#### CONCLUSIONS

The injection of sodium carbonate has been shown to be an effective method of preventing the emission of  $\text{N}_2\text{O}$  in combustion systems. This decomposition is catalytic but occurs in the gas phase. Computer modeling studies suggest that in this catalytic gas phase decomposition the reactions  $\text{Na} + \text{N}_2\text{O} = \text{NaO} + \text{N}_2$  and  $2\text{NaO} = 2\text{Na} + \text{O}_2$  are important.

#### REFERENCES

- 1 Weiss., R.F., J. Geophys. Res., 86,7185-7195 (1981).
- 2 Khalil, M.A. and Rasmussen, R.A., Tellus, 35B, 161-169 (1983).
- 3 Marland, G., and Rotty, R.M. J.A.P.C.A., 35, 1033-1038 (1985).
- 4 Weiss, R.F. and Craig, H., Geophys. Res. Lett., 3, 751-753, (1976).
- 5 Pierotti, D. and Rasmussen, R.A., Geophys. Res. Lett., 3, 265-267 (1976).
- 6 Hao, W.M., Wofsy, S.C., McElroy, N.B., Beer, J.M., Toqan, M.A., J. Geophys. Res., 92, 3098-3194 (1987).
- 7 Castaldini, C., Waterland, L.R., and Lips, H.I., EPA-600-7-86-003a, 1986.
- 8 Ryan, J. V., and R. K. Srivastava, EPA/IFP workshop on the emission of nitrous oxide from fossil fuel combustion (Rueil-Malmaison, France, June 1-2, 1988), Rep. EPA-600/9-89-089, Environ. Prot. Agency, Research Triangle Park, N.C., 1989. (Available as NTIS PB90-126038 from Natl. Technol. Inf. Serv., Springfield, Va.)
- 9 Lyon, R. K., Kramlich, J. C., et. al., 23rd Symposium (International) on Combustion, in press. also see Lyon, R. K., and Cole, J. A., Combustion and Flame, 77, 139 (1989) and Kramlich, J. C. and Muzio, L.-J., Geophysical Research Letters, 15, 1369-1372, (1988)
- 10 Levine, J. S., 1991 Joint Symposium on Stationary Combustion NOx Control -- EPA/EPRI March 1991, Washington, D.C.
- 11 Amand, L. E., and Leckner, B., Combustion and Flames, 84, 181-196, (1991) Also see references 8 and 10.
- 12 S. L. Chen, M. P. Heap, D. W. Pershing, and G. B. Martin, Fuel 61, 1218 (1982)



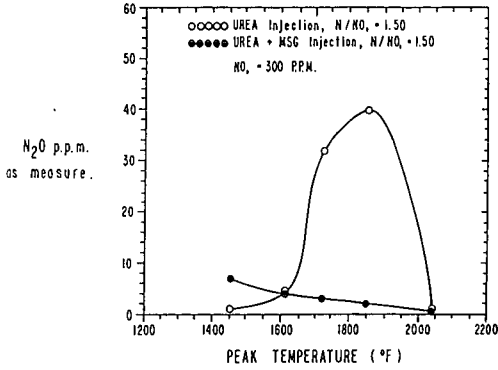


Figure 2

### N<sub>2</sub>O Reduction

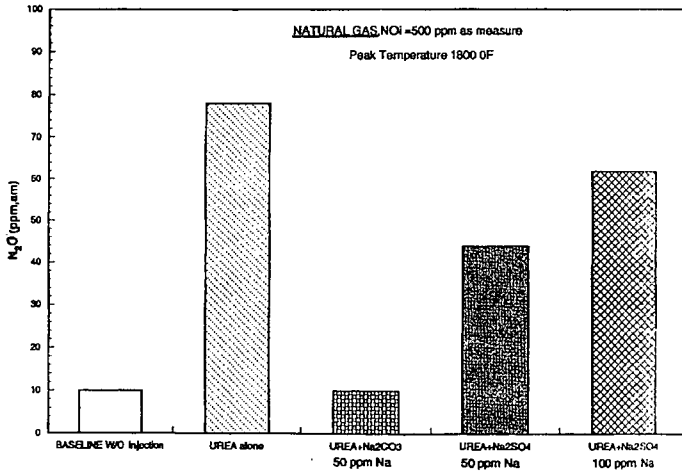


Figure 3

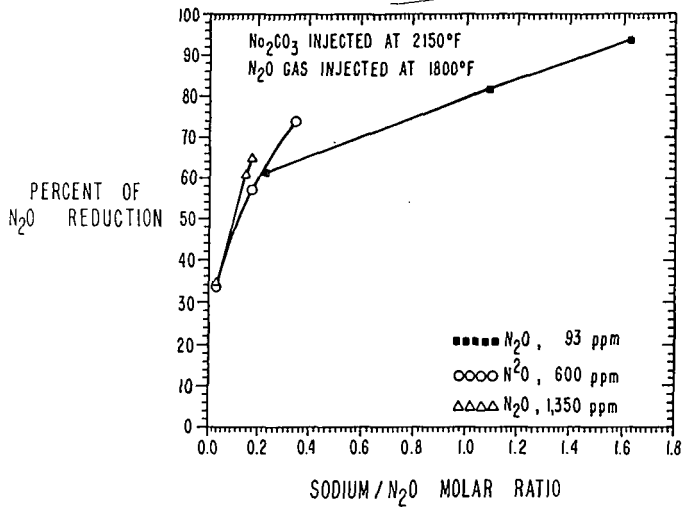
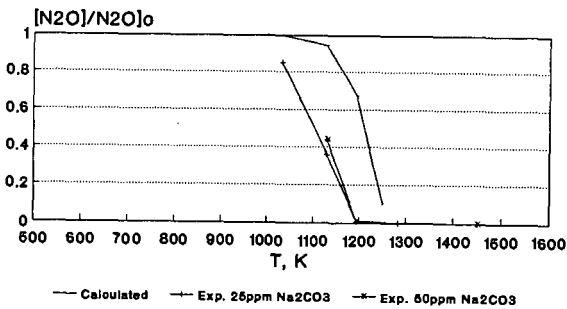


FIG. 4

Temperature Dependence of  $\text{Na}_2\text{CO}_3$  Catalyzed Decomposition of  $\text{N}_2\text{O}$



Calculations done for  $[\text{N}_2\text{O}]_0 = 100\text{ppm}$ ,  
 $t = 0.1\text{sec}$ , 3.8%  $\text{O}_2$ , 8.1%  $\text{CO}_2$ , 16.2%  $\text{H}_2\text{O}$   
 $[\text{Na}] = \text{equilibrium for } \text{Na}_2\text{CO}_3$

Figure 5

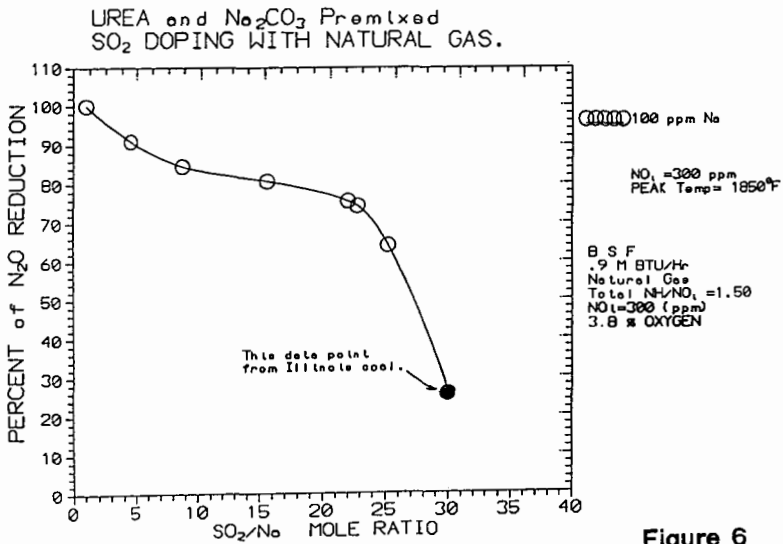


Figure 6

Equilibrium Calculation for  
 $\text{Na}_2\text{CO}_3 = 2\text{Na} + 1/2\text{O}_2 + \text{CO}_2$

